RIHAN(

PE 4613 - Lecture Notes

GAS RESERVOIR ENGINEERING

by

Djebbar Tiab, Ph.D.
Professor
School of Petroleum and Geological Engineering
The University of Oklahoma
Norman, Oklahoma, U.S.A.

Summer University 2000

Djebbar TIAB, Ph.D.

Professor, School of Petroleum & Geological Engineering, the University of Oklahoma

Director, *the University of Oklahoma Graduate Program in Petroleum Engineering in Algeria*

Dr. Tiab is the Senior Professor of Petroleum Engineering at the University of Oklahoma. He received his B.Sc. (May 1974) and M.Sc. (May 1975) degrees from the New Mexico Institute of Mining and Technology, and Ph.D. degree (July 1976) from the University of Oklahoma - all in Petroleum Engineering, with a minor in mathematics. He is also the Director of "The University of Oklahoma Graduate Program in Petroleum Engineering in Algeria", which started in July 1997 on the campus of the Algerian Petroleum Institute (IAP) in Boumerdess, and is expected to last 8 years.

Before joining the University of Oklahoma in 1977, he worked as an assistant professor at the New Mexico School of Mining and Technology, where he taught drilling & well completion, production engineering, well logging and natural gas engineering. At the University of Oklahoma, Dr. Tiab taught various petroleum and general engineering courses including: oil reservoir engineering, natural gas engineering, well test analysis, fluid mechanics, properties of reservoir fluids, fluid flow through porous media, introduction to engineering, advanced reservoir engineering, advanced natural gas engineering, petrophysics, advanced petrophysics, and advances in pressure transient analysis.

Dr. Tiab was president of the consulting firm United Petroleum Technologies Corporation (UPTEC) for fourteen years: 1980 - 1984 and 1990 – present. He has consulted for a number of oil companies and offered training programs in petroleum engineering in the USA and overseas. He worked for over two years in the oil fields of Algeria for Alcore, S.A., an association of Sonatrach and Core Laboratories. He has also worked and consulted for Core Laboratories and Western Atlas in Houston, Texas, for four years (1989-1993) as a Senior Reservoir Engineer Advisor.

As a researcher at the University of Oklahoma, Dr. Tiab received several research grants from the National Science Foundation (NSF), United States Department of Energy (DoE), U.S. Department of HEW, oil companies, Oklahoma Mining and Mineral Resources Institute, EPSCoR and the Energy Resources Institute. He is a member of the U.S. Research Council, SPE, Core Analysis Society, Pi Epsilon Tau, and American Men and Women of Science. He served as a technical editor of various SPE journals. He is currently a member of the SPE Pressure Analysis Transaction Committee.

Dr. Tiab is the author of over 100 journal and conference technical papers in the area of pressure transient analysis, petrophysics, natural gas engineering, reservoir characterization, reservoir engineering and injection processes. In **1975** (M.S. thesis) and **1976** (Ph.D. dissertation), **Tiab introduced the pressure derivative technique** which revolutionized the interpretation of pressure transient tests. He received several patents in the area of reservoir characterization (identification of flow units). He is the senior author of the textbook "**PETROPHYSICS**", published by Gulf Publishing Company, 1st Edition in October 1996 and 2nd Edition in 2000. He is currently working on two new books: "Advances in Pressure Transient Analysis" and "Advances in Petrophysics."

Dr. Tiab supervised 21 Ph.D. and 47 M.Sc. students at the University of Oklahoma. He received the Outstanding Young Men of America Award (1983), the SUN Award for Education Achievement (1984), Kerr-McGee Distinguished Lecturer Award (1985), the College of Engineering Faculty Fellowship of Excellence (1986), the Halliburton Lectureship Award (1987-89), Who's Who in Engineering (1989) and the UNOCAL Centennial Professorship (1995-1998).

He also received the prestigious 1995 SPE Distinguished Achievement Award for Petroleum Engineering Faculty. The citation read, ***"He is recognized for his role in student development and his excellence in classroom instruction. He pioneered the pressure derivative technique of well testing and has contributed considerable understanding to petrophysics and reservoir engineering through his research and writing."***

Table of contents

PART 1

Introduction

1. INTRODUCTION

Note to students: These lecture notes are based on Chapters 1, 6, 7 and 10 of the SPE Textbook Series Vol. 5, by J. Lee and R. A. Wattenberger. This book is used as a required textbook for the course PE 4463 - Natural Gas Engineering, which I teach at the University of Oklahoma. These notes are solely used to prepare transparencies for classroom presentation, and not intended for commercial use.

Part 2 presents methods for estimating reservoir fluid properties required for gas-reservoir-engineering calculations. First, PVT diagrams are used to define different types of gas reservoirs such as (1) dry gas, (2) wet gas, and (3) gas-condensate reservoirs. Then, the equations of state are presented, followed by a large number of correlations used to determine physical properties of the gas. Fluid sampling techniques are finally presented for each type of the gas reservoirs mentioned above.

Part 3 focuses on estimating original gas in place, gas reserves, and recovery factors for a variety of reservoir drive mechanisms. The first section discusses volumetric methods, including data requirements, calculation techniques, and limitations of the methods. This first section includes equations for volumetric dry reservoirs, dry-gas reservoirs with water influx, and volumetric wet-gas and gas-condensate reservoirs. Next, analysis techniques based on material-balance concepts are discussed. An equation for a volumetric gas reservoir is first derived in which gas expansion is the primary source of energy. This equation is then modified to include other external and internal energy sources (e.g., water influx, compressibility of connate water, and rock PV) and the effects of water vaporization and hydrocarbon phase changes. Applications of both volumetric and material-balance methods are illustrated with examples.

In Part 4 the theory and practical applications of pressure-transient testing in gas wells are presented. Beginning with the line-source (Ei-function) solution to the diffusivity equation, analysis techniques are presented for flow and buildup tests in homogeneous--acting reservoirs. Both semilog and log-log plotting analysis techniques are discussed and illustrated with examples. Non-Darcy flow effects that are more pronounced in gas-well testing are also discussed. Application of the pressure derivative concept in gas well testing is introduced only briefly, because this modern method is covered in a separate course (PE 5553 - Well Test Analysis)

Part 5 discusses the implementation and analysis of the four most common types of gas-well deliverability tests: flow-after-flow, single-point, isochronal, and modified isochronal tests. First, fundamental gas-flow equations, both theoretical and empirical, used to analyze deliverability tests are presented in terms of either pressure squared or the real-gas pseudopressure function. Next, the discussion focuses on specific tests and testing procedures, advantages and disadvantages of each testing method, and common analysis techniques.

SI METRIC CONVERSION FACTORS

acre	x 4.046 873	E+03 = m^2
acre	x 4.046 873	E–01 = ha
acre-ft	x 1.233 489	E+03 = m^3
ampere-hr	x 3.6*	E+03 = C
Å	x 1.0*	E–01 = nm
°API	141.5/(131.5+°API)	= g/cm^3
atm	x 1.013 250*	E+05 = Pa
bar	x 1.0*	E+05 = Pa
bbl	x 1.589 874	E–01 = m^3
Btu	x 1.055 056	E+00 = kJ
Ci	x 3.7*	E+10 = Bq
cp	x 1.0*	E–03 = Pa•s
cycles/sec	x 1.0*	E+00 = Hz
dyne	x 1.0*	E–02 = mN
eV	x 1.602 19	E–19 = J
ft	x 3.048*	E–01 = m
ft^2	x 9.290 304*	E–02 = m^2
ft^3	x 2.831 685	E–02 = m^3
°F	(°F – 32)/1.8	= °C
°F	(°F + 459.67)/1.8	= K
gal	x 3.785 412	E–03 = m^3
hp	x 7.460 43	E–01 = kW
hp-hr	x 2.684 520	E+00 = MJ
in.	x 2.54*	E+00 = cm
$in.^2$	x 6.451 6*	E+00 = cm^2
$in.^3$	x 1.638 706	E+01 = cm^3
kip	x 4.448 222	E+03 = N
knot	x 5.144 444	E–01 = m/s
ksi	x 6.894 757	E+03 = kPa
kW-hr	x 3.6*	E+00 = J
lbf	x 4.448 222	E+00 = N
lbm	x 4.535 924	E–01 = kg
mL	x 1.0*	E+00 = cm^3
mho	x 1.0*	E+00 = S
mile	x 1.609 344*	E+00 = km
oz	x 2.957 353	E+01 = cm^3
psi	x 6.894 757	E+00 = kPa
psi^2	x 4.753 8	E+01 = kPa^2
sq mile	x 2.589 988	E+00 = km^2
stokes	x 1.0*	E–04 = m^2/s
ton	x 9.071 847	E–01 = Mg
ton (metric)	x 1.0*	E+00 = Mg
tonf	x 8.896 444	E+03 = N
tonne	x 1.0*	E+00 = Mg

*Conversion factor is exact.

PART 2

PHYSICAL PROPERTIES OF GAS

2. PHYSICAL PROPERTIES OF GAS

The primary difference between a gas reservoir and an oil reservoir is the difference in composition in which the hydrocarbon material occurs at the original reservoir P and T:

- Oil reservoirs are usually a mixture in which heavier hydrocarbon components (normally liquid at atmospheric temperature and pressure) comprise the major fraction of the fluid.
- Gas reservoirs are a mixture in which the dominant constituents are lighter components.
- PVT diagrams, such as Figures 2.1.1-5 and Fig. 2.2, are commonly used to represent the phase behavior of hydrocarbon fluids and classify petroleum reservoirs.
- Understanding how properties of oil and gas change with pressure and temperature is undoubtedly the key to reservoir engineering and production.

2.1 - PVT DIAGRAM

2.1.1 - SOLUTION OR DISSOLVED GAS RESERVOIR

- Consider (as an example) a reservoir initially at P_i = 3000 psia and T_i = 125 °F, represented by point 1_i on Fig. 2.2
- Because point 1_i is in the single phase region above the bubble point line and $T_i < T_c$ the *HYDROCARBON MIXTURE* is in the liquid phase, 1.e. an oil reservoir.
- This type of reservoir is referred to by several names: *bubble point, dissolved gas, undersaturated oil, depletion, solution gas drive, expansion, and internal gas drive reservoir!*

- As the pressure declines in the reservoir (due to oil production) at a constant T, the *bubble point* will be reached (in Fig. 2.2 at point S where P = 2550 psia).
- *Bubble point pressure P_b (or saturation pressure)* refers to the highest pressure at which the first gas bubble comes out of solution from the oil and exists as free gas in the reservoir.
- Below this pressure, a free gas phase will appear. Eventually the free gas evolved begins to flow to the wellbore in ever-increasing quantities. Conversely, the oil flows in ever-decreasing quantities.
- The actual amount of free gas liberated will depend on the composition of the original oil:

  (a) *High API gravity* oil reservoirs, which contain relatively large amounts of the lighter and intermediate hydrocarbons, will release large amounts of gas.

  -- These reservoirs are also called *volatile* or *high- shrinkage oil* reservoirs (Fig. 2.1.2)

  (b) *Low API gravity* oil reservoirs, which contain small amounts of the lighter hydrocarbons, will release much smaller amounts of gas.

  -- These reservoirs are referred to as *black oil* or *low- shrinkage oil* reservoirs (Fig. 2.1.1)

2.1.2 - GAS CAP

- If the same *HYDROCARBON MIXTURE* in the above discussion occured (for instance) at P_i = 2000 psia and T_i = 215 °F, as shown in Fig. 2.2 (point 2), it would be an oil reservoir with a gas cap, or *gas cap reservoir.*

- The slightest reduction in pressure causes liberation of gas from oil (because $P_i \simeq P_b$), making this a saturated oil reservoir. Hence, anytime $P_i \simeq P_b$, we can conclude that the reservoir has an initial gas cap.

2.1.3 - GAS CONDENSATE

- Most known gas-condensate reservoirs are in the range of 3000-6000 psia and 200-400 °F. They exist primarily as vapor phase (gas not liquid). Fig. 2.1.3 is a typical phase diagram of a gas condensate or "retrograde gas" reservoir ($P_{pc} << P_{cric}$).
- Gas-condensate reservoirs may be approximately defined as those which produced liquid with gravity above 45 ° API at gas-oil ratios in the range of 5000 to 1000,000 scf/bbl.
- A gas condensate reservoir typically contains:
  - methane (as the major component),
  - intermediate components: propane, butane, pentane and hexane, and
  - small fraction of heavy components: heptane and heavier
- Consider a reservoir at, for instance, P_i = 3300 psia and T_i = 230 °F, shown as point 3_i in Fig. 2.2
- Since point 3_i is outside the two-phase envelope and $P_i > P_c$ and $T_{cric} > T_i > T_c$, this reservoir exists initially in the gaseous state, and is referred to as a *gas condensate reservoir* (T_{cric} is the cricondentherm or the maximum temperature of the two-phase envelope).
- As production begins from the reservoir and pressure declines, no change in the state of the reservoir fluid occurs until the dew point pressure is reached (in this example, at 2700 psia, point D).
- As the reservoir pressure drops with production and the dew point line is crossed, a liquid condenses out of the reservoir fluid.

  -- At the surface, this is normally indicated by the fact that the gas produced has a lower liquid content and the producing GOR rises.
- This condensation is NOT a normal phenomenon. Normally (or theoretically) one expects vaporization to occur with decreasing pressure. It is for this reason that this abnormal behavior is commonly referred to as "*retrograde*" condensation.

- At the molecular level, retrograde condensation results from the fact that the attraction between light and heavy hydrocarbon components decreases as the pressure drops and the lighter molecules become separated. As the attraction between the heavier molecules becomes dominant, they coalesce and form a liquid, as shown in Fig. 2.2B.
- Retrograde condensation continues until a low enough pressure is reached so that the hydrocarbon molecules begin to vaporize and leave the condensed liquid, at which point normal vaporization begins and continues until the condensed liquid becomes a gas.
- In Fig. 2.2 the process of retrograde condensation continues until a point of maximum liquid volume is reached (10% at 2250 psia, point E).

  -- As production continues from point E to the abandonment pressure (point 3_a), vaporization of the retrograde liquid occurs.

  -- This revaporization aids liquid recovery, and may be evidenced by decreasing GOR on the surface.
- Unfortunately, in the reservoir the production process inhibits total revaporization and recovery of condensed heavy hydrocarbons, because:

(a) As retrograde condensation occurs, the reservoir fluid composition changes and the P-T envelope shifts toward a higher percentage of heavy hydrocarbons.

This in turn, causes the phase envelope to shift downward and to the right, requiring increasingly lower pressures for revaporization.

(b) The reservoir rock structure requires that the liquid saturation reaches a critical percentage (15 to 20%) of the pore space before liquid flow can begin.

- This percentage of oil becomes trapped as an immobile phase.
- In some cases, a sufficient volume of liquid will be condensed in the reservoir to provide mobility of the liquid phase.

- In such cases, the surface fluid composition depends on the relative mobilities (k/μ) of gas and oil in the reservoir.

- If the reservoir-wide pressure drop with production is kept to a minimum, retrograde condensation may only be a problem in the near-wellbore area, where pressure drawdown is of course significant.

  Near-wellbore condensation can inhibit gas flow (because of the change in relative permeabilty) and therefore reduce productivity. It is a form of skin damage.

- If retrograde condensation occurs on a reservoir-wide scale, significant amounts of valuable hydrocarbon liquids can be left unrecovered (50 to 60%) which, of course, could substantially reduce the ultimate profit.

- Operating problems associated with gas condensate reservoirs are:

  (c) Obtaining optimum liquid recovery from gas produced to the surface.

  As the liquifiable portions of the reservoir fluids is normally the most valuable components, the loss of part of these fluids could substantially reduce the ultimate income from the reservoir (which must be considered in an economic evaluation)

  (b) Economically preventing loss of liquids condensed in the reservoir (typically by recycling produced gas); although some loss is unavoidable.

- Consider Fig. 2.2A: 19 bbl of oil per 1MMscf ($=10^6$scf) have condensed in the reservoir, after pressure has declined from 4500 psi to 3500 psl. Assume the initial gas in place is one million MMscf or one billion Mscf. In this case the volume of the condensate is 19 million bbl.

- If, for instance, 50% of this liquid is lost to the reservoir (1.e. cannot be recovered), it may have a major negative impact on the profitability of the project: 19,000,000 (bbl) x 50% $20/bbl = $190,000,000 loss!

2.1.4 - WET GAS RESERVOIR

- Fig. 2.1.4 shows the phase diagram of a typical wet gas.
- Consider a reservoir initially at 350 °F and 3600 psia, represented by point 4_i in Fig. 2.2
- Since this point is outside the two-phase envelope and $P_i > P_c$ the reservoir fluid is 100% gas. Also, since $T_i > T_{cricon}$, at no point the isothermal depletion line (path 4_i - 4_a) is crossed.
- Therefore the fluid in the RESERVOIR never changes composition; it is always in the gaseous state.
- During production, the reservoir fluid leaves the reservoir and enters the wellbore and then the separators along line 4_i - 4_s.
- Point 4_s is at surface T and P conditions and is inside the two-phase envelope. This accounts for the recovery of condensate liquid in the separator.

2.1.5 - DRY GAS RESERVOIR

- Fig. 2.1.5 is the phase diagram of a typical dry gas reservoir.
- If the phase diagram is such that point A_1 (Fig.2.2), i.e. separator conditions of P and T lies outside the two-phase envelope and in the single-phase (gas) region, then only gas will be produced at the surface.
- No liquid will be formed in the reservoir or at the surface, during isothermal production, and the gas is called "dry gas" reservoir.
- It contains very little (if any) heavy hydrocarbons. This is true because at high pressure the molecules composing the mixture are close together, and attractive forces of the light for the heavier components are so high that the heavier components are carried into the gas phase.
- A dry gas is composed principally of methane with only minor amounts of ethane, propane and butane.

- The word "dry" really indicates that the reservoir fluid does not contain enough of the heavier hydrocarbons to form a liquid at surface conditions.
- The gas cap of an oil reservoir may contain either gas condensate, wet gas or dry gas [wells completed in both oil and gas zones will produce a mixture of two types of fluids].

2. 2 - EQUATIONS OF STATE OR GAS LAWS

2.2.1 - IDEAL GAS EQUATION OF STATE (EOS)

An EOS seeks to describe specific PVT relationships of fluids mathematically. There are hundreds of these equations ranging from those for a specific pure compound to generalized forms that claim to relate the properties of multicomponent mixtures. Naturally, there is a large range of complexity from the simple ideal-gas law to modern equations with 15 or more universal constants plus adjustable parameters. Historically, use of these equations has been limited to applications by researchers having large computing facilities.

Recently, however, operating engineers have been provided with the same computing tools previously reserved only for researchers and special projects.

The use of EOS's, therefore, has become relatively common. Some applications, such as calcul factors, are possible on hand-held programmable calculators.

The modern engineer should not forget the use of EOS s when the need arises for calculation or estimation of fluid properties.

- The normal starting point for any discussion of the properties of gases is the ideal gas equation of state, or *ideal gas law*.
- This equation is a combination of several fundamental gas laws: Boyle's law, Charles' law and Avogadro's law.

Boyles' law: $V_2 = P_1V_1 / P_2$ (T = constant) (2.2.1)

Charles' law: $V_2 = T_2V_1 / T_1$ (P = constant) (2.2.2)

$$P_2 = P_1 T_2 / T_1 \quad (V = \text{constant}) \tag{2.2.3}$$

Combining these two laws yields:

$$P_2 V_2 / T_2 = P_1 V_1 / T_1 \tag{2.2.4}$$

Avogadro's law:

- "Under the same conditions of P and T, equal V of ideal gases contain the same number (n) of molecules".

  As a result of this law:

- There are 2.733×10^{26} molecules in one pound-mole of any gas.
- One pound-mole of an ideal gas occupies 378.6 cuft at standard pressure and temperature .
- Note that Standard temperature and pressure vary from country to country, but the most common values used are:

  $T_{SC} = 60\ ^{o}F,\ P_{SC} = 14.73$ psia

- Although none of the hydrocarbon gases behaves as ideal gas at reservoir conditions, the behavior of most gases at low pressure condition (close to atmospheric pressure) is represented reasonably well by the *ideal gas law*:

$$pV = n R T \tag{2.2.5}$$

where: $n = m / M$ (2.2.6)

p =pressure, V=Volume, T=Temperature

n = moles of gas

m = mass of gas, lb

M = molecular weight of gas, lbm/lb-mole

R = Universal gas constant (Table 2.4)

- The value of R depends on the unit of pressure, volume, temperature and moles. With pressure specified in atmosphere, volume in cm^3, n in gm-moles, and temperature in Kelvins, R = 82.057 atm cm^3/gm-mole/K
- With pressure specified in psia, volume in ft^3, n in lb-moles, and temperature in Rankine, R = 10.732 psia ft^3/lb-mole/°R
- Since the number (n) of pound-moles of a gas is equal to the mass (m) of the gas divided by the molecular weight (M) of the gas (Eq. 2.2.6) the ideal gas law can be expressed as:

$$pV = (m/M) R T \qquad (2.2.7)$$

This equation can be rearranged to calculate the mass and density of the gas:

$$m = MpV / RT \qquad (2.2.8)$$

$$\rho = m/V = Mp / RT \qquad (2.2.9)$$

EXAMPLE 2.1

- *Problem:*

  A quantity of gas at P_1 = 50 psig has a volume V_1 = 1000 cuft. If the gas is compressed to P_2 = 100 psig, what volume (V_2) would it occupy, assuming the temperature is kept constant and P_{sc} = 14.73 psia?

- *Solution:*

  Using Eq. 2.2.1 (Boyle's law), we have:

  $V_2 = 1000x(50+14.73)/(100+14.73) = 564.19$ cuft

EXAMPLE 2.2

- *Problem:*

(a) *A given mass of gas has a volume of 500 cuft when the temperature is 50 °F and the pressure is 10 psig. If P remains constant and T is changed to 100 °F, what will be the volume of the gas?*

(b) *What would be the new P of this gas if V remains constant and T is increased from 50 °F to 100 °F?*

- *Solution:*

(a) Using Eq. 2.2.2 (Charles' law) we have:

$V_2 = 500x(100 + 460)/(50 + 460) = 549.02$ *cuft*

(b) Using Eq. 2.2.2 (Charles' law) we have:

$P_2 = (10 + 14.73)x(100 + 460)/(50 + 460) = 27.15$ *psia*

EXAMPLE 2.3

Problem:

How many SCF of an ideal gas are required to fill a 100 cuft tank to a pressure of 40 psig when the temperature of the gas in the tank is 90 °F?

Solution:

Using Eq. 2.2.4, we have:

$V_2 = T_2P_1V_1 / T_1P_2$ *(2.2.4a)*

Where: $T_1 = 90 + 460 = 550\ °R$

$T_2 = T_{sc} = 60 + 460 = 520\ °R$

$P_1 = 14.73 + 40 = 54.73$ *psia*

$P_2 = P_{sc} = 14.73$ *psia*

$V_1 = 100$ *cuft*

Substituting these values into Eq. 2.2.4a gives

$V_2 = 351$ *SCF*

EXAMPLE 2.4

Problem:

Repeat Example 2.3 using the ideal gas law, Eq. (2.2.5)

Solution:

Since one pound-mole (lb-mole) of an ideal gas occupies 378.6 SCF, the gas volume (in SCF) needed to fill a 100cuft tank is:

$V_{sc} = 378.6\ n$ *(2.2.10)*

Combining Eqs. 2.2.5 and 2.2.10 gives

$V_{sc} = 378.6\ (PV/RT)$ *(2.2.11)*

$= 378.6\ (54.73x100 / 10.732x550)$

$= 378.6x0.927 = 351$ scf

EXAMPLE 2.5

Problem:

Calculate the contents of a 500 ft^3 tank of ethane at 100 psia and 100 °F in: moles, pounds, molecules, and SCF

Solution

- *Assuming ideal gas behavior:*

Moles =(100x500)/(10.73x560)=8.32

Pounds= 8.32x30.07=250.2

Molecules=8.32x2.733x10^{26} = 22.738x10^{26}

SCF=8.32x379.4=3157

- *Alternate solution using the ideal gas law:*

$V_{sc} = nRT/p=(8.32x10.73x520/14.7)=3158$ *SCF*

2.2.2 - REAL GAS LAW

- At very low pressures, many gases exhibit ideal behavior and the ideal gas law is valid. At higher pressures, such as those found in gas reservoirs, the ideal gas is not valid.
- Many attempts have been made to modify the ideal gas law so that it can be used to describe real gases over a wide range of P and T.
- The van der Waals equation and the Benedict-Webb-Rubin equation are examples of such equations.
- However these type of equations still lose accuracy at higher pressures and are generally cumbersome to work with.
- The real gas equation most commonly used in practice by the industry is:

$$pV = znRT \qquad (2.2.12)$$

which is obtained by introducing a correction factor- compressibility factor, z, in the ideal gas law.

- The z-factor, which is also referred to as the "gas deviation factor", is the ratio of the volume of real gas to the volume that would be occupied if the gas behaved as an ideal gas under the same conditions of P and T.
- This factor varies with P, T, and composition, and should be (preferably) determined experimentally or from charts and/or empirical correlations.

Van der Waals' Equation

Van der Waals added terms to the ideal-gas law in an attempt to take into account forces between molecules as well as volume of the molecules themselves.

His equation becomes

$$\left(p+\frac{a}{V_M^2}\right)(V_M-b)=RT \qquad (2.2.13)$$

where V_M is the molar volume and a and b are constants characteristic of the gas.
The term b is a constant to correct for the volume occupied by the molecules themselves.
The term al V_M is a correction factor to account for the attraction between molecules as a function of the average distance between them (which is related to the molar volume).
When an EOS such as the van der Waals equation is applied to mixtures, either special constants for a and b must be developed for each mixture or constants for each gas in the mixture must be included in the equation along with adjustments for the interaction between unlike gases. The latter is the more common approach.
Van der Waals' law extends the range of pressures and temperatures for describing gas behavior beyond that of the ideal-gas law. However, it has two disadvantages in actual application.
The correction factors are inadequate at very high pressures and it is not always easy to obtain the mixture coefficients and interaction constants.
In addition, this two-parameter formulation does not really treat the attractive and repulsive forces correctly. Despite these criticisms, modifications of the van der Waals equation have been used successfully in industry for many years.
Redlich and Kwong developed the first major extension of the two-parameter EOS when they proposed their own form and showed how they related the a and b terms to R, Pc, and Tc.
Other researchers since have modified the original Redlich and Kwong equation to improve its accuracy and generality further. Most notable of the modifications are those of Soave, Zudkevitch and Joffe, and Peng and Robinson.
Some companies have their own versions, such as the one published by Yarborough.
The most common equations of state in use today and the computer programs available are the following.

1. The Starling-Hon extension of the Benedict Webb-Rubin EOS:

$$p = RT_M + \left(B_o RT - A_o - \frac{C}{T^2} + \frac{D_o}{T^3} - \frac{E_o}{T^4} \right) \rho_M^2 + \left(bRT - a - \frac{d}{T} \right) \rho_M^3 + \alpha(a+d)\rho_M^6 + \left(\frac{c\rho_M^2}{T^2} \right) \left(1 + \gamma\rho_M^2 \right) \exp\left(-\gamma\rho_M^2 \right) \tag{2.2.14}$$

where Ao, Bo, Co, Do, Eo a, b, c, d, α, and γ are empirical constants, and P_M equals n/V_M (subscript M refers to molar values).

This equation usually is called the "BWRS" and is available from Exxon Corp.

2. The Peng-Robinson EOS

$$p = \frac{RT}{V_M - b} - \frac{a(T)}{V_M(V_M + b) + b(V_M - b)} \tag{2.2.15}$$

where a and b are constants characteristic of the fluid, a(T) is a functional relationship, and V_M is the molar volume. It is available from the Gas Processors Suppliers Assn. (GPSA).

3. The Soave modification of the Redlich-Kwong EOS:

$$p = \frac{RT}{V_M - b} - \frac{a(T)}{V_M(V_M + b)} \tag{2.2.16}$$

where a(T) is a functional relationship. It, too, is available from the GPA.

The first equation, BWRS, is an empirical form using 11 constants. The values of these constants have been determined from properties measured on many different fluids. It is extremely accurate in the prediction of most thermodynamic ,properties. Eqs. 2.2.15 and 2.2.16 are variations of the original equation proposed by van der Waals and as such are not as accurate as the BWRS for calculation of pure component properties or properties of mixtures of light hydrocarbons. Both the Peng-Robinson and the Soave RK EOS's are more reliable for phase equilibrium calculations or for calculation of properties of gas condensate systems. One cannot assess their accuracy directly because it is dependent on how well the constants repre sent the specific components.

The Redlich-Kwong EOS and its extension are cubic in compressibility factor. J.J. Martin proposed a generalized cubic equation that, through suitable adjustment of parameters, can be used to obtain any other cubic including those that have been proposed after his work was published.

All cubic equations have limitations in their ability to represent behavior at near-critical conditions They are incorrect in the prediction of the critical compressibility factor and/or the shape of the critical isotherm. They can be manipulated by additional terms to circumvent this problem but errors then appear in some other region of pressure-temperature-composition space.

In general, however, EOS's can be used routinely to calculate gas properties for both hydrocarbon and non-hydrocarbon systems and their mixtures.

One particularly useful application of EOS's in gas property estimations is the direct calculation of the compressibility factor, z. As noted previously, the principle of corresponding states can be used to obtain compressibilities with reasonable accuracy. However, one can solve an EOS directly for z quite readily.

The most reliable methods for typical natural gases are those of Robinson and Jacoby and Hall and Yarborough. Robinson and Jacoby proposed the following equations.

$$p = \frac{RT}{V_M - b} - \frac{a}{\sqrt{T}V_M(V_M + b)} \tag{2.2.17}$$

$$a_i = \alpha_i + \beta_i T \tag{2.2.18}$$

and

$$b_i = \gamma_i + \delta_i T \tag{2.2.19}$$

where α, β, γ, and δ are constants for Substance i, and for mixtures

$$a_{ij} = 1/2\left[k_{ij}a_i + (1 - k_{ij})a_j\right]$$

$$a_m = \sum_i \sum_j y_i y_j a_{ij}$$

and

$$b_m = \sum_i y_i b_i$$

where K_{ij} is a constant for each binary pair when used for mixtures.

Their equations are another modification of the Redlich-Kwong equation designed specifically for the region of temperatures from 70 to 250°F and pressures below 1,500 psia. It is untested for gas mixtures containing large amounts of C_{4+} material. Within these stated limits, it should be expected to calculate compressibility factors with less than 2% error.

2.2.3 - SPECIFIC GRAVITY AND DENSITY OF GAS

The density of gas is obtained by experimentally measuring the specific gravity of the gas, and then using the following relationship:

$$\rho_g = \rho_{air}\gamma_g \tag{2.2.20}$$

- Since density is defined as mass of gas per unit volume (m/V), the real gas equation of state can also be used to calculate the z-factor:

$$\rho_g = \frac{m}{V} = \frac{pM}{zRT} \qquad (2.2.21)$$

where, M is the molecular mass of the gas.

For a gas mixture, an apparent molecular weight (M_a) is used (instead of M) in the above equation, which is obtained as the weighted average of the molecular weight of its components:

$$M_a = \Sigma y_i M_i \qquad (2.2.22)$$

where,

M_a = Apparent molecular weight of a gas mixture,

y_i = Mole fraction of a component with a mol. weight M_i

It is obvious from Eq. 2.2.14 that , at constant T, the density of gas increases with pressure. However the z-factor also influences the behavior of the gas density.

- The specific gravity is defined as the ratio of the density of the gas to the density of air at the same pressure and temperature conditions.
- At standard conditions, both air and the gas mixtures can be treated as ideal gases, therefore:

$$\gamma_g = \frac{\rho_g}{\rho_{air}} = \frac{\left(\frac{pM_a}{RT}\right)}{\left(\frac{pM_{air}}{RT}\right)} = \frac{M_a}{M_{air}} = \frac{M_a}{29} \qquad (2.2.23)$$

Note that ρ_{air} and ρ_g must be determined at the same pressure and temperature.

2.3 - GAS DEVIATION FACTOR Z

- This section presents several correlations of physical properties of hydrocarbon gases. These correlations can be used when laboratory data are not available.
- However, to ensure the best possible reservoir engineering results, laboratory data should be obtained and used.
- Unfortunately, various surveys of PVT laboratories revealed that (too) often laboratory data are of poor quality due to: poorly trained lab. technicians, poor maintenance of instruments and poor fluid sampling techniques.
- In some cases, correlations yielded more representative values of fluid properties than those obtained from several commercial lab. measurement.
- With change in composition, the important engineering properties of gases vary over a wide range. Properties of gases such as gas deviation factor (z), density (ρ), compressibility (c_g) and viscosity are important for:
  - calculating gas in place and well flow rates,
  - simulating the gas volume changes
  - analyzing reservoir pressure behavior, and
  - design of hydrocarbon-handling systems

2.3.1 - THEOREM OF CORRESPONDING STATES

- According to The *theorem of corresponding states*: "If the pressure relative to the critical pressure and the temperature relative to the critical temperature are the same for two different substances, then the substances are in corresponding states and any other property, like the density relative to the critical density, will be the same for both substances".

- In other words, "the deviation of a real gas from the ideal gas law is the same for different gases at the same corresponding conditions of reduced T and reduced P".

The principle of corresponding states has been useful in correlating the properties of gases. This principle was developed because observers noticed that the behavior of pure gases was qualitatively similar when compared (on p-V plots, for instance) even though the quantitative values of P and V were very dissimilar. The idea was advanced that the properties of substances could be correlated if they were all compared at corresponding" values of T and P, which could be referenced easily.

In the application of the principle of corresponding states to a single component gas, the critical state of the gas is used as the reference point.

The following terms are used.

$$P_r = \frac{P}{P_c} \tag{2.3.1a}$$

$$T_r = \frac{T}{T_c}, \tag{2.3.1b}$$

$$V_r = \frac{V}{V_c} \tag{2.3.1c}$$

and

$$\rho_r = \frac{\rho}{\rho_c} \tag{2.3.1d}$$

where

p_r = reduced pressure,

T_r = reduced temperature,

V_r = reduced volume,

ρ_r = reduced volume,

P_c = critical pressure,

T_C = critical temperature, and

V_c = critical volume.

ρ_c = critical density.

Compressibility factors of many pure compounds are available as functions of pressure in most handbooks dealing with gas properties. While the principle of corresponding states is not entirely rigorous, its application has been used widely in the determination of gas volumes for engineering purposes. It also has application in the estimation of gas viscosities. In application of the principle of corresponding states to a mixture of gases, the true critical temperature and pressure for the gas cannot be used because the paraffinic hydrocarbon series does not strictly follow the principle as stated above. "Pseudocritical" temperature and pressure are defined for use in place of the true crit temperature and pressure to determine the compressibility factor for a mixture.

The pseudocritical temperature and pseudocritical pressure normally are defined as the molal average critical temperature and pressure of the m~xture components.

Thus

$$P_{pc} = \Sigma y_i P_{ci} \qquad (2.3.2a)$$

and

$$T_{pc} = \Sigma y_i T_{ci} \qquad (2.3.2b)$$

where

P_{pc} = pseudocritical pressure of the gas mixture,

T_{pc} = pseudocritical temperature of the gas mixture,

P_{ci} = critical pressure of Component i in the gas mixture,

T_{ci} = critical temperature of Component i in the gas mixture, and

y_i = mole fraction of Component i in the gas mixture.

These relations are known as "Kay's rule" after W.B. Kay, who first suggested their use. The pseudocritical pressure and temperature are then Used to determine the pseudoreduced conditions:

$$P_{pr} = \frac{P}{P_{pc}} \qquad (2.3.3a)$$

$$T_{pr} = \frac{T}{T_{pc}}, \qquad (2.3.3b)$$

where P_{pr} = the pseudoreduced pressure, and

T_{pr} = the pseudoreduced temperature.

These reduced conditions are used to determine the compressibility factor, z, from Fig. 2.3, which was developed by Standing and Katz from data collected on methane and natural gases. The data used to develop Fig. 2.3.1 ranged up to 8,200 psia and 250°F.

Compressibility factors of high-pressure natural gases (10,000 to 20,000 psia) may be obtained from Fig. 2.3.1, which was developed by Katz et al. Figs. 2.3.2 and 2.3.3 may be used for low pressure applications after Brown et al.

Fig. 2.4 presents a correlation developed by Brown et al. between the pseudocritical temperatures and pseudocritical pressures of naturally occurring systems with their specific gravities. Values from this chart then can be used to determine the compressibility factor of a gas whose complete analysis is not known but should be used with caution since many different compositions can result in similar gravities. It should be used only when small amounts of non-hydrocarbons are present.

Figs.2.3.1, 2.3.2 and 2.3.3 do not consider the presence of large quantities of non-hydrocarbons such as nitrogen, carbon dioxide, and hydrogen sulfide. Wichert and Aziz's have proposed corrections for the pseudocritical constants for natural gases with significant con-

centrations of carbon dioxide and hydrogen sulfide. Their procedure involves calculation of corrected pseudocritical constants for mixtures.

2.3.2 - FACTOR Z FROM VOLUME CHANGE

Step 1. Some quantity of gas (n moles) is charged into a cylinder maintained at the same temperature T throughout the experiment.

Step 2. Measure the initial volume of gas at an atmospheric pressure of 14.7 psia, V_o.

Step 3. Apply the real gas law at the atmospheric pressure

$(Z \cong 1)$: $14.7xV_o=nRT$

Step 4. Vary the volume of the gas in the cylinder by moving the piston in the cylinder and read the pressure p and the corresponding volume V. The corresponding equation for each pair of p,V will be pV=ZnRT.

Step 5. Divide the two equations for each pair p,V to the initial one and find $Z=(pV)/(14.7xV_o)$. Therefore, by varying p and measuring V, the isothermal Z(p) function can be readily obtained.

2.3.3 - FACTOR Z FROM SPECIFIC GRAVITY AND DENSITY OF GAS

Knowing the gas composition the specific gravity and density of any gas is determined as follows:

Step 1 - Calculate the apparent molecular weight (M_a) of the hydrocarbon components from Eq. 2.2.15:

$$M_a = \sum_i y_i M_i$$

where

y_i = mole fraction of component I in gaseous state

p_{ci} = pseudo critical pressure of component i

T_{ci} = pseudo critical temperature of component i

Step 2 - Calculate the specific gravity of gas from Eq. 2.2.16:

$$\gamma_g = \frac{M_a}{29}$$

Step 3 - The density of gas is obtained from Eq. 2.2.13

$$\rho_g = \rho_{air}\gamma_g$$

Step 4 - Calculate z from the gas law

$$\rho_g = \frac{m}{V} = \frac{pM_a}{zRT} \qquad (2.3.4)$$

- The specific gravity of gas is useful in determining (in addition of gas density) the gas pseudo-critical pressure and temperature from Fig. 2.4 (or correlations such as Eqs. 2.3.8 to 2.3.13).

EXAMPLE 2.6

Problem: Dry air is a mixture of nitrogen, oxygen, and small amount of other inert gases as given in the following table:

(a) *Calculate its apparent molecular weight and density of air*

(b) *Calculate the specific gravity of methane*

Component	*mole fract.*	*M*
Nitrogen	*0.78*	*28.01*
Oxygen	*0.21*	*32*
Argon	*0.01*	*39.94*
Total:	*1.0*	

Solution

(a) The apparent molecular mass of air is obtained from Eq. 2.2.15, 1.e.:

$$M_a = \sum_i y_i M_i = (yM)_{nitrogen} + (yM)_{oxygen} + (yM)_{argon}$$

$$M_{air} = (0.78)(28.01) + (0.21)(32.00) + (0.01)(39.94)$$

$$= 28.97 \text{ lb/lb-mole or } 28.97 \text{ kg/kg-mole}$$

- *For all practical purposes, $M_{air} = 29$ is used for calculating specific gravity of gases.*
- *The density of air at standard conditions of P and T is obtained from Eq.2.2.9:*

$$\rho = Mp / RT = [28.97x14.73] / [10.732x(60+460)]$$

$$\rho_{air} = 0.07646 \text{ lb/cuft}$$

(b) *The specific gravity of pure methane is calculated from Eq. 2.2.16 (where $M_{methane} = 16.04$, from table 2.5)*

$$\gamma_g = \frac{M_a}{M_{air}} = \frac{M_a}{29}$$

$$= 16.04 / 29 = 0.553$$

2.3.4 - FACTOR Z FOR DRY SWEET GAS

For our purpose a dry sweet gas is defined as a gas reservoir in which:

- The C_{7+} fraction is negligible, and
- The mole fraction of CO_2, H_2S, N_2 and H_2O are negligible

As stated earlier, the principle of corresponding states suggests that:

- pure gases have the same z-factor at the same values P_{pr} and T_{pr}
- mixtures of similar gases can also be correlated with P_{pr} and T_{pr}

Where the pseudo-reduced temperature and pressure are defined as:

$$p_{pr} = \frac{P}{P_{pc}}$$

$$T_{pr} = \frac{T}{T_{pc}} \qquad (2.3.6)$$

All charts and correlations for determining the z-factor require P_{pr} and T_{pr} values.

This section discusses methods for calculating the pseudocritical pressure and temperature of a gas mixture:

(1) Gas Composition is Known

A - Ppc,Tpc and z from Graphs

If the gas does not contain significant non-hydrocarbon components and γ_g is known from lab. data, then

Step 1 - Determine Ppc and Tpc from Fig. 2.4

Step 2 - Calculate Ppr and Tpr from Eqs. 2.3.3a and 2.3.3b:

$$p_{pr} = \frac{P}{P_{pc}} \qquad T_{pr} = \frac{T}{T_{pc}}$$

Step 3 - Obtain the gas deviation factor z from the Standing-Katz Chart, Fig.2.3, or one of several correlations (presented in section 2.4).

B - Ppc and Tpc from Gas Composition

Step 1 - Obtain the critical pressures (P_c) and temperatures (T_c) of the components of the gas mixture from Table 2.5

Step 2 - Determine the pseudo-critical pressure(P_{pc}) and temperature (T_{pc}), and

$$p_{pc} = \sum_i y_i p_{ci} \qquad (2.3.7)$$

$$T_{pc} = \sum_i y_i T_{ci}$$

Step 3 - Calculate the pseudoreduced pressure (P_{pr}) and temperature (T_{pr})

$$p_{pr} = \frac{P}{P_{pc}} \qquad T_{pr} = \frac{T}{T_{pc}}$$

Step 4 - The factor z is then determined either from the Standing-Katz chart or one of several correlations in the next section (i.e. 2.4).

EXAMPLE 2.7

Problem: Given the gas mixture whose composition is shown in the following table

(a) *Calculate the specific gravity of this gas mixture*

(b) *Calculate the density of this gas mixture at 1000 psia and 150 °F, treating it as*

(i) Ideal gas, and

(ii) Real gas

Component	*Mole fraction, y_i*
Methane (C_1)	*0.800*
Ethane (C_2)	*0.120*
Propane (C_3)	*0.060*
n-Butane (C_4)	*0.020*

Solution

(a) Specific gravity of gas mixture:

First calculate the apparent molecular weight (M_a) of the gas mixture

Component	*Mole fraction, y_i*	*Molecular wt., M_i*	*$y_i M_i$*
Methane (C_1)	*0.800*	*16.04*	*12.832*
Ethane (C_2)	*0.120*	*30.07*	*3.6084*
Propane (C_3)	*0.060*	*44.10*	*2.646*
n-Butane, C_4	*0.020*	*58.12*	*1.1624*
TOTAL:	*1.000*		*M_a = 20.249*

- *The apparent molecular weight of the gas mixture is 20.249*
- *Specific gravity of gas mixture*

$$\gamma_g = \frac{M_a}{M_{air}} = \frac{M_a}{29} = 20.249/29 = 0.698$$

(b) Density of gas mixture, 1000 psia and 150 °F:

$$\rho_g = \frac{m}{V} = \frac{pM}{zRT}$$

(i) *If the gas mixture is treated as an ideal gas, i.e. z = 1, the gas density is:*

$$\rho_g = \frac{1000x20.249}{1x10.732x(460+150)} = 3.095 \ lb/ft^3$$

(ii) *In order to correct the gas density for non-ideal behavior, the gas deviation factor, z, is needed* and is calculated as follows:

Comp.	*Mole fraction,* y_i	*Critical Temp., (°R)* T_{ci}	$y_i T_{ci}$	*Critical Pres., (psia)* p_{ci}	$y_i p_{ci}$
(C_1)	0.800	343.3	274.64	666.4	533.12
(C_2)	0.120	549.9	65.99	706.5	84.78
(C_3)	0.060	666.1	39.66	616	36.96
$(n\text{-}C_4)$	0.020	765.6	15.31	550.6	11.01
TOTAL:	1.000		T_{pc} =395.6		p_{pc} =665.87

- Thus, the pseudo-critical temperature and pressure are:

$T_{pc} = 395.6\ ^{\circ}R$

$p_{pc} = 665.87$ psia

- The pseudo-reduced temperature and pressure are:

$T_{pr} = (460 + 150) / 395.6 = 1.54$

$p_{pr} = (1000) / (665.87) = 1.502$

- From the Standing-Katz chart (Fig.2.3) the gas deviation factor is:

  $z = 0.89$

- The gas density of this (real) gas is:

$$\rho_g = \frac{1000x20.249}{0.89x10.732x(460+150)} = 3.477\ lb / ft^3$$

- Comparing the two values of the density of gas, we find that the assumption of ideal gas leads to an (unacceptable) error of:

$$error = \frac{3.477 - 3.095}{3.477} = 11\%$$

(2) Gas composition is <u>NOT known</u>

Step 1 - Determine experimentally the specific gravity of gas

Step 2 - Knowing the gas gravity use Table 2.2, Fig. 2.4 <u>or</u> the following Sutton correlations (for dry gas) to calculate P_{pc} [psia] and T_{pc} [°R]:

$$p_{pc} = 756.8 - 131.0\gamma_g - 3.6\gamma_g^2 \qquad (2.3.8)$$

$$T_{pc} = 169.2 + 349.5\gamma_g - 74.0\gamma_g^2 \qquad (2.3.9)$$

Where: T_{pc}, P_{pc}, and γ_g are the pseudo-critical T and P, and specific gas gravity (air=1) of the hydrocarbon components

- If the gas is dry (1.e. no condensate is formed) and contains less than 12%CO_2, less than 3%N_2, and no H_2S, then γ_g in the above correlation is the separator gas gravity or the gravity of the wellstream fluid
- These equations are valid only if the total impurity content is 7% or less.

For California dry gas reservoirs (~ similar to Algeria gases), these equations become:

$$p_{pc} = 677 + 15\gamma_g - 37.5\gamma_g^2 \qquad (2.3.10)$$

$$T_{pc} = 168 + 325\gamma_g - 12.5\gamma_g^2 \qquad (2.3.11)$$

For condensate gases, the following correlations should be used:

$$p_{pc} = 706 - 51.7\gamma_g - 11.1\gamma_g^2 \qquad (2.3.12)$$

$$T_{pc} = 187 + 330\gamma_g - 71.5\gamma_g^2 \qquad (2.3.13)$$

Step 3 - Calculate the pseudo-reduced temperature and pressure

Step 4 - Determine the z-factor using the Standing_Katz chart or one of the correlations in Section 2.4

2.3.5 - Z FACTOR OF DRY SOUR GAS

- Fig. 2.3 is a correlation of the Z-factor as a function of pseudo-reduced temperature (T_{pr}) and pseudo-reduced pressure (P_{pr})

Fig. 2.3 is generated for sweet natural gases and corrected for those containing H_2S, N_2 and CO_2.

- If the gas contains more than 15% of non-hydrocarbon components (y_{CO2}>12%, y_{N2}>3%, and/or any H_2S), P_{pc} and T_{pc} of the TOTAL gas mixture (1.e. hydrocarbon components plus impurities) and the gas deviation factor z are calculated as follows:

Step 1 - Calculate the total mole fraction of non-hydrocarbon components, including water vapor (y_{H2O}):

$$y_T = y_{CO2} + y_{H2S} + y_{N2} + y_{H2O} \quad (2.3.15)$$

Step 2 - Calculate the specific gravity correction factor:

$$\gamma_{wcor} = 1.1767y_{H2S} + 1.5196y_{CO2} + 0.9672y_{N2} + 0.622y_{H2O} \quad (2.3.16)$$

Step 3 - Calculate the specific gas gravity of the hydrocarbon components:

$$\gamma_{gh} = \frac{\gamma_w - \gamma_{wcor}}{1 - y_T} \quad (2.3.17)$$

where: γ_w = specific gas gravity of the well-stream fluid (methods for calculating this parameter will be discussed later); if a separator is used then γ_w is the separator gas gravity

Step 4 - Calculate P_{pc} and T_{pc} of the <u>hydrocarbon mixture</u> (only) using Sutton's correlations (Eqs. 2.3.8 and 2.3.9):

$$P_{pch} = 756.8 - 131.0\gamma_{gh} - 3.6\gamma_{gh}^2 \quad (2.3.18)$$

$$T_{pch} = 169.2 + 349.5\gamma_{gh} - 74.0\gamma_{gh}^2$$

Step 5 - Calculate the pseudo-critical pressure and temperature of the <u>ENTIRE gas mixture</u> (including contaminants):

$$P_{pc} = (1 - y_T)P_{pch} + (1306y_{H2S} + 1071y_{CO2} + 493y_{N2} + 3200y_{H2O})$$

$$T_{pc} = (1 - y_T)T_{pch} + (672.4y_{H2S} + 547.6y_{CO2} + 227y_{N2} + 1165y_{H2O}) \quad (2.3.19)$$

- Where the constants are actually the critical pressures and temperatures of the corresponding contaminants (e.g., 1306 and 672.4 are respectively the critical pressure and temperature of H_2S, etc.)

Step 6 - *Adjust* the pseudo-critical properties for H_2S and CO_2 by the Wichert and Aziz factor ε_3, which can be obtained from Fig.2.5, or from the following expression:

$$\varepsilon_3 = 120\left(y_{c+h}^{0.9} - y_{c+h}^{1.6}\right) + 15\left(y_h^{0.5} - y_h^4\right) \qquad (2.3.20)$$

y_{c+h} = *sum of mole fractions of* CO_2 *and* H_2S *and*

y_h = *mole fraction of* H_2S

Step 7 - Calculate the adjusted (for CO_2 and H_2S) pseudo-critical values

$$T'_{pc} = T_{pc} - \varepsilon_3 \qquad (2.3.21)$$

$$p'_{pc} = \frac{p_{pc} T'_{pc}}{T_{pc} + y_{H_2S}\left(1 - y_{H_2S}\right)\varepsilon_3} \qquad (2.3.22)$$

where:

P_{pc} = *pseudo-critical pressure of the* <u>entire</u> *gas mixture, psia (from step 5)*

T_{pc} = *pseudo-critical temperat. of the entire gas mixture,* °R *(from step 5)*

- Eqs. 2.3.20 through 2.3.22 yield z factors within 5% of experimental value of z (at temperatures and pressures of up to 300^0F and 7,000 psia, respectively) and for: $y_{CO2} \leq 55\%$ and $y_{H2S} \leq 75\%$
- These correlations assume that the Z-factor values are not greatly affected by the presence of nitrogen.

Step 8 - Assuming y_{N2} and y_{H2O} are negligible, 1.e. $y_{N2}+y_{H2O}<5\%$ (if they are not go to Step 9), calculate the adjusted pseudo-reduced pressure and temperature from the

following expressions, then determine the z-factor, either from the Standing-Katz chart or one of the correlations for z (see next section)

$$T_{pr} = \frac{T}{T'_{pc}} \qquad (2.3.23)$$

$$P_{pr} = \frac{P}{P'_{pc}}$$

Step 9 - If y_{N2} and y_{H2O} are NOT negligible, P'_{pc} and T'_{pc} (in step 7) and P'_{pr} and T'_{pr} (in step 8) must further be adjusted for nitrogen and water vapor content

(a) The adjusted (for all 4 contaminants) pseudo- critical properties are:

$$T_{pc}'' = \frac{T_{pc}' - (227y_{N2} + 1165y_{H2O})}{1 - (y_{N2} + y_{H2O})} - (246y_{N2} - 400y_{H2O})$$

$$P_{pc}'' = \frac{P_{pc}' - (493y_{N2} + 3200y_{H2O})}{1 - (y_{N2} + y_{H2O})} - (162y_{N2} - 1270y_{H2O}) \qquad (2.3.24)$$

(b) The adjusted (for all 4 contaminants) pseudo-reduced properties are:

$$T_{pr} = \frac{T}{T''_{pc}} \qquad (2.3.25)$$

$$P_{pr} = \frac{P}{P''_{pc}}$$

(c) The gas deviation factor is then calculated either from the Standing-Katz chart or from one of the correlations in the next section.

- The z-factor values calculated as described above are about as accurate as can be

measured in the laboratory. This is true even for wet gases and retrograde gases with specific gravity as high as 1.6.

EXAMPLE 2.8

Problem:

The composition of a sour gas mixture at 1623 psia (11.2 kPa) and 100^{0}F (37.8^{0}C) is hown in the following table.

(a) *Use the Wichert and Aziz adjustment factor method and the Standing and Katz chart to calculate the gas deviation factor of this mixture. Compare with the lab. measured value of Z = 0.822.*

(b) Determine the specific gravity and density of this sour gas mixture

Table. E.

Component	*Mole Fraction Yi*
C_1	*0.8303*
C_2	*0.013*
C_3	*0.007*
CO_2	*0.0744*
H_2S	*0.0735*
N_2	*0.0081*

Solution:

(a) The gas deviation factor z is determined as follows:

Step 1 - Obtain the critical temperature and critical pressure values of the constituents from Table 2.5

Step 2 - Calculate the pseudo-critical properties for the mixture using Eqs. 2.3.7

$$p_{pc} = \sum_i y_i p_{ci} = 748.3 \text{ psia}$$

$$T_{pc} = \sum_i y_i T_{ci} = 384.5\,^{\circ}R$$

Step 3 - From Fig. 2.5 , read the critical adjustment factor:

$$\varepsilon_3 = 20\,^{\circ}R$$

- *Eq. 1.3.20 gives a similar value for y_h = 7.35% and*

  y_{c+h} = 7.44 + 7.35 = 14.79%:

$$\varepsilon_3 = 120\left(y_{c+h}^{0.9} - y_{c+h}^{1.6}\right) + 15\left(y_h^{0.5} - y_h^{4}\right)$$

$$= 120(0.1479^{0.9} - 0.1479^{1.6}) + (0.0735^{0.5} - 0.0735^{4}) = 19.91\,^{\circ}R$$

Step 4 - The adjusted pseudo-critical pressure and temperature are obtained from Eqs. 2.3.21 and 2.3.22:

$$T'_{pc} = T_{pc} - \varepsilon_3 = 384.5 - 20 = 364.5\ ^{0}R$$

$$P'_{pc} = \frac{P_{pc}T'_{pc}}{T_{pc} + y_h(1-y_h)\varepsilon_3} = \frac{(748.3)(364.5)}{384.5 + 0.0735(1-0.0735)(20)} = 678.7 \text{ psia}$$

Step 5 - The pseudo-reduced pressure and temperature are:

$$T_{pr} = \frac{T}{T'_{pc}} = \frac{560}{364.5} = 1.54$$

$$P_{pr} = \frac{P}{P'_{pc}} = \frac{1623}{678.7} = 2.39$$

Step 6 - Obtain the gas deviation factor z from the Standing Katz chart, 1.e. Fig.2.3

z = 0.82. Thus the calculated value of z is in good agreement with the lab. measured value (0.8211).

(b) *The specific gravity and density of this sour gas is obtained as follows:*

1. *The apparent molecular weight (M_a) of this sour gas mixture is calculated from Eq. 2.2.15:*

$$M_a = \sum_i y_i M_i = 20.03$$

Where the mole fractions (y_i) and molecular weights M_i of the gas components are respectively shown in the Table E (above) and Table 2.5.

2. The specific gravity of this sour gas is calculated from Eq. 2.2.16:

$$\gamma_g = \frac{M_a}{29} = \frac{20.03}{29} = 0.69$$

3. *The density of this gas at reservoir pressure of 1623 psia and temperature of 100 ° F (z = 0.82) is obtained from Eq. 2.3.4:*

$$\rho_g = \frac{pM_a}{zRT} = \frac{1623x20.03}{0.82x10.732x(460+100)} = 6.6\ lb/cuft$$

Table. E.

Component	Mole Fract. Y_i	Tc_i ^0R	Y_iTc_i ^0R	Pc_i psia	Y_iPc_i
C_1	0.8303	343.3	285.0	673.1	558.9
C_2	0.0130	549.8	7.1	708.3	9.2
C_3	0.0007	666.0	0.5	617.4	0.4
CO_2	0.0744	547.7	40.7	1073	79.8
H_2S	0.0735	672.4	49.4	1306	96.0
N_2	0.0081	226.9	1.8	492	4.0
			T_{pc}= 384.5		P_{pc}= 748.3

Component	Mole Fract.	Mol. weight

	Y_i	M_i	Y_i*M_i
C_1	0.8303	16.04	13.32
C_2	0.0130	30.07	0.39
C_3	0.0070	44.10	0.31
CO_2	0.0744	44.01	3.28
H_2S	0.0735	34.08	2.50
N_2	0.0081	28.01	0.23
			M_a=20.03

2.4-CORRELATIONS OF Z FOR COMPUTER PROGRAMMING

- There are many computer programs for calculating z at designated pressures and temperatures for a given gas composition or gas gravity.
- Many programs rely on statistical correlations that may or may not represent your particular case.
- The following correlations require the pseudo-reduced properties T_{pr} *and* P_{pr} *that have already been adjusted for impurities(if any).*

(1) - *Dranchuk, Purvis and Robinson (DPR) Equation*

- The following equation is a correlation of the Standing-Katz chart by means of an eight coefficient Benedict-Webb-Rubin type equation of state:

$$z = 1 + \left(A_1 + \frac{A_2}{T_{pr}} + \frac{A_3}{T_{pr}^3} \right) \rho_{pr} + \left(A_4 + \frac{A_5}{T_{pr}} + \right) \rho_{pr}^2 \qquad (2.4.1)$$

$$+ \frac{A_5 A_6}{T_{pr}} \rho_{pr}^5 + \frac{A_7}{T_{pr}^3} \rho_{pr}^3 \left(1 + A_8 \rho_{pr}^2 \right) e^{\left(- A_8 \rho_{pr}^2 \right)}$$

$$\rho_{pr} = 0.27 \left[\frac{p_{pr}}{z T_{pr}} \right] \qquad (2.4.2)$$

where the constant 0.27 is the z factor of the gas at the critical point (which is true for most gases).

The correlation constants are:

$$A_1 = 0.31560237, \qquad A_2 = -1.0467099,$$

$$A_3 = -0.57832729, \qquad A_4 = 0.53530771,$$

$$A_5 = -0.61232032, \qquad A_6 = -0.10488813,$$

$$A_7 = 0.68157001, \qquad A_8 = 0.68446549,$$

For higher accuracy use the following form of DPR equation:

$$z = 1 + \left(A_1 + \frac{A_2}{T_{pr}} + \frac{A_3}{T_{pr}^3} + \frac{A_4}{T_{pr}^4} + \frac{A_5}{T_{pr}^5} \right) \rho_{pr}$$
$$+ \left(A_6 + \frac{A_7}{T_{pr}} + \frac{A_8}{T_{pr}^2} \right) \rho_{pr}^2 - A_9 \left(\frac{A_7}{T_{pr}} + \frac{A_8}{T_{pr}^2} \right) \rho_{pr}^5 \qquad (2.4.3)$$
$$+ A_{10} \left(1 + A_{11} \rho_{pr}^2 \right) \left(\frac{\rho_{pr}^2}{T_{pr}^3} \right) e^{\left(- A_{11} \rho_{pr}^2 \right)}$$

$$A_1 = 0.3265, \quad A_2 = -1.0700, \quad A_3 = -0.5339, \quad A_4 = 0.01569, \quad A_5 = -0.05165,$$
$$A_6 = 0.5472, \quad A_7 = -0.7361, \quad A_8 = 0.1844, \quad A_9 = 0.1056, \quad A_{10} = 0.6134,$$
$$A_{11} = 0.7210$$

- The DPR correlation is ideal for computer programming purposes.
- Note that since z is on both sides of the equation, Eq. 2.4.1 can only be solved by using the iterative technique.
- Eqs. 2.4.1 and 2.4.2 produce z factors that are well within 2% of experimental values

for temperatures up to 360^0F, pressures up to 12,500 psia, and gas specific gravities up to 2.2.

- Eq. 2.4.1 represents Standing-Katz correlation to within 1% for $0.2 < p_{pr} < 15$ and $0.7 < T_{pr} < 3.0$ and to within 3% for $15 < p_{pr} < 30$.
- This equation is also a good representation of the Standing-Katz chart, and is capable of generating z-values with a standard deviation of 0.00445.

(2) - Gopal Method

This method fits straight line equations to different portions of the Z- factor chart. It uses a general equation of the form:

$$Z = P_{pr}(At_{pr} + B) + CT_{pr} + D \qquad (2.4.3)$$

- The values of constants A, B, C, and D for various combinations of P_r and T_r are shown in the Table 2.1
- For $P_r > 5.4$, Gopal uses an equation of a different form (see Table 2.1).

(3) - The Hall-Yarborough method

The Hall-Yarborough equations, developed using the Starling-Carnahan equation of state, are:

$$Z = \frac{0.06125 p_{pr} t e^{-1.2(1-t)^2}}{y} \qquad (2.4.4)$$

where:

p_{pr} = the pseudo reduced pressure

t = the reciprocal pseudo-reduced temperature, 1.e.

$$t = T_{pc}/T \tag{2.4.5}$$

y = the reduced density, which can be obtained as the solution of the following non-linear equation:

$$F = -0.06125 p_{pr} t e^{-1.2(1-t)^2} + \frac{y + y^2 + y^3 - y^4}{(1-y)^3} - (14.76t - 9.76t^2 + 4.58t^3)y^2$$
$$+ (90.7t - 242.2t^2 + 42.4t^3)y^{(2.18+2.82t)} = 0 \tag{2.4.6}$$

- The non-linear equation 2.4.6 can be solved for y, using Newton-Raphson iterative technique. Substitution of the correct value of y in Eq. 2.4.4 will give the Z-factor.

Procedure For Calculating y:

Solve Eq. 2.4.6 for y, using the Newton-Raphson iterative technique:

Step 1. A guess is made for the value of y, call it $y^{(0)}$.

Step 2. Using this value in Eq. 2.4.6, $F^{(0)}$ can be evaluated, but because $y^{(0)}$ is only a guess, $F^{(0)}$ will not equal zeros as required.

Step 3. Approximate F by a first-order Taylor's series expansion about $F^{(0)}$.

$$F \cong F^{(0)} + \frac{dF^{(0)}}{dy}(y - y^0) = 0 \tag{2.4.7}$$

Step 4. Solving this equation, obtain a new value for y which can be used to reevaluate F and iterate until $F^{(0)}$ is less than some small number:

$$y = y^0 - \frac{F^{(0)}}{dF^{(0)}/dy} \tag{2.4.8}$$

where:

$$\frac{dF}{dy} = \frac{1 + 4y + 4y^2 - 4y^3 + y^4}{(1-y)^4} - (29.52t - 19.52t^2 + 9.16t^3)$$

$$+ (2.18 + 2.82t)(90.7t - 242.2t^2 + 42.4t^3)y^{(1.18+2.82t)} \qquad (2.4.9)$$

- These equations can be solved at all conditions by starting with a small value of y (=0.5)and converging to the answer.
- Since the gas constant R does not appear in any of the required equations, any consistent units may be included for pressure, volume and temperature.

(4) - Matthews, Roland, and Katz.

- In the methods outlined above, the C_{7+} fraction is generally considered as a single component.
- If the molecular weight and specific gravity of the C_{7+} fraction are known, the pseudo-critical pressure of this fraction may be obtained by using Fig. 2.6.

(5) - Beggs and Brill Correlations (valid only if $1.2 < T_{pr} < 2.4$)

$$Z = A + \frac{(1-A)}{e^B} + CP_{pr}^D \qquad (2.4.10)$$

$$A = 1.39(T_{pr} - 0.92)^{0.5} - 0.36T_{pr} - 0.101$$

$$B = (0.62 - 0.23T_{pr})p_{pr} + \left[\frac{0.066}{(T_{pr} - 0.86)} - 0.037\right]p_{pr}^2$$

$$+ \frac{0.32}{10^9(T_{pr} - 1)}p_{pr}^6 \qquad (2.4.11)$$

$$C = (0.132 - 0.32\log T_{pr})$$

$$D = 10^{(0.3106 - 0.49T_{pr} + 0.1824T^2{}_{pr})}$$

2.5 - PSEUDOCRITICAL PROPERTIES FOR GAS CONDENSATE AND WET GAS

- The Stewart et al. Mixing rule is recommended for determining the pseudo-critical properties of gas reservoirs in which the C7+ fraction is significant, such as gas condensate and wet gas reservoirs.

(1) - Negligible Non-hydrocarbon Components

(yco_2, y_{H2S}, y_{N2} and y_{H2O})

Step 1 - Obtain experimentally the molecular weight and gravity of the C_{7+} fraction

Step 2 - Estimate the boiling temperature of the C_{7+} fraction from:

$$T_{bC_{7+}} = (4.5579 M_{C_{7+}}^{0.15178} \gamma_{C_{7+}}^{0.15427})^3 \qquad (2.5.1)$$

Step 3 - Estimate the pseudocritical pressure of the C_{7+} fraction:

$$P_{pcC_{7+}} = \exp[8.3634 - \frac{0.0566}{\gamma_{C_{7+}}} - \left(0.24244 + \frac{2.2898}{\gamma_{C_{7+}}} + \frac{0.11857}{\gamma^2_{C_{7+}}}\right)\frac{T_{bC_{7+}}}{1{,}000}$$
$$+ \left(1.4685 + \frac{3.648}{\gamma_{C_{7+}}} + \frac{0.47227}{\gamma^2_{C_{7+}}}\right)\frac{T^2_{bC_{7+}}}{10^7} - \left(0.42019 + \frac{1.6977}{\gamma^2_{C_{7+}}}\right)\frac{T^3_{bC_{7+}}}{10^{10}}] \quad (2.5.2)$$

Step 4 - Estimate the pseudocritical temperature of the C_{7+} fraction:

$$T_{pc_{C_{7+}}} = (341.7 + 811\gamma_{C_{7+}}) + (0.4244 + 0.1174\gamma_{C_{7+}})T_{bc_{7+}}$$
$$+ (0.4669 - 3.2623\gamma_{C_{7+}})\frac{10^5}{T_{bc_{7+}}} \quad (2.5.3)$$

Step 5 - Determine the correction factors F_0, F_1 and F_2 for C_{7+} fraction:

$$F_0 = \frac{1}{3}\left(\frac{yT_{pc}}{p_{pc}}\right)_{C_{7+}} + \frac{2}{3}\left(\frac{y^2T_{pc}}{p_{pc}}\right)_{C_{7+}} \quad (2.5.4)$$

$$F_1 = 0.6081F_0 + 1.1325F_0^2 - 14.004F_0y_{C_{7+}} + 64.434F_0y^2_{C_{7+}} \quad (2.5.5)$$

$$F_2 = \left(\frac{T_{pc}}{\sqrt{p_{pc}}}\right)_{C_{7+}}\left(0.3129y_{C_{7+}} + 4.8156y^2_{C_{7+}} + 27.375y^3_{C_{7+}}\right) \quad (2.5.6)$$

Step 6 - Obtain the critical pressures (P_c) and temperatures (T_c) of the other components of the gas mixtures from Table 2.5.

Step 7 - Calculate the parameters J_1 and J_2:

$$J_1 = \frac{1}{3}\sum_{i=1}^{n_c}\left(\frac{yT_c}{p_c}\right)_i + \frac{2}{3}\left[\sum_{i=1}^{n_c}\left(y\sqrt{\frac{T_c}{p_c}}\right)_i\right]^2$$

$$J_2 = \sum_{i=1}^{n_c} \left(\frac{yT_c}{\sqrt{p_c}} \right)_i \qquad (2.5.7)$$

Step 8 - Correct the parameters J_1 and J_2 for the C_{7+} fraction:

$$J_1' = J_1 - F_1 \qquad (2.5.8)$$
$$J_2' = J_2 - F_2$$

Step 9 - Calculate the pseudocritical pressure (P_{pc}) and temperature (T_{pc}) of the total gas mixture:

$$p_{pc} = \left(\frac{J_2'}{J_1'} \right)^2$$
$$T_{pc} = \frac{(J_2')^2}{J_1'} \qquad (2.5.9)$$

Step 10 - Calculate the pseudo-reduced pressure and temperature of the gas mixture:

$$p_{pr} = \frac{P}{P_{pc}}$$
$$T_{pr} = \frac{T}{T_{pc}} \qquad (2.5.10)$$

Step 11 - Determine the factor z from the Standing-Katz chart or anyone of the correlations discussed in the next section.

Step 12 - Calculate the apparent molecular weight of the gas mixture:

$$M_a = \sum_i y_i M_i \qquad (2.5.11)$$

Step 13 - Calculate the specific gravity of gas:

$$\gamma_g = \frac{M_a}{M_{air}} = \frac{M_a}{29} \qquad (2.5.12)$$

Note that the values of P_{pc} and T_{pc}, and, therefore, the values of P_{pr} and T_{pr}, must be adjusted for non-hydrocarbon content (as shown in section 2.3.3)

EXAMPLE 2.9

Calculate the apparent molecular weight, gas gravity, and pseudocritical pressure and temperature of the sour gas (mole fraction of H_2S is 0.1841) with the composition given in Table 2.6. The molecular weight and gravity of the C_{7+} fraction are 114.2 lbm/lbm-mol and 0.7070, respectively.

Solution

Since the gas composition contains C_{7+} components, the Stewart et al. Mixing Rule is applicable.

Step 1 - Obtain experimentally the molecular weight and gravity of the C_{7+} fraction

$M_{C7+} = 114.2$

$\gamma_{C7+} = 0.707$

Step 2 - Estimate the boiling temperature of the C_{7+} fraction from:

$$T_{bC_{7+}} = (4.5579 \cdot M_{C_{7+}}^{0.15178} \gamma_{C_{7+}}^{0.15427})^3$$

$$T_{bC_{7+}} = (4.5579 \text{x} 114.2^{0.15178} \text{x} 0.707^{0.15427})^3 = 697.6\ ^\circ\text{R}$$

Step 3 - Estimate the pseudocritical pressure of the C_{7+} fraction:

$$P_{pcC_{7+}} = \exp[8.3634 - \frac{0.0566}{0.707} - \left(0.24244 + \frac{2.2898}{0.707} + \frac{0.11857}{0.707^2}\right)\frac{697.6}{1{,}000} + \left(1.4685 + \frac{3.648}{0.707} + \frac{0.47227}{0.707^2}\right)\frac{697.6^2}{10^7} - \left(0.42019 + \frac{1.6977}{0.707^2}\right)\frac{697.6^3}{10^{10}}] = 375.5 \text{ psia}$$

Step 4 - Estimate the pseudocritical temperature of the C_{7+} fraction:

$$T_{pcC_{7+}} = (341.7 + 811x0.707) + (0.4244 + 0.1174x0.707)697.6$$

$$+ (0.4669 - 3.2623x0.707)\frac{10^5}{697.6} = 1005.3\ ^{\circ}R$$

Step 5 - Determine the correction factors F_0, F_1 and F_2 for C_{7+} fraction:

$$F_0 = \frac{1}{3}\left(\frac{0.0005x1005.3}{375.5}\right) + \frac{2}{3}\left(\frac{0.0005^2 x1005.3}{375.5}\right) = 4.466x10^{-4}$$

$$F_1 = 0.6081x4.466x10^{-4} + 1.1325x4.466x10^{-4^2} - 14.004x4.466x10^{-4}x0.0005$$
$$+ 64.434x4.466x10^{-4}x0.0005^2 = 0.000269$$

$$F_2 = \left(\frac{1005.3}{\sqrt{375.5}}\right)\begin{pmatrix} 0.3129x0.0005 \\ -4.8156x0.0005^2 \\ +27.375x0.0005^3 \end{pmatrix} = 0.008054$$

Step 6 - Obtain the critical pressures (P_c) and temperatures (T_c) of the other components of the gas mixtures from Table 2.5.

Step 7 - Calculate the parameters J_1 and J_2:

$$J_1 = \frac{1}{3}\sum_{i=1}^{nC}\left(\frac{yT_c}{p_c}\right)_i + \frac{2}{3}\left[\sum_{i=1}^{nC}\left(y\sqrt{\frac{T_c}{p_c}}\right)_i\right]^2$$

$$J_1 = \frac{1}{3}(0.5405) + \frac{2}{3}[0.7318]^2 = 0.5372$$

$$J_2 = \sum_{i=1}^{nC}\left(\frac{yT_c}{\sqrt{p_c}}\right)_i = 13.88$$

The summation terms are calculated as shown in Table 2.7

Step 8 - Correct the parameters J_1 and J_2 for the C_{7+} fraction:

$J_1' = J_1 - F_1 = 0.5372 - 0.000269 = 0.5369$

$J_2' = J_2 - F_2 = 13.88 - 0.008054 = 13.87$

Step 9 - Calculate the pseudocritical pressure (P_{pc}) and temperature (T_{pc}) of the total gas mixture:

$$p_{pc} = \left(\frac{J_2'}{J_1'}\right)^2 = \left[\frac{13.87}{0.5369}\right]^2 = 667.4\,\text{psia}$$

$$T_{pc} = \frac{(J_2')^2}{J_1'} = \frac{(13.87)^2}{0.5369} = 358.3\,^{\circ}\text{R}$$

Step 10 - Calculate the pseudo-reduced pressure and temperature of the gas mixture:

$$p_{pr} = \frac{P}{P_{pc}}$$

$$T_{pr} = \frac{T}{T_{pc}}$$

Step 11 - Determine the factor z from the Standing-Katz chart

Step 12 - Calculate the apparent molecular weight of the gas mixture:

$$M_a = \sum_i y_i M_i$$

Step 13 - Calculate the specific gravity of gas:

$$\gamma_g = \frac{M_a}{M_{air}} = \frac{M_a}{29}$$

Note that the values of P_{pc} and T_{pc}, and therefore the values of P_{pr} and T_{pr}, must be adjusted for non-hydrocarbon content (as shown in the section 2.3.5)

(2) Systematic Procedure for Calculating P_{pc} and T_{pc}

- The following procedure summarizes the techniques outlined earlier and should be used to calculate pseudocritical pressure and temperature for estimating z factor, gas compressibility (c_g), and gas viscosity:

Step 1 - Estimate pseudocritical pressure, P_{pc}, and temperature, T_{pc} of the entire gas mixture:

A. If laboratory analysis of a reservoir fluid sample is available, then

- Calculate P_{pc} and T_{pc} with the Stewart *et al* mixing rules.
- If the composition of both the separator liquid and gas are known, then the reservoir fluid composition must first be determined from recombination calculations outlined earlier.

B. If no laboratory analysis of hydrocarbon composition is available or if speed is more important than precision, estimate P_{PC} and T_{pc} with Sutton's correlation.

(1) Estimate the hydrocarbon gas gravity, γ_h

a. - If the gas contains no contaminants, then:

- If separator gas gravity, γ_g, is used, then $\gamma_h = \gamma_g$ for a dry gas.
- If the gravity of the wellstream fluid, γ_w, is used, then $\gamma_h = \gamma_w$ for a wet gas or a gas condensate.

If the gas/liquid ratio and separator gas gravity of each separation

stage and the stock-tank-liquid gravity are known, calculate γ_w with Eq. 2.9.1 or 2.9.3

- Otherwise, calculate γ_w with Eq. 2.9.4.

b. - If the gas contains more than 12 mol% of CO_2, more than 3 mol% of N_2, or any H_2S, then calculate the hydrocarbon gas gravity, γ_h, with Eq. 2.3.17.

(2) Calculate P_{pch} and T_{pch} with Eqs. 2.3.18

(3) Calculate P_{pc} and T_{pc} with Eqs. 2.3.19

Step 2 - Correct the pseudocritical properties for H_2S and CO_2 contamination.

A. If the gas does not contain H_2S or CO_2, then $P'_{pc} = P_{pc}$ and $T'_{pc} = T_{pc}$.

B. If the gas contains H_2S and/or CO_2, then calculate the corrected pseudocritical properties, P'_{pc} and T'_{PC}, with the Wichert and Aziz correlation (Eqs. 2.3.20 - 2.3.22)

Step 3 - Correct the pseudocritical properties for nitrogen and water vapor using Casey's method.*

A. If the gas does not contain nitrogen or water vapor, then $P''_{PC} = P'_{PC}$ *and* $T''_{PC} = T'_{PC}$.

B. If the gas contains nitrogen and/or water vapor, then calculate P''_{PC} and T''_{PC} with Eqs. 2.3.24

Step 4 - P''_{pc} and T''_{pc} are the appropriate values to use in correlations

for z factor, compressibility, and viscosity.

2.6 - COMPRESSIBILITY OF GAS (c_g)

- The compressibility of a gas is defined as the fractional change of volume as pressure is changed at constant temperature:

$$c_g = -\frac{1}{V}\left(\frac{\partial V}{\partial p}\right) \tag{2.6.1}$$

where: V = Volume of one mole of the gas

From the real gas law equation, the volume of gas can be expressed as:

$$V = nRT\left(\frac{z}{p}\right) \tag{2.6.2}$$

Differentiating V with respect to pressure and substituting into Eq. 2.6.1 yields:

$$c_g = \frac{1}{p} - \frac{1}{z}\left(\frac{\partial z}{\partial p}\right) \tag{2.6.3}$$

Where *dz/dp* is the slope of a straight line tangent to the z vs p curve at a point where pressure is p.

- For an ideal gas, i.e. z=1, Eq. 2.6.3 becomes:

$$c_g = \frac{1}{p} \qquad (psia^{-1}) \tag{2.6.4}$$

From the definition of pseudo-reduced pressure the pressure is:

$$P = P_{pr}P_{pc} \tag{2.6.5}$$

Substitution of this expression into Eq. 2.6.4 gives:

$$c_g = \frac{1}{p_{pc}}\left[\frac{1}{p_{pr}} - \frac{1}{z}\left(\frac{\partial z}{\partial p_{pr}}\right)\right] \qquad (2.6.6)$$

Moving P_{pc} to the left hand side of the equation, and calling the product $c_g P_{pc}$ the pseudo-reduced compressibility c_r:

$$c_r = c_g P_{pc} \qquad (2.6.7)$$

Therefore, the pseudo-reduced compressibility for any gas mixtures can be expressed as:

$$c_r = \frac{1}{p_{pr}} - \frac{1}{z}\left(\frac{\partial z}{\partial p_{pr}}\right) \qquad (2.6.8)$$

This relationship was used to develop charts in which $c_r T_r$ is plotted as a function of T_r and P_r on a loglog graph (Figures 2.8a and 2.8b).

Note, in these figures: $T_r = T_{pr}$ and $P_r = P_{pr}$

- These figures are used to determine the gas compressibility c_g as follows:

Step 1: Calculate the pseudo-critical P and T from Eqs. 2.3.7 (if the gas composition is known), 1.e.

$$p_{pc} = \sum_i y_i p_{ci}$$

$$T_{pc} = \sum_i y_i T_{ci}$$

If gas composition is unknown, then use Eqs. 2.3.8 - 2.3.13.

Step 2: Calculate the pseudo-reduced P and T from:

$$p_{pr} = p / p_{pc}$$

$$T_{pr} = T / T_{pc}$$

Step 3 - Determine the value of $c_r T_r$ from Fig 2.8a or 2.8b

Step 4 - Calculate the compressibility of gas from Eq. 2.6.7:

$$c_g = \frac{c_r}{p_{pc}} \tag{2.6.9}$$

For programming purposes, c_r can be obtained from the following expression:

$$c_r = \frac{1}{p_{pr}} - \frac{0.27}{z^2 T_{pr}} \left(\frac{\left(\partial z / \partial P_{pr} \right)}{1 + \left(\rho_{pr} / z \right) \left(\partial z / \partial P_{pr} \right)} \right) \tag{2.6.10}$$

where

$$\rho_{pr} = 0.27 \left[\frac{p_{pr}}{z T_{pr}} \right]$$

and $\left(\partial z / \partial P_{pr} \right)$ is the derivative of z (in Eq. 2.6.8) with respect to P_{pr}.

$$\left(\partial z/\partial P_{pr}\right) = \left(A_1 + \frac{A_2}{T_{pr}} + \frac{A_3}{T_{pr}^3} + \frac{A_4}{T_{pr}^4} + \frac{A_5}{T_{pr}^5}\right)$$
$$+ 2\rho_{pr}\left(A_6 + \frac{A_7}{T_{pr}} + \frac{A_8}{T_{pr}^2}\right) - 5\rho_{pr}^4 A_9\left(\frac{A_7}{T_{pr}} + \frac{A_8}{T_{pr}^2}\right) \qquad (2.6.11)$$
$$+ \frac{2A_{10}\rho_{pr}}{T_{pr}^3}\left(1 + A_{11}\rho_{pr}^2 - A_{11}^2\ \rho_{pr}^4\right)e^{\left(-A_{11}\rho_{pr}^2\right)}$$

Eqs. 2.6.10 and 2.6.11 should not be used when $T_{pr} < 1.4$ and $0.4 < p_{pr} < 3.0$.

The accuracy of these equations is unknown; however, the results should be suitable for engineering calculations.

EXAMPLE 2.10

Problem: What is the gas compressibility of the sweet gas mixture in EXAMPLE 2.7

Solution:

- The pseudo-critical and pseudo-reduced pressure and temperature values in EXAMPLE 2.7 are:

  $T_{pc} = 395.6$ °R $T_{pr} = 1.54$

  $p_{pc} = 665.87$ psia $P_{pr} = 1.502$ @ p = 1000 psia

- From Fig. 2.8b the product $c_r T_r$ at $P_r = 1.5$ and $T_r = 1.54$ is approximately:

  $c_r T_r = 1.14$

- The pseudo-reduced compressibility value is:

  $c_r = T_r / 1.14 = 1.54 / 1.14 = 1.35$

- The compressibility of the sweet gas mixture in EXAMPLE 2.7 is obtained from Eq. 2.6.9:

$$c_g = \frac{c_r}{p_{pc}} = \frac{1.35}{665.87} = 2.027 \times 10^{-3} \text{ psia}^{-1}$$

- Note: If the gas mixture had been assumed to be an ideal gas, c_g is:

$$c_g = \frac{1}{p} = \frac{1}{1000} = 1.0 \times 10^{-3} \text{ psia}^{-1}$$

which is only <u>half</u> of the correct value of c_g. This approximation should always be avoided.

EXAMPLE 2.11

Problem: What is the gas compressibility of the sour gas mixture in EXAMPLE 2.8

Solution:

- The pseudo-crtical and pseudo-reduced pressure and temperature of this sour gas mixture are:

$T_{pc} = 364.5\ ^\circ R$ $\quad T_{pr} = 1.54$

$P_{pc} = 678.7\ psia$ $\quad P_{pr} = 2.39$ $\quad @\ p = 1623$ psia

- From Fig. 2.8b the product c_rT_r at $P_r = 2.39$ and $T_r = 1.54$ is approximately:

$$c_rT_r = 0.74$$

- The pseudo-reduced compressibility value is:

$c_r = T_r / 0.74 = 1.54 / 0.74 = 2.08$

- The compressibility of the sour gas mixture in EXAMPLE 2.8 is obtained from Eq. 2.6.9:

$$c_g = \frac{c_r}{p_{pc}} = \frac{2.08}{678.7} = 3.066 \times 10^{-3} \text{ psia}^{-1}$$

2.7 - VISCOSITY OF GASES

Viscosity is a measure of the resistance to flow exerted by a fluid.

- At high reservoir pressures (Fig. 2.9), gas viscosity increases as the reservoir pressure increases, and decreases with increasing temperature.
- At low pressure ($p<1000$ psi) as shown in Fig. 2.10, gas viscosity increases with increasing temperature ($T>200°F$).
- Measuring gas viscosities at reservoir conditions of pressure and temperature is a difficult procedure. Correlations based on gas gravity are commonly used in place of actual laboratory measurements.

METHOD 1

- The **NGSMA chart**, Fig. 2.16 , is one of the simplest graphs for determining gas viscosity. This figure gives gas viscosity as a function of reservoir gas gravity, p and T.
- Its use is illustrated by the arrows: For a 0.7 gravity gas at reservoir p and T of 750 psia and 220 °F, respectively, the gas viscosity is 0.0158 cp.

METHOD 2

Carr-Kobayashi-Burrow (CKB) developed one of the most common equation for determining viscosity of gas mixtures.

- It requires knowledge of the gas composition and of the viscosity of each component at atmospheric pressure and reservoir temperature
- The CKB equation for viscosity of a gas mixture at atmospheric P and reservoir T is:

$$\mu_{ga} = \frac{\Sigma[\mu_{gi} y_i (M_i^{1/2})]}{\Sigma[y_i (M_i^{1/2})]} \qquad (2.7.1)$$

where,

$\mu_{ga} = \mu_{gl}$ = Viscosity of the gas mixture at 1 atm.

μ_{gi} = Viscosity of the component i (Fig. 2.17)

M_i = Molecular mass of component i

y_i = Mole fraction of component i

- If the gas composition is not known, Fig. 2.11 may be used to estimate the gas viscosity at atmospheric pressure and reservoir temperature, where the apparent molecular weight of the gas mixture is obtained from:

$$M = 29\gamma_g \qquad (2.7.2)$$

The following procedure is recommended for determining gas viscosity (from the CKB equation) at reservoir conditions of P and T:

(A) Sweet Gas

Step 1 - Determine the pseudo-critical pressure (P_{pc}) and pseudo-critical temperature (T_{pc})

Step 2 - Determine the pseudo-reduced pressure (P_{pr}) and pseudo-reduced temperature (T_{pr})

Step 3 - Determine the viscosity of the gas mixture at atmospheric and reservoir T, μ_{ga}, using either Eq. 2.7.1 (or Fig. 2.11 knowing M_a)

Step 4 - Obtain the ratio μ_g/μ_{ga} from Figures 2.8a or 2.8b

Step 5 - Calculate the gas viscosity at reservoir P and T from:

$$\mu_g = [\mu_g/\mu_{ga}] \times \mu_{ga} \qquad (2.7.3)$$

(B) Sour gas

- The inserts in Fig. 2.11 are corrections for the presence of carbon dioxide (CO_2), hydrogen sulfide (H_2S) and nitrogen (N_2) and for 4 gas gravity values: 0.6, 1, 1.5, and 2.

- The effect of each of the non-hydrocarbon gases is to increase the viscosity of the gas mixture.

- The corrections are (reasonably) accurate only if the mole fractions of CO_2, H_2S and N_2 are less than 15%. If the mole fractions are higher than 15% and up to 25%, corrections (less accurate) are still possible by linearly extrapolating the lines in the inserts.

The procedure for calculating the viscosity of a sour gas at reservoir P and T is:

Step 1 - Determine the pseudo-critical pressure (P_{pc}) and pseudo-critical temperature (T_{pc}) of the total gas mixture

Step 2 - The pseudo-critical properties are adjusted with a factor ε_3, using Eqs. 2.3.20 - 22: T'_{pc} and P'_{pc}

Step 3 - Determine the adjusted pseudo-reduced pressure (P_{pr}) and pseudo-reduced temperature (T_{pr}) from:

$$p_{pr} = p / p_{pc}'$$
$$T_{pr} = T / T_{pc}' \qquad (2.7.4)$$

Step 4 - Determine the (uncorrected) viscosity of the gas mixture at atmospheric and reservoir T, μ_{gau}, using either Eq. 2.7.1 (or Fig. 2.11 knowing M_a)

Step 5 - Knowing the gas gravity γ_g and the mole fractions of the non-hydrocarbon components, 1.e. y_{CO2}, y_{H2S} and y_{N2}, obtain the viscosity correction factors from the vertical axis of the inserts in Fig. 2.11:

$$\mu_{corCO2}, \quad \mu_{corH2S}, \text{ and } \mu_{corN2}$$

Step 6 - Calculate the total viscosity correction factor for non-hydrocarbon components:

$$\mu_{corNH} = \mu_{corCO2} + \mu_{corH2S} + \mu_{corN2} \qquad (2.7.5)$$

Step 7 - Calculate the <u>corrected</u> viscosity of the gas mixture at atmospheric and reservoir T, μ_{ga}:

$$\mu_{ga} = \mu_{gau} + \mu_{corNH} \qquad (2.7.6)$$

Step 8 - Using the adjusted pseudo-reduced pressure (P'_{pr}) and pseudo-reduced temperature (T'_{pr}) from step 3, determine the ratio μ_g / μ_{ga} from Figures 2.8a or 2.8b

Step 9 - Calculate the gas viscosity at reservoir P and T from Eq. 2.7.3, 1.e.

$$\mu_g = [\mu_g / \mu_{ga}] \times \mu_{ga}$$

EXAMPLE 2.12

Problem: Calculate the viscosity of the gas described in EXAMPLE 2.7

Solution:

Since the gas only contains hydrocarbon components, the procedure for sweet gas is applicable.

Step 1 - From EXAMPLE 2.7:

P_{pc}= 665.87 psia, T_{pc}=395.6 °R

Step 2 - From EXAMPLE 2.7:

P_{pr}= 1.502, T_{pr}= 1.54

Step 3 - From EXAMPLE 2.7, the apparent molecular weight of the gas mixture is 20.249.

Using Fig. 2.11 the viscosity of the gas mixture at atmospheric pressure and reservoir T= 150 °F is:

μ_{ga} = 0.0122 cp

Step 4 - Obtain the ratio μ_g/μ_{ga}*:*

μ_g/μ_{ga} = 3.72

Step 5 - Calculate the gas viscosity at reservoir P = 1000 psia and T = 150 from Eq. 2.7.3:

$\mu_g = [\mu_g/\mu_{ga}] \times \mu_{ga} = 3.72 \times 0.0122 = 0.0454$ cp

EXAMPLE 2.13

Problem: Calculate the viscosity of the gas described in EXAMPLE 2.8

Solution:

Since the gas contains non-hydrocarbon components, the procedure for sour gas is applicable:

Step 1 - From EXAMPLE 2.8:

P_{pc}= 748.3 psia, T_{pc} = 384.5 °R

Step 2 - From EXAMPLE 2.8, the adjusted values are:

P'_{pc}= 678.7 psia, T'_{pc} = 364.5 °R

Step 3 - From EXAMPLE 2.8:

P_{pr}= 2.39, T_{pr}= 1.54

Step 4 - From EXAMPLE 2.11, M_a = 20.03. Using Fig. 2.11 the (uncorrected) viscosity of the gas mixture at atmospheric pressure and reservoir

T = 100 °F is:

μ_{ga} = *0.0108 cp*

Step 5 - From EXAMPLE 2.11, γ_g = *0.69 The viscosity correction factors from the vertical axis of the inserts in Fig. 2.11:*

y_{CO2} = *7.44%*	μ_{corCO2} = 0.0004
y_{H2S} = *7.35%*	μ_{corH2S} = 0.00015
y_{N2} = *0.81%*	μ_{corN2} = 0.00008

Step 6 - Calculate the total viscosity correction factor for non-hydrocarbon components from Eq. 2.7.5

$\mu_{corNH} = \mu_{corCO2} + \mu_{corH2S} + \mu_{corN2}$

= 0.0004 + 0.00015 + 0.00008 = 0.00063 cp

Step 7 - Calculate the corrected viscosity of the gas mixture at atmospheric and reservoir T, μ_{ga} from Eq. 2.7.6:

$\mu_{ga} = \mu_{gau} + \mu_{corNH}$

= 0.0108 + 0.00063 = 0.01143 cp

Step 8 - Using the adjusted values of P_{pr} and T_{pr} from step 3 (P_{pr}= 2.39, T_{pr}= 1.54), obtain the ratio μ_g/μ_{ga} *:*

μ_g/μ_{ga} = *1.32*

Step 9 - Calculate the gas viscosity at reservoir P = 1623 psia and T = 100 °F from Eq. 2.7.3:

$\mu_g = [\mu_g/\mu_{ga}] \times \mu_{ga} = 1.32 \times 0.01143 = 0.0151$ *cp*

METHOD 3

For programming purposes μ_g can be obtained from the **CKB - Dempsey procedure**:

Step 1 - Knowing the gas gravity γ_g determine the (uncorrected) viscosity of the gas mixture at atmospheric and reservoir T, μ_{gau}:

$$\mu_{gau} = \left[\left(\left(1.709\text{x}10^{-5}\right) - \left(2.062\text{x}10^{-6}\right)\gamma_g\right)\right]T + \left[\left(8.188\text{x}10^{-3}\right) - \left(6.15\text{x}10^{-3}\right)\log\gamma_g\right] \quad (2.7.7)$$

Where T = reservoir temperature, °F

γ_g = specific gas gravity (air = 1)

- This equation is primarily valid for the case where the specific gas gravity value is less than or equal to 1.5 (region of interest in reservoir engineering calculations).

Step 2 - Knowing the mole fractions of the non-hydrocarbon components, 1.e. y_{CO2}, y_{H2S} and y_{N2}, obtain the viscosity correction factors from:

$$\mu_{corN2} = y_{N2}\left(\left(8.48\text{x}10^{-3}\right)\log\gamma_g - \left(9.59\text{x}10^{-3}\right)\right)$$
$$\mu_{corCO2} = y_{CO2}\left(\left(9.08\text{x}10^{-3}\right)\log\gamma_g - \left(6.24\text{x}10^{-3}\right)\right) \quad (2.7.8)$$
$$\mu_{corH2S} = y_{H2S}\left(\left(8.49\text{x}10^{-3}\right)\log\gamma_g - \left(3.73\text{x}10^{-3}\right)\right)$$

Step 3 - Calculate the total viscosity correction factor for non-hydrocarbon components:

$$\mu_{corNH} = \mu_{corCO2} + \mu_{corH2S} + \mu_{corN2} \qquad (2.7.9)$$

Step 4 - Calculate the corrected viscosity of the gas mixture at atmospheric pressure and reservoir T, μ_{ga}:

$$\mu_{ga} = \mu_{gau} + \mu_{corNH} \qquad (2.7.10)$$

Step - 5 Calculate the adjusted Dempsey factor (D_{fr}) from the following expression, where P_{pr} and T_{pr} are the adjusted values (which may be obtained from Step 3 of the previous procedure, Eq. 2.7.4)

$$\begin{aligned} D_{fr} = {} & a_0 + a_1 p_{pr} + a_2 p_{pr}^2 + a_3 p_{pr}^3 \\ & + T_{pr}\left(a_4 + a_5 p_{pr} + a_6 p_{pr}^2 + a_7 p_{pr}^3\right) \\ & + T_{pr}^2\left(a_8 + a_9 p_{pr} + a_{10} p_{pr}^2 + a_{11} p_{pr}^3\right) \\ & + T_{pr}^3\left(a_{12} + a_{13} p_{pr} + a_{14} p_{pr}^2 + a_{15} p_{pr}^3\right) \end{aligned} \qquad (2.7.11)$$

Where the correlation constants are:

$a_0 = -2.4621$

$a_1 = 2.9705$

$a_2 = -2.8626 \times 10^{-1}$

$a_3 = 8.0542 \times 10^{-3}$

$a_4 = 2.8086$

$a_5 = 3.4980$

$a_8 = -7.9338 \times 10^{-1}$

$a_9 = 1.3964$

$a_{10} = -1.4914 \times 10^{-1}$

$a_{11} = 4.4101 \times 10^{-3}$

$a_{12} = 8.3938 \times 10^{-2}$

$a_{13} = -1.8640 \times 10^{-1}$

$a_6 = 3.6037$ $a_{14} = 2.0336 \times 10^{-2}$

$a_7 = -1.0443 \times 10^{-2}$ $a_{15} = -6.0957 \times 10^{-4}$

Step 6 - Calculate the gas viscosity at reservoir P and T from

$$\ln\left(\frac{\mu_g}{\mu_{ga}} T_{pr}\right) = D_{fr} \qquad (2.7.12)$$

solving Eq. 2.7.12 for μ_g yields:

$$\mu_g = (\mu_{ga}/T_{pr}) EXP(D_{fr}) \qquad (2.7.13)$$

METHOD 4

- The **Lee, Eakin and Gonzales (LEG)** correlation was believed to be valid only for sweet natural gases.
- However, if the gas density or the z-factor has been corrected for noo-hydrocarbon contaminants, the LEG correlation can accurately estimates of the gas viscosity at reservoir P and T.

The LEG correlation for viscosity is:

$$\mu_g = A * 10^{-4} \left[e^{\left(B\rho_g^C \right)} \right] \qquad (2.7.14)$$

Where:

μ_g = gas viscosity at reservoir temperature and pressure, cp

ρ_g = gas density, gm/cc

$$\rho_g = 1.4935x10^{-3}\frac{pM_a}{zT} \qquad (2.7.15)$$

p = reservoir pressure, psia

T = reservoir temperature, °R

M_a = apparent molecular weight, lbm/lb-mol

z = gas deviation factor (which is corrected for contaminants as discussed in section 1.3)

A, B, C = correlation constants, given by the following expressions:

$$A = \frac{(9.379 + 0.01607M_a)T^{1.5}}{209.2 + 19.26M_a + T} \qquad (2.7.16)$$

$$B = 3.448 + \left(\frac{986.4}{T}\right) + 0.01009M_a \qquad (2.7.17)$$

$$C = 2.447 - 0.2224B \qquad (2.7.18)$$

- The standard deviation in the calculated gas viscosity compared with experimental data was 2.7% and the maximum error was 9%.
- in general, the LEG coorrelation is valid for $100<p<8000$ psia, and $100<T<340$ °F.
- The LEG correlation gives accurate results for $0.9<y_{co2}<3.2$ percent.
- The results of these equations agree with the limited published data of gas viscosity to within 2% at low pressure and to within 4% at high pressure when the specific gravity of the gas is <1.0.
- The equations are less accurate for gases of higher specific gravities, usually giving low estimates by up to 20% for retrograde gases with specific gravities over 1.5.

EXAMPLE 2.14

Problem: Calculate gas viscosity for the sour gas reservoir described in EXAMPLE 2.8 with the LEG correlation

Solution:

- *The apparent molecular weight and z-factor were estimated in Example 8, where the reservoir P = 1623 psia and T=100 °F:*

  M_a = *20.03 lbm/lb-mol*

  z = *0.89*

Step 1 - Calculate the gas density with Eq. 2.7.15

$$\rho_g = 1.4935 \times 10^{-3} \frac{pM_a}{zT}$$

$$\rho_g = 1.4935 \times 10^{-3} \frac{1623 \times 20.03}{0.82 \times (100 + 460)}$$

$$= 0.1057 \, g / cm^3$$

Step 2 - Calculate the correlation constant A with Eq. II.7.16

$$A = \frac{(9.379 + 0.01607 \times 20.03)560^{1.5}}{209.2 + 19.26 \times 20.03 + 560} = 111.31$$

Step 3 - Calculate the correlation constant B with Eq. 2.7.17

$$B = 3.448 + \left(\frac{986.4}{560}\right) + 0.01009 \times 20.03 = 5.41$$

Step 4 - Calculate the correlation constant C with Eq.2.7.18

C = 2.447- 0.2224x5.41 = 1.24

Step 5 - Calculate the gas viscosity with Eq. 2.7.14

$$\mu_g = A * 10^{-4} \left[\exp\left(B\rho_g^C\right)\right]$$

$$\mu_g = 111.31 * 10^{-4}\left[e^{5.41\left(0.1057^{1.24}\right)}\right] = 0.0155cp$$

- This value of gas viscosity is practically similar to that obtained in EXAMPLE 2.13 (ie. 0.0151 cp) using Method 2, which is based on the CKB equation for sour gases.
- The minor difference (less than 3% error) is due to the fact that the mole fraction of CO_2 is greater than 3.20% (where the LEG correlation is less precise)

METHOD 5 - THODOS METHOD

Thodos et al. have shown that the residual viscosity function can be well correlated against density, therfeby making it a useful tool for both gas and liquid viscosities. The Thodos method requires two steps, as does the technique of Carr et al. First μ^* must be estimated, then the effect of pressure can be calculated from another correlation. The correlation for μ^* is shown in Fig. 2.17a, and the effects of pressure can be estimated from Fig. 2.17b. viscosities calculated using the correlations of Thodos et al. can be expected to have an accuracy on order of 3%.

To use of Figs. 2.17a and 2.17b, one must first calculate the average mole weight of the mixture, $\overline{M}_g = \sum y_i M_i$, and the pseudo-critical temperature, pressure, and volume by Kay's rules (T_c in units of Kelvin and V_c in $cm^3/gmol$) or Fig.2.18 if C_{7+} concentration is small. Alternatively, the correlation of Matthews et al. (Fig. 2.6) may be used to get T_c and p_c for C_{7+} fractions. The following may be used for V_C of the C_{7+} fraction.

$$(V_C)_{C7+} = 1.561(M_{C7+}/\rho_R)^{1.15} \qquad (2.7.19)$$

where M_{C7+} is the molecular weight of the C_{7+}fraction, and

ρ_R is the relative density of the C_{7+} fraction.

Calculation of the pseudocritical density, ρ_{pc}, and the viscosity parameter, ξ, are as follows

$$\rho_{pc} = \frac{\overline{M}_g}{V_{pc}} \tag{2.7.20}$$

and

$$\xi = \frac{\left(T_{pc}\right)^{1/6}}{\left(\overline{M}_g\right)^{1/2}\left(p_{pc}\right)^{2/3}} \tag{2.7.21}$$

where T_{pc} is the pseudocritical temperature, K, and

p_{pc} is the pseudocritical pressure, atm.

If gas density is not known it can be obtained from the compressibility factor through

$$\rho_g = \frac{\overline{M}_g p}{z\ RT} \tag{2.7.22}$$

where compressibility, z, factor can be determine.

Reduced conditions can be determined making sure that ρ and ρ_{pc} are in the same units.

Fig. 2.17a can be used to obtain $\mu^*\xi$ and then calculate

$$\mu^* = \mu^*\xi/\xi \tag{2.7.23}$$

The final step is to obtain $\left(\mu - \mu^*\right)\xi$ from Fig. 2.17b and solve for μ with

$$\mu = \mu^* + \left[\left(\mu - \mu^*\right)\xi\right]/\xi \tag{2.7.24}$$

The Thodos et al. correlation is a more general relationship and can be used for both gases and liquids, making it the preferred method for phase equilibrium calculations or for the near-critical region.

2.8 - FORMATION VOLUME FACTOR

- In gas reservoir engineering, the main use of the real gas equation of state is to relate surface volumes to reservoir volumes of hydrocarbons.
- This is accomplished by the use of the "gas formation volume factor" B_g or the "gas expansion factor":

$$E = 1/B_g \tag{2.8.1}$$

- The gas formation volume factor is the ratio of the volume of gas in the reservoir to its volume at standard conditions:

$$B_g = \frac{V_r}{V_{sc}} = \frac{\text{Volume of gas in the reservoir}}{\text{Same volume of gas at } T_{sc} \text{ and } P_{sc}} \tag{2.8.2}$$

From the real gas law, the volume gas at reservoir P and T is:

$$V_r = \frac{znRT}{P} \tag{2.8.3}$$

The volume of gas at surface P_{sc} and T_{sc} is:

$$V_{sc} = \frac{z_{sc}nRT_{sc}}{P_{sc}} \tag{2.8.4}$$

Combining Eqs. 2.8.2,3, and 4 gives:

$$B_g = \frac{V_r}{V_{sc}} = \frac{p_{sc}}{p} x \frac{T}{T_{sc}} x \frac{Z}{Z_{sc}} \qquad (2.8.5)$$

Where:

P_{sc}= 14.7 psia = 101 kPa

T_{sc}= 60 °F = 520 °R = 289 °K

z_{sc} = gas deviation factor at T_{sc} and P_{sc} = 1.0

Thus, at standard conditions, Eq. 2.8.5 becomes:

$$B_g = \frac{zT(14.7)}{1.0x520p} = 0.0283\frac{ZT}{p} \qquad (ft^3 / scf) \qquad (2.8.6)$$

- Dividing reservoir cubic feet by 5.615 (to convert to reservoir barrels) gives:

$$B_g = 0.00504\frac{ZT}{p} \quad (bbl / scf) \qquad (2.8.7)$$

- In SI units, the gas formation volume factor is:

$$B_g = \frac{zT(101)}{1.0x289p} = 0.3495\frac{ZT}{p} \qquad (m^3 / scm^3) \qquad (2.8.8)$$

- Because the production from a volumetric gas reservoir is due solely to gas expansion, the recovery can be expressed in terms of the gas formation volume factor:

$$\%Recovery = 100\ (1 - \frac{B_{gi}}{B_{ga}}) \qquad (2.8.9)$$

Where:

B_{gi} = gas formation volume factor at initial reservoir pressure, P_i

B_{ga} = gas formation volume factor at abandonment reservoir pressure, P_a

EXAMPLE 2.15

Problem: At initial reservoir pressure of 2500 psia and temperature of 180 °F, the gas deviation factor z = 0.85.

(a) *Calculate the gas formation volume factor*

(b) *How many SCF of this gas are contained in the reservoir with gas pore volume of 10^9 cuft?*

Solution:

(a) Using Eq. 2.8.6, the gas FVF is

$$B_{gi} = 0.0283\frac{ZT}{p_i} = 0.0283\frac{0.85x(180+460)}{2500} = 0.00616\frac{scf}{ft^3}$$

(b) The initial gas in place is:

$$IGIP = \frac{V_r}{B_{gi}} = \frac{10^9}{0.00616} = 162.388x10^9 \text{ scf}$$

(c) In SI units, B_{gi} is calculated from Eq. 2.8.8:

$$B_{gi} = 0.3495\frac{ZT}{p_i} = \frac{0.3495x0.85x355.55}{17237.5} = 6.128x10^{-3} \quad (m^3 / scm^3)$$

where temperature and pressure are converted to SI units as follows:

$$T \text{ (in °K)} = 0.5555\ [T \text{ (in °F)} + 460] \qquad (2.8.10)$$

$$= 0.5555\ [\ 180 + 460] = 355.55$$

$$P \text{ (in kPa)} = 6.895 \times P \text{ (in psi)} \qquad (2.8.11)$$

$$= 6.895 \times 2500 = 17237.5$$

$$V_r \text{ (in m}^3\text{)} = 0.028317 \times V_r \text{ (in ft}^3\text{)} \qquad (2.8.12)$$

$$= 0.028317 \times 10^9 = 28.317 \times 10^6$$

The initial gas in place in SI units is:

$$IGIP = \frac{V_r}{B_{gi}} = \frac{28.31710^6}{6.128x10^{-3}} = 4.621x10^9 \text{ m}^3$$

The IGIP in SI units could have also been obtained by simply converting $162.388x10^9$ scf:

$$IGIP = 162.388x10^9(\text{ft}^3) \times 0.028317 (\text{m}^3/\text{ft}^3) = 4.6x10^9 \text{ m}^3$$

2.9 - SPECIFIC GRAVITY OF GAS AND GAS CONDENSATE RESERVOIRS

(a) Three-stage separation

Eq. 2.9.1 is the recombination expression for the reservoir gas gravity, γ_w, for a three-stage separation system consisting of a primary (high pressure) separator, secondary (low-pressure) separator, and stock tank.

$$\gamma_w = \frac{R_1\gamma_1 + 4{,}602\gamma_0 + R_2\gamma_2 + R_3\gamma_3}{R_1 + \frac{133{,}316\gamma_0}{M_0} + R_2 + R_3} \qquad (2.9.1)$$

Eq. 2.9.1 is applicable (and rigorously correct) if the gas/liquid ratio and gas specific gravity of each separation stage and the stock tank liquid gravity are known.

Where:

R_1 = primary (high-pressure) separator gas/stock-tank-liquid ratio, scf/STB;

R_2 = secondary (low-pressure) separator gas/stock-tank-liquid ratio, scf/STB;

R_3 = stock-tank-gas/stock-tank-liquid ratio, scf/STB;

γ_1 = specific gravity of primary-separator gas (air= 1.0);

γ_2 = specific gravity of secondary-separator gas (air= 1.0);

γ_3 = specific gravity of stock-tank gas (air= 1.0);

γ_o = specific gravity of the liquid hydrocarbons (water=1.0); and

M_O = molecular weight of stock-tank liquid, lbm/lbm-mol.

- If *Mo* is unknown, then it can be approximated with either API gravity (Eq. 2.9.2a) or specific gravity (Eq. 2.9.2b):

$$M_0 = \frac{5{,}954}{\gamma_{API} - 8.811} \qquad (2.9.2a)$$

$$\text{or } M_0 = \frac{42.43\gamma_0}{1.008 - \gamma_0} \qquad (2.9.2b)$$

where γ_{API} is the specific gravity (in °API) of the stock-tank hydrocarbon liquid.

(b) Two-stage separation

Eq. 2.9.3 is the recombination expression for a two-stage separation system consisting of a primary separator and a stock tank.

$$\gamma_w = \frac{R_1\gamma_1 + 4{,}602\gamma_0 + R_3\gamma_3}{R_1 + \frac{133{,}316\gamma_0}{M_0} + R_3} \qquad (2.9.3)$$

(c) Gas Specific Gravity Correlations

Because gas rates and specific gravities from low-pressure separators and the stock tank frequently are not measured, this gas production must be estimated for Eq. 2.9.1 or 2.9.2. These estimates are made with **correlations** for additional gas production, G_{pa}, and vapor equivalent, V_{eq}, in conjunction with Eq. 2.9.4

The correlations are based on generally available production parameters, specifically the primary-separator pressure, temperature, and gas gravity; the secondary-separator temperature; and the stock-tank-liquid gravity.

- In terms of G_{pa} and V_{eq}, the reservoir gas specific gravity, γ_w, is estimated by

$$\gamma_w = \frac{R_1\gamma_1 + 4{,}602\gamma_0 + G_{pa}}{R_1 + V_{eq}} \qquad (2.9.4)$$

where

V_{eq} = volume of secondary-separator gas and stock-tank gas plus the volume that would be occupied by 1 bbl of stock-tank liquid if it were gas, scf/STB; and

Gpa = additional gas production, scf/STB.

(1) **Three-stage separation**

The correlation equation for Gpa and Veq are:

$$G_{pa} = 2.9922\left(p_{sl} - 14.65\right)^{0.97050} \gamma_1^{6.8049} \gamma_{API}^{1.0792} T_{sl}^{-1.1960} T_{s2}^{0.55367} \qquad (2.9.5)$$

$$V_{eq} = 535.92 + 2.6231 p_{sl}^{0.79318} \gamma_1^{4.6612} \gamma_{API}^{1.2094} T_{sl}^{-0.84911} T_{s2}^{0.26987} \qquad (2.9.6)$$

(2) **Two-stage separation:**

The correlation equations for G_{pa} and V_{eq} are:

$$G_{pa} = 1.4599\left(p_{sl} - 14.65\right)^{1.3394} \gamma_1^{7.0943} \gamma_{API}^{1.1436} T_{sl}^{-0.93446} \qquad (2.9.7)$$

$$V_{eq} = 635.53 + 0.36182 p_{sl}^{1.0544} \gamma_1^{5.0831} \gamma_{API}^{1.5812} T_{sl}^{-0.79130} \qquad (2.9.8)$$

(d) Wellstream gas flow rate

The wellstream gas flow rate, representing all gas and liquid produced at the surface and including the high- and low-pressure separator and stock-tank gas, can be calculated with Eq. 2.9.9 or 2.9.10:

$$q = q_g + 133.316\left(\frac{\gamma_o q_o}{M_o}\right) \qquad (2.9.9)$$

$$\text{or} \qquad q = q_{sl}\left(1 + \frac{V_{eq}}{R_1}\right) \qquad (2.9.10)$$

where

q=total wellstream gas flow rate, Mscf/D;

q_g=total gas surface gas flow rate, Mscf/D;

q_O=oil flow rate, STB/D; and

q_{sl}=*gas* flow rate from primary separator, Mscf/D.

- Eq. 2.9.9 should be used if the total surface gas flow rate is known.
- Eq. 2.9.10 is applicable when the secondary-separator (low-pressure) and/or stock-tank gas production is not known.

(e) Cumulative wellstream gas produced

If the gas/liquid ratio and liquid and gas gravities remain constant with time and if the cumulative surface production of gas, $Q_{g,dry}$, and cumulative stock-tank-liquid production, Q_O are known, then the cumulative gas produced at the sandface is:

$$Q_{g,wet} = Q_{g,dry} + 133.316\left(\frac{\gamma_O Q_O}{M_O}\right) \tag{2.9.11}$$

Otherwise,

$$Q_{g,wet} = Q_{g,dry}\left(1+\frac{V_{eq}}{R_1}\right) \tag{2.9.12}$$

where

$Q_{g,wet}$ = cumulative wellstream gas produced at the sandface, Mscf;

$Q_{g,dry}$ = cumulative surface gas production, Mscf; and

Q_O=cumulative stock-tank liquid production, STB.

When the gas/liquid ratio and/or the gas and liquid compositions change with time, the wet-gas cumulative production can be calculated by integrating the wet-gas rate over time.

EXAMPLE 2.16

Calculating Wellstream Gas Gravity and Flow Rate With Known Fluid Properties. Calculate the wellstream gas gravity, the total wellstream gas flow rate, and the cumulative wellstream production for a three-stage separation system. Measured production data and fluid properties, including the gas and liquid from the stock tank, are summarized below.

$R_1 = 7{,}040$ scf / STB

$\gamma_1 = 0.712$

$\gamma_o = 0.755$

$Q_{g,dry} = 767$ MMscf

$R_2 = 510$ scf / STB

$\gamma_2 = 1.02$

$M_o = 125$ lb / lbm – mol

$Q_o = 100{,}000$ STB

$R_3 = 120$ scf / STB

$\gamma_3 = 1.55$

$q_o = 50$ STB / D

$q_g = 384$ Mscf / D

Solution

1. Eq. 2.9.1 is applicable because every term in the recombination expression is known. The specific gravity of the reservoir gas (air=1.0) is

$$\gamma_w = \frac{R_1\gamma_1 + 4{,}602\gamma_0 + R_2\gamma_2 + R_3\gamma_3}{R_1 + \dfrac{133{,}316\gamma_0}{M_0} + R_2 + R_3} =$$

$$\frac{(7{,}040)(0.712) + 4{,}602(0.755) + (510)(1.02) + (120)(1.55)}{7{,}040 + \dfrac{(133{,}316)(0.755)}{125} + 510 + 120} = 1.08$$

2. The total wellstream gas rate (Eq. 2.9.9) is

$$q = q_g + 133.316\left(\frac{\gamma_o q_o}{M_o}\right)$$

$$= 384 + 133.316\frac{(0.755)(50)}{125} = 424 \text{ Mscf / D}$$

3. Cumulative wellstream gas production is calculated with Eq. 2.9.11:

$$Q_{g,wet} = Q_{g,dry} + 133.316\left(\frac{\gamma_o Q_o}{M_o}\right) = 767{,}000 + 133.316\frac{(0.755)(100{,}000)}{125} = 847{,}523 \text{ Mscf}$$

$$= 848 \text{ MMscf}$$

EXAMPLE 2.17

Estimating Wellstream Gas Gravity and Flow Rate Correlations. Calculate the wellstream gas gravity, total wellstream gas flow rate, and cumulative wellstream production for a two-stage separation system.

$R_1 = 7{,}040$ scf / STB

$P_{s1} = 700$ psia

$\gamma_{API} = 55.8^0$ API

$\gamma_1 = 0.712$

$T_{s1} = 90\ ^0F$

$q_{s1} = 352$ MMscf / D

$Q_{g,dry} = 680$ MMscf

Solution

1. First, calculate G_{pa} with Eq. 2.9.7

$$G_{pa} = 1.4599\left(p_{s1} - 14.65\right)^{1.3394} \gamma_1^{7.0943} \gamma_{API}^{1.1436} T_{s1}^{-0.93446}$$

$$= 1.4599(700 - 14.65)^{1.3394}(0.712)^{7.0943}(55.8)^{1.1436}(90)^{-0.93446}$$

$$= 1{,}223.2 \text{ scf / STB}$$

2. Similarly, we can calculate V_{eq} with Eq. 2.9.8

$$V_{eq} = 635.53 + 0.36182 p_{sl}^{1.0544} \gamma_1^{5.0831} \gamma_{API}^{1.5812} T_{sl}^{-0.79130}$$

$$= 635.53 + 0.36182(700)^{1.0544}(0.712)^{5.0831}(55.8)^{1.5812}(90)^{-0.79130}$$

$$= 1{,}692.1 \text{ scf / STB}$$

3. The specific gravity of the stock-tank liquid, γ_o, is

$$\gamma_o = \frac{141.5}{131.5 + \gamma_{API}} = \frac{141.5}{131.5 + 55.8} = 0.756$$

4. Calculate the reservoir gas specific gravity, γ_w, with Eq. 2.9.4

$$\gamma_w = \frac{R_1 \gamma_1 + 4{,}602 \gamma_0 + G_{pa}}{R_1 + V_{eq}}$$

$$= \frac{(7{,}040)(0.712) + 4{,}602(0.756) + 1{,}223.2}{7{,}040 + 1{,}692.1}$$

$$= 1.112$$

5. The total wellstream gas flow rate is

$$q = q_{sl}\left(1 + \frac{V_{eq}}{R_1}\right)$$

$$= 352\left(1 + \frac{1{,}692.1}{7{,}040}\right) = 437 \text{ Mscf / D}$$

6. The cumulative wellstream gas is

$$Q_{g,wet} = Q_{g,dry}\left(1+\frac{V_{eq}}{R_1}\right) = 680\left(1+\frac{1{,}692.1}{7{,}040}\right) = 843 \text{ MMscf.}$$

Once we have estimated the specific gas gravity of the reservoir gas, we then use Sutton's method for calculating pseudocritical pressure and temperature. Sec. 2.6.7 outlines a systematic procedure, including corrections for H_2S, CO_2, nitrogen, and water vapor contamination, for estimating the pseudocritical properties of a natural gas.

2.10 VAPOR PRESSURE

At a given temperature, the vapor pressure of a pure component is the pressure at which vapor and liquid coexist at equilibrium. The term "vapor pressure" should be used only in conjunction with pure compounds and is usually considered as a liquid (rather than gas) property. For a pure compound, there is only one vapor pressure at any temperature. A plot of these pressures is shown in Fig. 2.12.1. for n-butane. The temperature at which the vapor pressure is equal to 1 atm (14.696 psia or 101.32 kPa) is known as the normal boiling point.

The Clapeyron equation gives a rigorous quantitative relationship between vapor pressure and temperature:

$$\frac{dp_v}{dT} = \frac{L_v}{T \cdot \Delta V} \qquad (2.10.1)$$

where

p_v = vapor pressure,

T = absolute temperature,

ΔV = increase in volume while vaporizing 1 mole, and

L_v = mole latent heat of vaporization.

Assuming ideal-gas behavior of the vapor and neglecting the liquid volume, the Clapeyron equation can be simplified over a small temperature range to give the approximation

$$\frac{d\ln(p_v)}{dT} = \frac{L_v}{RT^2} \qquad (2.10.2)$$

which is known as the Clausius-Clapeyron equation.

This equation suggests that a plot of logarithm of vapor pressure against the reciprocal of the absolute temperature would approximate a straight line. Such a plot is useful in interpolating data over short ranges. However, the shape of this relationship for real substances is not a straight line but rather S-shaped. Therefore, the use of the Clausius-Clapeyron equation is not recommended when other methods are available.

2.10.1 Cox Chart

Cox further improved the method of estimating vapor pressure by plotting the logarithm of vapor pressure against an arbitrary temperature scale. The vapor-pressure/temperature plot forms a straight line, at least for the reference compound, and usually for the most of the materials related to the reference compound. This is especially true for petroleum hydrocarbons. A Cox chart using water as a reference material is shown in Fig. 2.12.2.

In addition to forming nearly straight lines, compounds of the same family appear to converge on a single point. Thus, it is necessary to know only vapor pressure at one temperature to estimate the position of the vapor-pressure line. This approach is very handy and can be much better than the previous method. Its accuracy is dependent to a large degree on the readability of the chart.

2.10.2 Calingeart and Davis Equation

The Cox chart was fit with a three-parameter function by Calingeart and Davis. Their equation is

$$\ln(p_V) = A - \frac{B}{T - C} \qquad (2.10.3)$$

where A and B are empirical constants, and, for compounds boiling between 32 and 212°F, C is a constant with a value of 43 when T is in K, and C is a constant with a value of 77.4 when T is in °R.

This equation generally is known as the Antoine equation because Anfoine proposed one of very similar nature that used 13K for the constant C. Knowledge of the vapor pressure at two temperatures will fix A and B and permit approximations of vapor pressures at other temperatures.

Generally, the Antoine approach can be expected to have less than 2 % error and is the preferred approach if the vapor pressure is expected to be less than 1,500 mmHg [200kPa] and if the constants are available.

2.10.3 Lee-Kesler

Vapor pressures also can be calculated by corresponding states principles. The most common expansions of the Clapeyron equation lead to a two-parameter expression. Pitzer extended the expansion to contain three parameters:

$$\ln(p_{VT}) = f^0 T_r + \omega f^1 T_r \qquad (2.10.4)$$

where

p_{vr} is the reduced vapor pressure (vapor pressure /critical pressure),

f^0 and f^1 are functions of reduced temperature, and

ω is the acentric factor.

Lee and Kesler have expressed f^0 and f^1 in analytical forms:

$$f^0 = 5.92714 - (6.09648 / T_r) - 1.28862 \ln(T_r) + 0.169347(T_r)^6 \qquad (2.10.5)$$

and

$$f^1 = 15.2518 - (15.6875 / T_r) - 13.4721 \ln(T_r) + 0.43577(T_r)^6 \qquad (2.10.6)$$

which can be solved easily by high speed computer or a hand-held calculator.

Lee-Kesler is the preferred method of calculation but should be used only for nonpolar liquids. The advent of computers and calculators makes use of approximations and charts much less advantageous than they were in the 1960's. Values of acentric factors can be found in literature, together many other available vapor-pressure correlations and calculation techniques with comments about their advantages and limitations.

2.11 FLUID SAMPLING TECHNIQUES

SURFACE SAMPLES

1. Gas Condensates
2. Wet Gases
3. Dry Gases

2.11.1 - FLUID SAMPLING OF GAS-CONDENSATE WELLS

WELL CONDITIONING

When a gas condensate well is produced, the pressure in the formation near the wellbore is often reduced below the dewpoint pressure of the reservoir fluid. This pressure drop causes a liquid phase to be formed in the pores of the formation in this area.

As a result, the vapor phase (which is the fluid produced) has a lower concentration of condensable hydrocarbons and is said to be leaner than the original reservoir fluid.

This loss of condensable hydrocarbons results in an increase in the producing gas-liquid ratio. Since the largest part of the pressure drop occurs close to the wellbore, retrograde liquid saturation near the wellbore can build up enough to allow the liquid to become mobile. This mobile liquid will cause significant, but unpredictable changes in the producing gas-liquid ratio.

There are many situations where special procedures must be used in order to prepare a well for the collection of proper fluid samples. Also, there are unique situations in which the wells are conditioned for sampling without any special procedures.

It is always helpful to communicate the production history, formation characteristics, production rates, ratios and related stock tank liquid gravity data, etc. with appropriate laboratory personnel before and during the conditioning period for evaluation and advice.

Before collecting fluid samples, a new well must have had sufficient production to remove all drilling fluids, acids, etc.

The well should not be produced rapidly during the cleaning period because high production rates could cause a large pressure drawdown in the formation around the wellbore. A large pressure drawdown usually provokes the need for a long conditioning period prior to sample collection.

Although there are those unique situations where the well does not require any special conditioning procedures; however, the well is usually conditioned by placing it on a producing schedule consisting of a series of successively lower flow rates. After each rate reduction, flow is continued until the gas-liquid ratio becomes stabilized.

The trend of the resulting stabilized gas-liquid ratio data will generally be found to decrease as the producing flow rate is decreased.

The well is considered to be conditioned when the stabilized gas-liquid ratio does not change after the producing rate is reduced. However, one must realize the producing rate must be sufficient to prevent heading.

SAMPLE COLLECTION

Gas condensate are difficult to sample reliable because:

- Large quantities of gas are associated with small quantities of liquid. The phase behavior of the system may be highly sensitive to the amount and composition of the liquid phase.
- The flowing system invariably becomes two-phase before reservoir fluid reaches the surface, and frequently before it enters the wellbore.

Because the liquid phase standing in the tubing of a shut-in gas condensate well is not representative of the reservoir fluid, sampling during gas condensate testing is usually carried out at surface.

The considerations and procedures of collecting separator gas and liquid samples of fluids producing from a gas condensate well are identical to those used for collecting separator gas and liquid samples for black oil wells described before.

The most common way of obtaining reservoir fluid is to recombine samples taken from the test separator streams. These samples have the advantage of being comparatively inexpensive and plentiful.

It is often the case that samples are taken when the above criteria are not satisfied completely and PVT studies are carried out using unrepresentative samples.

Assuming, however, that these criteria are satisfied, the major sources of uncertainty in obtaining representative reservoir fluid by recombining separator samples are:

- Separator design and efficiency,
- Gas and liquid flow rate measurements, and
- Sampling technique.

O the above, it is likely that the liquid flow rate measurement is the largest source of uncertainty. The accuracy of the volumetric condensate-gas-ratio (CGR) is generally in the range ±5 to 10%.

The following are basic data requirements, prior to conducting a PVT study:

1. Reservoir conditions,
2. Separator conditions, and
3. CGR and metering conditions.

After validation of separator gas and condensate samples, these fluids are recombined in the corrected filed CGR to obtain reservoir fluid.

The filed fluid-measured gas flow rate is corrected using laboratory measured gas properties at metering conditions. Constant composition expansions (CCE's) and constant volume depletion studies (CVD's) are carried out in visual cells, using recombined reservoir fluids.

Depleted Gas Condensate Reservoirs

Consider the depletion of a gas condensate reservoir without pressure maintenance. Once the pressure falls below dewpoint, at any point in the reservoir, differential mobility of the two phases will result in the production of fluid which differs in composition from that of the original reservoir fluid.

With the separator products produced from such a reservoir, it is not only impossible (too late) to recreate a reservoir fluid which would be representative of the original fluid, but also any recombination of these products would not even approach the original reservoir fluid nor its properties.

Constant volume depletion CVD studies are carried out in the laboratory to model an extreme case, in which it is assumed that the reservoir can be treated as a single cell; the liquid phase has zero mobility and, therefore, only single phase gas is produced.

Practical Limitations in Obtaining PVT Data for Gas Condensate Systems.

There are recognized difficulties in obtaining representative samples from gas condensate reservoirs and there are also significant uncertainties in the results of laboratory studies performed using the samples.

The largest uncertainties are associated with the measurements of small liquid volumes, dewpoints and chemical compositions. Reservoir engineers should be aware of these uncertainties and should weight PVT data accordingly, when used as input parameters to reservoir models.

Because compositional simulation models are being used increasingly to study gas condensate reservoir depletion process, particularly when gas injection and recycling are used for pressure maintenance, the development of the reservoir simulation models is dependent on the quality of experimental PVT data.

If experimental data are not used to tune the EOS, then the quantitative prediction of the phase behavior of petroleum systems using the traditional cubic equation of state (EOS) is of little value, due to a poor theoretical basis of the model and to a lack of detail in the reservoir fluid analysis and heavy end (hepthane-plus) characterization.

PVT data are generated in the laboratory using samples taken in the field during well testing.

There are practical limitations in both obtaining the samples from a gas condensate reservoir and, subsequently, measuring the physical and chemical properties of the samples which should be considered because they are associated with the uncertainties in the results of standard PVT studies. Quantification of these uncertainties is extremely important. When tuning EOS models to experimental PVT data, in case of CCE study, it should be considered that the measurement of low liquid volumes has a high associated uncertainty. At lower pressures below the maximum retrograde liquid volume, measurements are more accurate. The data should be weighted accordingly.

Although exact specification of gas condensate dewpoints is of considerable academic interest, it has to be asked whether the presence of small (less than 1% by volume) amounts of liquid has a significant effect on reservoir flow processes.

When tuning to the results of CVD, it should be considered that, on average, liquid volumes, gas densities and gas Z-factors will be underestimated. Some liquid will be lost during the study on the walls of the catchment system and some will remain traped in the cell at the end of the study.

The accuracy of CVD results is increased by increasing the size of charge.

It is common practice for laboratories to use correlations for calculating gas Z-factors and viscosities. If a correlation is used to calculate the Z-factor of a separator gas, prior to charging a gas condensate visual cell, then the accuracy of the reported physical properties of the reservoir fluid is significantly decreased.

Conclusions and Recommendations

1. Reservoir engineers should be aware of the precision of experimental gas condensate PVT data which are used to tune EOS models. Some data are more accurate than others and these should be weighted accordingly.

2. It is impractical for a single laboratory to establish the absolute accuracy of the PVT data it generates; however a laboratory can either estimate the repeatability of the data or, at least, highlight the presence of systematic errors. Repeatability data are specific to an individual study and should be reported along with the experimental results.

3. There are invariably systematic losses of liquid in PVT equipment, due to wetting of the walls which leads to uncertainty of the measurement of small liquid volumes and dewpoints. Therefore it is not possible to achieve 100 % mass balance during CVD studies, although molar balances can approach this value.

4. There are significant uncertainties in the chemical analysis of reservoir fluids. Analytically undetectable variations in the amount and properties of the heavy end

(heptanes-plus) fraction are known to have large effect upon the observed and predicted phase behavior.

5. If, during a PVT study, correlations are used to estimate the physical properties of the gas condensate system, then this should be clearly stated along with the reported accuracies of the correlations.

2.11.2 - FLUID SAMPLING OF WET GAS WELLS

WELL CONDITIONING

Because the effluent from a wet gas reservoir does not change as the reservoir is depleted, a sample can be collected at any convenient time and no conditioning of the well is necessary.

The well effluent should be processed through a conventional separator because small amounts of liquid hydrocarbons condense from the wellstream at surface pressure and temperature.

Once the producing gas/liquid ratio is monitored for a period of time sufficient to properly define the true ratio, the separator gas and liquid samples are to be collected using considerations and procedures outlined for collecting such samples for black oil wells.

2.11.3 - FLUID SAMPLING OF DRY GAS WELLS

A sample can be taken at any convenient time. No conditioning of the well is necessary.

Samples of surface gas are collected and used in the laboratory to determine the various PVT properties.

2.12 ADDITIONAL EXAMPLES

EXAMPLE 2.1

(a) Determine the volume occupied by 1 lb-mole of a natural gas at standard conditions

(b) Determine the volume occupied by 1 gm-mole of a natural gas at standard conditions (25 °C and 1 atm.)

Solution

It is reasonable to treat any gas as ideal gas at standard pressure (low pressure) and temperature conditions

Therefore, the volume of one mole of gas is:

$V_M = RT/p$

(a): $V_M = (10.732)(459.7 + 60) / (14.65) = 380.7$ SCF/ lb-mole

1 SCF of any gas is equivalent to (1/380.7) lb-mole

(b) $V_M = (82.057)(273 + 25) / (1.0)$

$V_M = 24.453$ litters/ gm-mole or

$V_M = 24.453$ m^3/ kg-mole

1 Std. Cubic Meter of any gas is equivalent to (1/24.453) Kg-mole

For all practical purposes, SCF or SCM are units of amount of gas

EXAMPLE 2.2

Dry air is a mixture of nitrogen, oxygen, and small amount of other inert gases as given in Table below.

(a) Calculate its apparent molecular weight

Component	Composition, mole fraction
Nitrogen	0.78
Oxygen	0.21
Argon	0.01
Total:	1.00

(b) Calculate the specific gravity of pure methane

(c) Calculate the specific gravity of the gas mixture whose composition is given in the following Table.

(d) Calculate the density of this gas mixture at 1000 psia and 150 °F, treating it as (i) an ideal gas; (2) Real gas

Component	Mole fraction, y_i
Methane (C_1)	0.800
Ethane (C_2)	0.120
Propane (C_3)	0.060
n-Butane (C_4)	0.020

Solution

(a) Apparent molecular mass of air:

M_{air} = (0.78)(28.01) + (0.21)(32.00) + (0.01)(39.94)

= 28.97 lb/lb-mole or 28.97 kg/kg-mole

For all practical purposes, M_{air} = 29 is used for calculating specific gravity of gases

(b) Specific gravity of methane = $M_{methane}$ / M_{air} = 16.04 / 29 = 0.553

(C) Specific gravity of gas mixture:

Component	Mole fraction, y_i	Molecular wt., M_i	$y_i M_i$
Methane (C_1)	0.800	16.04	12.832
Ethane (C_2)	0.120	30.07	3.6084
Propane (C_3)	0.060	44.10	2.646
n-Butane (C_4)	0.020	58.12	1.1624
TOTAL:	1.000		$M_a = 20.249$

Apparent Molecular weight of the gas mixture is 20.249

Specific gravity of gas mixture $= M_a / M_{air}$ = 20.249 / 29 = 0.698

(d) Density of gas mixture, 1000 psia and 150 °F:

$$\rho_g = \frac{m}{V} = \frac{pM}{zRT}$$

(i) Since, we are treating this gas as an ideal gas, z = 1, and,

Gas density = (1000) (20.249) / (10.732) (459.7 + 150) = 3.095 Lbs. / ft^3 (Ideal)

(2) In order to correct the gas density for non-ideal behavior, a compressibility factor, z, is needed.

Comp.	Mole fraction, y_i	Critical Temp., (°R) T_{ci}	$y_i T_{ci}$	Critical Pres., (psia) p_{ci}	$y_i p_{ci}$
(C_1)	0.800	343.3	274.64	666.4	533.12
(C_2)	0.120	549.9	65.99	706.5	84.78
(C_3)	0.060	666.1	39.66	616	36.96
(n-C_4)	0.020	765.6	15.31	550.6	11.01
TOTAL:	1.000	T_{ci} =	395.6	p_{ci} =	665.87

T_{pc} = (459.7 + 150) / (395.6) = 1.54

p_{pc} = (1000) / (665.87) = 1.502

From the chart for compressibility factor, z = 0.89.

Gas density = (1000) (20.249) / [(0.89)(10.732) (609.7) = 3.477 LBS. / ft^3 (Real)

compared to 3.095 LBS. / ft^3 with the assumption of ideal gas.

The ideal gas assumption leads to an error of 11% !

EXAMPLE 2.3

Calculate the compressibility of methane at 1500 psia and 120 °F

1. Treating methane as an ideal gas
2. Accounting for non-ideal effects

Solution

Treating methane as an ideal gas, compressibility of methane at 1500 psia ,

$$c_g = \frac{1}{p}$$

c_g = 1/(1500) = 667 x 10^{-6} psi^{-1}

1. Accounting for non-ideal effects,

$$c_g = \frac{1}{p_{pc}}\left[\frac{1}{p_{pr}} - \frac{1}{z}\left(\frac{\partial z}{\partial p_{pr}}\right)\right]_{T_{pr}}$$

For methane, T_c = 343.3 °R and p_c = 666.4 psia

at 120 °F, T_r = (459.7+120)/343.3 = 1.688

at 1500 psia, p_r = (1500)/(666.4) = 2.251,

From compressibility factor chart (Fig. 2.3),

$z = 0.87$ and $\left(\frac{\partial z}{\partial p_{pr}}\right) = 0.0375$

$c_g = [1/(2.251) - (1/0.87)(0.0375)]/(666.4) = (0.401)/(666.4) = 602 \times 10^{-6}$ psi^{-1}

Assumption of ideal gas leads to an error of 11%.

EXAMPLE (2.4)

Given the composition of a gas mixture and the viscosity values of its component gases, determine the viscosity of the mixture at atmospheric pressure and 200 °F

Component	Mole fraction, y_i	Molecular Mass, M_i	μ_{gi} cp
Methane	0.9712	16.043	0.0130
Ethane	0.0242	30.07	0.0111
Propane	0.0031	44.097	0.0097
i-Butane	0.0005	58.123	0.0091
n-Butane	0.0002	58.123	0.0090
Hexane	0.0002	86.177	0.0076
Heptane +	0.0006	128	0.0071

Solution

Comp.	Mole fraction, y_i	M_i	$y_i \cdot M_i^{1/2}$	μ_{gi}(cp)	$\mu_{gi} y_i \cdot M_i^{1/2}$
Methane	0.9712	16.043	3.890	0.0130	5.057E-02
Ethane	0.0242	30.07	0.133	0.0111	1.473E-03
Propane	0.0031	44.097	0.021	0.0097	1.997E-04
i-Butane	0.0005	58.123	0.004	0.0091	3.469E-05
n-Butane	0.0002	58.123	0.002	0.0090	1.372E-05
Hexane	0.0002	86.177	0.002	0.0076	1.411E-05
Heptane $^+$	0.0006	128	0.007	0.0071	4.820E-05
Total:	1.000		Sum= 4.0573		Sum= 0.0524

μ_g = = (0.0524)/ (4.0573) = 0.0129 cp

EXAMPLE 2.5

a). Compute the pseudocritical properties (P_{pc} and T_{pc}) and the gravity of a sour natural gas of known composition:

Component	Mole Fraction, %
N_2	2.36
CO_2	1.64
H_2S	18.41
C_1	77.00
C_2	0.42
C_3	0.05
iC_4	0.03
nC_4	0.03
iC_5	0.01
nC_5	0.01
C_6	0.01
C_{7+}	0.03

b). Calculate the gas deviation factor Z for the following pressure data: 300, 600, 900, 1200, 1500, 1800, 2100, 2400, 2700, 3000, 3300, 3600, 4200, 4500, 4800, 5100 psia. - T=149^{0}F. Use Dranchuk et al., Gopal, Brill and Beggs, Standing - Katz, and Hall and Yarbourough correlations.

Solution

$P_{pc} = \sum y_i P_{ci} = 791.74$ psia

$T_{pc} = \sum y_i T_{ci} = 406.77\ ^0R$

$$\gamma_g = \frac{Mg}{Mair} = \frac{\sum y_i M_i}{Mair} = \frac{19.58301}{29} = 0.675$$

Because H_2S and CO_2 are present, the pseudocritical properties are adjusted by

$$T'_{pc} = T_{pc} - \varepsilon,$$

$$p'_{pc} = \frac{p_{pc}T'_{pc}}{T_{pc} + y_{H_2S}\left(1 - y_{H_2S}\right)\varepsilon}$$

where $\varepsilon = 120\left(A^{0.9} + A^{1.6}\right) + 15\left(B^{0.5} + B^{4}\right)$

$A = 0.0164+0.184=0.2005$

$B = 0.1841$

$$\varepsilon = 120\left(0.2005^{0.9} + 0.2005^{1.6}\right) + 15\left(0.1841^{0.5} + 0.1841^{4}\right) = 25.5$$

$$T'_{pc} = T_{pc} - \varepsilon = 406.77 - 25.5 = 381.27\ {}^{0}R,$$

$$p'_{pc} = \frac{(791.74)(381.27)}{406.77 + 0.1841(1 - 0.1841)25.5} = 735.18 \text{ psia}$$

For these values of pseudocritical parameters,

$\gamma_g = 0.554$

b). $T = 149\ {}^{0}F = 459.7+149=608.7\ {}^{0}R$

$P_{pc}=735.18$ psia,

$P_{pr}=P/P_{pc}=P/735.18$

$T_{pr}=T/T_{pc}=608.7/381.27=1.5965$

Table E 2.5.2 shows the values of the gas deviation factor calculated by using different correlations, and Fig. E 2.5.1 is a plot of Z vs P.

EXAMPLE 2.6

Given the following analysis of a natural gas:

Component	Mole %
C_1	83.19
C_2	8.48
C_3	4.37
iC_4	0.76
nC_4	1.68
iC_5	0.57
nC_5	0.32
C_6	0.63

Compute:

(a) Gas gravity

(b) Pseudo-critical pressure and temperature

(c) What is the ratio of actual volume to ideal volume for this gas at 4000 psig and 200 ^{0}F?

(d) What volume will 100 lb of this gas occupy at the conditions in (c)?

(e) What is the gas density at the same conditions?

Solution

As shown in Table E 2.6.1,

$$M = \sum y_i M_i = 20.42 \text{ lb / lbmole}$$

a) $$\gamma_g = \frac{M}{M_{air}} = \frac{\sum y_i M_i}{M_{air}} = \frac{20.42}{29} = 0.704$$

b) $$P_{pc} = \sum y_i P_{ci} = 663.05 \text{ psia}$$

$$T_{pc} = \sum y_i T_{ci} = 393.56 \ ^0R$$

c) $P_{pr} = \frac{P}{P_{pc}} = \frac{4015}{663.05} = 6.055$

$T_{pr} = \frac{T}{T_{pc}} = \frac{660}{393.56} = 1.677$

Therefore, from Fig. 2.3, z=0.91

d) PV = znRT = z m/M RT

$V = \frac{zmRT}{pM} = \frac{0.91(100)(10.73)(660)}{(20.42)(4015)} = 7.86 \text{ ft}^3$

e) $\rho = \frac{pM}{zRT} = \frac{(20.42)(4015)}{0.91(10.73)(660)} = 12.7 \text{ lb / ft}^3$

EXAMPLE 2.7

Partial analysis from CO_2 gas reservoir indicates the following hydrocarbon composition:

C_1 - 10.8 % mole

C_2 - 6.7 % mole

C_3 - 4.3 % mole

The rest is believed to be CO_2 and H_2S.

Find:

(a) If the corrected pseudocritical temperature of the gas, T'_{pc}, is 522^{0}R, what are the percentages of CO_2 and H_2S in the mixture?

(b) Calculate the volume of 1 MSCF of gas at reservoir conditions of 1938 psig and 48^{0}C.

Solution

a) Percentages of CO_2 and H_2S.

$$P_{pc} = \sum y_i P_{ci} = 146.6 + 1071x_c + 1306x_H \text{ psia} \quad (1)$$

$$T_{pc} = \sum y_i T_{ci} = 102.7 + 548x_c + 672x_H \ ^0R \quad (2)$$

From

$$1 = \sum y_i = 0.108 + 0.067 + 0.043 + x_c + x_H = 0.218 + x_c + x_H,$$

we have

$$x_c = 0.782 - x_H \quad (3)$$

and the pseudocritical temperature is:

$$T_{pc} = T'_{pc} + \varepsilon = 522 + \varepsilon \quad (4)$$

where $\varepsilon = 15.08 + 15(x_H^{0.5} - x_H^4)$ (5)

Combining Eqs. 2,4 and 5:

$$0 = x_H^4 - x_H^{0.5} + 8.32x_H - 0.433 \quad (6)$$

or

$$f(x) = 0 = x_H^4 - x_H^{0.5} + 8.32x_H - 0.433$$

Using Newton-Raphson technique,

$$x_H = 0.087 = 8.7\ \%$$

Substituting this value of x_H into Eq. 3,

$$x_c = 0.782 - 0.087 = 0.645 = 69.5\ \%.$$

Therefore, we have the percentages of CO_2 and H_2S contained in the gas mixture.

(b) The volume of 1 MSCF of gas at reservoir conditions of 1938 psig and 48^{0}C.

If write the real gas law at both standard and reservoir conditions,

$$\left(\frac{PV}{znRT}\right)_{St.cond.} = \left(\frac{PV}{znRT}\right)_{Res.cond.}$$

and

$$V_{St.cond} = \frac{P_{res}}{P_{Stand}} \frac{z_{stand}}{z_{res}} \frac{T_{stand}}{T_{res}} V_{res}$$

where Z_{res} is unknown.

In order to find Z_{res}, we need to compute the pseudocritical and pseudoreduced parameters.

$$p'_{pc} = \frac{p_{pc} T'_{pc}}{T_{pc} + y_{H_2S}\left(1 - y_{H_2S}\right)\varepsilon}$$

where

$$P_{pc} = \sum y_i P_{ci} = 1003.5 \text{ psia}$$

$$T_{pc} = T'_{pc} + \varepsilon = 522 + 19.58 = 541.5 \ ^0R$$

$$p'_{pc} = \frac{(1003.5)(522)}{541.5 + 0.695(1 - 0.695)19.58} = 964.6 \text{ psia}$$

$$p_{pr} = \frac{p}{P_{pc}} = \frac{1938}{964.6} = 2,$$

$$T_{pr} = \frac{T}{T_{pc}} = \frac{459.7 + 1.8 * 48 + 32}{522} = 1.108$$

From Fig. 2.3, Z = 0.388, and

$$V_{St.cond} = 1000SCF = \frac{1938}{14.7}\frac{1}{0.388}\frac{(459.7+60)}{459.7+118.4}V_{res} = (305.478)V_{res}$$

and

$V_{res} = 1000/305.478 = 3.273\ ft^3$

EXAMPLE 2.8

a) If Sabine Field gas gravity is 0.65 calculate the deviation factors from zero to 6000 psia at 160^{0}F, in 1000 psi increments, using the gas gravity correlation of Fig. 2.4.

b) Recalculate, then plot the deviation factors at the same pressures as in part (a), using the Standing-Katz correlation chart.

Component	Mole Fraction
C_1	0.875
C_2	0.083
C_3	0.021
iC_4	0.006
nC_4	0.008
iC_5	0.003
nC_5	0.002
C_6	0.001
C_{7+}	0.001*

* For C_{7+} use M, T_C and P_C of normal octane.

c) Below what pressure at 16^{0}F may be the ideal gas law to be used for the gas of the Sabine Gas Field, if errors are to be kept within 2%?

d) Will a reservoir contain more SCF of a real or an ideal gas at similar conditions? Explain.

e) Calculate the viscosity of this gas mixture, and plot versus pressure.

Solution.

$\gamma_g = 0.65$

$T = 160^0F = 460 + 160 = 620\ ^0R$

a) From Fig. 2.4,

$P_{pc} = 670$ psia

$T_{pc} = 374\ ^0R$

Table E 2.8.a shows the calculated values of P_{pr} and the corresponding $Z=f(T_{pr},P_{pr})$, obtained from Fig. 2.7.3, for any pressure P from 0 to 6000 psia.

b) Table E 2.8.b shows the calculated values of pseudocritical and pseudeoreduced pressures and temperatures:

$P_{pc} = 667$ psia,

$T_{pc} = 376\ ^0R$,

Because the calculated pseudocritical values are within 1 % of those read from Fig. 2.4, there is no need to redo the reading of Fig. 2.7.3. Fig. E.2.8. b is a plot of Z vs P.

c) The ideal gas law assumes no deviation of z from unity (z=1.0). Two different areas of 2% or better accuracy are apparent Fig. 2.7.3:

1) from $P_r = 0$ to $P_r = 0.3$, which corresponds to P from 0 to 180 psia, and

2) from $P_r = 7.45$ to $P_r = 8.2$, which corresponds to P from 4,970 to 5,470 psia.

d) Because n, the number of moles of the gas contained in a reservoir, can be defined as

$n = \frac{PV}{zRT}$, we can see that, for the same reservoir conditions (P,V,T), n will be:

d1) $n = n_{ideal}$, the number of moles of an ideal gas, for z=1

d2) $n > n_{ideal}$, for $z < 1$

d3) $n < n_{ideal}$, for $z > 1$

e) Table E 2.8.e shows the mole fractions, the molecular weights and the viscosities for all the components of the gas mixture.

The following equation allows calculation of the viscosity of a gas mixture at atmospheric pressure.

$$\mu_1 = \frac{\sum y_i \sqrt{m_i}\mu_i}{\sum y_i \sqrt{m_i}} = \frac{5.1527}{4.345} = 0.01186 \text{ cp},$$

From Fig. 2.17, we can obtain the viscosity, $\mu_{gs} = \mu_1 = 0.01195$ cp. The viscosity at a particular pressure different from the atmospheric pressure is given by the following equation:

$\mu = \mu_1 \frac{\mu}{\mu_1}$, where $\frac{\mu}{\mu_1}$ can be obtained from Fig. 2.18 as a function of pressure.

Table E 2.8 e.2 shows the values of $\frac{\mu}{\mu_1}$ and the corresponding μ for each pressure P from 0 to 6000 psia, in 1000 psi increments.

EXAMPLE 2.9

Given the analysis in the table below of a natural gas produced from an oil well,

1. Calculate the gas gravity and pseudo-critical T and P,
2. What volume will 100 lb of this gas occupy at P=3000 psig and T=170^{0}F ?
3. Calculate the gas density and specific volume at these conditions of P and T.
4. A 10 ft^3 cylindrical tank is filled with this gas at 2500 psig and 100^{0}F.
   a) How many moles of gas are in the tank?
   b) What standard volume (in SCF) of gas is in this?
   c) 750 scf of gas is released from the tank, this causes the temperature to fall to 60^{0}F. What is the final tank pressure?

Component	Mole Fraction, %
C_1	79.05
C_2	10.85
C_3	4.61
iC_4	1.28
nC_4	2.04
iC_5	0.21
nC_5	0.34
C_6	0.84
C_{7+}	0.78

$M_{C7+}=140$

$SG_{C7+}=0.85$

Solution:

Gas gravity.

Since one mole of any gas ocupies the same volume at standard conditions (379 ft^3),

$$\gamma_g = \frac{M}{M_{air}} = \frac{\sum y_i M_i}{M_{air}}$$

where

$M = \sum y_i M_i = 22.13$, from Table E 2.9 1, and

$M_{air}=29$

Therefore,

$$\gamma_g = \frac{M}{M_{air}} = \frac{22.13}{29} = 0.76$$

b) The pseudo-critical parameters are

$P_{pc} = \sum y_i P_{ci} = 664$ psia

$T_{pc} = \sum y_i T_{ci} = 409\ {}^0R$

as shown in Table E 2.9.1.

2. From the real gas law, we can determine the volume occupied by 100 lb of the gas at P=3000 psig, T=170^{0}F.

$$V = \frac{znRT}{p},$$

where:

$$n = \frac{100}{22.1} = 4.52 \text{ moles}$$

$T = 460 + 170 = 630\ {}^0R$

$p = 3000 + 14.7 \cong 3015$ psia

R = 10.7, and

Z can be determined:

a) from Fig. 2.3 as a function of pseudoreduced pressure and temperature:

$$p_{pr} = \frac{p}{P_{pc}} = \frac{3015}{664} = 4.54,$$

$$T_{pr} = \frac{T}{T_{pc}} = \frac{630}{409} = 1.54$$

we have z = 0.81.

b) From Fig. 2.7.4 and 2.7.5

γ_g	Z
0.70	0.84
0.80	0.79

Therefore Z for 0.76 gas gravity = 0.79+(4/10+0.05) = 0.81, which is the same as that in part a, and the volume will be:

$$V = \frac{(0.81)(4.52)(10.7)(630)}{3015} = 8.2 \text{ ft}^3$$

3. The gas density is

$$\rho = \frac{PM}{zRT} = \frac{(3000)(22.13)}{(0.81)(10.7)(630)} = 12.11 \text{ lb/ft}^3$$

The specific volume at these conditions is

$$V_s = \frac{1}{\rho} = \frac{1}{12.11} = 0.08 \text{ ft}^3/\text{lb}$$

4. a) The number of moles in the tank is

$$n = \frac{PV}{zRT}$$

where:

Z can be determined from Fig. 2.3 as a function of pseudoreduced pressure and temperature:

$$p_{pr} = \frac{p}{P_{pc}} = \frac{2515}{664} = 3.787,$$

$$T_{pr} = \frac{T}{T_{pc}} = \frac{560}{409} = 1.37$$

From this, z = 0.69, and then n can be calculated

$$n = \frac{PV}{zRT} = \frac{(2515)(10)}{(0.69)(10.7)(560)} = 6.07 \text{ moles}$$

b) Standard volume of gas (in SCF) in the tank.

$$V_{St.cond} = \frac{P_{res}}{P_{Stand}} \frac{z_{stand}}{z_{res}} \frac{T_{stand}}{T_{res}} V_{res}$$

$$V_{St.cond} = \frac{(2515)}{14.7} \frac{1}{0.69} \frac{520}{560} 10 = 2302 \text{ SCF}, \text{ or}$$

$$V_{St.cond} = (6.25)(379) = 2300 \text{ SCF}$$

c) The final tank pressure, at T=520 ^{0}R, after 750 SCF of gas is released from the tank,

$$P = \frac{zRT}{V}$$

where $n = 6.07 - \frac{750}{379} = 4.09$ moles remaining in the reservoir

$$P = \frac{zRT}{V} = z\frac{(4.09)(10.73)(520)}{10} = (2282) \cdot Z$$

Because Z = f(P), the equation requires a trial and error procedure in order to be solved for pressure P.

Assume:

(1) p = 1500 psia

Then

$$p_{pr} = \frac{p}{P_{pc}} = \frac{1500}{664} = 2.23,$$

$$T_{pr} = \frac{T}{T_{pc}} = \frac{520}{409} = 1.27,$$

$z = 0.63$, and

$p = 2282 \times 0.63 = 1437$ psia

(2) p=1450 psia

Then

$$p_{pr} = \frac{p}{P_{pc}} = \frac{1450}{664} = 2.18,$$

$$T_{pr} = \frac{T}{T_{pc}} = \frac{520}{409} = 1.27,$$

$z = 0.633$, and

$p = 2282 \times 0.633 \approx 1450$ psia (close enough)

EXAMPLE 2.10.

Given the following gas deviation factor curve, Fig. E 2.10.1, calculate the compressibility (c_g) at:

(a) P = 1000 psia

(b) P = 2400 psia

(c) P = 4000 psia

Solution

The compressibility of the gas can be calculating by using the following equation:

$$c_g = \frac{1}{P} - \frac{1}{z}\frac{dz}{dp}$$

Therefore, we have:

(a) At p=1000 psia, the slope dz/dp=(0.75-0.98)/(1850-0)=-12.4x10^{-5} psi^{-1}, z=0.855, and

$$c_g = \frac{1}{1000} - \frac{1}{0.855}(-12.4\text{x}10^{-5}) = 8.55\text{x}10^{-4}\ \text{psi}^{-1}$$

(b) At p=2400 psia, the slope dz/dp=0 psi^{-1}, z=0.765, and

$$c_g = \frac{1}{2400} = 4.17\text{x}10^{-4}\ \text{psi}^{-1}$$

(c) At p=4000 psia, the slope dz/dp=(0.95-0.77)/(5000-3000)=-9x10^{-5} psi^{-1}, z=0.765, and

$$c_g = \frac{1}{4000} - \frac{1}{0.855}(9\text{x}10^{-5}) = 14.5\text{x}10^{-5}\ \text{psi}^{-1}$$

EXAMPLE 2.11

Estimate the viscosity of a gas condensate fluid at 7000 psia and 220 ^{0} F.

It has a specific gravity of 0.90, and contains 2% nitrogen, 4% carbon dioxide and 6 % hydrogen sulfide.

Solution

$\gamma_g = 0.9$

P = 7000 psia

T = 220^{0}F = 680 ^{0} R

$y_{N_2} = 0.02$

$y_{CO_2} = 0.04$

$y_{H_2S} = 0.06$

The pseudo-critical parameters can be determined from Fig. 2.4.

$$P_{pc} = 649 - 5 + 19 + 39 = 702 \text{ psia}$$

$$T_{pc} = 428 - 5 - 4 + 8 = 427^0 R$$

Then, the pseudoreduced parameters can be calculated as follows

$$p_{pr} = \frac{p}{P_{pc}} = \frac{7000}{702} \cong 10,$$

$$T_{pr} = \frac{T}{T_{pc}} = \frac{680}{427} = 1.59,$$

and, from Fig. 2.17, we can obtain the viscosity $\mu_{gau} = 0.0119$, then

$$\mu_1 = 0.0119 + 0.0002 + 0.00025 + 0.0002 = 0.01255 \text{ cp}.$$

The viscosity at a particular pressure different from the atmospheric pressure is given by the following equation:

$\mu = \mu_1 \frac{\mu}{\mu_1}$, where $\frac{\mu}{\mu_1}$ can be obtained from Fig. 2.18 as a function of pressure.

For $\frac{\mu}{\mu_1} = 2.82$, the corresponding μ=(0.01255)(2.82)=0.0354 cp.

EXAMPLE 2.12.

At a pressure of 2,500 psia and reservoir temperature of 180^{0}F, the gas deviation factor for the sour natural gas is 0.850.

a. Calculate the formation volume factor and gas expansion factor.

b. How many standard cubic feet of this gas are contained in a reservoir with a gas pore volume of 1.0×10^9 ft^3?

Solution.

a. The gas formation volume factor:

$$B_g = 0.0283\frac{(0.850)(640)}{(2{,}500)} = 0.00616 \ ft^3 / scf$$

$$E = \frac{1}{B_g} = 162.39 \ scf / ft^3$$

$$\text{b. Gas in place} = \frac{1.0x10^9}{0.00616} = 162.39x10^9 \ scf$$

EXAMPLE 2.13

Calculate relative density(specific gravity) of the following natural gas. All compositions are in mole percent.

Component	Mole %, y_i	Mole fraction, y_i	Molecular Mass, M_i	y_iM_i
Methane	83.19	0.8319	16.04	13.344
Ethane	8.48	0.0848	30.07	2.55
Propane	4.37	0.0437	44.10	1.927
i-Butane	0.76	0.0076	58.12	0.442
n-Butane	1.58	0.0158	58.12	0.976
i-Pentane	0.57	0.0057	72.15	0.411
n-Pentane	0.32	0.0032	72.15	0.231
Hexanes	0.63	0.0063	86.18	0.543
Total	1.00			20.424

Solution

First calculate the apparent mole weight from information in the table above.

$\overline{M}_g = \Sigma M_i y_i = 20.424$

Then

$\gamma_g = \overline{M}_g / M_a = 20.424 / 28.966 = 0.705$

where M_a is the molecular weight of air = 28.966

EXAMPLE 2.14

Calculate actual density of the following natural gas at 1,525 psia and 75^{0}F.

Component	Mole %, y_i	T_c ^{0}R	P_c psia	M_i
Methane	83.19	343	668	16.04
Ethane	8.48	550	708	30.07
Propane	4.37	666	616	44.10
i-Butane	0.76	735	529	58.12
n-Butane	1.58	766	551	58.12
i-Pentane	0.57	829	490	72.15
n-Pentane	0.32	846	489	72.15
Hexanes	0.63	914	437	86.17
Total	1.00			20.424

Solution

$$\rho_g = \frac{p\overline{M}_g}{zRT}$$

p=1,525 psia,

$\overline{M}_g = 20.424$

R = 10.73 (psiaxft^3)/(^{0}Rxlbm mol)

$T = 75^0F + 460 = 535^0R$ and

z must be obtained from Fig. 2.3.

Calculate z from known composition or gas gravity in the table above. From the known gas composition we obtain:

$$T_{pc} = \sum y_i T_{ci} = 393.8\ ^0R$$

$$P_{pc} = \sum y_i P_{ci} = 662.6\ \text{psia}$$

$$T_{pr} = \frac{T}{T_{pc}} = \frac{535}{393.8} = 1.36$$

$$P_{pr} = \frac{P}{P_{pc}} = \frac{1{,}525}{662.6} = 2.3$$

Therefore, from Fig. 2.3, z=0.712

From gas gravity we obtain

$$\overline{M}g = \sum M_i y_i = 20.424$$

and

$$\gamma_g = \overline{M}_g / M_a = 20.424 / 28.966 = 0.705$$

From Fig. 2.8 we obtain

$$T_{pc} = 392\ ^0R$$

$$P_{pc} = 663\ \text{psia}$$

$$T_{pr} = \frac{T}{T_{pc}} = \frac{535}{392} = 1.36$$

$$P_{pr} = \frac{P}{P_{pc}} = \frac{1{,}525}{663} = 2.3$$

and z = 0.712

Conclusion. Composition and gas gravity methods yield results for this hydrocarbon gas at surface processing conditions. Then,

$$\rho_g = \frac{1{,}525 \text{x} 20.424}{0.172 \text{x} 10.73 \text{x} 535} = 7.62 \text{ lbm} / \text{ft}^3 = 0.122 \text{g} / \text{cm}^3$$

EXAMPLE 2.15

Calculate the z factor for the reservoir fluid in table below at of the following natural gas at 6,098 psia and 307^{0}F.

Component	Mole %, y_i	T_c ^{0}R	P_c psia	M_i
Nitrogen	0.1186	228	493	28.02
Methane	0.3836	343	668	16.04
Carbon Dioxide	0.0849	548	1071	44.01
Ethane	0.0629	550	708	30.07
Hydrogen Sulfide	0.2419	673	1306	34.08
Propane	0.0261	666	616	44.10
i-Butane	0.0123	735	529	58.12
n-Butane	0.0154	766	551	58.12
i-Pentane	0.0051	829	490	72.15
n-Pentane	0.0052	846	489	72.15
Hexanes	0.0067	914	437	86.17
Heptanes plus	0.0373	1,116	453	119.00
Total	1.000			20.424

For C_{7+} fraction:

$\gamma = 0.825(40\ ^\circ\text{API})$

$\overline{M}_g = 119$, and

z = 0.998

Solution

$T_{pc} = \sum y_i T_{ci} = 487\ ^0R$

$P_{pc} = \sum y_i P_{ci} = 822$ psia

$$T_{pr} = \frac{T}{T_{pc}} = \frac{767}{487} = 1.58$$

$$P_{pr} = \frac{P}{P_{pc}} = \frac{6,098}{824} = 7.42$$

z= 0.962 (-4% error)

From gas gravity we obtain

$\overline{M}_g = \sum M_i y_i = 31.87$

and

$\gamma_g = \overline{M}_g / M_a = 31.87 / 28.966 = 1.100$

$T_{pc} = 524\ ^0R$

$P_{pc} = 652$ psia

$$T_{pr} = \frac{T}{T_{pc}} = \frac{767}{524} = 1.464$$

$$P_{pr} = \frac{P}{P_{pc}} = \frac{6,098}{652} = 9.35$$

and z = 1.087 (9% error)

By including corrections to calculate criticals with Wichert and Aziz's chart we obtain

$\varepsilon = 31.2$ (Fig.2.5)

$T'_{pc} = 487\text{-}31 = 456\ ^oR$

$p'_{pc} = (822)(456)/[487+(0.2419)(1-0.2419)(31.2)]=762$ psia

$$T_{pr} = \frac{T}{T_{pc}} = \frac{767}{456} = 1.68$$

$$P_{pr} = \frac{P}{P_{pc}} = \frac{6,098}{762} = 8.00$$

and $z = 1.010$ (1% error)

EXAMPLE 2.16

A new discovery in the Lower Tuscalosa formation produces a gas consisting of 96% C_1 and 4% C_2. There is no liquid production at the surface. Reservoir conditions are 6,000 psia and 245 °F. Calculate the gas formation volume factor and the coefficient of isothermal compressibility.

Solution

The pseudocritical pressure and temperature of the mixture are

$T_{pc} = 0.96x\ 343 = 329.3$

$+0.04x550 = 22.0$

$= 351.3\ ^0R$

$p_{pc} = 0.96x668 = 641.3$

$+0.04x550 = 28.3$

$= 351.3\ ^0R$

The reduced quantities at reservoir (subscript rc) and surface (subscript sc) conditions are

$$\left(T_{pr}\right)_{rc} = \frac{245+459.6}{351.3} = 2.00$$

$$\left(T_{pr}\right)_{sc} = \frac{60+459.6}{351.3} = 1.48$$

$$\left(p_{pr}\right)_{rc} = \frac{6{,}000}{669.6} = 8.96$$

and

$$\left(p_{pr}\right)_{sc} = \frac{14.7}{669.6} = 0.022$$

From Fig. 2.3, z_{rc}=1.095, z_{sc}=0.998 (probably could have assumed 1.0), and

$$B_g = 0.005035\frac{T_{rc}z_{rc}}{p_{rc}z_{sc}} = \frac{(0.005035)(704.6)(1{,}095)}{(6{,}000)(0.998)} = 0.00065 \text{ RB/scf}$$

From Fig. 2.9, by using T_{pr}=2.00 and p_{pr}=8.96, we obtain:

c_{pr}= 0.074

c_{pr}= c_g x p_{pc},

and

$$c_g = \frac{c_{pr}}{p_{pc}} = \frac{0.074}{669.6} = 0.0001105\,\text{psi}^{-1}$$

By using a computer to calculate the numerical derivative of z with respect to pressure, we get c_g=107.4 x 10^{-6} psi-1, which indicates Trube's correlation to be in error by about 3%.

EXAMPLE 2.17

The vapor pressure of pure hexane as a function of temperature is 54.04 kPa at 50 ^{0}C and 88 188.76 kPa at 90^{0}C, using all the methods outlined in the text.

Solution

a) Calusius-Clapeyron

The Calusius -Clapeyron equation can be solved graphically by plotting log of vapor pressure vs. reciprocal absolute temperature and extrapolating.

It also can be solved by slopes.

T_1 = 50°C [581.67°R]

$1/T_1$ = 0.001719

T_2 = 90°C [617.67°R]

$1/T_2$ = 0.001619

p_v at T_1 = 54.04 kPa = 7.8374 psia,

$\log(p_v)$ = 0.89417

p_v at T_2 = 105.37 kPa = 15.2826 psia,

$\log(p_v)$ = 1.18420

$D\log(p_v)$ =-0.29003

$1/T_1 - 1/T_2$ = 0.0001

and

$$\text{slope} = \Delta\log(p_v)/\left(\frac{1}{T_1}-\frac{1}{T_2}\right) = \frac{-0.29003}{0.0001} = -2900.3$$

Solving for p_v = -2900.3(1/T) +b for b yields

b=5.87977,

T_3 = 100°C = 671.67 °R, and

$1/T_3$ = 0.001489

Solving for p_v at 100 °C:

$\log(p_v)$ = -2900.3(0.001489) +5.87977=1.56122,

and

p_v = 36.4102 psia [251.04 kPa].

However, if you know that the vapor pressure at 70 °c is 105.37 kPa, you can use the 70 to 90°C temperature differential to calculate the slopes and ultimately will calculate p_v = 35.81 psia = 246.7 kPa

b) Cox Chart

From Fig. 2.10 , the vapor pressure at 100°C can be approximated between 35 and 36 psia. A larger chart is required for more precise readings.

c) The Calingeart and Davis or Antoine Equation.

This can be used by obtaining the antoine constants from Reid et al. For n=hexane, with temperature in K, these constants are A=15.8366, B=2697.55, and C=-48.78.

Then,

$$\ln(p_v) = A - \frac{B}{T+C} = 15.8366 - \frac{2697.55}{373-48.78} = 3.60223$$

and

p_v = 36.68 psia [252.73kPa]

d) Lee-Kesler

The use of the Lee-Kesler equation requires p_c, T_c, and ω for n-hexane. These can be obtained from Table 2.8 (page II.A-38)

p_c = 436.9 psia [29.7 atm]

T_c = 453.7°F or 913.3 °R or 507.4 K, and

ω = 0.3007

For 100°C,

T_r=0.7351

$\ln(T_r)$ = -0.30775

$$f^0 = 5.92714 - (6.09648/0.7351) + 1.28862(0.30775) + 0.169347(0.7351)^6 = -1.94296$$

and

$$f^1 = 15.2518 - (15.6875/0.7351) + 13.4721(0.30775) + 0.43577(0.7351)^6 = -1.87402$$

$$\ln(p_{VR}) = f^0 T_r + \omega f^1 T_r = -1.94296 + 0.3007(-1.87402) = -2.50648,$$

$$p_{VR} = \frac{p_v}{p_c} = 0.0816$$

and

$p_v = 0.0816 \times 29.7 = 2.4235$ atm $= 35.62$ psia $= 245.59$ kPa

Experimental value: $p_v = 35.69$ psia $= 246.90$ kPa

Conclusions. Lee-Kesler gives the best answer, but the Clausius-Clapeyron method can be more accurate if the extrapolation is short.

EXAMPLE 2.18

Calculate the viscosity at 150°F and 2.012 psia for the gas of the composition shown in the following table

Component	Mole %, y_i	T_c ^{0}R	P_c psia	M_i
Nitrogen	0.158	228	493	28.02
Methane	0.739	343	668	16.04
Ethane	0.061	550	708	30.07
Propane	0.034	666	616	44.10
i-Butane	0.002	735	529	58.12
n-Butane	0.006	766	551	58.12
Total	1.000			20.424

Solution

a) Carr-Kobayashi-Burrows Method

$T_{pc} = \Sigma y_i T_{ci} = 350$ ^{0}R

$$P_{pc} = \Sigma y_i P_{ci} = 639 \text{ psia}$$

$$T_{pr} = \frac{T}{T_{pc}} = \frac{460+150}{350} = 1.74$$

$$P_{pr} = \frac{P}{P_{pc}} = \frac{2{,}012}{639} = 3.15$$

$$\overline{M}_g = \Sigma M_i y_i = 19.98$$

and

$$\gamma_g = \overline{M}_g / M_a = 19.98 / 28.966 = 0.690$$

Viscosity at 150°F, 1 atm (Fig. 2.11) = 0.0116 cp

Correction for N_2 (Fig. 2.11) = +0.0013 cp

Viscosity $\mu_1 = 0.0129$ cp

Viscosity ratio $\mu / \mu_1 = 0.0129$ cp (Fig. 2.15) = 1.32

Viscosity $\mu = 0.0170$ cp

b) Thodos Method

$$\nu_{pc} = \Sigma y_i \nu_{ci} = 104.5 \text{ cm}^3 / \text{gmol}$$

Viscosity parameter

$$\xi = \frac{\left(T_{pc}\right)^{1/6}}{\left(\overline{M}_g\right)^{1/2}\left(p_{pc}\right)^{2/3}} = \frac{(350/1.8)^{1/6}}{(19.98)^{1/2}(639/14.7)^{2/3}} = 0.0435$$

Pseudocritical density,

$$\rho_g = \frac{\overline{M}_g}{V_{pc}} = \frac{19.98}{104.5} = 0.1912 \text{ g/cm}^3$$

Viscosity factor, from Fig. 2.17a

$\mu^* \xi = 55 \times 10^{-5}$

$$\mu^* = \mu^* \xi / \xi = 55 \cdot 10^{-5} / 0.0435 = 0.0126 \text{ cp}$$

Density,

$z = 0.876$, from Fig. 2.3.

$$\rho_g = \frac{\overline{M}_g p}{zRT} = \frac{(19.98)(2{,}012)}{(0.876)(10.73)(610)} = 7.017 \text{ lbm/ft}^3 = 0.112 \text{ g/cm}^3, \text{ and}$$

$$\rho_{pr} = \frac{0.112}{0.1912} = 0.58$$

Viscosity factor, $\left(\mu - \mu^*\right)\xi = 18.9 \times {}^{10\text{-}}5$ (from Fig. 2.17b)

Viscosity

$$\mu = \mu^* + \left[\left(\mu - \mu^*\right)\xi\right] / \xi = 0.0126 + 18.9 \cdot 10^{-5} / 0.0435 = 0.0169 \text{ cp}$$

Results:

Carr et al. $\mu = 0.0170$ cp

Thodos et al. $\mu = 0.0169$ cp

Excellent results are obtained from either correlation for viscosity of a natural gas.

APPENDIX II.A

TABLES AND FIGURES

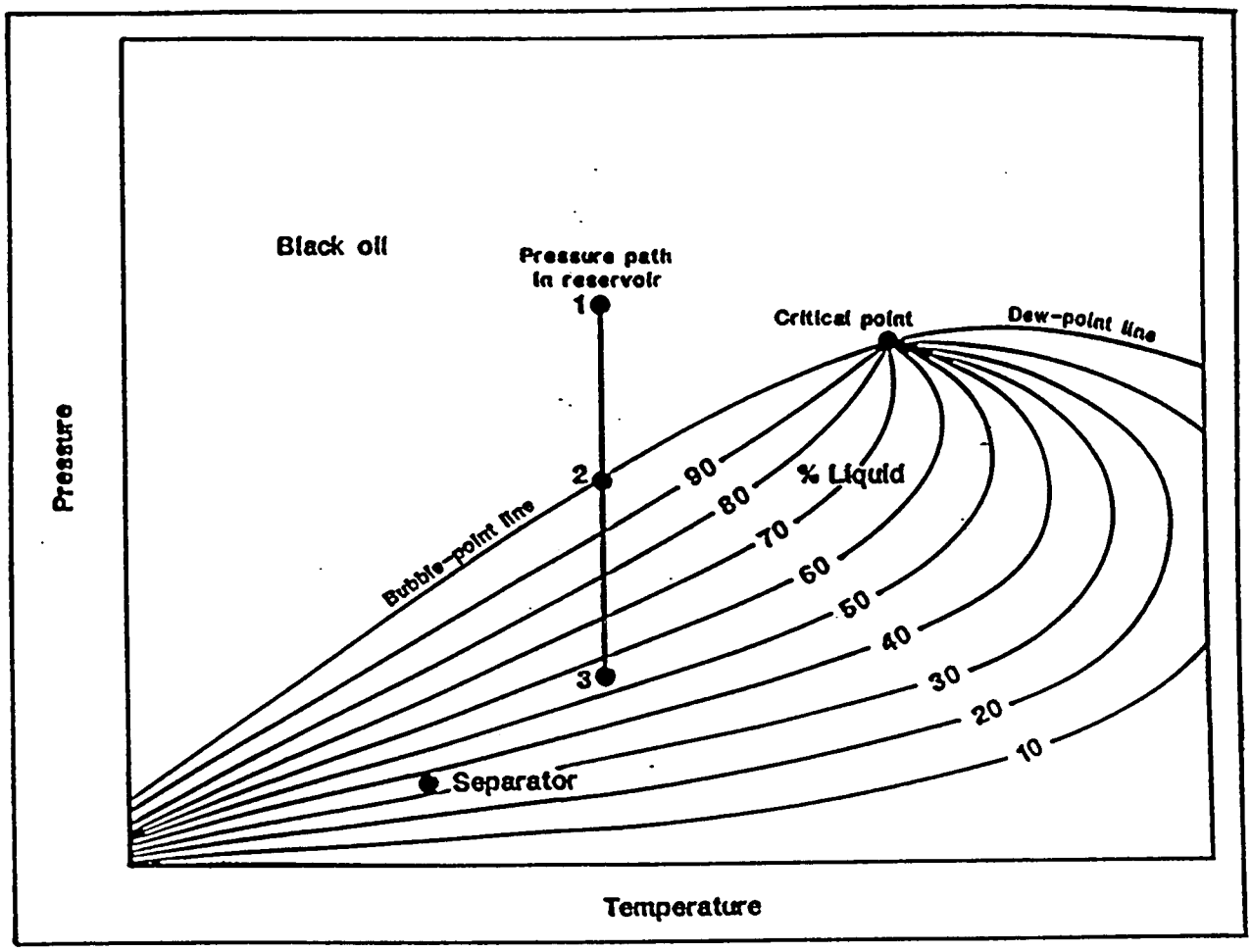

Fig. [illegible]. Phase diagram of a typical black oil with line of isothermal reduction of reservoir pressure, 123, and surface separator conditions.

Figure 2.1.1

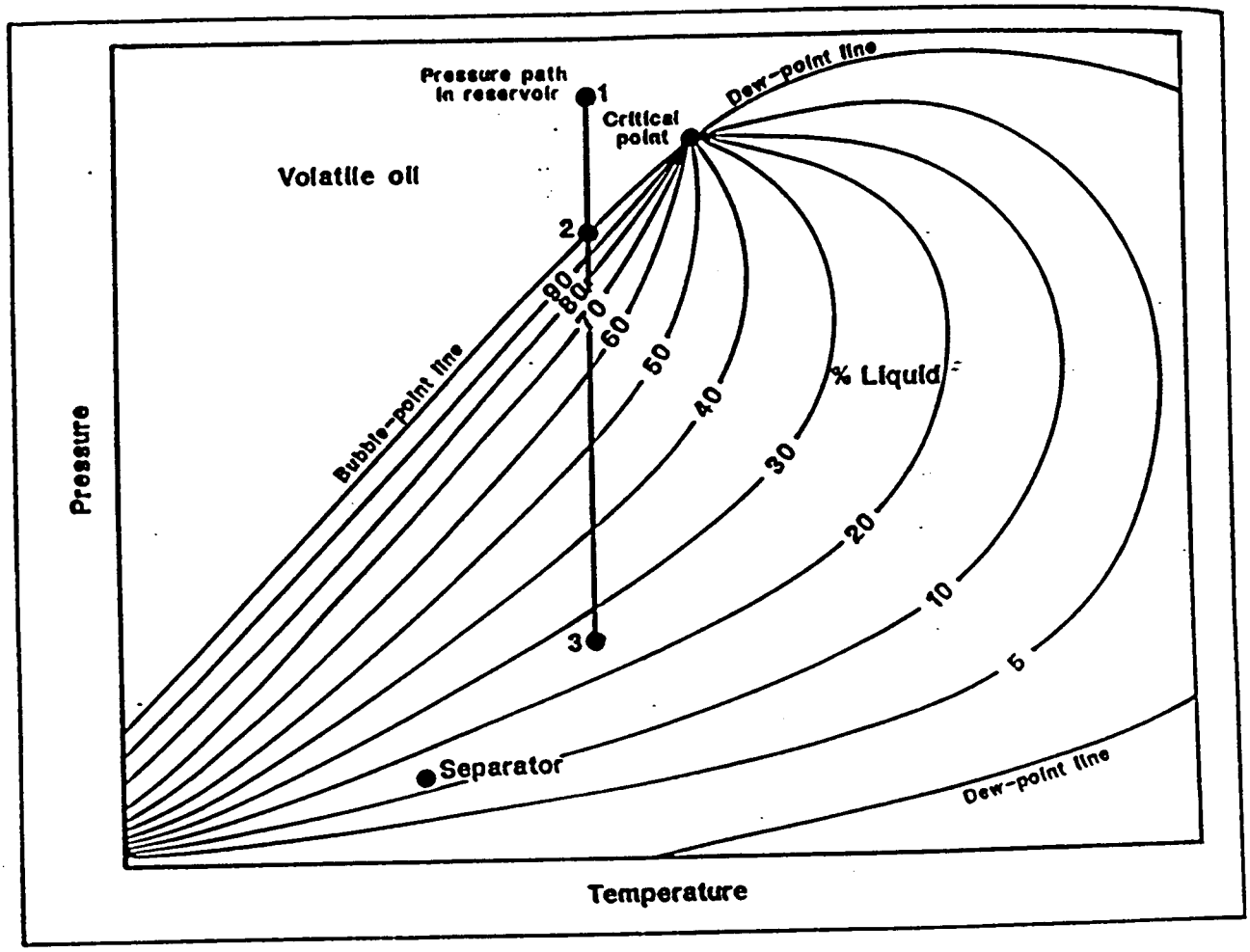

Fig. [illegible] Phase diagram of a typical volatile oil with line of isothermal reduction of reservoir pressure, 123, and surface separator conditions.

Figure 2.1.2

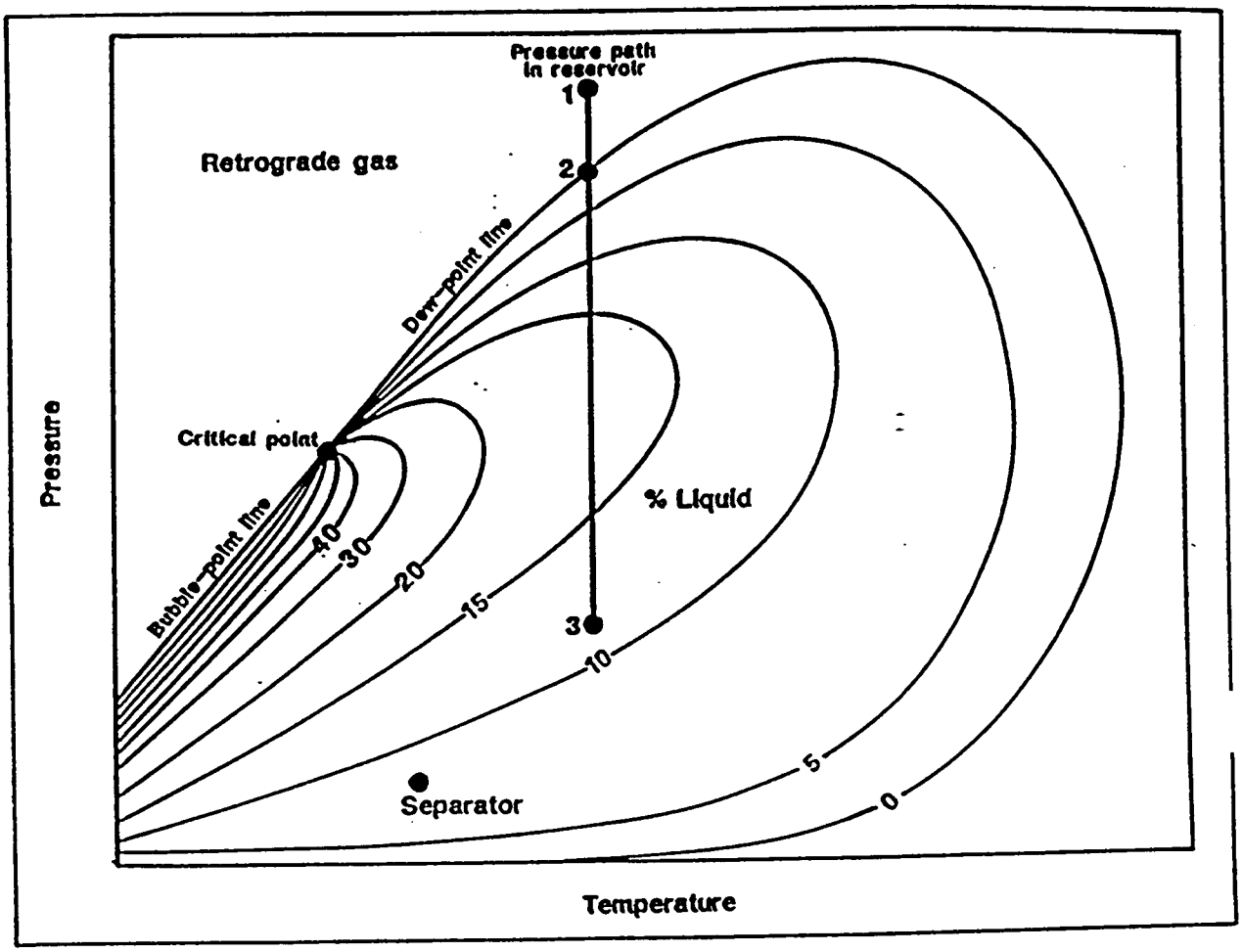

Fig. Phase diagram of a typical retrograde gas with line of isothermal reduction of reservoir pressure, 123, and surface separator conditions.

Figure 2.1.3

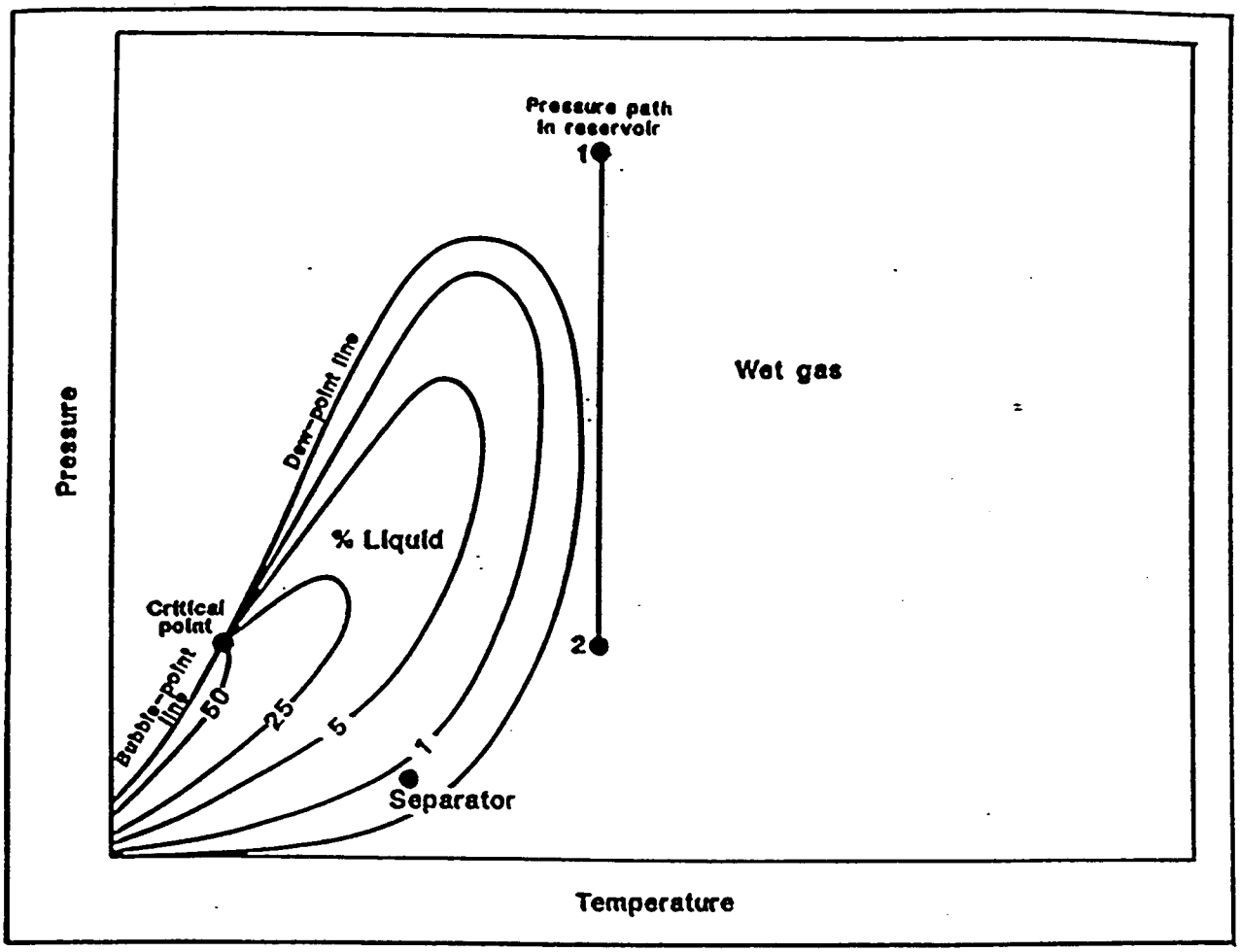

Fig. 12 Phase diagram of a typical wet gas with line of isothermal reduction of reservoir pressure, 12 , and surface separator conditions.

Figure 2.1.4

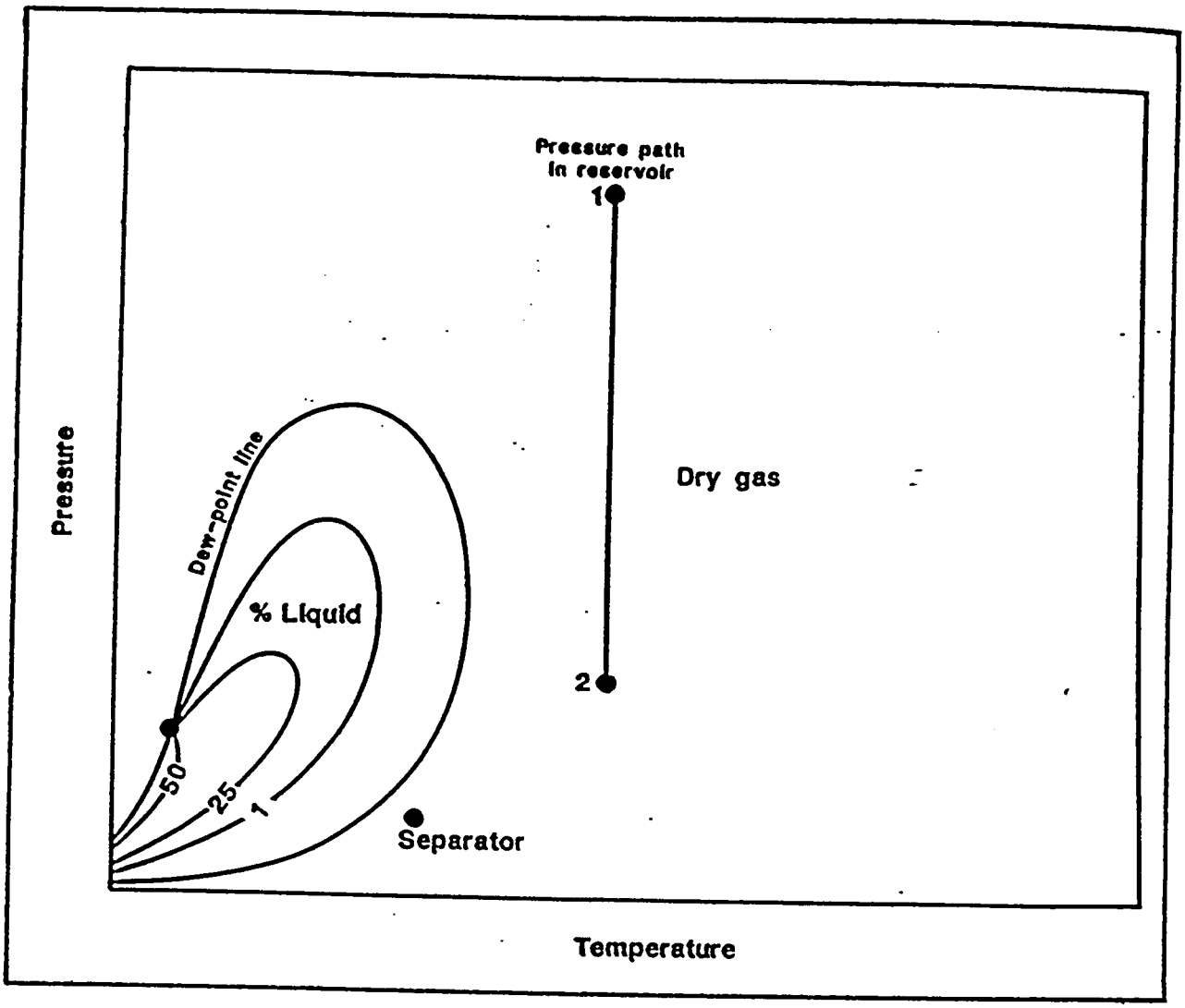

Fig. Phase diagram of a typical dry gas with line of isothermal reduction of reservoir pressure, 12 , and surface conditions.

Figure 2.1.5

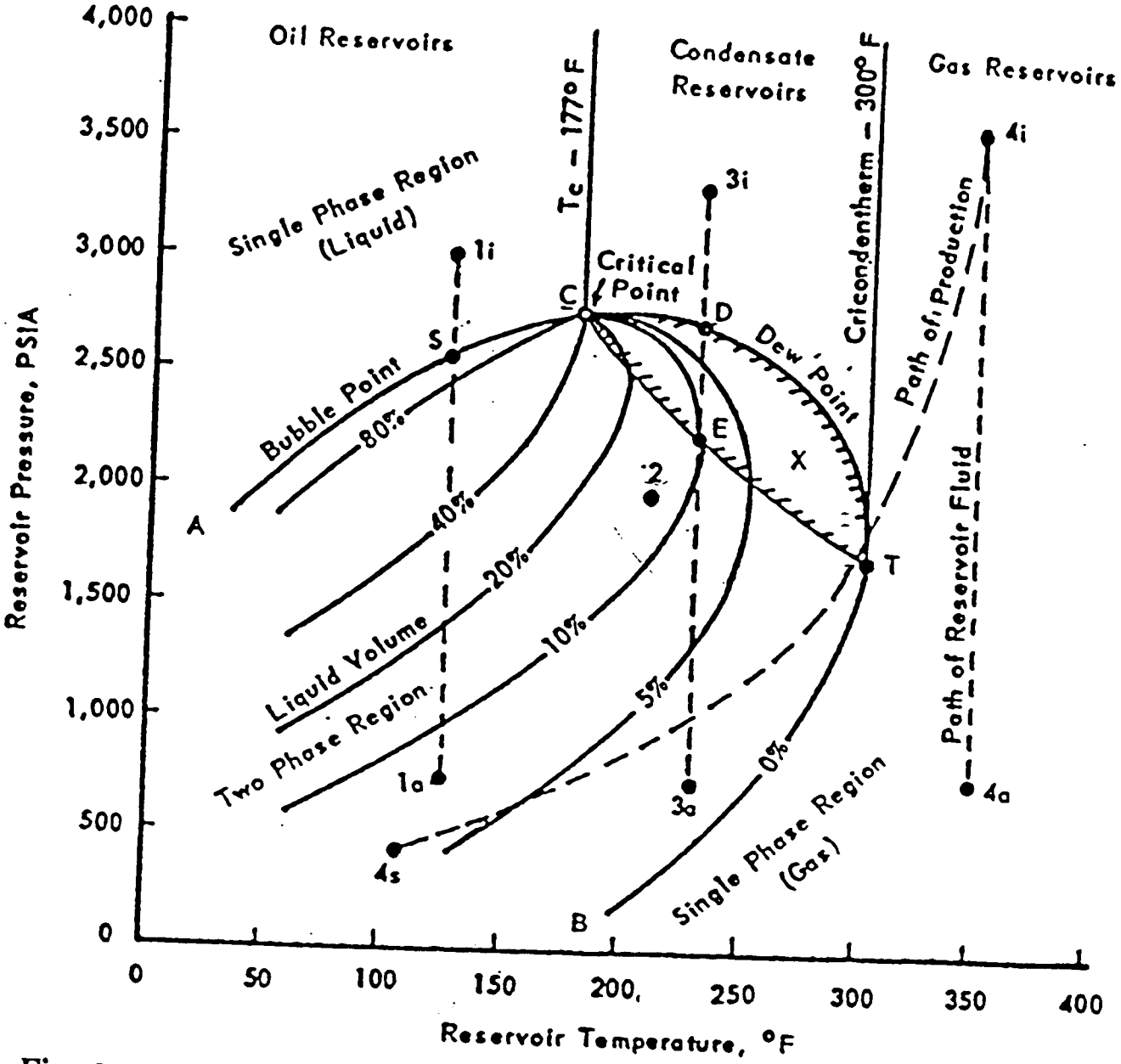

Fig. 2.2 Pressure-temperature phase diagram of a reservoir fluid

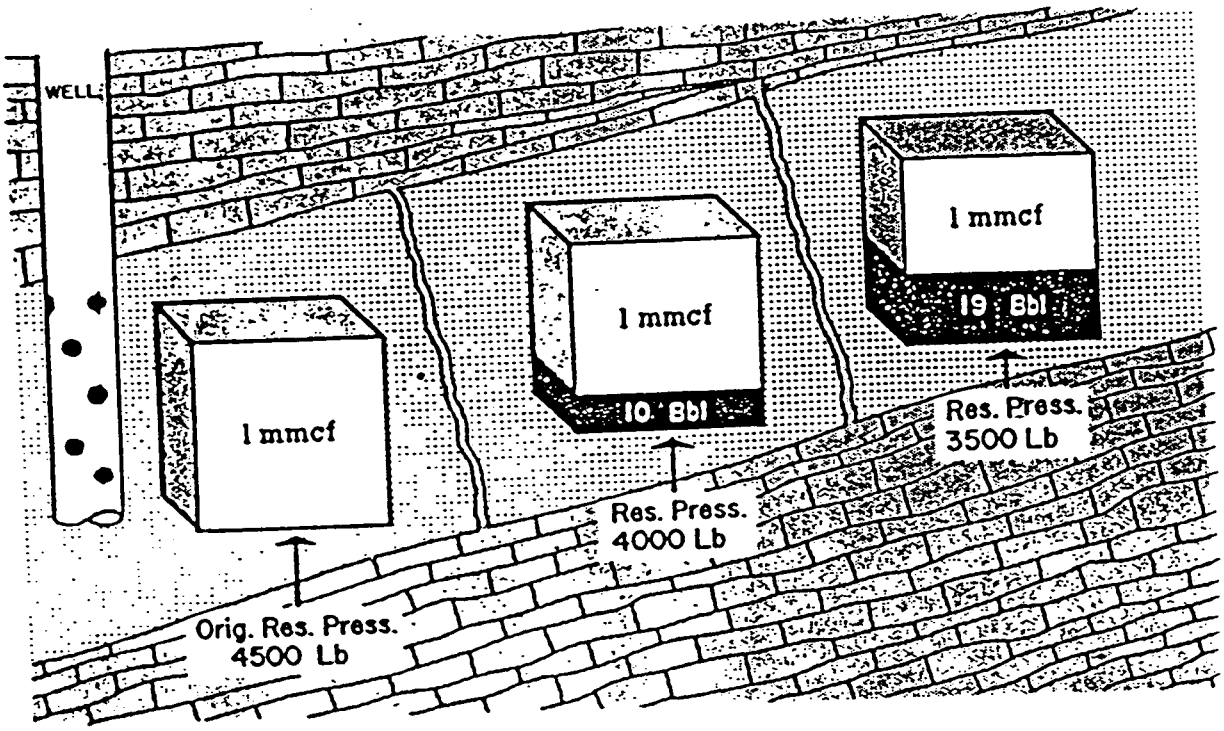

—Retrograde condensation of liquid from gas in a reservoir. (Courtesy WORLD OIL*—June, 1951.)*

Figure 2.2A

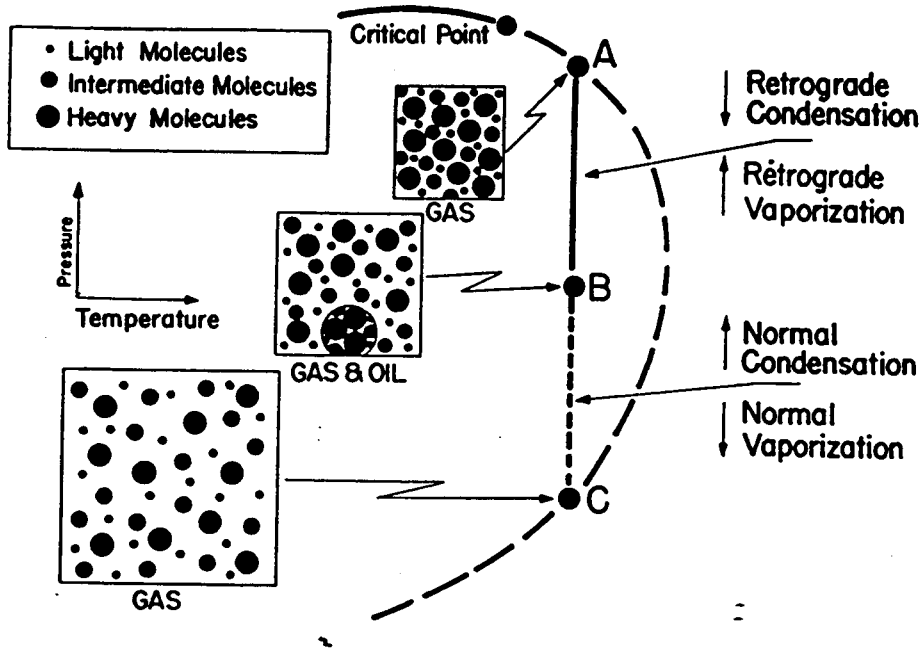

Figure 2.2B —*Equilibrium retrograde behavior of condensate gas.*

- As pressure drops (at constant temperature) below dew-point pressure (A), the attraction between light and heavy component molecules decreases because the light molecules move farther apart.

- As this occurs, attraction between the heavy component molecules becomes more effective; thus, these heavy molecules coalesce into a liquid.

- This process continues until a pressure (B) is reached where a maximum amount of liquid is formed.

- Further reduction in pressure permits the heavy molecules to commence normal vaporization-the process whereby fewer gas molecules strike the liquid surface; this causes more molecules to leave than to enter the liquid phase, until complete vaporization of the liquid again occurs(C).

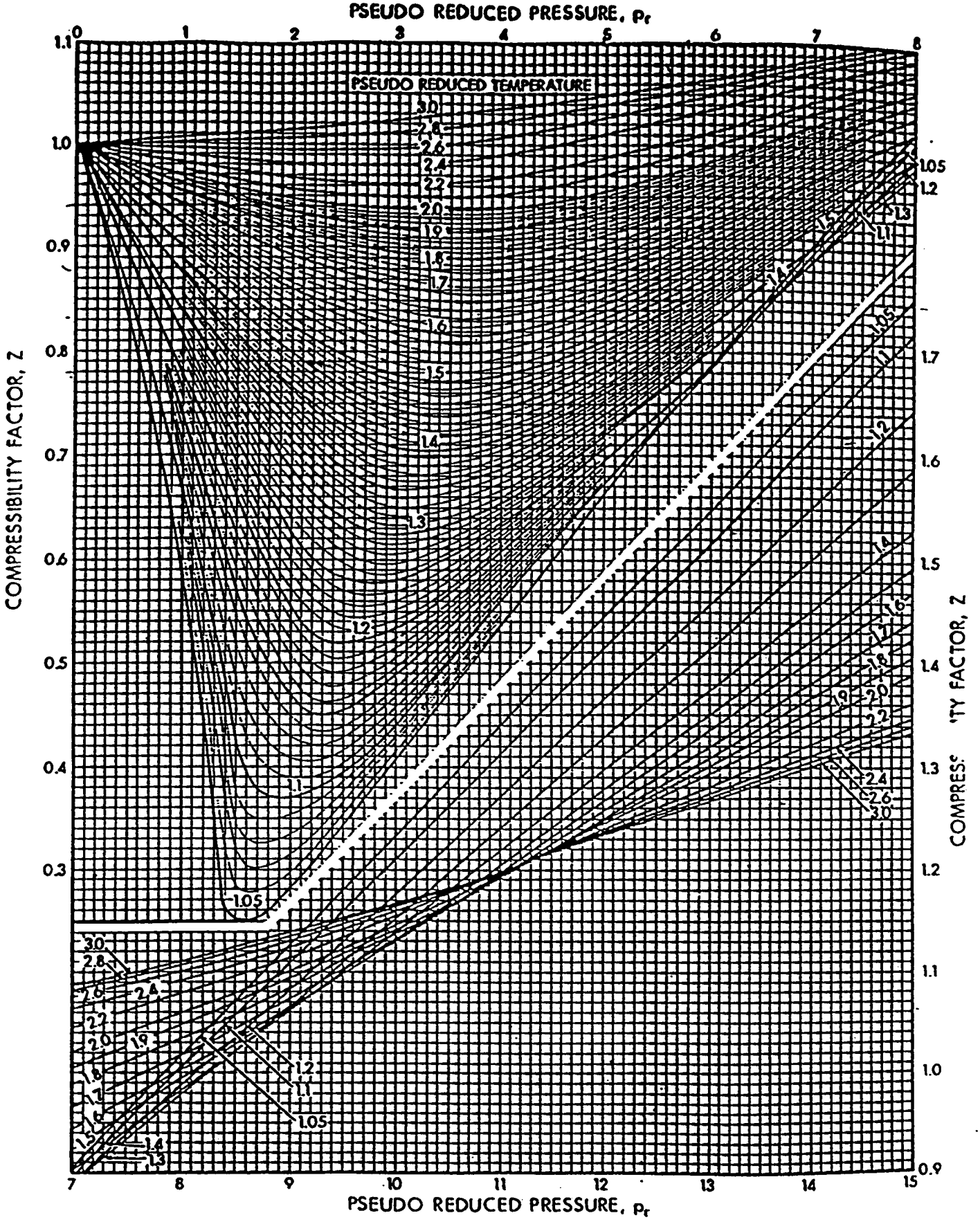
PSEUDO REDUCED PRESSURE, p_r
PSEUDO REDUCED TEMPERATURE
COMPRESSIBILITY FACTOR, Z
PSEUDO REDUCED PRESSURE, p_r

Fig. 2.3

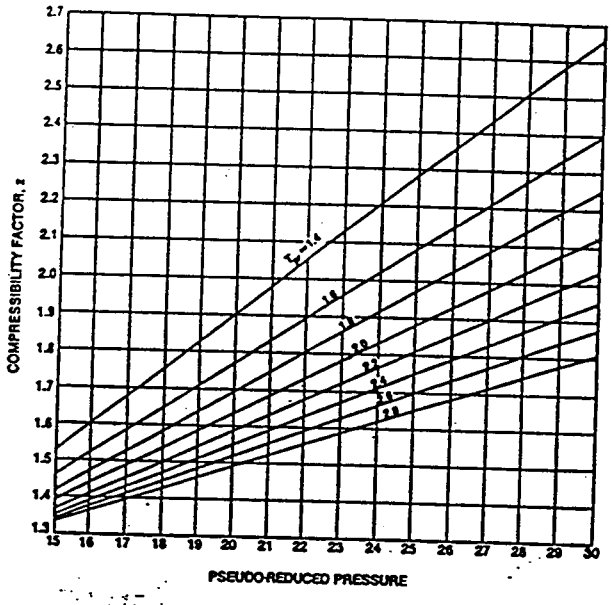

Fig. 2. 3.1 Compressibility factor for natural gases at pressures of 10,000 to 20,000 psia (from Ref. 2).

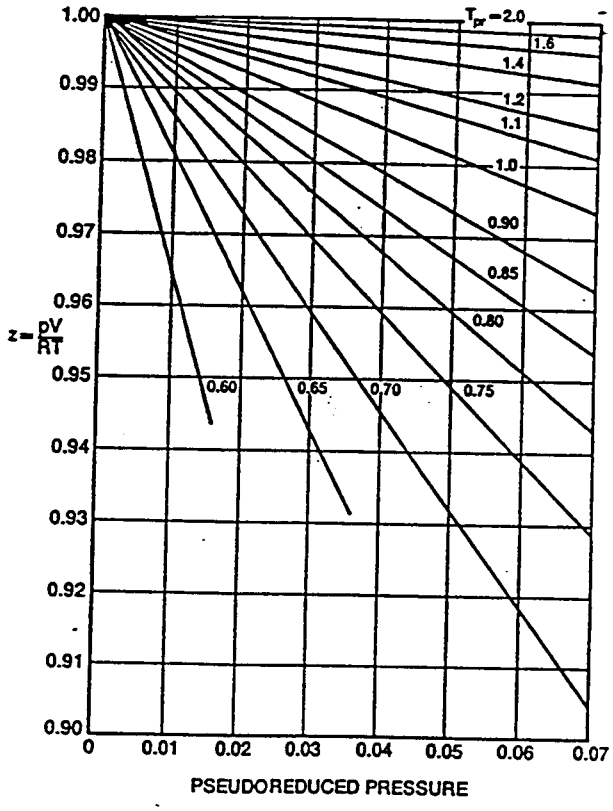

Fig. 2. 3.2 Compressibility factors for natural gases near atmospheric pressures.

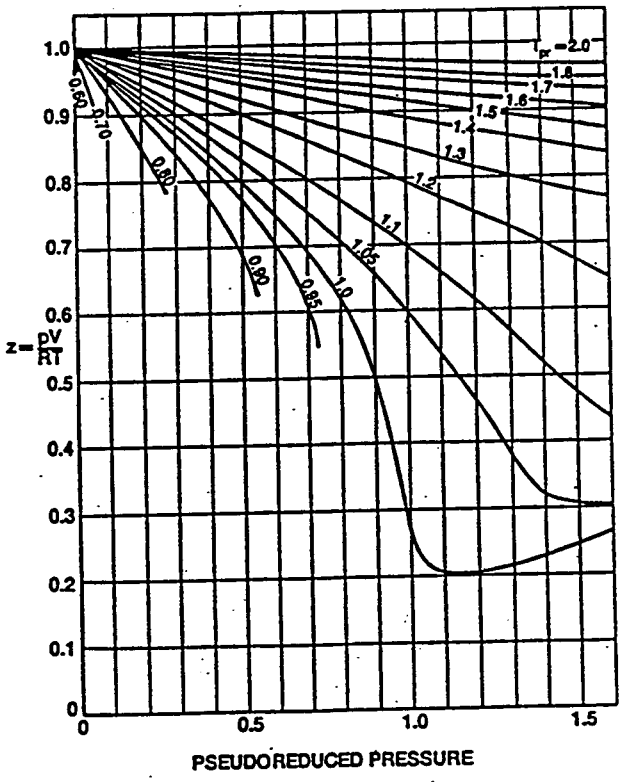

Fig. 2. 3.3 Compressibility factors for natural gases at low reduced pressures.

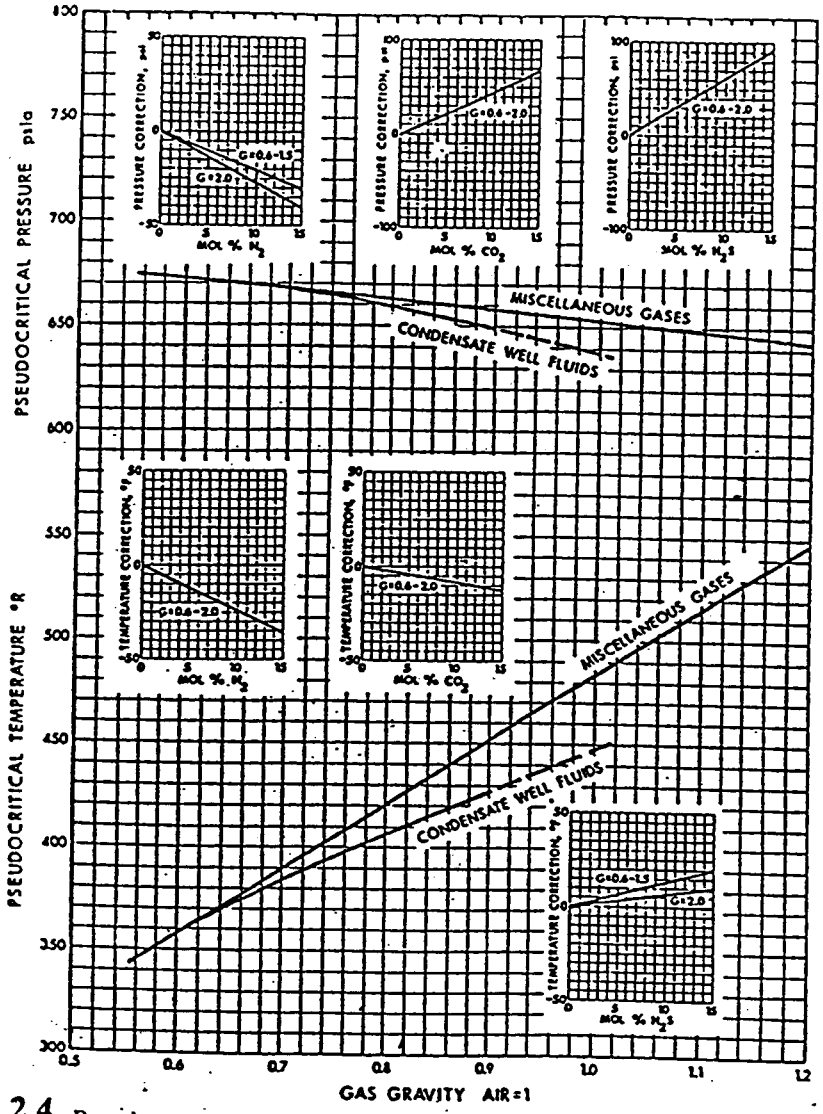

Fig. 2.4 Pseudo critical properties of miscellaneous natural gases (after Brown et al.)

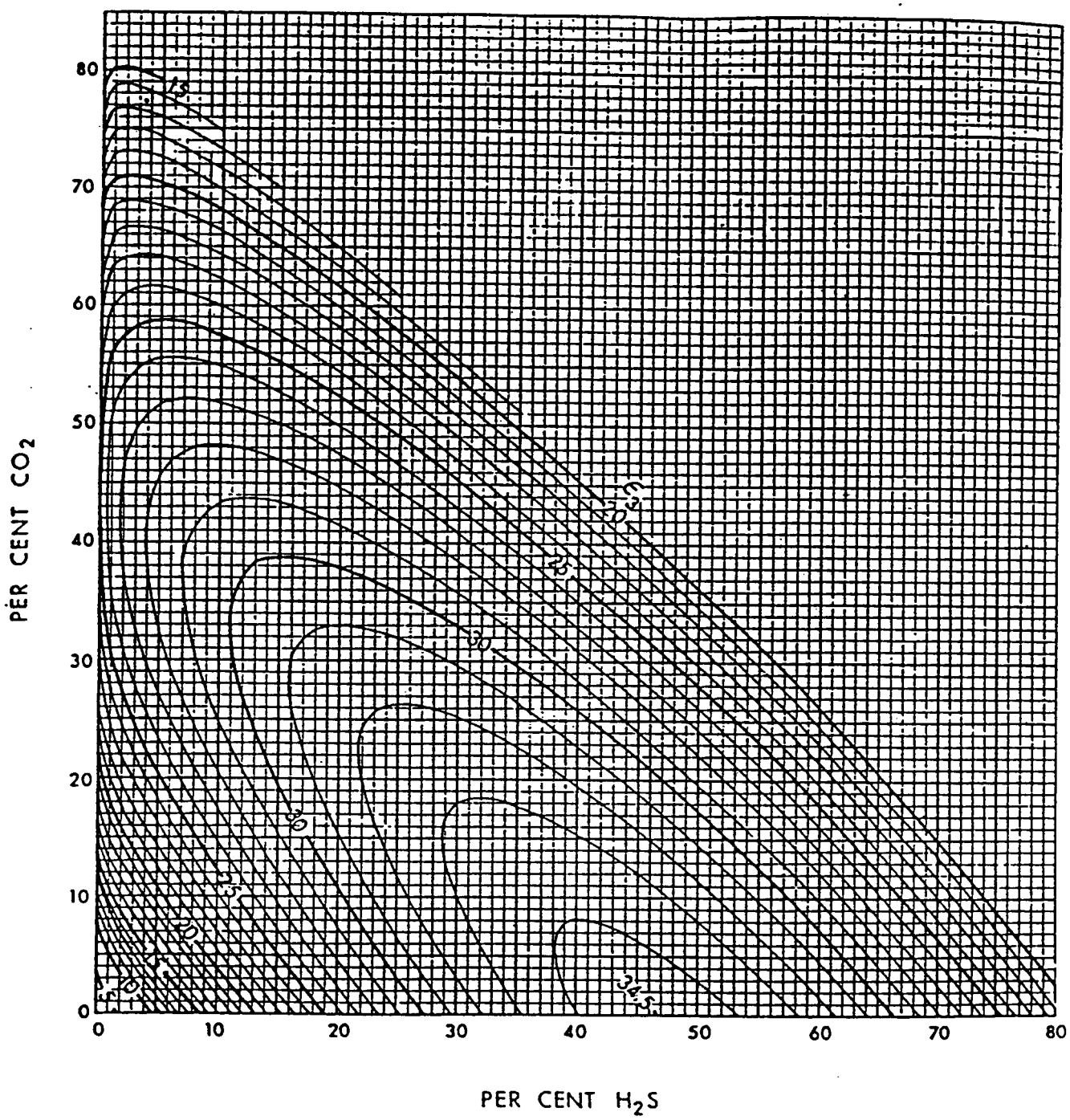
PER CENT CO_2
PER CENT H_2S
0
10
20
30
40
50
60
70
80
5
10
15
20
25
30
35
40
45

Figure 2.5

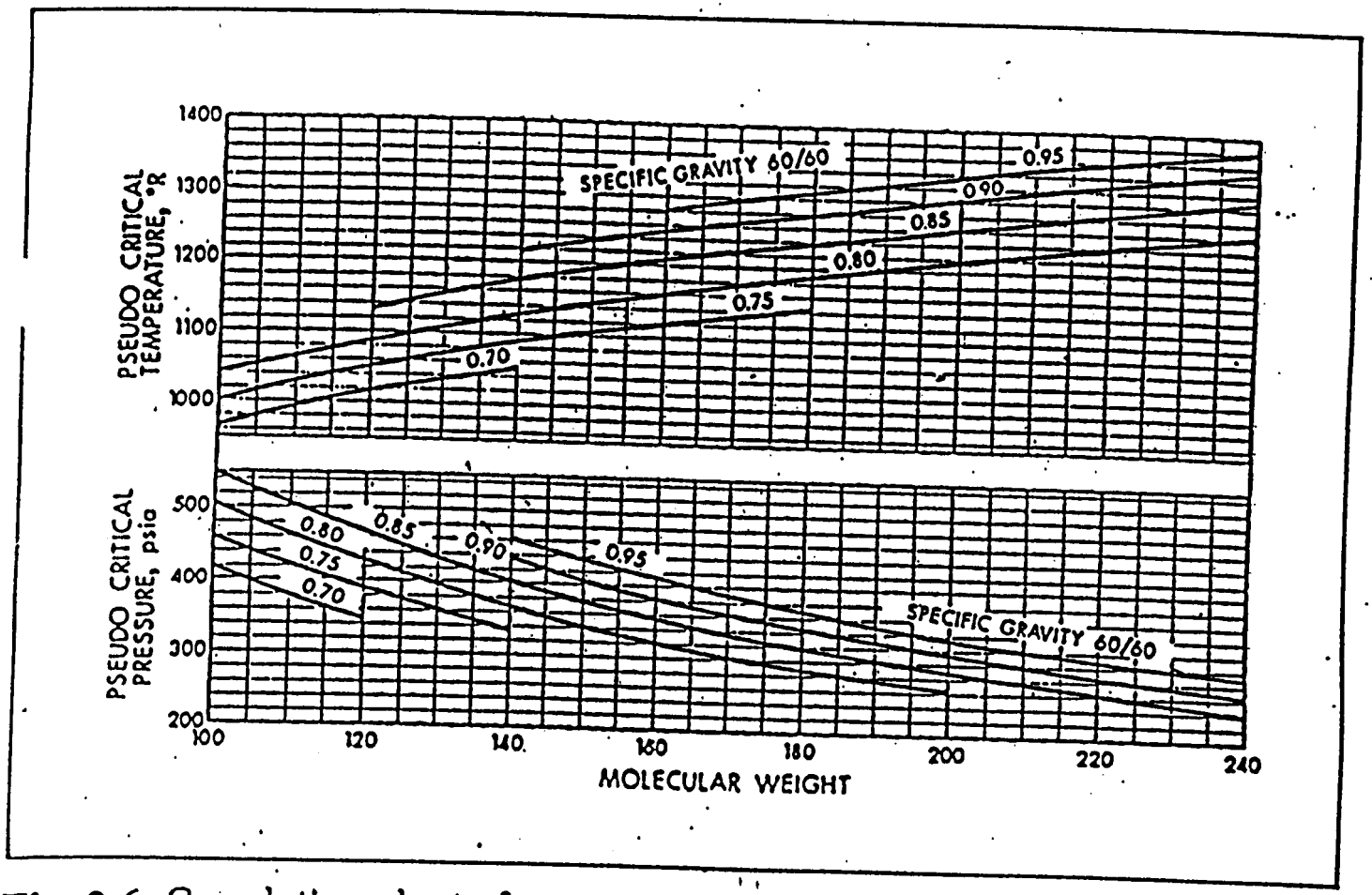

Fig. 2.6 Correlation charts for estimation of the pseudo critical temperature and pressure of heptanes plus fractions from molecular weight and specific gravity (courtesy Mathews, Roland, and Katz)

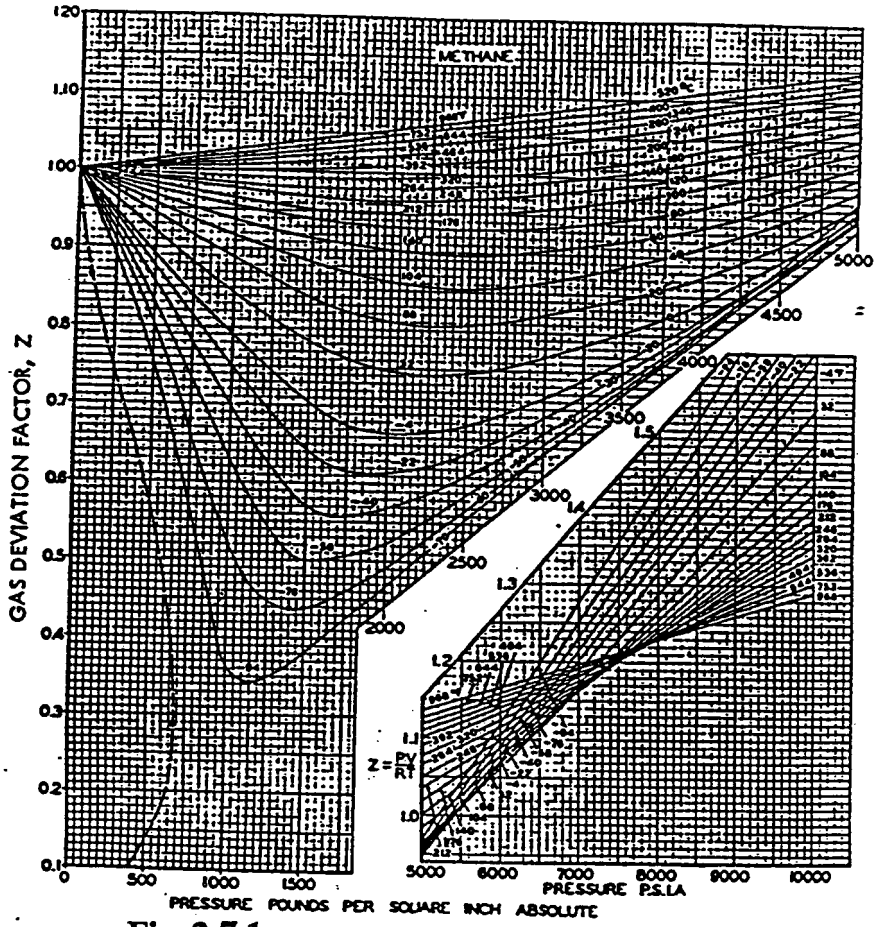

Fig. 2.7.1 Gas deviation factor for methane

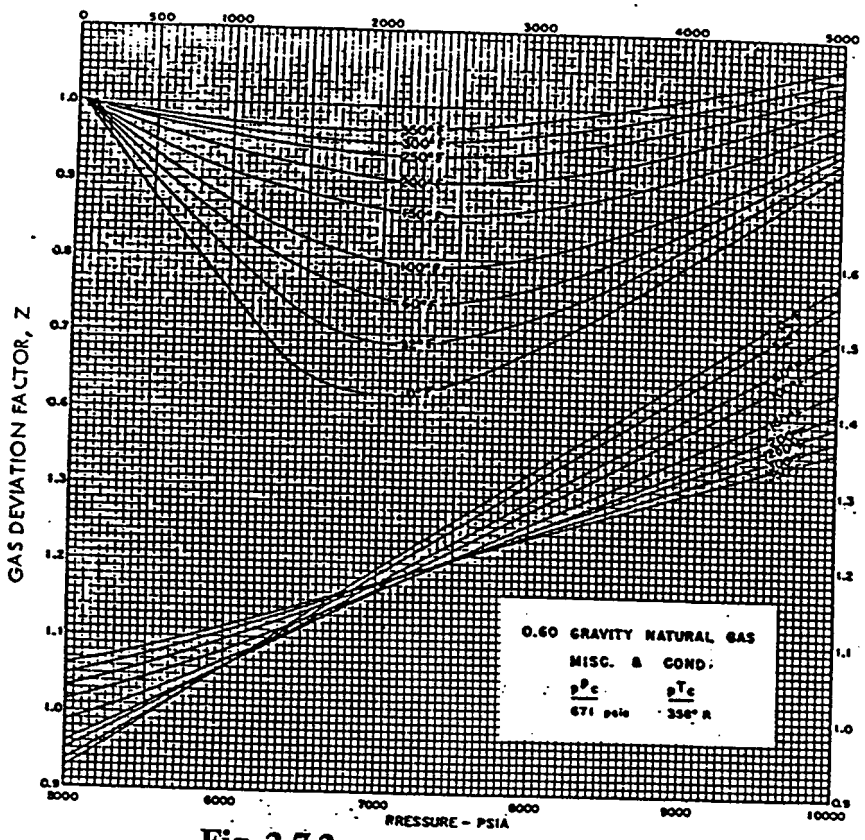

Fig. 2.7.2 0.60 gravity natural gas

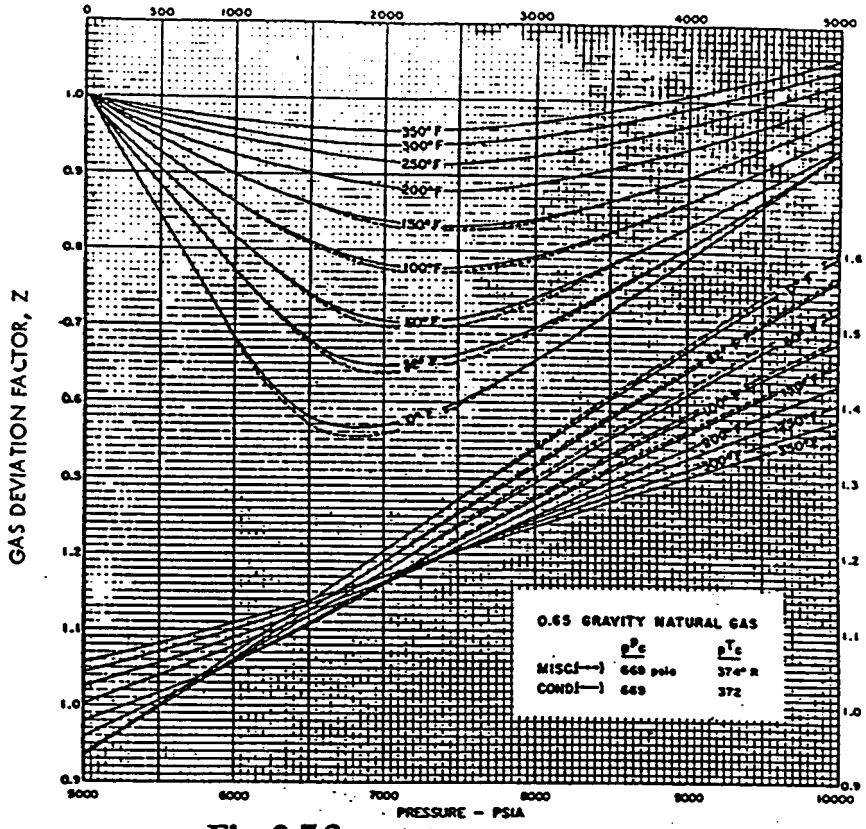

Fig. 2.7.3 0.65 gravity natural gas

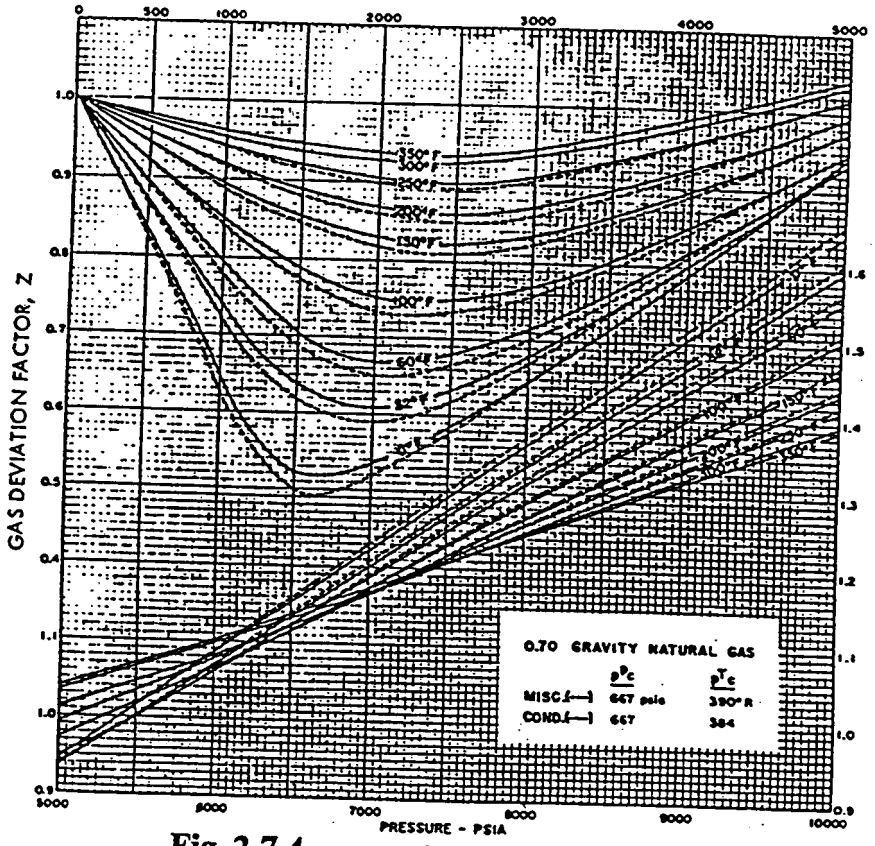

Fig. 2.7.4 0.70 gravity natural gas

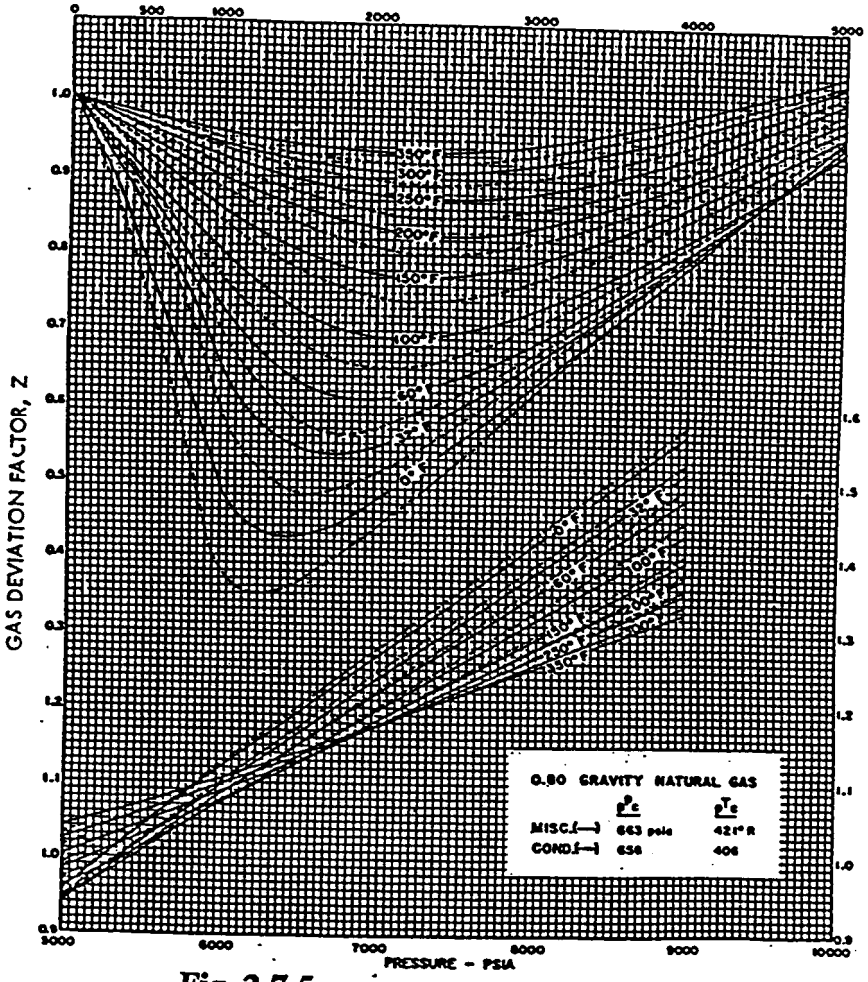

Fig. 2.7.5 0.80 gravity natural gas

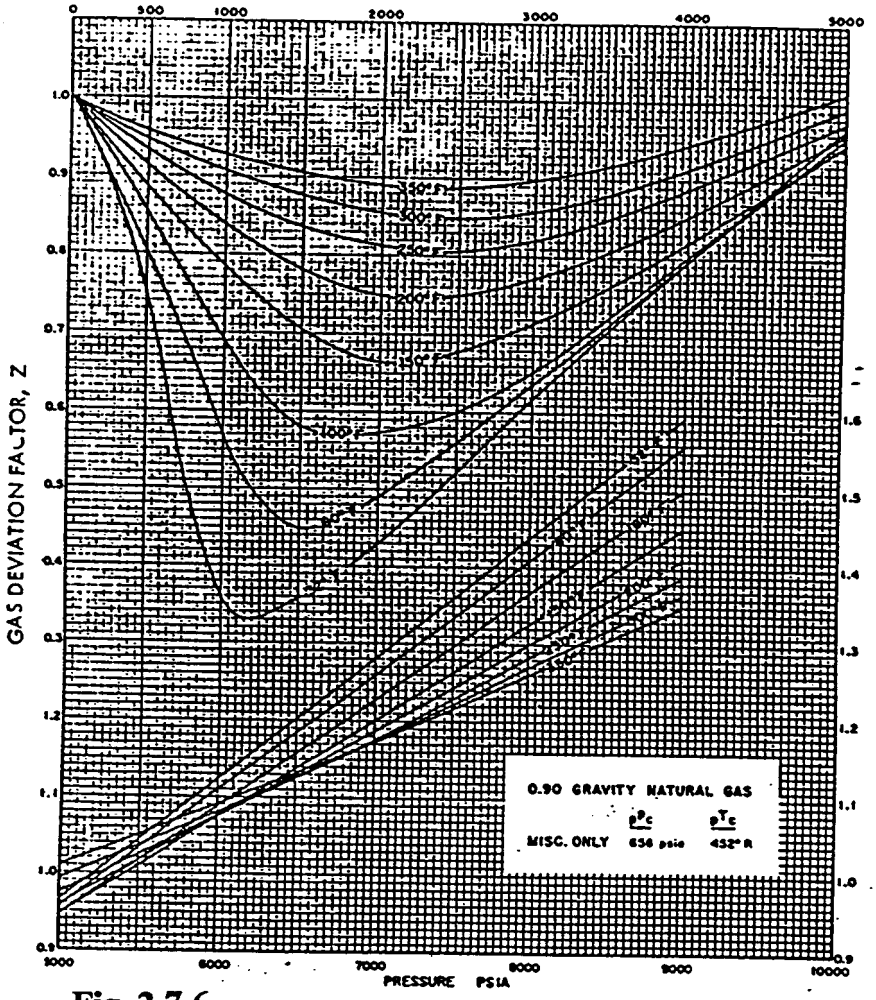

Fig. 2.7.6 0.90 gravity natural gas, miscellaneous only

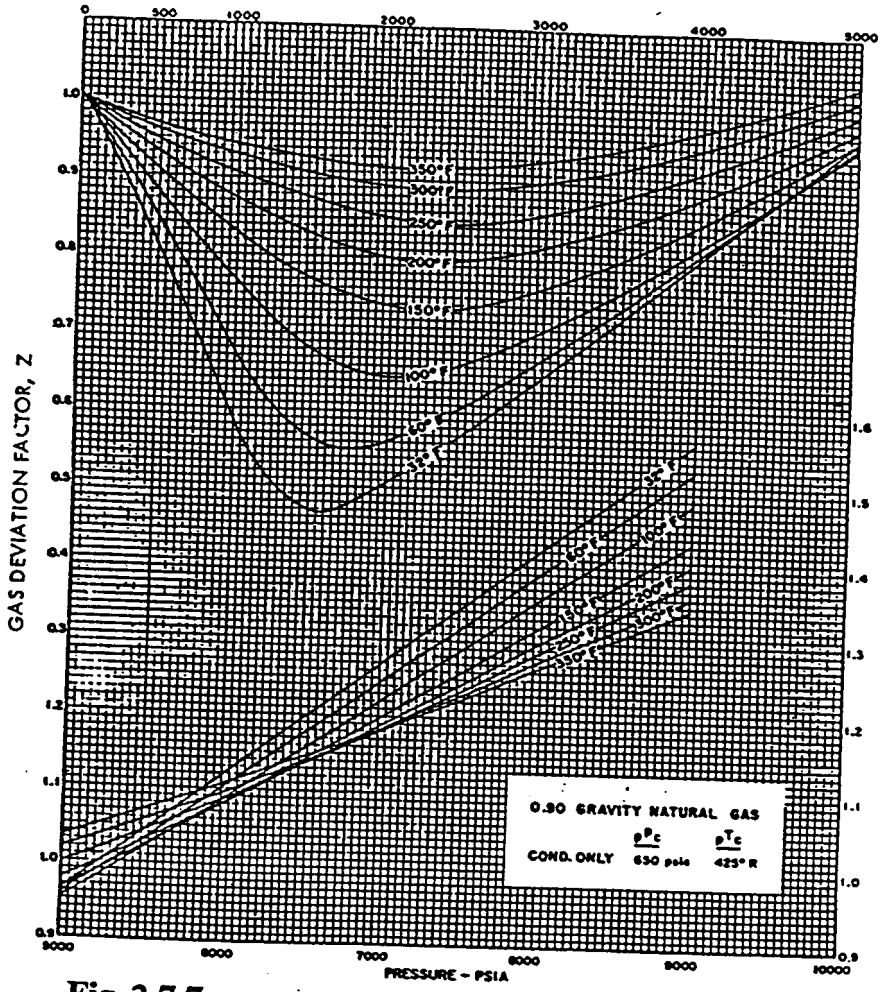

Fig. 2.7.7 0.90 gravity natural gas, condensate only

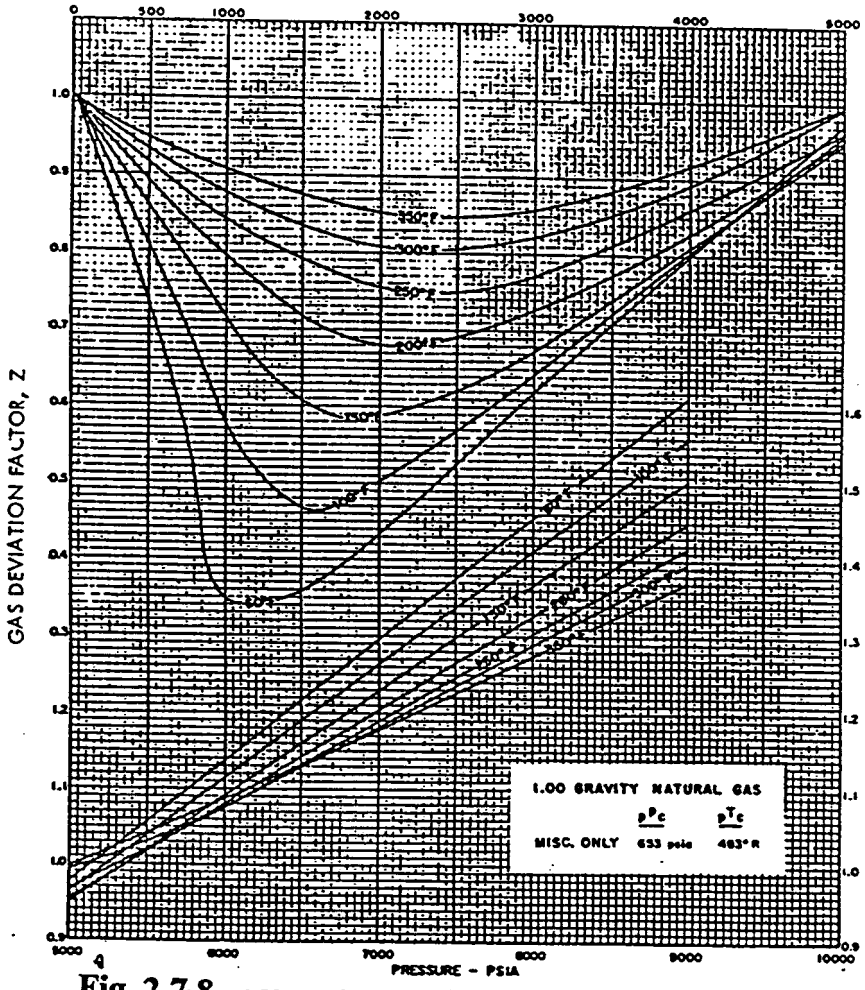

Fig. 2.7.8 1.00 gravity natural gas, miscellaneous only

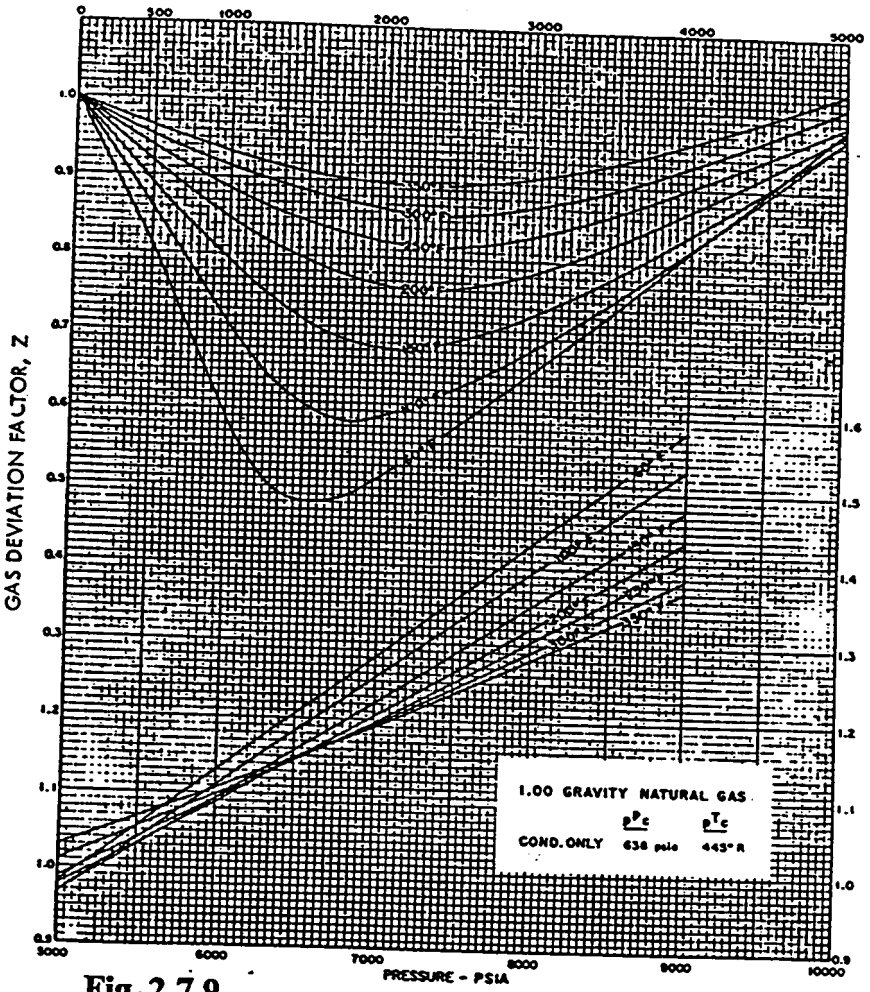

Fig. 2.7.9 1.00 gravity natural gas, condensate only

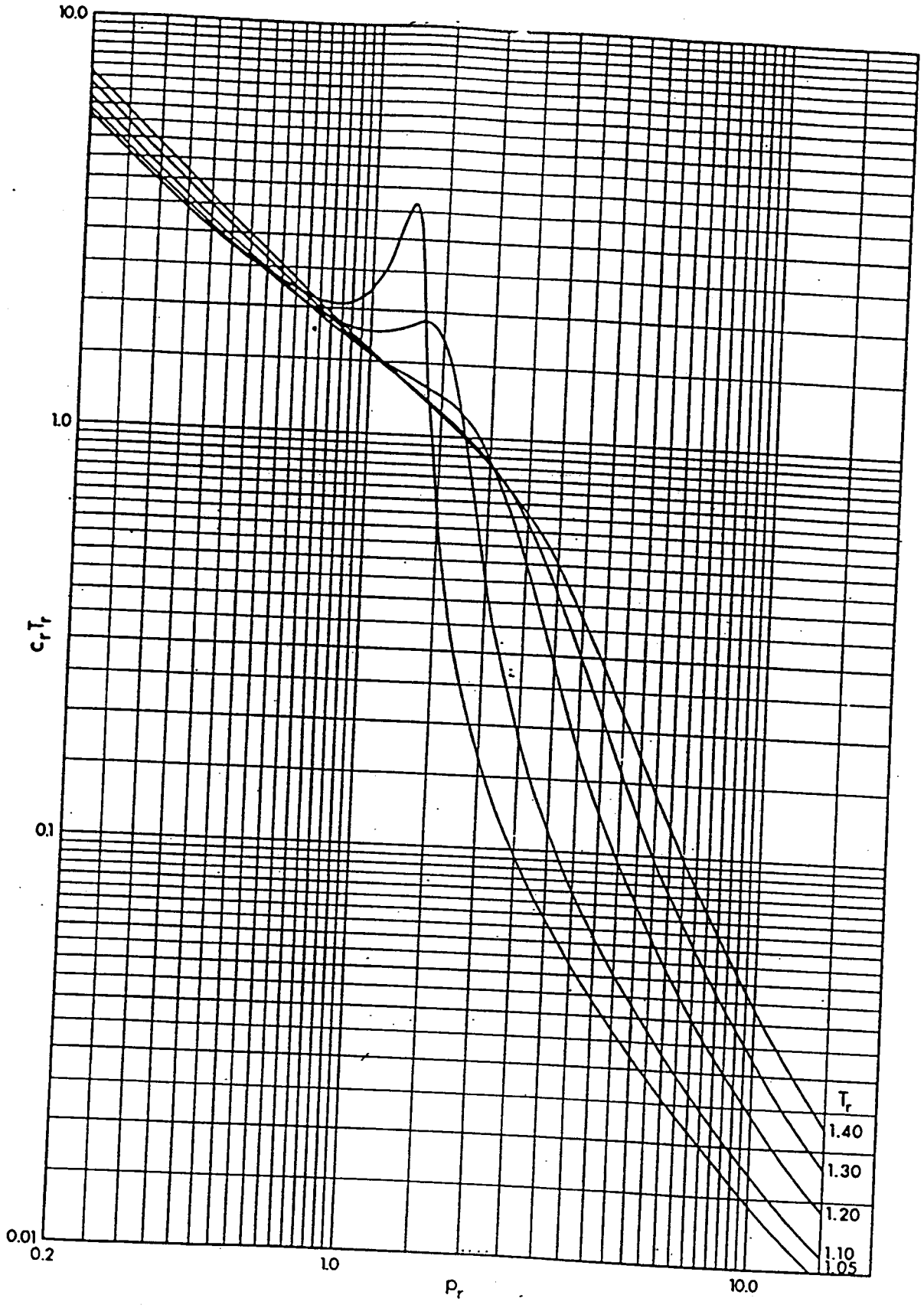

Fig. 2.8a

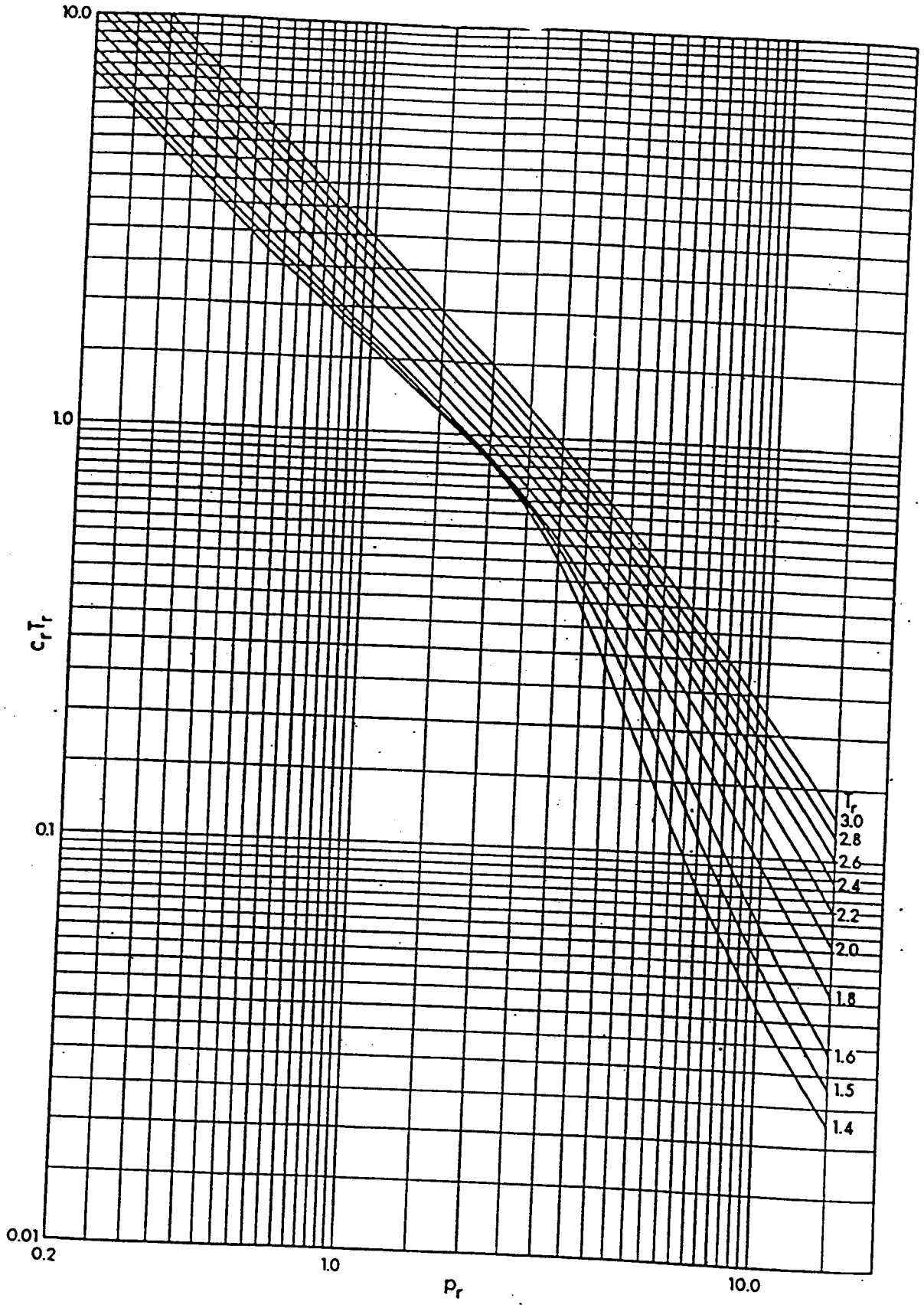

Fig. 2.8b

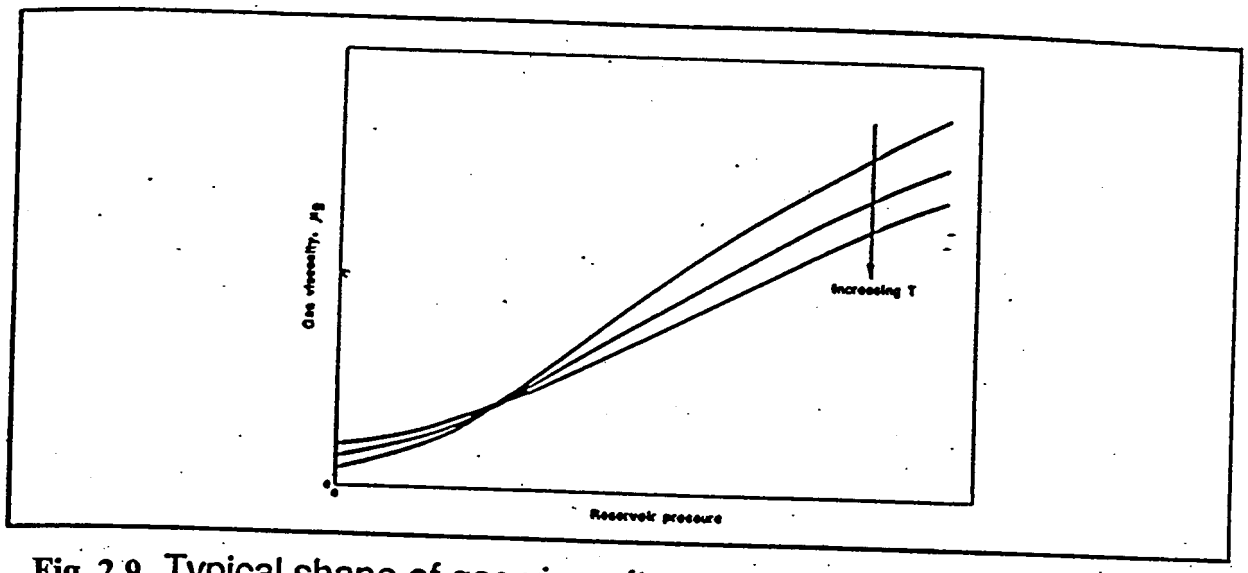

Fig. 2.9 Typical shape of gas viscosity as a function of pressure at three reservoir temperatures.

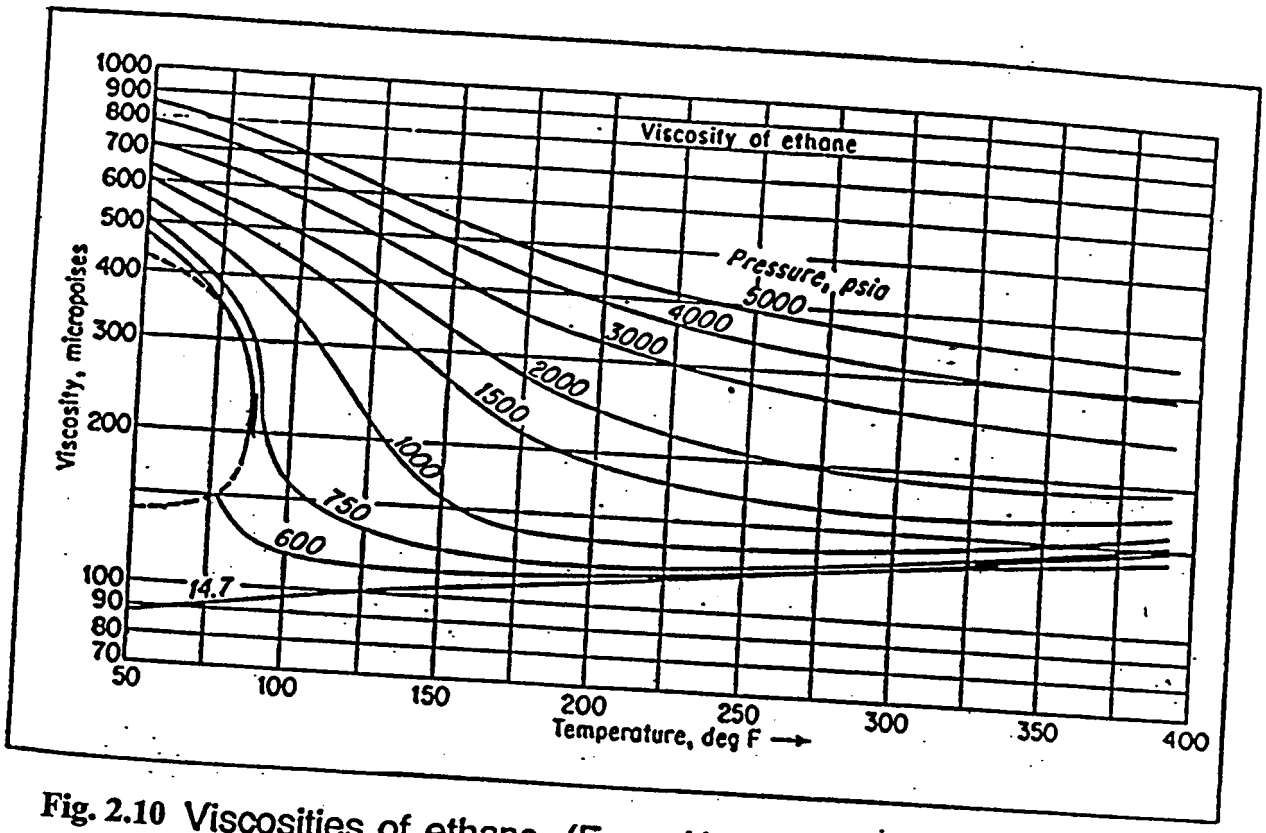

Fig. 2.10 Viscosities of ethane. (From *Handbook of Natural Gas Engineering* by Katz et al. Copyright 1959 by McGraw-Hill Book Co. Used with permission of McGraw-Hill Book Co.)

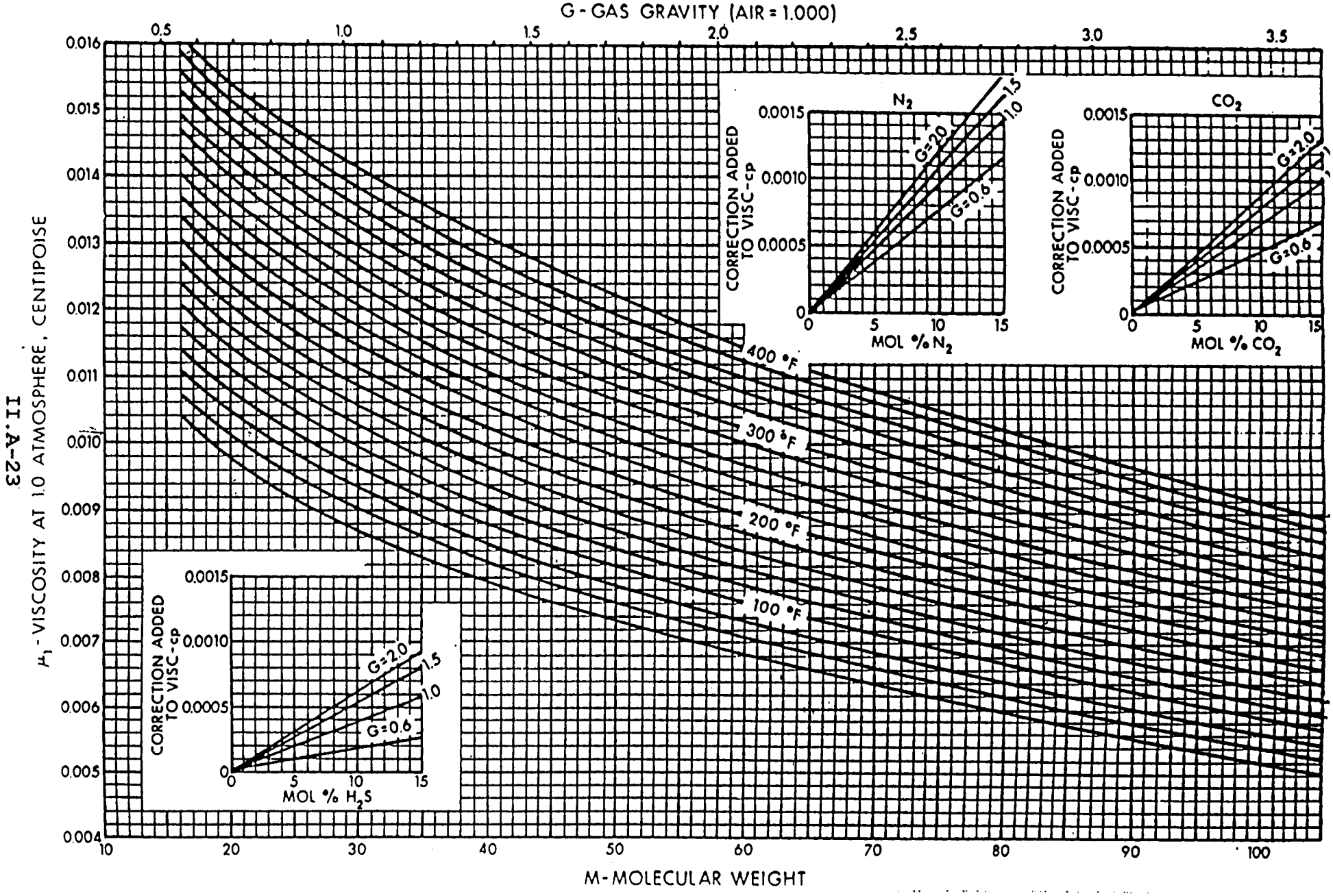
G - GAS GRAVITY (AIR = 1.000)
0.5
1.0
1.5
2.0
2.5
3.0
3.5
0.016
0.015
0.014
0.013
0.012
0.011
0.010
0.009
0.008
0.007
0.006
0.005
0.004
μ_1 - VISCOSITY AT 1.0 ATMOSPHERE, CENTIPOISE
400 °F
300 °F
200 °F
100 °F
10
20
30
40
50
60
70
80
90
100
M - MOLECULAR WEIGHT
N_2
CORRECTION ADDED TO VISC - cp
0.0015
0.0010
0.0005
0
G=2.0
1.5
1.0
G=0.6
0
5
10
15
MOL % N_2
CO_2
CORRECTION ADDED TO VISC - cp
0.0015
0.0010
0.0005
0
G=2.0
G=0.6
0
5
10
15
MOL % CO_2
CORRECTION ADDED TO VISC - cp
0.0015
0.0010
0.0005
0
G=2.0
1.5
1.0
G=0.6
0
5
10
15
MOL % H_2S

Figure 2.11

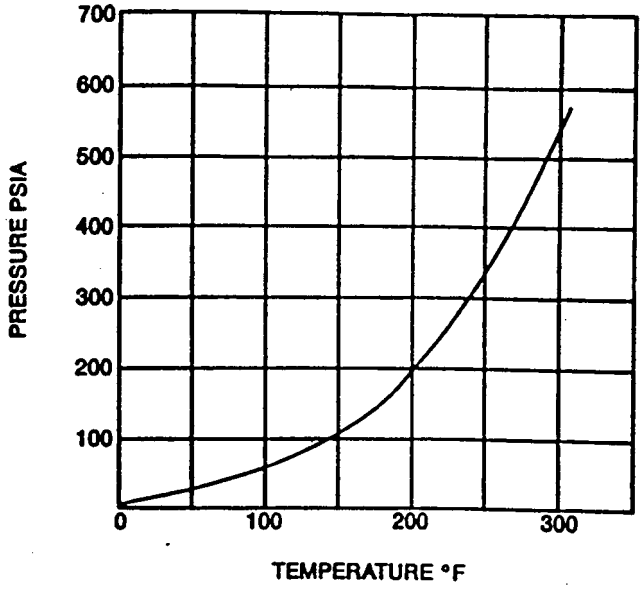

Vapor pressure of n-butane.

Fig. 2.12.1

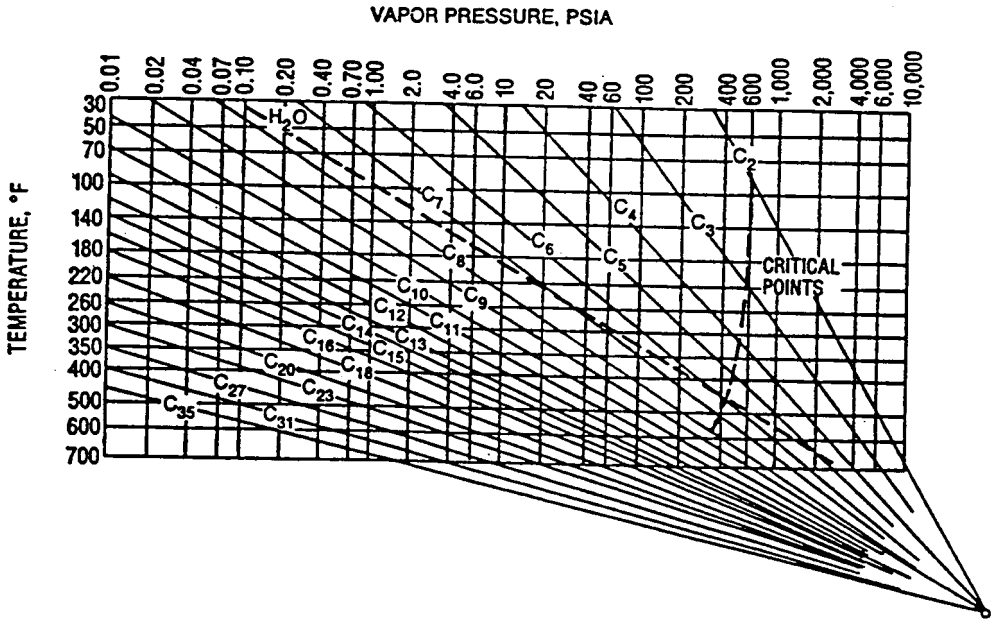

Fig. 2.12.2

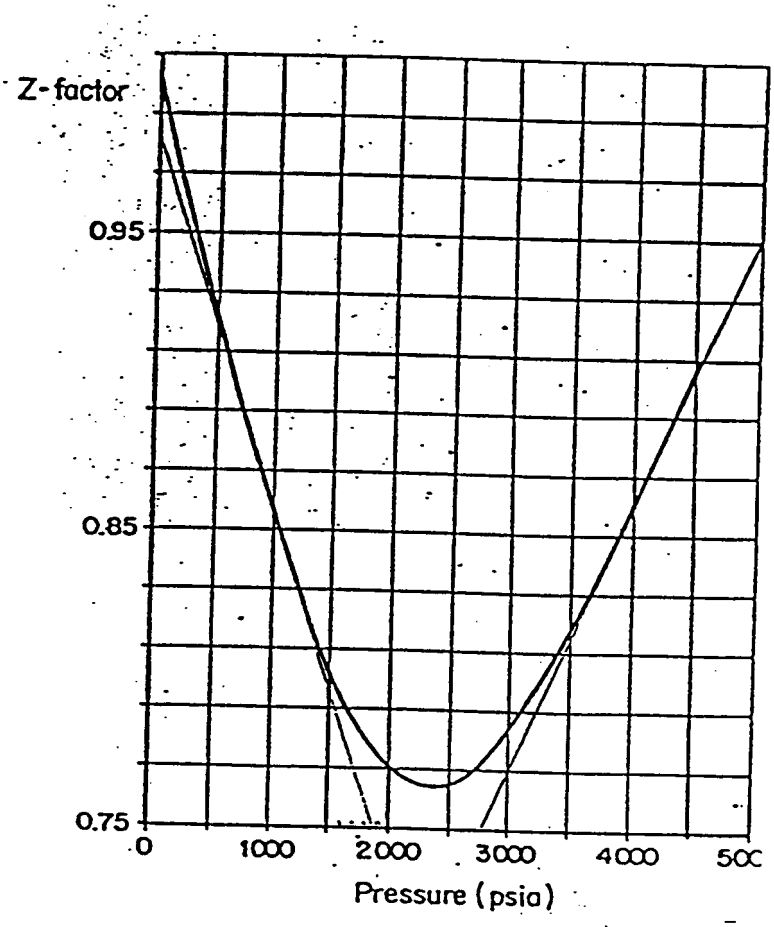

Fig. 2.13

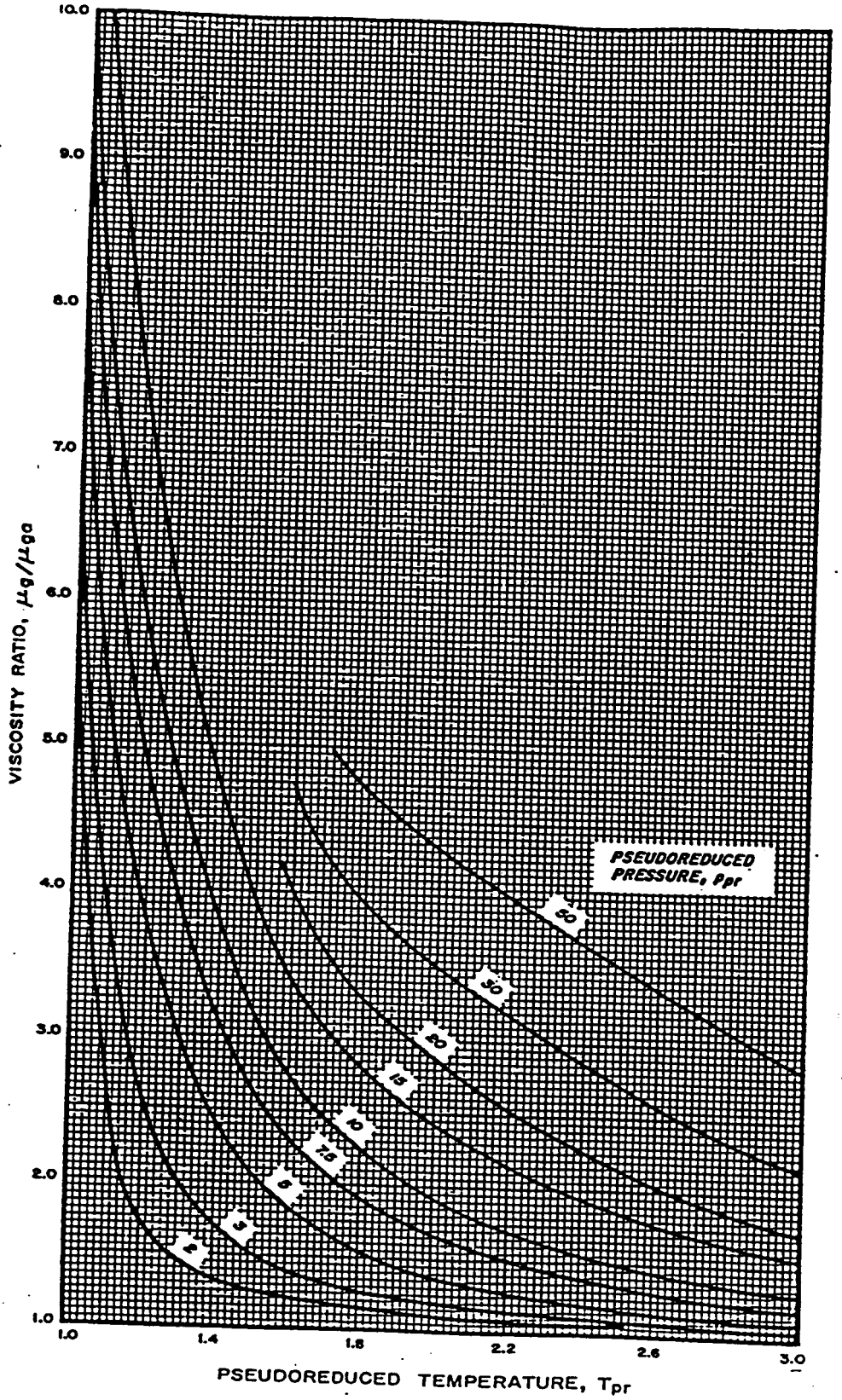
VISCOSITY RATIO, μ_g/μ_{ga}
10.0
9.0
8.0
7.0
6.0
5.0
4.0
3.0
2.0
1.0
PSEUDOREDUCED PRESSURE, p_{pr}
80
50
30
15
10
7.5
5
3
2
1.0
1.4
1.8
2.2
2.6
3.0
PSEUDOREDUCED TEMPERATURE, T_{pr}

Fig. 2.15

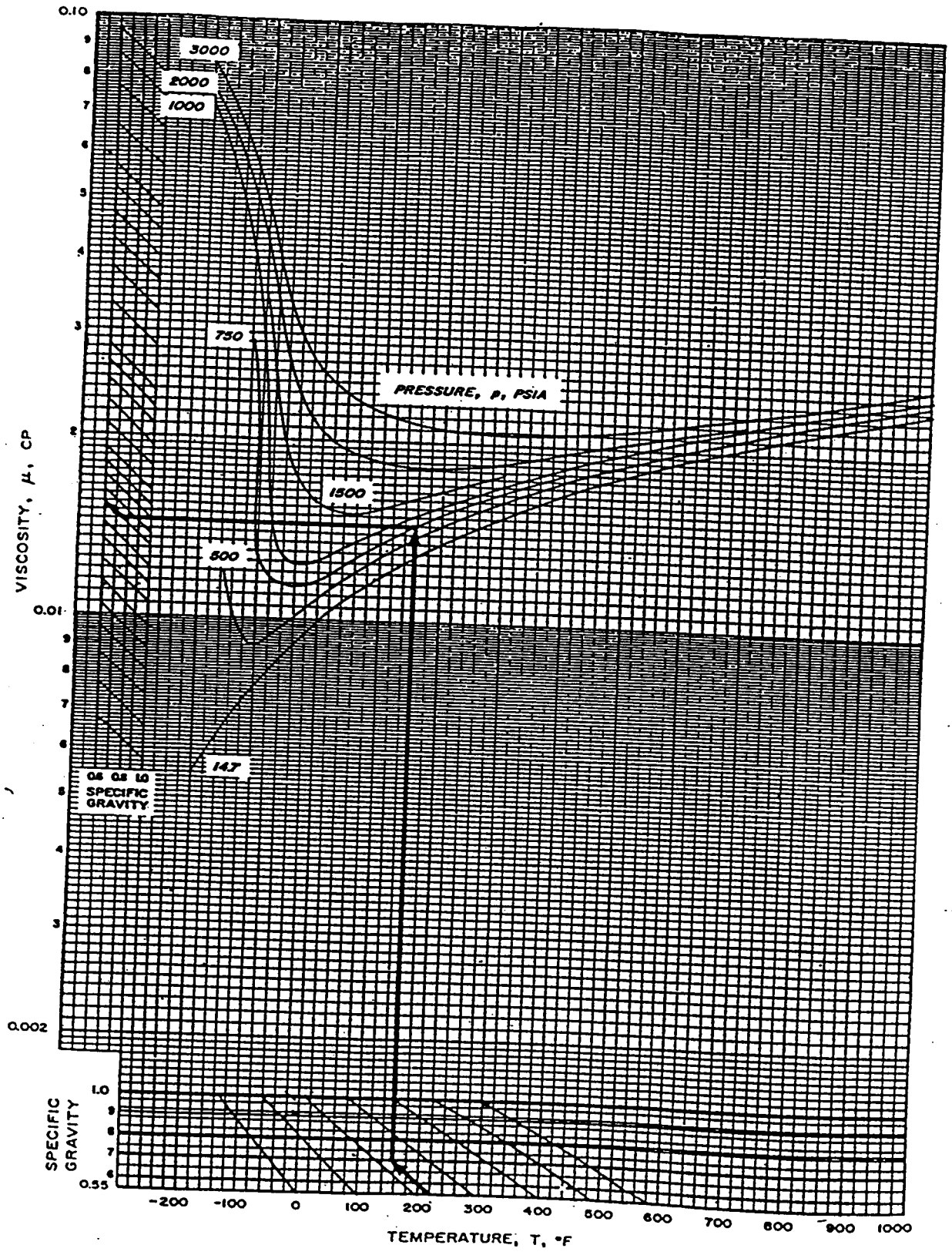
VISCOSITY, μ, CP
0.10
0.01
0.002
3000
2000
1000
750
500
147
1500
PRESSURE, P, PSIA
0.6 0.8 1.0
SPECIFIC GRAVITY
SPECIFIC GRAVITY
1.0
0.55
-200 -100 0 100 200 300 400 500 600 700 800 900 1000
TEMPERATURE, T, °F

Fig. 2.16

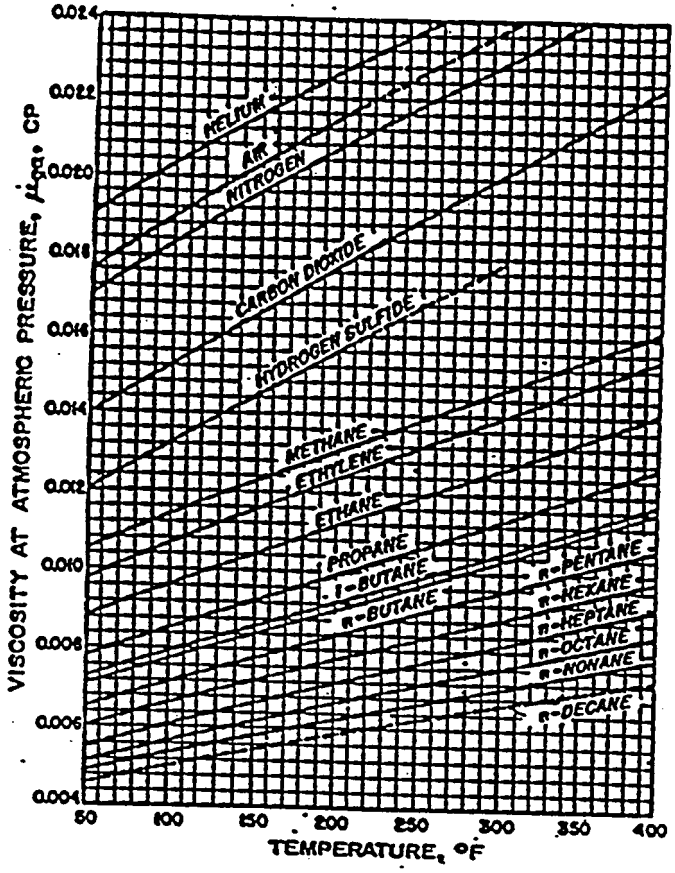
VISCOSITY AT ATMOSPHERIC PRESSURE, μ_{atm}, CP
0.024
0.022
0.020
0.018
0.016
0.014
0.012
0.010
0.008
0.006
0.004
HELIUM
AIR
NITROGEN
CARBON DIOXIDE
HYDROGEN SULFIDE
METHANE
ETHYLENE
ETHANE
PROPANE
i-BUTANE
n-BUTANE
n-PENTANE
n-HEXANE
n-HEPTANE
n-OCTANE
n-NONANE
n-DECANE
50
100
150
200
250
300
350
400
TEMPERATURE, °F

Fig. 2.17

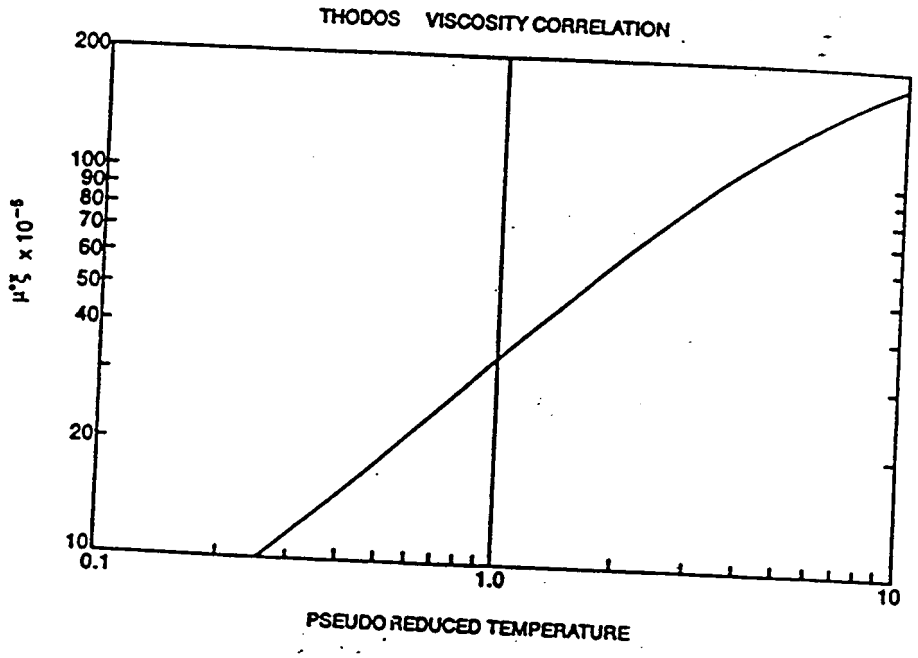

Fig. 2.17a Thodos viscosity correlation.

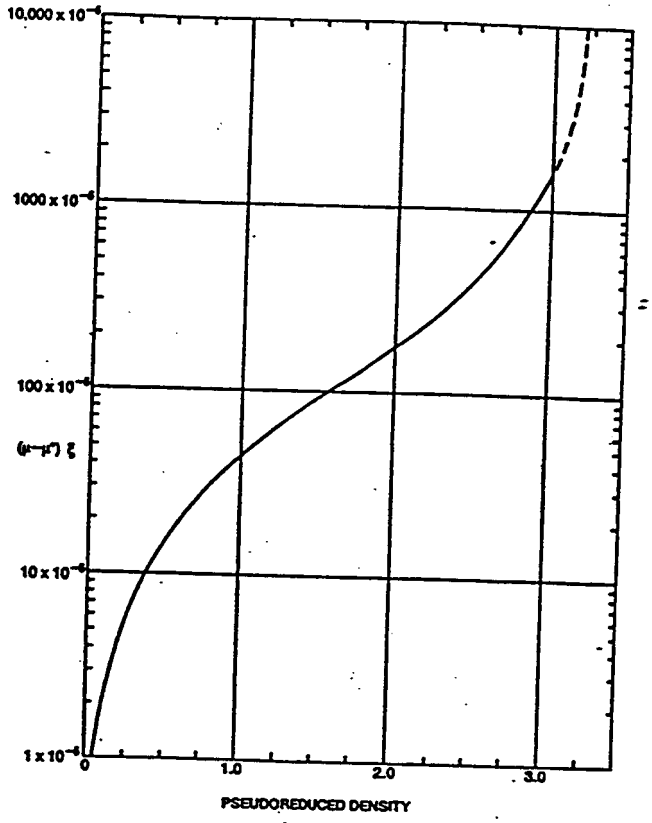

Fig. 2.17b Thodos viscosity correlation—pressure correction.

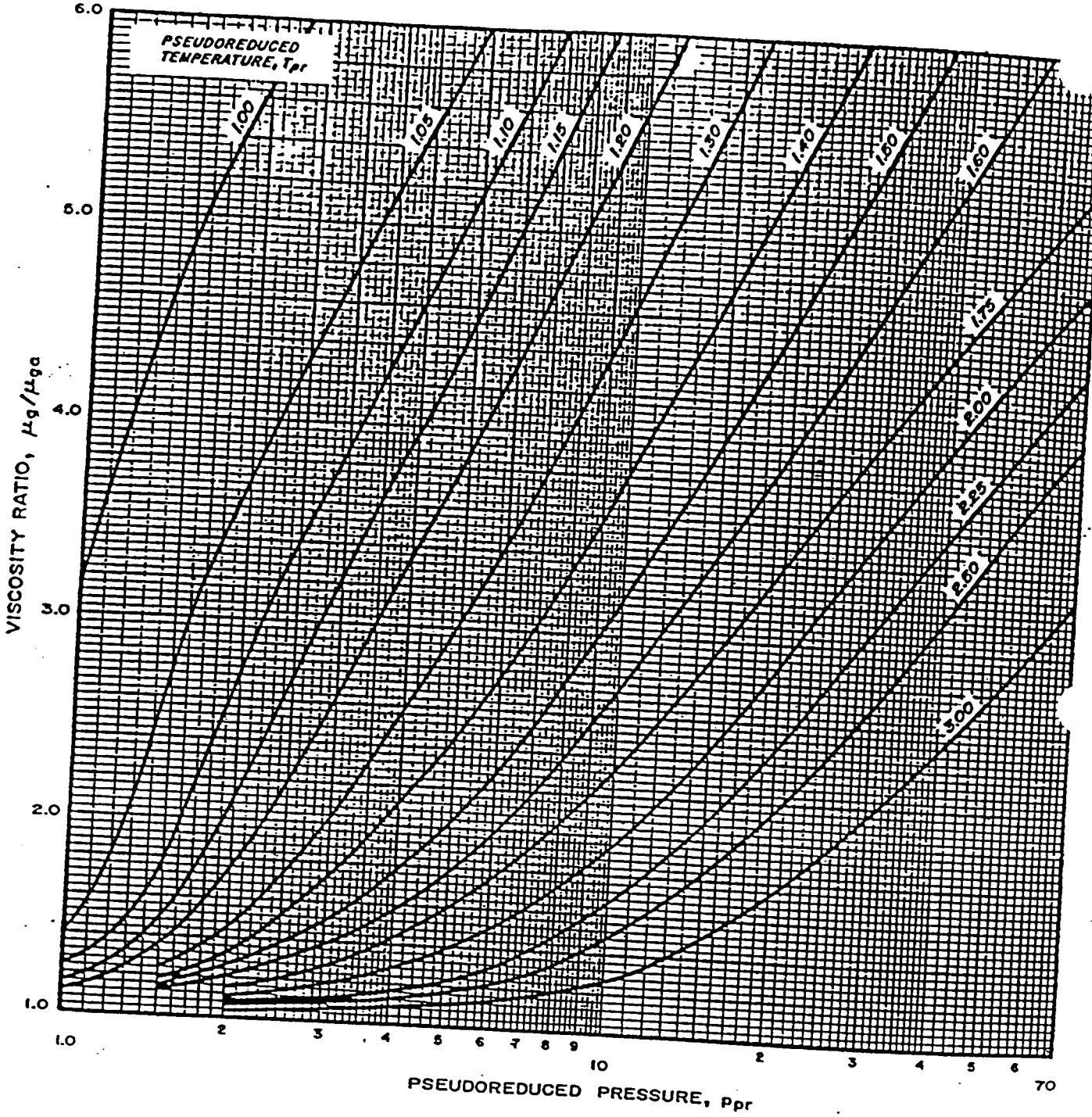
PSEUDOREDUCED TEMPERATURE, T_{pr}
1.00
1.05
1.10
1.15
1.20
1.30
1.40
1.50
1.60
1.75
2.00
2.25
2.50
3.00
VISCOSITY RATIO, μ_g/μ_{ga}
6.0
5.0
4.0
3.0
2.0
1.0
1.0
2
3
4
5
6
7
8
9
10
2
3
4
5
6
70
PSEUDOREDUCED PRESSURE, p_{pr}

Fig. 2.18

Table 2.1

Reduced Pressure P_r Range Between	Reduced Temperature, T_r Range Between	Equations	Equation Number
0.2 and 1.2	1.05 and 1.2	$P_r(1.6643T_r - 2.2114) - 0.3647T_r + 1.4385$	1
	1.2+ and 1.4	$P_r(0.5222T_r - 0.8511) - 0.0364T_r + 1.0490$	2
	1.4+ and 2.0	$P_r(0.1391T_r - 0.2988) + 0.0007T_r^a + 0.9969$	3[b]
	2.0+ and 3.0	$P_r(0.0295T_r - 0.0825) + 0.0009T_r^a + 0.9967$	4[b]
1.2+ and 2.8	1.05 and 1.2	$P_r(-1.3570T_r + 1.4942) + 4.6315T_r - 4.7009$	5[c]
	1.2+ and 1.4	$P_r(0.1717T_r - 0.3232) + 0.5869T_r + 0.1229$	6
	1.4+ and 2.0	$P_r(0.0984T_r - 0.2053) + 0.0621T_r + 0.8580$	7
	2.0+ and 3.0	$P_r(0.0211T_r - 0.0527) + 0.0127T_r + 0.9549$	8
2.8+ and 5.4	1.05 and 1.2	$P_r(-0.3278T_r + 0.4752) + 1.8223T_r - 1.9036$	9[b]
	1.2+ and 1.4	$P_r(-0.2521T_r + 0.3871) + 1.6087T_r - 1.6635$	10[b]
	1.4+ and 2.0	$P_r(-0.0284T_r + 0.0625) + 0.4714T_r - 0.0011^a$	11
	2.0+ and 3.0	$P_r(0.0041T_r + 0.0039) + 0.0607T_r + 0.7927$	12
5.4+ and 15.0	1.05 and 3.0	$P_r(0.711 + 3.66T_r)^{-1.4667} - 1.637/(0.319\,T_r + 0.522) + 2.071$	13

[a]These terms may be ignored.

[b]For a very slight loss in accuracy, Eqs. 3 and 4 and 9 and 10 can, respectively, be replaced by the following two equations:

$z = P_r(0.0657T_r - 0.1751) + 0.0009\,T_r^a + 0.9968$

$z = P_r(-0.2384\,T_r + 0.3695) + 1.4517\,T_r - 1.4580$

[c]Preferably use this equation for P_r up to 2.6 only. For $P_r = 2.6+$, Eq. 9 will give slightly better results. Also, preferably,use Eq. 1 for $1.08 \leqq T_r \leqq 1.19$ and $P_r \leqq 1.4$.

Table 2.2

*Pseudocritical Properties of Hydrocarbon Gases, p_{pc} and T_{pc} **

γ_g	p_{pc}	T_{pc}	γ_g	p_{pc}	T_{pc}
0.55	673	336	0.85	664	441
0.56	673	341	0.86	664	444
0.57	672	346	0.87	663	448
0.58	672	350	0.88	663	451
0.59	672	354	0.89	662	454
0.60	671	358	0.90	662	457
0.61	671	362	0.91	662	461
0.62	671	365	0.92	662	464
0.63	670	368	0.93	661	467
0.64	670	372	0.94	661	471
0.65	670	375	0.95	660	474
0.66	670	378	0.96	660	477
0.67	669	382	0.97	659	481
0.68	669	385	0.98	659	484
0.69	669	388	0.99	659	487
0.70	668	392	1.00	658	491
0.71	668	395	1.01	658	494
0.72	668	398	1.02	657	497
0.73	668	401	1.03	656	500
0.74	667	405	1.04	656	504
0.75	667	408	1.05	655	507
0.76	667	411	1.06	655	510
0.77	666	415	1.07	654	514
0.78	666	418	1.08	654	517
0.79	666	421	1.09	653	520
0.80	665	424	1.10	652	524
0.81	665	428	1.11	652	527
0.82	665	431	1.12	651	530
0.83	665	434	1.13	651	534
0.84	664	438	1.14	650	537

Do not interpolate; values are inclusive to the next higher value.

* Used by permission of the Pacific Energy Association (formerly the California Natural Gasoline Association), taken from Bulletin No. TS-461, 1947. Data are for the average of the natural gas mixtures occuring in the western states—primarily California.

Table 2.3

*Correction for Pseudocritical Properties of Hydrocarbon Gases for Carbon Dioxide, Nitrogen, and Hydrogen Sulfide**

Add if positive or subtract if negative from values in table A–1.

Volume Percent of CO_2 or N_2 in Gas	Carbon Dioxide, CO_2		Nitrogen, N_2		Hydrogen sulfide, H_2S	
	P_{pc}	T_{pc}	P_{pc}	T_{pc}	P_{pc}	T_{pc}
1	+ 4	− 1	− 1	− 3	+ 2	−2
2	+ 8	− 3	− 3	− 6	+ 4	−2
3	+ 12	− 5	− 5	− 9	+ 7	−3
4	+ 17	− 7	− 7	−11	+10	−3
5	+ 21	− 9	− 9	−14	+15	−4
6	+ 25	−11	−11	−17		
7	+ 30	−12	−12	−20		
8	+ 34	−14	−14	−22		
9	+ 39	−16	−16	−25		
10	+ 44	−17	−17	−28		
11	+ 48	−19	−19	−30		
12	+ 53	−21	−21	−33		
13	+ 57	−22	−22	−36		
14	+ 61	−24	−24	−39		
15	+ 66	−26	−26	−42		
16	+ 70	−27	−27	−44		
17	+ 74	−29	−29	−47		
18	+ 79	−31	−31	−50		
19	+ 83	−32	−32	−52		
20	+ 87	−34	−34	−55		
21	+ 92	−36	−36	−58		
22	+ 96	−37	−37	−60		
23	+100	−39	−39	−63		
24	+104	−41	−41	−66		
25	+109	−42	−42	−68		
26	+113	−44	−44	−71		
27	+117	−46	−46	−74		
28	+122	−47	−47	−77		
29	+126	−49	−49	−79		
30	+130	−51	−51	−82		
31	+134	−52	−52	−85		
32	+139	−54	−54	−87		
33	+143	−56	−56	−90		
34	+147	−57	−57	−93		
35	+152	−59	−59	−95		
36	+156	−61	−61	−98		

* Values for carbon dioxide and nitrogen are based on data from the California Natural Gasoline Association Bulletin No. TS–461. Used by permision of the Interstate Oil Compact Commission. Values for hydrogen sulfide are supplied by the author.

TABLE 2.4

Values of the universal gas constant, R (from *Engineering Data Book*, GPSA, 1987, with permission)

Basis of units listed below is 22.4140 liters at 0°C and 1 atm for the volume of 1g mole. All other values were calculated from conversion factors.

n	Temperature	Pressure	Volume	R	n	Temperature	Energy	R
g mole	K	atm	liter	0.082057477	g mole	K	calorie	1.9859
g mole	K	atm	cc	82.057	g mole	K	joule	8.3145
g mole	K	mm Hg	liter	62.364				
g mole	K	bar	liter	0.083145	lb mole	°R	BTU	1.9859
g mole	K	kg/sq cm	liter	0.084784	lb mole	°R	hp-hr	0.00078048
g mole	K	k Pa	cu m	0.0083145	lb mole	°R	kw-hr	0.00058200
lb mole	°R	atm	cu ft	0.73024	lb mole	°R	ft-lb	1545.3
lb mole	°R	in Hg	cu ft	21.850				
lb mole	°R	mm Hg	cu ft	554.98	k mole	K	joule	8314.5
lb mole	°R	lb/sq in	cu ft	10.732				
lb mole	°R	lb/sq ft	cu ft	1545.3				
lb mole	K	atm	cu ft	1.3144				
lb mole	K	mm Hg	cu ft	998.97				
k mole	K	k Pa	cu m	8.3145				
k mole	K	bar	cu m	0.083145				

TABLE 2.5

TABLE . —PHYSICAL PROPERTIES OF GASES AT 14.7 psia AND 60°F

Component	Chemical Formula	Molecular Weight (lbm/lbm-mol)	Critical Temperature (°R)	Critical Pressure (psia)	Liquid Density* (lbm/ft^3)	Gas Density (lbm/ft^3)	Gas Viscosity (cp)
Hydrogen	H_2	2.109	59.36	187.5	4.432	0.005312	0.00871
Helium	He	4.003	9.34	32.9	7.802	0.01055	0.01927
Water	H_2O	18.015	1,164.85	3,200.1	62.336	—	~1.122
Carbon monoxide	CO	28.013	227.16	493.1	50.479	0.07381	0.01725
Nitrogen	N_2	28.010	239.26	507.5	49.231	0.07382	0.01735
Oxygen	O_2	31.999	278.24	731.4	71.228	0.08432	0.02006
Hydrogen sulfide	H_2S	34.08	672.35	1,306.0	49.982	0.08981	0.01240
Carbon dioxide	CO_2	44.010	547.58	1,071.0	51.016	0.1160	0.01439
Air	—	28.963	238.36	546.9	54.555	0.07632	0.01790
Methane	CH_4	16.043	343.00	666.4	18.710	0.04228	0.01078
Ethane	C_2H_6	30.070	549.59	706.5	22.214	0.07924	0.00901
Propane	C_3H_8	44.097	665.73	616.0	31.619	—	0.00788
I-Butane	C_4H_{10}	58.123	734.13	527.9	35.104	—	0.00732
n-Butane	C_4H_{10}	58.123	765.29	550.6	36.422	—	0.00724
I-Pentane	C_5H_{12}	72.150	828.77	490.4	38.960	—	—
n-Pentane	C_5H_{12}	72.150	845.47	488.6	39.360	—	—
n-Hexane	C_6H_{14}	86.177	913.27	436.9	41.400	—	—
n-Heptane	C_7H_{16}	100.204	972.37	396.8	42.920	—	—
n-Octane	C_8H_{18}	114.231	1,023.89	360.7	44.090	—	—
n-Nonane	C_9H_{20}	128.258	1,070.35	331.8	45.020	—	—
n-Decane	$C_{10}H_{22}$	142.285	1,111.67	305.2	45.790	—	—

*Values given are liquid densities for those components that can exist as liquids at 60°F and 14.7 psia and estimated liquid densities for components that are naturally gases at these conditions.

TABLE 2.6

TABLE —COMPOSITION OF SOUR NATURAL GAS, EXAMPLE 1.2				
Component	Mole Fraction	Molecular Weight (lbm/lbm-mol)	Critical Temperature (°R)	Critical Pressure (psia)
N_2	0.0236	28.013	227.16	493.1
CO_2	0.0164	44.010	547.58	1,071.0
H_2S	0.1841	34.080	672.35	1,306.0
CH_4	0.7700	16.043	343.00	666.4
C_2H_6	0.0042	30.070	549.59	706.5
C_3H_8	0.0005	44.097	665.73	616.0
i-C_4H_{10}	0.0003	58.123	734.13	527.9
n-C_4H_{10}	0.0003	58.123	765.29	550.6
i-C_5H_{12}	0.0001	72.150	828.77	490.4
n-C_5H_{12}	0.0001	72.150	845.47	488.6
C_6H_{14}	0.0001	86.177	913.27	436.9
C_{7+}	0.0003	114.231	—	—

TABLE 2.7

TABLE —PSEUDOCRITICAL PROPERTY CALCULATIONS USING THE STEWART *et al.*[5] MIXING RULES, EXAMPLE 1.2								
Component	Mole Fraction, y_i	Molecular Weight, M_i	y_iM_i	Critical Temperature, T_{cl} (°R)	Critical Pressure, p_{cl} (psia)	y_iT_{cl}/p_{cl}	$y_i\sqrt{T_{cl}/p_{cl}}$	$y_iT_{cl}/\sqrt{p_{cl}}$
N_2	0.0236	28.013	0.6611	227.16	493.1	0.0109	0.0160	0.2414
CO_2	0.0164	44.010	0.7218	547.58	1071.0	0.0084	0.0117	0.2744
H_2S	0.1841	34.080	6.2741	672.35	1306.0	0.0948	0.1321	3.4251
CH_4	0.7700	16.043	12.353	343.00	666.4	0.3963	0.5524	10.231
C_2H_6	0.0042	30.070	0.1263	549.59	706.5	0.0033	0.0037	0.0868
C_3H_8	0.0005	44.097	0.0220	665.73	616.0	0.0005	0.0005	0.0134
i-C_4H_{10}	0.0003	58.123	0.0174	734.13	527.9	0.0004	0.0004	0.0096
n-C_4H_{10}	0.0003	58.123	0.0174	765.29	550.6	0.0004	0.0004	0.0098
i-C_5H_{12}	0.0001	72.150	0.0072	828.77	490.4	0.0002	0.0001	0.0037
n-C_5H_{12}	0.0001	72.150	0.0072	845.47	488.6	0.0002	0.0001	0.0038
C_6H_{14}	0.0001	86.177	0.0086	913.27	436.9	0.0002	0.0001	0.0044
C_{7+}	0.0003	114.23	0.0343	1005.3	375.5	0.0008	0.0005	0.0156
Σ=	1.0000	—	20.250	—	—	0.5163	0.7181	14.319

TABLE 20.2—SOME PHYSICAL CONSTANTS OF HYDROCARBONS

Number	Compound	Formula	Molecular Weight	Vapor Pressure (100°F, psia)	Critical Constants			Gas Density (60°F, 14.696 psia) Calculated as Ideal Gas* (cu ft gas/gal liquid)
					Pressure (psia)	Temperature (°F)	Volume (cu ft/lbm)	
1	methane	CH_4	16.043	(5000)	667.8	−116.68	0.0988	59.1*
2	ethane	C_2H_6	30.070	(800)	707.8	90.1	0.0788	37.48**
3	propane	C_3H_8	44.097	188.0	616.3	206.01	0.0737	36.49**
4	n-butane	C_4H_{10}	58.124	51.54	550.7	305.62	0.0703	31.80**
5	isobutane	C_4H_{10}	58.124	72.39	529.1	274.96	0.0724	30.65**
6	n-pentane	C_5H_{12}	72.151	15.575	488.6	385.6	0.0674	27.67
7	isopentane	C_5H_{12}	72.151	20.4444	490.4	369.03	0.0679	27.38
8	neopentane	C_5H_{12}	72.151	36.66	464.0	321.08	0.0673	26.16**
9	n-hexane	C_6H_{14}	86.178	4.960	436.9	453.6	0.06887	24.38
10	2-methylpentane	C_6H_{14}	86.178	6.767	436.6	435.74	0.0682	24.16
11	3-methylpentane	C_6H_{14}	86.178	6.103	453.1	448.2	0.0682	24.56
12	neohexane	C_6H_{14}	86.178	9.859	446.9	420.04	0.0668	24.02
13	2,3-dimethylbutane	C_6H_{14}	86.178	7.406	453.5	440.0	0.0665	24.47
14	n-heptane	C_7H_{16}	100.205	1.620	396.8	512.7	0.0690	21.73
15	2-methylhexane	C_7H_{16}	100.205	2.2719	396.5	494.89	0.0673	21.56
16	3-methylhexane	C_7H_{16}	100.205	2.131	408.1	503.67	0.0646	21.84
17	3-ethylpentane	C_7H_{16}	100.205	2.013	419.3	513.36	0.0665	22.19
18	2,2-dimethylpentane	C_7H_{16}	100.205	3.494	402.2	477.12	0.0665	21.41
19	2,4-dimethylpentane	C_7H_{16}	100.205	3.293	397.0	475.84	0.0668	21.39
20	3,3-dimethylpentane	C_7H_{16}	100.205	2.774	427.1	505.74	0.0662	22.03
21	triptane	C_7H_{16}	100.205	3.375	428.4	496.33	0.0636	21.93
22	n-octane	C_8H_{18}	114.232	0.537	360.6	564.10	0.0690	19.58
23	diisobutyl	C_8H_{18}	114.232	1.1017	360.6	530.31	0.0676	19.33
24	isooctane	C_8H_{18}	114.232	1.709	372.5	519.33	0.0657	19.28
25	n-nonane	C_9H_{20}	128.259	0.1796	331.8	610.54	0.0684	17.81
26	n-decane	$C_{10}H_{22}$	142.286	0.0609	304.4	651.6	0.0679	16.32
27	cyclopentane	C_5H_{10}	70.135	9.914	653.0	461.6	0.0594	33.85
28	methylcyclopentane	C_6H_{12}	84.162	4.503	549.0	499.24	0.0607	28.33
29	cyclohexane	C_6H_{12}	84.162	3.266	590.9	536.6	0.0589	29.45
30	methylcyclohexane	C_7H_{14}	98.189	1.6093	503.6	570.15	0.0601	24.92
31	ethylene	C_2H_4	28.054	—	731.1	48.56	0.0748	—
32	propene	C_3H_6	42.081	227.6	667.2	197.06	0.0689	39.25**
33	1-butene	C_4H_8	56.108	62.10	583.5	295.48	0.0686	33.91**
34	cis-2-butene	C_4H_8	56.108	45.95	612.1	324.37	0.0668	35.36**
35	trans-2-butene	C_4H_8	56.108	49.94	587.1	311.86	0.0679	34.40**
36	isobutene	C_4H_8	56.108	63.64	580.0	292.55	0.0682	33.86**
37	1-pentene	C_5H_{10}	70.135	19.117	591.8	376.93	0.0676	29.13**
38	1,2-butadiene	C_4H_6	54.092	36.5	(653.0)	(340.0)	(0.0649)	38.4**
39	1,3-butadiene	C_4H_6	54.092	59.4	628.0	305.0	0.0655	36.69**
40	isoprene	C_5H_8	68.119	16.68	(558.4)	(412.0)	(0.0650)	31.87
41	acetylene	C_2H_2	26.038	—	890.4	95.32	0.0695	—
42	benzene	C_6H_6	78.114	3.225	710.4	552.22	0.0525	35.82
43	toluene	C_7H_8	92.141	1.033	595.5	605.57	0.0549	29.94
44	ethylbenzene	C_8H_{10}	106.168	0.376	523.4	651.29	0.0565	25.97
45	o-xylene	C_8H_{10}	106.168	0.263	541.6	674.92	0.0557	26.36
46	m-xylene	C_8H_{10}	106.168	0.325	512.9	651.02	0.0567	25.88
47	p-xylene	C_8H_{10}	106.168	0.3424	509.2	649.54	0.0570	25.80
48	styrene	C_8H_8	104.152	0.238	580.0	706.0	0.0541	27.68
49	isopropylbenzene	C_9H_{12}	120.195	0.188	465.4	676.3	0.0572	22.80
50	methyl alcohol	CH_4O	32.042	4.63	1,174.4	463.08	0.0589	78.61
51	ethyl alcohol	C_2H_6O	46.069	2.125	925.3	465.39	0.0580	54.36
52	carbon monoxide	CO	28.010	—	507.5	−220.4	0.0532	—
53	carbon dioxide	CO_2	44.010	—	1,071.0	87.87	0.0342	59.78**
54	hydrogen sulfide	H_2S	34.076	387.1	1,306.0	212.6	0.046	73.07
55	sulfur dioxide	SO_2	64.059	85.46	1,145.0	315.8	0.0306	69.01
56	ammonia	NH_3	17.031	211.9	1,636.0	270.4	0.0681	114.71
57	air	N_2O_2	28.964	—	546.9	−221.4	0.0517	—
58	hydrogen	H_2	2.016	—	188.1	−399.9	0.5164	—
59	oxygen	O_2	31.999	—	736.9	−181.2	0.0367	—
60	nitrogen	N_2	28.013	—	493.0	−232.7	0.0516	—
61	chlorine	Cl_2	70.906	154.9	1,118.4	291.0	0.0280	63.53
62	water	H_2O	18.015	0.9495	3,207.9	705.5	0.0509	175.6
63	helium	He	4.003	—	32.99	−450.308	0.230	—
64	hydrogen chloride	HCl	36.461	906.3	205.1	124.8	0.0356	74.88

*Apparent value at 60°F
**Saturation pressure at 60°F

Table 2.8

PART 3

GAS RESERVES

GAS RESERVES AND MATERIAL-BALANCE CALCULATIONS

3.1 VOLUMETRIC METHODS

Volumetric methods consider the reservoir PV occupied by hydrocarbons at initial conditions and at later conditions after some fluid production and associated pressure reduction. The later conditions often are defined as the reservoir pressure at which production is no longer economical. Volumetric methods are used early in the life of a reservoir before significant development and production. These methods, however, can also be applied later in a reservoir's life and often are used to confirm estimates from material-balance calculations. The accuracy of volumetric estimates depends on the availability of sufficient data to characterize the reservoir's areal extent and variations in net thickness and, ultimately, to determine the gas-bearing reservoir PV. Obviously, early in the productive life of a reservoir when few data are available to establish subsurface geologic control, volumetric estimates are least accurate. As more wells are drilled and more data become available, the accuracy of these estimates improves.

Data used to estimate the gas-bearing reservoir PV include, but are not limited to, well logs, core analyses, bottomhole pressure (BHP) and fluid sample information, and well tests. These data typically are used to develop various subsurface maps. Of these maps, structural and stratigraphic cross-sectional maps help to establish the reservoir's areal extent and to identify reservoir discontinuities, such as pinchouts, faults, or gas/water contacts. Subsurface contour maps, usually drawn relative to a known or marker formation, are constructed with lines connecting points of equal elevation and therefore portray the geologic structure. Subsurface isopachous maps are constructed with lines of equal net gas-bearing formation thickness. With these maps, the reservoir PV can then be estimated by planimetering the areas between the isopachous lines and using an approximate volume calculation technique, such as the pyramidal or trapezoidal methods.

After the gas-bearing reservoir PV has been estimated, we can calculate the original gas in place and, for some abandonment conditions, estimate the gas reserves. The form of the volumetric equations varies according to the drive mechanism and type of gas. In the following sections, we present equations for dry-gas reservoirs, dry-gas reservoirs with water influx, and wet-gas reservoirs.

3.2 VOLUMETRIC RESERVOIRS.

3.2.1 Volumetric Dry-Gas Reservoirs.

As the name implies, a volumetric reservoir is completely enclosed by low-permeability or completely impermeable barriers and does not receive pressure support from external sources, such as an encroaching aquifer. In addition, if the expansion of rock and the connate water are negligible, then the primary source of pressure maintenance is gas expansion resulting from gas production and the subsequent pressure reduction.

When we use "dry gas," we are referring to a reservoir gas made up primarily of methane with some intermediate-weight hydrocarbon molecules. The dry-gas-phase diagram in Fig. 3.1 indicates that, because of this composition, dry gases do not undergo phase changes following a pressure reduction and therefore are solely gases in the reservoir and at the surface separator conditions. In this sense, "dry" does not refer to the absence of water but indicates that no liquid hydrocarbons form in the reservoir, wellbore, or surface equipment during production.

Beginning with the real-gas law, the gas volume at initial reservoir conditions is

$$V_{gi} = \frac{z_i nRT}{p_i} \tag{3.1}$$

Similarly. the gas volume at standard conditions is

$$V_{sc} = G = \frac{z_{sc} n R T_{sc}}{p_{sc}} \tag{3.2}$$

Equating the number of moles of gas at initial reservoir conditions to the number at standard conditions and rearranging, we can solve for the initial volume of gas at standard conditions:

$$G = \frac{p_i V_{gi}}{z_i T} \frac{z_{sc} T_{sc}}{p_{sc}} \tag{3.3}$$

Assuming that the PV occupied by the gas is constant during the producing life of the reservoir gives

$$V_{gi} = 43.56 A h \phi \ (1\text{-}S_{wi}) \tag{3.4}$$

Substituting Eq. 3.4 into Eq. 3.3 yields

$$G = 43.56 A h \phi (1 - S_{wi}) \ \frac{p_i z_{sc} T_{sc}}{p_{sc} z_i T} \tag{3.5}$$

If we express the reservoir PV in barrels, Eq. 3.5 becomes

$$G = \frac{7{,}758 A h \phi (1 - S_{wi})}{B_{gi}} \tag{3.6}$$

where

$$B_{gi} = \frac{1{,}000 \cdot p_{sc} z_i T}{5.615 \cdot p_i z_{sc} T_{sc}} = \frac{5.02 z_i T}{p_i} \tag{3.7}$$

Eq. 3.7, which assumes standard conditions of P_{sc} = 14.65 psia, T_{sc} = 60°F = 520°R, and Z_{SC} = 1.0, also was derived in Chap. 1.

We can estimate the gas reserve or the total cumulative gas production, G_p, over the life of the reservoir as the difference between original gas in place, G, and gas in place at some abandonment conditions, G_a:

$$G_p = G - G_a, \tag{3.8}$$

In terms of Eq. 3.6, the gas reserve is

$$G_p = \frac{7{,}758 A h \phi (1 - S_{wi})}{B_{gi}} - \frac{7{,}758 A h \phi (1 - S_{wi})}{B_{ga}} \tag{3.9}$$

$$\text{or } G_p = \frac{7{,}758 A h \phi (1 - S_{wi})}{B_{gi}} \left(1 - \frac{B_{gi}}{B_{ga}}\right) \tag{3.10}$$

where the gas recovery factor $F = \left(1 - \frac{B_{gi}}{B_{ga}}\right)$

Simple gas expansion is a very efficient drive mechanism. Even though gas saturations at abandonment can be quite high, ultimate recoveries of 80% to 90% of the original gas in place are routinely achieved in volumetric gas reservoirs. The percentage of the original volume of gas in place that can be recovered depends on the abandonment pressure, which usually is determined by economical rather than technical considerations. Note that we developed Eq. 3.10 with the assumption that the initial connate water saturation does

not change. This assumption is valid in volumetric gas reservoirs where the initial connate water saturation is immobile. (See Example 3.1)

3.1.2 Dry-Gas Reservoirs With Water Influx.

Many gas reservoirs are not completely closed but are subjected to some natural water influx from an aquifer. Water encroachment occurs when the pressure at the reservoir/aquifer boundary is reduced following gas production from the reservoir. Recall that we derived the equation for a volumetric reservoir with the assumption that the reservoir PV occupied by gas remained constant over the reservoir's productive life. However, in gas reservoirs with water influx, this PV decreases by an amount equal to the net volume of water entering the reservoir and remaining unproduced. Therefore, if we can estimate both the initial gas saturation and the residual gas saturation at abandonment (i.e., the endpoint saturations), we can use volumetric equations to calculate the gas reserves in a gas reservoir with water influx.

Under these conditions, we consider the initial gas volume and the remaining gas volume plus the volume of water that has entered the reservoir. Beginning with Eq. 3.8, the equation for the cumulative gas production in terms of the initial and final water

$$G_p = \frac{7{,}758Ah\phi(1-S_{wi})}{B_{gi}} - \frac{7{,}758Ah\phi(1-S_{wa})}{B_{ga}} \qquad (3.11)$$

In terms of the residual gas saturation, S_{gr}, at abandonment, Eq. 3.11 becomes

$$G_p = \frac{7{,}758Ah\phi\left(1-S_{wi}\right)}{B_{gi}} - \frac{7{,}758Ah\phi\left(S_{gr}\right)}{B_{ga}} \qquad (3.12)$$

$$G_p = \frac{7{,}758Ah\phi(1-S_{wi})}{B_{gi}}\left(1-\frac{B_{gi}S_{gr}}{B_{ga}(1-S_{wi})}\right) \tag{3.13}$$

Here, the recovery factor, $F = \left(1-\frac{B_{gi}S_{gr}}{B_{ga}(1-S_{wi})}\right)$

Eqs. 3.11 through 3.13 were derived with the implicit assumption that the volumetric sweep efficiency for gas is 100%. In fact water may displace gas inefficiently in some cases. Results from early coreflood studies suggest that significant gas volumes can be bypassed and eventually trapped by an advancing water front. In addition, because of reservoir heterogeneities (i.e., natural fractures and layering) and discontinuities (i.e., sealing faults and low permeability shale stringers), the encroaching water does not sweep some portions of the reservoir effectively, resulting in high residual gas saturations in these unswept areas and higher abandonment pressures than for volumetric dry-gas reservoirs. To account for the unswept portions of the reservoir, we introduce a volumetric sweep efficiency, E_V, into the volumetric equation. With E_V, Eq. 3.8 can be rewritten as

$$G_p = G-[E_V G_a + (1-E_V)G_t]. \cdot \tag{3.14}$$

Eq. 3.14 can be rewritten in a form similar to Eq. 3.10,

$$G_p = \frac{7{,}758Ah\phi(1-S_{wi})}{B_{gi}} - \left[E_V\frac{7{,}758Ah\phi(1-S_{wa})}{B_{ga}} + (1-E_V)\frac{7{,}758Ah\phi(1-S_{wi})}{B_{ga}}\right] \tag{3.15}$$

Eq. 3.15 can be rearranged to yield

$$G_p = \frac{7{,}758Ah\phi(1-S_{wi})}{B_{gi}}\left[1 - E_V \frac{B_{gi}}{B_{ga}}\left(\frac{S_{gr}}{S_{gi}} + \frac{(1-E_V)}{E_V}\right)\right] \tag{3.16}$$

Here

$$F = \left[1 - E_V \frac{B_{gi}}{B_{ga}}\left(\frac{S_{gr}}{S_{gi}} + \frac{(1-E_V)}{E_V}\right)\right]$$

Because gas often is bypassed and trapped by the encroaching water, recovery factors for gas reservoirs with water drive can be significantly lower than for volumetric reservoirs produced by simple gas expansion. In addition, the presence of reservoir heterogeneities, such as low-permeability stringers or layering, may reduce gas recovery further. As noted previously, ultimate recoveries of 80% to 90% are common in volumetric gas reservoirs, while typical recovery factors in water drive gas reservoirs can range from 50% to 70%.

Eq. 3.16 requires estimates of S_{gr}, and E_V. Coreflood studies of representative reservoir samples are the best method for determining residual gas saturations. In the absence of laboratory studies Agarwal[6] proposed the following correlations for estimating the gas saturation in gas reservoirs with water influx. These correlations, based on multiple regression analyses of 320 experimental measurements of imbibition residual gas saturations, are presented in terms of porosity, absolute permeability, initial gas saturation, and lithology for consolidated sandstones, limestones, and unconsolidated sandstones.

For consolidated sandstones,

$$S_{gr} = \frac{A_1(100S_{gi}) + A_2(100S_{gi}^2)}{100} \tag{3.16b}$$

where $A_1 = 0.80841168$ and $A_2 = -0.0063869116$.

For limestones,

$$S_{gr} = \frac{A_1(100\phi) + A_2\log(k) + A_3(100S_{gi}) + A_4}{100} \tag{3.16c}$$

where $A_1 = -0.53482234$, $A_2 = 3.3555165$, $A_3 = 0.15458573$, and $A_4 = 14.403977$.

For unconsolidated sandstones,

$$S_{gr} = \frac{A_1(100S_{gi}) + A_1(10^4\phi S_{gi}) + A_3(100\phi) + A_4}{100} \tag{3.16d}$$

where $A_1 = -0.51255987$, $A_2 = 0.026097212$, $A_3 = -0.26769575$, and $A_4 = 14.796539$.

where

k = absolute permeability, L^2, md

S_{gr} = residual gas saturation, fraction

S_{gi} = initial gas saturation, fraction

ϕ = porosity, fraction

They may not be accurate for all situations and should be applied judiciously. We also can use numerical simulation to estimate volumetric sweep efficiencies if sufficient reservoir data are available. (See Examples 3.2 and 3.3)

3.2.3 Volumetric Wet-Gas and Gas-Condensate Reservoirs

Like dry gases, the primary composition of a wet gas is methane; however, unlike dry gases, wet gases have more of the intermediate and heavier-weight hydrocarbon molecules. Because of this composition, formation of a liquid phase in the wellbore and surface production equipment accompanies pressure and temperature reductions during production. In this context, "wet" does not mean that a gas is wet with water but refers to the hydrocarbon liquid that condenses at surface conditions.

The behavior of wet-gas systems is best illustrated with the phase diagram[3] in Fig. 3.2. The reservoir fluid is classified as a wet gas if it is single-phase gas at reservoir conditions but surface pressure and temperature conditions fall within the two-phase region.The reservoir pressure path in Fig. 3.2 does not enter the two phase envelope; thus, no liquid hydrocarbons are formed in the reservoir. The separator conditions, however, lie within the two phase envelope, and some gas condenses at the surface.

For a wet-gas reservoir, the total initial gas in place, G_T which includes gas and the gaseous equivalent of produced liquid hydrocarbons. is

$$G_T = \frac{7{,}758Ah\phi(1-S_{wi})}{B_{gi}} \tag{3.17}$$

where B_{gi} is defined by Eq. 3.7. Because of the gas condensation at the surface, the surface and reservoir gas properties are different. Consequently, the use of Eq. 3.17 requires knowledge of the gas properties at reservoir conditions. A laboratory analysis of the recombined surface fluid production is the most accurate source of these properties; however, in the absence of such an analysis, we can estimate these properties using correlations of surface production data. These correlations are recommended for fluids in

which the total non-hydrocarbon components (i.e., CO_2, H_2S, and N_2) do not exceed 20%.[7]

According to Gold et al., for a three-stage separation system consisting of a high-pressure separator, a low-pressure separator, and a stock tank, the reservoir gas gravity is estimated from a recombination of the Produced well stream.

$$\gamma_w = \frac{R_1\gamma_1 + 4{,}602\gamma_0 + R_2\gamma_2 + R_3\gamma_3}{R_1 + \frac{133{,}316\gamma_0}{M_0} + R_2 + R_3} \tag{3.18}$$

Similarly, for a two-stage separation system consisting of a high pressure separator and stock tank, the reservoir gas gravity is estimated with

$$\gamma_w = \frac{R_1\gamma_1 + 4{,}602\gamma_0 + R_3\gamma_3}{R_1 + \frac{133{,}316\gamma_0}{M_0} + R_3} \tag{3.19}$$

If the molecular weight of the stock-tank liquid (i.e., the condensates produced at the surface) is unknown, we can estimate it using either

$$M_0 = \frac{5{,}954}{\gamma_{API} - 8.811} \tag{3.20}$$

$$\text{or } M_0 = \frac{42.43\gamma_0}{1.008 - \gamma_0} \tag{3.21}$$

Accurate estimates of gas properties at reservoir conditions require that all surface gas and liquid production be recombined according to Eq. 3.18 or 3.19. However, gas production from low-pressure separators and stock tanks often is not measured.

Gold et al. developed correlations for estimating the additional gas production from the secondary separator and stock tank, G_{pa} , and the vapor equivalent of the primary

separator liquid, V_{eq}. These correlations, expressed in terms of generally available production data, are presented in Chap. 1 and are used in Eq. 3.22 to estimate the reservoir gas gravity:

$$\gamma_w = \frac{R_l\gamma_l + 4{,}602\gamma_0 + G_{pa}}{R_l + V_{eq}} \tag{3.22}$$

After the gas gravity at reservoir conditions is known, we can use the method established previously to estimate the gas deviation factor. Using this value, we can estimate the total original gas in place with Eq. 3.17.

Because of condensation, some gas at reservoir conditions is produced as liquids at the surface. The fraction of the total initial gas in place that will be produced in the gaseous phase at the surface is

$$f_g = \frac{R_t}{R_t + \dfrac{132{,}800\gamma_0}{M_0}} \tag{3.23}$$

where R_t includes gas and condensate production from all separators and the stock tank. The fraction of the original total gas in place, G_T that will be produced in the gaseous phase is

$$G = f_g G_T, \tag{3.24}$$

and the original oil (condensate) in place is

$$N = \frac{1{,}000 \cdot f_g G_T}{R_t} \tag{3.25}$$

Note that this calculation procedure is applicable to gas-condensate reservoirs only when the reservoir pressure is above the original dewpoint pressure. Gas-condensate reservoir fluids also are characteristically rich with intermediate- and heavier-weight hydrocarbon molecules. Because of this composition, a liquid phase forms not only in the wellbore and surface equipment but also in the reservoir.

The behavior of a gas-condensate fluid is illustrated with the phase diagram in Fig. 3.3.

Upon discovery, if the reservoir pressure is above the dewpoint pressure and if the temperature lies between the critical temperature and the cricondentherm, then a single-phase fluid (i.e., gas) exists in the reservoir.

Once the reservoir pressure falls below the dewpoint pressure, however, liquid hydrocarbons form in the reservoir, and we cannot use surface production data to estimate reservoir fluid properties accurately. Under these conditions, accurate estimates of the gas and condensate in place require a laboratory analysis of the reservoir fluid.

3.3 MATERIAL BALANCE METHOD

Material-balance methods provide a simple, but effective, alternative to volumetric methods for estimating not only original gas in place but also gas reserves at any stage of reservoir depletion. A material-balance equation is simply a statement of the principle of conservation of mass, or

(original hydrocarbon mass) - (produced hydrocarbon mass) = (remaining hydrocarbon mass).

In 1941, Schilthuis presented a general form of the material balance equation derived as a volumetric balance based on the simple assumption that the reservoir PV either remains constant or changes in a manner that can be predicted as a function of change in reservoir pressure. With this assumption, he equated the cumulative observed surface production

(expressed in terms of fluid production at reservoir conditions) to the expansion of the remaining reservoir fluids resulting from a finite decrease in pressure. We also can include the effects of water influx, changes in fluid phases, or PV changes caused by rock and water expansion.

Sometimes called production methods, material-balance methods are developed in terms of cumulative fluid production and changes in reservoir pressure and therefore require accurate measurements of both quantities.

Unlike volumetric methods, which can be used early in a reservoir's life, material-balance methods cannot be applied until after some development and production. However, an advantage of material-balance methods is that they estimate only the gas volumes that are in pressure communication with and that may be ultimately recovered by the producing wells. Conversely, volumetric estimates are based on the total gas volume in place, part of which may not be recoverable with the existing wells because of unidentified reservoir discontinuities or heterogeneities. Therefore, comparisons of estimates from both methods can provide a qualitative measure of the degree of reservoir heterogeneity and allow a more accurate assessment of gas reserves for a given field-development strategy.

Another advantage of material-balance methods is that, if sufficient production and pressure histories are available, application of these methods can provide insight into the predominant reservoir drive mechanism, whereas the correct use of volumetric methods requires a priori knowledge of the primary source of reservoir energy. As we shall see in the next section, a plot of p/z vs. G_p will be a straight line for a volumetric gas reservoir in which gas expansion is the primary reservoir drive mechanism. However, consistent deviations from this straight line indicate other internal or external energy sources.

Once the predominant reservoir drive mechanism has been identified, we can apply the correct material-balance plotting functions to estimate original gas in place and gas reserves.

Like volumetric methods, the form of the material-balance equation varies depending on the drive mechanism. In the following sections, we present the material-balance equations

for volumetric dry-gas reservoirs, dry-gas reservoirs with water influx, volumetric geopressured gas reservoirs, and volumetric gas-condensate reservoirs.

3.3.1 Volumetric Dry-Gas Reservoirs.

As stated, volumetric reservoirs are completely enclosed and receive no external energy from other sources, such as aquifers. If rock and connate water expansions are negligible sources of internal energy, then the dominant drive mechanism is gas expansion as reservoir pressure decreases. Comparison of typical values of gas and liquid compressibilities shows that gases can be as much as 100 or even 1,000 times more compressible than relatively incompressible liquids, so simple gas expansion is a very efficient drive mechanism, often allowing up to 90% of in-place gas to be recovered.

Assuming a constant reservoir PV over the producing life of the reservoir, we can derive a material-balance equation by equating the reservoir PV occupied by the gas at initial conditions to that occupied by the gas at some later conditions following gas production and the associated pressure reduction. Referring to the tank-type model in Fig. 3.4, we write the material-balance equation as

$$GB_{gi} = (G-G_p)B_g, \tag{3.26}$$

where

GB_{gi} = reservoir volume occupied by gas at initial reservoir pressure, res bbl, and $(G-G_p)B_g$ = reservoir volume occupied by gas after gas production at a pressure below the initial reservoir pressure, res bbl.

We can rewrite Eq. 3.26 as

$$G_p = G\left(1 - \frac{B_{gi}}{B_g}\right) \tag{3.27}$$

If we substitute the ratio of the gas FVF evaluated at initial and later conditions, $B_{gi}/B_g = (z_i p)/(z p_i)$, into Eq. 3.27, we obtain an equation in terms of the measurable quantities, surface gas production. and BHP:

$$G_p = G\left(1 - \frac{z_i p}{z p_i}\right) \tag{3.27}$$

where the gas recovery factory is

$$\left(1 - \frac{z_i p}{z p_i}\right)$$

Further, we can rewrite Eq. 3.28 as

$$\frac{p}{z} = \frac{p_i}{z_i}\left(1 - \frac{G_p}{G}\right) = \frac{p_i}{z_i} - \frac{p_i}{z_i G} G_p \tag{3.29}$$

Similar to van Everdingen et al.'s and Havlena and Odeh's graphical analysis techniques, the form of Eq. 3.29 suggests that, if the reservoir is volumetric, a plot of p/z vs. Gp will be a straight line, from which we can estimate both original gas in place and gas reserve at some abandonment conditions.

As stated earlier, if sufficient pressure and production data are available to define the line fully, we also can determine the dominant drive mechanism from the shape of the plot. Although consistent deviations from a straight line suggest other sources of reservoir

energy, errors in pressure and production measurements also can cause departures from a straight line. Obviously, early in the productive life of a reservoir when few data are available, this plotting technique may not be accurate. Fig. 3.5 shows typical shapes of p/z plots for selected gas reservoir drive mechanisms.

The same material balance is applicable to wet-gas reservoirs, but we must base z and z_i on the reservoir gas gravity and Gp must include the vapor equivalent of the condensate produced. The original gas in place, G, and the gas reserve to abandonment includes the vapor equivalent of liquid and must be corrected to determine dry-gas and gas-condensate reserves. (See Example 3.5)

3.3.2 Dry-Gas Reservoirs With Water Influx.

In the previous section, we derived a material-balance equation for a volumetric gas reservoir. A critical assumption in this derivation is that the reservoir PV occupied by the gas remained constant throughout the productive life of the reservoir. However, if the reservoir is subjected to water influx from an aquifer, this PV is reduced by an amount equal to the volume of encroaching water. In addition, the water entering the reservoir provides an important source of energy (i.e., pressure support) that must be considered in material balance calculations.

We can derive a material-balance equation for a water drive system by equating the reservoir PV occupied by the gas at initial conditions to that occupied by the gas at later conditions plus the change in PV resulting from water influx (Fig. 3.7). A general form of the material-balance equation is

$$GB_{gi} = (G-G_p)B_g + \Delta V_p \qquad (3.30)$$

where

GB_{gi} = reservoir PV occupied by gas at initial reservoir pressure, res bbl;

$(G-G_p)$ = reservoir PV occupied by gas following gas production at a pressure below the initial pressure, res bbl; and

ΔV_p = change in reservoir PV occupied by gas at later conditions due to water influx, res bbl.

Referring to Fig. 3.7, we can see that the change in reservoir PV at some reduced pressure is affected not only by the volume of water influx but also by the amount of water produced at the surface:

$$\Delta V_p = W_e - W_p B_w \tag{3.31}$$

Combining Eqs. 3.30 and 3.31 yields

$$GB_{gi} = (G-G_p)B_g + W_e - W_p B_W \tag{3.32}$$

If water influx and production are ignored, a plot of p/z vs. Gp may appear as a straight line initially but eventually will deviate from the line. The deviation will occur early for a strong water drive and later for a weak aquifer support system. Chierici and Pizzi[12] studied the effects of weak or partial water drive systems and concluded that accurate gas-in-place estimates are difficult to obtain, especially early in the production period or when the aquifer characteristics are unknown. Similarly, Bruns et al. [13] showed that significant errors in gas-in-place estimates occur if the effects of water encroachment are ignored in the material-balance calculations.

Before the effects of water influx on gas reservoir behavior were completely understood, early deviations from a straight line on a plot of p/z vs. G_p often were attributed to measurement errors. In some instances, errors in field pressure measurements can mask the effects of water influx, especially if a weak water drive is present; however, consistent deviations from a straight line suggest that the reservoir is not volumetric and that additional energy is being supplied to the reservoir. Bruns et a/.

studied the effects of water influx on the shape of the plot of p/z vs. G_p and showed that the shape and direction of the deviation from straight line depend on the strength of the aquifer support system and on the aquifer properties and the reservoir/aquifer geometry.

If the initial gas in place is known from other sources, such as volumetric estimates, we can calculate W_e from Eq. 3.32. In practice, however, usually both W_e and G are unknown, and calculation of initial gas in place requires an independent estimate of water influx. Therefore, in the next section we discuss three methods for estimating water influx.

Methods For Estimating Water Influx.

Water influx results from a reduction in reservoir pressure following gas production. Water influx tends to maintain, either partially or wholly, the reservoir pressure.

In general, both the effectiveness of the pressure support system and the water influx rates are governed by the aquifer characteristics, which principally include the permeability, thickness, areal extent, and the pressure history along the original reservoir/aquifer boundary.

Note that, in practice, estimating water influx is very uncertain, primarily because of the lack of sufficient data to characterize the aquifer (especially its geometry and areal continuity) completely.

Because wells are seldom drilled intentionally into an aquifer to gain information, these data must be either assumed or inferred from the geologic and reservoir characteristics.

Generally, reservoir/aquifer systems are classified as either edgewater or bottomwater drive. In edgewater-drive systems, water moves into the reservoir flanks, while bottomwater drive occurs in reservoirs with large areal extents and gently dipping structures where the aquifer completely underlies the reservoir. van Everdingen and Hurst's and Carter and Tracy's methods are applicable only to edgewater-drive geometries or for combined geometries that can be modeled as edgewater-drive systems, while the Fetkovich method[16] is applicable for all geometries

1. van Everdingen-Hurst's Method.

In 1949, van Everdingen and Hurst presented an unsteady-state model for predicting water influx. As Fig. 3.8 shows, the reservoir/aquifer system is modeled as two concentric cylinders or sectors of cylinders. The inside cylindrical surface, defined by radius r_r, represents the reservoir/aquifer boundary, while the outer surface is the aquifer boundary defined by r_a. Radial flow of water from the aquifer to the reservoir is described mathematically with the radial diffusivity equation '

$$\frac{\partial^2 p_D}{\partial r_D^2} + \frac{1}{r_D}\frac{\partial p_D}{\partial r_D} = \frac{\partial p_D}{\partial t_D} \tag{3.33}$$

where the dimensionless variables are defined in terms of the aquifer properties. The dimensionless pressure for constant-rate conditions at the reservoir/aquifer boundary is

$$P_D = \frac{0.00708kh(p_i - p)}{q\mu} \tag{3.34}$$

For constant-terminal-pressure conditions,

$$P_D = \frac{p_i - p}{p_i - p_r} \tag{3.35}$$

The dimensionless radius is defined in terms of r_r:

$$r_D = r/r_r \cdot \tag{3.36}$$

and for t in days,

$$t_D = \frac{0.00633kt}{\phi\mu c_t r_r^2} \tag{3.37}$$

van Everdingen and Hurst derived solutions to Eq. 3.33 for two reservoir/aquifer boundary conditions—constant terminal rate and constant terminal pressure. The water influx rate for the constant terminal-rate case is assumed constant for a given period, and the pressure drop at the reservoir/aquifer boundary is calculated. For the constant-pressure case, the water influx rate is determined for a constant pressure drop over some finite time period. Reservoir engineers usually are more interested in determining the water influx than the pressure drop at the reservoir/aquifer boundary, so
we will focus on water-influx calculations under constant-pressure conditions.

van Everdingen and Hurst derived the constant-pressure solutions in terms of a dimensionless water influx rate defined by

$$q_D = \frac{q_w \mu}{0.00708kh\Delta p} \tag{3.38}$$

Integrating both sides of Eq. 3.38 with respect to time yields

$$\int_0^{t_D} q_D dt_D = \left(\frac{\mu}{0.00708kh\Delta p}\right)\left(\frac{0.00633k}{\phi\mu c_t r_r^2}\right) \cdot \int_0^t q_w dt = \frac{1}{1.119\phi\mu c_t h r_r^2 \Delta p} \int_0^t q_w dt \tag{3.39}$$

In material-balance calculations, we are more interested in the cumulative water influx than in influx rate. Therefore, because cumulative water influx, W_e, is

$$W_e = \int_0^t q_w dt \tag{3.40}$$

and dimensionless cumulative water influx is

$$Q_{pD} = \int_0^{t_D} q_D dt_D \tag{3.41}$$

we can combine Eqs. 3.39 through 3.41 to obtain

$$Q_{pD} = \frac{W_e}{1.119 \phi \mu c_t h r_r^2 \Delta p} \tag{3.42}$$

Thus, $W_e = 1.1\ 19 \phi c_t h r^2 \Delta_P Q_{pD}$ (3.43)

If the total productive reservoir life is divided into a finite number of pressure reductions or increases, we can use superposition of the solution given by Eq. 3.43 to model the water-influx behavior for a given pressure history. This method assumes that the pressure history at the original reservoir/aguifer boundary can be approximated by a series of step-by-step pressure changes. Fig. 18.9 shows the modeling of a pressure history.

Referring to Fig. 3.9, we define the average pressure in each period as the arithmetic average of the pressures at the beginning and end of the period. Thus, for an initial aquifer pressure, p_i, the average pressure during the first time period $\overline{p_1} = \frac{1}{2}(p_i + p_1)$

Similarly, for the second time period, $\overline{p_2} = \frac{1}{2}(p_1 + p_2)$. In general, for the n^{th} time period,

$$\overline{p_n} = \frac{1}{2}(p_{n-1} + p_n)$$

We can then calculate the pressure changes between time periods as follows. Between the initial and first time periods,

$$\Delta p_0 = \left(p_i - \bar{p}_1\right) = p_i - \frac{1}{2}(p_i + p_1) = \frac{1}{2}(p_i - p_1)$$

Similarly, between the first and second time periods,

$$\Delta p_0 = \bar{p}_1 - \bar{p}_2 = \frac{1}{2}(p_i + p_1) - \frac{1}{2}(p_1 + p_2) = \frac{1}{2}(p_i - p_2)$$

In general, for the (n-1) and n^{th} time periods,

$$\Delta p_0 = \bar{p}_{n-1} - \bar{p}_n = \frac{1}{2}(p_{n-2} + p_{n-1}) - \frac{1}{2}(p_{n-1} + p_n) = \frac{1}{2}(p_{n-2} - p_n)$$

During each time increment, the pressure is assumed constant (i.e., constant-pressure solution), and the cumulative water influx for n time periods is

$$W_e(t_n) = B\sum_{i=1}^{n} \Delta p_i Q_{pD}(t_n - t_{i-1})_D \qquad (3.44)$$

where $B = 1.1\ 19\phi c_t h r_r^2$ (3.45)

If the angle subtended by the reservoir is less than 360° (Fig. 3.8). then B is adjusted as follows:

$$B = 1.119\phi c_t h r_r^2\left(\frac{\theta}{360}\right) \tag{3.46}$$

The pressure change during each time increment, as explained above, is calculated with

$$\Delta p_i = \frac{1}{2}(p_{i-2} - p_i),\ i = 1,2...n \tag{3.47}$$

and $p_{i-2} = p_O$ = initial pressure. Each Δp_i in Eg. 3.44 is multiplied by the dimensionless cumulative water influx, Q_{PD}. evaluated at a dimensionless time corresponding to the time for which Δp_i has been in effect. For example, Δp_i will have been in effect for the total productive life of the reservoir, so Q_{PD} will be evaluated at $(t_1 - 0)_D$. In general, Δp_n will have been in effect for the time period $t-t_{n-1}$ so Q_{PD} that multiplies Δp_n will be evaluated at $(t-t_{n-1})_D$.

To simplify calculations, Tables 3.1 and 3.2 present values for dimensionless cumulative water influx as a function of time for both infinite-acting and finite aquifers.

Alternatively, for the special case of infinite-acting aquifers, Edwardson et al. developed polynomial expressions for calculating Q_{PD}. These expressions, Eqs. 3.48 through 3.50, depend on dimensionless time:

For $t_D < 0.01$,

$$Q_{pD}(t_D) = 2\sqrt{\frac{t_D}{\pi}} \tag{3.48}$$

For $0.01 < t_D < 200$,

$$Q_{PD}(t_D) = \frac{1.2838t_D^{1/2} + 1.19328t_D + 0.269872t_D^{3/2} + 0.00855294t_D^2}{1 + 0.616599t_D^{1/2} + 0.0413008t_D} \tag{3.49}$$

For $t_D > 200$,

$$Q_{PD}(t_D) = \frac{-4.29881 + 2.02566t_D}{\ln(t_D)} \tag{3.50}$$

Similarly, Klins et al.[21] developed polynomial approximations for both infinite-acting and finite aquifers.

The van Everdingen and Hurst method also is applicable to linear flow geometries (Fig. 3.10). For linear flow, we define a dimensionless time in terms of the reservoir length, L, as

$$t_D = \frac{0.00633kt}{\phi\mu c_t L^2} \tag{3.51}$$

Following a derivation similar to that presented for radial flow, we find that the cumulative water influx for n time periods is

$$W_e(t_n) = B \sum_{i=1}^{n} \Delta p_i Q_{pD}\left(t_n - t_{i-1}\right)_D \tag{3.52}$$

where the parameter R is defined in terms of the reservoir length,

$$B = 0.178\phi\mu c_t hL \tag{3.53}$$

Derived from exact solutions to the diffusivity equation, the van Everdingen and Hurst method models all aquifer flow regimes (i.e., transient and pseudosteady-state) and is

applicable to both infinite acting and finite aquifers. Example 3.6 illustrates the following calculation procedure.

1. First, calculate the parameter B for radial flow,

$$B = 1.1\,19\phi c_t h r_r^2 \left(\frac{\theta}{360}\right) \tag{3.46}$$

or for a linear flow geometry,

$$B = 0.178\phi\mu c_t hL \tag{3.53}$$

2. Calculate the pressure change, Δp_i. between each time period,

$$\Delta p_i = \frac{1}{2}(p_{i-2} - p_i),\ i = 1,2...n$$

3. Calculate the t_D that correspond to each time period on the production history. For a radial flow geometry,

$$t_D = \frac{0.00633kt}{\phi\mu c_t r_r^2} \tag{3.37}$$

and for a linear geometry,

$$t_D = \frac{0.00633kt}{\phi\mu c_t L^2} \tag{3.51}$$

4. For each t_D computed in Step 3, calculate a dimensionless water cumulative influx, $Q_{pD}(t_D)$. For an infinite-acting aquifer we can use Eqs. 3.50 through 3.52, use Klins et al.'s[21] equations, or read the values directly from Table 3.1. For finite aquifers, we must use Klins et al.'s equations or Table 3.2.

5. Calculate the water influx:

$$W_e(t_n) = B\sum_{i=1}^{n}\Delta p_i Q_{pD}(t_n - t_{i-1})_D \tag{3.44}$$

3. Carter-Trapy Method.

van Everdingen and Hurst's method was developed from exact solutions to the radial diffusivity equation and therefore provides a rigorously correct technique for calculating water influx. However, because superposition of solutions is required, their method involves rather tedious calculations. To reduce the complexity of water influx calculations, Carter and Tracy proposed a calculation technique that does not require superposition and allows direct calculation of water influx.

If we approximate the water influx process by a series of constant influx intervals, then the cumulative water influx during the j^{th} interval is

$$W_e(t_{DJ}) = \sum_{n=0}^{J-1} q_{Dn}(t_{Dn+1} - t_{Dn}) \tag{3.54}$$

Eq. 3.54 can be rewritten as the sum of the cumulative water influx through the ith interval and between the ith and jth intervals:

$$W_e(t_{DJ}) = \sum_{n=0}^{J-1} q_{Dn}(t_{Dn+1} - t_{Dn}) + \sum_{n=i}^{J-1} q_{Dn}(t_{Dn+1} - t_{Dn}) \tag{3.55}$$

$$W_e(t_{Dj}) = W_e(t_{Di}) + \sum_{n=i}^{J-1} q_{Dn}(t_{Dn+1} - t_{Dn}) \tag{3.56}$$

Using the convolution integral, we also can express the cumulative water up to the j^{th} interval as a function of variable pressure:

$$W_e(t_{Dj}) = B \int_0^{t_{Dj}} \Delta p(\lambda) \frac{d}{d\lambda}\left[Q_{pD}(t-\lambda)\right] d\lambda \qquad (3.57)$$

Combining Eqs. 3.56 and 3.57, we use Laplace transform methods to solve for the cumulative water influx in terms of the cumulative pressure drop, ΔPn:

$$W_{en} = W_{en-1} + (t_{Dn} - t_{Dn-1})\left[\frac{B\Delta p_n - W_{en-1} p'_D(t_{Dn})}{p_D(t_{Dn}) - t_{Dn-1} p'_D(t_{Dn})}\right] \qquad (3.58)$$

where B and t_D are the same variables defined previously for the van Everdingen-Hurst method. The subscripts n and n-1 refer to the current and previous timesteps, respectively, and

$$\Delta p_n = p_{aq,i} - p_n \qquad (3.59)$$

P_D is a function of t_D and for an infinite-acting aquifer, can be computed from the following curve-fit equation:

$$P_D(t_D) = \frac{370.529(t_D)^{1/2} + 137.582(t_D) + 5.69549(t_D)^{3/2}}{328.834 + 265.488(t_D)^{1/2} + 45.2157(t_D) + (t_D)^{3/2}} \qquad (3.60)$$

In addition, the dimensionless pressure derivative, P'_D, can be approximated by a curve-fit equation.

$$P'_D(t_D) = \frac{716.441 + 46.7984(t_D)^{1/2} + 270.038(t_D) + 71.0098(t_D)^{3/2}}{1{,}296.86(t_D)^{1/2} + 1{,}204.73(t_D) + 618.618(t_D)^{3/2} + 538.072(t_D)^2 + 142.41(t_D)^{5/2}} \quad (3.61)$$

Eqs. 3.60 and 3.61 model infinite-acting aquifers; however Klins et al. developed similar polynomial approximations for both infinite and finite aquifers.

We should stress that, unlike the van Everdingen-Hurst technique,- the Carter-Tracy method is not an exact solution to the diffusivity equation, but is an approximation. Research conducted by Agarwal, however, suggests that the Carter-Tracy method is an accurate alternative to the more tedious van Everdingen-Hurst calculation technique. The primary advantage of the Carter-Tracy method is the ability to calculate water influx directly without superposition.

The Carter-Tracy method, which also is applicable to infinite acting and finite aquifers, is illustrated with the following calculation procedure and Example 3.7.

1. First, calculate the van Everdingen-Hurst parameter B for radial flow,

$$B = 1.119\phi c_t h r_r^2 \left(\frac{\theta}{360}\right) \quad (3.46)$$

or for a linear flow geometry,

$$B = 0.178\phi c_t h L \quad (3.53)$$

2. Calculate the pressure change, Δp_n, for each time period,

$$\Delta p_n = p_{aq,i} - p_n \tag{3.59}$$

3. Calculate the van Everdingen-Hurst dimensionless times, t_D, that correspond to each time period on the production history. For a radial flow geometry,

$$t_D = \frac{0.00633kt}{\phi\mu c_t r_r^2} \tag{3.37}$$

and for a linear geometry,

$$t_D = \frac{0.00633kt}{\phi\mu c_t L^2} \tag{3.51}$$

4. For each t_D computed in Step 3, calculate a P_D and a P'_D. For infinite-acting radial aquifer, we can use Eqs. 3.60 and 3.61 to calculate P_D and P'_D, respectively:

$$P_D(t_D) = \frac{370.529(t_D)^{1/2} + 137.582(t_D) + 5.69549(t_D)^{3/2}}{328.834 + 265.488(t_D)^{1/2} + 45.2157(t_D) + (t_D)^{3/2}} \tag{3.60}$$

In addition, the dimensionless pressure derivative, P'_D, can be approximated by a curve-fit equation.

$$P'_D(t_D) = \frac{716.441 + 46.7984(t_D)^{1/2} + 270.038(t_D) + 71.0098(t_D)^{3/2}}{1{,}296.86(t_D)^{1/2} + 1{,}204.73(t_D) + 618.618(t_D)^{3/2} + 538.072(t_D)^2 + 142.41(t_D)^{5/2}} \tag{3.61}$$

We also can use Klins et al's equations. For infinite aquifers, we must use Klins et al's equations

5. Calculate the water influx:

$$W_{en} = W_{en-1} + (t_{Dn} - t_{Dn-1})\left[\frac{B\Delta p_n - W_{en-1}p'_D(t_{Dn})}{p_D(t_{Dn}) - t_{Dn-1}p'_D(t_{Dn})}\right] \qquad (3.58)$$

3. Ferkovich Method.

To simplify water influx calculations further, Fetkovich proposed a model that uses a pseudosteady-state aquifer Pl and an aquifer material balance to represent the system compressibility. Like the Carter-Tracy method, Fetkovich's model eliminates the use of superposition and therefore is much simpler than van the Everdingen-Hurst method. However, because Fetkovich neglects the early transient time period in these calculations, the calculated water influx will always be less than the values predicted by the previous two models.

Similar to fluid flow from a reservoir to a well, Fetkovich used an inflow equation to model water influx from the aquifer to the reservoir. Assuming constant pressure at the original reservoir/aquifer boundary, the rate of water influx is

$$q_w = \frac{dW_e}{dt} = J\left(\overline{P_{aq}} - P_r\right)^n \qquad (3.62)$$

where

n = exponent for inflow equation (for flow obeying Darcy's law, n = l; for fully turbulent flow, n = 0.5).

Assuming that the aquifer flow behavior obeys Darcy's law and is at pseudosteady-state conditions, n = 1. Based on an aquifer material balance, the cumulative water influx resulting from aquifer expansion is

$$W_e = c_t W_i \left(P_{aq,i} - \overline{P_{aq}} \right) \tag{3.63}$$

Eq. 3.63 can be rearranged to yield an expression for the average aquifer pressure,

$$\overline{P_{aq}} = P_{aq,i}\left(1 - \frac{W_e}{c_t W_i P_{aq,i}} \right) = P_{aq,i}\left(1 - \frac{W_e}{W_{ei}} \right) \tag{3.64}$$

where $W_{ei} = c_t P_{aq,i} W_i$ (3.65)

is defined as the initial amount of encroachable water and represents the maximum possible aquifer expansion.

After differentiating Eq. 3.64 with respect to time and rearranging, we have

$$\frac{dW_e}{dt} = -\frac{W_{ei}}{p_i}\frac{d\overline{P_{aq}}}{dt} \tag{3.66}$$

Combining Eqs. 3.62 and 3.66 and integrating yields

$$\int_{P_{aq,i}}^{\overline{P}_{aq}} \frac{d\overline{P}_{aq}}{\overline{P}_{aq} - P_r} = -\int_0^t \frac{JP_i}{W_{ei}} dt' \tag{3.67}$$

$$\text{or } \overline{P_{aq}} - P_r = \left(P_{aq} - P_{aq,i} \right) e^{-\frac{JP_i t}{W_{ei}}} \tag{3.69}$$

Table 3.10 summarizes the equations for calculating the aquifer PI for various reservoir/aquifer boundary conditions and aquifer geometries. Note that we must use the aquifer properties to calculate J.

From Eq. 3.67, we can derive an expression for ($\overline{P_{aq}}$ -P_r), and following substitution into Eq. 3.68 and rearranging, we have

$$\frac{dW_e}{dt} = J\left(P_{aq,i} - P_r\right)e^{-\frac{JP_i t}{W_{ei}}} \tag{3.69}$$

which is integrated to obtain the cumulative water influx. W_e:

$$W_e = \frac{W_{ei}}{P_{aq,i}}\left(P_{aq,i} - P_r\right)\left(1 - e^{-\frac{JP_{aq,i} t}{W_{ei}}}\right) \tag{3.70}$$

Recall that we derived Eq. 3.10 for constant pressure at the reservoir/aquifer boundary. In reality, this boundary pressure changes as gas is produced from the reservoir. Rather than using superposition, Fetkovich assumed that, if the reservoir/aquifer boundary pressure history is divided into a finite number of time intervals, the incremental water influx during the nth interval is

$$\Delta W_{en} = \frac{W_{ei}}{P_{aq,i}}\left(\overline{P}_{aq,n-1} - \overline{P_{rn}}\right)\left[1 - e^{-\frac{JP_{aq,i}\Delta t_n}{W_{ei}}}\right] \tag{3.71}$$

where

$$\bar{P}_{aq,n-1} = P_{aq,i}\left(1 - \frac{W_{e,n-1}}{W_{ei}}\right) \tag{3.72}$$

$$\bar{P}_m = \frac{P_{m-1} + P_m}{2} \tag{3.73}$$

Although it was developed for finite aquifers, Fetkovich's method can be extended to infinite-acting aquifers. For infinite-acting aquifers, the method requires the ratio of water influx rate to pressure drop to be approximately constant throughout the productive life of the reservoir. Under these conditions, we must use the aquifer PI for an infinite-acting aquifer.

The following **calculation procedure** illustrates this method.

1. Calculate the maximum water volume, W_{ei}, from the aquifer that could enter the gas reservoir if the reservoir pressure were reduced to zero.

$$W_{ei} = c_t P_{aq,i} W_i \tag{3.65}$$

where W_i depends on the reservoir geometry and the PV available to store water.

2. Calculate J. Note that the equations summarized in Table 3.10 depend on the boundary conditions and aquifer geometry.

3. Calculate the incremental water influx, ΔW_{en}, from the aquifer during the nth time interval.

$$\Delta W_{en} = \frac{W_{ei}}{P_{aq,i}}\left(\bar{P}_{aq,n-1} - \bar{P}_m\right)\left[1 - e^{-\frac{JP_{aq,i}\Delta t_n}{W_{ei}}}\right] \tag{3.71}$$

4. Calculate W_{en}:

$$W_{en} = \sum_{i=1}^{n} \Delta W_{ei}$$

Estimating Original Gas In Place With Material Balance For A Dry-Gas Reservoir With Water Influx

Once the water influx has been calculated, we can estimate the original gas in place with material-balance concepts. The general form of the material-balance equation including water influx:

$$GB_{gi} = (G-G_p)B_g+W_e-B_WW_P, \tag{3.74}$$

which can be rearranged to yield

$$\frac{G_pB_g + W_pB_w}{(B_g - B_{gi})} = G + \frac{W_e}{(B_g - B_{gi})} \tag{3.75}$$

If we define a water influx constant, C, in terms of the cumulative water influx as

$$W_e = Cf(p,t), \tag{3.76}$$

then Eq. 3.75 becomes

$$\frac{G_pB_g + W_pB_w}{(B_g - B_{gi})} = G + \frac{Cf(p,t)}{(B_g - B_{gi})} \tag{3.77}$$

The form of Eq. 3.77 suggests that, if water influx is the predominant reservoir drive mechanism, then a plot of $[(G_eB_g)+(W_pB_W)]/(B_g - B_{gi})$ vs. $f(p,t)/(B_g-B_{gi})$ will be a straight line with a slope equal to C and an intercept equal to G. The functional form of f(p,t) varies according to the water influx model used. Any water influx model, such as steady state, unsteady state, or pseudosteady state, can be used with Eq. 3.77.

Note that, if the incorrect water influx model is assumed, the data may not exhibit a straight line. Example 3.9 illustrates the application of Eq. 3.77 for an unsteady-state water influx model.

3.3.3 Volumetric Geopressured Gas Reservoirs.

We developed the material-balance equation for a volumetric dry-gas reservoir assuming that gas expansion was the dominant drive mechanism and that expansions of rock and water are negligible during the productive life of the reservoir. These assumptions are valid for normally pressured reservoirs (i.e., reservoirs with initial pressure gradients between 0.43 and 0.5 psi/ft) at low to moderate pressures when the magnitude of gas compressibilities greatly exceeds the effects of rock and connate water compressibilities. However, for abnormally or geopressured reservoirs, pressure gradients often approach values equal to the overburden pressure gradient (i.e., ~ 1.0 psi/ft). In these and other higher-pressure reservoirs, the changes in rock and water compressibilities may be important and should be considered in material-balance calculations.

Following Ramagost et al.'s[23] derivation, we begin with Eq. 3.26 for a normally pressured volumetric gas reservoir and include the effects of changing water volume, ΔV_w, and formation (rock) volume, ΔV_f. As Fig. 3.12 shows, the general form of the material-balance equation for a volumetric geopressured reservoir is

$$GB_{gi} = (G-G_p)B_g + \Delta V_w + \Delta V_f, \qquad (3.78)$$

where

GB_{gi} = reservoir volume occupied by gas at initial reservoir pressure, RB;

$(G-G_p)B_g$ = reservoir volume occupied by gas after gas production at a pressure below the initial reservoir pressure, RB;

ΔV_w = increase in reservoir PV occupied by connate water and following water expansion at a pressure below the initial reservoir pressure, RB; and

ΔV_f = increase in reservoir PV occupied by formation (rock) at a pressure below the initial reservoir pressure, RB.

The expansion of the connate water following a finite pressure decrease can be modeled with isothermal water compressibility:

$$c_w = -\frac{1}{V_w}\left(\frac{\partial V_w}{\partial p}\right)_T \cong -\frac{1}{V_{wi}}\frac{\Delta V_w}{\Delta p}, \tag{3.79}$$

where V_{wi} = initial reservoir volume occupied by the connate water.

We can arrange Eq. 3.79 in terms of the change in water volume,

$$\Delta V_w = -c_w V_{wi} \Delta p, \tag{3.80}$$

where $\Delta p = p-p_i$. We can also write the original water volume in terms of the original gas in place:

$$V_{wi} = \frac{S_{wi} GB_{gi}}{(1-S_{wi})} \tag{3.81}$$

Substituting Eq. 3.81 into Eq. 3.80 and noting that $-\Delta p = p_i-p$ yields

$$\Delta V_w = c_w(p_i - p)\frac{S_{wi}GB_{gi}}{(1-S_{wi})} \tag{3.82}$$

Similarly, the decrease in PV, Δp, caused by a finite reduction in pore pressure can be modeled with

$$c_f = -\frac{1}{V_p}\left(\frac{\partial V_p}{\partial p}\right)_T, \tag{3.83a}$$

and thus,

$$\bar{c}_f = \frac{1}{V_{pi}}\frac{\Delta V_p}{\Delta p}, \tag{3.83b}$$

where $\bar{c}_f$ = average formation compressibility over the finite pressure interval, Δp.
In terms of the change in PV, Eq. 3.83 becomes

$$\Delta V_p = \bar{c}_f V_{pi} \Delta p \tag{3.84}$$

where $\Delta p = p - p_i$. Again, we can write the original rock PV in terms of the original gas in place as

$$V_{pi} = \frac{GB_{gi}}{(1-S_{wi})} \tag{3.85}$$

Substituting V_{pi} from Eq. 3.85 into Eq. 3.84 and noting that $-\Delta p = p_i - p$, and $\Delta V_p = -\Delta V_f$ (the change in rock volume) yields

$$-\Delta V_p = \bar{c}_f (p_i - p)\frac{GB_{gi}}{(1-S_{wi})} = \Delta V_f \tag{3.86}$$

Substituting Eqs. 3.82 and 3.86 into Eq. 3.78, we can now write a general material-balance equation for a volumetric geopressured reservoir:

$$GB_{gi} = (G - G_p)B_g + \frac{c_w (p_i - p) S_{wi} GB_{gi}}{(1-S_{wi})} + \frac{\bar{c}_f (p_i - p) GB_{gi}}{(1-S_{wi})} \tag{3.87}$$

After simplification, Eq. 3.87 becomes

$$GB_{gi} = (G - G_p)B_g + \frac{GB_{gi}(p_i - p)}{(1-S_{wi})}(c_w S_{wi} + \bar{c}_f) \tag{3.88}$$

$$\text{or } G\left[1 - \frac{(c_w S_{wi} + \bar{c}_f)(p_i - p)}{(1-S_{wi})}\right]\frac{B_{gi}}{B_{gi}} = G - G_p \tag{3.89}$$

Substituting $B_{gi}/B_g = pz_i/p_i z$ into Eq.3.89 and rearranging, we have

$$\frac{p}{z}\left[1 - \frac{(c_w S_{wi} + \bar{c}_f)(p_i - p)}{(1-S_{wi})}\right] = \frac{p_i}{z_i} - \frac{p_i}{z_i}\frac{G_p}{G} \tag{3.90}$$

Note that, when the effects of rock and water compressibility are negligible, Eq. 3.90 reduces to the material-balance equation in which gas expansion is the primary source of reservoir energy (Eq. 3.29).

Failure to include the effects of rock and water compressibilities in the analysis of high-pressure reservoirs can result in errors in both original gas in place and subsequent gas reserve estimates.

We present two analysis techniques based on Eq. 3.90 for volumetric geopressured reservoirs.

Estimating Original Gas in Place When Average Formation compressibility Is Known.

If $\bar{c}_f$ is assumed to be constant with time, the form of Eq. 3.90 suggests that a plot of

$$\frac{p}{z}\left[1-\frac{\left(c_w S_{wi}+\bar{c}_f\right)\left(p_i-p\right)}{\left(1-S_{wi}\right)}\right] \text{ vs } G_p$$

will be a straight line with slope equal to $-p_i/z_i\, G$ and an intercept equal to p_i/z_i.

At $p/z = 0$, $G_p = G$, so extrapolation of the line to $p/z = 0$ provides an estimate of original gas in place. Example 3.10 illustrates this analysis technique.

Simultaneous Determination of Average Formation Compressibility and Original Gas in Place.

Roach developed a material-balance technique for simultaneously estimating formation compressibility and original gas in place in geopressured reservoirs. Beginning with Eq. 3.90, Roach presented the material-balance equation in the following form:

$$\frac{1}{\left(p_i-p\right)}\left(\frac{p_i z}{p z_i}-1\right)=\frac{1}{G}\left[\frac{G_p}{\left(p_i-p\right)}\frac{p_i z}{p z_i}\right]-\frac{c_w S_{wi}+\bar{c}_f}{1-S_{wi}} \qquad (3.91)$$

Again, if $\overline{c_f}$ is constant, the form of Eq. 3.91 suggests that a plot of

$$\frac{1}{(p_i - p)}\left(\frac{p_i z}{z_i p} - 1\right) \text{ vs } \left[\frac{G_p}{(p_i - p)}\frac{p_i z}{z_i p}\right]$$

will be a straight line with a slope that equals 1/G and an intercept that equals $-(S_{wi}c_w + \overline{c_f}/1-S_{wi})$.

We can then calculate the original gas in place, G, and the average formation compressibility, $\overline{c_f}$, using the slope and intercept, respectively.

Poston and Chen[26] applied this method to the geopressured gas reservoir data presented in Example 3.10. Their analysis is reproduced in Example 3.11. ◦

3.3.4 VOLUMETRIC GAS-CONDENSATE RESERVOIRS.

In this section, we develop material-balance equations for a volumetric gas reservoir with gas condensation during pressure depletion. We also include the effects of connate water vaporization. Both phenomena are most prevalent in deep, high-temperature, high-pressure gas reservoirs and must be included for accurate material-balance calculations.

Depending on whether the pressure is above or below the dewpoint, two or three fluid phases may be present in a gas-condensate reservoir. Above the dewpoint, the vapor phase consists of not only hydrocarbon and inert gases but also water vapor. As the reservoir pressure declines, the water in the liquid phase continues to vaporize to remain in equilibrium with the existing water vapor, thus decreasing the saturation of the liquid water in the reservoir and increasing the PV occupied by the vapor phases. As the reservoir pressure declines further, the amount of water vapor present in the gas phase may increase significantly. However, as the reservoir pressure decreases below the

dewpoint, the fraction of PV available for the vapor phases decreases as liquids condense from the hydrocarbon vapor phase.

To develop á material-balance equation that considers the effects of gas condensation and water vaporization requires that we include the changes in reservoir PV resulting from these phenomena. We begin with a material-balance equation for gas-condensate reservoirs. We then extend this equation to include the effects of connate water vaporization. In addition, because changes in formation compressibilities often are significant in these deep, high-pressure gas reservoirs, we include geopressured effects.

Gas-Condensate Reservoirs.

We derived the material-balance equations in previous sections for dry gases with the inherent assumption that no changes in hydrocarbon phases occurred during pressure depletion. Unlike dry-gas reservoirs, gas-condensate reservoirs are characteristically rich with intermediate and heavier hydrocarbon molecules. At pressures above the dewpoint, gas condensates exist as a single-phase gas; however, as the reservoir pressure decreases below the dewpoint, the gas condenses and forms a liquid hydrocarbon phase. Often, a significant volume of this condensate is immobile and remains in the reservoir. Therefore, correct application of material-balance concepts requires that we consider the liquid volume remaining in the reservoir and any liquids produced at the surface.

Assuming that the initial reservoir pressure is above the dewpoint, the reservoir PV is occupied initially by hydrocarbons in the gaseous phase (Fig. 3.16), or

$$V_{pi} = V_{hvi} \tag{3.92}$$

The reservoir PV occupied by hydrocarbons in the gaseous phase also can be written as

$$V_{hVi} = G_T B_{gi} \tag{3.93}$$

where G_T includes gas and the gaseous equivalent of produced condensates and B_{gi} is defined by Eq. 3.7.

At later conditions following a pressure reduction below the dewpoint, the reservoir PV is now occupied by both gas and liquid hydrocarbon phases, or

$$V_p = V_{hv} + V_{hL} \tag{3.94}$$

where

V_p = reservoir PV at later conditions, RB;

V_{hv} = reservoir volume occupied by gaseous hydrocarbons at later conditions, RB; and

V_{hL} = reservoir PV occupied by liquid hydrocarbons at later conditions, RB.

Eq. 3.94 assumes that rock expansion and water vaporization are negligible. In terms of the condensate saturation, S_O, we can write

$$V_{hv} = (1-S_O)V_P \,. \tag{3.95}$$

$$\text{and } V_{hL} = S_o V_p. \tag{3.96}$$

In addition, the hydrocarbon vapor phase at later conditions is

$$V_{hv} = \left(G_T - G_{pT}\right)B_g \tag{3.97}$$

where B_g is evaluated at later conditions.

Equating Eqs. 3.95 and 3.97, the reservoir PV is

$$V_p = \frac{(G_T - G_{pT})B_g}{(1-S_o)} \tag{3.98}$$

Substituting Eq. 3.98 into Eq. 3.95 and combining with Eq. 3.97 yields an expression for the reservoir PV at later conditions:

$$(G_T - G_{pT})B_g + \frac{S_o(G_T - G_{pT})B_g}{(1-S_o)} \tag{3.99}$$

Now, combining Eqs. 3.92 and 3.99 yields the following material-balance equation:

$$G_T B_{gi} = (G_T - G_{pT})B_g + \frac{S_o(G_T - G_{pT})B_g}{(1-S_o)} \tag{3.100}$$

or, if we substitute $B_{gi}/B_g = (pz_i)/(p_i z)$ into Eq. 3.100 and rearrange,

$$(1-S_o)\frac{p}{z} = \frac{p_i}{z_i}\left(1 - \frac{G_{pT}}{G_T}\right) \tag{3.101}$$

which suggests that a plot of $(1-S_0)(p_i z)$ vs. G_{pT} will be a straight line from which G_T can be estimated.

Correct application of Eq. 3.101, however, requires estimates of the liquid hydrocarbon volumes formed as a function of pressure below the dewpoint. The most accurate source of these estimates is a laboratory analysis of the reservoir fluid samples. Unfortunately, laboratory analyses of fluid samples often are not available.

An **alternative material-balance technique** is

$$G_T B_{2gi} = \left(G_T - G_{pT}\right) B_{2g} \tag{3.102}$$

where

$G_T B_{2gi}$ = reservoir PV occupied by the total gas, which includes gas and the gaseous equivalent of the produced condensates, at the initial reservoir pressure above the dewpoint, RB;

$(G_T - G_{pT})B_{2g}$ = reservoir PV occupied by hydrocarbon vapor phase and the vapor equivalent of liquid phase after some production at a pressure below the initial reservoir pressure and dewpoint pressure, RB; and B_{2gi} and B_{2g} = gas FVF's based on two-phase z factors at initial and later conditions, respectively, RB/Mscf.

If we substitute $B_{2gi}/B_{2g} = (PZ_{2i})/(P_i Z_2)$ into Eq. 3.102 and rearrange, we have

$$\frac{p}{z_2} = \frac{p_i}{z_{2i}}\left(1 - \frac{G_{pT}}{G_T}\right) \tag{3.103}$$

where z_{2i} and z_2 = two-phase gas deviation factors evaluated at initial reservoir pressure and at a later pressure, respectively.

The form of Eq. 3.103 suggests that a plot of P/Z_2 vs. G_{pT} will be a straight line for a volumetric gas-condensate reservoir when two-phase gas deviation factors are used.

Two-phase gas deviation factors account for both gas and liquid phases in the reservoir. Fig. 3.17 is an example of the relationship between the equilibrium gas (i.e., single-phase gas) and two phase deviation factors for a gas-condensate reservoir.

At pressures above the dewpoint, the single- and two-phase z factors are equal; at pressures below the dewpoint, however, the two-phase z factors are lower than those for the single-phase gas.

Ideally, two-phase gas deviation factors are determined from a laboratory analysis of reservoir fluid samples. Specifically, these two-phase z factors are measured from a

constant-volume depletion study. However, in the absence of a laboratory study, correlations are available for estimating two-phase z factors from properties of the well-stream fluids.

Gas-Condensate Reservoirs With Water Vaporization.

In this section, we develop a material-balance equation for gas-condensate reservoirs in which both phase changes and water vaporization occur. Similar to Humphreys' work, we include the effects of rock and water compressibilities, which are often significant in deep, high-pressure reservoirs. The reservoir PV is occupied initially by hydrocarbon and water vapor phases as well as the connate liquid phase, or

$$V_{pi} = V_{vi} + V_{wi} \tag{3.104}$$

where

V_{vi} = initial reservoir PV occupied by hydrocarbon and water vapors, RB, and

V_{wi} = initial reservoir PV occupied by the liquid water, RB.

If the reservoir pressure is above the dewpoint, connate water is the only liquid phase present. From the definition of water saturation, we can write the initial reservoir PV occupied by the liquid phase as

$$V_{wi} = S_{wi} V_{pi} \tag{3.105}$$

Similarly, we can express the initial reservoir volume of the vapor phases as

$$V_{vi} = (1-S_{wi})V_{pi} . \tag{3.106}$$

Now, we define the fraction of the initial vapor phase volume that is water vapor as

$$y_{wi} = V_{wvi}/V_{vi} \tag{3.107}$$

and the fraction occupied by the hydrocarbon gases as

$$(1-y_{wi}) = V_{hvi}/V_{vi} \tag{3.108}$$

where

V_{wvi} = initial reservoir PV occupied by water vapor, RB, and

V_{hvi} = initial reservoir PV occupied by hydrocarbon vapor, RB.

Substituting Eq. 3.106 into Eq. 3.108 gives an expression for the hydrocarbon vapor-phase volume in terms of the initial reservoir PV:

$$V_{hvi} = V_{pi}(1-S_{wi})(1-y_{wi}). \tag{3.109}$$

Finally, because the initial hydrocarbon vapor phase is the original gas in place.

$$V_{hvi} = G\,B_{gi}, \tag{3.110}$$

$$\text{then } V_{pi} = \frac{GB_{gi}}{(1-S_{wi})(1-y_{wi})} \tag{3.111}$$

The form of the material-balance equation at some pressure lower than the initial reservoir pressure depends on the value of the dewpoint. Therefore, we will develop material-balance equations for depletion at pressures above and below the dewpoint.

Depletion at Pressures Above the Dewpoint.

Because the reservoir pressure is still above the dewpoint, no hydrocarbon gas has condensed. However, as the pressure declines, more of the liquid water vaporizes, thus reducing the liquid water saturation.

Therefore, the volume of liquid phase becomes (Fig. 3.18)

$$V_w = S_w V_p. \tag{3.112}$$

where S_w = current value of connate water saturation. Similarly, the volume of the vapor phase is

$$V_v = (1-S_w)V_p \tag{3.113}$$

In addition, we define the fraction of the vapor phase that is water vapor as

$$y_w = V_{wv}/ V_v \tag{3.114}$$

and the fraction of vapor phase that is hydrocarbon as

$$(1-y_w) = V_{hv}/ V_v \tag{3.114}$$

If we substitute Eq. 3.113 into Eq. 3.115, we can write an expression for the hydrocarbon vapor phase in terms of the current reservoir PV:

$$V_{hv} = V_p(1-S_w)(1-y_w). \tag{3.116}$$

The current hydrocarbon vapor phase is

$$V_{hV} = (G - G_p)B_g. \tag{3.117}$$

Combining Eqs. 3.116 and 3.117 gives the current reservoir

$$V_p = \frac{\left(G - G_p\right) B_g}{(1-S_w)(1-y_w)} \tag{3.118}$$

Like geopressured gas reservoirs, deep, high-pressured gascondensate reservoirs often experience significant changes in PV during pressure depletion. Therefore, using a method similar to that presented in the section on geopressured gas reservoirs, we can express the change in reservoir formation (rock) volume in terms of the formation compressibility as

$$\Delta V_f = \frac{\overline{c_f}\left(p_i - p\right) GB_{gi}}{(1-S_{wi})(1-y_{wi})} \tag{3.119}$$

In terms of Eq. 3. 119, the material-balance equation for pressures above the dewpoint becomes

$$\frac{G\,B_{gi}}{(1-S_{wi})(1-y_{wi})} = \frac{\left(G - G_p\right) B_g}{(1-S_w)(1-y_w)} + \frac{\overline{c_f}\left(p_i - p\right) GB_{gi}}{(1-S_{wi})(1-y_{wi})} \tag{3.120}$$

Rearranging terms gives

$$G\frac{(1-S_w)}{(1-S_{wi})}\frac{(1-y_w)}{(1-y_{wi})}\frac{B_g}{B_{gi}}\left[1-\overline{c_f}(p_i-p)\right]=\left(G-G_p\right) \tag{3.121}$$

Substituting $B_{gi}/B_g = PZ_i/P_iZ$ into Eq. 3.121 and rearranging yields

$$\frac{(1-S_w)}{(1-S_{wi})}\frac{(1-y_w)}{(1-y_{wi})}\left[1-\overline{c_f}(p_i-p)\right]\frac{p}{z}=\frac{p_i}{z_i}-\frac{p_i}{z_i}\frac{G_p}{G} \tag{3.122}$$

The form of Eq. 3.122 suggests that a plot of

$$\frac{(1-S_w)}{(1-S_{wi})}\frac{(1-y_w)}{(1-y_{wi})}\left[1-\overline{c_f}(p_i-p)\right]\frac{p}{z} \text{ vs } G_p$$

will be a straight line with a slope equal to $-p_i/z_iG$ and an intercept equal to P_i/Z_i- At $p/z = O$, $Gp = G$, so extrapolation of the straight line to $p/z = 0$ provides an estimate of original gas in place. Note that, if the water saturation remains constant during the life of the reservoir (i.e., $S_w = S_{wi}$ and $Y_w = Y_{wi}$) and when formation compressibility is negligible, Bq. 3.122 reduces to Eq. 3.29 for a volumetric dry-gas reservoir.

Depletion at Pressures Below the Dewpoint.

When reservoir pressures decrease below the dewpoint, the gas phase condenses. In many gas-condensate reservoirs, the liquid hydrocarbons formed in the reservoir remain immobile. Therefore, we must modify Eq. 3.120 to include this additional liquid phase (Fig. 3.19).

Adding the liquid phase gives

$$\frac{G\,B_{gi}}{(1-S_{wi})(1-y_{wi})}=\frac{\left(G-G_p\right)B_g}{(1-S_w-S_o)(1-y_w)}+\frac{\overline{c_f}(p_i-p)\,GB_{gi}}{(1-S_{wi})(1-y_{wi})} \tag{3.123}$$

where S_O = liquid hydrocarbon phase (i.e., condensate) saturation.

After rearranging Eq. 3.123, we write a material-balance equation similar in form to Eq. 3.122:

$$\frac{(1-S_w-S_o)}{(1-S_{wi})}\frac{(1-y_w)}{(1-y_{wi})}\left[1-\bar{c}_f(p_i-p)\right]\frac{p}{z}=\frac{p_i}{z_i}-\frac{p_i}{z_i}\frac{G_p}{G} \qquad (3.123)$$

Again, the form of Eq. 3.124 suggests that a plot of

$$\frac{(1-S_w-S_o)}{(1-S_{wi})}\frac{(1-y_w)}{(1-y_{wi})}\left[1-\bar{c}_f(p_i-p)\right]\frac{p}{z} \text{ vs } G_p$$

will be a straight line with a slope equal to p_i/z_iG and an intercept equal to p_j/z_i.

At $p/z = 0$, $G_p = G$, so extrapolation of the straight line to $p/z = 0$ provides an estimate of original gas in place. Again, the gas deviation factors in Eqs. 3.122 and 3.124 should be two-phase z factors representing both gas and liquid hydrocarbon phases in the reservoir. In addition, gas production should include not only production from all separators and the stock tank but also the gaseous equivalent of the produced condensates.

The water vapor content of a gas has been shown[31] to be dependent on pressure, temperature, and gas composition. Gas composition also has more effect on water vapor content at higher pressures. Unfortunately, laboratory analyses of gas usually do not quandfy the amount of water vapor; however , empirical methods are available for estimating the water vapor content of a gas.

Correct application of Eq. 3.124 also requires estimates of the liquid hydrocarbon volumes formed at pressures below the dewpoint. The most accurate source of these estimates is a laboratory analysis of the reservoir fluid samples. These liquid saturations are obtained from a constant-volume depletion study. Note that this type of laboratory fluid study assumes that the liquid hydrocarbons formed in the reservoir are immobile.

This assumption is valid for most gas-condensate reservoirs; however, some very rich gascondensate fluids may be characterized by mobile liquid saturations. For these conditions, compositional simulators are required to model the multiphase flow and predict future performance accurately.

3.4. NUMERICAL APPLICATIONS

EXAMPLE 3.4.1

Calculating Original Gas In Place in a Volumetric Dry-Gas Reservoir.

The following reservoir data were estimated from subsurface maps, core analysis, well tests, and fluid samples obtained at several wells. Use these data with the volumetric method to estimate original gas in place.

Assume a volumetric dry-gas reservoir.

P_i = 2,500 psia.

A = 1,000 acres.

T = 180°F.

ϕ = 20%.

S_{wi}= 25%.

h = 10 ft.

z_i = 0.860.

Solution.

1. First, calculate B_{gi}. Z_i was estimated with methods presented in Chap. 1.

$$B_{gi} = \frac{5.02 z_i T}{p_i} = \frac{5.02(0.860)(180+460)}{2{,}500} = 1105 \text{ RB / Mscf.}$$

2. The original gas in place for a volumetric dry-gas reservoir is given by Eq. 3.6:

$$G_p = \frac{7{,}758 A h \phi (1 - S_{wi})}{B_{gi}} = \frac{7{,}758(1{,}000)(10)(0.20)(1 - 0.25)}{1.105} = 10{,}531 \times 10^3 \text{ Mscf} = 10.5 \text{ Bscf}$$

EXAMPLE 3.4.2

Calculating Gas Reserves and Recovery Factor for a Gas Reservoir With Water Influx.

Calculate the gas reserve and the gas recovery factor using the data given in Example 3.1 and assuming that the residual gas saturation is 35% at an abandonment pressure of 750 psia. Assume that the volumetric sweep efficiency is 100%.

p_i = 2,500 psia.

A = 1.000 acres.

Z_i = 0.860.

S_{wi} = 0.25

P_a = 750 psia.

h = 10 ft.

Za = 0.550.

S_{gr} = 0. 35

ϕ = 20%.

T = 180 ^{0}F

E_V = 100

Solution

1. First, calculate the gas FVF at initial and abandonment conditions. The gas FVF at initial conditions, calculated in Example 3.1, is B_{gi} = 1.105 Mscf.

The gas FVF at abandonment is

$$B_{ga} = \frac{5.02 z_a T}{p_a} = \frac{5.02(0.550)(180+460)}{750} = 2.356 \text{ RB / Mscf.}$$

2. The gas reserve at an abandonment pressure of 750 psia is estimated with Eq. 3.16:

$$G_p = \frac{7{,}758Ah\phi(1-S_{wi})}{B_{gi}}\left[1-E_V\frac{B_{gi}}{B_{ga}}\left(\frac{S_{gr}}{S_{gi}}+\frac{(1-E_V)}{E_V}\right)\right]=$$

$$\frac{7{,}758(1{,}000)(10)(0.20)(1-0.25)}{1.105}\left[1-\frac{1.105}{2.356}\left(\frac{0.35}{(1-0.25)}\right)\right]=8{,}226\text{x}10^3 \text{ Mscf}=8.2 \text{ Bscf}$$

EXAMPLE 3.4.3

Calculating Gas Reservoir and Recovery Factor for a Gas Reservoir With Water Influx.

Using the same data from Example 3.2, calculate the gas reserve and the gas recovery factor if S_{gr} = 35% at P_a = 750 psia and E_V = 60%.

A = 1,000 acres.

z_i = 0.860.

S_{wi} = 25%.

p_i = 2,500 psia.

B_{gi} =1.105 RB/Mscf.

h = 10 ft.

Za = 0.550

S_{gr} = 0.35

Pa = 750 psia.

Bga = 2.356 RB/Mscf.

ϕ = 20%.

T = 180°F.

Ev = 60%.

Solution

1. Gp is calculated with Eq. 3.16.

$$G_p = \frac{7{,}758Ah\phi(1-S_{wi})}{B_{gi}} - \left[1 - E_V \frac{B_{gi}}{B_{ga}}\left(\frac{S_{gr}}{S_{gi}} + \frac{(1-E_V)}{E_V}\right)\right] =$$

$$= \frac{7{,}758(1{,}000)(10)(0.20)(1-0.25)}{1.105} x\left[1-(0.60)\frac{1105}{2.356}\left(\frac{(0.35)}{(0.75)} + \frac{1-0.60}{0.60}\right)\right] = 7{,}172x10^3 \text{ Mscf} = 7.2 \text{ B}$$

2. The gas recovery factor is

$$F = \left[1 - E_V \frac{B_{gi}}{B_{ga}}\left(\frac{S_{gr}}{S_{gi}} + \frac{(1-E_V)}{E_V}\right)\right] = \left[1 - (0.60)\frac{1.105}{2.356}\left(\frac{(0.35)}{(0.75)} + \frac{1-0.60}{0.60}\right)\right] = 0.681 =$$

68.1%

EXAMPLE 3.4.4

Calculating Original Gas and Condensate in Place for a Volumetric Wet-Gas Reservoir.

Estimate the total initial gas in place, the fraction of the total initial gas in place that will be produced in the gaseous phase, and the initial oil (condensate) in place using the data given below. Table 3.1 gives the initial surface production data.

P_i = 5,500 psia.

h = 50 ft

T = 288°F

ϕ = 0.21.

A = 1,000 acres.

S_{wi} = 0.32.

Solution

1. First, calculate the properties of the stock-tank oil (i.e., condensate). The specific gravity is

$$\gamma_0 = \frac{141.5}{131.5 + \gamma_{API}} = \frac{141.5}{131.5 + 54.5} = 0.76$$

From Eq. 3.20, the molecular weight of the condensate is

$$M_0 = \frac{5{,}954}{\gamma_{API} - 8.811} = \frac{5{,}954}{54.5 - 8.811} = 130.3 \text{ lbm / lbm} - \text{mol}$$

2. For a two-stage separation system, use Eq. 3.19 to calculate the gas gravity at reservoir conditions:

$$\gamma_w = \frac{R_1\gamma_1 + 4{,}602\gamma_0 + R_3\gamma_3}{R_1 + \frac{133{,}316\gamma_0}{M_0} + R_3} = \frac{(59{,}550)(0.72) + (4{,}602)(0.76) + (415)(1.23)}{(59{,}550) + \frac{133{,}316(0.76)}{(130.3)} + (415)} = 0.77$$

3. Using the method presented in Chap. I, the pseudocritical pressure and temperature are estimated to be p_{pc} = 655 psia and T_{PC} = 395°R. With these pseudocritical values, calculate the pseudoreduced pressure and temperature, respectively:

$$P_{pr} = \frac{P_i}{P_{pc}} = \frac{5{,}500}{655} = 8.40$$

and $$T_{pr} = \frac{T_i}{T_{pc}} = \frac{288 + 460}{395} = 1.89$$

Finally, using the method in Part II to estimate the gas deviation factor at original reservoir conditions gives Z_i = 1.06.

4. The gas FVF at initial reservoir conditions is

$$B_{gi} = \frac{5.02 z_i T}{p_i} = \frac{5.02(1.06)(288 + 460)}{5{,}500} = 0.72 \text{ RB / Mscf.}$$

From Eq. 3.17, the total initial gas in place, which includes gas and the gaseous equivalent of condensates, is

$$G_p = \frac{7{,}758Ah\phi(1 - S_{wi})}{B_{gi}} = \frac{7{,}758(1{,}000)(50)(0.21)(1 - 0.32)}{0.72} = 76.9 \times 10^6 \text{ Mscf} = 76.9 \text{ Bscf}$$

5. The fraction of the total initial gas in place that will be produced in the gaseous phase at the surface is

$$f_g = \frac{R_t}{R_t + \frac{132{,}800\gamma_0}{M_0}}$$

where the total producing GOR is R_t, = R_1+R_3 = 59,550+415 = 59,965 scf/STB. Therefore,

$$f_g = \frac{59{,}965}{59{,}965 + \frac{132{,}800(0.76)}{130.3}} = 0.99$$

The volume of surface gas production is

$G = f_g G_T = (0.99)(76.9) = 76.1$ Bcf.

6. The original volume of condensate in place is

$$N = \frac{1{,}000 \cdot f_g G_T}{R_t} = \frac{1{,}000 \cdot (0.99)(76.9)}{59{,}965 \text{ scf / STB}} = 1.3\text{x}10^6 \text{ STB}$$

EXAMPLE 3.4.5

Calculating Original Gas in Place Using Material Balance for a Volumetric Dry-Gas Reservoir.

Estimate the original gas in place for the reservoir described below using the material-balance equation for a volumetric dry-gas reservoir where the original reservoir pressure at discovery was p_i = 4,000 psia. Table 3.2 gives the reservoir pressure and production history.

Solution

1. First, prepare a plot of p/z vs. G_p (Fig. 3.6) using the data in Table 3.3.

2. Extrapolation of the best-fit line through the data to p/z = 0 indicates that *G = 42* MMscf. Note that, if no measurements of initial reservoir pressure are available, we also can estimate p_i from the extrapolation of the line to *Gp = 0.* For this example, p_i = 4,000 psia or p_i/z_i = 5,000 psia.

In addition, the trend of the data (i.e., a straight line) suggests that the reservoir is volumetric. As mentioned, consistent deviations from a straight line often indicate that gas expansion is not the predominant reservoir drive mechanism.

EXAMPLE 3.4.6

Estimating Water Influx With the van Everdingen-Hurst Method.

Calculate the water influx for the reservoir/aquifer system given below. Assume an infinite-acting aquifer. The estimated properties of the aquifer are given below; Table 3.4 summarizes the reservoir/aquifer pressure history.

ϕ = 0.209.

μ = 0.25 cp.

θ = 180°.

k = 275 md.

$C_t = 6x10^{-6}$ $psia^{-1}$.

h = 19.2 ft.

r, = 5,807 ft.

Solution

1. Calculate *B* using Ea. 3.46:

$$B = 1.119\phi c_t hr^2\left(\frac{\theta}{360}\right) = 1.119(0.209)(6x10^{-6})(19.2)(5,807)^2\left(\frac{180}{360}\right) = 454.3 \text{ RB/psi}$$

2. For each time period, calculate ΔP_i defined by

$$\Delta p_n = \frac{1}{2}(p_{n-2} - p_n),$$

For example, at n = 1

$$\Delta p_1 = \frac{1}{2}(p_{1-2} - p_1) = \frac{1}{2}\ (3{,}793 - 3{,}788)\ =\ 2.5 \text{ psi}$$

For n = 6,

$$\Delta p_6 = \frac{1}{2}(p_{6-2} - p_6) = \frac{1}{2}(3{,}709 - 3{,}643) = 33.0 \text{ psi.}$$

3. Calculate dimensionless times that correspond to each time on our schedule. Use the dimensionless time defined by Eq. 3.37 for a radial system:

$$t_D = \frac{0.00633kt}{\phi\mu c_t r_r^2} = \frac{0.00633(275)t}{(0.29)(0.25)\left(6x10^{-6}\right)(5{,}807)^2} = 0.165 \cdot t$$

For example, at t = 91.5 days, $t_D = 0.165(91.5) = 15.1$.

4. For each t_D computed in Step 3, calculate a dimensionless cumulative water influx. Because we are assuming an infinite-acting aquifer, we can use either Eqs. 3.48 through 3.50 or Table E-4. For this example, we have chosen to use the equations.

The value of t_D determines which equation to use. For example, at 91.5 days (n = 1), t_D = 15.1, so we use Eq. 3.49.

$$Q_{pD}(t_D) = \frac{1.2838t_D^{1/2} + 1.19328t_D + 0.269872t_D^{3/2} + 0.00855294t_D^2}{1 + 0.616599t_D^{1/2} + 0.0413008t_D} =$$

$$= \frac{1.2838(15.1)^{1/2} + 1.19328(15.1) + 0.269872(15.1)^{3/2} + 0.00855294(15.1)^2}{1 + 0.616599(15.1)^{1/2} + 0.0413008(15.1)} = 10.1$$

Table 3.5 summarizes the intermediate results from Steps 2 through 4.

5. Next, calculate W_e, using Eq. 3.44. Note that, although this calculation procedure assumes *equal* time intervals, the method also is applicable for unequal time intervals with slight modifications.

$$W_e(t_{Dn}) = B\sum_{i=1}^{n}\Delta p_i Q_{pD}(t_n - t_{i-1})_D$$

For example, at n = 1

$$W_e(t_{Dn}) = B\left[\Delta p_1 Q_{pD}(t_1 - t_0)_D\right] = B\left[\Delta p_1 Q_{pD}(t_{D1})\right] = 454.3\left[2.5(10.1)\right] = 11.471 \text{ RB}$$

Similarly, for n = 6,

$$W_e(t_{Dn}) = B\sum_{i=1}^{n}\Delta p_i Q_{pD}(t_n - t_{i-1})_D = B[\Delta p_1 Q_{pD}(t_6 - t_0)_D + \Delta p_2 Q_{pD}(t_6 - t_1)_D + \Delta p_3 Q_{pD}(t_6 - t_2)_D$$
$$+ \Delta p_4 Q_{pD}(t_6 - t_3)_D + \Delta p_5 Q_{pD}(t_6 - t_4)_D + \Delta p_6 Q_{pD}(t_6 - t_5)_D =$$

$$= 454.3[(2.5)(40.0) + (9.5)(34.5) + (20)(29.0) + (32.5)(23.1) + (34)(17.0) + (33)(10.1)]$$
$$= 1{,}212{,}890 \text{ RB}.$$

6. Table 3.6 summarizes the final results

EXAMPLE 3.4.7

Estimating Water Influx With the Carter-Tracy Method.

Calculate the water influx for the reservoir/aquifer system described in Example 3.6 and compare the results with those from the van Everdingen-Hurst method. Assume an infinite-acting aquifer. The properties of the aquifer are given below; Table 3.7 summarizes the reservoir/aquifer pressure history.

$\phi = 0.209$

$\mu = 0.25$ cp.

$\theta = 180°$.

$k = 275$ md.

$c_t = 6x10^{-6}$ psia^{-1}.

$h = 19.2$ ft.

$r_r = 5{,}807$ ft.

Solution.

1. Calculate the parameter *B* using Eq. 3.46:

$$B = 1.1\,19\phi c_t h r^2\left(\frac{\theta}{360}\right) = 1.119(0.209)(6x\ 10^{-6})(19.2)(5{,}807)^2\left(\frac{180}{360}\right) = 454.3$$

RB/psi.

2. For each time period, calculate Δp_n defined by Eq. 3.59:

$$\Delta p_n = p_{aq,i} - p_n$$

For example, at $n = 1$,

$$\Delta p_n = p_{aq,i} - p_1 = 3{,}793 - 3{,}788 = 5 \text{ psi}$$

For $n = 2$,

$$\Delta p_n = p_{aq,i} - p_2 = 3{,}793 - 3{,}774 = 19 \text{ psi}$$

3. Calculate dimensionless times that correspond to each time on the schedule. Use the dimensionless time defined by Eq. 3.37 for a radial geometry:

$$t_D = \frac{0.00633kt}{\phi\mu c_t r_r^2} = \frac{0.00633(275)t}{(0.209)(0.25)(6\text{x}10^{-6})(5{,}807)^2} = 0.165 \cdot t$$

For example, at t = 91.5 days,

$t_D = 0.165(91.5) = 15.1.$

4. Calculate dimensionless pressures and pressure derivatives at each of the dimensionless times computed in Step 3. The dimensionless pressures are calculated with Eq. 3.60. For example, at

$t_D = 15.1,$

$$P_D(t_D) = \frac{370.529(t_D)^{1/2} + 137.582(t_D) + 5.69549(t_D)^{3/2}}{328.834 + 265.488(t_D)^{1/2} + 45.2157(t_D) + (t_D)^{3/2}} =$$

$$= \frac{370.529(15.1)^{1/2} + 137.582(15.1) + 5.69549(15.1)^{3/2}}{328.834 + 265.488(15.1)^{1/2} + 45.2157(15.1) + (15.1)^{3/2}} = 1.83$$

Similarly, the dimensionless pressure derivatives are calculated with Eq. 3.61. For example, at $t_D = 15.1$,

$$P'_D(t_D) = \frac{716.441 + 46.7984(t_D)^{1/2} + 270.038(t_D) + 71.0098(t_D)^{3/2}}{1{,}296.86(t_D)^{1/2} + 1{,}204.73(t_D) + 618.618(t_D)^{3/2} + 538.072(t_D)^2 + 142.41(t_D)^{5/2}} =$$

$$= \frac{716.441 + 46.7984(15.1)^{1/2} + 270.038(15.1) + 71.0098(15.1)^{3/2}}{1{,}296.86(15.1)^{1/2} + 1{,}204.73(15.1) + 618.618(15.1)^{3/2} + 538.072(15.1)^2 + 142.41(15.1)^{5/2}} = 0.02$$

Table 3.8 summarizes the intermediate results.

5. Calculate the water influx using Eq. 3.58:

$$W_{en} = W_{en-1} + (t_{Dn} - t_{Dn-1})\left[\frac{B\Delta p_n - W_{en-1}p'_D(t_{Dn})}{p_D(t_{Dn}) - t_{Dn-1}p'_D(t_{Dn})}\right],$$

For example, at n = 1,

$$W_{e1} = W_{e0} + (t_{D1} - t_{D0})\left[\frac{B\Delta p_1 - W_{e0}p'_D(t_{D1})}{p_D(t_{D1}) - t_{D0}p'_D(t_{D1})}\right] =$$

$$= 0 + (15.1 - t_{Dn-1})\left[\frac{(454.3)(5) - 0}{1.83 - 0}\right] = 18{,}743 \text{ RB}$$

For n = 2,

$$W_{e2} = W_{e1} + (t_{D2} - t_{D1})\left[\frac{B\Delta p_1 - W_{e1}p'_D(t_{D2})}{p_D(t_{D2}) - t_{D1}p'_D(t_{D2})}\right] =$$

$$= 18{,}743 + (15.1)\left[\frac{(454.3)(19) - (18{,}743)(0.155)}{2.15 - 15.1(0.0155)}\right] = 84{,}482 \text{ RB}$$

6. Table 3.9 gives the final results.

EXAMPLE 3.4.8

Estimating Water Influx With the Fetkovich Method.

Calculate the water influx for the reservoir/aquifer system described below. Assume a finite radial aquifer with an area of 250,000 acres and having a no-flow outer boundary. The estimated aquifer properties are given below; Table 3.11 summarizes the pressure history at the reservoir/aquifer boundary. Note that the aquifer is a sector of a cylinder where $\theta = 180°$.

$\phi = 0.209$.

$r_r = 5{,}807$ ft

$\mu = 0.25$ cp.

$k = 275$ md.

$\theta = 180°$.

$c_r = 6 \times 10^{-6}$ psia^{-1}.

$h = 19.2$ ft.

Solution.

1. Calculate the maximum volume of water from the aquifer, W_{ei}, that could enter the reservoir if the reservoir pressure were reduced to zero. Note that the aquifer shape is a sector of a cylinder, so the initial volume of water in the aquifer is

$$W_i = \frac{\pi\left(r_a^2 - r_r^2\right)\phi h(\theta/360)}{5.615}$$

where

$$r_a = \sqrt{\left(\frac{43{,}560 \cdot A}{\pi}\right)\left(\frac{360}{\theta}\right)} = \sqrt{\frac{(43{,}560)(250{,}000)}{\pi}\left(\frac{360}{180}\right)} = 83{,}260 \text{ ft}$$

Therefore,

$$W_i = \frac{\pi\left(83{,}260^2 - 5{,}807^2\right)(19.2)(0.209)(180/360)}{5.615} = 7.744\text{x}10^9 \text{ RB}$$

From Eq. 3.65,

$W_{ei} = c_t p_{aq,i} W_i = (6\text{x}10^{-6})(3{,}793)(7.744\text{x}10^9) = 176.3\text{x}10^6$ RB.

2. Calculate J. For radial flow in an aquifer with a finite no-flow outer boundary, from Table 3.10,

$$J = \frac{0.00708kh(\theta/360)}{\mu\left[\ln(r_a/r_r) - 0.75\right]} = \frac{(0.00708)(275)(19.2)(180/360)}{0.25\left[\ln(83{,}260/5{,}807) - 0.75\right]} = 39.1 \text{ STB/D} - \text{psi}$$

3. For each time period, calculate the incremental water influx using Eq. 3.71.

$$\Delta W_{en} = \frac{W_{ei}}{P_{aq,i}}\left(\overline{P}_{aq,n-1} - \overline{P_m}\right)\left[1 - e^{-\frac{JP_{aq,i}\Delta t_n}{W_{ei}}}\right]$$

where (from Eq. 3.72)

$$\overline{P}_{aq,n-1} = P_{aq,i}\left(1 - \frac{W_{e,n-1}}{W_{ei}}\right)$$

and from Eq. 3.73,

$$\bar{P}_m = \frac{P_{m-1} + P_m}{2}$$

For example. at n = 1.

$$\bar{P}_{aq,0} = P_{aq,i}\left(1 - \frac{W_{e,n-1}}{W_{ei}}\right) = 3{,}793\left(1 - \frac{0}{176.254\text{x}10^6}\right) = 3{,}793 \text{ psi}$$

The average pressure at the aquifer/reservoir boundary is

$$\bar{P}_{r1} = \frac{P_{r0} + P_{r1}}{2} = \frac{3{,}793 + 3{,}788}{2} = 3{,}790.5 \text{ psia}$$

Therefore, the incremental water influx during Timestep I is

$$\Delta W_{e1} = \frac{W_{ei}}{P_{aq,i}}\left(\bar{P}_{aq,0} - \bar{P}_{r1}\right)\left[1 - e^{-\frac{JP_{aq,i}\Delta t_1}{W_{ei}}}\right] =$$

$$= \frac{176.3\text{x}10^6}{3{,}793}(3{,}793 - 3{,}790.5)\left[1 - e^{-\frac{(39.1)(3{,}793)(91.5)}{176.3\text{x}10^6}}\right] = 8{,}587 \text{ RB}$$

Similarly, at n = 2,

$$\bar{P}_{aq,1} = P_{aq,i}\left(1 - \frac{W_{e,1}}{W_{ei}}\right) = 3{,}793\left(1 - \frac{8{,}587}{176.254\text{x}10^6}\right) = 3{,}792.8 \text{ psi}$$

The average pressure at the aquifer/reservoir boundary is

$$\overline{P}_{r2} = \frac{P_{r1} + P_{r2}}{2} = \frac{3{,}788 + 3{,}774}{2} = 3{,}781 \text{ psia}$$

Therefore, the incremental water influx during Timestep 1 is

$$\Delta W_{e2} = \frac{W_{ei}}{P_{aq,i}}\left(\overline{P}_{aq,1} - \overline{P_{r2}}\right)\left[1 - e^{-\frac{JP_{aq,i}\Delta t_2}{W_{ei}}}\right] =$$

$$= \frac{176.3\text{x}10^6}{3{,}793}(3{,}792.8 - 3{,}781)\left[1 - e^{-\frac{(39.1)(3{,}793)(91.5)}{176.3\text{x}10^6}}\right] = 40{,}630 \text{ RB}$$

4. Calculate the cumulative water influx during each time step. For example, at the end of the first time step, n = 1

$$W_{e1} = \sum_{i=1}^{n=1} \Delta W_{ei} = \Delta W_{e1} = 8{,}587 \text{ RB}$$

Similarly, the cumulative water influx at the end of the second time step is n = 2

$$W_{e2} = \sum_{i=1}^{n=2} \Delta W_{ei} = \Delta W_{e1} + \Delta W_{e2} = 8{,}587 + 40{,}630 = 49{,}217 \text{ RB}$$

Table 3.12 summarizes the final results.

EXAMPLE 3.4.9

Estimating Original Gas in Place With Material Balance for a Dry-Gas Reservoir With Water Influx.

Estimate the original gas in place and water influx constant using the material balance equation developed for water influx in a dry-gas reservoir. Assume an unsteady-state, infinite-acting aquifer. According to McEwen [22], the volumetric estimate of original gas in place is 200x 10^6 Mscf. Table 3.13 gives the pressure and production histories; the estimated aquifer properties are summarized below.

$\phi = 0.24$.

$\mu = 1.0$ cp.

$r_r = 3{,}383$ ft.

$k = 50$ md.

$c_t = 6x10^{-6}$ $psia^{-1}$.

$\theta = 360^{O}$.

$h = 20.0$ ft.

$B_W = 1.0$ RB/STB.

Solution.

Using a procedure similar to that illustrated for the van Everdingen and Hurst method, estimate water influx for each timestep as described below.

1. Calculate ΔP_n, where

$$\Delta p_n = \frac{1}{2}(p_{n-2} - p_n)$$

For example, at n = 1 (i.e., t = 182.5 days),

$$\Delta p_1 = \frac{1}{2}(p_0 - p_1) = \frac{1}{2}(5{,}392 - 5{,}368) = 12.0 \text{ psi.}$$

At n = 5 (i.e., t = 912.5 days),

$$\Delta p_5 = \frac{1}{2}(p_3 - p_5) = \frac{1}{2}(5{,}245 - 5{,}147) = 49.0 \text{ psi.}$$

2. Calculate dimensionless times for each of the real times given. Use the dimensionless time defined by Eq. 3.37 for a radial geometry.

$$t_D = \frac{0.00633kt}{\phi\mu c_t r_r^2} = \frac{(0.00633)(50)t}{(0.24)(1.0)(6x10^{-6})(3{,}383)^2} = 0.019 \cdot t$$

For example, at n = 1 (i.e., t = 182.5 days), $t_D = (0.019)(182.5) = 3.5$.

3. For each dimensionless time computed in Step 2, calculate a dimensionless cumulative water influx. We-are assuming an infiniteacting aquifer, so we can use Eq. 3.49.

$$Q_{PD}(t_D) = \frac{1.2838(t_D)^{1/2} + 1.19328(t_D) + 0.269872(t_D)^{3/2} + 0.00855294(t_D)^2}{1 + 0.616599(t_D)^{1/2} + 0.0413008(t_D)}$$

For example, at n = 1

$$Q_{pD} = \frac{1.2838(3.5)^{1/2} + 1.19328(3.5) + 0.269872(3.5)^{3/2} + 0.00855294(3.5)^2}{1 + 0.616599(3.5)^{1/2} + 0.0413008(3.5)} = 3.68.$$

4. Now, estimate the original gas in place and water influx constant using the material-balance plotting method. Calculate the plotting functions defined in the previous section,

$[(G_pB_g)+(W_pB_w)]/(B_g-B_{gi})$ vs. $f(p,t)/(B_g-B_{gi})$,

where $f(p,t) = \Sigma \Delta p\, Q_{pD}$.

For example, at n = 1 the plotting function for the vertical axis, y, is

$$y = \frac{G_pB_g + W_pB_w}{(B_t - B_{gi})} = \frac{(677.7x10^3)(0.6796)+(3)(1.0)}{(0.6796-0.6775)} = 2.913x10^6 \text{ Mscf} = 219.3 \text{ Bscf}$$

The plotting function for the horizontal axis, x, is

$$y = \frac{\Sigma \Delta_p Q_{pD}}{(B_t - B_{gi})} = \frac{(12)(3.68)}{(0.6796-0.6775)} = 21x10^3 \text{ Mscf}$$

5. The material-balance plotting functions, summarized in Table 3.14, are plotted in Fig. 3.11.

6. From the slope of the line through the data points in Fig. 3.11, C is estimated to be 1195 RB/psi, and the original gas in place estimated from the intercept is G = 197 Bscf = 197 x 10^6 Mscf, which agrees with the volumetric estimate of G = 200x10^6 Mscf.

The general problem that reservoir engineers face when analyzing gas reservoirs with water influx is simultaneous determination of G, C, aquifer size or an aquifer/reservoir size ratio, r_a/r_r, and the relationship between real time, *t*, and dimensionless time, t_D. Simultaneous determination of these variables that best fit a pressure/production history is a complex problem in regression analysis.

EXAMPLE 3.4.10

Estimating Original Gas in Place With Material Balance for a Volumetric Geopressured Gas Reservoir.

For the following data taken from an abnormally pressured reservoir (the Anderson "L" sand[24]), estimate the original gas in place using the material-balance equation developed for a high-pressure gas reservoir. In addition, use the material-balance equation for a normally pressured gas reservoir, and compare the initial gas estimates from both equations. Table 3.15 gives the pressure and production histories.

p_i = 9,507 psia.

$C_W = 3.2 \times 10^{-6}$ psi^{-1}.

S_{wi} = 0.24.

Original pressure gradient = 0.843 psi/ft.

$\overline{c_f} = 19.5 \times 10^{-6}$ psi^{-1} (assumed constant).

Solution

1. Calculate the geopressured and normally pressured pressure plotting functions for each data point (Table 3.16).
2. From the two plots, estimate original gas in place from the intercept with the horizontal axis: high-pressure reservoir analysis (Fig.3.13) - G = 70.7 Bcf; normally pressured reservoir analysis (Fig. 3.14) - G = 89.3 Bcf.

The results show that, if we analyze this geopressured reservoir using techniques for normally pressured reservoirs, we will overestimate the original gas in place by more than 25 %. In addition, note that the data in Fig. 3.14 are beginning to trend downward, which indicates that a normally pressured analysis of the available data is not valid.

We developed the material-balance equation for a high-pressure gas reservoir using a single value for formation compressibility over the life of the reservoir. In reality, formation compressibility may vary during pressure depletion, especially at the highest pressures. Further, the previous derivation assumed that values for formation compressibility are readily available. However, these values are very difficult to measure accurately in the laboratory, especially as a function of changes in pore pressure. Therefore, in the next section, we present a graphical technique for simultaneously estimating original gas in place and an average value of formation compressibility.

EXAMPLE 3.4.11

Simultaneous Determination of Average Formation Compressibility and Original Gas in Place With Material Balance in a Volumetric Geopressured Gas Reservoir.

For the following data taken from the Anderson "L" sand,[24] estimate original gas in place using Eq. 3.91 and an average value for formation compressibility. Table 3.17 gives the pressure and production histories.

$P_i = 9{,}507$ psia.

$C_w = 3.2\text{x}10^{-6}$ psi^{-1}.

$S_{wi} = 0.24$.

Original pressure gradient = 0.843 psi/ft.

Solution.

1. First, we must generate the plotting functions developed by Roach.[25] Example calculations for $G_p = 392.5$ MMscf $= 3.925\text{x}10^5$ Mscf follow.

For the variable on the vertical axis, we plot

$$\frac{1}{(p_i - p)}\left(\frac{p_i z}{p z_i} - 1\right) = \frac{1}{(9{,}507 - 9{,}292)}\left(\frac{(9{,}507)(1.418)}{(9{,}292)(1.440)} - 1\right) = 34.9\text{x}10^{-6}\ psi^{-1}$$

For the variable on the horizontal axis, we plot

$$\left[\frac{G_p}{(p_i - p)}\frac{p_i z}{p z_i}\right] = \left[\frac{3.92\text{x}10^5}{(9{,}507 - 9{,}292)}\frac{(9{,}507)(1.418)}{(9{,}292)(1.440)}\right] = 1.84\text{x}10^3\ \text{Mscf / psi}$$

2. Prepare a plot (Fig. 3.15) of the plotting functions summarized in Table 3.18.

3. Estimate the original gas in place and average formation compressibility from Fig. 3.15.

A. The original gas in place, G, is estimated from the slope of the line, m:

$$\frac{1}{G} = \text{slope} = 13.3\text{x}10^{-6}\ (\text{MMscf})^{-1},$$

or $G = 1/(13.3\text{x}10^{-6}) = 75{,}190$ MMscf.

Note that, in Example 3.10, we estimated the original gas in place assuming an average value of formation compressibility, while in this example we calculated the original gas in place and formation compressibility simultaneously. As a result, the two estimates of gas in place are slightly different.

B. The average formation compressibility is determined from the intercept of the line. b:

$$b = -\left[\frac{c_w S_{wi} + \bar{c}_f}{1 - S_{wi}}\right] = -18.5\text{x}10^{-6}\ \text{psi}^{-1} = -\left[\frac{(3.2\text{x}10^{-6})(0.24) + \bar{c}_f}{(1 - 0.24)}\right]$$

$$\bar{c}_f = 13.3\text{x}10^{-6}\ \text{psi}^{-1}$$

The data plotted in Fig. 3.15 do not lie completely on a straight line. Poston and Chen[26] concluded that, initially, most of the formation resistance to the overburden pressure is provided by the fluids in the pore spaces. However, as fluids are withdrawn from these pore spaces, the formation compacts, resulting in more resistance to the overburden being transferred to the rock matrix. Under these conditions, the formation compressibility is not a constant but changes with time, as indicated by the initial nonlinear portion of the data in Fig. 3.15.

3.4 SUMMARY

Reading this chapter should prepare you to do the following.

1. Calculate original gas in place in a volumetric dry-gas reservoir using volumetric methods.
2. Calculate gas reserves and recovery factor for a gas reservoir with water influx using volumetric methods.
3. Calculate original gas in place and condensate in place for a volumetric wet-gas reservoir using volumetric methods.
4. State the principle of conservation of mass and derive a general material-balance equation from that principle.
5. Calculate original gas in place using material balance for a volumetric dry-gas reservoir.
6. Estimate water influx using the van Everdingen-Hurst, Carter Tracy, and Fetkovich methods and state the assumptions and limitations of each method.
7. Estimate original gas in place using material balance for a dry-gas reservoir with water influx.
8. Estimate original gas in place using material balance for a volumetric geopressured gas reservoir.
9. Determine average formation compressibility and original gas in place simultaneously using material balance in a volumetric geopressured gas reservoir.
10. Derive material-balance relationships for volumetric gascondensate reservoirs, gas-condensate reservoirs with water vaporization, gas-condensate reservoirs with depletion at pressures above the dewpoint, and gas-condensate reservoirs with depletion at pressures below the dewpoint.

Questions for Discussion

1. Your company is planning to drill a wildcat well in an area believed to have great potential for natural gas. In planning for the well (and assuming gas is discovered), what data should be gathered? Why?

2. The well does discover gas. Using information from the discovery well alone, you are asked to estimate reserves and forecast future production. What methods will you use? What additional data will you need?

3. Several additional wells are planned. What sort of information should be obtained from these wells? Why?

4. Two years after the discovery well was drilled, the field is highly developed. You are again asked to estimate reserves and forecast future production. What methods will you use? What data will you need?

5. How would your strategy be affected if the reservoir is geopressured? Is a retrograde gas reservoir Has a waterdrive? Is the gas cap of a oil reservoir, a fact discovered only much later? How can you determine whether any of these possibilities is a fact?

6. How would you determine optimal well spacing? Optimal depletion plan? In answer to both these questions, what data would you need, and what study methods would you use?

7. What are the potential errors in the volumetric method? The materiall-balance method?

8. What are typical recovery factors for volumetric gas reservoirs? How may we estimate abandonment pressure to calculate recovery factor? At what point does abandonment pressure enter the recovery factor calculation?

9. Compare typical recoveries in waterdrive gas reservoirs with those from volumetric gas reservoirs and explain the reasons for the difference.

10. Explain two methods for improving the recovery from waterdrive gas reservoirs.

11. Describe the different types of aquifer that may be in association with a reservoir.

12. How does the aquifer offset pressure decline in the reservoir?

13. If the time elapsed since production began doubled, do you think the amount of water influx into a gas reservoir would double? Or would it be more or less than double? Why? If additional information is required to answer this question, what is that additional information?

Nomenclature

A = well drainage area, L^2, acres

b = intercept

B = van Everdingen-Hurst constant, RB/psi

B_g = gas FVF, RB/Mscf

B_{ga} = gas FVF at reservoir abandonment pressure and temperature conditions, RB/Mscf

B_{gi} = gas FVF at initial reservoir pressure and temperature, RB/Mscf

B_W = water FVF, RB/STB

B_{2g} = gas FVF based on two-phase gas deviation factor, RB/Mscf

B_{2gi} = gas FVF based on two-phase gas deviation factor at initial reservoir pressure and temperature, RB/Mscf

C = water influx constant from material-balance calculations, RB/psi

C_f = in-situ formation compressibility, Lt^2/m, $psia^{-1}$

c_t = total aquifer compressibility, $C_f + C_w$, Lt^2/m, $psia^{-1}$

C_W = water compressibility, Lt^2/m, $psia^{-1}$

Ev = volumetric sweep efficiency, fraction

fg = fraction of reservoir gas produced as liquid at surface, fraction

F = gas recovery factor

G = original gas in place, L^3, Mscf

G_a = gas in place at reservoir abandonment, L^3, Mscf

G_p = cumulative gas production, L^3, Mscf

G_{pa} = additional gas production from secondary separator and stock tank, L^3/L^3, scf/STB

GPT = cumulative gas production from primary and secondary separators, stock tank, and the gaseous equivalent of produced condensates, L^3, Mscf

G_{pT} = cumulative gas production from primary separator, L^3, Mscf

G_{p2} = cumulative gas production from secondary separator, L^3, Mscf

G_{p3} = cumulative gas production from stock tank, L^3, Mscf

G_t = reservoir volume occupied by gas trapped by encroaching water, L^3, Mscf

G_T = total initial gas in place, including gas and gaseous equivalent of produced condensates, L^3, Mscf

h = net formation thickness, L, ft

J = aquifer PI, L^3t/m, STB/D-psi

k = reservoir permeability, L^2, md

L = length of linear-shaped reservoir, L, R

m = slope

M_o = molecular weight of stock tank liquids, m, I b m/ lb m- mol n = number of moles of gas

N = original oil (condensate) in place, L^3, STB

N_p = cumulative oil (condensate) production, L^3, STB p = reservoir pressure, m/Lt^2, psia

P_a = abandonment pressure, m/Lt^2, psia

p_{aq} = aquifer pressure, m/Lt^2, psia

P_{aqi} = initial aquifer pressure, m/Lt^2, psia

P_d = dewpoint pressure of gas-condensate reservoir, m/Lt^2, psia

P_D = dimensionless pressure

P_D = dimensionless pressure derivative

p_i = initial reservoir pressure, m/Lt^2, psia

p_n = pressure at time interval n, m/Lt^2, psia

p_r = pressure at aquifer/reservoir interface, m/Lt^2, psia

P_{sc} = pressure at standard conditions, m/Lt^2, psia

A_p = difference between initial aquifer pressure and pressure at original reservoir/aquifer boundary. m/Lt^2, psia

q_D = dimensionless water influx rate

q_w = water influx rate, L^3/t, STB/D

Q_{PD} = dimensionless cumulative water influx

r_a = radius of aquifer, L, ft

r_e = outer radius of reservoir, L, ft

r_r = radius to aquifer/reservoir interface, L, ft

R = universal gas constant, 10.73 psia-ft^3/lbm-mol-°R

R_t = total gas/stock-tank liquid ratio, scf/STB

R_1 = ratio of high-pressure separator gas volume to stocktank liquid volume, L^3/L^3, scf/STB

R_2 = ratio of low-pressure separator gas volume to stocktank liquid volume, L^3/L^3, scf/STB

R_3 = ratio of stock-tank gas volume to stock-tank liquid volume, L^3/L^3, scf/STB

S_{gi} = initial gas saturation, fraction

S_{gr} = residual gas saturation, fraction

S_O = condensate saturation, fraction

S_w = connate water saturation, fraction

S_{Wa} = water saturation at abandonment conditions, fraction

S_{wi} = initial connate water saturation, fraction t = time, t, days

t_D = dimensionless time

T = reservoir temperature, T, °R

T_{sc} = temperature at standard conditions, T, °R

V_{cq} = vapor equivalent of primary separator liquid, L^3/L^3, scf/STB

V_f = reservoir formation (rock) volume, L^3, res bbl

V_{gf} = gas volume at initial conditions, L^3, res bbl

V_{hL} = volume of hydrocarbon liquids, L^3, res bbl

V_{hv} = volume of hydrocarbon vapors, L3, res bbl

V_{hvi} = initial volume of hydrocarbon vapors, L^3, res bbl

V_p = reservoir PV, L^3, res bbl

V_{pi} = initial reservoir PV, L^3, res bbl

V_{sc} = gas volume at standard conditions, L^3, res bbl

V_v = volume of vapor phase, L^3, res bbl

V_{vi} = initial volume of vapor phase, L^3, res bbl

V_w = volume of water, L^3, res bbl

V_{wi} = initial volume of water, L^3, res bbl

V_w = volume of water vapor phase, L^3, res bbl

V_{wvi} = initial volume of water vapor phase, L^3, res bbl

ΔV_f = change in reservoir formation (rock) volume, L^3, res bbl

ΔV_w = change in water volume, L^3, res bbl

w = width of linear reservoir, L, R

W_e = cumulative water influx volume, L^3, res bbl

W_{ei} = initial "encroachable" volume of water in aquifer, L^3, res bbl

W_i = initial volume of water in aquifer, L^3, res bbl

W_p = cumulative water production, L^3,STB

Y_w = fraction of total vapor-phase volume that is water

Y_{wi} = initial fraction of total vapor phase volume that is water

z = gas compressibility factor, dimensionless

Z_a = gas compressibility factor at abandonment, dimensionless

Z_i = gas compressibility factor evaluated at initial conditions, dimensionless Z,c = gas compressibility factor at standard conditions, dimensionless

Z_2 = two-phase gas compressibility factor, dimensionless

Z_{2i} = two-phase gas compressibility factor evaluated at initial conditions, dimensionless

γ_o = specific gravity of condensate (water = 1.0 g/cm3)

γ_g = specific gravity of reservoir gas at reservoir eonditions (air = 1.0)

γ_1 = speeific gravity of high-pressure separator gas (air = 1.0)

γ_2 = speeific gravity of low-pressure separator gas (air = 1.0)

γ_3 = speeific gravity of stock-tank gas (air = 1.0)

θ = angle encompassed by aquifer, degrees

λ = dummy integration variable for Eq. 10.57

μ = viscosity, m/Lt, ep

ϕ = Porosity, fraction

Subscript

aq = aquifer

Superscript

$\bar{}$ = average

References

1. Amyx, J.W., Bass, D.M., and Whiting, R.L.: Petroleum Reservoir Engineering, Physical Properties, McGraw-Hill Book Co. Inc., New York City (1961).
2. Craft, B.C. et al.: Applied Petroleum Reservoir Engineering, second edition, Prentice-Hall Inc., Englewood Cliffs, NJ (1991).
3. McCain, W.D. Jr.: The Properties of Petroleum Fluids, second edition, PennWell Publishing Co., Tulsa, OK (1989).
4. Geffen, T.M. et al.: "Efficiency of Gas Displacement From Porous Media by Liquid Flooding," Trans., AIME (1952) 195, 29.
5. Keelan, D.K. and Pugh, V.J.: "Trapped-Gas Saturations in Carbonate Formations," SPEJ (April 1975) 149-60; Trans., AIME, 259.
6. Agarwal, R.G.: "Unsteady-State Performance of Water-Drive Gas Reservoirs," PhD. dissertation, Texas A&M U., College Station (1967).
7. Gold, D.K., McCain, W.D. Jr., and Jenamgs, J.W.: "An Improved Method for the Determination of the Resenoir-Gas Gravity for Retrograde Gases," JPT (July 1989) 747-52; Trans., AIME, 287.
8. Schilthuis, R.J.: "Active Oil and Resenoir Energy," Trans., AIME (1936) 118, 33-52.
9. Katz, D.L. et al.: Handbook of Natural Gas Engineering, McGrawHill Book Co. Inc., New York City (1959).
10. van Everdingen, A.F., Timmerman, E.H., and McMahon, J.J.: "Application of the Material-Balance Equation to a Partial Water-Drive Resenoir," Trans., AIME (1953) 198, 51.
11. Havlena, D. and Odeh, A.S.: "The Material-Balance Equation as an Equation of a Straight Line," lPT(Aug. 1963) 896 900; Trans., AIME, 228.
12. Chierici, G.L. and Pizzi, G.: "Water-Drive Gas Resenoirs: Uncertainty in Resenes Evaluation From Past History," JPT (Feb. 1967) 237-44; Trans., AIME, 240.

13. Bruns, J.R, Fetkovich, M.J., and Meitzen, V.C.: "The Effect of Water on p/z Cwoulative Gas Production Cunes," JPT(March 1965) 287-91.
14. van Everdingen, A.F. and Hurst, W.: "Application of the Laplace Transformation to Flow Problems m Resenoirs," Trans., AIME (1994) 1K, 305-24.
15. Carter, R.D. and Tracy, G.W.: "An Improved Method for Calculating Water Influx," JPT (Dec. 1960) 415-17; Trans., AIME, 219.
16. Fetkovich, M.J.: "A Simplified Approach to Water Influx Calculations—Finite Aquifer Systems," JPT (July 1971) 814-28.
17. Allard, D.R. and Chen, S.M.: "Calculation of Water Influx for Bottomwater Drive Resenoirs," SPERE (May 1988) 369-79.
18. Olarewaju, J.S.: "A Mathematical Model of Edgewater and Bottomwater Drives for Water Influx Cslculations," paper SPE 18764 presented at the 1989 SPE California Regional Meeting, Bakersfidd, April 5-7.
19. Lee, W.J.: Well Testing, SPE Textbook Series, Richardson, TX (1982) 1.
20. Edwardson, M.J. et al.: "Calculation of Formation Temperature Disturbances Caused by Mud Circulation," JPT (April 1962) 416-26; Trans., AIME, 225.
21. Klins, M.A., Bouchard, A.J., and Cable, C.L.: "A Polynomial Approach to the van Everdingen-Hurst Dimensionless Variables for Water Encorachment," SPERE (Feb. 1988) 320-26.
22. McEwen, C.R.: "Material Balance Calculations With Water Influx in the Presence of Uncertainty in Pressures," JPT(June 1962) 120-28; Trans., AIME, 225.
23. Ramagost, B.P. and Farshad, F.F.: "p/z Abnormally Pressured Gas Reservoirs," paper SPE 10125 presented at the 1981 SPE Annual Tech nical Conference and Exhibition, San Antonio, Oct. 5-7.
24. Duggan, J.O.: "The Anderson "L"—An Abnormally Pressured Gas Resenoir in South Texas," JPT (Feb. 1972) 132-38.
25. Roach, R.H.: "Analyzing Geopressured Resenoirs—A MaterialBalance Technique," paper SPE 9968 available at SPE, Richardson, TX.

26. Poston, S.W. and Chen, H.Y: "Simultaneous Determination of Formation Compressibility and Gas-in-Place in Abnormally Pressured Resenoirs," paper SPE 16227 presented at the 1987 SPE Production Operations Symposium, Oklahoma City, March 8-10.

27. Moses, P.L.: "Engineering Applications of Phase Behavior of Crude Oil and Condensate Systems," JPT (July 1986) 715-23.

28. Moses, P.L. and Donohoe, C.W.: Petroleum Engineering Handbook, H.B. Bradley et aL (eds.), SPE, Richardson, TX (1987) 39-1-39-28.

29. Rayes, D.G. et al.: "Two-Phase Compressibility Factors for Retrograde Gases," SPEFE (March 1992) 87-92; Trans., AIME, 293.

30. Humphreys, N.V.: "Material-Balance Equation for a Gas-Condensate Resenoir With Significant Water Vaporization," paper SPE 21514 presented at the 1991 SPE Gas Technology Symposium, Houston, Jan. 22-24.

31. GPSA Engineering Data Book, 10th edition, Gas Processors Suppliers Assn., Tulsa, OK (1987).

32. McKetta, J.J. and Wehe, A.H.: "Use This Chart for Water Vapor Content of Natural Gases," Petroleum Refiner (Aug. 1958) 153-54.

33. Bukacek, R.F.: "Equilibrium Moisture Content of Natural Gases," Inst. Of Gas Technology Bulletin (1955) 8.

APPENDIX A

FIGURES AND TABLES

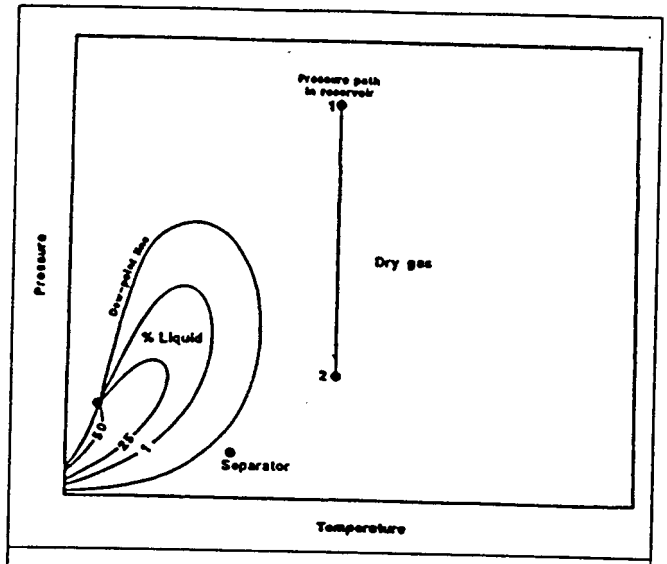

Phase diagram for a dry-gas reservoir fluid (after William D. McCain Jr.'s *Properties of Petroleum Fluids*, Second Edition, Copyright Pennwell Books, 1990[3]).

FIG. 3.1

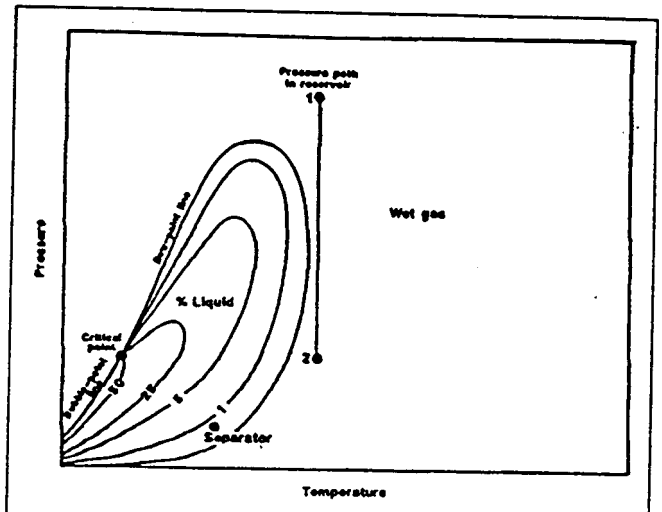

Phase diagram for a wet-gas reservoir fluid (after William D. McCain Jr.'s *Properties of Petroleum Fluids*, Second Edition, Copyright Pennwell Books, 1990[3]).

FIG. 3.2

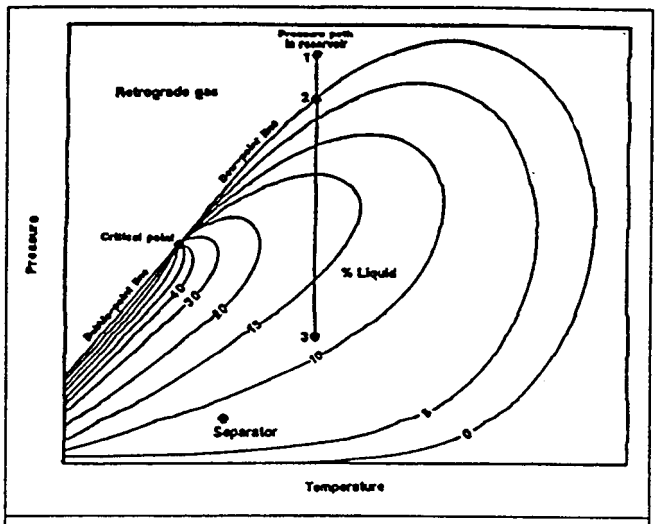

Phase diagram for a gas-condensate reservoir (after William D. McCain Jr.'s *Properties of Petroleum Fluids*, Second Edition, Copyright Pennwell Books, 1990[3]).

FIG. 3.3

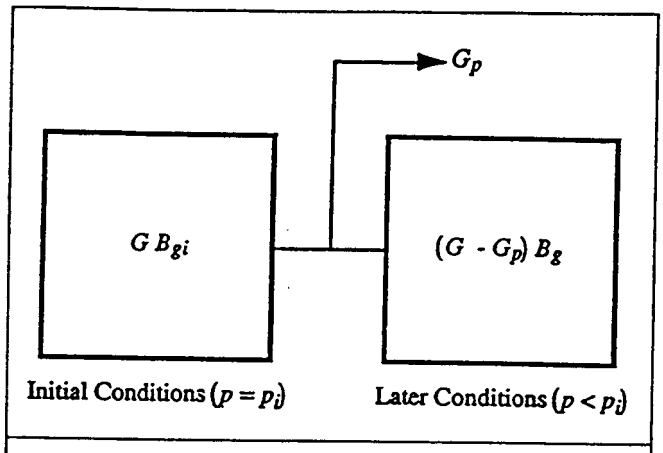

Material-balance model for a volumetric dry-gas reservoir showing reservoir PV occupied by gas at initial and later conditions.

FIG. 3.4

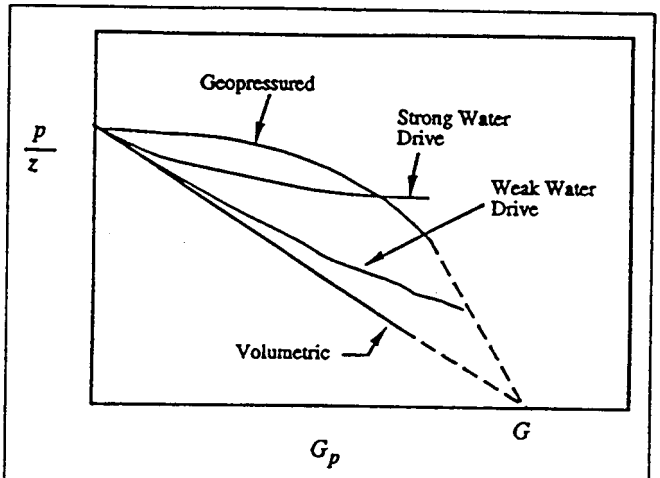

Shapes of p/z plots for various drive mechanisms.

FIG. 3.5

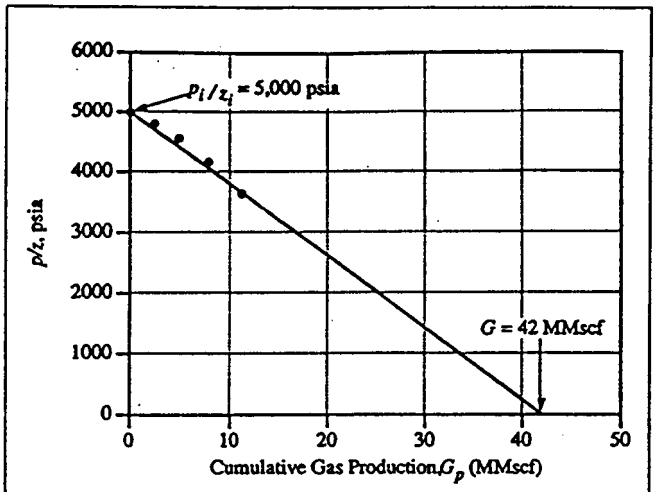

Graphical solution to the material-balance equation for a volumetric dry-gas reservoir, Example 5.

FIG. 3.6

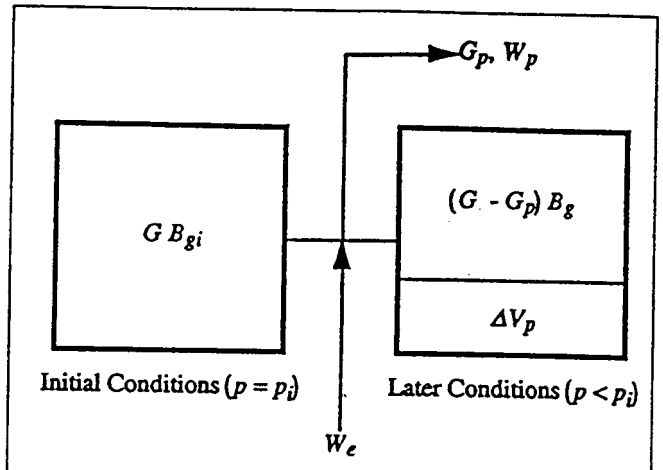

Material-balance model showing reservoir PV occupied by gas at initial and later conditions for a dry-gas reservoir with water influx.

FIG. 3.7

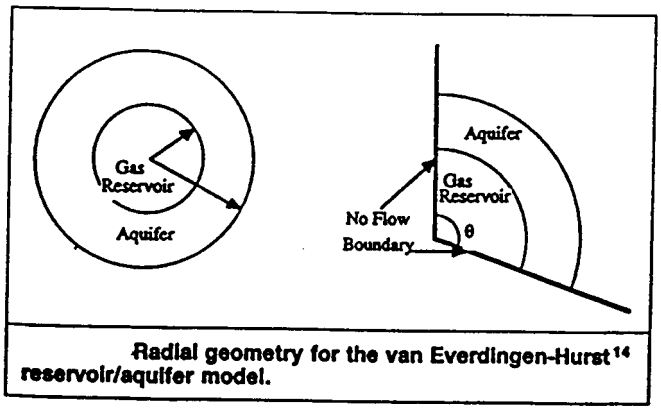

Radial geometry for the van Everdingen-Hurst[14] reservoir/aquifer model.

FIG. 3.8

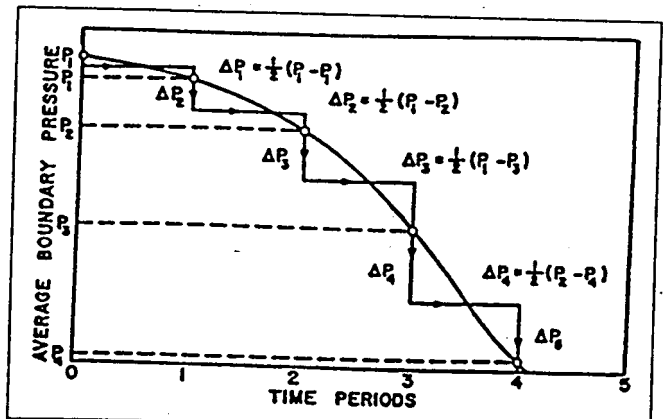

Step-by-step pressure-history approximation used in the van Everdingen-Hurst[14] model (after Craft and Hawkins[2]).

FIG. 3.9

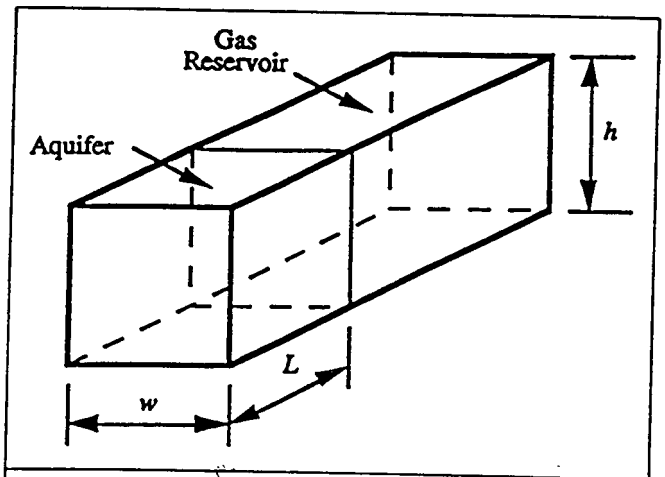

Linear geometry for the van Everdingen-Hurst[14] reservoir/aquifer model.

FIG. 3.10

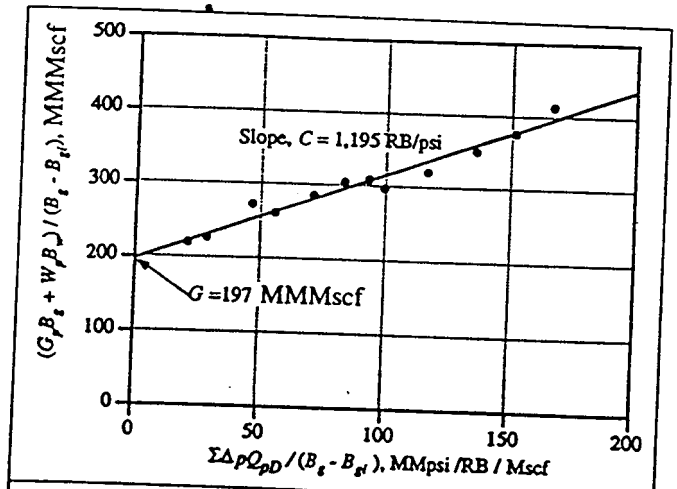

Graphical solution to the material-balance equation for a dry-gas reservoir with water influx, Example 9.

FIG. 3.11

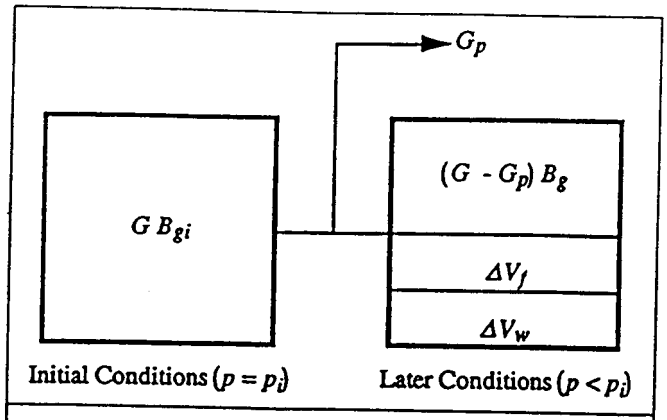

Material-balance model showing reservoir PV occupied by gas at initial and later conditions for a volumetric geopressured gas reservoir.

FIG. 3.12

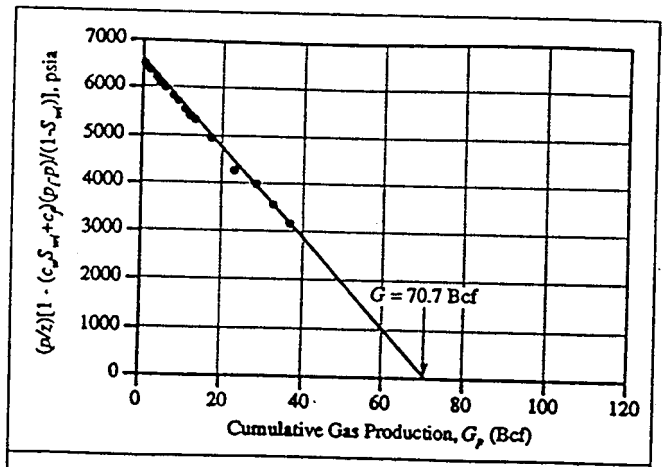

Graphical solution to the material-balance equation for a volumetric geopressured gas reservoir, Example 3.10.

FIG. 3.13

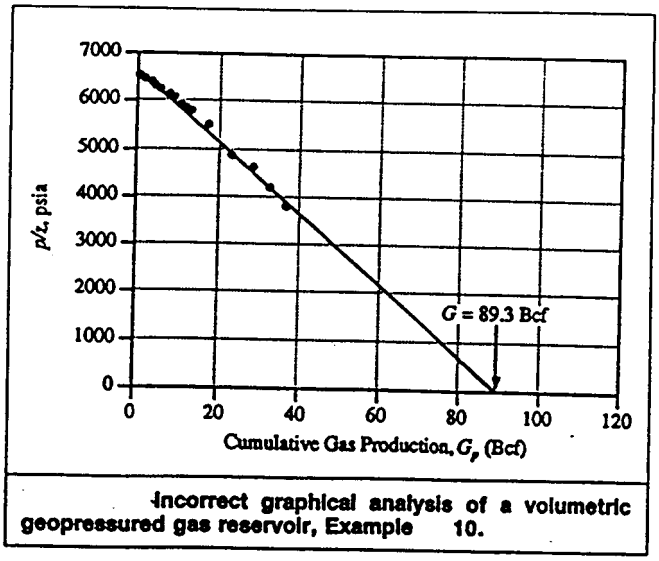

Incorrect graphical analysis of a volumetric geopressured gas reservoir, Example 10.

FIG. 3.14

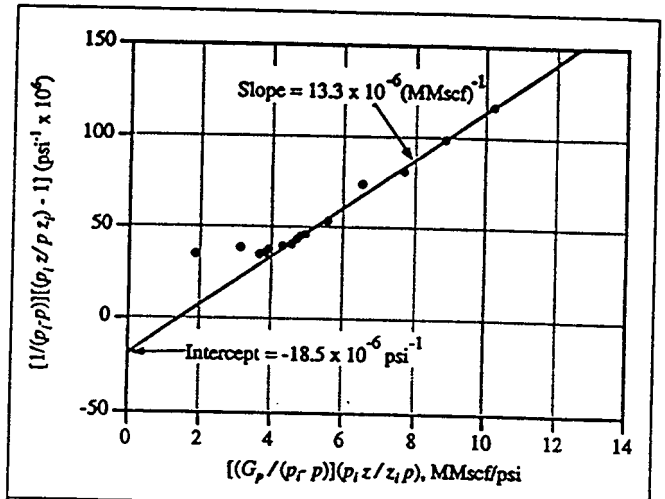

Graphical solution to the material-balance equation for simultaneous estimation of original gas in place and formation compressibility in volumetric geopressured gas reservoirs, Example 11.

FIG. 3.15

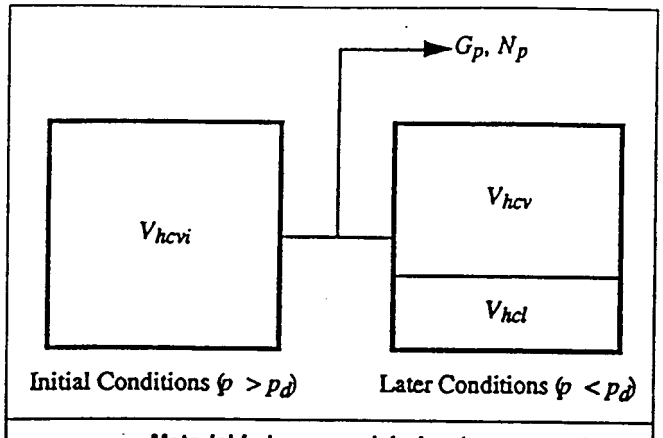

Material-balance model showing reservoir PV occupied by gas and liquid hydrocarbon phases at initial and later conditions for a gas-condensate reservoir.

FIG. 3.16

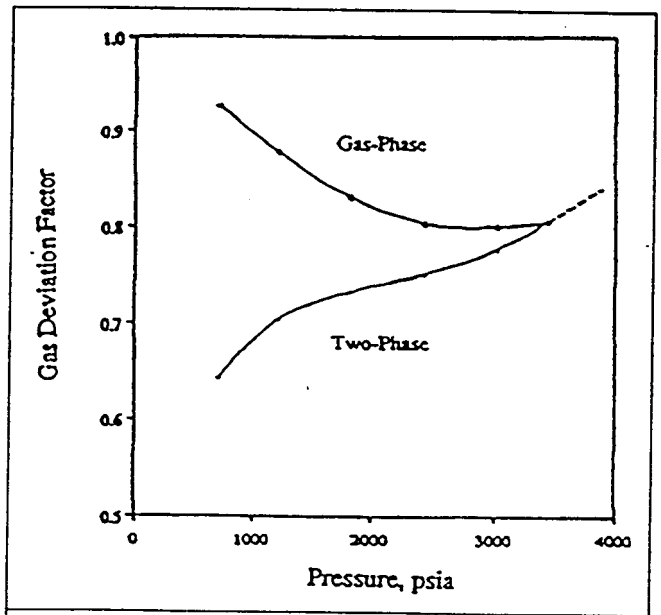

Example of equilibrium and two-phase gas deviation factors for a gas-condensate reservoir.

FIG. 3.17

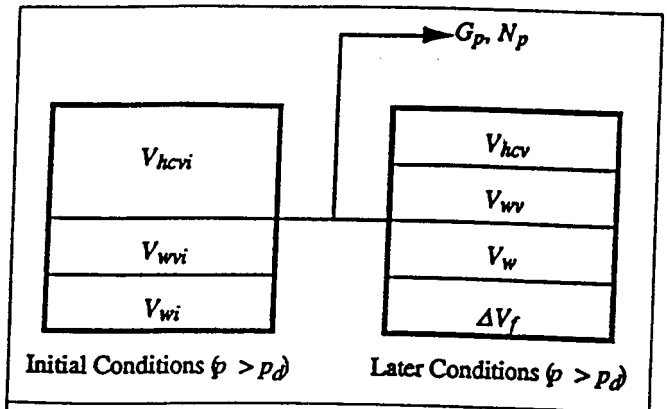

Material-balance model showing reservoir PV occupied by hydrocarbons and water at initial and later conditions for a gas-condensate reservoir with water vaporization.

FIG. 3.18

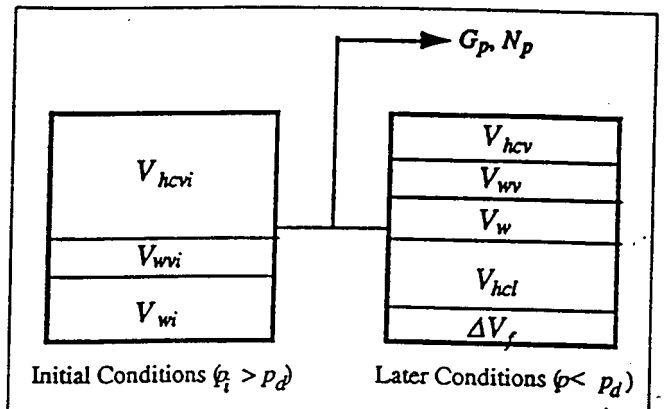

Material-balance model showing reservoir PV occupied by hydrocarbons and water at initial and later conditions for a gas-condensate reservoir with water vaporization.

FIG. 3.19

TABLE 3.1

INITIAL SURFACE PRODUCTION DATA, EXAMPLE 4				
			Separator Conditions	
	Specific Gravity of Surface Fluids	Field Production	Pressure (psia)	Temperature (°F)
Primary separator	0.72	59,550 scf/STB	200	62
Stock-tank gas	1.230	415 scf/STB	14.7	60
Stock-tank oil	54.5 °API	1,050 STB/D	14.7	60

TABLE 3.2

RESERVOIR PRESSURE AND PRODUCTION HISTORY, EXAMPLE 5		
p_I (psia)	G_p (MMscf)	z
4,000	0	0.80
3,500	2.460	0.73
3,000	4.920	0.66
2,500	7.880	0.60
2,000	11.200	0.55

TABLE 3.3

MATERIAL-BALANCE PLOTTING FUNCTIONS, EXAMPLE 5	
G_p (MMscf)	p/z (psia)
0	5,000
2.460	4,795
4.920	4,545
7.880	4,167
11.200	3,636

TABLE 3.4

PRESSURE HISTORY AT THE RESERVOIR/ AQUIFER BOUNDARY, EXAMPLE .6

Time (days)	p_r (psia)
0	3,793
91.5	3,788
183.0	3,774
274.5	3,748
366.0	3,709
457.5	3,680
549.0	3,643

TABLE 3.5

SUMMARY OF INTERMEDIATE RESULTS, EXAMPLE 6

n	Time (days)	t_{Dn}	p (psia)	Δp_n (psi)	$Q_{pD}(t_{Dn})$
0	0	0	3,793	0	0
1	91.5	15.1	3,788	2.5	10.1
2	183.0	30.2	3,774	9.5	17.0
3	274.5	45.3	3,748	20.0	23.1
4	366.0	60.4	3,709	32.5	29.0
5	457.5	75.5	3,680	34.0	34.5
6	549.0	90.6	3,643	33.0	40.0

TABLE 3.6

SUMMARY OF FINAL RESULTS, EXAMPLE 6

n	Time (days)	p (psia)	W_e (RB)
0	0	3,793	0
1	91.5	3,788	11,471
2	183.0	3,774	62,898
3	274.5	3,748	191,374
4	366.0	3,709	436,219
5	457.5	3,680	781,237
6	549.0	3,643	1,212,890

TABLE 3.7

PRESSURE HISTORY AT THE RESERVOIR/ AQUIFER BOUNDARY, EXAMPLE .7

t (days)	p_r at Reservoir/ Aquifer Boundary (psia)
9	3,793
91.5	3,788
183.0	3,774
274.5	3,748
366.0	3,709
457.5	3,680
549.0	3,643

TABLE 3.8

SUMMARY OF INTERMEDIATE RESULTS, EXAMPLE .7

n	t (days)	t_{Dn}	t_{Dn-1}	$t_{Dn}-t_{Dn-1}$	Δp_n (psi)	$p_D(t_{Dn})$	$p_{D'}(t_{Dn})$
0	0	0	0	0	0	0	0
1	91.5	15.1	0	15.1	5	1.83	0.0296
2	183.0	30.2	15.1	15.1	19	2.15	0.0155
3	274.5	45.3	30.2	15.1	45	2.34	0.0105
4	366.0	60.4	45.3	15.1	84	2.48	0.0080
5	457.5	75.5	60.4	15.1	113	2.59	0.0064
6	549.0	90.6	75.5	15.1	150	2.67	0.0054

TABLE 3.9

SUMMARY OF FINAL RESULTS, EXAMPLE .7

n	Time (days)	p (psia)	W_e (RB)
1	91.5	3,788	18,743
2	183.0	3,774	84,482
3	274.5	3,748	230,461
4	366.0	3,709	489,431
5	457.5	3,680	819,766
6	549.0	3,643	1,245,061

TABLE 3.10

AQUIFER PI's		
Type of Outer Aquifer Boundary	J for Radial Flow (STB/D-psi)	J for Linear Flow (STB/D-psi)
Finite, no flow	$J=\frac{0.00708kh(\theta/360)}{\mu[\ln(r_e/r_r)-0.75]}$	$J=\frac{3(0.001127)kwh}{\mu L}$
Finite, constant pressure	$J=\frac{0.00708kh(\theta/360)}{\mu \ln(r_e/r_r)}$	$J=\frac{0.001127kwh}{\mu L}$
Infinite	$J=\frac{0.00708kh(\theta/360)}{\mu \ln\sqrt{0.0142kt/\phi\mu c_t r_r^2}}$	$J=\frac{kwh}{1{,}000\mu\sqrt{0.0633kt/\phi\mu c_t}}$

TABLE 3.11

PRESSURE HISTORY AT THE RESERVOIR/ AQUIFER BOUNDARY, EXAMPLE 8	
t (days)	p_r (psia)
0	3,793
91.5	3,788
183.0	3,774
274.5	3,748
366.0	3,709
457.5	3,680
549.0	3,643

TABLE 3.12

SUMMARY OF FINAL RESULTS, EXAMPLE 8						
n	p_{rn} (psia)	$\bar{p}_{rn}$ (psia)	$p_{aq,n}$ (psia)	$p_{aq,n-1}-\bar{p}_{rn}$ (psia)	ΔW_e (RB)	W_e (RB)
0	3,793	3,793.0	3,793	0	0	0
1	3,788	3,790.5	3,792.8	2.5	8,587	8,587
2	3,774	3,781.0	3,791.9	11.8	40,630	49,217
3	3,748	3,761.0	3,789.7	30.9	106,399	155,616
4	3,709	3,728.5	3,785.1	61.2	210,285	365,901
5	3,680	3,694.5	3,778.4	90.6	311,642	677,543
6	3,643	3,661.5	3,769.8	116.9	402,060	1,079,603

TABLE 3.13

PRESSURE AND PRODUCTION HISTORIES, EXAMPLE 9

t (days)	p (psia)	G_p (MMscf)	W_p (STB)	z	B_g (RB/Mscf)
0	5,392	0	0	1.0530	0.6775
182.5	5,368	677.7	3	1.0516	0.6796
365	5,292	2,952.4	762	1.0470	0.6864
547.5	5,245	5,199.6	2,054	1.0442	0.6907
730	5,182	7,132.8	3,300	1.0404	0.6965
912.5	5,147	9,196.9	4,644	1.0383	0.6999
1,095	5,110	11,171.5	5,945	1.0360	0.7033
1,277.5	5,066	12,999.5	7,148	1.0328	0.7072
1,460	5,006	14,769.5	8,238	1.0285	0.7127
1,642.5	4,994	16,317.0	9,289	1.0276	0.7138
1,825	4,997	17,868.0	10,356	1.0278	0.7136
2,007.5	4,990	19,416.0	11,424	1.0273	0.7142
2,190	4,985	21,524.8	12,911	1.0270	0.7147

TABLE 3.14

MATERIAL-BALANCE PLOTTING FUNCTIONS, EXAMPLE 9

t (days)	t_{Dn}	Q_{pDn}	Δp_n (psia)	$\Sigma \Delta p Q_{pD}/(B_g - B_{gi})$ (1,000 psi/RB-Mscf)	$(G_p B_g + W_p B_w)/(B_g - B_{gi})$ (Bscf)
0	—	—	0	—	—
182.5	3.5	3.68	12.0	21.0	219.3
365	6.9	5.82	50	28.5	227.7
547.5	10.4	7.76	61.5	46.3	272.6
730	13.9	9.56	55.0	55.8	260.9
912.5	17.3	11.21	49.0	71.0	287.6
1,095	20.8	12.84	36.0	83.1	304.5
1,277.5	24.3	14.42	40.5	93.1	309.3
1,460	27.7	15.91	52.0	99.1	298.8
1,642.5	31.2	17.40	36.0	116.7	320.8
1,825	34.7	18.87	4.5	136.0	352.9
2,007.5	38.1	20.26	2.0	151.7	378.3
2,190	41.6	21.68	6.0	166.7	413.6

TABLE 3.15

PRESSURE AND PRODUCTION HISTORIES, EXAMPLE 10

p (psia)	z	G_p (MMscf)
9,507	1.440	0
9,292	1.418	392.5
8,970	1.387	1,642.2
8,595	1.344	3,225.8
8,332	1.316	4,260.3
8,009	1.282	5,503.5
7,603	1.239	7,538.1
7,406	1.218	8,749.2
7,002	1.176	10,509.3
6,721	1.147	11,758.9
6,535	1.127	12,789.2
5,764	1.048	17,262.5
4,766	0.977	22,890.8
4,295	0.928	28,144.6
3,750	0.891	32,566.7
3,247	0.854	36,819.9

TABLE 3.16

PLOTTING FUNCTIONS FOR EXAMPLE 10

G_p (MMscf)	p/z (psia)	$p/z[1-(c_w S_{wi}+c_f)(p_i-p)/(1-S_{wi})]$ (psia)
0	6,602	6,602
392.5	6,553	6,515
1,642.2	6,467	6,374
3,225.8	6,395	6,239
4,260.3	6,331	6,133
5,503.5	6,247	5,998
7,538.1	6,136	5,825
8,749.2	6,081	5,740
10,509.3	5,954	5,556
11,758.9	5,860	5,424
12,789.2	5,799	5,339
17,262.5	5,500	4,951
22,890.8	4,878	4,261
28,144.6	4,628	3,985
32,566.7	4,209	3,563
36,819.9	3,802	3,167

TABLE 3.17

PRESSURE AND PRODUCTION HISTORIES, EXAMPLE 11

p (psia)	z	G_p (MMscf)
9,507	1.440	0
9,292	1.418	392.5
8,970	1.387	1,642.2
8,595	1.344	3,225.8
8,332	1.316	4,260.3
8,009	1.282	5,503.5
7,603	1.239	7,538.1
7,406	1.218	8,749.2
7,002	1.176	10,509.3
6,721	1.147	11,758.9
6,535	1.127	12,789.2
5,764	1.048	17,262.5
4,766	0.977	22,890.8
4,295	0.928	28,144.6
3,750	0.891	32,566.7
3,247	0.854	36,819.9

TABLE 3.18

PLOTTING FUNCTIONS, EXAMPLE 11

p/z (psia)	G_p (MMscf)	$1/(p_i-p)[(p_iz/pz_i)-1]$ 10^{-6} psi^{-1}	$G_p/(p_i-p)(p_iz/pz_i)$ (Mscf/psi)
6,602.1	0	—	—
6,552.9	392.5	34.9	1,840
6,467.2	1,642.2	38.9	3,120
6,395.1	3,225.8	35.5	3,650
6,331.3	4,260.3	36.4	3,780
6,247.3	5,503.5	37.9	3,880
6,136.4	7,538.1	39.9	4,260
6,080.5	8,749.2	40.8	4,520
5,954.1	10,509.3	43.4	4,650
5,859.6	11,758.9	45.4	4,760
5,798.6	12,789.2	46.6	4,900
5,500.0	17,262.5	53.5	5,540
4,878.2	22,890.8	74.5	6,530
4,628.2	28,144.6	81.8	7,700
4,208.8	32,566.7	98.8	8,870
3,802.1	36,819.9	117.6	10,210

TABLE 3.19

TABLE E-4—Q_{pD} vs. t_D—INFINITE RADIAL SYSTEM, CONSTANT PRESSURE AT INNER BOUNDARY

t_D	Q_{pD}	t_D	Q_{pD}	t_D	Q_{pD}	t_D	Q_{pD}	t_D	Q_{pD}
0.00	0.000	98	42.433	740	226.904	1,975	528.337	8,900	1,986.796
0.01	0.112	99	42.781	750	229.514	2,000	534.145	9,000	2,006.628
0.05	0.278	100	43.129	760	232.120	2,025	539.945	9,100	2,026.438
0.10	0.404	105	44.858	770	234.721	2,050	545.737	9,200	2,046.227
0.15	0.520	110	46.574	775	236.020	2,075	551.522	9,300	2,065.996
0.20	0.606	115	48.277	780	237.318	2,100	557.299	9,400	2,085.744
0.25	0.689	120	49.968	790	239.912	2,125	563.068	9,500	2,105.473
0.30	0.758	125	51.648	800	242.501	2,150	568.830	9,600	2,125.184
0.40	0.898	130	53.317	810	245.086	2,175	574.585	9,700	2,144.878
0.50	1.020	135	54.976	820	247.668	2,200	580.332	9,800	2,164.555
0.60	1.140	140	56.625	825	248.957	2,225	586.072	9,900	2,184.216
0.70	1.251	145	58.265	830	250.245	2,250	591.086	10,000	2,203.861
0.80	1.359	150	59.895	840	252.819	2,275	597.532	12,500	2,688.967
0.90	1.469	155	61.517	850	255.388	2,300	603.252	15,000	3,164.780
1	1.569	160	63.131	860	257.953	2,325	608.965	17,500	3,633.368
2	2.447	165	64.737	870	260.515	2,350	614.672	20,000	4,095.800
3	3.202	170	66.336	875	261.795	2,375	620.372	25,000	5,005.726
4	3.893	175	67.928	880	263.073	2,400	626.066	30,000	5,899.508
5	4.539	180	69.512	890	265.629	2,425	631.755	35,000	6,780.247
6	5.153	185	71.090	900	268.181	2,450	637.437	40,000	7,650.096
7	5.743	190	72.661	910	270.729	2,475	643.113	50,000	9,363.099
8	6.314	195	74.226	920	273.274	2,500	648.781	60,000	11,047.299
9	6.869	200	75.785	925	274.545	2,550	660.093	70,000	12,708.358
10	7.411	205	77.338	930	275.815	2,600	671.379	75,000	13,531.457
11	7.940	210	78.886	940	278.353	2,650	682.640	80,000	14,350.121
12	8.457	215	80.428	950	280.888	2,700	693.877	90,000	15,975.389
13	8.964	220	81.965	960	283.420	2,750	705.090	100,000	17,586.284
14	9.461	225	83.497	970	285.948	2,800	716.280	125,000	21,560.732
15	9.949	230	85.023	975	287.211	2,850	727.449	1.5×10^5	2.538×10^4
16	10.434	235	86.545	980	288.473	2,900	738.598	2.0×10^5	3.308×10^4
17	10.913	240	88.062	990	290.995	2,950	749.725	2.5×10^5	4.066×10^4
18	11.386	245	89.575	1,000	293.514	3,000	760.833	3.0×10^5	4.817×10^4
19	11.855	250	91.084	1,010	296.030	3,050	771.922	4.0×10^5	6.267×10^4
20	12.319	255	92.589	1,020	298.543	3,100	782.992	5.0×10^5	7.699×10^4
21	12.778	260	94.090	1,025	299.799	3,150	794.042	6.0×10^5	9.113×10^4
22	13.233	265	95.588	1,030	301.053	3,200	805.075	7.0×10^5	1.051×10^5
23	13.684	270	97.081	1,040	303.560	3,250	816.090	8.0×10^5	1.189×10^5
24	14.131	275	98.571	1,050	306.065	3,300	827.088	9.0×10^5	1.326×10^5
25	14.573	280	100.057	1,060	308.567	3,350	838.067	1.0×10^6	1.462×10^5
26	15.013	285	101.540	1,070	311.066	3,400	849.028	1.5×10^6	2.126×10^5
27	15.450	290	103.019	1,075	312.314	3,450	859.974	2.0×10^6	2.781×10^5
28	15.883	295	104.495	1,080	313.562	3,500	870.903	2.5×10^6	3.427×10^5
29	16.313	300	105.968	1,090	316.055	3,550	881.816	3.0×10^6	4.064×10^5
30	16.742	305	107.437	1,100	318.545	3,600	892.712	4.0×10^6	5.313×10^5
31	17.167	310	108.904	1,110	321.032	3,650	903.594	5.0×10^6	6.544×10^5
32	17.590	315	110.367	1,120	323.517	3,700	914.459	6.0×10^6	7.761×10^5
33	18.011	320	111.827	1,125	324.760	3,750	926.309	7.0×10^6	8.965×10^5
34	18.429	325	113.284	1,130	326.000	3,800	936.144	8.0×10^6	1.016×10^6
35	18.845	330	114.738	1,140	328.480	3,850	946.966	9.0×10^6	1.134×10^6
36	19.259	335	116.189	1,150	330.958	3,900	957.773	1.0×10^7	1.252×10^6
37	19.671	340	117.638	1,160	333.433	3,950	968.566	1.5×10^7	1.828×10^6
38	20.080	345	119.083	1,170	335.906	4,000	979.344	2.0×10^7	2.398×10^6
39	20.488	350	120.526	1,175	337.142	4,050	990.108	2.5×10^7	2.961×10^6
40	20.894	355	121.966	1,180	338.376	4,100	1,000.858	3.0×10^7	3.517×10^6
41	21.298	360	123.403	1,190	340.843	4,150	1,011.595	4.0×10^7	4.610×10^6
42	21.701	365	124.838	1,200	343.308	4,200	1,022.318	5.0×10^7	5.689×10^6
43	22.101	370	126.270	1,210	345.770	4,250	1,033.028	6.0×10^7	6.758×10^6
44	22.500	375	127.699	1,220	348.230	4,300	1,043.724	7.0×10^7	7.816×10^6
45	22.897	380	129.126	1,225	349.460	4,350	1,054.409	8.0×10^7	8.866×10^6
46	23.291	385	130.550	1,230	350.688	4,400	1,065.082	9.0×10^7	9.911×10^6
47	23.684	390	131.972	1,240	353.144	4,450	1,075.743	1.0×10^8	1.095×10^7
48	24.076	395	133.391	1,250	355.597	4,500	1,086.390	1.5×10^8	1.604×10^7
49	24.466	400	134.808	1,260	358.048	4,550	1,097.024	2.0×10^8	2.108×10^7
50	24.855	405	136.223	1,270	360.496	4,600	1,107.646	2.5×10^8	2.607×10^7
51	25.244	410	137.635	1,275	361.720	4,650	1,118.257	3.0×10^8	3.100×10^7
52	25.633	415	139.045	1,280	362.942	4,700	1,128.854	4.0×10^8	4.071×10^7
53	26.020	420	140.453	1,290	365.386	4,750	1,139.439	5.0×10^8	5.03×10^7
54	26.406	425	141.859	1,300	367.828	4,800	1,150.012	6.0×10^8	5.98×10^7
55	26.791	430	143.262	1,310	370.267	4,850	1,160.574	7.0×10^8	6.928×10^7
56	27.174	435	144.664	1,320	372.704	4,900	1,171.125	8.0×10^8	7.865×10^7
57	27.555	440	146.064	1,325	373.922	4,950	1,181.666	9.0×10^8	8.797×10^7
58	27.935	445	147.461	1,330	375.139	5,000	1,192.198	1.0×10^9	9.725×10^7
59	28.314	450	148.856	1,340	377.572	5,100	1,213.222	1.5×10^9	1.429×10^8
60	28.691	455	150.249	1,350	380.003	5,200	1,234.203	2.0×10^9	1.880×10^8

TABLE E-4—Q_{pD} vs. t_D—INFINITE RADIAL SYSTEM, CONSTANT PRESSURE AT INNER BOUNDARY (continued)

t_D	Q_{pD}	t_D	Q_{pD}	t_D	Q_{pD}	t_D	Q_{pD}	t_D	Q_{pD}
61	29.068	460	151.460	1,360	382.432	5,300	1,255.141	2.5×10^9	2.328×10^8
62	29.443	465	153.029	1,370	384.859	5,400	1,276.037	3.0×10^9	2.771×10^8
63	29.818	470	154.416	1,375	386.070	5,500	1,296.893	4.0×10^9	3.645×10^8
64	30.192	475	155.801	1,380	387.283	5,600	1,317.709	5.0×10^9	4.510×10^8
65	30.565	480	157.184	1,390	389.705	5,700	1,338.486	6.0×10^9	5.366×10^8
66	30.937	485	158.565	1,400	392.125	5,800	1,359.225	7.0×10^9	6.220×10^8
67	31.308	490	159.945	1,410	394.543	5,900	1,379.927	8.0×10^9	7.066×10^8
68	31.679	495	161.322	1,420	396.959	6,000	1,400.593	9.0×10^9	7.909×10^8
69	32.048	500	162.698	1,425	398.167	6,100	1,421.224	1.0×10^{10}	8.747×10^8
70	32.417	510	165.444	1,430	399.373	6,200	1,441.820	1.5×10^{10}	1.288×10^9
71	32.785	520	168.183	1,440	401.786	6,300	1,462.383	2.0×10^{10}	1.697×10^9
72	33.151	525	169.549	1,450	404.197	6,400	1,482.912	2.5×10^{10}	2.103×10^9
73	33.517	530	170.914	1,460	406.606	6,500	1,503.408	3.0×10^{10}	2.505×10^9
74	33.883	540	173.639	1,470	409.013	6,600	1,523.872	4.0×10^{10}	3.299×10^9
75	34.247	550	176.357	1,475	410.214	6,700	1,544.305	5.0×10^{10}	4.087×10^9
76	34.611	560	179.069	1,480	411.418	6,800	1,564.706	6.0×10^{10}	4.868×10^9
77	34.974	570	181.774	1,490	413.820	6,900	1,585.077	7.0×10^{10}	5.643×10^9
78	35.336	580	184.473	1,500	416.220	7,000	1,605.418	8.0×10^{10}	6.414×10^9
79	35.697	590	187.166	1,525	422.214	7,100	1,625.729	9.0×10^{10}	7.183×10^9
80	36.058	600	189.852	1,550	428.196	7,200	1,646.011	1.0×10^{11}	7.948×10^9
81	36.418	610	192.533	1,575	434.168	7,300	1,666.265	1.5×10^{11}	1.17×10^{10}
82	36.777	620	195.208	1,600	440.128	7,400	1,686.490	2.0×10^{11}	1.55×10^{10}
83	37.136	625	196.544	1,625	446.077	7,500	1,706.688	2.5×10^{11}	1.92×10^{10}
84	37.494	630	197.878	1,650	452.016	7,600	1,726.859	3.0×10^{11}	2.29×10^{10}
85	37.851	640	200.542	1,675	457.945	7,700	1,747.002	4.0×10^{11}	3.02×10^{10}
86	38.207	650	203.201	1,700	463.863	7,800	1,767.120	5.0×10^{11}	3.75×10^{10}
87	38.563	660	205.854	1,725	469.771	7,900	1,787.212	6.0×10^{11}	4.47×10^{10}
88	38.919	670	208.502	1,750	475.669	8,000	1,807.278	7.0×10^{11}	5.19×10^{10}
89	39.272	675	209.825	1,775	481.558	8,100	1,827.319	8.0×10^{11}	5.89×10^{10}
90	39.626	680	211.145	1,800	487.437	8,200	1,847.336	9.0×10^{11}	6.58×10^{10}
91	39.979	690	213.784	1,825	493.307	8,300	1,867.329	1.0×10^{11}	7.28×10^{10}
92	40.331	700	216.417	1,850	499.167	8,400	1,887.298	1.5×10^{11}	1.08×10^{11}
93	40.684	710	219.046	1,875	505.019	8,500	1,907.243	2.0×10^{11}	1.42×10^{11}
94	41.034	720	221.670	1,900	510.861	8,600	1,927.166		
95	41.385	725	222.980	1,925	516.695	8,700	1,947.065		
96	41.735	730	224.289	1,950	522.520	8,800	1,966.942		
97	42.084								

For $t_D < 0.01$, $Q_{pD} = \dfrac{2\sqrt{t_D}}{\pi}$.

For $t_D > 200$, $Q_{pD} = \dfrac{-4.29881 + 2.02566 t_D}{\ln t_D}$.

TABLE 3.20

TABLE E-5—Q_{pD} vs. t_D—FINITE RADIAL SYSTEM WITH CLOSED EXTERIOR BOUNDARY, CONSTANT PRESSURE AT INNER BOUNDARY

$r_{eD} = 1.5$		$r_{eD} = 2.0$		$r_{eD} = 2.5$		$r_{eD} = 3.0$		$r_{eD} = 3.5$		$r_{eD} = 4.0$	
t_D	Q_{pD}	t_D	Q_{pD}	t_D	Q_{pD}	t_D	Q_{pD}	t_D	Q_{pD}	t_D	Q_{pD}
0.05	0.276	0.05	0.278	0.10	0.408	0.30	0.755	1.00	1.571	2.00	2.442
0.06	0.304	0.075	0.345	0.15	0.509	0.40	0.895	1.20	1.761	2.20	2.598
0.07	0.330	0.10	0.404	0.20	0.599	0.50	1.023	1.40	1.940	2.40	2.748
0.08	0.354	0.125	0.458	0.25	0.681	0.60	1.143	1.60	2.111	2.60	2.893
0.09	0.375	0.150	0.507	0.30	0.758	0.70	1.256	1.80	2.273	2.80	3.034
0.10	0.395	0.175	0.553	0.35	0.829	0.80	1.363	2.00	2.427	3.00	3.170
0.11	0.414	0.200	0.597	0.40	0.897	0.90	1.465	2.20	2.574	3.25	3.334
0.12	0.431	0.225	0.638	0.45	0.962	1.00	1.563	2.40	2.715	3.50	3.493
0.13	0.446	0.250	0.678	0.50	1.024	1.25	1.791	2.60	2.849	3.75	3.645
0.14	0.461	0.275	0.715	0.55	1.083	1.50	1.997	2.80	2.976	4.00	3.792
0.15	0.474	0.300	0.751	0.60	1.140	1.75	2.184	3.00	3.098	4.25	3.932
0.16	0.486	0.325	0.785	0.65	1.195	2.00	2.353	3.25	3.242	4.50	4.068
0.17	0.497	0.350	0.817	0.70	1.248	2.25	2.507	3.50	3.379	4.75	4.198
0.18	0.507	0.375	0.848	0.75	1.299	2.50	2.646	3.75	3.507	5.00	4.323
0.19	0.517	0.400	0.877	0.80	1.348	2.75	2.772	4.00	3.628	5.50	4.560
0.20	0.525	0.425	0.905	0.85	1.395	3.00	2.886	4.25	3.742	6.00	4.779
0.21	0.533	0.450	0.932	0.90	1.440	3.25	2.990	4.50	3.850	6.50	4.982
0.22	0.541	0.475	0.958	0.95	1.484	3.50	3.084	4.75	3.951	7.00	5.169
0.23	0.548	0.500	0.983	1.0	1.526	3.75	3.170	5.00	4.047	7.50	5.343
0.24	0.554	0.550	1.028	1.1	1.605	4.00	3.247	5.50	4.222	8.00	5.504
0.25	0.559	0.600	1.070	1.2	1.679	4.25	3.317	6.00	4.378	8.50	5.653
0.26	0.565	0.650	1.108	1.3	1.747	4.50	3.381	6.50	4.516	9.00	5.790
0.28	0.574	0.700	1.143	1.4	1.811	4.75	3.439	7.00	4.639	9.50	5.917
0.30	0.582	0.750	1.174	1.5	1.870	5.00	3.491	7.50	4.749	10	6.035
0.32	0.588	0.800	1.203	1.6	1.924	5.50	3.581	8.00	4.846	11	6.246
0.34	0.594	0.900	1.253	1.7	1.975	6.00	3.656	8.50	4.932	12	6.425
0.36	0.599	1.000	1.295	1.8	2.022	6.50	3.717	9.00	5.009	13	6.580
0.38	0.603	1.1	1.330	2.0	2.106	7.00	3.767	9.50	5.078	14	6.712
0.40	0.606	1.2	1.358	2.2	2.178	7.50	3.809	10.00	5.138	15	6.825
0.45	0.613	1.3	1.382	2.4	2.241	8.00	3.843	11	5.241	16	6.922
0.50	0.617	1.4	1.402	2.6	2.294	9.00	3.894	12	5.321	17	7.004
0.60	0.621	1.6	1.432	2.8	2.340	10.00	3.928	13	5.385	18	7.076
0.70	0.623	1.7	1.444	3.0	2.380	11.00	3.951	14	5.435	20	7.189
0.80	0.624	1.8	1.453	3.4	2.444	12.00	3.967	15	5.476	22	7.272
		2.0	1.468	3.8	2.491	14.00	3.985	17	5.506	24	7.332
		2.5	1.487	4.2	2.525	16.00	3.993	18	5.531	26	7.377
		3.0	1.495	4.6	2.551	18.00	3.997	19	5.551	30	7.434
		4.0	1.499	5.0	2.570	20.00	3.999	20	5.579	34	7.464
		5.0	1.500	6.0	2.599	22.00	3.999	25	5.611	38	7.481
				7.0	2.613	24.00	4.000	30	5.621	42	7.490
				8.0	2.619			35	5.624	46	7.494
				9.0	2.622			40	5.625	50	7.497
				10.0	2.624						

TABLE E-5—Q_{pD} vs. t_D—FINITE RADIAL SYSTEM WITH CLOSED EXTERIOR BOUNDARY, CONSTANT PRESSURE AT INNER BOUNDARY (Continued)

$r_{eD} = 4.5$		$r_{eD} = 5.0$		$r_{eD} = 6.0$		$r_{eD} = 7.0$		$r_{eD} = 8.0$		$r_{eD} = 9.0$		$r_{eD} = 10.0$	
t_D	Q_{pD}	t_D	Q_{pD}	t_D	Q_{pD}	t_D	Q_{pD}	t_D	Q_{pD}	t_D	Q_{pD}	t_D	Q_{pD}
2.5	2.835	3.0	3.195	6.0	5.148	9.00	6.861	9	6.861	10	7.417	15	9.965
3.0	3.196	3.5	3.542	6.5	5.440	9.50	7.127	10	7.398	15	9.945	20	12.32
3.5	3.537	4.0	3.875	7.0	5.724	10	7.389	11	7.920	20	12.26	22	13.22
4.0	3.859	4.5	4.193	7.5	6.002	11	7.902	12	8.431	22	13.13	24	14.09
4.5	4.165	5.0	4.499	8.0	6.273	12	8.397	13	8.930	24	13.98	26	14.95
5.0	4.454	5.5	4.792	8.5	6.537	13	8.876	14	9.418	26	14.79	28	15.78
5.5	4.727	6.0	5.074	9.0	6.795	14	9.341	15	9.895	28	15.59	30	16.59
6.0	4.986	6.5	5.345	9.5	7.047	15	9.791	16	10.36	30	16.35	32	17.38
6.5	5.231	7.0	5.605	10.0	7.293	16	10.23	17	10.82	32	17.10	34	18.16
7.0	5.464	7.5	5.854	10.5	7.533	17	10.65	18	11.26	34	17.82	36	18.91
7.5	5.684	8.0	6.094	11	7.767	18	11.06	19	11.70	36	18.52	38	19.65
8.0	5.892	8.5	6.325	12	8.220	19	11.46	20	12.13	38	19.19	40	20.37
8.5	6.089	9.0	6.547	13	8.651	20	11.85	22	12.95	40	19.85	42	21.07
9.0	6.276	9.5	6.760	14	9.063	22	12.58	24	13.74	42	20.48	44	21.76
9.5	6.453	10	6.965	15	9.456	24	13.27	26	14.50	44	21.09	46	22.42
10	6.621	11	7.350	16	9.829	26	13.92	28	15.23	46	21.69	48	23.07
11	6.930	12	7.706	17	10.19	28	14.53	30	15.92	48	22.26	50	23.71
12	7.208	13	8.035	18	10.53	30	15.11	34	17.22	50	22.82	52	24.33
13	7.457	14	8.339	19	10.85	35	16.39	38	18.41	52	23.36	54	24.94
14	7.680	15	8.620	20	11.16	40	17.49	40	18.97	54	23.89	56	25.53
15	7.880	16	8.879	22	11.74	45	18.43	45	20.26	56	24.39	58	26.11
16	8.060	18	9.338	24	12.26	50	19.24	50	21.42	58	24.88	60	26.67
18	8.365	20	9.731	25	12.50	60	20.51	55	22.46	60	25.36	65	28.02
20	8.611	22	10.07	31	13.74	70	21.45	60	23.40	65	26.48	70	29.29
22	8.809	24	10.35	35	14.40	80	22.13	70	24.98	70	27.52	75	30.49
24	8.968	26	10.59	39	14.93	90	22.63	80	26.26	75	28.48	80	31.61
26	9.097	28	10.80	51	16.05	100	23.00	90	27.28	80	29.36	85	32.67
28	9.200	30	10.98	60	16.56	120	23.47	100	28.11	85	30.18	90	33.66
30	9.283	34	11.26	70	16.91	140	23.71	120	29.31	90	30.93	95	34.60
34	9.404	38	11.46	80	17.41	160	23.85	140	30.08	95	31.63	100	35.48
38	9.481	42	11.61	90	17.27	180	23.92	160	30.58	100	32.27	120	38.51
42	9.532	46	11.71	100	17.36	200	23.96	180	30.91	120	34.39	140	40.89
46	9.565	50	11.79	110	17.41	500	24.00	200	31.12	140	35.92	160	42.75
50	9.586	60	11.91	120	17.45			240	31.34	160	37.04	180	44.21
60	9.612	70	11.96	130	17.46			280	31.43	180	37.85	200	45.36
70	9.621	80	11.98	140	17.48			320	31.47	200	38.44	240	46.95
80	9.623	90	11.99	150	17.49			360	31.49	240	39.17	280	47.94
90	9.624	100	12.00	160	17.49			400	31.50	280	39.56	320	48.54
100	9.625	120	12.00	180	17.50			500	31.50	320	39.77	360	48.91
				200	17.50					360	39.88	400	49.14
				220	17.50					400	39.94	440	49.28
										440	39.97	480	49.36
										480	39.98		

TABLE E-5—Q_{pD} vs. t_D—FINITE RADIAL SYSTEM WITH CLOSED EXTERIOR BOUNDARY, CONSTANT PRESSURE AT INNER BOUNDARY (Continued)

$r_{eD} = 20$

t_D	q_D	Q_{pD}
100	0.3394	42.91
130	0.3174	52.76
160	0.2975	61.98
200	0.2728	73.38
240	0.2502	83.83
300	0.2197	97.91
400	0.1770	117.7
500	0.1426	133.6
600	0.1148	146.4
700	0.0925	156.7
800	0.0745	165.1
1,000	0.0483	177.1
1,300	0.0483	187.8
1,600	0.0132	193.4
2,000	0.0056	196.9
3,000	0.0006	199.2

$r_{eD} = 50$

t_D	q_D	Q_{pD}
600	0.2652	189.0
800	0.2915	241
1,000	0.2393	290
1,300	0.2220	359
1,600	0.2060	473
2,000	0.1865	502
2,400	0.1682	573
3,000	0.1543	667
4,000	0.1133	795
5,000	0.0833	895
6,000	0.0682	974
8,000	0.0418	1,082
1×10^4	0.0254	1,148
1.3×10^4	0.0120	1,201
1.6×10^4	0.0056	1,227
2×10^4	0.0021	1,241
2.4×10^4	0.0006	1,246
3×10^4	0.0002	1,249

$r_{eD} = 100$

t_D	q_D	Q_{pD}
2,000	0.2304	532
3,000	0.2179	757
4,000	0.2070	969
5,000	0.1967	1,171
6,000	0.1869	1,363
8,000	0.1686	1,718
1×10^4	0.1536	2,000
1.3×10^4	0.1304	2.46×10^3
1.6×10^4	0.1118	2.82×10^3
2×10^4	0.0910	3.23×10^3
2.4×10^4	0.0741	3.56×10^3
3×10^4	0.0645	3.94×10^3
4×10^4	0.0326	4.37×10^3
5×10^4	0.0195	4.62×10^3
6×10^4	0.0117	4.77×10^3
8×10^4	0.0042	4.92×10^3
1×10^5	0.0015	4.97×10^3
1.1×10^5	0.0009	4.98×10^3

$r_{eD} = 200$

t_D	q_D	Q_{pD}
1×10^4	0.1943	2.19×10^3
1.3×10^4	0.1860	2.77×10^3
1.6×10^4	0.1820	3.33×10^3
2×10^4	0.1742	4.04×10^3
2.4×10^4	0.1668	4.72×10^3
3×10^4	0.1562	5.69×10^3
4×10^4	0.1401	7.17×10^3
5×10^4	0.1236	8.50×10^3
6×10^4	0.1126	9.68×10^3
8×10^4	0.0905	1.17×10^4
1×10^5	0.0728	1.33×10^4
1.3×10^5	0.0524	1.52×10^4
1.6×10^5	0.0378	1.65×10^4
2×10^5	0.0244	1.78×10^4
2.4×10^5	0.0138	1.86×10^4
3×10^5	0.0082	1.92×10^4
4×10^5	0.0028	1.97×10^4
5×10^5	0.0009	1.99×10^4

$r_{eD} = 500$

t_D	q_D	Q_{pD}
1×10^5	0.1566	1.75×10^4
1.3×10^5	0.1498	2.21×10^4
1.6×10^5	0.1435	2.65×10^4
2×10^5	0.1354	3.21×10^4
2.4×10^5	0.1277	3.73×10^4
3×10^5	0.1170	4.47×10^4
4×10^5	0.1012	5.56×10^4
5×10^5	0.0875	6.50×10^4
6×10^5	0.0756	7.31×10^4
8×10^5	0.0565	8.62×10^4
1×10^6	0.0422	9.60×10^4
1.3×10^6	0.0273	1.06×10^5
1.6×10^6	0.0176	1.13×10^5
2×10^6	0.0098	1.18×10^5
2.4×10^6	0.0055	1.21×10^5
3×10^6	0.0023	1.23×10^5
4×10^6	0.0005	1.25×10^5
5×10^6	0.0001	1.25×10^5

$r_{eD} = 1{,}000$

t_D	q_D	Q_{pD}
3×10^4	0.1773	5.89×10^3
4×10^4	0.1729	7.64×10^3
5×10^4	0.1697	9.35×10^3
1×10^5	0.1604	1.76×10^4
2×10^5	0.1518	3.32×10^4
3×10^5	0.1464	4.80×10^4
4×10^5	0.1416	6.24×10^4
5×10^5	0.1371	7.64×10^4
6×10^5	0.1327	8.98×10^4
7×10^5	0.1285	1.03×10^5
8×10^5	0.1244	1.16×10^5
9×10^5	0.1204	1.23×10^5
1×10^6	0.1166	1.40×10^5
1.4×10^6	0.1024	1.83×10^5
2×10^6	0.0844	2.39×10^5
2.4×10^6	0.0741	2.71×10^5
3×10^6	0.0610	3.11×10^5
4×10^6	0.0442	3.63×10^5
5×10^6	0.0320	4.01×10^5
7×10^6	0.0167	4.48×10^5
8.4×10^6	0.0106	4.67×10^5
1×10^7	0.0063	4.80×10^5
1.4×10^7	0.0017	4.95×10^5
2×10^7	0.0004	4.99×10^5
3×10^7	0.0000	5.00×10^5

TABLE E-5—Q_{pD} vs. t_D—FINITE RADIAL SYSTEM WITH CLOSED EXTERIOR BOUNDARY, CONSTANT PRESSURE AT INNER BOUNDARY (Continued)

r_{eD} = 2,000			r_{eD} = 4,000			r_{eD} = 1 × 10⁴		
t_D	q_D	Q_{pD}	t_D	q_D	Q_{pD}	t_D	q_D	Q_{pD}
1×10^5	0.1604		9×10^5	0.1366		3×10^6	0.1263	4.06×10^5
2×10^5	0.1520		1×10^6	0.1356		4×10^6	0.1240	5.31×10^5
3×10^5	0.1475		1.3×10^6	0.1333		5×10^6	0.1222	6.76×10^5
4×10^5	0.1445	6.27×10^4	1.6×10^6	0.1315	2.26×10^5	6×10^6	0.1210	7.76×10^5
5×10^5	0.1422	7.70×10^4	2×10^6	0.1296	2.78×10^5	8×10^6	0.1188	1.02×10^6
6×10^5	0.1404	9.11×10^4	2.4×10^6	0.1280	3.30×10^5	1×10^7	0.1174	1.25×10^6
7×10^5	0.1389	1.05×10^5	3×10^6	0.1262	4.06×10^5	1.2×10^7	0.1162	1.49×10^6
8×10^5	0.1375	1.19×10^5	4×10^6	0.1237	5.31×10^5	1.4×10^7	0.1152	1.72×10^6
9×10^5	0.1363	1.33×10^5	5×10^6	0.1215	6.54×10^5	1.6×10^7	0.1143	1.95×10^6
1×10^6	0.1352	1.46×10^5	6×10^6	0.1194	7.74×10^5	1.8×10^7	0.1135	2.17×10^6
1.3×10^6	0.1320	1.86×10^5	8×10^6	0.1155	1.01×10^6	2×10^7	0.1128	2.40×10^6
1.6×10^6	0.1291	2.25×10^5	1×10^7	0.1118	1.24×10^6	2.4×10^7	0.1115	2.85×10^6
2×10^6	0.1254	2.76×10^5	1.2×10^7	0.1081	1.46×10^6	3×10^7	0.1098	3.51×10^6
2.4×10^6	0.1216	3.26×10^5	1.4×10^7	0.1046	1.67×10^6	4×10^7	0.1071	4.60×10^6
3×10^6	0.1166	3.97×10^5	1.6×10^7	0.1012	1.87×10^6	5×10^7	0.1050	5.66×10^6
4×10^6	0.1084	5.10×10^5	1.8×10^7	0.0979	2.07×10^6	7×10^7	0.0998	7.70×10^6
5×10^6	0.1008	6.14×10^5	2×10^7	0.0948	2.27×10^6	8×10^7	0.0975	8.69×10^6
7×10^6	0.0872	8.02×10^5	2.3×10^7	0.0902	2.54×10^6	9×10^7	0.0952	9.65×10^6
1×10^7	0.0701	1.04×10^6	3×10^7	0.0803	3.14×10^6	1×10^8	0.0930	1.06×10^7
1.3×10^7	0.0563	1.23×10^6	4×10^7	0.0681	3.88×10^6	1.2×10^8	0.0887	1.24×10^7
1.7×10^7	0.0421	1.42×10^6	5×10^7	0.0577	4.51×10^6	1.4×10^8	0.0846	1.41×10^7
2×10^7	0.0339	1.53×10^6	7×10^7	0.0415	5.49×10^6	1.7×10^8	0.0788	1.66×10^7
2.4×10^7	0.0253	1.65×10^6	8×10^7	0.0352	5.87×10^6	2×10^8	0.0734	1.89×10^7
3×10^7	0.0164	1.78×10^6	9×10^7	0.0298	6.20×10^6	2.4×10^8	0.0668	2.17×10^7
4×10^7	0.0079	1.89×10^6	1×10^8	0.0252	6.47×10^6	3×10^8	0.0580	2.54×10^7
5×10^7	0.0038	1.95×10^6	1.2×10^8	0.0181	6.90×10^6	4×10^8	0.0458	3.06×10^7
7×10^7	0.0009	1.99×10^6	1.4×10^8	0.0130	7.21×10^6	5×10^8	0.0362	3.47×10^7
1×10^8	0.0001	2.00×10^6	1.7×10^8	0.0079	7.52×10^6	6×10^8	0.0286	3.79×10^7
1.3×10^8	0.0000	2.00×10^6	2×10^8	0.0048	7.71×10^6	7×10^8	0.0226	4.04×10^7
			2.3×10^8	0.0029	7.82×10^6	8×10^8	0.0178	4.24×10^7
			2.6×10^8	0.0018	7.89×10^6	1×10^9	0.0111	4.53×10^7
			3×10^8	0.0009	7.94×10^6	1.4×10^9	0.0043	4.82×10^7
			4×10^8	0.0002	7.99×10^6	2×10^9	0.0011	4.96×10^7
			5×10^8	0.0000	8.00×10^6	3×10^9	0.0001	5.00×10^7

TABLE E-5—Q_{pD} vs. t_D—FINITE RADIAL SYSTEM WITH CLOSED EXTERIOR BOUNDARY, CONSTANT PRESSURE AT INNER BOUNDARY (Continued)

$r_{eD} = 2.5 \times 10^4$			$r_{eD} = 1 \times 10^5$		
t_D	q_D	Q_{pD}	t_D	q_D	Q_{pD}
3×10^7	0.1103		1.4×10^8	0.1017	
4×10^7	0.1086		2×10^8	0.1000	
6×10^7	0.1064	6.77×10^6	2.4×10^8	0.0990	
7×10^7	0.1054	7.83×10^6	3×10^8	0.0980	3.10×10^7
8×10^7	0.1047	8.86×10^6	3.5×10^8	0.0971	3.59×10^7
9×10^7	0.1041	9.93×10^6	4×10^8	0.0966	4.07×10^7
1×10^8	0.1035	1.10×10^7	5×10^8	0.0956	5.03×10^7
1.4×10^8	0.1016	1.51×10^7	6×10^8	0.0948	5.98×10^7
2×10^8	0.0993	2.11×10^7	7×10^8	0.0941	6.93×10^7
2.6×10^8	0.0973	2.70×10^7	8×10^8	0.0935	7.87×10^7
3×10^8	0.0960	3.09×10^7	8.4×10^8	0.0933	8.24×10^7
3.3×10^8	0.0950	3.37×10^7	9×10^8	0.0930	8.80×10^7
3.6×10^8	0.0940	3.66×10^7	1×10^9	0.0925	9.73×10^7
4×10^8	0.0927	4.03×10^7	1.4×10^9	0.0911	1.34×10^8
4.4×10^8	0.0915	4.40×10^7	2×10^9	0.0896	1.80×10^8
5×10^8	0.0896	4.94×10^7	3×10^9	0.0877	2.77×10^8
5.4×10^8	0.0804	5.30×10^7	4×10^9	0.0861	3.64×10^8
6×10^8	0.0866	5.82×10^7	5×10^9	0.0845	4.49×10^8
6.4×10^8	0.0855	6.17×10^7	6×10^9	0.0829	5.33×10^8
7×10^8	0.0837	6.67×10^7	7×10^9	0.0814	6.15×10^8
7.4×10^8	0.0826	7.01×10^7	8×10^9	0.0799	6.95×10^8
8×10^8	0.0809	7.50×10^7	9×10^9	0.0784	7.75×10^8
8.4×10^8	0.0798	7.82×10^7	1×10^{10}	0.0770	8.52×10^8
9×10^8	0.0782	8.29×10^7	1.3×10^{10}	0.0728	1.08×10^9
1×10^9	0.0756	9.06×10^7	1.6×10^{10}	0.0689	1.29×10^9
1.3×10^9	0.0683	1.12×10^8	2×10^{10}	0.0639	1.56×10^9
1.6×10^9	0.0616	1.32×10^8	2.4×10^{10}	0.0594	1.80×10^9
2×10^9	0.0538	1.55×10^8	3×10^{10}	0.0531	2.14×10^9
2.4×10^9	0.0469	1.75×10^8	4×10^{10}	0.0441	2.62×10^9
3×10^9	0.0382	2.00×10^8	5×10^{10}	0.0366	3.03×10^9
4×10^9	0.0272	2.33×10^8	6×10^{10}	0.0304	3.36×10^9
5×10^9	0.0193	2.56×10^8	7×10^{10}	0.0253	3.64×10^9
6×10^9	0.0138	2.72×10^8	8×10^{10}	0.0210	3.87×10^9
8×10^9	0.0070	2.92×10^8	9×10^{10}	0.0174	4.06×10^9
1×10^{10}	0.0035	3.02×10^8	1×10^{11}	0.0145	4.22×10^9
1.4×10^{10}	0.0009	3.10×10^8	1.3×10^{11}	0.0083	4.55×10^9
2×10^{10}	0.0001	3.12×10^8	1.6×10^{11}	0.0048	4.74×10^9
3×10^{10}	0.0000	3.12×10^8	2×10^{11}	0.0023	4.88×10^9
			2.4×10^{11}	0.0011	4.94×10^9
			3×10^{11}	0.0004	4.98×10^9
			3.4×10^{11}	0.0002	4.99×10^9
			4×10^{11}	0.0001	5.00×10^9

TABLE E-5—Q_{pD} vs. t_D—FINITE RADIAL SYSTEM WITH CLOSED EXTERIOR BOUNDARY, CONSTANT PRESSURE AT INNER BOUNDARY (Continued)

$r_{eD} = 2.5 \times 10^5$			$r_{eD} = 1 \times 10^6$		
t_D	q_D	Q_{pD}	t_D	q_D	Q_{pD}
2×10^9	0.0897		2×10^{10}	0.0813	
3×10^9	0.0881		3×10^{10}	0.0800	
4×10^9	0.0870		4×10^{10}	0.0791	
5×10^9	0.0861	4.51×10^8	6×10^{10}	0.0778	
6×10^9	0.0854	5.37×10^8	8×10^{10}	0.0770	
7×10^9	0.0849	6.22×10^8	1×10^{11}	0.0763	7.95×10^9
8×10^9	0.0844	7.07×10^8	1.3×10^{11}	0.0756	1.02×10^{10}
1×10^{10}	0.0836	8.75×10^8	1.6×10^{11}	0.0750	1.25×10^{10}
1.4×10^{10}	0.0824	1.21×10^9	2×10^{11}	0.0743	1.55×10^{10}
2×10^{10}	0.0809	1.70×10^9	2.4×10^{11}	0.0737	1.84×10^{10}
3×10^{10}	0.0787	2.49×10^9	3×10^{11}	0.0730	2.28×10^{10}
4×10^{10}	0.0766	3.27×10^9	4×10^{11}	0.0719	3.21×10^{10}
4.4×10^{10}	0.0757	3.58×10^9	5×10^{11}	0.0709	3.72×10^{10}
4.7×10^{10}	0.0751	3.80×10^9	6×10^{11}	0.0697	4.42×10^{10}
5×10^{10}	0.0745	4.03×10^9	7×10^{11}	0.0686	5.11×10^{10}
5.4×10^{10}	0.0737	4.32×10^9	8×10^{11}	0.0676	6.32×10^{10}
6×10^{10}	0.0725	4.76×10^9	1×10^{12}	0.0656	7.13×10^{10}
7×10^{10}	0.0705	5.48×10^9	1.2×10^{12}	0.0636	8.42×10^{10}
7.4×10^{10}	0.0698	5.76×10^9	1.4×10^{12}	0.0617	9.67×10^{10}
8×10^{10}	0.0686	6.17×10^9	1.5×10^{12}	0.0607	1.03×10^{11}
8.4×10^{10}	0.0679	6.42×10^9			
9×10^{10}	0.0668	6.85×10^9	$> 1.5 \times 10^{12}$ not determined.		
1×10^{11}	0.0658	7.51×10^9			
1.1×10^{11}	0.0632	8.15×10^9			
1.3×10^{11}	0.0593	9.38×10^9			
1.6×10^{11}	0.0551	1.11×10^{10}			
2×10^{11}	0.0494	1.32×10^{10}			
2.4×10^{11}	0.0443	1.51×10^{10}			
3×10^{11}	0.0376	1.75×10^{10}			
4×10^{11}	0.0286	2.08×10^{10}			
5×10^{11}	0.0217	2.33×10^{10}			
7×10^{11}	0.0126	2.67×10^{10}			
1×10^{12}	0.0055	2.92×10^{10}			
1.3×10^{12}	0.0024	3.04×10^{10}			
1.6×10^{12}	0.0011	3.09×10^{10}			
2×10^{12}	0.0004	3.11×10^{10}			

For t_D smaller than values listed in this table for a given r_{eD}, the reservoir is infinite-acting. Find Q_{pD} in Table E-4.

For t_D larger than values listed in this table,

$$Q_{pD} \cong \frac{(r_{eD}^2 - 1)}{2}.$$

For t_D larger than values listed in this table, $q_D \cong 0$.

FIGURE 3.21

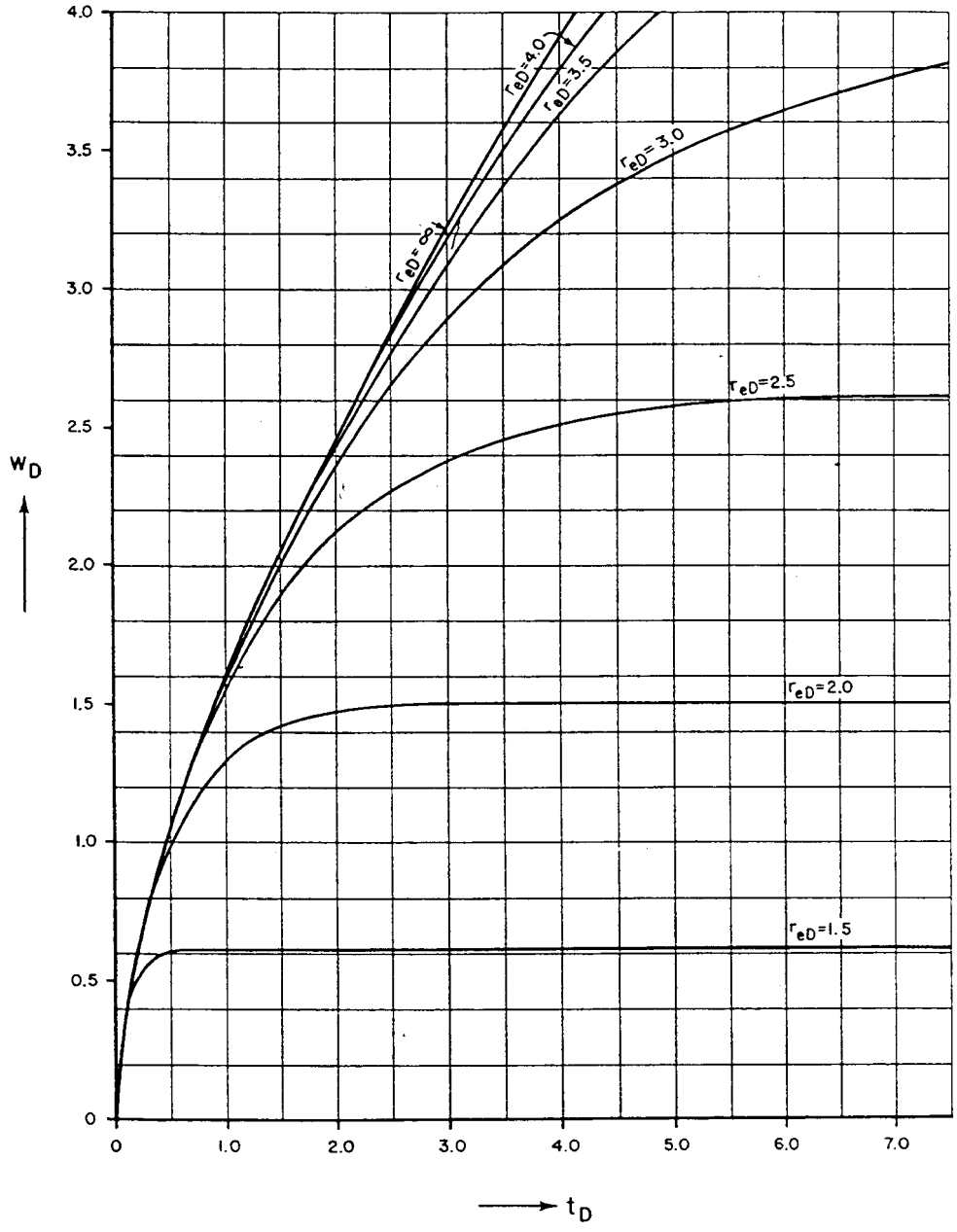

Fig. . Dimensionless water influx, constant terminal pressure case, radial flow. (After Hurst and van Everdingen, ref. 1).

FIGURE 3.22

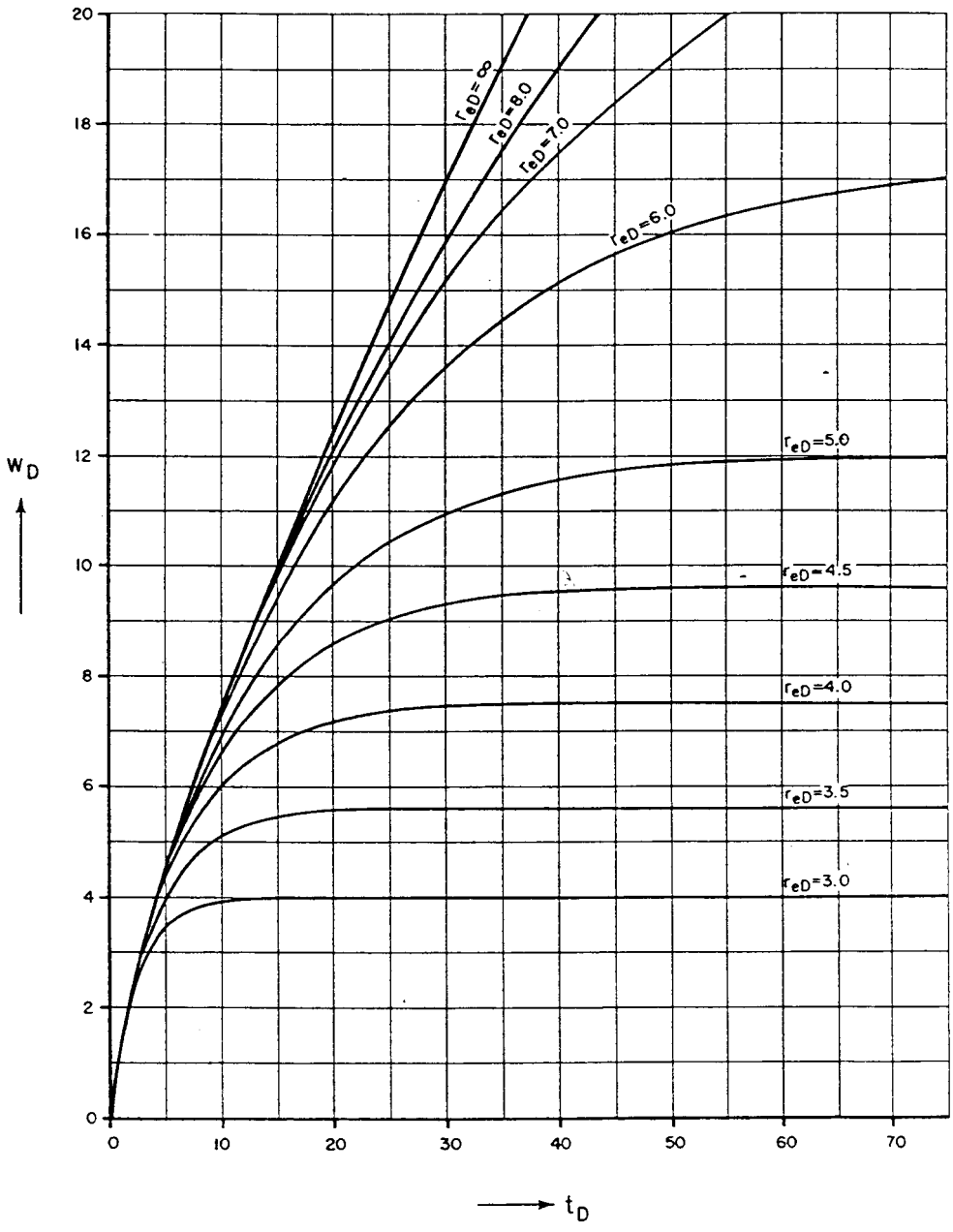

Fig. . . Dimensionless water influx, constant terminal pressure case, radial flow. (After Hurst and van Everdingen, ref. 1).

FIGURE 3.23

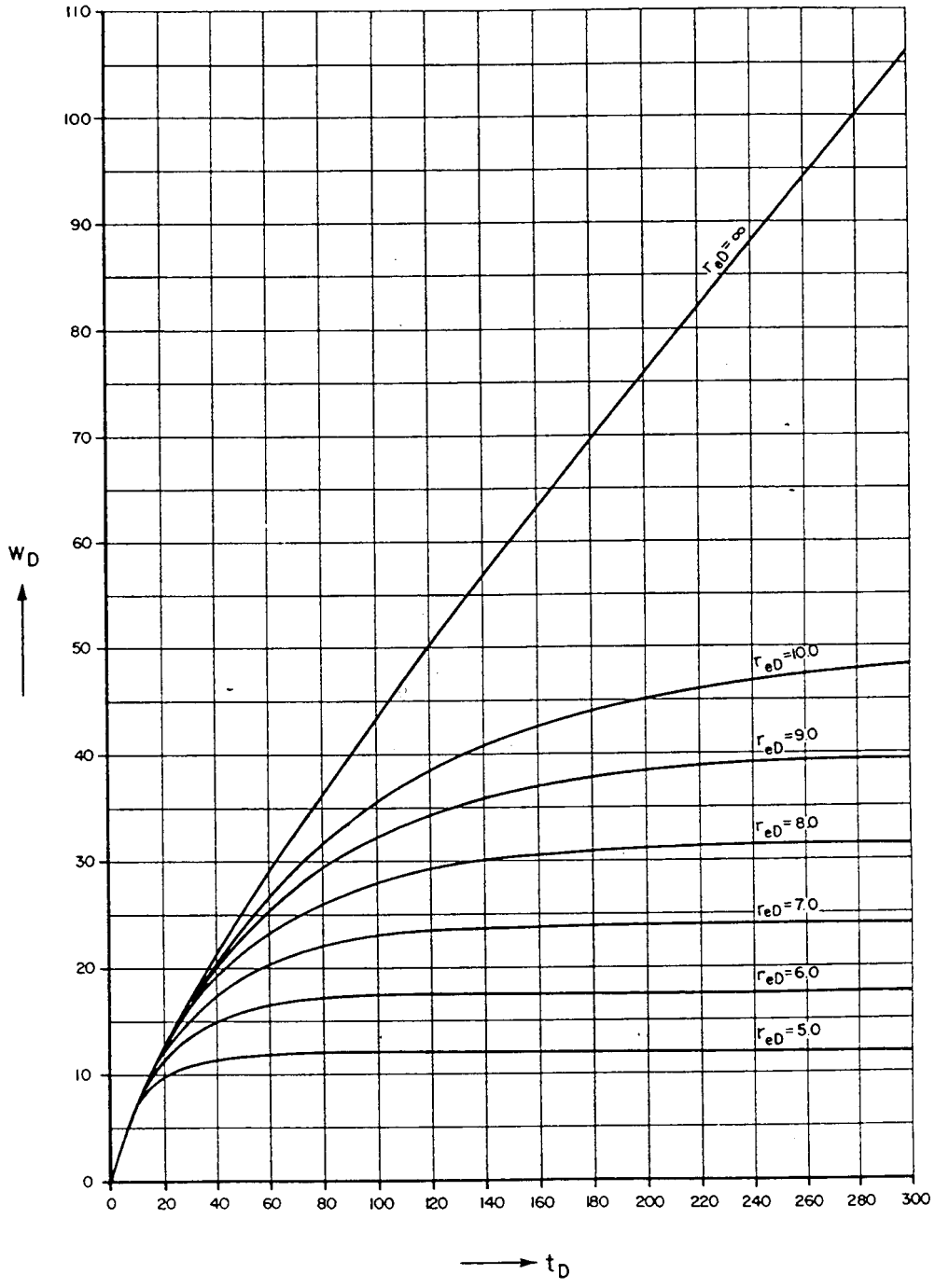

Fig. Dimensionless water influx, constant terminal pressure case, radial flow. (After Hurst and van Everdingen, ref. 1).

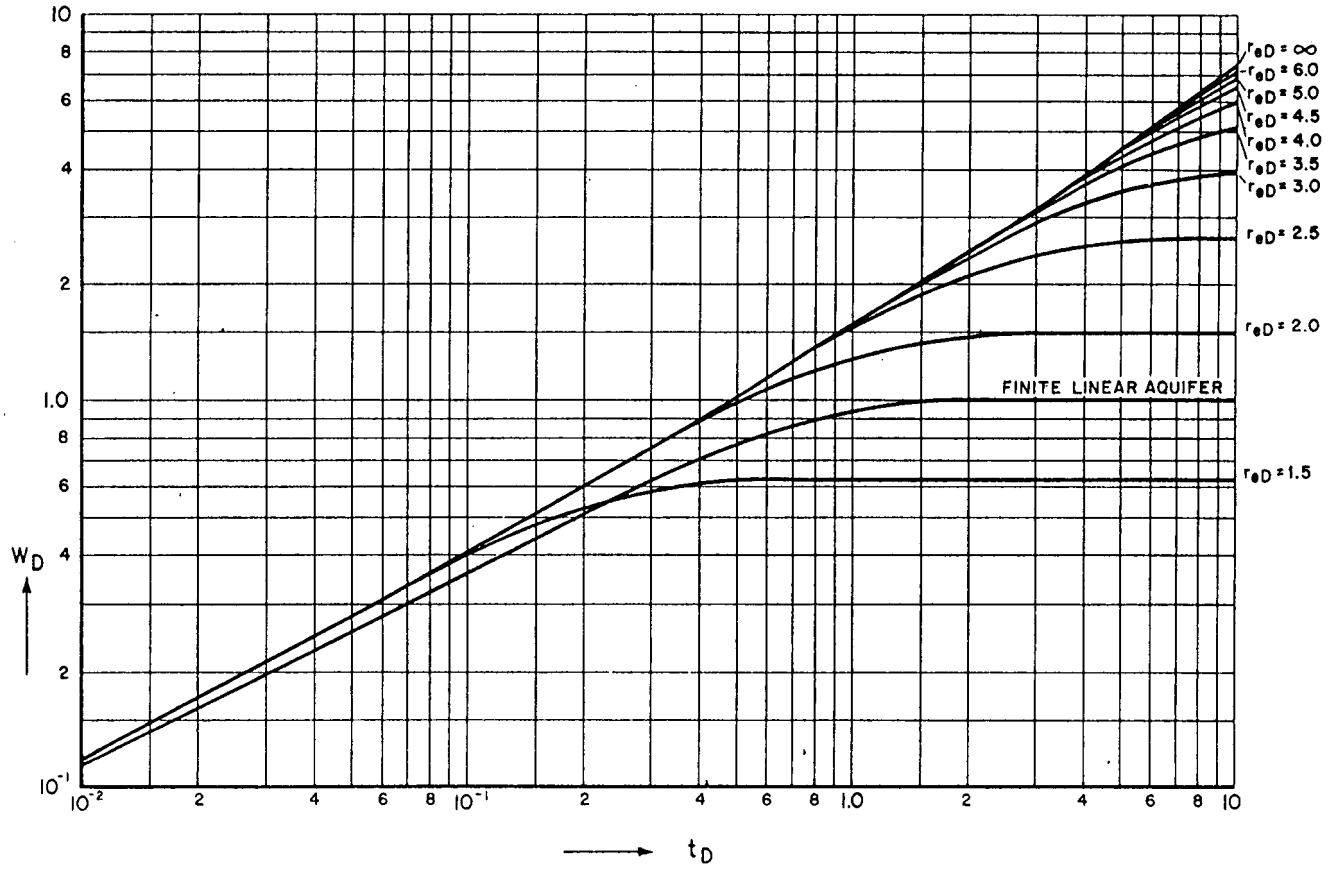

Fig. Dimensionless water influx, constant terminal pressure case, radial and linear flow. (After Hurst and van Everdingen, ref. 1).

FIGURE 3.24

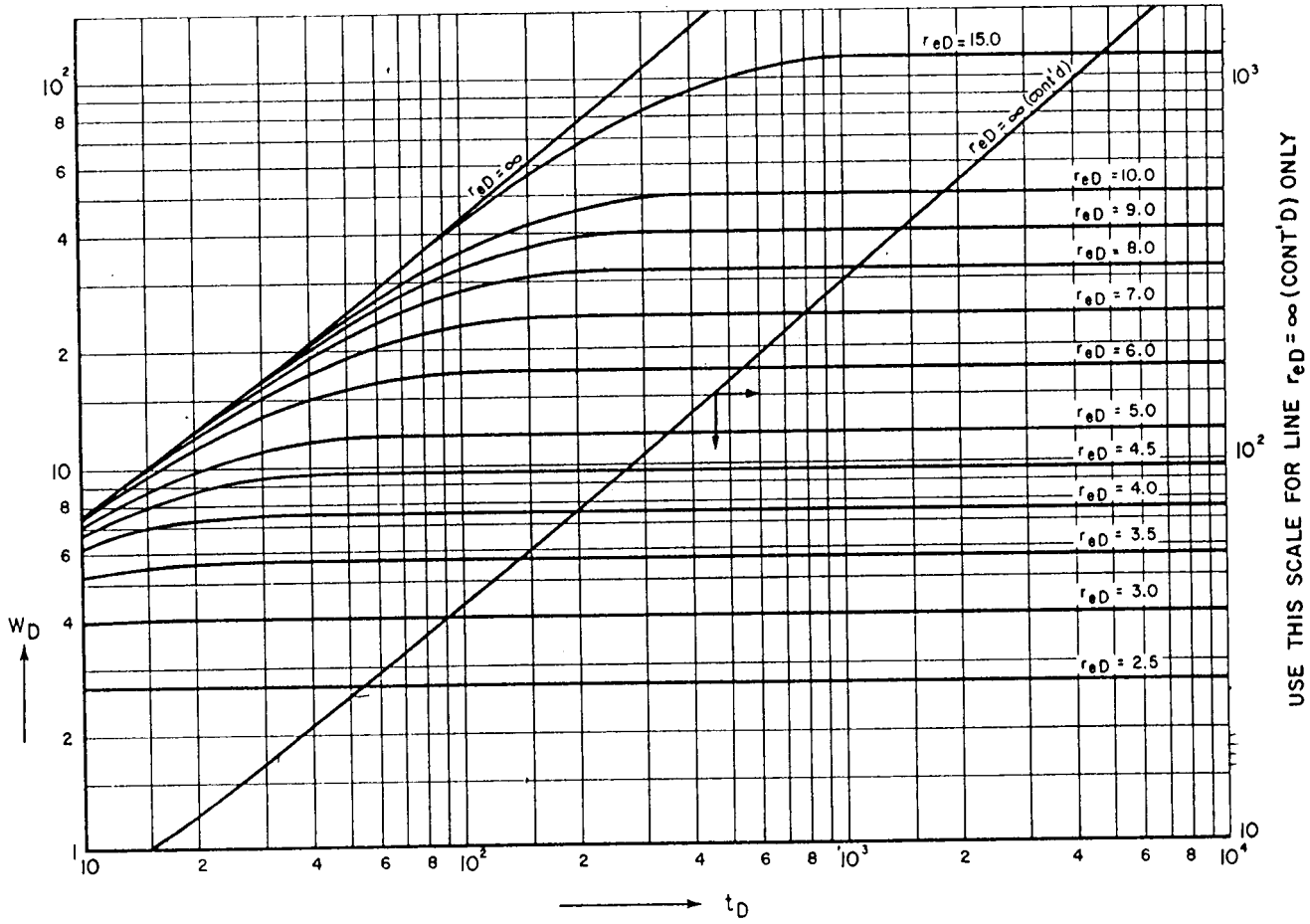

Fig. Dimensionless water influx, constant terminal pressure case, radial flow. (After Hurst and van Everdingen, ref. 1).

FIGURE 3.25

PART 4

PRESSURE TRANSIENT TESTING OF GAS WELLS

PRESSURE TRANSIENT TESTING OF GAS WELLS

4.1 TYPES AND PURPOSES OF PRESSURE TRANSIENT TESTS

The term pressure-transient test refers to a test in which we generate and measure pressure changes in a well as a function of time. From this measured pressure response, we can determine important formation properties of potential value in optimizing either an individual completion or a depletion plan for a reservoir. Pressure transient tests can be grouped into two broad categories: singlewell and multiwell tests.

Single-well tests measure pressure buildup, drawdown, and falloff, as well as injectivity. In these tests, we use the measured pressure response to determine average properties in part or all of the drainage area of the tested well.

Multiwell tests, which include interference and pulse tests, are used to estimate properties in a region centered along a line connecting pairs of wells. Therefore, they are more sensitive to directional variations in properties. In a multiwell test, the approach is to produce from (or inject into) one well, called the active well, and observe the pressure response in one or more offset wells, or observation wells. Although we concentrate in this chapter on analysis techniques for single-well tests, the fundamental principles presented can be extended to develop methods for analyzing multiwell tests.

4.2 HOMOGENEOUS RESERVOIR MODEL - SLIGHTLY COMPRESSIBLE LIQUIDS

The basis of well-test analysis techniques for homogeneous-acting reservoirs is the line-source (Ei-function) solution to the diffusivity equation.

The relationship between bottomhole flowing pressure (BHFP), P_{wf}, and the formation and well characteristics for a well producing a slightly compressible liquid at a constant rate is

$$P_{wf} = P_i + \frac{70.6q\mu B}{kh}\left[\log\frac{1{,}688\phi\mu c_t r_w^2}{kt} - 2s\right] \tag{4.1}$$

If we change from natural logarithms to base 10 logarithms and simplify, we can rewrite Eq. 4.1 in a more familiar form,

$$P_{wf} = P_i - \frac{162.6q\mu B}{kh}\left[\log\frac{kt}{\phi\mu c_t r_w^2} - 3.23 + 0.869 \cdot S\right] \tag{4.2}$$

where the skin factor, s, is used to quantify either formation damage or stimulation. Skin effects are discussed later.

4.2.1 Analysis of Constant-Rate Flow Tests

Eq. 4.2 describes the variation of the wellbore pressure with time when a well is produced at constant rate. Production at a constant rate can be considered a pressure-drawdown or -flow test. Comparing Eq. 4.2 with the equation of a straight line, y = mx+b, suggests an analysis technique in which the following terms are analogous:

$$y \sim p_{wf}$$

$$x \sim \log t$$

$$m \sim -\frac{162.6q\mu B}{kh}$$

$$b \sim P_i - \frac{162.6q\mu B}{kh}\left[\log\left(\frac{kt}{\phi\mu c_t r_w^2}\right) - 3.23 + 0.869 \cdot s\right] \tag{4.3}$$

These analogies indicate that a plot of P_{wf} vs. log t will exhibit a straight line from which the slope, m, allows us to estimate k and s. Fig. 4.1 is an example semilog graph of constant-rate flow test data. The slope of the line, m, is the difference between two pressures, $p_{wf,1}$ and $P_{wf,2}$, one log cycle apart, or $m = p_{wf,2} - p_{wf,1}$.

For single-phase flow, the formation permeability in the drainage area of the well is computed from

$$k = \frac{162.6q\mu B}{mh} \tag{4.4}$$

$$S = 1.151\left[\left(\frac{P_i - P_{wf}}{m}\right) - \log\frac{kt}{\phi\mu c_t r_w^2} + 3.23\right] \tag{4.5}$$

where the absolute value of m is used. Rearranging Eq. 4.2 and combining with Eq. 4.3 gives. For convenience, we set the flow time, t, equal to 1 hour, and use the symbol P_{1hr} for the BHFP at this time. Note that P_{1hr} necessarily lies on the semilog straight line. Substituting these into Eq. 4.4 yields

$$S = 1.151\left[\left(\frac{P_i - P_{1hr}}{m}\right) - \log\left(\frac{k}{\phi\mu c_t r_w^2}\right) + 3.23\right] \tag{4.6}$$

In summary, from the straight line predicted by theory for a plot of constant-rate flow test data on semilog graph paper, we can estimate k and s.

4.2.2 Analysis of Pressure-Buildup Tests

An equation modeling a pressure-buildup test can be developed by use of superposition in time. In terms of the line-source solution given by Eq 4.2, the bottomhole pressure (BHP) for the rate history shown in Fig. 4.2 is

$$P_{wf} = P_i - \frac{162.6q\mu B}{kh}\left\{\log\left[\frac{k\left(t_p + \Delta t\right)}{\phi\mu c_t r_w^2}\right] - 3.23 + 0.869 \cdot s\right\} - \frac{162.6(-q)\mu B}{kh}\left\{\log\left[\frac{k\Delta t}{\phi\mu c_t r_w^2}\right] - 3.23 + 0.869 \cdot s\right\} \quad (4.6)$$

where

p_{ws} = shut-in BHP,

t_p = duration of the constant-rate production period before shut-in, and

Δt = duration of the shut-in period.

If we combine terms and simplify, Eq. 4.6 can be rewritten as

$$P_{ws} = P_i - \frac{162.6q\mu B}{kh}\left\{\log\left[\frac{\left(t_p + \Delta t\right)}{\Delta t}\right]\right\} \quad (4.7)$$

Comparing Eq. 4.7 to the equation of a straight line, y = mx+b, gives

$y \sim p_{ws}$

$b \sim p_i$

$m \sim -\frac{162.6q\mu B}{kh}$

and $x \sim \log\left[\frac{\left(t_p + \Delta t\right)}{\Delta t}\right]$

This suggests that a plot of shut-in BHP, P_{ws}, from a buildup test as a function of the log of the Horner time ratio function, $(t_p + \Delta t)/\Delta t$, will exhibit a straight line with slope m. The slope is the difference between two values of pressure, $P_{ws,1}$ and $P_{ws,2}$ one log cycle apart. To calculate permeability, we use the absolute value of the slope, or

$$k = \frac{162.6q\mu B}{mh} \tag{4.8}$$

From the semilog graph, the original reservoir pressure, p_i, is estimated by extrapolating the straight line to infinite shut-in time where $(t_p + \Delta t)/\Delta t = 1$. Fig. 4.3 illustrates calculation of the slope and original reservoir pressure.

We also can solve for the skin factor, s, from a pressure-buildup test. At the instant a well is shut-in, the BHFP is

$$P_{wf} = P_i - \frac{162.6q\mu B}{kh}\left[\log\left(\frac{kt_p}{\phi\mu c_t r_w^2}\right) - 3.23 + 0.869 \cdot s\right] \tag{4.9}$$

Combining Eqs. 4.7. 4.8, and 4.9, we can derive an expression for the skin factor:

$$S = 1.151\left[\left(\frac{P_{ws} - P_{wf}}{m}\right) - \log\frac{k\Delta t}{\phi\mu c_t r_w^2} + 3.23 + \log\left[\frac{(t_p + \Delta t)}{t_p}\right]\right] \tag{4.10}$$

where m = slope of the semilog straight line. Setting $\Delta t = 1$ hour, introducing the symbol p_{1hr} for P_{ws} at $\Delta t = 1$ hour on the semilog straight line, and neglecting the term log $[(t_p + \Delta t)/t_p]$ gives

$$S = 1.151\left[\left(\frac{P_{1hr} - P_{wf}}{m}\right) - \log\left(\frac{k}{\phi\mu c_t r_w^2}\right) + 3.23\right] \tag{4.11}$$

where p_{wf} = BHFP at the instant of shut-in. In summary, using information obtained from a plot of p_{ws} vs log $[(t_p + \Delta t)/t_p]$, we can estimate k, p_i, and s.

4.3 COMPLICATIONS IN ACTUAL TESTS

The analysis techniques presented in the previous section were derived assuming a homogeneous reservoir model and therefore represent ideal conditions. In reality, reservoirs are not homogeneous, and the actual pressure response during a flow or buildup test deviates from the ideal behavior (i.e., the semilog straight line predicted by theory may not be present). These deviations usually are caused by conditions in the wellbore and drainage radius of the reservoir that are not considered in the simple model described by Eq. 4.2. We use the concept of radius of investigation to understand the causes of the nonideal behavior.

4.3.1 Radius of Investigation Concept.

Consider a graph (Fig. 4.4) of pressure as a function of radius for constant-rate flow at various times since the beginning of flow. The pressure in the wellbore continues to decrease as flow time increases. Simultaneously, the area from which fluid is drained increases, and the pressure transient moves further out into the reservoir. The radius of investigation, defined as the point in the formation beyond which the pressure drawdown is negligible, is a measure of how far a transient has moved into a formation following any rate change in a well and physically represents the depth to which formation properties are being investigated at any time in a test. The approximate position of the radius of investigation at any time is estimated with the relation

$$r_i = \sqrt{\frac{kt}{948\phi\mu c_t}} \tag{4.12}$$

Similarly, for a buildup test, pressure distributions following shut-in have the profiles illustrated in Fig. 4.5. The radius at which the rate of pressure change becomes negligible by a particular shut-in time moves farther into the reservoir with time, and the radius reached by this pressure level is given by

$$r_i = \sqrt{\frac{k\Delta t}{948\phi\mu c_t}} \tag{4.13}$$

As an example, if the permeability encountered by the radius of investigation near the wellbore at earliest times in a buildup or flow test is different from that encountered later (away from the well), we should not be surprised that the slope of the curve of pressure vs. the appropriate time function on a semilog graph is different at early and late times. Similarly, because the Ei function solution assumes an infinite-acting reservoir, we should expect the slope of a buildup or flow test plot to change shapes at late times when the radius of investigation reaches the reservoir drainage boundaries.

4.3.2 Time Regions on Test Plots.

On an actual flow or buildup test plot, the straight line predicted by ideal theory rarely occurs over the entire range of test times. Instead, the curve is shaped more as illustrated in Fig. 4.6 or 4.7. To help understand the causes of the nonlinear portions of the curve, we subdivide the flow test data into three time regions - early, middle, and late time-based on the radius-of-investigation concept.

1. Early time. The pressure transient is near the wellbore in a damaged or stimulated

zone. Wellbore unloading or afterflow of fluid stored in the wellbore also distorts the test data during this period.

2. Middle time. The pressure transient has moved into the undamaged formation. A straight line, with a slope related to the effective permeability of the flowing phase, usually occurs during this period. This flow period, called the radial flow or middle-time region, is the basis of conventional well-test analysis techniques.

3. Late time. The pressure transient encounters reservoir boundaries, interference effects from other producing wells, or massive changes in reservoir properties. The flow test curve deviates from the straight line established during the middle-time region.

4.3.3 Wellbore-Storage Effects.

Only in rare cases is the time required for the radius of investigation to move through the altered zone near the wellbore of significant duration. In most cases, the length of the early-time region is determined by the duration of wellbore-storage distortion of test data. In flow tests, a special case of the wellbore-storage phenomenon is called wellbore unloading which occurs because the initial fluid production measured at the surface originates from fluids stored in the wellbore rather than from the formation. Only after what may be a prolonged time does the bottomhole flow rate approximately equal the surface rate (Fig. 4.8). Until then, the assumption of constant bottomhole rate, on which the flow equation and graphing technique are based, is not satisfied.

Wellbore storage also affects the early buildup pressure response. Following shut-in at the surface, fluid continues to flow from the reservoir into the wellbore, compressing the gas and liquid already in the wellbore and storing more fluid. This continued production, which also is a special type of wellbore storage, is called afterflow (Fig. 4.9). Until the rate of afterflow diminishes to less than about 1% of the rate before shut-in, the straight line predicted by ideal theory for a Homer plot of buildup test data does not appear.

Following a mass balance in the wellbore, we define a wellbore-storage coefficient, C, as

$$C = \Delta V / \Delta p \tag{4.14}$$

where

ΔV = change in wellbore fluid volume at wellbore conditions, bbl, and

Δp = change in BHP, psi.

The form of C depends on the fluid phases in the wellbore. For a well with a liquid/gas interface that is either rising or falling,

$$C = \frac{25.64 A_{wb}}{\rho_{wb}} \tag{4.15}$$

where A_{wb} = wellbore area. If the wellbore contains only a single phase fluid (either liquid or gas), then

$$C = V_{wb} C_{wb} \tag{4.16}$$

where

V_{wb} = wellbore volume and

c_{wb} = fluid compressibility evaluated at wellbore conditions.

4.3.4 Damage and Stimulation Analysis

Many wells either have a zone of reduced permeability near the wellbore resulting from drilling or completion operations or have been stimulated by acidization or hydraulic fracturing. A common technique for incorporating the effects of altered conditions near the wellbore is with a skin factor.

Historically, skin effects have been modeled as an infinitesimally small zone of reduced

permeability on the formation face. Another modeling technique considers the formation to be a two region reservoirs (Fig. 4.10) in which the damaged or stimulated zone is considered equivalent to an altered zone of uniform permeability, k_S, extending out to a radius, r_S; outside this zone of altered permeability, the formation has a permeability, k, unaffected by drilling or completion operations. With this model the skin factor to quantify either formation damage or stimulation in terms of the properties of the altered zone is

$$s = \left(\frac{k}{k_s} - 1 \right) \ln \frac{r_s}{r_w} \tag{4.17}$$

According to the sign convention used in this book, a positive skin factor indicates damage or a permeability reduction, and a negative skin factor indicates an improvement in permeability from acidizing or hydraulic fracturing. If the formation near the wellbore is neither damaged nor stimulated, the skin factor is zero. If the radial depth of formation damage, r_S, can be determined or assumed, then we can estimate the corresponding value of permeability in the altered zone, k_S. Alternatively, if the permeability reduction ratio, k_S/k, is available from laboratory measurements the depth of damage, r_S, can be calculated directly with Eq. 4.17.

Another use of the skin factor is in terms of an effective wellbore radius, r_{wa}.

$$r_{wa} = r_w e^{-s} \tag{4.18}$$

Note that, for positive skin factors (i.e., damaged zones), the effective wellbore radius models a well with no damage but with a smaller radius and a larger pressure drop at the well. Conversely, for stimulated wells, the effective wellbore radius models an unstimulated well with a very large wellbore. An application of the

effective-wellbore-radius concept is based on the observation that for vertically fractured wells with infinitely conductive fractures having two wings each of equal length, L_f, the relationship between r_{wa} and L_f is

$$L_f = 2r_{wa} \tag{4.19}$$

Thus, if the skin factor for a fractured well can be estimated from a well test, and if the fracture is assumed to be infinitely conductive, then L_f can be estimated.

We also can quantify the skin factor in terms of the additional pressure drop associated with the damaged zone, or

$$\Delta p_s = \frac{141.2q\mu B}{kh}s \tag{4.20}$$

For example, if the total drawdown is 1,500 psi and Δp_s = 1,000 psi, then the skin factor has provided some useful information regarding the incentive for well stimulation. Either the pressure drawdown can be reduced by about 1,000 psi and the same flow rate maintained, or the same pressure drawdown can be maintained and the rate increased By a factor of about three.

4.4 FUNDAMENTALS OF PRESSURE-TRANSIENT TESTING IN GAS WELLS

The basis of flow-test analysis techniques for gas wells is the line source (Ei function) solution to the diffusivity equation given by Eq. 4.2. Eq. 4.2 is valid for a slightly compressible liquid with relatively constant properties. However, for flow of compressible gases in which the properties are strong functions of pressure, Eq. 4.2 often is not sufficiently accurate for analyzing gas-well tests. In this section, we introduce pressure and time transformation variables that account for the variation of gas properties with pressure.

4.4.1 Pseudopressure and Pseudotime Variables

The equations developed for slightly compressible fluids (i.e., liquids) can be altered by replacing pressure and time with real-gas pseudopressure and pseudotime variables, respectively. These transformations account for variations in gas properties with pressure. Accuracy is improved for both semilog and type-curve analysis of gas-well tests by replacing pressure with the real-gas pseudopressure function, p_p,

$$p_p(p) = 2\int_0^p \frac{p}{\mu_g(p)z(p)}dp, \tag{4.21}$$

For type-curve, particularly of wellbore-storage-distorted data from both flow and buildup tests, accuracy also is improved by replacing time with pseudotime, $t_{ap}(p)$,[8]

$$t_{ap}(p) = \int_0^t \frac{dt}{\mu_g(p)c_t(p)}, \tag{4.22}$$

For convenience, although not by necessity, p_p and t_{ap} can be normalized to have units of psia and hours, respectively, like the original variables, p and t. Normalization also gives the pseudopressure and pseudotime variables magnitudes comparable with those of the untransformed pressure and time, the unnormalized variables p_p and t_{ap} typically have values of 10^5 to 10^8. Reference values of pressure used for normalization are arbitrary. In this chapter. we define normalized variables as

$$p_n = \frac{1}{2}\left(\frac{\mu_g z}{p}\right)_r p_p = \left(\frac{\mu_g z}{p}\right)_r \int_0^p \frac{p}{\mu_g z}dp, \tag{4.23}$$

$$\text{and } t_n = \left(\mu_g c_t\right)_r t_{ap} = \left(\mu_g c_t\right)_r \int_{r_0}^{t} \frac{dt}{\mu_g c_t}, \tag{4.24}$$

where the subscript n refers to the normalized variables and r refers to the reference values of properties used in the normalization process.

Some engineers prefer properties evaluated at original reservoir pressure, p_i. Because BHFP can be measured directly, others prefer at the end of a flow period. In this chapter, we use the current static drainage area pressure, $\bar{p}$. Although $\bar{p}$ may not be available at the start of an analysis, using the pressure p* (the pressure on the semilog straight line extrapolated to a Homer time ratio of unity) as an estimate of $\bar{p}$ is quite satisfactory for buildup tests because the choice of a reference pressure is completely arbitrary (i.e., the value of P_r has no effect on results). For a flow test, of course, the pressure at the start of the test is p. We shall call our normalized variables adjusted pressure, P_a, and adjusted time, t_a and we define them as

$$p_a = \frac{1}{2}\left(\frac{\bar{\mu}_g \bar{z}}{\bar{p}}\right) p_p = \frac{\bar{\mu}_g \bar{z}}{\bar{p}} \int_0^p \frac{p}{\mu_g z} dp, \tag{4.25}$$

$$\text{and } t_a = \left(\bar{\mu}_g \bar{c}_t\right) t_{ap} = \left(\bar{\mu}_g \bar{c}_t\right) \int_0^t \frac{dt}{\mu_g c_t}, \tag{4.26}$$

where $\bar{p} \cong p^*$ and $\bar{p} = p_i$, for a new well. In terms of adjusted variables, the unsteady-state equation for slightly compressible liquids (Eq. 4.2) becomes

$$P_{a,i} - P_{a,wf} = \frac{162.6 q_g \bar{\mu}_g \bar{B}_g}{kh}\left[\log\left(\frac{kt}{\phi \bar{\mu}_g \bar{c}_t r_w^2}\right) - 3.23 + 0.869 \cdot S'\right] \tag{4.27}$$

where s' = total skin factor that includes the skin resulting from true formation damage or stimulation, s, and a non-Darcy effect.

For semilog analysis of buildup tests, adjusted pressure and adjusted time should be used, but the adjusted producing time, t_{pa} used in the Homer time ratio is evaluated at current average drainage area pressure,

$$t_{pa} = \frac{\bar{\mu}_g \bar{c}_t}{\bar{\mu}_g \bar{c}_t} t_p = t_p \tag{4.28}$$

Consequently, $t_{pa} = t_p$. Adjusted shut-in time, Δt_a is evaluated from the integral

$$\Delta t_a = \left(\bar{\mu}_g \bar{c}_t\right) \int_0^{\Delta t} \frac{d(\Delta t)}{\mu_g c_t}, \tag{4.29}$$

with μ_g and c_t, evaluated at shut-in BHP, P_{ws}, at values of Δt_a during the test. For semilog analysis of a flow test, adjusted pressure should be used, but adjusted flowing time, t_a is evaluated at $\bar{p}$. Consequently, Eq. 4.29, which involves no numerical integration can be used to calculate adjusted flowing time. This is equivalent to using actual rather than adjusted flowing time, and we will write all working equations using this result.

The logic behind these rules is that, for semilog analysis (data not distorted by wellbore storage), gas properties should be evaluated at the pressure at the radius of investigation reached at the time under consideration. The pressure at the radius of investigation is $\bar{p}$ for flow tests and P_{ws} (the current shut-in pressure in the wellbore) for buildup tests.

4.4.2 Pressure and Time Variables

Use of adjusted time and adjusted pressure in formulating equations for analysis of transient tests in gas wells is not always necessary. For some (although certainly not all) gases at high pressure (e.g., above 3,000 psia), an adequate approximation is $p/\mu_g z$ = constant $= \bar{p}/\bar{\mu}_g \bar{z}$. When this approximation is valid, Eq. 4.25 becomes

$$p_a = \frac{\bar{\mu}_g \bar{z}}{\bar{p}} \int_0^p \frac{p}{\mu_g z} dp = p, \tag{4.30}$$

Thus, in the unsteady-state flow equation given by Eq. 4.27 commonly used unsteady-state flow equation for pressure-drawdown terms of adjusted pressure, P_a can be replaced by ordinary presure- analysis with constant-rate gas production is based on the solution

$$P_i - P_{wf} = \frac{162.6 q_g \bar{\mu}_g \bar{B}_g}{kh} \left[\log\left(\frac{kt}{\phi \bar{\mu}_g \bar{c}_t r_w^2} \right) - 3.23 + 0.869 \cdot S' \right] \tag{4.31}$$

where the average gas FVF, $\bar{B}_g$, and viscosity, $\bar{\mu}_g$, are evaluated at the average pressure in the drainage area of the well.

4.4.3 Pressure-Squared and Time Variables

An adequate approximate for some gases at low pressures (e.g., below 2,000 psia) is $\mu_g z$ = constant = $\bar{\mu}_g \bar{z}$. When this approximation is valid, Eq. 4.25 becomes

$$p_a = \left(\frac{\bar{\mu}_g \bar{z}}{\bar{p}} \right)_r \int_0^p \frac{p}{\mu_g z} dp = \frac{p^2}{2p}, \tag{4.32}$$

and the unsteady-state flow equation can be written in terms of pressure-squared,

$$P_i^2 - P_{wf}^2 = \frac{57{,}910 q_g p_{sc} T \bar{\mu}_g \bar{z}}{khT_{sc}} \left[\log\left(\frac{kt}{\phi \bar{\mu}_g \bar{c}_t r_w^2} \right) - 3.23 + 0.869 \cdot S' \right] \tag{4.33}$$

For $p_{SC} = 14.7$ psia and $T_{SC} = 520^0$R, Eq. 4.33 becomes

$$P_i^2 - P_{wf}^2 = \frac{1{,}637 q_g T \bar{\mu}_g \bar{z}}{kh} \left[\log\left(\frac{kt}{\phi \bar{\mu}_g \bar{c}_t r_w^2} \right) - 3.23 + 0.869 \cdot S' \right] \tag{4.34}$$

4.4.4 Summary of Working Equations for Gas-Well-Test Analysis

The modified unsteady-state flow equations for gas wells (Eqs. 4.27, 4.31, and 4.34) serve as the basis for buildup- and flow-test analysis techniques for gas wells. Table 4.1 summarizes the interpretation and analysis equations for the variables frequently used in gas-well-test analysis. We included variables for well-test analysis of slightly compressible liquids for comparison.

4.5 NON-DARCY FLOW

The transient pressure response of a gas well may be affected by high-velocity or non-Darcy flow near the wellbore. The commonly used unsteady-state flow equation for pressure-drawdown analysis with constant-rate gas production is based on the solution for slightly compressible liquid flow with pressure replaced by pseudopressure:

$$P_p(p_{wf}) = P_p(p_i) - \frac{1{,}637 q_g T}{kh}\left[\log(t) + \log\left(\frac{k}{\phi\bar{\mu}_g\bar{c}_t r_w^2}\right) - 3.23 + 0.869 \cdot S'\right] \quad (4.35)$$

for slightly compressible liquid flow with pressure replaced by pseudopressure:

sure, p. The unsteady-state flow equation then becomes.

In terms of normalized pseudopressure (adjusted pressure), P_a, the unsteady-state flow equation becomes

$$P_{a,wf} = P_{a,i} - \frac{162.6 q_g \bar{\mu}_g \bar{B}_g}{kh}\left[\log(t) + \log\left(\frac{k}{\phi\bar{\mu}_g\bar{c}_t r_w^2}\right) - 3.23 + 0.869 \cdot S'\right] \quad (4.36)$$

where $s' = s + Dq_g$ is an effective skin factor that includes true formation damage (or stimulation) and the effects of non-Darcy flow. Eq. 4.35 can be written in dimensionless form:

$$P_{pD}(1, t_D) = 0.5\left[\log(t_D) + 0.80907\right] + s + Dqg, \quad (4.37)$$

where $P_{PD}(1,t_D)$ is the dimensionless (or normalized) pseudopressure at the wellbore and dimensionless time

$$t_D = \frac{0.0002637kt}{\phi\bar{\mu}_g\bar{c}_t r_w^2}, \ldots \quad (4.38)$$

The usual assumption in conventional calculations is that the non-Darcy flow effect can be represented as a rate-dependent pseudoskin defined as Dq_g where D is a constant known as the non-Darcy flow coefficient (in D/Mscf) and q_g is the flow rate (in Mscf/D).

The true skin factor, s, reflecting formation damage or stimulation near the wellbore cannot be determined from a single drawdown or buildup test. Rather, the apparent or total skin factor, $s' = s + Dq_g$, is obtained. If s and D are to be determined separately, then two flow tests can be run at different rates so that two equations (given by Eq. 4.37) can be solved simultaneously for the two unknowns, s and D. If only one test is available, then D can be estimated by

$$D = \frac{2.715 \times 10^{-15} \beta k M p_{sc}}{h r_w T_{sc} \mu_{g,wf}} \tag{4.39}$$

where

M = gas molecular weight and

$\mu_{g,wf}$ = pressure-dependent gas viscosity evaluated at p_{wf}.

β which is a turbulence parameter inversely proportional to permeability, can be determined experimentally or from

$$\beta = 1.88 \times 10^{10} k^{-1.47} \phi^{-0.53} \tag{4.40}$$

4.6 ANALYSIS OF GAS-WELL FLOW TESTS

Gas wells are produced at conditions approximating constant wellhead pressure or variable bottomhole rates, rather than at constant bottomhole rates, in most gas field operations. In addition, many gas-well tests, especially deliverability tests, are conducted under variable-rate conditions. In this section, we begin with a brief discussion of constant-rate gas flow tests, but we concentrate on analysis techniques for variable gas rates, including gas-well tests with discrete rate changes and tests in which the rates are smoothly changing. We also address non-Darcy flow effects in flow tests. Finally, we briefly discuss the effects of reservoir boundaries on gas-well testing.

4.6.1 Constant-Rate Gas Flow Tests.

In terms of adjusted variables, Eq. 4.27 describes the pressure drop at the wellbore as a function of time when a well is produced at a constant rate. Similar to the analysis of slightly compressible liquids, the form of Eq. 4.27 suggests that a plot of $P_{a,wf}$ vs. log t will form a straight line from which the slope, m, allows estimation of k and s.

For single-phase gas flow, the formation permeability in the drainage area of the well is computed from

$$k = \frac{162.6 q_g \bar{\mu}_g \bar{B}_g}{mh} \tag{4.41}$$

Combining Eqs. 4.27 and 4.41, we also can develop an expression for s:

$$s = 1.151\left[\frac{P_{a,i} - P_{a,wf}}{m} - \log\left(\frac{kt}{\phi \bar{\mu}_g \bar{c}_t r_w^2}\right) + 3.23\right] \tag{4.42}$$

For convenience, we set the flow time, t, equal to 1 hour and use $P_{a,1hr}$ for the adjusted BHFP, $P_{a,wf}$, at this time. Substituting these into Eq. 4.42 yields

$$s = 1.151\left[\frac{P_{a,i} - P_{a,1hr}}{m} - \log\left(\frac{k}{\phi \bar{\mu}_g \bar{c}_t r_w^2}\right) + 3.23\right] \tag{4.43}$$

Note that $P_{a,1hr}$ necessarily lies on either the semilog straight line or its extrapolation. Table 4.1 summarizes the working equations for semilog analysis of gas flow tests in terms of pressure and pressure-squared.

4.6.2 Gas Flow Tests With Discrete Rate Changes

We model a variable-rate gas flow test using superposition in time. First, we consider the pressure drawdown in terms of adjusted pressures in an infinite-acting gas reservoir resulting from a single production rate. We assume, for now, negligible non-Darcy flow effects. Eq. 4.27 can be rewritten as

$$P_{a,i} - P_{a,wf} = \frac{162.6 q_g \bar{\mu}_g \bar{B}_g}{kh}\left[\log(t) + \log\left(\frac{kt}{\phi \bar{\mu}_g \bar{c}_t r_w^2}\right) - 3.23 + 0.869s\right] \quad (4.44)$$

or

$$P_{a,i} - P_{a,wf} = m' q_g\left[\log(t) + \bar{s}\right] \quad (4.45)$$

where

$$m' = \frac{162.6 \bar{\mu}_g \bar{B}_g}{kh} \quad (4.46)$$

and

$$\bar{s} = \log\left(\frac{kt}{\phi \bar{\mu}_g \bar{c}_t r_w^2}\right) - 3.23 + 0.869s \quad (4.47)$$

Now, for the variable-rate production history in Fig. 4.11, the pressure drawdown resulting from n discrete rate changes and for time $t > t_{n-1}$ is

$$P_{a,i} - P_{a,wf} = m' q_1\left(\log(t) + \bar{s}\right) + m'\left(q_2 - q_1\right)\left(\log(t - t_1) + \bar{s}\right) + m'\left(q_3 - q_2\right)\left[\log\left(t - t_2\right) + \bar{s}\right]$$
$$+ \ldots + m'\left(q_n - q_{n-1}\right)\left[\log\left(t - t_{n-1}\right) + \bar{s}\right]$$

(4.48)

Eq. 4.48 can be rewritten as

$$\frac{P_{a,i}-P_{a,wf}}{q_n}=m'\sum_{j=1}^{n}\frac{\left(q_n-q_{j-1}\right)}{q_n}\log\left(t_n-t_{j-1}\right)+m'\bar{s},\ q_n\neq 0 \qquad (4.49)$$

The form of Eq. 4.49 suggests that we plot

$$\frac{P_{a,i}-P_{a,wf}}{q_n}\ \text{vs.}\ \frac{1}{q_n}\sum_{j=0}^{n-1}\Delta q_j\left[\log\left(t_n-tj\right)\right]$$

on Cartesian coordinate paper, where $p_{a,i}$ = adjusted initial reservoir pressure, psia; $P_{a,wf}$ = adjusted FBHP at time t_n, psia; q_n = last of n different flow rates, Mscf/D; $\Delta q_j = q_{j+1} - q_j (q_o = 0)$; t_n = total (cumulative) flowing time for n constant-rate flow periods, hours; and t_j = time at which rate was changed, hours.

A straight line with slope m' proportional to k should result from this plot. Specifically,

$$k=\frac{162.6\bar{\mu}_g\bar{B}_g}{m'h} \qquad (4.50)$$

where m' is defined by Eq. 4.46. The skin factor also can be determined from this plot. If b is the intercept of the plot (the value of $\Delta p / q$ at which the time plotting function is zero), then

$$s = 1.151\left[\frac{b}{m'} - \log\left(\frac{k}{\phi\bar{\mu}_g\bar{c}_t r_w^2}\right) + 3.23\right] \qquad (4.51)$$

The plotting method assumes that the reservoir is infinite-acting at all times up to t_n. Once boundary effects are felt by the pressure transient, the method is invalid. This analysis method can be used with four-point deliverability or backpressure tests, which are simply variable-rate tests with discrete changes in flow rate.

Non-Darcy flow effects in a gas-well test can be included by plotting

$$\frac{P_{a,i} - P_{a,wf} - D'q_n^2}{q_n} \text{ vs. } \frac{1}{q_n}\sum_{j=0}^{n-1}\Delta q_j\left[\log\left(t_n - t_j\right)\right]$$

where $D' = \dfrac{141.2\bar{B}_g\bar{\mu}_g D}{kh}$ is a constant, and D is the non-Darcy flow coefficient defined by Eq. 4.39. With the non-Darcy flow term, $D'q_n^2$, we are forced either to assume D' = 0 or to find, by trial and error, the value of D' that results in the best straight-line plot. The slope of the straight line, m', provides an estimate of permeability and skin factor by use of Eqs. 4.50 and 4.51, respectively.

Although this method is potentially quite useful because backpressure data are available for virtually all gas wells, it has at least two limitations. First, a well may not be cleaned up at the time of testing, especially when the well is tested following a workover operation or a hydraulic fracture treatment. Second, the method assumes negligible wellbore-storage distortion; however, wellbore storage almost certainly distorts some of the test data, particularly for short-duration flow periods and in low-permeability formations.

4.6.3 Variable-Rate Gas Flow Tests With Smoothly Changing Rates.

In many testing situations, a strictly constant producing rate is impractical or impossible to maintain. A more probable mode of operation is production at a constant surface pressure, and if tubing friction effects are negligible, the BHP also is constant. At early times, however, both BHP and bottomhole rate may be changing rapidly. Data obtained under these nonideal test conditions can be analyzed accurately with a simple modification of the transient flow equation for constant-rate production.

For slightly compressible liquids, Winestock and Colpitts showed that, even when both P_{wf} and q vary with time, Eq. 4.52 can be used as long as the rate is changing slowly and smoothly rather than abruptly:

$$\frac{P_i - P_{wf}}{q} = \frac{162.6B\mu}{kh}\left[\log\left(\frac{kt}{\phi\mu c_t r_w^2}\right) - 3.23 + 0.869s\right] \qquad (4.52)$$

To analyze transient data, we prepare a semilog graph of $(P_i - P_{wf})/q$ as a function of t. To analyze variable-rate tests in gas wells in which non-Darcy effects are important, we can rewrite Eq. 4.52 in terms of adjusted pressures:

$$\frac{P_{a,i} - P_{a,wf} - D'q_g^2}{q} = \frac{162.6\bar{\mu}_g\bar{B}_g}{kh}\left[\log\left(\frac{kt}{\phi\bar{\mu}_g\bar{c}_t r_w^2}\right) - 3.23 + 0.869s\right] \qquad (4.53)$$

where

$$D' = \frac{141.2\bar{B}_g\bar{\mu}_g D}{kh}$$

Either the non-Darcy flow effects (the $D'q_g^2$ term) must be neglected or the value of D' that leads to the best straight line in the middle-time region must be found iteratively. Once we have identified the semilog straight line indicative of the middle-time region, k is

estimated from the m' of this line:

$$k = \frac{162.6\bar{\mu}_g \bar{B}_g}{m'h} \qquad (4.54)$$

and

$$s = 1.151\left[\frac{1}{m'}\left(\frac{P_{a,i} - P_{a,wf}}{q}\right)_{1hr} - \log\left(\frac{k}{\phi\bar{\mu}_g \bar{c}_t r_w^2}\right) + 3.23\right] \qquad (4.55)$$

where $[(P_{a,i}-P_{1,wf})/q]_{1hr}$ must lie on the semilog straight line or its extrapolation to 1 hour. Similar to constant-rate production data the variable-rate data may be affected by wellbore storage at early times and reservoir boundaries at late times, thus distorting the pressure response and possibly masking the correct semilog straight line indicative of the radial flow or middle-time region.

4.6.4 Gas Flow Tests With Non-Darcy Flow.

As noted previously, the pressure drawdown in a gas well can be affected by high velocity, non-Darcy flow near the wellbore. Unsteady-state, constant-rate gas flow can be modeled in terms of dimensionless pseudopressure:

$$P_{PD}(1,t_D) = 0.5[\ln(t_D) + 0.80907] + s + Dq_g, \qquad (4.56)$$

where D frequently is treated as a constant. In reality, D is not constant.

Fig. 4.14 show the effects of non-Darcy flow and skin damage on the pressure response. The dimensionless pseudopressure Responses A, B, and C are simulated with Eq. 4.56 for the conditions shown. The lowest solid line is the liquid-flow response with a slope of 1.151. Response B, with a slope of 1.163, shows only the effect of non-Darcy flow. Response C is a translation of Response A with a positive skin factor, assuming that the

non-Darcy pseudoskin effect is an additive term to the pressure response. Response D, with a slope of 1.183, is the actual response with turbulent flow and a positive skin factor, indicating that the non-Darcy term is not additive and thereby confirming that D is not constant. Fligelman et al. presented a method to estimate k and true s from pressure-drawdown data for a gas well. Their equations, written in terms of pseudopressures, are modified here for use with adjusted pressures.

They define the dimensionless group

$$Bq_D = \frac{2.715x10^{-15}\beta kMp_{sc}q_g}{T_{sc}hr_w\bar{\mu}_g} \qquad (4.57)$$

where $\bar{\mu}_g$ = gas viscosity evaluated at $\bar{p}$. For a constant skin factor, the dimensionless intercept of the semilog straight line in a plot of dimensionless pseudopressure as a function of the log of dimensionless time is defined as

$$b_D = \frac{p_{a,i} - m\log\left(\frac{0.0002637k}{\phi\bar{\mu}_g\bar{c}_t r_w^2}\right) - p_{a,1hr}}{q_D p_{a,i}} \qquad (4.58)$$

where m and $P_{a,1hr}$ are the slope and intercept, respectively, of the semilog straight line in a plot of P_a vs. log(t) . The dimensionless form of the slope is

$$m_D = \frac{m}{q_D p_{a,i}} \qquad (4.59)$$

and the dimensionless flow rate is

$$q_D = \frac{0.138 q_g p_{sc} T}{k h T_{sc} p_{a,i}} \qquad (4.60)$$

The intercept b_D is related to B_{qD} by the correlation

$$b_D = c(Bq_D) + c_2 \qquad (4.61)$$

Table 4.6 summarizes selected values of the constants c_1 and c_2. The correlation of b_D and B_{qD} is shown in Fig. 4.15 for a range of skin factors.

A second correlation relates the pseudopressure response with non-Darcy flow to the group B_{qD}. The dimensionless wellbore pressure response over dimensionless time is given by

$$P_{aD} = (m_D\text{-}1.15\ 1)\log t_D + b_D\text{-}0\ 4045\text{-}s, \qquad (4.62)$$

where m_D = slope of the straight line in a plot of P_{PD} vs. log t_D.

The time t^*_D is defined as

$$t^*_D = \frac{0.0002637k}{\bar{\mu}_g \bar{c}_t r_w^2} \qquad (4.63)$$

The pressure response with turbulent flow, P^*_{aD} is related to B_{qD} by the correlation

$$P^*_{aD} = C_3(B_{qD}) + C_4(B_{qD})^2 + c_5(B_{qD})^3 \qquad (4.64)$$

where selected values of the constants C_3, C_4, and C_5 are summarized in Table 4.7. The correlation of P^*_{aD} and B_{qD} also is shown in Fig. 4.16 for a range of skin factors.

When non-Darcy flow effects are significant, we suggest the following procedure for pressure-drawdown analysis in terms of adjusted pressures.

1. Convert the sandface pressures, measured at a constant flow rate, to adjusted pressures, $P_a(P)$ Construct a log-log plot of adjusted pressure change as a function of time. Use conventional type-curve matching with a wellbore-storage/skin type curve to estimate the beginning of the semilog straight line.

2. Plot Pa as a function of log t. Draw a straight line through the semilog-straight-line data on the semilog plot. Find the slope, m, and the intercept, $P_{a,1hr}$ Calculate a first approximation of formation permeability by

$$k = \frac{162.6 q_g \bar{\mu}_g \bar{B}_g}{mh} \qquad (4.65)$$

3. Calculate the total skin factor, s'.

$$S = s + Dq_g = 1.151\left[\left(\frac{P_{a,i} - P_{a,1hr}}{m}\right) - \log\left(\frac{k}{\phi \bar{\mu}_g \bar{c}_t r_w^2}\right) + 3.23\right] \qquad (4.66)$$

4. Calculate β, B_{qD}, b_D, and q_D using Eqs. 4.40, 4.57, 4.58, and 4.60, respectively. Find the true skin factor, s, from Fig. 4.15.

5. Using B_{qD} and s, find P^*_{aD} from Fig. 4.16. Calculate an approximation of m_D by rearranging Eq. 4.62 to

$$m_D = 1.151 + \frac{\left(p^*_{aD} - b_D + 0.4045 + s\right)}{\log t^*_D} \qquad (4.67)$$

6. Using m_D, calculate a second approximation of k by

$$k = \frac{0.138 T p_{sc} q_g}{mhT_{sc}} m_D \qquad (4.68)$$

7. Repeat Steps 4 through 6 until the k estimate from Eq. 4.65 converges. The convergent value is the correct estimate of k, and the associated value of s is the correct skin factor.

Note that this procedure has certain limitations. First, only non-Darcy flow effects are considered. The method does not consider the effects of D on a phase change (i.e., condensation of the gaseous phase) as the pressure is reduced near the wellbore. Second, because the correlations are based on positive skin factors, the procedure applies only when $s > 0$. Third, the correlations were developed for a damaged-region/wellbore radius ratio greater than 10. For a higher ratio and a given value of skin factor, the slope of the semilog straight line is unaffected, but the non-Darcy effect is smaller.

Finally, the accuracy of this method depends on the applicability of the empirical correlation for β (Eq. 4.40), which is subject to considerable uncertainty.

4.6.5 Gas Flow Tests in Bounded Reservoirs.

When a pressure transient encounters reservoir boundaries during a gas-well test, the liquid solution no longer describes the pressure behavior. With boundary effects, variations in pressure-dependent gas properties affect the pressure response. In the semilog plot in Fig. 4.18, dimensionless pseudopressure solutions are compared with the liquid solution.

Dimensionless time is

$$t_{AD} = \frac{0.0002637kt_{\bar{p}}}{\phi\bar{\mu}_g\bar{c}_tA}$$

with fluid properties evaluated at $\bar{p}$.

Afler about one log cycle of dimensionless time, the gas solutions deviate substantially from the liquid solution. Because the gas physical properties are significantly affected by boundary effects, PV cannot be found with techniques developed for slightly compressible fluids (i.e., liquids).

However, Fraim and Wattenbarger developed an iterative procedure that accounts for variations in fluid properties during pseudosteady-state flow in a gas well producing at constant BHP.

4.7 ANALYSIS OF GAS WELL - BUILDUP TESTS

This section discusses analysis techniques for pressure-buildup tests in wells completed in gas reservoirs. We begin with buildup tests with constant-rate production before shut-in but then discuss the more probable testing scenarios-discrete rate changes or constant-pressure production before shut-in. Finally, we illustrate how average drainage area pressure is determined from a gas-well buildup test.

4.7.1 Buildup Tests With Constant-Rate Production Before Shut-In

An equation modeling a pressure-buildup test in a gas well also can be developed by use of superposition in time. In terms of adjusted variables, Eq. 4.7 for a slightly compressible liquid becomes

$$P_{a,ws} = P_{a,i} - \frac{162.6 q_g \bar{\mu}_g \bar{B}_g}{kh} \left\{ \log \left[\frac{k\left(t_p + \Delta t_a\right)}{\Delta t_a} \right] \right\} \tag{4.70}$$

where

$P_{a,ws}$ = adjusted shut-in BHP,

t_p = duration of the constant rate production period before shut-in, and

Δt_a = adjusted shut-in time.

Comparison of Eq. 4.70 to the equation of a straight line suggests that a plot of adjusted shut-in BHP, $P_{a,ws}$, from a buildup test as a function of the log of the adjusted Horner time ratio function, $\left(t_p + \Delta t_a\right) / \Delta t_a$, will exhibit a straight line with slope m. To calculate permeability, we use the absolute value of the slope, or

$$k = \frac{162.6 q_g \bar{\mu}_g \bar{B}_g}{mh} \tag{4.71}$$

From the semilog graph, the original reservoir pressure, Pi, is estimated by extrapolating the straight line to infinite shut-in time where $\left(t_p + \Delta t_a\right) / \Delta t_a = 1$

We also can solve for the apparent skin factor, s', from a pressure buildup test. At the instant that a well is shut in,

$$P_{a,wf} = P_{a,i} - \frac{162.6 q_g \bar{\mu}_g \bar{B}_g}{kh} \left[\log \left(\frac{kt}{\phi \bar{\mu}_g \bar{c}_t r_w^2} \right) - 3.23 + 0.869 s' \right] \tag{4.72}$$

Combining Eqs. 4.70 and 4.72 yields an expression for the apparent skin factor,

$$S' = 1.151\left[\left(\frac{P_{a,ws} - P_{a,wf}}{m}\right) - \log\left(\frac{k\Delta t_a}{\phi\bar{\mu}_g\bar{c}_t r_w^2}\right) + 3.23 + \log\left(\frac{t_p + \Delta t_a}{\Delta t_a}\right)\right] \tag{4.73}$$

where m = slope of the semilog straight line.

Setting Δt_a = 1 hour, introducing the symbol $P_{a,1hr}$ for $P_{a,ws}$ at Δt_a = 1 hour on the semilog straight line, and neglecting the term $\log\left(t_p + \Delta t_a\right) / \Delta t_a$ we can rewrite Eq. 4.73:

$$S' = 1.151\left[\left(\frac{P_{a,1hr} - P_{a,wf}}{m}\right) - \log\left(\frac{k}{\phi\bar{\mu}_g\bar{c}_t r_w^2}\right) + 3.23\right] \tag{4.74}$$

wnere $P_{a,wf}$ = adjusted BHFP at the instant of shut-in.

Similar to the technique for slightly compressible liquids, we can estimate k, Pi, and s' by using information obtained from a graph of $P_{a,ws}$ vs. $\log\left(t_p + \Delta t_a\right) / \Delta t_a$. Although presented in terms of adjusted variables, similar analysis techniques are possible with either pressure or pressure-squared variables. Table 4.1 gives the appropriate working equations.

4.7.2 Buildup Tests With Discrete Changes in Rate Before Shut-In

Superposition Method

We can develop an analysis technique for buildup tests with discrete rate changes before shut-in using superposition in time for (n-1) rates preceding the pressure-buildup test (Fig. 4.19).

For the general case where $q_n = 0$ and for (n- 1) different rates before shut-in,

$$P_i - P_{ws} = \frac{162.6q_{n-1}\mu B}{kh}\left[\left(\frac{q_1}{q_{n-1}}\right)\log\left(\frac{t}{t-t_1}\right)+\left(\frac{q_2}{q_{n-1}}\right)\log\left(\frac{t-t_1}{t-t_2}\right)\right.$$
$$\left.+\left(\frac{q_{n-2}}{q_{n-1}}\right)\log\left(\frac{t-t_{n-3}}{t-t_{n-2}}\right)+\log\left(\frac{t-t_{n-2}}{t-t_{n-1}}\right)\right] \tag{4.75}$$

where $t - t_{n-1} = \Delta t$ (time elapsed since shut-in) and q_{n-1} is the gas production rate just before shut-in.

Note the fundamental assumption on which Eq. 4.75 is based (that, for $t = t_{p1} + t_{p2} + \ldots + t_{p,n-1} + \Delta t$, the reservoir is infinite-acting) rarely will be valid for large values of t. Nevertheless, when Eq. 4.75 is used to model a buildup test, the following analysis procedure in terms of adjusted variables is recommended.

1. Calculate the plotting function.

$$X = \left[\left(\frac{q_1}{q_{n-1}}\right)\log\left(\frac{t}{t-t_1}\right) + .. + \log\left(\frac{t-t_{n-2}}{t-t_{n-1}}\right)\right]$$

2. Plot $P_{a,ws}$ vs. X on Cartesian coordinate graph paper.
3. Determine the slope m of the straight line.
4. Calculate permeability to gas using the slope from Step 2.

$$k = \frac{162.6q_{n-1}\bar{\mu}_g\bar{B}_g}{mh} \tag{4.76}$$

5. Calculate the skin factor.

$$S = 1.151\left[\left(\frac{P_{a,1hr} - P_{a,wf}}{m}\right) - \log\left(\frac{k}{\phi\bar{\mu}_g\bar{c}_t r_w^2}\right) + 3.23\right] \tag{4.77}$$

4. The initial adjusted formation pressure, $P_{a,i}$, is the value of $P_{a,ws}$ on the straight line extrapolated to X = 0.

Odeh-Selig Method. As an alternative to superposition, Odeh and Selig suggested that a buildup test following n different rates could be analyzed by a method similar to the Homer method. The shut-in pressure response is

$$P_{a,i} - P_{a,ws} = \frac{162.6q^*\bar{\mu}_g\bar{B}_g}{kh}\left\{\log\left[\frac{k\left(t_p^* + \Delta t_a\right)}{\Delta t_a}\right]\right\} \tag{4.78}$$

where the modified production time, t^*_p, and flow rate, q*, are

$$t_p^* = 2\left[t_n - \frac{\sum_{j=1}^{n} q_j\left(t_j^2 - t_{j-1}^2\right)}{2\sum_{j=1}^{n} q_j\left(t_j - t_{j-1}\right)}\right] \tag{4.79}$$

and

$$q^* = \frac{1}{t_p^*} \sum_{j=1}^{n} q_j \left(t_j - t_{j-1} \right) \tag{4.80}$$

The Odeh-Selig method, approximate but accurate, is applicable only for pressures at Δt_a values greater than actual producing time. This condition is likely only in a drillstem test or short production test.

Horner's Approximation

Homer reported an approximation that can be used in many cases to avoid the use of superposition in modeling the production history of a variable-rate well. He defined a producing time, t_p, for production from a gas well as

$$t_p = \frac{G_p}{q_{last}} \tag{4.81}$$

where

G_p = cumulative production from the well, Mscf, and

q_{last} = the most recent production rate, Mscf/D.

For t_p in hours, Eq. 4.81 then becomes

$$t_p = \frac{24 G_p}{q_{last}} \tag{4.82}$$

Homer proposed to model the effect of the entire rate history by

$$P_{a,wf} = P_{a,i} - \frac{162.6 q_{last} \bar{\mu}_g \bar{B}_g}{kh} \left[\log\left(\frac{kt_p}{\phi \bar{\mu}_g \bar{c}_t r_w^2} \right) - 3.23 + 0.869 s' \right] \tag{4.83}$$

An equation modeling a pressure-buildup test can be written by noting that pressure buildup is a special case of variable-rate production.

Assuming that Homer's approximation adequately models the production history before shut-in, the entire production history can be modeled as production at q_{last} for t_p.

If Δt_a denotes time elapsed since shut-in, then superposition in time with Eq. 4.27 yields Eq. 4.84, which describes $P_{a,ws}$

$$P_{a,wf} = P_{a,i} - \frac{162.6 q_{last} \bar{\mu}_g \bar{B}_g}{kh} \left\{ \log\left(\frac{k\left(t_p + \Delta t_a\right)}{\phi \bar{\mu}_g \bar{c}_t r_w^2} \right) - 3.23 + 0.869 s' \right\} -$$
$$\frac{162.6\left(-q_{last}\right) \bar{\mu}_g \bar{B}_g}{kh} \left\{ \log\left(\frac{k\left(\Delta t_a\right)}{\phi \bar{\mu}_g \bar{c}_t r_w^2} \right) - 3.23 + 0.869 s' \right\} \tag{4.84}$$

Combining terms and simplifying yields

$$P_{a,ws} = P_{a,i} - \frac{162.6 q_{last} \bar{\mu}_g \bar{B}_g}{kh} \left\{ \log\left[\frac{\left(t_p + \Delta t_a\right)}{\Delta t_a} \right] \right\} \tag{4.85}$$

As in the analysis technique for pressure-buildup tests preceded by a constant-rate production period, we simply plot $P_{a,ws}$ as a function of the log of the Horner time ratio function based on the pseudoproducing time, $\left(t_p + \Delta t_a\right) / \Delta t_a$.

To calculate permeability, we use the absolute value of m of the semilog straight line,

$$k = \frac{162.6 q_{last} \bar{\mu}_g \bar{B}_g}{mh} \tag{4.86}$$

From the semilog graph, the original adjusted reservoir pressure, $P_{a,i}$ is estimated by extrapolating the straight line to infinite shut-in time, where $\left(t_p + \Delta t_a\right)/\Delta t_a = 1$.

The apparent skin factor is estimated from

$$S' = 1.151\left[\left(\frac{P_{a,1hr} - P_{a,wf}}{m}\right) - \log\left(\frac{k}{\phi \bar{\mu}_g \bar{c}_t r_w^2}\right) + 3.23\right] \tag{4.87}$$

where

m = slope of the semilog straight line,

$P_{a,1hr} = P_{a,ws}$ at Δt_a = 1 hour on the semilog straight line, and

$P_{a,wf}$ = adjusted BHFP at the instant of shut-in.

4.7.3 Buildup Tests With Constant-Pressure Production Before Shut-In

Conventional buildup test analysis techniques have been developed primarily for wells producing at a constant rate before shut-in. However, some common situations involve production at constant BHP rather than at constant rate. Examples include declining-rate production during reservoir depletion, fluid flow into a constant-pressure separator, or open wells flowing at atmospheric pressure. With slight modification, conventional Homer and type-curve analyses can be used to analyze buildup test data following production at constant BHP. The Horner method gives the correct semilog straight line from which k, s, and average drainage area pressure can be found.

The usual Homer time plotting function uses a producing time defined by Eq. 4.82.

$$t_p = \frac{24G_p}{q_{last}}$$

where q_{last} is the last established flow rate before shut-in. For Homer analysis of a buildup test following constant-pressure production, the actual producing time, t_{actual}, rather than t_p defined by Eq. 4.82 is used. As an example, suppose that a gas well has been produced at constant BHP for 1 year (8,760 hours).

At the time of shut-in for a buildup test, G_p = 100,000 Mscf and q_{last} =. 100 Mscf/D.

From Eq. 4.82, the conventional Homer producing time is

$$t_p = \frac{24G_p}{q_{last}} = \frac{24(100{,}000)}{100} = 24{,}000 \text{ hours}$$

and at Δt_a = 10 hours, the Homer plotting function is

$$\frac{t_p + \Delta t_a}{\Delta t_a} = \frac{24{,}000 + 10}{10} = 2{,}401$$

Using t_{actual} = 8,760 hours rather than t_p = 24,000 hours, we obtain the Homer plotting function of

$$\frac{t_{actual} + \Delta t_a}{\Delta t_a} = \frac{8{,}760 + 10}{10} = 877 \text{ hours}$$

A plot of $P_{a,ws}$ vs. the adjusted Homer time ratio based on t_{actual} al gives the correct

semilog straight line with slope m. k is computed with

$$k = \frac{162.6 q_{last} \bar{\mu}_g \bar{B}_g}{mh} \tag{4.86}$$

where for the constant-pressure case q_{last} is the last established producing rate, not the average rate over the producing period.

The skin factor also is calculated in the usual way,

$$S' = 1.151\left[\left(\frac{P_{a,1hr} - P_{a,wf}}{m}\right) - \log\left(\frac{k}{\phi \bar{\mu}_g \bar{c}_t r_w^2}\right) + 3.23\right] \tag{4.87}$$

Extrapolation of the semilog straight line to infinite shut-in time (adjusted Homer time equal to one) gives $P_{a,i}$ for an infinite-acting reservoir.

For buildup tests following constant-pressure production, the effects of wellbore storage, skin damage, and non-Darcy (high velocity) gas flow usually are short-lived and do not affect the slope of the semilog straight line. However, in gas reservoirs with k > 0.1 md, non-Darcy flow effects may cause substantial errors in estimates of the apparent skin factor, s', from match-point data in type-curve analysis.

Under these conditions, semilog analysis must be used for reliable formation evaluation. Furthermore, when non-Darcy flow effects are significant, a buildup test gives more reliable results than a drawdown test.

4.7.4 Determining Average Drainage Area Pressure for Gas Wells.

The average pressure in the drainage area of a well represents the driving force for fluid flow and is useful in material-balance calculations. For a well in a new reservoir with negligible pressure depletion, extrapolation of buildup test data to infinite shut-in time on

a Homer semilog plot provides an estimate of original (and current) drainage area pressure, p_i. For a well in a reservoir where the average pressure has declined from its original value because of fluid production, the pressure extrapolated to infinite shut-in time, p*, is related but not equal to the current average pressure in the drainage area of the well.

We consider two possibilities for a well in a reservoir with negligible pressure depletion. First, if the pressure-transient data are not influenced by boundaries during the production period before the buildup test, a typical buildup test will have the shape shown in Fig. 4.20. The original reservoir pressure is obtained by extrapolating the middle-time semilog straight line to $\left(t_p + \Delta t_a\right)/\Delta t_a = 1$.

Second, for a well with one or more boundaries relatively near the well (and encountered by the radius of investigation during the production period), a buildup test will exhibit the shape shown in Fig. 4.21, and the late-time semilog straight line is extrapolated.

For a reservoir where the pressure has been depleted, the Matthews-Brons-Hazebroek (MBH) method can be used to estimate the average drainage-area pressure. The MBH method is based on theoretical correlations between the extrapolated pressure, p*, shown in Fig. 4.22 and current average drainage area pressure, $\bar{p}$, for various drainage area configurations.

Figs. 4.23 through 4.24 show two of the numerous correlation charts available. Fig. 4.23 applies to wells in various locations in square drainage areas. The most common approximation of drainage area is that the well is centered in a square drainage area with an area equal to the acreage assigned to the well. Fig. 4.24 applies to 2:1 rectangular drainage areas. Here, $(t_{AD})_{pss}$ indicates the beginning of pseudosteady-state flow, where t_{AD} is defined by Eq. 4.89. Similar charts for other drainage area shapes are available elsewhere.

A dimensionless pressure, P_{MBHD}, is plotted as a function of a dimensionless time, t_{AD}, in Figs. 4.23 and 4.24. The dimensionless variables are defined as

$$p_{MBHD} = \frac{kh\left(p^* - \bar{p}\right)}{70.6q\mu B} \tag{4.88}$$

and

$$t_{AD} = \frac{0.0002637kt_p}{\phi\mu c_t A} \tag{4.89}$$

where A = drainage area of the tested well, ft^2,

The advantages of the MBH method are that it does not require data beyond the middle-time region and that it is applicable to a wide variety of drainage area shapes. The disadvantages are that the drainage area size and shape must be known and that reliable estimates of rock and fluid properties, such as c_t and ϕ, must be available. In addition, the method is limited to well tests in single layer formations and cannot be applied accurately to multilayer formations.

Although developed for slightly compressible liquids, the average drainage area pressure, $\bar{p}$, for a gas well can be found with the MBH p* method. To find the correct $\bar{p}$, pressure-dependent fluid properties must be evaluated at $\bar{p}$. This suggests an iterative procedure.

For gas, we use p_a The procedure (outlined below) involves making an initial estimate of $\bar{p}_a$ (the adjusted pressure corresponding to $\bar{p}$), evaluating fluid properties at the pressure associated with F, calculating the MBH pressure function $P_{a,MBHD}$ on the basis of those properties, and obtaining another estimate of $\bar{p}_a$ from $P_{a,MBHD}$

1. Assume a value of $\bar{p}$, calculate the adjusted pressure and time, and make a Homer plot of the buildup data, using values of $P_{a,ws}$ and $\left(t_p + \Delta t_a\right)/\Delta t_a$

2. Extrapolate $P_{a,ws}$ to $\left(t_p + \Delta t_a\right)/\Delta t_a = 1$. The extrapolated adjusted pressure, P_a^*, may

be an improved estimate of $\bar{p}_a$; however, if P_a^* is clearly larger than the apparent level value of $\bar{p}_a$, continue to use the initial estimate of $\bar{p}_a$ in subsequent steps.

3. Estimate the drainage area shape. In practice, the drainage area usually is reasonably symmetrical.

4. Select the appropriate MBH chart, for the drainage area

5. Calculate the t_{AD} with Eq. 4.89 with μ and c_t at the pressure corresponding to the most recent estimate of $\bar{p}$.

6. From the MBH chart at the calculated value of t_{AD}, read the value of the MBH pressure function:

$$p_{a,MBHD} = \frac{kh\left(p_a^* - \bar{p}_a\right)}{70.6q\bar{\mu}_g\bar{B}g} = \frac{2.303\left(p_a^* - \bar{p}_a\right)}{m} \tag{4.90}$$

7. Calculate the next estimate of $\bar{p}_a$:

$$\bar{p}_a = p_a^* \frac{mp_{a,MBHD}}{2.303} \tag{4.91}$$

8. If the $\bar{p}_a$ estimate from Eq. 4.91 is different from the previous estimate, evaluate the gas properties at the pressure associated with the new estimate of $\bar{p}_a$. Repeat Steps 5 through 7, recalculating t_{AD} at the new values of the fluid properties, until the estimate $\bar{p}_a$ from Eq. 4.91 converges. The correct $\bar{p}$ is the pressure corresponding to the final $\bar{p}_a$ value.

Kazemi and Reynolds et al. presented other methods to estimate $\bar{p}$ for gas reservoirs. Kazemi's method requires an iterative procedure; Reynolds et al's technique requires a

Homer plot in terms of real time and pseudopressure rather than adjusted time and adjusted pressure.

4.8 Gas Well Test Analysis Using Pressure And Pressure Derivative

4.8.1 Type Curve Analysis

Type curves, which are plots of theoretical solutions to flow equations, are very useful in well-test analysis, particularly when used with semilog analysis techniques. Type curves can help identify the appropriate reservoir model, identify the appropriate flow regimes for analysis, and estimate reservoir properties. They are especially helpful for analyzing gas-well tests when the data are distorted by wellbore storage. In this section, we explain what type curves are, identify some of their more useful properties, and illustrate how they can be used to improve pressure-transient test analysis.

4.8.1.1 Development of Type Curves

Type curves can be generated for virtually any kind of reservoir model for which a general solution describing the flow behavior is available. For a type curve to be applied correctly, the assumptions underlying the solution must be understood. Furthermore, those assumptions must accurately model the well or reservoir conditions being analyzed. As a matter of convenience, type curves usually are presented in terms of dimensionless rather than real variables. The definition of the dimensionless variables varies according to the reservoir model. For example, recall the line-source or Ei-function solution for slightly compressible liquids,

$$p_i - p = \frac{70.6q\mu B}{kh} E_i\left(\frac{-948\phi\mu c_t r^2}{kt}\right) \tag{4.92}$$

If we rearrange Eq. 4.92 as

$$\frac{kh\left(p_i - p\right)}{141.2q\mu B} = -\frac{1}{2}E_i\left(-\frac{\left(r/r_w\right)^2}{4\left(\frac{0.0002637kt}{\phi\mu c_t r_w^2}\right)}\right) \tag{4.93}$$

then the form of Eq. 4.93 suggests the following convenient dimensionless variables

$$p_D = \frac{kh\left(p_i - p\right)}{141.2q\mu B} \tag{4.94}$$

$$r_D = \frac{r}{r_w} \tag{4.95}$$

$$\text{and } t_D = \frac{0.0002637kt}{\phi\mu c_t r_w^2} \tag{4.96}$$

In terms of these dimensionless variables, the line-source solution becomes

$$p_D = -\frac{1}{2}E_i\left(-\frac{r_D^2}{4t_D}\right) \tag{4.97}$$

At the well, where $r_D = 1$, the solution simplifies to

$$p_D = p_{wD} = -\frac{1}{2}E_i\left(-\frac{1}{4t_D}\right) \tag{4.98}$$

where

$$p_{wD} = -\frac{1}{2}E_i\left(-\frac{1}{4t_D}\right) \tag{4.99}$$

Eq. 4.98 implies that we can develop a type curve from a plot of P_{WD} as a function of the single variable t_D. Generating a single graph in terms of P_{WD} is much simpler than attempting to plot P_{wf} as a function of t for all reasonable values of the variables that appear in the dimensional form of the line-source solution (Eq. 4.92). Thus, with this type curve, we can analyze any pressure-transient test conducted under conditions satisfying the assumptions made in deriving the E_i-function solution. Again, before using any type curve, we must fully understand the assumptions inherent in the model being used.

The theory underlying type-curve matching is that the type curve and test data plots differ only by displacement of both coordinates by constants. This concept is illustrated as follows.

4.8.1.2 Type-Curve Analysis With Pressure Derivatives

Homogeneous-Reservoir Model, Slightly Compressible Liquids.

As discussed, type curves must accurately model the reservoir or well conditions being analyzed. Therefore, the key to using type curves is identifying the correct reservoir type (homogeneous, dual porosity, hydraulically fractured, etc.) so that we may select the appropriate type curves. Unfortunately, conventional log-log pressure/time plots are relatively insensitive to the changes in pressure data characteristic of various reservoir types. As a supplement to pressure/time plots, the pressure derivative is used widely, specifically to identify reservoir types. In this section, we introduce the basic concepts of

well-test analysis using pressure derivatives and illustrate how pressure derivatives can aid in reservoir identification.

Bourdet et al. Derivative Type Curve.

Although a number of pressure-derivative type curves have been presented, we have selected the derivative type curve developed by Bourdet et al. for illustration purposes. Their type curve is based on the analytical solution for a slightly compressible liquid derived by Agarwal et al. and plotted on the Gringarten et al. type curve. The Bourdet et al. type curve also includes a pressure-derivative function. The variable $p'_D(t_D/C_D)$ is plotted on the derivative type curve as a function of t_D/C_D for various values of C_De^{2S}, where

$$p'_D = \frac{dp_D}{d\left(t_D / p_D\right)} \qquad 4.100$$

The derivative type curve also has the following useful properties.

1. For test data on the unit-slope line, $p'_D = t_D/C_D$. Therefore,

$$\frac{dp_D}{d\left(t_D / p_D\right)} = p'_D = 1$$

$$\text{and} \quad p'_D\left(t_D / p_D\right) = t_D / p_D \qquad 4.101$$

Then, $\log[p_D(t_D/C_D)] = \log(t_D/C_D)$, and thus the slope of a plot of $[p_D(t_D/C_D)]$ vs. t_D/C_D on a log-log graph is unity. Therefore, at early times, for the same times during which a unit-slope line appears on a plot of P_D vs. t_D/C_D, a unit-slope line also will appear on a plot of $[P_D(t_D/C_D)]$ vs. t_D/C_D

2. For test data on the semilog straight line, P_D can be modeled with the logarithmic approximation to the line-source solution:

$$p_D=0.5[\ln t_D+0.80907+2S] \qquad 4.102$$

Adding and subtracting In C_D inside the parentheses in Eq. 4.102 gives

$$p_D=0.5[\ln t_D-\ln C_D+0.80907+\ln C_D+\ln(e^{2S})]= 0.5[\ln(t_D/C_D)+0.80907+\ln(C_De^{2S}) \qquad 4.103$$

Thus.

$$\frac{dp_D}{d\left(t_D/p_D\right)}=p'_D=\frac{0.5}{t_D/p_D}$$

$$\text{and} \quad p'_D\left(t_D/p_D\right)=0.5 \qquad 4.104$$

Data that lie on a straight line on a semilog graph will lie on a horizontal line at $p'_D(t_D/C_D)=0.5$ on the derivative type curve. Fig. 4.33 illustrates derivative curves with unit-slope lines at early times, a horizontal line at late times, and more complex shapes at intermediate times.

3. If a test data plot has both a unit-slope line on a logarithmic type-curve plot and a straight line on a semilog plot, then a match of the early and late test data is clearly and uniquely defined on the derivative type curve. A unique value of C_De^{2s} can then be determined, unlike Gringarten et al.'s type curve of P_D vs. t_D/C_D, which has uniqueness problems for large values of C_De^{2S}.

4. The type curves of P_D and P'_D vs. t_D/C_D can be plotted on a single graph, thus permitting simultaneous and less ambiguous type-curve analysis. Fig. 4.34 shows these curves.

4.8.1.3Gas-Well-Test Analysis With Derivative Type Curves

The following procedure, adapted from slightly-compressible-liquid analysis techniques using derivative type curves, can be applied to gaswell-test data analysis in terms of adjusted pressure and time variables:

1. From test data, calculate the following derivatives.

For a drawdown test,

$$\frac{dp_{a,wf}}{d(\ln t)} = -t\left(\frac{dp_{a,wf}}{d(\ln t)}\right) = t\Delta p'_a$$

and for a buildup test,

$$\frac{dp_{a,ws}}{d\left(\ln \Delta t_{ae}\right)} = \Delta t_{ae}\left(\frac{dp_{a,ws}}{d\left(\Delta t_{ae}\right)}\right) = \Delta t_{ae}\Delta p'_a$$

2 Plot $t\Delta p'_a$ (or $\Delta t_{ae}\Delta p'_a$) and Δp_a as functions of t (or Δt_{ae}) on either tracing paper or log-log graph paper the same size as the type-curve graph.

3. If possible, force a match of the data to the type curve in the vertical direction by aligning the flat region of the test data with the $p'_D(t_D/C_D)=0.5$ line on the type curve. The flat region is the middle-time or radial flow region. If this flat region is not present, semilog analysis is not possible.

4. If possible, force a match in the horizontal direction by aligning the unit-slope regions of the test data derivative plot and the derivative type curve.

5. Determine C_De^{2s} from the matching parameter of the derivative type-curve match. This same matching parameter characterizes the fit on the pressure-change type curve (P_D vs t_D/C_D).

6. With the test data plot fitted to the type curve, record values of (Δp_a,P_D) and (t,t_D/C_D) for a drawdown test or (Δp_{ae} t_D/C_D)for a buildup test at the match point. The match-point values are corresponding values of the pressure and time variables on the test data plot and the type curve.

7. Calculate permeability from the pressure match point.

$$k = \frac{141.2 q_g \bar{B}_g \bar{\mu}_g}{h}\left(\frac{p_D}{\Delta p_a}\right)_{MP}$$

where $\Delta p_a = (p_{a,i} - p_{a,wf})$ for a drawdown test or $\Delta p_a = (p_{a,ws} - p_{a,wf})$ for a buildup test.

8. Calculate or confirm C_D from the time match point.

$$C_D = \frac{0.0002637k}{\phi \bar{\mu}_g \bar{c} t r_w^2}\left(\frac{t \text{ or } \Delta t_{ae}}{t_D / C_D}\right)_{MP}$$

9. Calculate s using $C_D e^{2s}$ and C_D from Step 8.

$$S = 0.5 \ln\left(\frac{C_D e^{2S}}{C_D}\right)$$

Note that simultaneously matching both the adjusted pressure change and the adjusted pressure-derivative curves eliminates much of the ambiguity associated with conventional type-curve matching with only the pressure-change data. As an additional verification of

our analysis, we could precalculate a pressure match point using results from a semilog analysis. Further, we should not rely only on one well test analysis technique but should use the characteristics of each method. From these observations, the following general analysis procedure, which integrates conventional semilog analyses with type-curves, is suggested.

1. Perform a preliminary or qualitative analysis of the data using both the pressure-change and pressure-derivative data. The objective of this preliminary analysis is to identify the time regions(early-, middle-, and late-time regions).

2 Next, try a semilog analysis if the middle-time or radial flow region is present and is identified correctly from the preliminary type-curve analysis.

3. Finally, perform a quantitative type-curve analysis using both pressure and pressure-derivative data. Precalculate a pressure match point using k from the semilog analysis. If a reasonable match is obtained, we have confidence in our analysis. If we cannot obtain a reasonable match with the precalculated match point, we should iterate between the semilog and type-curve analyses until we obtain consistent results.

4.8.2 ANALYSIS OF PRESSURE AND PRESSURE DERIVATIVE WITHOUT TYPE-CURVE MATCHING

The current type-curve matching technique is essentially a trial-and-error procedure. A new technique for interpreting pressure tests using log-log plots of the pressure and pressure derivative versus time to calculate reservoir and well parameters *without* type-curve matching is presented. Wellbore storage and skin are present. Characteristic points are obtained of intersection of various straight line portions of the pressure and pressure derivative curve, slopes and starting times of these straight lines. These points, slopes and times are then used with appropriate equations to solve directly

for permeability, wellbore storage and skin. A step-by-step procedure for calculating these parameters without type-curve matching for five different cases is included in the paper.

The most important aspect of this new technique is its accuracy because it uses exact analytical solutions to calculate permeability, skin, and wellbore storage. The proposed technique is applicable to the interpretation of pressure buildup and drawdown tests and is illustrated by several numerical examples.

Appendices B discusses the basic equations and procedure for the case of slightly compressible fluid. Appendices C and D extend the direct synthesis technique to the gas-well test.

4.9 NUMERICAL APPLICATIONS

EXAMPLE 4.1

Determining Permeability and Skin Factor From a Multirate Test.

A gas well was tested with a conventional flow-after-flow backpressure test. Table 4.2 summarizes the measured pressures and rates. Assuming the non-Darcy flow effects ($D'q_n^2$) are negligible, estimate effective gas permeability and skin factor using the following well, rock, and gas properties.

γ_g =0.7

rw = 0.255 ft.

h = 19 ft.

T = 200°F.

$\bar{c}_t = 73.3 \times 10^{-6}$ psia^{-1},

Bg = 0.58778 RB/Mscf

ϕ = 0.176,

$\bar{\mu}$ = 0.0286 cp.

Solution

1. Our objective is to prepare a plot of

$$\frac{P_{a,i} - P_{a,wf} - D'q_n^2}{q_n} \text{ vs. } \frac{1}{q_n} \sum_{j=1}^{n} \Delta q_j \left[\log\left(t_n - t_{j-1}\right)\right]$$

Thus, the first step is to calculate the pressure/rate and time/rate plotting ffinctions for each of the four flow periods. For example at t=6 hours, n=1, t_1=6 hours, and q_1=2,711 Mscf/D,

$$\frac{P_{a,i} - P_{a,wf}}{q_n} = \frac{4{,}709.4 - 66.4}{2{,}711} = 1.713 \text{ psi / Mscf / D}$$

$$\frac{1}{q_n}\sum_{j=1}^{n} \Delta q_j \left[\log\left(t_n - t_{j-1}\right)\right] = \frac{1}{q_1}\Delta q_1\left[\log\left(t_1 - t_0\right)\right] = \frac{1}{2{,}711}(2{,}711 - 0)\left[\log(6-0)\right] = 0.7782$$

At t=9.5 hours, n=3, t_3 =9.5 hours, and q_3 =2,504 Mscf/D.

$$\frac{P_{a,i} - P_{a,wf}}{q_n} = \frac{4{,}709.4 - 258.9}{2{,}504} = 1.777 \text{ psi / Mscf / D}$$

$$\frac{1}{q_n}\sum_{j=1}^{n} \Delta q_j \left[\log\left(t_n - t_{j-1}\right)\right] = \frac{1}{q_3}\left[\Delta q_1 \log\left(t_3 - t_0\right) + \Delta q_2 \log\left(t_3 - t_1\right) + \Delta q_3 \log\left(t_3 - t_2\right)\right]$$

$$= \frac{1}{2{,}504}\left[(2{,}711 - 0)\log(9.5 - 0) + (2{,}607 - 2{,}711)\log(9.5 - 6) + (2{,}504 - 2{,}607)\log(9.5 - 8)\right] = 1.02$$

Calculated values of the pressure- and time-rate plotting functions (Table 4.3) are plotted in Fig. 4.12.

Using least-squares regression analysis, calculate the best-fit straight line through the data. From this line, we determine m'=0.236 and b=1.532.

2. The effective gas permeability is calculated with Eq. 4.50.

$$k = \frac{162.6(0.5878)(0.0286)}{(0.236)(19)} 0.61 \text{ md}$$

3. Next, calculate the skin factor using Eq. 4.51.

$$s = 1.151\left[\frac{b}{m'} - \log\left(\frac{k}{\phi \bar{\mu}_g \bar{c}_t r_w^2}\right) + 3.23\right] =$$

$$= 1.151\left\{\frac{1.532}{0.236} - \log\left[\frac{0.61}{(0.176)(0.0286)(7.33\text{x}10^{-5})(0.255)^2}\right] + 3.23\right\} = 2.6$$

A positive skin factor indicates damage resulting from a reduction in Permeability in the formation adjacent to the wellbore.

EXAMPLE 4.2

Analysis of a Variable-Rate Gas Flow Test.

A gas well was produced at a constant BHP of 1,000 psia. Known data are summarized below and in Table 4.4. Average gas and formation properties are evaluated at the arithmetic average of the initial and BHFPs, $\bar{p}$=2,825 psia. Assuming non-Darcy flow effects ($D'q_g^2$) are negligible, estimate formation permeability and skin factor using the semilog analysis technique for variable-rate gas flow tests.

$r_w = 0.365$ ft.

$\bar{\mu}_g = 0.0286$ cp.

$p_i = 4{,}560$ psia

$p_{wf} = 1{,}000$ psia

$h = 23$ ft

$\bar{c}_t = 21.55 \times 10^{-5}$ psia^{-1},

$p_{a,i} = 3{,}616.91$ psia

$p_{a,wf} = 231{,}71$ psia

$\phi = 0.14$,

$\bar{B}_g = 1.0485$ RB/Mscf

Solution

1. The first step is to prepare a plot of $(P_{a,i}-P_{a.wf} - D'q_g^2)/q_g$ vs. log t. Using the adjusted initial and BHP's in Table 4.4, calculate the plotting functions assuming negligible non-Darcy flow effects (i.e., D=0). For example, at t=4.8 hours, the plotting function is

$$\frac{P_{a,i} - P_{a,wf}}{q} = \frac{3{,}616.91 - 231.71}{405.9} = 8.34$$

Similarly, plotting functions for each measured rate are summarized in Table 4.5.

2. The data from Table 4.5 also were plotted in Fig. 4.13. From type-curve analysis we have identified the beginning of the middle-time region at approximately 30 hours. Therefore, the slope of the line drawn through data points afler this time is m'=1.09 psi/cycle.

3. The formation permeabilitv is

$$k = \frac{162.6(1.05)(0.0187)}{(1.09)(23)} = 0.13 \text{ md}$$

4. Next, calculate the skin factor. From Fig. 4.13, we see that the value of the pressure function at the extrapolation of the straight line to t=1 hour is

$$\left(\frac{P_{a,i} - P_{a,wf}}{q}\right)_{1hr} = 7.8 \text{ psi / Mscf / D}$$

and from Eq. 4.55,

$$s = 1.151\left[\frac{1}{m'}\left(\frac{P_{a,i} - P_{a,wf}}{q}\right)_{1hr} - \log\left(\frac{k}{\phi\bar{\mu}_g\bar{c}_t r_w^2}\right) + 3.23\right] =$$

$$= 1.151\left[\frac{1}{1.09}7.8 - \log\left(\frac{0.13}{(0.14)(0.0187)(21.55\text{x}10^{-5})(0.365^2)}\right) + 3.23\right] = 4.8$$

We assumed negligible non-Darcy effects, so the skin factor represents true formation damage.

EXAMPLE 4.3

Constant-Rate Gas-Well Drawdown Analysis With Non-Darcy Flow.

Table 4.8 summarizes pressure and time data from a constant-rate drawdown gas-well test ; other known data are summarized below. Determine k and s. In addition, estimate the skin factors caused by non-Darcy flow and by true formation damage or stimulation.

$q_g = 40{,}000$ Mscf/D

$\phi = 0.14$,

$T = 200°F$

$\bar{c}_t = 112 \times 10^{-6}$ psia^{-1},

$r_w = 0.365$ ft.

$\bar{\mu}_g = 0.0286$ cp.

$p_i = \bar{p} = 4{,}290$ psia

$h = 40$ ft

$S_w = 0.25$

$\bar{z} = 0.92$

$\bar{B}_g = 0.7163$ RB/Mscf

$p_{a,i} = \bar{p}_a = 3{,}056$ psia

$r_w = 0.3$ ft

$\gamma_g = 0.85$

$\bar{p}_{a,1hr} = 2{,}364$ psia

$\bar{\mu}_g = 0.0286$ cp.

Solution

With the high flow rate of 40,000 Mscf/D, the skin factor from conventional semilog analysis can be expected to reflect both a true skin factor (formation condition near the wellbore) and a pseudoskin resulting from non-Darcy flow near the wellbore. The procedure adapted from Fligelman et al. can be used to find k and true s when non-Darcy flow has a significant effect on the pressure response. For convenience in analyzing a gas-well drawdown test, we convert pseudopressures to adjusted pressures using viscosity, $\bar{\mu}_g$, compressibility factor, $\bar{z}$, and total compressibility, $\bar{c}_t$, evaluated at average pressure, $\bar{p}$. Table 4.8 gives plotting variables.

1. Qualitative type-curve analysis using adjusted pressure indicates that all data points are in the region of the semilog straight line.
2. Adjusted pressure is plotted as a function of real time in Fig. 4.17, and the semilog straight line drawn through the data points has a slope m=52.0 psi/cycle. Adjusted pressure at t=1 hour is $P_{a,1hr}$=2,364 psia.
The initial estimate of formation permeability is

$$k = \frac{162.6 q_g \bar{\mu}_g \bar{B}_g}{mh} = \frac{162.6(40{,}000)(0.7163)(0.0254)}{(52)(40)} = 57 \text{ md}$$

3. The total skin factor is estimated to be

$$s = 1.151\left[\left(\frac{P_{a,i} - P_{a,1hr}}{q}\right) - \log\left(\frac{k}{\phi \bar{\mu}_g \bar{c}_t r_w^2}\right) + 3.23\right] =$$

$$= 1.151\left[\frac{3{,}056 - 2{,}364}{52} - \log\left(\frac{57}{(0.10)(0.0254)(112\text{x}10^{-5})(0.3)^2}\right) + 3.23\right] = 8.3$$

4. The turbulence factor is estimated with Eq. 4.40.

$$\beta = 1.88x10^{10}k^{-1.47}\phi^{-0.53} = 1.88x10^{10}(57)^{-1.47}(0.10)^{-0.53} = 1.67x10^{8}\ ft^{-1}$$

The group B_{qD} is

$$Bq_D = \frac{2.715x10^{-15}\beta k M p_{sc} q_g}{T_{sc} h r_w \bar{\mu}_g} = \frac{(2.715x10^{-15})(1.67x10^{8})(57)(0.85)(29)(14.7)(40,000)}{(520)(40)(0.3)(0.02544)} = 2.36$$

The dimensionless rate is

$$q_D = \frac{0.138 q_g p_{sc} T}{khT_{sc} p_{a,i}} = \frac{(0.138)(40,000)(14.7)(660)}{(57)(40)(520)(3,056)} = 0.0148$$

The term b_D is

$$b_D = \frac{p_{a,i} - m\log\left(\frac{0.0002637k}{\phi\bar{\mu}_g\bar{c}tr_w^2}\right) - p_{a,1hr}}{q_D p_{a,i}} =$$

$$= \frac{3,056 - 52\log\left[\frac{0.0002637(57)}{(0.1)(0.02544)(0.000112)(0.3)^2}\right] - 2,364}{(0.0148)(3,056)} = 8.68$$

From Fig. 4.15 with B_{qD}=2.36 and b_D=8.68, estimate s=2.7.

5. From Fig. 4.16 with B_{qD}=2.36 and s=2.7, we find p^*_{aD}=5.8. The term t^*_D is

$$t_D^* = \frac{0.0002637k}{\bar{\mu}_g \bar{c}_t r_w^2} = \frac{(0.0002637)(57)}{(0.0254)(0.000112)(0.3)^2} = 58.615$$

And m_D is

$$m_D = 1.151 + \frac{\left(p_{aD}^* - b_D + 0.4045 + s\right)}{\log t_D^*} = 1.151 + \frac{(5.8 - 8.68 + 0.4045 + 2.7)}{\log(58.615)} = 1.12$$

6. Using m_D, calculate a second approximation of permeability

$$k = \frac{0.138 T p_{sc} q_g}{mhT_{sc}} m_D = \frac{0.138(660)(14.7)(40{,}000)}{(52)(40)(520)}(1.12) = 55.5 \text{ md}$$

7. For illustration purposes, consider the permeability estimate of 55.5 md from Step 5 sufficiently different from the initial estimation of 57 md that iteration is required.

First Iteration.

4A. The new value for the turbulence factor is

$$\beta = 1.88 \times 10^{10} k^{-1.47} \phi^{-0.53} = 1.88 \times 10^{10} (55.5)^{-1.47} (0.10)^{-0.53} = 1.74 \times 10^{8} \text{ ft}^{-1}$$

The group B_{qD} is

$$Bq_D = \frac{2.715 \times 10^{-15} \beta k M p_{sc} q_g}{T_{sc} h r_w \bar{\mu}_g} = \frac{(2.715 \times 10^{-15})(1.74 \times 10^{8})(55.5)(0.85)(29)(14.7)(40{,}000)}{(520)(40)(0.3)(0.02544)} = 2.4$$

The dimensionless rate is

$$q_D = \frac{0.138 q_g p_{sc} T}{k h T_{sc} p_{a,i}} = \frac{(0.138)(40{,}000)(14.7)(660)}{(55.5)(40)(520)(3{,}056)} = 0.0152$$

The term b_D is

$$b_D = \frac{p_{a,i} - m \log\left(\frac{0.0002637k}{\phi \bar{\mu}_g \bar{c}_t r_w^2}\right) - p_{a,1hr}}{q_D p_{a,i}} =$$

$$= \frac{3{,}056 - 52 \log\left[\frac{0.0002637(55.5)}{(0.1)(0.02544)(0.000112)(0.3)^2}\right] - 2{,}364}{(0.0148)(3{,}056)} = 8.45$$

From Fig. 4.15 with B_{qD}=2.39 and b_D=8.45, estimate s=2.5.

5A. From Fig. 4.16 with B_{qD}=2.39 and s=2.9, we find p^*_{aD}=6.0. The term t^*_D is

$$t^*_D = \frac{0.0002637k}{\bar{\mu}_g \bar{c}_t r_w^2} = \frac{(0.0002637)(55.5)}{(0.0254)(0.000112)(0.3)^2} = 57.162$$

And m_D is

$$m_D = 1.151 + \frac{\left(p^*_{aD} - b_D + 0.4045 + s\right)}{\log t^*_D} = 1.151 + \frac{(6.0 - 8.45 + 0.4045 + 2.5)}{\log(57.162)} = 1.25$$

6A. Using m_D, calculate a second approximation of permeability

$$k = \frac{0.138 T p_{sc} q_g}{m h T_{sc}} m_D = \frac{0.138(660)(14.7)(40{,}000)}{(52)(40)(520)}(1.25) = 61.9 \text{ md}$$

7A. The permeability estimate of 61.9 md from Step 5A still does not agree with the previously calculated value of 55.5 md. For better accuracy, another iteration will be made.

Second Iteration.

4B. The new value for the turbulence factor is

$$\beta = 1.88\text{x}10^{10}k^{-1.47}\phi^{-0.53} = 1.88\text{x}10^{10}(61.9)^{-1.47}(0.10)^{-0.53} = 1.48\text{x}10^{8}\ \text{ft}^{-1}$$

The group B_{qD} is

$$Bq_D = \frac{2.715\text{x}10^{-15}\beta k M p_{sc} q_g}{T_{sc} h r_w \bar{\mu}_g} = \frac{(2.715\text{x}10^{-15})(1.48\text{x}10^{8})(61.9)(0.85)(29)(14.7)(40{,}000)}{(520)(40)(0.3)(0.02544)} = 2.27$$

The dimensionless rate is

$$q_D = \frac{0.138 q_g p_{sc} T}{khT_{sc} p_{a,i}} = \frac{(0.138)(40{,}000)(14.7)(660)}{(61.9)(40)(520)(3{,}056)} = 0.0136$$

The term b_D is

$$b_D = \frac{p_{a,i} - m\log\left(\dfrac{0.0002637k}{\phi\bar{\mu}_g\bar{c}tr_w^2}\right) - p_{a,1hr}}{q_D p_{a,i}} =$$

$$= \frac{3{,}056 - 52\log\left[\dfrac{0.0002637(61.9)}{(0.1)(0.02544)(0.000112)(0.3)^2}\right] - 2{,}364}{(0.0136)(3{,}056)} = 9.39$$

From Fig. 4.15 with B_{qD}=2.27 and b_D=9.39, estimate s=3.0.

5B. From Fig. 4.16 with B_{qD}=2.37 and s=3.0, we find p^*_{aD}=6.3. The term t^*_D is

$$t_D^* = \frac{0.0002637k}{\bar{\mu}_g \bar{c}_t r_w^2} = \frac{(0.0002637)(61.9)}{(0.0254)(0.000112)(0.3)^2} = 63.754$$

And m_D is

$$m_D = 1.151 + \frac{\left(p_{aD}^* - b_D + 0.4045 + s\right)}{\log t_D^*} = 1.151 + \frac{(6.3 - 9.39 + 0.4045 + 3.0)}{\log(63.754)} = 1.22$$

6B. Using m_D, calculate a second approximation of permeability

$$k = \frac{0.138 T p_{sc} q_g}{mhT_{sc}} m_D = \frac{0.138(660)(14.7)(40{,}000)}{(52)(40)(520)}(1.22) = 60.4 \text{ md}$$

7B . The permeability estimate of 60.4 md from Step 5B differs from the previous estimate of 61.9 md, so iterations could continue; however, we will accept this result here because our main objective is to illustrate the computational procedure. Thus, formation permeability is k=60.4 md. From Step 3B, the corresponding "true" skin factor is s=3.0.

8. The error from the exclusion of non-Darcy flow effects in the drawdown analysis can be assessed by comparing these results with results from conventional calculations.

The non-Darcy coefficient is estimated to he

$$D = \frac{2.715x10^{-15} \beta k M p_{sc}}{T_{sc} h r_w \mu_{g,wf}} = \frac{(2.715x10^{-15})(1.67x10^{8})(57)(0.85)(29)(14.7)}{(520)(40)(0.3)(0.0244)} = 6.15x10^{-5} \text{ D / Mscf}$$

As an estimate, $\mu_{g,wf}$ is evaluated at the final flowing pressure during the test, P_{wf} = 3,570 psia, and is equal to 0.0244 cp. The pseudoskin, Dq_g, resulting from high-velocity flow near the wellbore is

$$Dq_g = (6.15 \times 10^{-5})(40{,}000) = 2.5$$

9. The true skin factor, s, resulting from formation damage near the wellbore is estimated to be

$$s = s' - Dq_g = 8.3 - 2.5 = 5.8$$

Note that the estimate of s=5.8 obtained with conventional calculations is almost twice that obtained when non-Darcy flow is included (s=3.0).

EXAMPLE 4.4

Analysis of a Gas-Well Pressure-Buildup Test With Constant-Rate Production Before Shut-In.

A pressure buildup test was run on a gas well in a newly discovered reservoir. Known and calculated data are summarized below and in Table 4.9. Because the reservoir pressure has not been depleted, the semilog straight line should extrapolate to original reservoir pressure at a Homer time ratio of unity; i.e., $p^*=p_i$. Prepare Homer plots of

(1) p_{ws} vs. $\left(t_p+\Delta t\right)/\Delta t$;

(2) p_{ws}^2 vs. $\left(t_p+\Delta t\right)/\Delta t$

(3) $p_{a,ws}$ vs. $\left(t_p+\Delta t_a\right)/\Delta t_a$;

Determine k and s from each plot.

$h = 21$ ft.

$t_p = 2{,}000$ hours.

$\bar{\mu}_g = 0.03403$ cp.

$p_i = 9{,}000$ psia

$\gamma_g = 0.85$

$r_w = 0.365$ ft

$q_g = 100$ Mscf/D

$\bar{c}_t = 35.5 \times 10^{-6}$ psia^{-1},

$p_{a,i} = 7{,}560$ psia

$S_w = 0.3$ ft

$\phi = 0.10$.

$T = 670°R\ (210°F)$

$\bar{B}_g = 0.4973$ RB/Mscf

$\bar{z} = 1.325$

Solution.

Figs. 4.25 through 4.27 give Homer plots in terms of pressure, pressure-squared, and adjusted pressures, respectively. Note that semilog straight lines passing through the later data and through Pi (equal to p* in this case) appear in each case.

Analysis Using Pressure Variables (Fig. 4.25).

1. Calculate the slope of the line drawn through the semilog straight line.

m=8,989.7-8,545.1 = 444.6 psi/cycle.

2. The permeability to gas is

$$k = \frac{162.6 q_g \bar{\mu}_g \bar{B}_g}{mh} = \frac{162.6(q_g)(100)(0.497)(0.3403)}{(444.61)(21)} = 0.029 \text{ md}$$

Calculate the skin factor. The pressure p_{1hr} at

$$\left(t_p + \Delta t\right)/\Delta t = (2{,}000+1)/1 = 2{,}001 \text{ is } 7{,}522 \text{ psia}$$

Thus,

$$S' = 1.151\left[\left(\frac{P_{1hr} - P_{wf}}{m}\right) - \log\left(\frac{k}{\phi \bar{\mu}_g \bar{c} t r_w^2}\right) + 3.23\right] =$$

$$1.151\left[\left(\frac{7{,}522 - 6{,}287.1}{444.6}\right) - \log\left(\frac{0.029}{(0.1)(0.03403)(0.0000355)(0.365)^2}\right) + 3.23\right] = -0.292$$

Analysis Using Pressure-Squared Variables (Fig. 4.26).

1. Calculate the slope of the line drawn through the semilog straight line.

$m=80.67x10^6-73.07x10^6 = 7.6 \times 10^6$ psi^2/cycle.

2. The permeability to gas is

$$k = \frac{1{,}637 q_g \bar{\mu}_g \bar{z}T}{mh} = \frac{1{,}637(100)(670)(1.325)(0.03403)}{(0.760x10^7)(21)} = 0.031 \text{ md}$$

Calculate the skin factor. The pressure p^2_{1hr} at

$\left(t_p + \Delta t\right)/\Delta t = (2{,}000+1)/1 = 2{,}001$ is $55.6x10^6$ psia^2, so

$$S' = 1.151\left[\left(\frac{P^2_{1hr} - P^2_{wf}}{m}\right) - \log\left(\frac{k}{\phi\mu c_t r^2_w}\right) + 3.23\right] =$$

$$1.151\left[\left(\frac{55.6x10^6 - 39.53x10^6}{7.6x10^6}\right) - \log\left(\frac{0.031}{(0.1)(0.03403)(0.0000355)(0.365)^2}\right) + 3.23\right] =$$

$$= -1.08$$

Analysis Using Adjusted Pressure Variables (Fig. 4.27).

1. Calculate the slope of the line drawn through the semilog straight line.

m=7,553.8-7,117.5= 436.3 psi/cycle.

2. The permeability to gas is

$$k = \frac{162.6 q_g \bar{\mu}_g \bar{B}_g}{mh} = \frac{162.6(100)(0.497)(0.3403)}{(436.3)(21)} = 0.030 \text{ md}$$

Calculate the skin factor. The pressure p_{1hr} at

$$\left(t_p + \Delta t\right) / \Delta t = (2{,}000 + 1)/1 = 2{,}001 \text{ is } 6{,}114 \text{ psia}$$

Thus,

$$S' = 1.151\left[\left(\frac{P_{a,1hr} - P_{a,wf}}{m}\right) - \log\left(\frac{k}{\phi \bar{\mu}_g \bar{c}_t r_w^2}\right) + 3.23\right] =$$

$$1.151\left[\left(\frac{6{,}114 - 4{,}804.1}{436.3}\right) - \log\left(\frac{0.030}{(0.1)(0.03403)(0.0000355)(0.365)^2}\right) + 3.23\right] = -0.04$$

In this example, there is little difference in results when the pressure, pressure-squared, or adjusted-pressure analysis is used on a Homer semilog graph. However, when wellbore-storage-distorted data are analyzed on a type curve, the differences can be significant.

EXAMPLE 4.5

Gas-Well Buildup Test Analysis With Pressure Derivative Type Curves.

With the gas-well buildup test data presented in Example 4.4, estimate k and s using the Bourdet et al. derivative type curves. Known and calculated data are summarized in Table 4.13. Use adjusted pressure and time variables as the plotting functions.

Solution.

1. Plot Δp_a and $\Delta t_{ae}\,\Delta p'_a$ vs. Δp_a on log-log paper (Fig. 4.35).

2. Using the Bourdet et al. type curve, try to match both Δp_a and $\Delta t_{ae}\,\Delta p'_a$.

Note that the early-time data form a unit-slope line, indicating wellbore-storage effects. Similarly, several adjusted pressure-derivative data points at the end of the test begin to flatten and appear to form a middle-time region. As Fig. 4.35 shows, we could match both adjusted pressure change and pressure derivative with the type curves characterized by $C_De^{2S} = 100$. In addition, we can match several of the last few pressure-derivative points on the type curve for $p_D(t_D/C_D)$=O.5, indicating the presence of the middle-time region.

3. From the match in Fig. 4.35, we obtain a pressure match point of Δp_a=380 psi, P_D=1, and a time match point of Δt_{ae}=2.7 hours, t_D/C_D=10.

4. Determine k using the pressure match point.

$$k = \frac{141.2 q_g \bar{B}_g \bar{\mu}_g}{h}\left(\frac{p_D}{\Delta p_a}\right)_{MP} = \frac{141.2(100)(0.497)(0.03403)}{21}\left(\frac{1}{380}\right) = 0.03 \text{ md}$$

8. Calculate or confirm C_D from the time match point.

$$C_D = \frac{0.0002637k}{\phi \bar{\mu}_g \bar{c}_t r_w^2}\left(\frac{t \text{ or } \Delta t_{ae}}{t_D / C_D}\right) = \frac{0.0002637(0.03)}{(0.1)(0.034)(0.0000355)(0.365)^2}\left(\frac{2.7}{10}\right) = 133$$

9. Calculate s using $C_D e^{2s}$ and C_D from Step 8.

$$S = 0.5 \ln\left(\frac{C_D e^{2S}}{C_D}\right) = 0.5 \ln\left(\frac{100}{133}\right) = -0.14$$

APPENDIX A

FIGURES AND TABLES

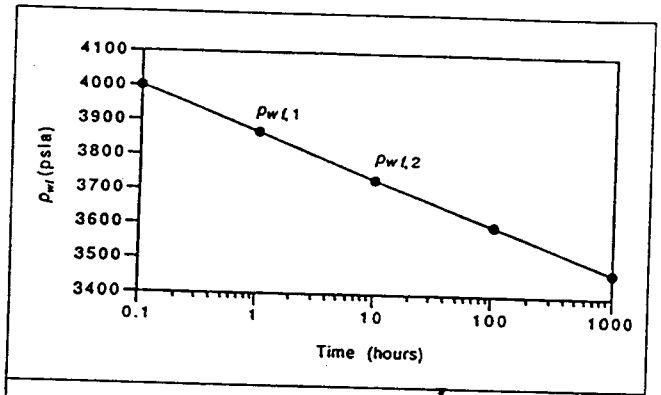

Analysis technique for constant-rate flow test data.

FIG. 4.1

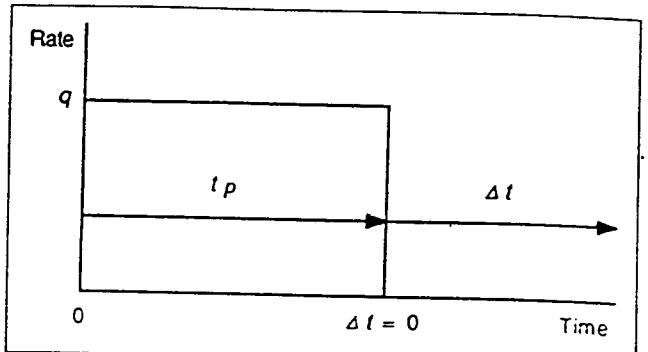

Modeling a pressure-buildup test in terms of variable-rate production.

FIG. 4.2

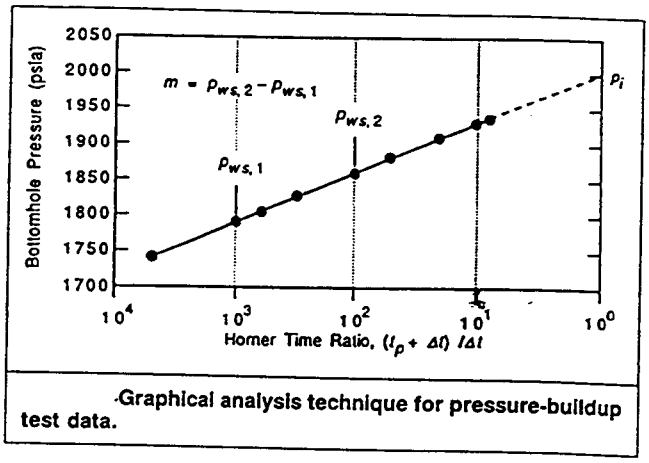

Graphical analysis technique for pressure-buildup test data.

FIG. 4.3

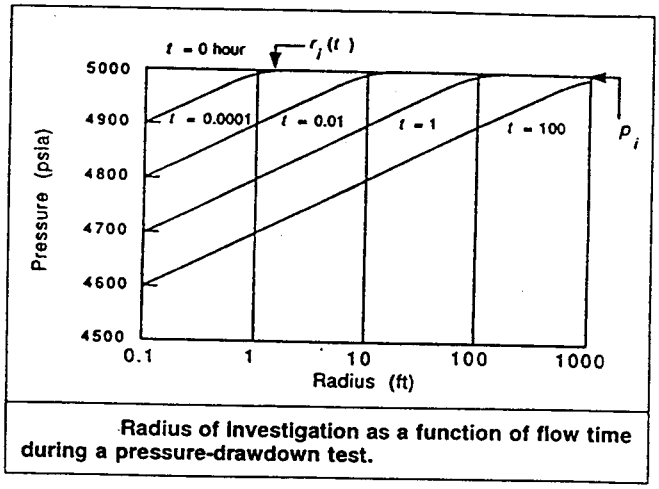

Radius of investigation as a function of flow time during a pressure-drawdown test.

FIG. 4.4

FIG. 4.5

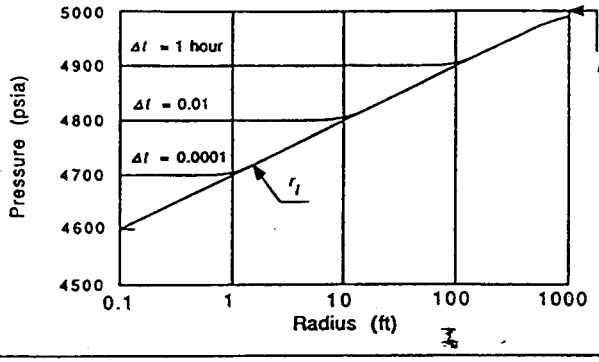

Radius of investigation as a function of shut-in time during a pressure-buildup test.

FIG. 4.6

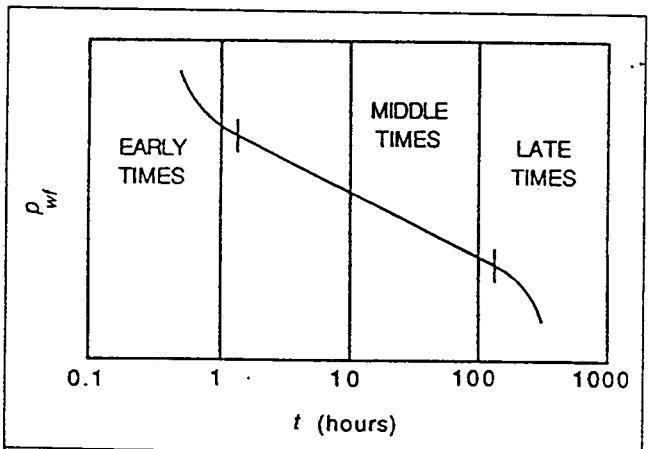

Characteristic curve shapes exhibited during a flow test.

FIG. 4.7

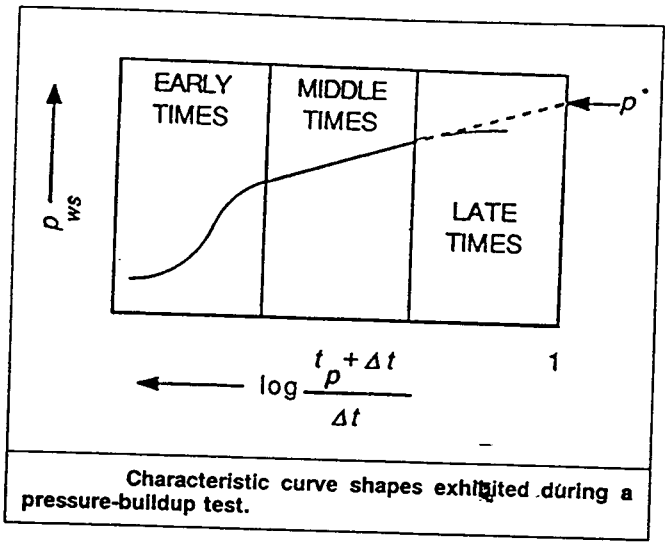

Characteristic curve shapes exhibited during a pressure-buildup test.

FIG. 4.8

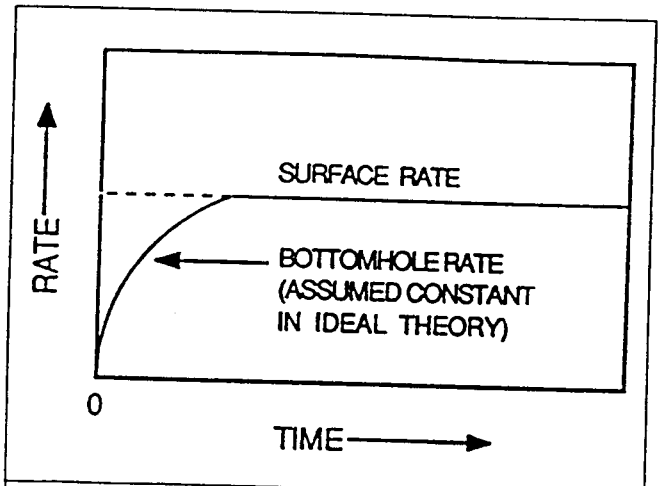

Surface production rate schedule during wellbore-storage period.

FIG. 4.9

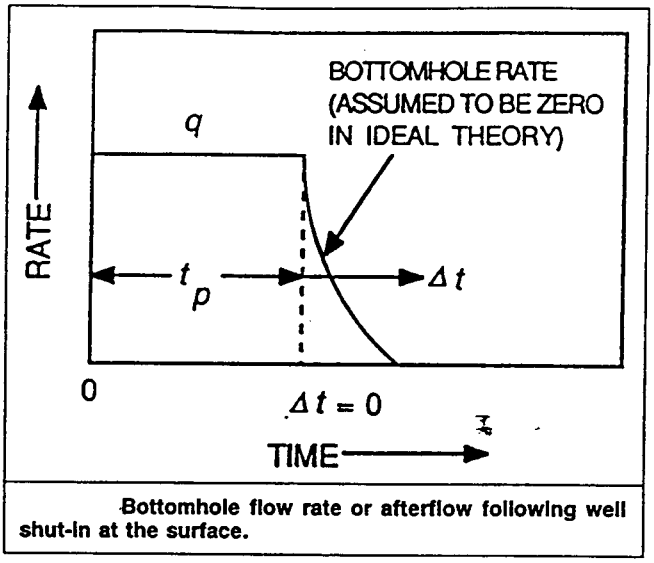

Bottomhole flow rate or afterflow following well shut-in at the surface.

FIG. 4.10

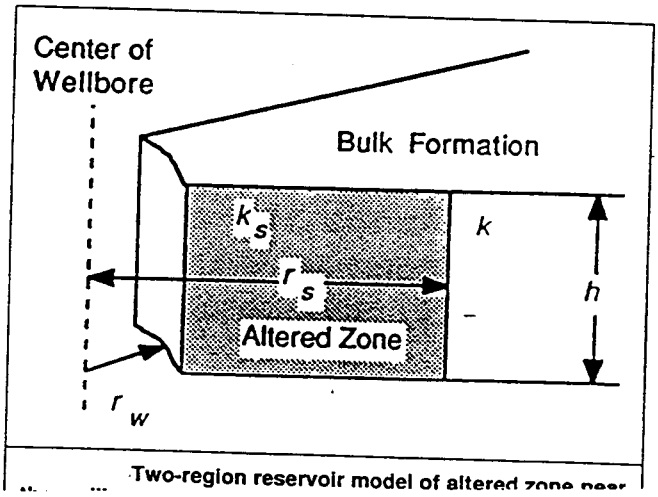

Two-region reservoir model of altered zone near

FIG. 4.11

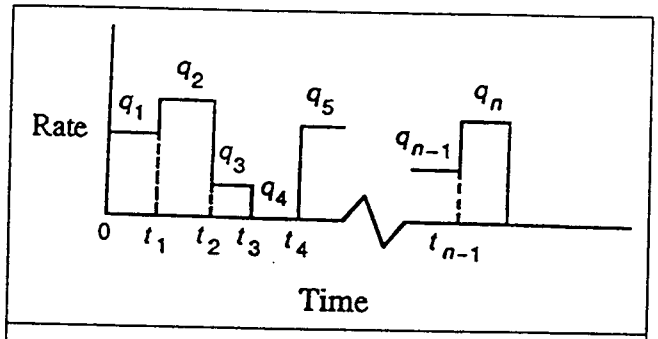

Variable-rate production history.

FIG. 4.12

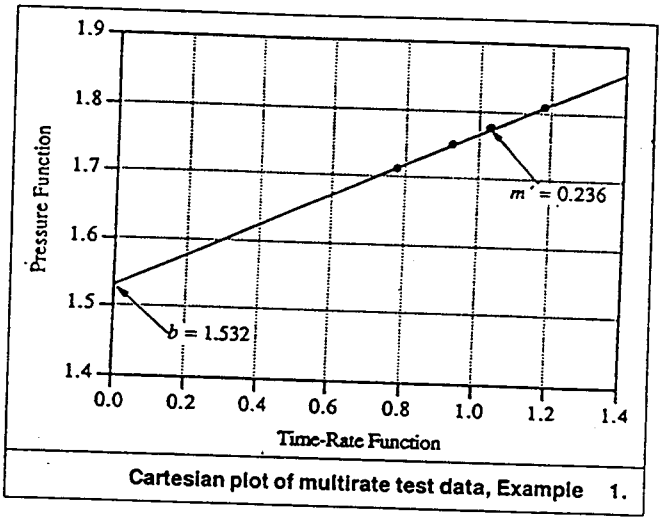

Cartesian plot of multirate test data, Example 1.

FIG. 4.13

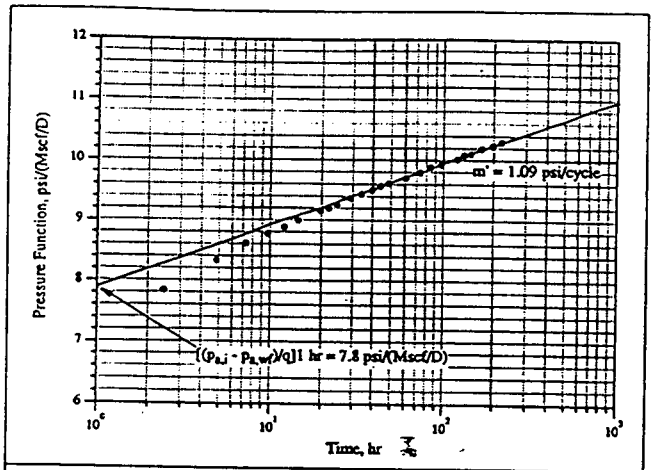

Semilog plot of variable-rate data for Example 2.

FIG. 4.14

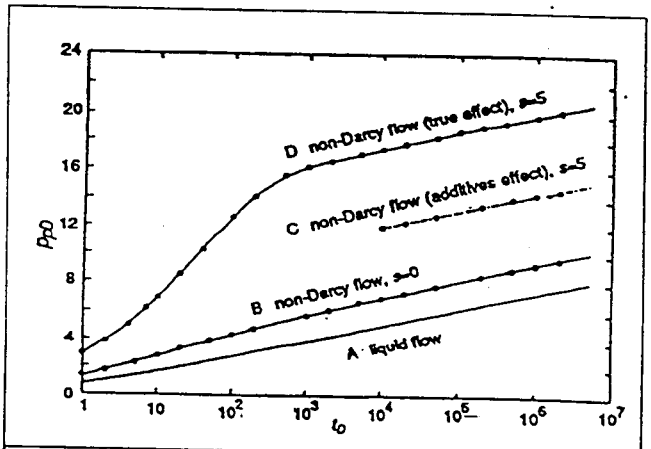

Effects of non-Darcy flow and skin factor on transient-pressure response (after Fligelman *et al.* [12]).

FIG. 4.15

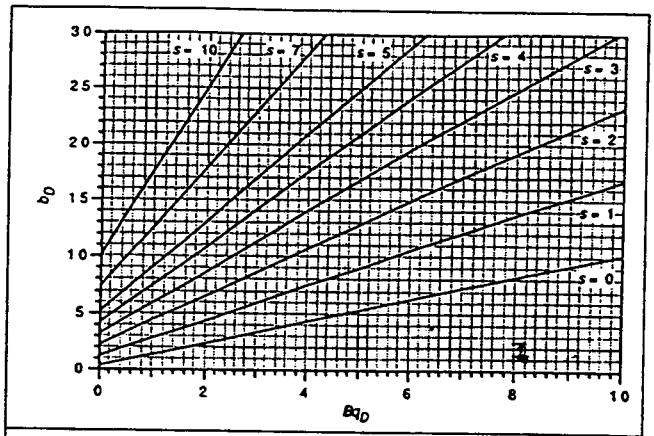

Correlation of b_D and Bq_D (after Fligelman et *al.*[12]).

FIG. 4.16

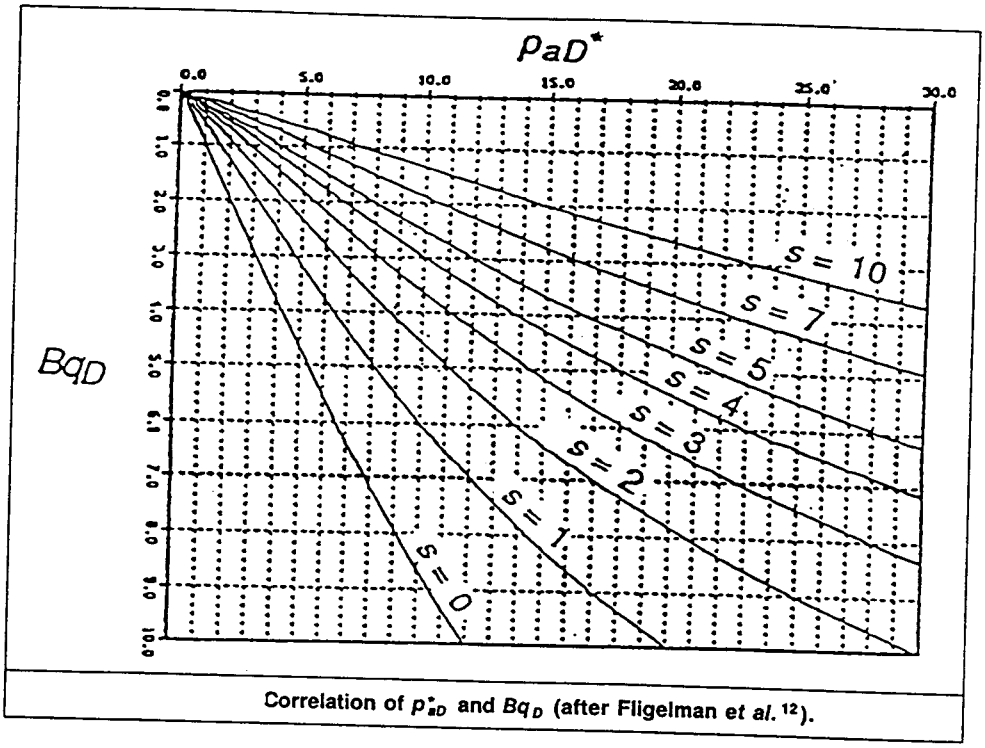

Correlation of p_{aD}^* and Bq_D (after Fligelman et *al.*[12]).

FIG. 4.17

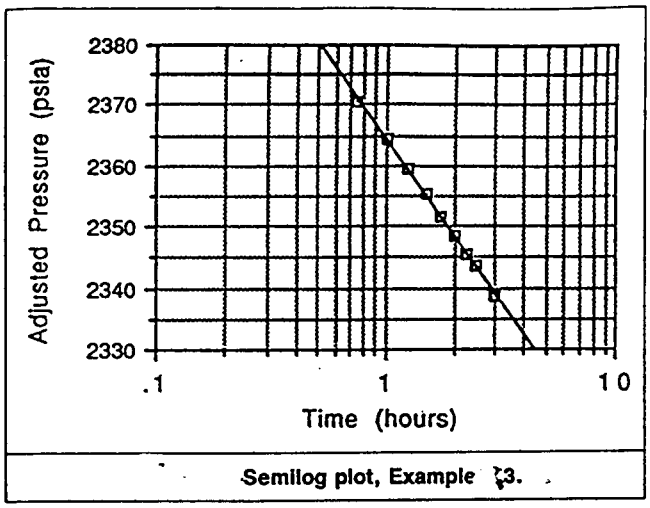

Semilog plot, Example 3.

$\bar{B}_g$ = 0.7163 RB/Mscf.
$p_{a,i}=\bar{p}_a$ = 3,056 psia.
r_w = 0.3 ft.

FIG. 4.18

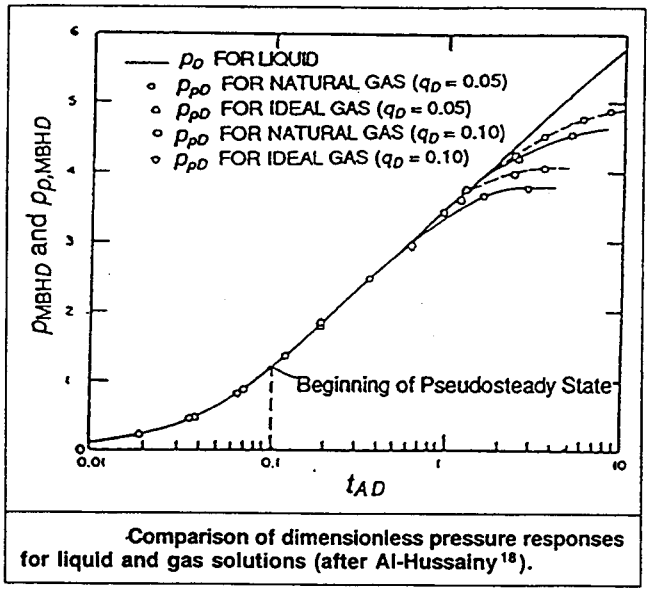

Comparison of dimensionless pressure responses for liquid and gas solutions (after Al-Hussainy[18]).

FIG. 4.19

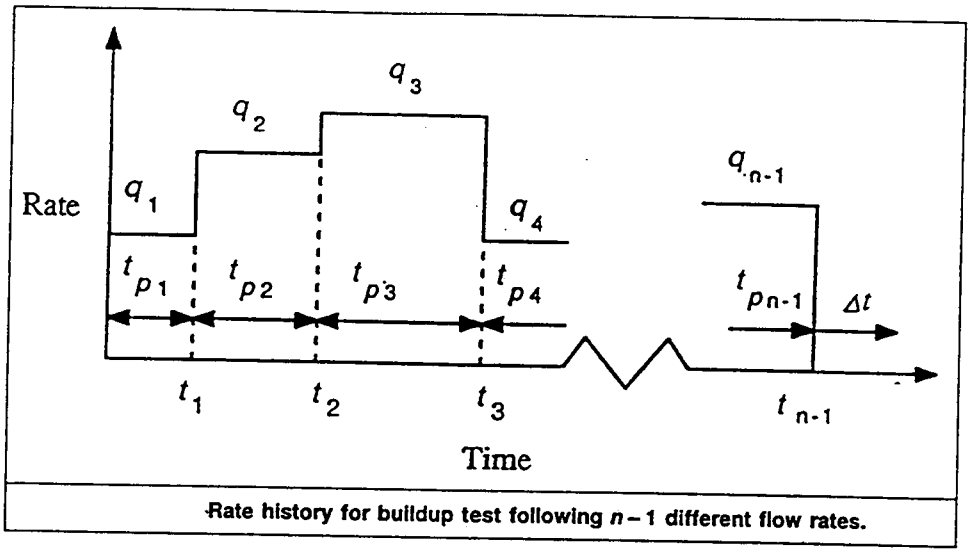

Rate history for buildup test following $n-1$ different flow rates.

FIG. 4.20

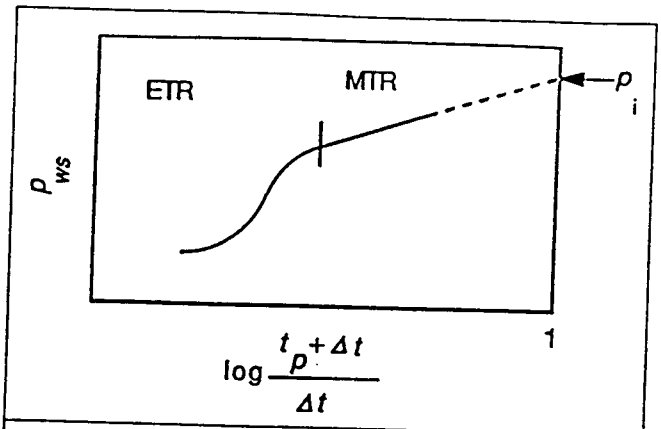

Buildup test plot for a well in an infinite-acting reservoir with negligible pressure depletion (ETR = early-time region; MTR = middle-time region).

FIG. 4.21

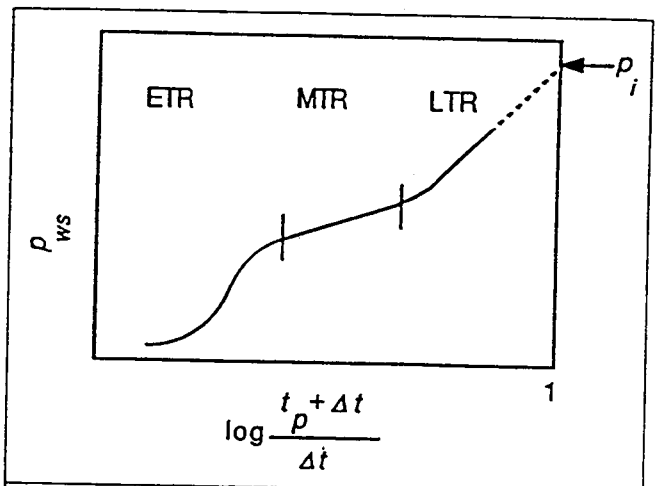

Buildup test plot for a well near a boundary in a reservoir with negligible pressure depletion (LTR = late-time region).

FIG. 4.22

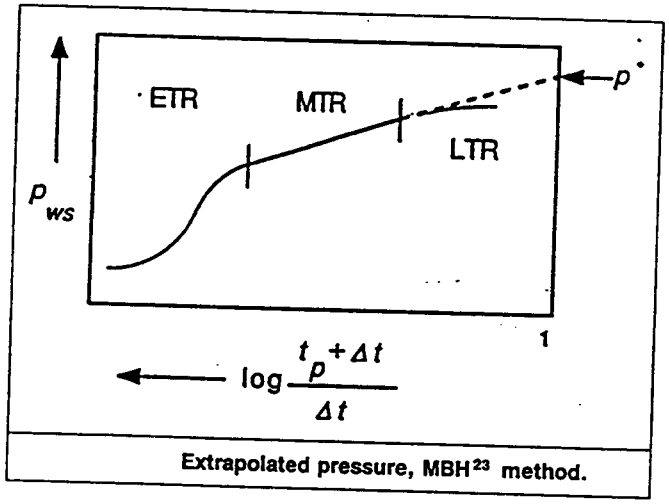

Extrapolated pressure, MBH[23] method.

FIG. 4.23

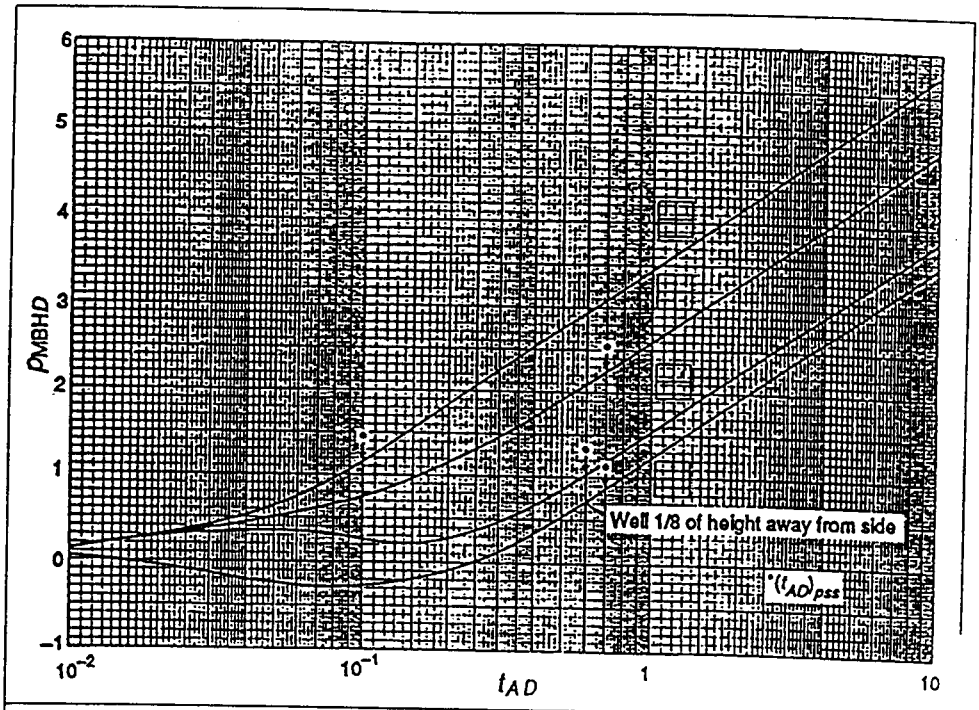

MBH[23] dimensionless pressures for various well locations in a square drainage area (after Earlougher[2]).

FIG. 4.24

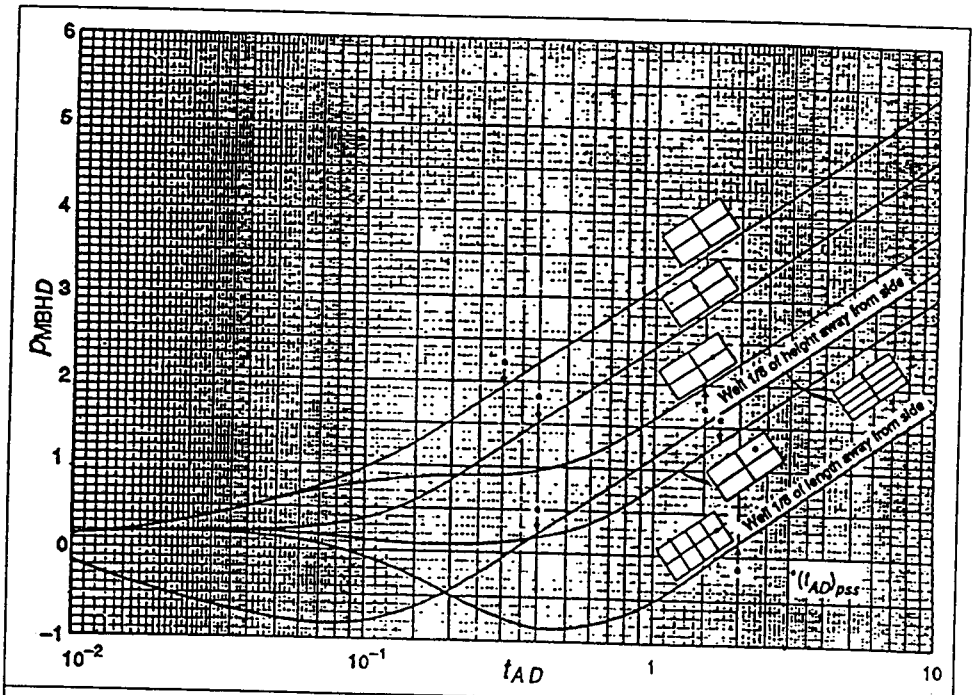

- MBH[23] dimensionless pressures for various well locations in a 2:1 rectangular drainage area (after Earlougher[1]).

FIG. 4.25

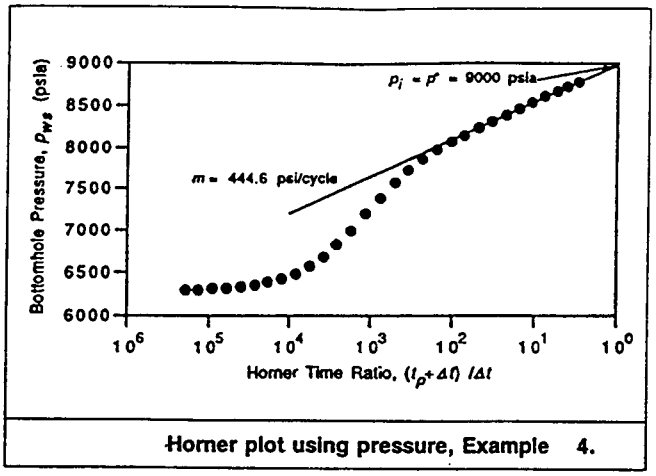

Horner plot using pressure, Example 4.

FIG. 4.26

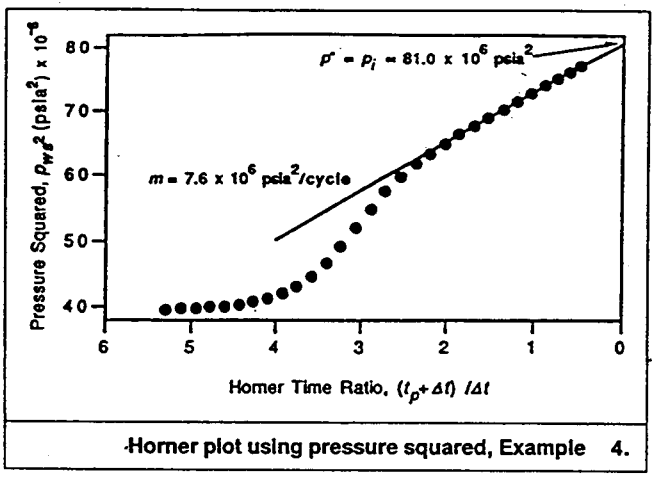

Horner plot using pressure squared, Example 4.

FIG. 4.27

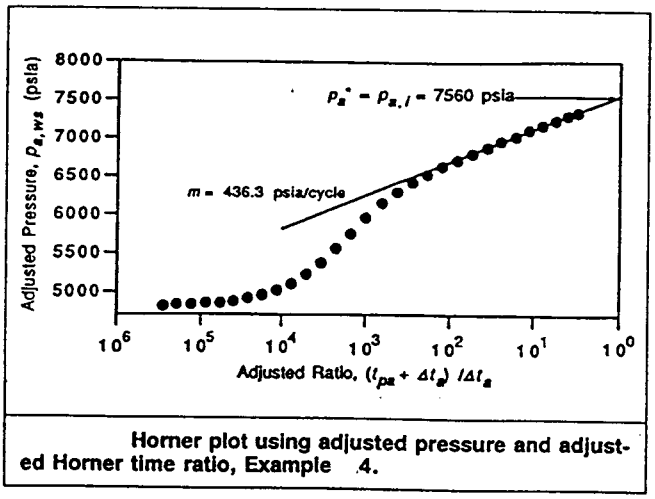

Horner plot using adjusted pressure and adjusted Horner time ratio, Example 4.

TABLE 4.1

SUMMARY OF WORKING EQUATIONS FOR PRESSURE-TRANSIENT TEST ANALYSIS IN GAS WELLS

	Oil	Gas, Using Adjusted Variables
Flow Test		
Semilog graph variables	p_{wf} vs. t	$p_{a,wf}$ vs. t
Permeability from m of semilog straight line	$k = \dfrac{162.6 q_o B_o \mu_o}{mh}$	$k = \dfrac{162.6 q_g \bar{B}_g \bar{\mu}_g}{mh}$
Skin factor calculation	$s = 1.151\left[\dfrac{p_i - p_{1hr}}{m} - \log\left(\dfrac{k}{\phi \mu_o c_t r_w^2}\right) + 3.23\right]$	$s = 1.151\left[\dfrac{p_{a,i} - p_{a,1hr}}{m} - \log\left(\dfrac{k}{\phi \bar{\mu}_g \bar{c}_t r_w^2}\right) + 3.23\right]$
Buildup Test		
Semilog graph variables	p_{ws} vs. $(t_p + \Delta t)/\Delta t$	$p_{a,ws}$ vs. $(t_p + \Delta t_a)/\Delta t_a$
Permeability from m of semilog straight line	$k = \dfrac{162.6 q_o B_o \mu_o}{mh}$	$k = \dfrac{162.6 q_g \bar{B}_g \bar{\mu}_g}{mh}$
Skin factor calculation	$s = 1.151\left[\dfrac{p_{1hr} - p_{wf}}{m} - \log\left(\dfrac{k}{\phi \mu_o c_t r_w^2}\right) + 3.23\right]$	$s = 1.151\left[\dfrac{p_{a,1hr} - p_{a,wf}}{m} - \log\left(\dfrac{k}{\phi \bar{\mu}_g \bar{c}_t r_w^2}\right) + 3.23\right]$
Definition of $p_{MBH,D}$	$\dfrac{kh(p^* - \bar{p})}{70.6 q_o B_o \mu_o}$	$\dfrac{kh(p_a^* - \bar{p}_a)}{70.6 q_g \bar{B}_g \bar{\mu}_g}$

TABLE 4.1

SUMMARY OF WORKING EQUATIONS FOR PRESSURE-TRANSIENT TEST ANALYSIS IN GAS WELLS (Continued)

	Gas, Using Pressure and Time	Gas, Using Pressure-Squared and Time
Flow Test		
Semilog graph variables	p_{wf} vs. t	p_{wf}^2 vs. t
Permeability from m of semilog straight line	$k = \dfrac{162.6 q_g \bar{B}_g \bar{\mu}_g}{mh}$	$k = \dfrac{1637 q_g T \bar{z} \bar{\mu}_g}{mh}$
Skin factor calculation	$s = 1.151\left[\dfrac{\bar{p} - p_{1hr}}{m} - \log\left(\dfrac{k}{\phi \bar{\mu}_g \bar{c}_t r_w^2}\right) + 3.23\right]$	$s = 1.151\left[\dfrac{\bar{p}^2 - p_{1hr}^2}{m} - \log\left(\dfrac{k}{\phi \bar{\mu}_g \bar{c}_t r_w^2}\right) + 3.23\right]$
Buildup Test		
Semilog graph variables	p_{ws} vs. $(t_p + \Delta t)/\Delta t$	p_{ws}^2 vs. $(t_p + \Delta t)/\Delta t$
Permeability from m of semilog straight line	$k = \dfrac{162.6 q_g \bar{B}_g \bar{\mu}_g}{mh}$	$k = \dfrac{1637 q_g T \bar{z} \bar{\mu}_g}{mh}$
Skin factor calculation	$s = 1.151\left[\dfrac{p_{1hr} - p_{wf}}{m} - \log\left(\dfrac{k}{\phi \bar{\mu}_g \bar{c}_t r_w^2}\right) + 3.23\right]$	$s = 1.151\left[\dfrac{p_{1hr}^2 - p_{wf}^2}{m} - \log\left(\dfrac{k}{\phi \bar{\mu}_g \bar{c}_t r_w^2}\right) + 3.23\right]$
Definition of $p_{MBH,D}$	$\dfrac{kh(p^* - \bar{p})}{70.6 q_g B_g \bar{\mu}_g}$	$\dfrac{kh(p^{*2} - \bar{p}^2)}{711 q_g T \bar{z} \bar{\mu}_g}$

TABLE 4.1

SUMMARY OF WORKING EQUATIONS FOR PRESSURE-TRANSIENT TEST ANALYSIS IN GAS WELLS (Continued)

	Gas, Using Pseudopressure and Time
Flow Test	
Semilog graph variables	p_p vs. t
Permeability from m of semilog straight line	$k = \dfrac{1637 q_g T}{mh}$
Skin factor calculation	$s = 1.151\left[\dfrac{\bar{p}_p - p_{p,1hr}}{m} - \log\left(\dfrac{k}{\phi\bar{\mu}_g\bar{c}_t r_w^2}\right) + 3.23\right]$
Buildup Test	
Semilog graph variables	p_p vs. $(t_p + \Delta t)/\Delta t$
Permeability from m of semilog straight line	$k = \dfrac{1637 q_g T}{mh}$
Skin factor calculation	$s = 1.151\left[\dfrac{p_{p,1hr} - p_{p,wf}}{m} - \log\left(\dfrac{k}{\phi\bar{\mu}_g\bar{c}_t r_w^2}\right) + 3.23\right]$
Definition of $p_{MBH,D}$	$\dfrac{kh(p_p^* - \bar{p}_p)}{711 q_g T}$

TABLE 4.2

FLOW-AFTER-FLOW TEST DATA, EXAMPLE 1			
t (hours)	p_{wf} (psia)	$p_{a,wf}$ (psia)	q (Mscf/D)
0	6,180	4,709.4	0
6	566	66.4	2,711
8	832	142.2	2,607
9.5	1,130	258.9	2,504
12.5	1,646	535.2	2,309

PRESSURE AND TIME FUNCTIONS, EXAMPLE 1	
Pressure Function (psi/Mscf-D)	Time/Rate Function
—	—
1.713	0.7782
1.752	0.9271
1.777	1.0287
1.808	1.1819

TABLE 4.3

TABLE 4.4

TIME AND FLOW DATA FOR EXAMPLE 2	
t (hours)	q (Mscf/D)
2.4	432.0
4.8	405.9
7.2	392.9
9.6	385.4
12.0	380.3
14.4	376.3
16.8	372.9
19.2	370.0
21.6	367.5
24.0	365.2
28.8	361.4
33.6	358.3
38.4	355.7
43.2	353.5
48.0	351.7
60.0	348.1
72.0	345.1
84.0	342.8
96.0	340.8
108.0	339.6
120.0	337.4
132.0	335.9
144.0	334.5
168.0	332.1
192.0	330.4
216.0	328.1

TABLE 4.5

PLOTTING FUNCTIONS FOR EXAMPLE 4.2	
t (hours)	$(p_{a,i} - p_{a,wf})/q_g$ (psi/Mscf-D)
2.4	7.84
4.8	8.34
7.2	8.62
9.6	8.78
12.0	8.90
14.4	9.00
19.2	9.15
21.6	9.21
24.0	9.27
28.8	9.37
33.6	9.45
38.4	9.52
43.2	9.58
48.0	9.63
60.0	9.72
72.0	9.81
84.0	9.88
96.0	9.93
120.0	10.03
132.0	10.08
144.0	10.12
168.0	10.19
192.0	10.25
216.0	10.32

TABLE 4.6

CONSTANTS c_1 AND c_2 FOR NON-DARCY FLOW CORRELATIONS		
s	c_1	c_2
0	1.0013	0.3205
5	3.96273	5.2411
10	7.4733	10.1993

TABLE 4.7

CONSTANTS c_3, c_4, AND c_5 FOR NON-DARCY FLOW CORRELATIONS			
s	c_3	c_4	c_5
0	0.002	−0.002	0.002
5	4.168	−0.202	0.049
10	7.624	−0.366	0.134

TABLE 4.8

PRESSURE DRAWDOWN DATA, EXAMPLE .3		
Time (hours)	Pressure (psia)	Adjusted Pressure (psia)
0.00	4,290	—
0.75	3,602	2,370.4
1.00	3,596	2,364.5
1.25	3,591	2,359.5
1.50	3,587	2,355.5
1.75	3,583	2,351.6
2.00	3,580	2,348.6
2.25	3,577	2,345.6
2.50	3,575	2,343.6
3.00	3,570	2,338.7

TABLE 4.9

GAS-WELL PRESSURE-BUILDUP TEST DATA, EXAMPLE 4

Δt (hours)	p_{ws} (psia)	p_{ws}^2 (psia$^2 \times 10^{-6}$)	Adjusted Pressure (psia)	Horner Time Ratio	Adjusted Horner Time Ratio
0	6,287.1	39.528	4,804.1	—	—
0.0100	6,296.6	39.647	4,813.9	200,000	286,370
0.0149	6,301.1	39.704	4,818.5	134,230	192,120
0.0221	6,307.8	39.788	4,825.4	90,499	129,460
0.0329	6,317.7	39.913	4,835.5	60,791	86,887
0.0489	6,332.1	40.095	4,850.3	40,901	58,386
0.0728	6,353.1	40.362	4,871.9	27,474	39,148
0.108	6,383.5	40.749	4,903.0	18,520	26,230
0.161	6,427.1	41.308	4,947.8	12,423	17,589
0.240	6,488.6	42.102	5,010.8	8,334.3	11,737
0.356	6,573.6	43.212	5,098.0	5,619.0	7,853.9
0.530	6,687.9	44.728	5,215.1	3,774.6	5,221.7
0.788	6,834.7	46.713	5,365.5	2,539.1	3,464.2
1.17	7,011.8	49.165	5,546.9	1,710.4	2,292.4
1.74	7,208.3	51.960	5,748.0	1,150.4	1,509.1
2.59	7,405.9	54.847	5,950.1	773.20	990.16
3.86	7,586.0	57.547	6,134.1	519.13	648.42
5.74	7,738.7	59.887	6,289.8	349.43	426.11
8.53	7,864.9	61.857	6,418.3	235.47	280.88
12.7	7,971.4	63.543	6,526.6	158.48	185.36
18.9	8,065.6	65.054	6.622.3	106.82	122.80
28.1	8,153.2	66.475	6,710.3	72.174	81.709
41.8	8,234.4	67.805	6,793.5	48.847	54.543
62.1	8,313.4	69.113	6,873.5	33.206	36.615
92.4	8,389.8	70.389	6,950.7	22.645	24.677
137	8,463.7	71.634	7,025.4	15.599	16.811
204	8,534.9	72.845	7,097.2	10.804	11.519
304	8,602.9	74.010	7,165.7	7.5789	7.9970
452	8,666.6	75.110	7,229.8	5.4248	5.6678
672	8,725.3	76.131	7,288.8	3.9762	4.1160
1,000	8,777.6	77.046	7,341.3	3.0000	3.0794

APPENDIX B

FUNDAMENTALS OF DIRECT SYNTHESIS FOR SLIGHTLY COMPRESSIBLE FLUIDS

ANALYSIS OF PRESSURE AND PRESSURE DERIVATIVE WITHOUT TYPE-CURVE MATCHING - HOMOGENEOUS-RESERVOIR MODEL, SLIGHTLY COMPRESSIBLE FLUIDS

1. INTRODUCTION AND BASIC EQUATIONS

Interpretation of pressure tests for a single well with wellbore storage and skin in a homogeneous reservoir considerably improved when the type-curve matching technique was published in the seventies (Ramey, 1970; Agarwal et al., 1970; Ramey and Agarwal, 1972; Earlougher and Kersch, 1974). Later that decade Tiab introduced the pressure derivative analysis (Tiab, 1975, 1976; Tiab and Crichlow, 1979; Tiab and Kumar, 1980a, b; Puthihgai and Tiab, 1982). He showed that a log-log plot of pressure derivative versus time is an important tool in identifying flow regimes and boundary effects. In the eighties type-curves which combine both the pressure and pressure derivative functions for various reservoir systems became an integral part of modern well test analysis (Bourdet et al., 1983; Clark and Van Golf-Racht, 1984; Wong et al., 1986; Ozkan et al., 1987; Mishra and Ramey, 1988; Onur and Reynolds, 1988; Vongvuthipornchai and Raghavan, 1988; Horne, 1990). Unless all flow regimes are definitely observed in the pressure derivative curve, type-curve matching is still a risky technique. Also, combinations of various boundary conditions may yield approximately similar pressure behavior. For a well producing from a bounded system, it is possible for inner and outer boundary effects to interact and considerably affect the well pressure behavior such that the infinite acting radial flow line is either too short or non-existent. Horne (1990) showed that log-log type curve matching is not as accurate as conventional semilog methods, because log-log axes tend to mask inaccuracies at late time, where 1 mm deviation of a pressure point may mean an actual error of 200 psia. Finally, the noise in the pressure derivative curve can be sever enough to make it impossible to draw the characteristic straight lines corresponding to flow regimes.

In this discussion, it is shown how a log-log plot of pressure and pressure derivatives versus time can be analyzed without using the type-curve matching technique. This new approach

is particularly useful when the early-time unit slope line and/or the late-time infinite acting radial flow line are not well developed due to the lack of points or any of the reasons discussed above. This new technique is also applicable to hydraulically fractured wells (Tiab, 1989, 1993). The classical assumptions normally used in conjunction with a single well producing at a constant rate from a homogeneous, isotropic and uniform porous media are applicable in this study. The fluid has a constant viscosity and is considered to be slightly compressible. The dimensionless wellbore pressure for a well with storage and skin, p_{wD}, and its derivative, dp_{wD}/dt, are obtained from

$$p_D = \frac{4}{\pi^2}\int_0^\infty \left(\frac{1-e^{-u2t_D}}{u^3 U_J}\right) du \tag{1.1}$$

and

$$\frac{dp_{wD}}{dt_D} = \frac{4}{\pi^2}\int_0^\infty \left(\frac{e^{-u2t_D}}{uU_J}\right) du \tag{1.2}$$

where

$$U_J = \left[uC_D J_0(u) - (1 - C_D s u^2) J_1(u)\right]^2 + \left[uC_D Y_0(u) - \left(1 - C_D s u^2\right) Y_1(u)\right]^2 \tag{1.3}$$

the dimensionless pressure, p_{wD}, dimensionless time, t_D and dimensionless wellbore storage coefficient are expressed as follows:

$$P_D = \left(\frac{kh}{141.2quB}\right)\Delta p \tag{1.4}$$

$$t_D = \left(\frac{0.0002637k}{\phi\mu c_t r_w^2}\right) t \tag{1.5}$$

$$C_D = \left(\frac{0.8935}{\phi c_t h r_w^2}\right) C \tag{1.6}$$

The factors C and S are respectively the wellbore storage coefficient and skin.

2. CHARACTERISTIC POINTS AND STRAIGHT LINES

The log-log plot of dimensionless pressure and pressure derivatives versus time, Fig. B1,

has several unique features:

(1) The pressure curve has a unit slope line during early time. This line corresponds to pure wellbore storage flow. The equation of this straight line is

$$p_D = \frac{t_D}{C_D} \tag{2.1}$$

Combining Eqs. 1.5 and 1.6 gives

$$\frac{t_D}{C_D} = \left(2.95\times10^{-4}\frac{h}{\mu}\right)\frac{t}{C} \tag{2.2}$$

Substituting Eqs. 1.4 and 2.2 into Eq. 2.1 and solving for the wellbore storage coefficient C we obtain:

$$C = \left(\frac{qB}{24}\right)\frac{t}{\Delta p} \tag{2.3}$$

For drawdown tests, $\Delta p = p_i - p_{wf}$ for buildup tests $\Delta p = p_{ws} - p_{wf}(\Delta t = 0)$.

2) The pressure derivative curve also has an early time straight line of unit slope. The equation of this line is obtained by taking the derivative of Eq. 2.1 with respect to the natural log of t_D/C_D Thus:

$$\left(\frac{t_D}{C_D}\right)p'_D = \frac{t_D}{C_D} \tag{2.4}$$

where the dimensionless pressure derivative is

$$p'_D = \left(\frac{26.856 r_w^2 \phi c_t h}{qB}\right)\Delta p' \tag{2.5}$$

The left-hand side of Eq. 2.4 can be expressed in real units by combining Eqs. 2.2 and 2.5

$$\left(\frac{t_D}{C_D}\right)p'_D = \left(\frac{kh}{141.2 q\mu B}\right)t\cdot\Delta p' \tag{2.6}$$

It is obvious from Fig. B.1 that the early-time unit slope line is the same for both pressure and pressure derivative curves. Combining Eqs. 2.4, 2.5 and 2.6 and solving for C we obtain an equation similar to Eq. 2.3 where Δp is replaced with $t\cdot\Delta p'$.

3) The infinite acting radial flow portion of the pressure derivative is a horizontal straight line. For a homogeneous reservoir, the equation of this line is:

$$\left[\left(\frac{t_D}{C_D}\right)p'_D\right]_r = 0.5 \tag{2.7}$$

Combining Eqs. 2.6 and 2.7 and solving for the permeability yields:

$$k = \frac{70.6q\mu B}{h(t\cdot\Delta p')_r} \tag{2.8}$$

where the subscript r stands for radial flow line. In terms of pressure, the equation of this line is:

$$p_{Dr} = 0.5\left[\ln\left(\frac{t_D}{C_D}\right)_r + 0.80907 + \ln\left(C_De^{2s}\right)\right] \tag{2.9}$$

4) The starting time of the infinite acting line of the pressure derivative curve is approximately given by:

$$\left(\frac{t_D}{C_D}\right)_{SR} = 10\log\left(C_De^{2s}\right)^{10} \tag{2.10}$$

This equation is obtained by plotting the values of t_D/C_D corresponding to the first point where Eq. 2.9 is valid, i.e. at the start of the horizontal line for different values of $C_De^{2s} > 10^2$. Values of t_D/C_{SR} were obtained from the second derivative of Eq. 1.1. Substituting for C_D and t_D and solving for t_{SR} gives:

$$t_{SR} = \frac{\mu C}{6.9\times10^{-5}kh}\left[\ln\left(\frac{0.8935C}{\phi c_t h r_w^2}\right) + 2s\right] \tag{2.11}$$

where t_{SR} is the starting time of the infinite acting radial flow line.

Vongvuthipornchai and Raghavan (1988) showed that the starting time of the semilog straight line is best determined from

$$\left(\frac{t_D}{C_D}\right)_{SR} = \frac{1}{\alpha}\left[\ln\left(C_De^{2s}\right) + \ln\left(\frac{t_D}{C_D}\right)_{SR}\right] \tag{2.12}$$

where α is the tolerance (fraction) used to determine the value of t_{DSR} at which Eq. 2.7 is valid. For α=0.05 they found that Eq. 2.12 (approximate solution) can predict the value of t_{DSR} within 8

percent of the value predicted by Eq. 1.2 (exact solution).

The semilog straight line will always appear to start earlier than the horizontal portion of the pressure derivative curve. The difference can be as much as fifty percent.

The wellbore storage coefficient may be estimated from Eq. 2.12 by letting α=0.05 and solving for C:

$$C = 0.056\phi c_t h r_w^2 \left(\frac{t_{DSR}}{2s + \ln t_{DSR}} \right) \tag{2.13}$$

where t_{DSR} is calculated from Eq. 1.5 at $t=t_{SR}$.

5) The early-time unit slope line and the late-time infinite acting line of the pressure derivative, i.e. the horizontal line, intersect at:

$$\left(\frac{t_D}{C_D} p'_D \right)_i = 0.5 \tag{2.14}$$

$$\left(\frac{t_D}{C_D} \right)_i = 0.5 \tag{2.15}$$

where the subscript i stands for "intersection". In real units the coordinates of this intersection point are obtained from

and

$$(t \cdot \Delta p')_i = \frac{70.6 q \mu B}{kh} \tag{2.16}$$

and

$$t_i = \frac{1695 \mu C}{kh} \tag{2.17}$$

These equations can be derived, respectively, from Eqs. 2.8, 2.2 and 2.15. Thus, the intersection point can be used to determine k from Eq. 2.16 and C from Eq. 2.17. Since the unit slope line is the same for pressure and pressure derivative curves, at the intersection point we have:

$$(\Delta p)_i = (t \cdot \Delta p')_i = (t \cdot \Delta p')_r \tag{2.18}$$

6) Between the early-time and late-time straight lines, the derivative curves have specific shapes for different values of C_De^{2s}. In this study, the coordinates of the "peaks" for $C_de^{2s} > 10^2$ were obtained from the second derivative and plotted on a cartesian graph. The equation of this line is

$$\left(\frac{t_D}{C_D}p'_D\right)_x = 0.36\left(\frac{t_D}{C_D}\right)_x - 0.42 \tag{2.19}$$

Combining Eqs. 2.2, 2.6 and 2.19 yields:

$$(t\cdot\Delta p')_x = \left(0.015\frac{qB}{C}\right)t_x - 0.42b_x \tag{2.20}$$

where b_x is given by:

$$b_x = 141.2q\mu B / kh \tag{2.21}$$

and $(t\cdot\Delta p')_x$ and t_x are the coordinates of the maximum point (peak) of the pressure derivative curve. It is obvious from Eq. 2.20 that we can calculate the wellbore storage coefficient or the permeability from the coordinates of the peak.

Solving Eq. 2.20 for k yields:

$$k = \left(\frac{59.3q\mu B}{h}\right)\frac{1}{(0.015qB/C)t_x - (t\cdot\Delta p')_x} \tag{2.22a}$$

This equation should be used to calculate k only if the late-time infinite acting radial flow line is not observed, such as in a short test, or there is too much noise in the late-time derivative values.

Solving Eq. 2.20 for C yields:

$$C = \frac{0.015qBt_x}{(t\cdot\Delta p')_x + 0.84(t\cdot\Delta p')_r} \tag{2.22b}$$

This equation should be used in cases where k is known from other sources and the early time unit slope line is not observed.

7) A log-log plot of log (C_De^{2s}) versus the coordinates of the peaks yielded the following equations:

$$\log\left(C_D e^{2s}\right)=0.35\left(\frac{t_D}{C_D}\right)_x^{1.24} \tag{2.23}$$

and

$$\log\left(C_D e^{2s}\right)=1.71\left(\frac{t_D}{C_D}p'_D\right)_x^{1.10} \tag{2.24}$$

Substituting Eqs. 2.2 and 2.6 into Eqs. 2.23 and 2.24 yields two new expressions. Combining these new expressions with Eqs. 2.16 and 2.17 gives:

$$\log C_D e^{2s} = 0.1485\left(\frac{t_x}{t_i}\right)^{1.24} \tag{2.25}$$

and

$$\log C_D e^{2s} = 0.80\left[\frac{(t\cdot\Delta p')_x}{(t\cdot\Delta p')_i}\right]^{1.10} \tag{2.26}$$

Thus the coordinates of the maximum point (peak) of the pressure derivative can be used also to calculate skin. Solving for skin Eqs. 2.25 and 2.26 give respectively:

$$s=0.171\left(\frac{t_x}{t_i}\right)^{1.24}-0.5\ln\left(\frac{0.8935C}{\phi hc_t r_w^2}\right) \tag{2.27}$$

and

$$s=0.921\left[\frac{(t\cdot\Delta p)_x}{(t\cdot\Delta p)_i}\right]^{1.1}-0.5\ln\left(\frac{0.8935C}{\phi hc_t r_w^2}\right) \tag{2.28}$$

Because in some pressure tests the wellbore storage hump may appear to be flat at the "peak", it is possible to read the right value of $(t\cdot\Delta p')_x$ but the wrong value of t_x. In this case, it is a good practice to calculate s from both equations. If they give different values then obtain a new value of t_x and repeat the calculations until the two equations give the same value of skin.

8) An expression relating the infinite-acting radial flow line portion of the pressure derivative curve and the peaks for different values of $C_D e^{2S}$ can be derived by dividing Eq. 2.19 with Eq. 2.7:

$$\frac{\left(\frac{t_D}{C_D}p'_D\right)_x}{\left(\frac{t_D}{C_D}p'_D\right)_r}=2\left[0.36\left(\frac{t_D}{C_D}\right)_x-0.42\right] \tag{2.29}$$

Using Eqs. 2.2 and 2.6 with Eq. 2.29 we have:

$$\frac{(t\cdot\Delta p')_x}{(t\cdot\Delta p')_r}=2\left[1.062\times10^{-4}\left(\frac{kh}{\mu}\right)\frac{t_x}{C}-0.42\right] \tag{2.30}$$

Eq. 2.30 can be used to calculate C or k. Substituting for kh/μ from Eq. 2.8 and solving for C gives:

$$C=\frac{0.015qBt_x}{(t\cdot\Delta p')_x+0.84(t\cdot\Delta p')_r} \tag{2.31}$$

Thus, the wellbore storage coefficient can be determined even if the unit slope line is not observed for mechanical reasons or due to lack of early time pressure data. Solving for k Eq. 2.30 yields:

$$k=9416.2\frac{\mu C}{ht_x}\left[0.5\frac{(t\cdot\Delta p')_x}{(t\cdot\Delta p')_r}+0.42\right] \tag{2.32}$$

9) An expression relating the infinite-acting radial flow line portions of the pressure and pressure derivative curves can be derived by dividing Eq. 2.9 with Eq. 2.7:

$$\frac{p_{Dr}}{(t_D/C_D)p'_D)_r}=\ln t_{Dr}+2s+0.80907 \tag{2.33}$$

Using Eqs. 1.4, 2.2 and 2.6 with Eq. 2.33 and solving for skin we have:

$$s=0.5\left[\frac{\Delta p_r}{(t\cdot\Delta p')_r}-\ln\left(\frac{kt_r}{\phi\mu c_t r_w^2}\right)+7.43\right] \tag{2.34}$$

where t_r is any convenient time during the infinite acting radial flow line and Δpr is the value of Δp corresponding to t_r.

3. PROCEDURES

Normally, a well designed single-well pressure test in a homogeneous reservoir will show all the necessary flow regimes to determine permeability, skin and wellbore storage from conventional analysis techniques. However, in many cases conventional techniques cannot be used for various reasons: the test is too short to observe the infinite-acting radial flow line, or the wellbore storage unit-slope line is not observed because of lack of early-time pressure points, or there is too much noise in the pressure derivative curve, or both the unit-slope line and the infinite-acting line are missing. In such cases type-curve matching was the only alternative to conventional semilog techniques. However, even with the addition of the pressure derivative curve, finding a unique match by a simple comparison of shapes is still one of the main problems of the type-curve matching technique. The technique proposed here analyzes log-log plots of pressure and pressure derivatives versus time without type-curve matching. The five cases discussed below, with examples, illustrate the effectiveness and simplicity of this new technique.

3.1. Case 1 (basic case) - Unit-slope and infinite-acting lines are observed

The following step-by-step procedure is for the ideal case where both the early time unit-slope line and the late time infinite acting radial flow line have **definitely** been observed, and are **well defined**.

Step 1 - Plot Δp and $t \cdot \Delta p'$ versus time on a log-log graph.

Step 2 - Draw the unit-slope line corresponding to the wellbore storage flow regime using early-time pressure and pressure derivative points. If there is too much noise in the derivative values, it is recommended to draw the unit-slope line using only pressure points.

Step 3 - Draw the infinite acting radial flow line using late-time pressure derivative points. This line is, of course, horizontal.

Step 4 - Read the coordinates of the point where the unit-slope line and the infinite-acting horizontal line intersect: t_i and Δp_i. Note that $\Delta p_i = (t \cdot \Delta p')_i = (t \cdot \Delta p')_r$ in all steps.

Step 5 - Read the coordinates of the maximum point (peak) on the pressure derivative curve: t_x and $(t \cdot \Delta p')_x$

Step 6 - Select any convenient time t_r during infinite acting radial flow and read Δp_r from the pressure curve.

Step 7 - Calculate the permeability from Eq. 2.8.

Step 8 -Calculate the wellbore storage coefficient from Eq. 2.3 using t_i and Δp_i , or any convenient t and Δp values on the unit slope line.

Step 9 - Calculate the skin factor from Eq. 2.34.

Step 10 - This step is used to verify the correctness and accuracy of the permeability, skin and wellbore storage. This step is necessary only if there is considerable noise in the pressure derivative value. Recalculate permeability using Eq. 2.32. If the values of k obtained from Eqs. 2.8 and 2.32 are approximately equal, this means the peak, the unit-slope and horizontal lines are in their correct "location", and therefore, the values of k, s and C are correct. However, if the two values of k are significantly different, obtain a new peak and/or shift one or both straight lines and repeat Steps 4 through 9 until the values of t_i and Δp_i give similar values of k. The decision of which straight lines should be shifted or whether a new peak should be obtained is really a function of the quality of data. For instance, if the infinite-acting line (horizontal line) portion of the derivative curve is well defined, the value of k and s obtained in Steps 7 and 9 are correct. In this case the unit slope line should be shifted and/or a new peak selected and a new value of C calculated such that the value of k obtained from Eq. 2.32 is similar to the one obtained in Step 7.

Example 1

A pressure drawdown test in a new oil well is strongly influenced by skin and wellbore storage. The measured pressure data as a function of time are listed in Table 1 (Horne). Other known reservoir and well data are:

$q = 2500 STB/D$ $\quad\quad$ $\phi = 0.21$

$\mu = 0.92 cp$ $\quad\quad$ $c_t = 8.72 \cdot 10^{-6} psi^{-1}$

$B = 1.21 RB/STB$ $\quad\quad$ $h = 23 ft$

$r_w = 0.401 ft$ $\quad\quad$ $p_i = 6009 psi$

Calculate permeability, skin factor and wellbore storage coefficient.

Solution

The derivative values are calculated from the following algorithm, which uses a weighted central difference approximation to calculate $t \cdot \Delta p'$ at any point i

$$\left(\frac{dp}{dx}\right)_t = \left[\frac{P_i - P_{i-1}}{X_i - X_i - 1}(X_{i+1} - X_i) + \frac{P_{i+1} - P_i}{X_{i+1} - X_i}(X_i - X_{i-1})\right] \Big/ (X_{i+1} - X_{i-1}) \quad (3.1)$$

where X is the natural logarithm of the appropriate time function and Points i-1 and $i+1$ are the points preceding and following Point i respectively.

While Eq. 3.1 is simple to use, this algorithm has several shortcomings: (1) estimates for the derivative are not obtained throughout the entire interval (i.e., they are available only at those points with abscissa values that correspond to measured data, which may be widely spaced); (2) calculated derivative values may contain high levels of noise, even after smoothing; (3) truncation errors associated with Eq. 3.1 will increase as Δx increases, causing the approximation for the derivative to deteriorate so that the curve may begin to lose its characteristic shape; and (4) so-called end effects may arise when data corresponding to early and late times are differentiated.

To avoid the noise problems associated with the differentiation of measured data, Lane et. al. presented an algorithm for fitting a set of measured pressure data with a spline function that effectively filters out the measurement noise so that the true underlying pressure function can be approximated. The first and second derivatives of the resulting spline function can then be calculated analytically to produce smooth, continuous functions that are free of the noise typically associated with discrete pressure derivatives.

A spline is a collection of piecewise polynomial segments with every two consecutive pieces joining smoothly at the knots (segment join points). The spline function and some of its derivatives are required to be continuous across the knots.

Step 1 - Figs. B.2a and B.2b are log-log plots of Δp and $t \cdot \Delta p'$ versus time. The late-time pressure derivative portion in Fig. B.2a was calculated by the spline technique while the derivative curve in Fig. B.2b was calculated by the more commonly used numerical differentiation method (Bourdet et al., 1989). Fig. B.2a is used to illustrate steps 1 through 9 of this case while Fig. B.2b is used to illustrate the importance of step 10.

Step 2 - Draw the unit-slope line corresponding to the wellbore storage flow region using only pressure data, because there is some noise in the early-time derivative values.

Step 3 - The infinite acting radial flow line is well defined in the pressure derivative curve, as shown in Fig. B.2a. This horizontal line corresponds to $(t \cdot \Delta p') = 110\ psi$

Step 4 - The coordinates of the point of intersection of the unit slope line and the horizontal line are:

$$t_i = 1.35 \cdot 10^{-2}\ h$$

$$(t \cdot \Delta p')_i = (t \cdot \Delta p')_r = 110\ psi$$

Step 5 - The coordinates of the maximum (peak) point on the derivative curve are:

$$t_x = 0.36\ h$$

$$(t \cdot \Delta p')_x = 965\ psi$$

Step 6 - During the infinite acting radial flow regime, we have

$$t_r = 40.4\ h$$

$$(\Delta p)_r = 2947\ psi$$

Step 7 - Calculate the permeability from Eq. 2.8:

$$k = \frac{(70.6)(2500)(0.92)(1.21)}{(23)(110)} = 77.6\ mD$$

Step 8 - Using Eq. 2.3, the wellbore storage coefficient is

$$C = \left(\frac{(2500)(1.21)}{24}\right)\frac{1.35 \cdot 10^{-2}}{110} = 0.0154\frac{bbl}{psi}$$

Step 9 - Calculate the skin factor using Eq. 2.34 and values of t_r and Δp_r (from Step 6):

$$s = 0.5\left[\frac{2947}{110} - \ln\left(\frac{(77.6)(10.6)}{(0.21)(0.92)(8.72 \cdot 10^{-6})(0.401)^2}\right) + 7.43\right] = 6.2$$

Step 10 - Since the noise in the derivative curve of Fig. B.2a is negligible , Step 10 may not be necessary. However, it is a good practice to recalculate k anyway. Using Eq. 2.30, $k = 77.4\ md$. Since Eqs. 2.8 and 2.30 give practically the same value of permeability, we can conclude that the values of k, s and C are correct.

Similar results were obtained from Fig. B.2b. However, because of the noise in the late-time pressure derivative curve, it took several iterations to find the correct "location" of the horizontal

line. In this example, it was not necessary to shift the unit-slope line or the maximum point, as they are well defined. The computer program, however, can shift any of the three characteristic features, i.e. the unit-slope line, the maximum point and the infinite acting line, then recalculate k, C and s until the requirement in Step 10 is satisfied. That is, until Eqs. 2.8 and 2.30 give similar values of permeability. The values of k, C and s obtained here are similar to the values obtained by type-curve matching and semilog analysis (Horne, 1990).

3.2. Case 2 - The unit-slope line is not observed

Pure wellbore storage flow regime, which causes the early-time pressure and pressure derivative points to yield a unit slope line is not a very common occurrence. Also, in many pressure tests there are not enough early-time points to draw the unit slope line. It is important to emphasize that wellbore storage is not an essential parameter to determine as long the infinite acting line is well defined. In this case, the following step-by-step procedure is recommended.

Step 1 - Plot Δp and $t \cdot \Delta p'$ versus time on a log-log graph.

Step 2 - Draw the infinite acting radial flow line (horizontal line) using the late-time pressure derivative points, and read its corresponding value on the pressure derivative axis $(t \cdot \Delta p')_r$. This value is of course equal to $(t \cdot \Delta p')_i$ and Δp_i had the unit-slope line been observed.

Step 3 - Determine from the graph the coordinates of the maximum point (peak) on the $t \cdot \Delta p'$ versus time curve, i.e. t_x and $(t \cdot \Delta p')_x$.

Step 4 - Select t_r as discussed in Step 6 of Case 1, and read the corresponding value of Δp_r.

Step 5 - Calculate the permeability from Eq. 2.8.

Step 6 - Calculate the wellbore storage coefficient from Eq. 2.31.

Step 7 - Calculate skin from Eq. 2.34.

Step 8 - Recalculate s from Eqs. 2.27 or 2.28. If the two values of s obtained in Steps 5 and 8 are approximately equal, then k, s and C are correct. The two values of s are significantly different, which is very possible if there is considerable noise in the derivative curve, then either select a new peak or shift up or down the infinite acting (horizontal) line, and repeat Steps 5, 6 and 7 until the two values of s are approximately equal. Obviously, if needed, the early-time unit slope line can now be drawn.

Example 2

Using the reservoir and well characteristics in Example 1, and the pressure and pressure derivative data in Fig. B.3, calculate k, s and C.

Solution

Step 1 - Plot Δp and $t \cdot \Delta p'$ versus time on a log-log graph. Fig. B.3 is actually drawn using the pressure data in Example 1, but without the early-time pressure and pressure derivative points.

Step 2 - The infinite acting radial flow line on the pressure derivative curve yields

$$(t \cdot \Delta p')_r = 110 psi$$

Step 3 - The coordinates of the maximum point of the wellbore storage hump are:

$$t_x = 0.36h$$

$$(t \cdot \Delta p')_x = 965 psi$$

Step 4 - From the infinite acting radial flow line of the pressure curve, we have

$$t_r = 10.4h$$

$$\Delta p_r = 2947 psi$$

Step 5 - Calculate the permeability from Eq. 2.8

$$k = 77.6\ mD$$

Step 6 - The wellbore storage coefficient is obtained by substituting the coordinates of the maximum point into Eq. 2.31:

$$C = \frac{0.015qBt_x}{(t \cdot \Delta p')_x + 0.84(t \cdot \Delta p')_r} = \frac{(0.015)(2500)(1.21)(0.36)}{(965 + 0.84 \cdot 110} = 0.0154\, bbl / psi$$

Step 7 - Calculate skin from Eq. 2.34

$$s = 0.5\left[\frac{\Delta p_r}{(t \cdot \Delta p')_r} - \ln\left(\frac{kt_r}{\phi \mu c_t r_w^2}\right) + 7.43\right] = 0.5\left[\frac{2947}{110} - \ln\left(\frac{(77.6)(10.4)}{(0.21)(0.92)(8.72 \cdot 10^{-6})(0.401)^2}\right) + 7.43\right] = 6.2$$

Step 8 - Verification: Recalculate k from Eq. 2.32 and compare with the value of k obtained in

Step 5:

$$k = 9416.2\frac{\mu C}{ht_x}\left[0.5\frac{(t\cdot\Delta p')_x}{(t\cdot\Delta p')_r}+0.42\right] = \frac{(9416.2)(0.92)(0.0154)}{(23)(0.36)}\left[\frac{(0.5)(965)}{110}+0.42\right] = 77.4mD$$

Since the two values of k (77.6 and 77.4MD) are essentially equal, we can conclude that the values of s, k and C are correct.

3.3. Case 3 - The infinite acting line is not observed (short test)

If the pressure test is too short to observe the infinite acting radial flow line, or there is too much scatter in the late-time derivative points, or the boundary effects are felt before the infinite acting flow regime is fully developed, then the following step-by-step procedure is recommended.

Step 1 - Plot Δp and $t\cdot\Delta p'$ versus time on a log-log graph.

Step 2 - Draw the early-time unit slope line as discussed in Step 2 of Case 1.

Step 3 - Read the coordinates of the maximum point (peak) i.e. t_x and $(t\cdot\Delta p')_x$.

Step 4 - Calculate the wellbore storage coefficient from Eq. 2.3, where t and Δp are the coordinates of any convenient point on the unit-slope line.

Step 5 - Calculate the permeability from Eq. 2.22.

Step 6 - Calculate the coordinates of the point of intersection of the unit-slope line and infinite-acting line (had the test been run long enough to observe it) from Eqs. 2.16 and 2.17, i.e. $(t\cdot\Delta p')_i$ and t_i.

Step 7 - Determine the skin factor from Eq. 2.27 or 2.28.

Step 8 - Recalculate k from Eq. 2.32. If the two values of k obtained in Steps 5 and 8 are approximately equal, then k, s and C are correct. If not, obtain a new peak and/or shift the unit slope line (left or right) and repeat the process until the two values of k obtained from Eqs. 2.21 and 2.32 are approximately identical. If needed, the infinite acting radial line can now be drawn.

Example 3

Using the reservoir, well characteristics and the pressure buildup data in Table 2 Example 1 of Bourdet et al. 1983, calculate k, s and C.

$q = 174\ STB/D$ $\phi = 0.25$

$\mu = 2.5\,cp$ $c_t = 4.2 \cdot 10^{-6}\ psi^{-1}$

$B = 1.06\ RB/STB$ $h = 107\ ft$

$r_w = 0.29\ ft$

Solution

Step 1 - Fig. B.4 is log-log plot of Δp and $t \cdot \Delta p'$ versus test time, without the late-time points (to illustrate the procedure of Case 3).

Step 2 - The unit slope line (on the pressure curve) is well defined.

Step 3 - The coordinates of the maximum point corresponding to the wellbore storage hump are:

$t_x = 1.06\ h$

$(t \cdot \Delta p')_x = 291 psi$

Step 4 - Calculate the wellbore storage coefficient from Eq. 2.3 using $t=0.1h$and $\Delta p=83psi$ (obtained from unit-slope line):

$$C = \left(\frac{qB}{24}\right)\frac{t}{\Delta p} = \left(\frac{(174)(1.06)}{24}\right)\frac{0.1}{83} = 9.3 \cdot 10^{-3}\ bbl/psi$$

Step 5 - The permeability of the formation is obtained from Eq. 2.22a

$$k = \left(\frac{59.3q\mu B}{h}\right)\frac{1}{(0.015qB/C)t_x - (t \cdot \Delta p')_x}$$

$$k = \left(\frac{(59.3)(174)(2.5)(1.06)}{107}\right)\frac{1}{\left((0.015)(174)(1.06)/(9.3 \cdot 10^{-3})\right)1.06 - 2.91} = 105\ mD$$

Step 6 - Calculate the coordinates of the point of intersection of the unit-slope line and the infinite acting horizontal line (had the first been run long enough to observe it) from Eqs. 2.16 and 2.17:

$$(t \cdot \Delta p')_i = \frac{70.6q\mu B}{kh} = \frac{(70.6)(174)(1.06)}{(10.5)(107)}$$

and

$$t_i = \frac{1695\mu C}{kh} = \frac{(1695)(2.5)(9.3 \cdot 10^{-3})}{(10.5)(107)} = 0.035h$$

Step 7 - The skin factor is calculated from Eq. 2.27 or Eq. 2.28

$$s = 0.171\left(\frac{t_s}{t_i}\right)^{1.24} - 0.5\ln\left(\frac{0.8935C}{\phi h c_t r_w^2}\right) = 0.171\left(\frac{1.06}{0.035}\right)^{1.24} - 0.5\ln\left(\frac{(0.8935)(9.3)(16^{-3})}{(0.25)(107)(4.2)(10^{-6})(0.29)^2}\right) = 8.3$$

Equation 2.8 also yields $s = .83$

Step 8 - Verification: Recalculate k from Eq. 2.32, when

$(t\cdot\Delta p')_r = (t\cdot\Delta p')_i = 28.97\,psi$

$$k = 9416.2\frac{\mu C}{ht_x}\left[0.5\frac{(t\cdot\Delta p')_x}{(t\cdot\Delta p')_r} + 0.42\right] = \frac{(9416.2)(2.5)(9.3\cdot10^{-3})}{(107)(1.06)}\left[\frac{(0.50)(291)}{28.97} + 0.42\right] = 105\ mD$$

Since the two values of k (from Step 5 and Step 8) are equal, we can conclude that the values of k, s and C are correct.

The values of k, s and C obtained here are approximately equal to the values obtained by Bourdet et al. using the type-curve matching technique *(k=10.67 mD, s=7.7, C=9.3x10^{-3} bbl/psi).*

3.4. Case 4 - The unit-slope line and the peak are not observed

In some pressure tests, the first pressure reading occurred well after the end of wellbore storage flow regime, such that the peak or maximum point of the pressure derivative is not observed. In this case, if the pressure test is run long enough to observe the infinite acting radial flow (horizontal) line the following procedure is recommended.

Step 1 - Plot Δp and $t\cdot\Delta p'$ versus time on a log-log graph

Step 2 - Draw the infinite acting radial flow (horizontal) line. The straight line of course has a constant value on the pressure derivative axis $(t\cdot\Delta p')_r$.

Step 3 - Determine from the graph the starting time, t_{SR}, of the infinite acting line of the pressure derivative curve.

Step 4 - Determine Δp_r as discussed in Step 6 of Case 1.

Step 5 - Calculate the permeability from Eq. 2.8.

Step 6 - Calculate the skin factor from Eq. 2.34.

Step 7 - Calculate the dimensionless time at the start of the infinite acting line, t_{DSR}, from Eq. 1.5 where $t=t_{SR}$; then estimate the wellbore storage coefficient from Eq. 2.13.

The starting time t_{SR} is almost impossible to determine, if there is too much noise in the infinite acting portion of the pressure derivative curve. In this case the following procedure is recommended:

(1) Calculate k from the conventional semilog analysis,

(2) Compute $(t \cdot \Delta p')_r$ from Eq. 2.8,

(3) Calculate s from Eq. 2.34, where t_r and Δp_r are determined as discussed above, and

(4) Calculate C from Eq. 2.13 where t_{SR} is obtained from the semilog plot.

Example 4

A pressure buildup test in the Ness formation sand of the Osberg Field, North Sea, is influenced by skin and wellbore storage. The measured shut-in pressure and $t \cdot \Delta p'$ data as a function of time are listed in Table 3 (Clark and Van Golf-Racht, 1984). Other reservoir, fluid and well characteristics are listed below:

$q = 3000\,STB/D$ $\qquad$ $\phi = 0.23$

$\mu = 0.445\,cp$ $\qquad$ $c_t = 16.8 \cdot 10^{-6}\,psi^{-1}$

$B = 1.49\,RB/STB$ $\qquad$ $h = 33\,ft$

Solution

Step 1 - Fig. B.5 is a log-log plot of Δp and $t \cdot \Delta p'$ versus time.

Step 2 - The infinite acting radial flow (horizontal) line yields $(t \cdot \Delta p')_r = 1.332\,psi$

Step 3 - The starting time of the horizontal line (pressure derivative curve) is approximately:

$t_{SSR} = 0.06\,h$

Step 4 - From the infinite acting line portion of the pressure curve; we have

$t_r = 15.2\,h$

$\Delta p_r = 48.47\ psi$

Step 5 - Calculate the permeability from Eq. 2.8

$$k = \frac{70.6q\mu B}{h(t\cdot\Delta p')_r} \quad \frac{(70.6)(3000)(0.445)(1.49)}{(33)(48.47)} = 3195mD$$

Step 6 - Calculate the skin factor from Eq. 2.34:

$$s=0.5\left[\frac{\Delta p_r}{(t\cdot\Delta p')_r}-\ln\left(\frac{kt_r}{\phi\mu c_t r_w^2}\right)+7.43\right]=0.5\left[\frac{48.47}{1.332}-\ln\left(\frac{(31.95)(15.2)}{(0.23)(0.445)(16.8\cdot10^{-6})(0.51)^2}\right)+7.43\right]=9.2$$

Step 7 - The wellbore storage coefficient can only be estimated from Eq. 2.13

$$C = 0.056\phi c_t h r_w^2\left(\frac{t_{DSR}}{2s+\ln t_{DSR}}\right)$$

$$C = (0.056)(0.23)(16.8\cdot10^{-6})(33)(0.51)^2\left(\frac{1.13\cdot10^5}{(2)(9.2)+\ln(1.13\cdot10^5)}\right) = 6.97\cdot10^{-3}\ bbl/psi$$

t_{SSR} is calculated from Eq. 1.5, where $t=t_{SSR}$.

The values of k, s and C obtained here are similar to those obtained by Clark and Van Golf-Racht using the type-curve matching technique ($k=3115\ mD$, $s=9.3$, $C=6.8x10^{-3}\ bbl/psi$)

3.5. *Case 5 - The unit-slope and infinite-acting lines have not been observed*

In some short tests, both the unit slope line and the infinite acting radial flow line are missing. In other tests the first pressure reading was taken after the unit-slope line. For wells with wellbore storage and skin producing from a small bounded reservoir it is possible for boundary effects to be felt before the infinite acting line develops. In these situations, the pressure test can be analyzed as in Case 2 or Case 3, depending on the quality of early and/or late time pressure derivative values. If the wellbore storage coefficient can be calculated from well completion data, then the following procedure is recommended:

Step 1 - Plot Δp and $t\cdot\Delta p'$ versus time on a log-log graph.

Step 2 - Estimate the wellbore storage coefficient from well completion data. For a wellbore with changing liquid level $C=144V_u/p$, where V_u is the wellbore volume per unit length. When the wellbore is completely filed with a single phase fluid $C=c_wV_w$, where V_w is the total wellbore volume and c_w is the compressibility of the fluid in the wellbore.

Step 3 - Obtain the coordinates of the maximum point (peak) from the derivative curve: t_x and $(t \cdot \Delta p')_x$.

Step 4 - Calculate permeability from Eq. 2.22a.

Step 5 - Calculate $(t \cdot \Delta p')_i$ and t_i from Eqs. 2.16 and 2.17, respectively. If needed, draw the infinite acting line portion of the derivative curve, and the unit slope line.

Step 6 - Calculate the skin factor from Eq. 2.27 and 2.28. If they give different values of s, obtain a new peak and recalculate s until the two equations agree (within 5 percent).

If permeability is known from other sources, then calculate C from Eq. 2.22b and skin as discussed in Steps 5 and 6 (Case 5).

Example 5

Fig. B.6 shows pressure (Table 4) and pressure derivative data of a highly damaged well. Calculate the wellbore storage coefficient, permeability and skin. Known reservoir, fluid and well properties are:

$q = 250\,STB/D$ $\qquad$ $\phi = 0.13$

$\mu = 1.2\,cp$ $\qquad$ $c_t = 2.4 \times 10^{-6}\,psi^{-1}$

$B = 1.229\,RB/STB$ $\qquad$ $h = 16\,ft$

$r_w = 3.2\,in.$ $\qquad$ $\rho = 42.5\,lbm/cuft$

$V_u = 0.0134\,bbl/ft$

Solution

Step 1 - Fig. B.6 is a log-log plot of Δp and $t \cdot \Delta p'$ data. This is obviously a short pressure test. Both the unit-slope and the infinite acting lines have not been observed.

Step 2 - The wellbore storage coeffecient can be estimated either by type-curve matching or from well completion data:

$$C = \left(\frac{144}{\rho}\right) V_u = \left(\frac{144}{42.5}\right) 0.0134 = 0.0454\,bbl/psi$$

Step 3 - The coordinates of the maximum points from Fig. b are:

$$t_x = 1.55h$$

$$(t \cdot \Delta p')_x = 146.88 psi$$

Step 4 - Calculate the permeability from Eq. 22a

$$k = \left(\frac{59.3q\mu B}{h}\right)\frac{1}{(0.015qB/C)t_x - (t \cdot \Delta p')_x}$$

$$k = \left(\frac{(59.3)(250)(1.2)(1.229)}{16}\right)\frac{1}{(0.015)(250)(1.229/0.0454)1.55 - 146.88} = 206mD$$

Step 5 - Calculate the coordinates of the point of intersection of the unit-slope and the infinite acting lines (had they been observed) from Eqs. 2.1 and 2.17

$$(t \cdot \Delta p')_i = \frac{70.6q\mu B}{kh} = \frac{(70.6)(250)(1.2)(1.229)}{206)(16} = 7.88 psi$$

$$t_i = \frac{1695\mu C}{kh} = \frac{(1695)(1.2)(0.0454)}{(206)(16)} = 0.028 \ hour$$

Step 6 - Estimate the skin factor from Eq. 2.27

$$s = 0.171\left(\frac{t_x}{t_i}\right)^{1.24} - 0.5\ln\left(\frac{0.8935C}{\phi h c_t r_w^2}\right) = 0.171\left(\frac{1.55}{0.028}\right)^{1.24} - 0.51n\left(\frac{(0.8935)(0.0454)}{(0.13)(16)(2.4 \cdot 10^{-6})(0.27)^2}\right) = 192$$

Equation 2.28 gives a similar value of s.

4. CONCLUSIONS

1. A log-log plot of pressure and pressure derivative versus time can be analyzed without using the type-curve matching technique.

2. This new technique is particularly useful when the early-time unit slope line and/or the late-time infinite acting radial flow line have not been observed or are not well defined due to a variety of reasons, such as lack of points, severe noise problem, and interference of outer boundaries.

3. Several unique features of the pressure derivative plot have been identified, including the point of intersection of the unit slope and the infinite acting lines, the maximum point (or peak) or the transition period, and the starting time of the infinite acting line.

4. Equations corresponding to these unique features have been derived and their usefulness has been demonstrated.

5. Unlike type-curve matching, the results of the new technique are verifiable. Any two parameters calculated from two independent equations corresponding to two different features of the pressure derivative curve are verified by a third equation which corresponds to a third feature relating the two parameters.

6. The technique is presented as a step-by-step procedure for five different cases. Each case is illustrated by a numerical example.

7. The spline technique should be used to smooth the pressure derivative curve, especially the portions corresponding to the peak of the wellbore storage hump and the infinite acting radial flow line.

8. The new technique is applicable to the interpretation of pressure drawdown and buildup tests.

5. NOMENCLATURE

b_x	See Eq. 2.21
c_t	Total system compressibility, psi^{-1}
C	Wellbore storage coefficient, RB/psi
C_D	Dimensionless storage constant
h	Formation thickness, feet
$J_0(u)$	Bessel function of the first kind, order zero
$J_1(u)$	Bessel function of the first kind, order one
k	Formation permeability
P_D	Dimensionless wellbore pressure drop
P_D'	Dimensionless wellbore pressure derivative
P_i	Initial pressure, psi
P_{wf}	Wellbore flowing pressure, psi
q	Surface rate, STB/day
r_w	Wellbore radius, ft
s	skin factor
t	Test time, h
t_D	Dimensionless time
t_{DSR}	Dimensionless time reflecting time at which storage effects can be assumed to be negligible or start of infinite acting line
$Y_0(u)$	Bessel function of second kind, order zero
$Y_1(u)$	Bessel function of second kind, order one
α	Tolerance, fraction
m	Viscosity, cp
f	Porosity, fraction of bulk volume

Subscripts

D	Dimensionless quantity
i	Initial conditions or intersection

w	Well
wf	Flowing conditions
ws	Shut-in condition
x	Maximum point or peak
r	radial flow
SR	Start of radial flow line

ACKNOWLEDGMENTS

This study was originally presented as SPE 25426 at the 1993 SPE Production Operations Symposium held March 21-23 in Oklahoma City, Oklahoma.

REFERENCES

Agarwal, R.G., Al-Hussainy, R. and Ramey, H.J., Jr., 1970. An investigation of wellbore storage and skin effect in unsteady liquid flow: I. Analytical treatment. Soc. Pet. Eng. J.: 279-290.

Bourdet, D., Whittle, T.M., Douglas, A.A. and Pirard, Y, M., 1983. A new set of type curves simplifies well test analysis. World Oil: 95-106.

Bourdet, D. et al., 1989. Use of pressure derivative in well test interpretation. SPE Form. Eval.: 293.

Clark, G. and Van Golf-Racht, T.D., 1984. Pressure derivative approach to transient test analysis: a high permeability north sea reservoir example. Paper SPE 12959, European Petr. Conf., London, England, Oct. 25-28.

Earlougher, R.C., Jr., and Kersch, K.M., 1974. Analysis of short-time transient test data by type-curve matching. J. Petrol. Tech.: 793-800.

Horne, R.N., 1990. Modern Well Test Analysis. Petroway Inc., Palo Alto, CA.

Lane, H.S. et al., 1991. An algorithm for determining smooth, continuous pressure derivatives from well test-test data. SPE Form. Eval.: 493.

Mishra, S. and Ramey, H.J., 1988. A new derivative type-curve for pressure buildup analysis with boundary effect. J. Petr. Sci. Eng.: 271-275.

Onur, M. and Reynolds, A.C., 1988. A new approach for constructing derivative type curves for well test analysis. SPE Form. Eval.: 197-206.

Ozkan, E. Vo, D.T. and Raghavan, R., 1987. Some applications of pressure derivative analysis procedure. SPE 16811, 62nd Annual Conf. of SPE, Dallas, TX Sept. 27-30.

Puthigai, S.K. and Tiab, D., 1982, application of P_D' function to vertically fractured wells-field cases. Paper SPE 11028 presented at the SPE 5th Annual Fall Meeting, New Orleans, LA, Sept. 26-29.

Ramey, H.J., Jr., 1970. Short-time well test data interpretation in the presence of skin effects and wellbore storage. J. Petrol. Tech.: 97-104.

Ramey, H.J., Jr. and Agarwal, R.G., 1972. Annulus unloading rates as influenced by wellbore storage and skin effect. Soc. Pet. Eng. J.: 453-462.

Tiab, D., 1975. A new approach (pressure derivative) to detect and locate multiple reservoir boundaries by transient well pressure data. M.S. Thesis, New Mexico Tech.

Tiab, D., 1976. Analysis of multiple-sealing faults systems and bounded reservoirs by type-curve matching (using pressure and pressure derivative). Ph.D. Dissertation, University of Oklahoma.

Tiab, D. and Crichlow, H.B., 1979. Analysis of multiple-sealing fault systems and bounded reservoirs by type curve matching. Soc. Pet. Eng. J.: 378-392.

Tiab, D. and Kumar, A., 1980a. Application of P_D'-function to interference analysis. J. Petrol. Tech.: 1465-1470.

Tiab, D. and Kumar, A., 1980b. Detection of location of two parallel sealing faults around a well. J. Petrol. Tech.: 1701-1708.

Tiab, D., 1989. Direct Type Curve Synthesis. SPE 18992, Proceedings, SPE Rocky Mountain Conf., Denver, Colorado, March.

Tiab, D., 1993. Analysis of pressure and pressure derivatives without type-curve matching-III. Vertically fractured wells in closed systems. SPE 26138, SPE Western Regional Meeting, Anchorage, Alaska, May 26-28.

Vongvuthipornchai, S. and Raghavan, R., 1988. A note on the duration of the transitional period of responses influenced by wellbore storage and skin. SPE Form. Eval.: 207-214.

Wong, D.W., Harrington, A.G. and Cinco-Ley, H., 1986. Application of the pressure-derivative function in the pressure-transient testing of fractured wells. SPE Form. Eval.:470-480

CHARACTERISTIC POINTS AND STRAIGHT LINES OF p_D AND p_D' TYPE-CURVES
(9 characteristics)

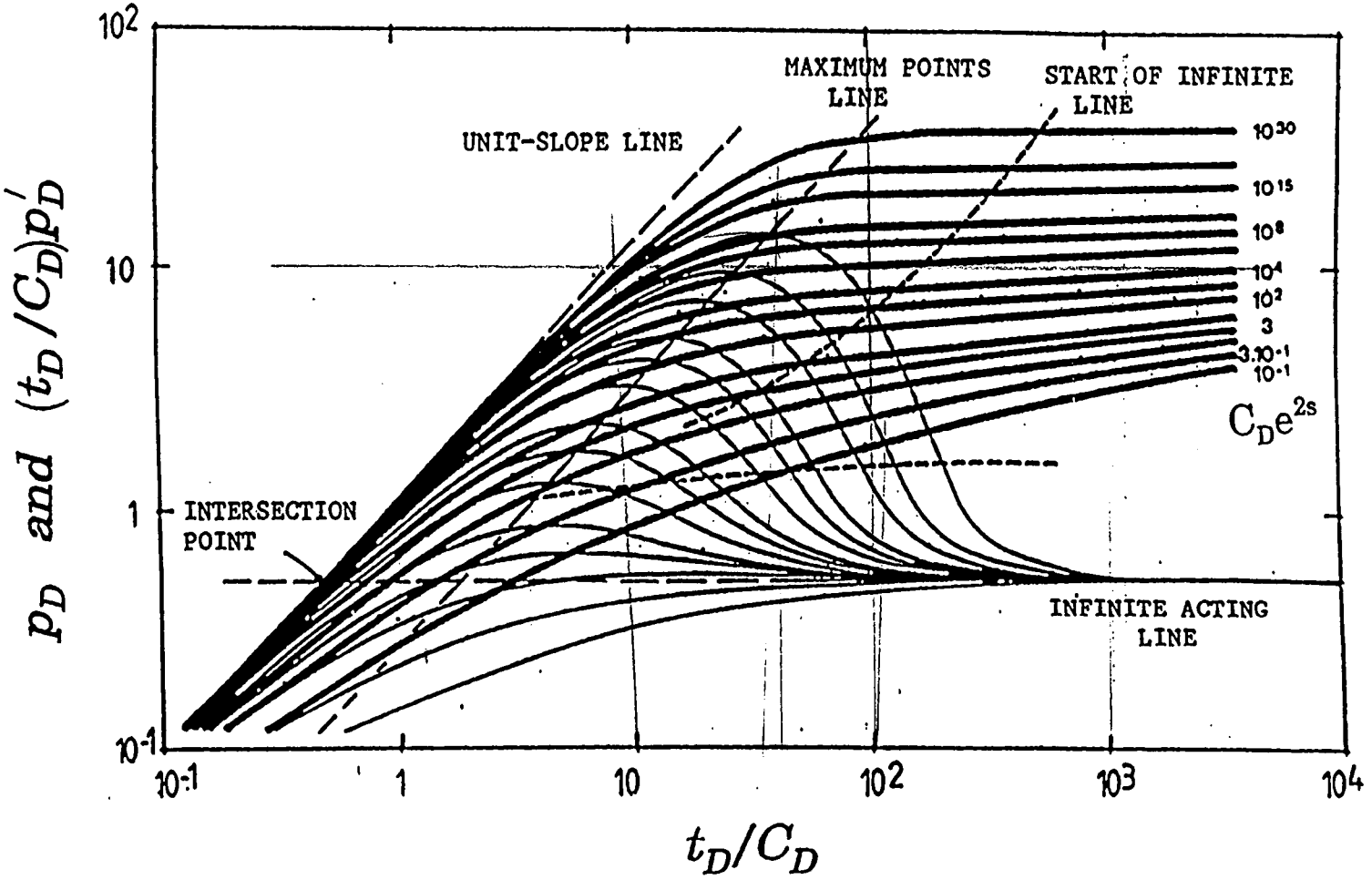

Fig. B.1

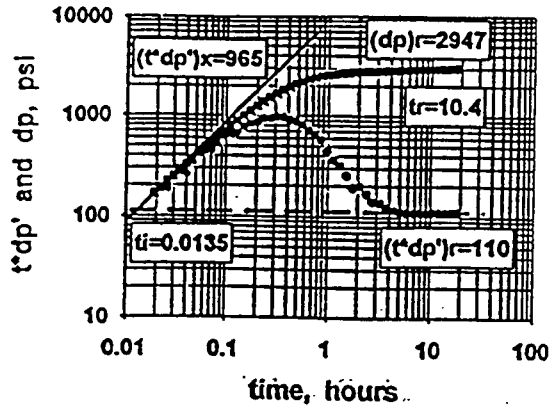

Fig. B.2a - Pressure and pressure derivative curves for Example 1. The late time portion of the derivative curve is smoothed by the Spline technique.

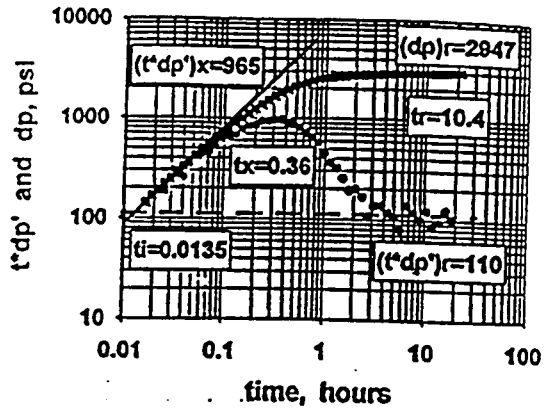

Fig. B.2b Pressure and Pressure derivative curves for Example 1. The pressure derivative points were calculated by numerical differentiation.

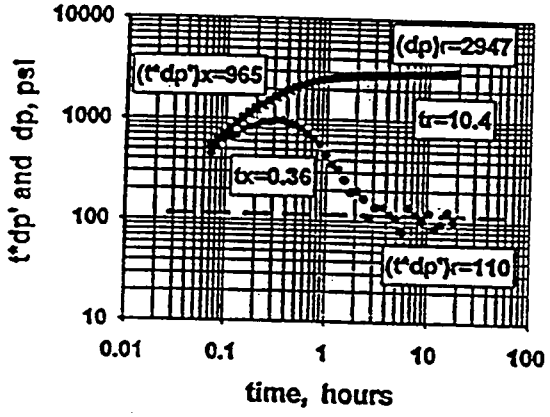

Fig. B.3 Pressure and pressure derivative curves for Example 2.

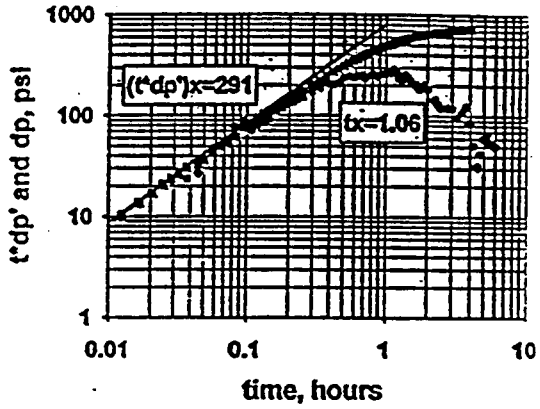

Fig. B.4 Pressure and pressure derivative curves for Example 3.

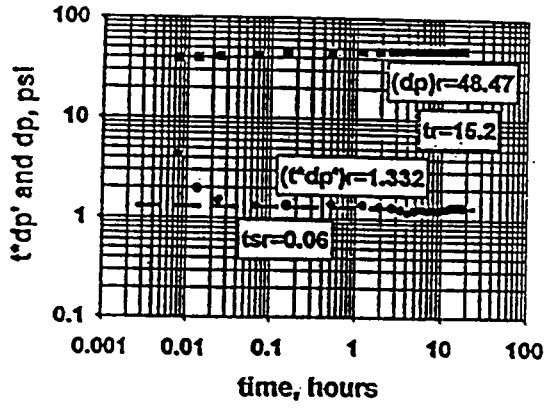

Fig. B.5 Pressure and pressure derivative curves for Example 4.

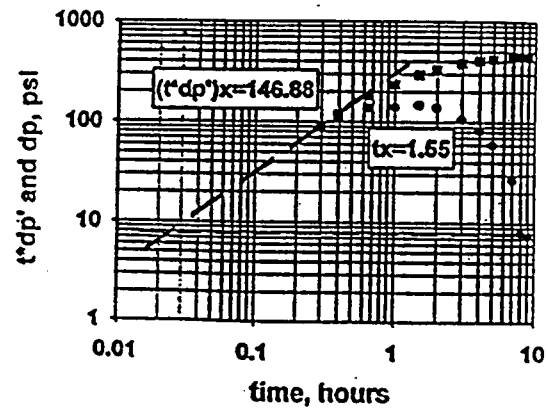

Fig. B.6 Pressure and pressure derivative curves for Example 5.

APPENDIX C

PSEUDO-PRESSURE THEORY AND DIRECT SYNTHESIS

I. GAS WELL PRESSURE TRANSIENT ANALYSIS

1. INTRODUCTION:

A confined reservoir is in the state of static equilibrium. When a new well is put on production, it disturbs static equilibrium of the reservoir and a pressure wave is initiated at the wellbore heading towards the boundaries of the reservoir just like a stone, when thrown into a static pond of water, creates splash waves heading towards the external boundaries of the pond. Time, just before the pressure wave touches external boundary of the reservoir, is called the *Transient Period* or *Transient State*.

Pressure response at the well bore changes rapidly at the instant when a well is put on production and begins to stabilize as the wave reaches the boundaries of the reservoir. The degree of pressure response depends upon the reservoir rock and fluid properties. Thus, a pressure response during this state in some form, is representative of the reservoir rock and fluid properties and can be analyzed.

Pressure at any time after transient state then declines with natural logarithm of time and the change is very small almost undetectable in short periods of time. This period is called *Pseudosteady state*.

Transient state provides a good opportunity to analyze the reservoir for its properties by putting the new wells on production and by shutting-in the old flowing wells. Pressure response is then recorded at the wellbore with pressure recording equipment or electronic gauges which transmit the data on the surface through a conductor wire directly. Pressure data is then analyzed with the help of diffusivity equation by solving it for the reservoir rock and fluid properties.

Purpose of Transient Testing:

To determine following reservoir properties:

- Permeability, K
- Skin, S

- Wellbore storage coefficient, C_{ws}
- Wellbore flowing Pressure, P_{wf}
- Average drainage area pressure, P_e
- Drainage area, A_d
- Shape of reservoir
- To estimate AOF
- Flow Efficiency
- Turbulent flow factor, D
- Damage ratio, R_d
- Radius of investigation, r_i

Types:

- Pressure Drawdown Test
- Pressure Buildup Test
- Isochronal Test
- Reservoir Limit Test
- Interference Test
- Pulse Test

2. PRESSURE DRAWDOWN TEST

Introduction:

Pressure drawdown test is conducted in newly drilled wells or in old wells that are shut-in for very long period of time where pressure is fully developed throughout the reservoir. It can also be performed in wells that can not be shut-in for economic reasons.

A drawdown test is conducted by flowing well and recording pressure response at the wellbore with the help of pressure gauges.

Governing equation in terms of pseudopressure function, *m(P)*

$$m(P_{wf}) = \bar{m(P)} + 50{,}300\frac{P_{SC}}{T_{SC}}\frac{qT}{kh}\left[1.151\log\left(\frac{1{,}688\phi\mu c_t r_w^{\,2}}{kt_p}\right) - S + D|q_g|\right] \quad (1)$$

Where

$$m(P) = 2\int_{P_{wf}}^{P}\frac{P}{\mu Z}dp \quad (2)$$

At $t = 0$, $P_{wf} = P_e$ throughout the reservoir and $P<2000$

$\mu z_g \approx \mu_p z_p \approx$ Constant and pseudopressure function is nearly equal to:

$$m(P) = \frac{2}{\mu_p Z_p}\left(\frac{p^2}{2} - \frac{p_{wf}^{\,2}}{2}\right) \quad (3)$$

Therefore eq: 1 becomes:

$$P_{wf}^{\,2} = P^2 + 1{,}637\frac{q_g Z_g \mu_g}{kh}\left[\log\left(\frac{1{,}688\phi\mu c_t r_w^{\,2}}{kt}\right) - \left(\frac{S + D|q_g|}{1.151}\right)\right] \quad (4)$$

Eq: 4 is drawdown eq. in terms of press- squired terms.When P is between 2000 and 3ooo psia use eq.1, otherwise both equations can be used. Main purpose of using psuedopressure function is to linearize diffusivity equation. Pressure dependence of viscosity causes nonlinearity in diffusivity equation.

Assumptions:

- Homogeneous and isotropic reservoir
- Infinite acting reservoir
- Well fully penetrates the producing formation
- Turbulent factor, D, is constant

Test Procedure:

- Drawdown test is performed in wells shut in for a long period so that P_{ws} equalizes P.
- If the well is a producing it should be shut in for enough time so that P_{ws} equalizes P
- Lower the pressure recording equipment in the well
- Produce the well at stabilized rate (q_g) by adjusting choke size
- Read P_{wf}
- A stage will be observed where pressure drop is almost negligible
- Finish the test and pull out the equipment.

How to calculate Pseudopressure function, *m(P):*

$$m(P) = 2\int_{P_{wf}}^{P_i} \frac{P}{\mu Z} dp \approx \frac{2\left[\left(\frac{P}{\mu Z}\right)_0 + \left(\frac{P}{\mu Z}\right)_1\right]}{2}(P_1 - P_0) \approx$$

$$\approx \frac{2\left[\left(\frac{0}{\mu Z}\right)_0 + \left(\frac{150}{0.01238 * 0.9856}\right)_1\right]}{2}(150 - 0) = 1.844x10^6\, psia^2 / cp \qquad (5)$$

Analysis procedure:

1. Plot $m(P_{wf})$ Vs log t on a Cartesian graph or $m(P_{wf})$ Vs t on a semi-log graph.
2. Calculate the slope (m)
3. Read $m(P_{1hr})$ and m(P_i), y-intercept by extrapolating it.
4. Calculate k:

$$k = 50{,}330 \frac{P_{SC}}{T_{SC}} \frac{q_g T}{mh} \qquad (6)$$

5. Calculate turbulent coefficient, β:

$$\ln(\beta) = -1.201 \ln(k) + 23.83 \qquad (7)$$

6. Apparent skin factor (S_a)

$$S_a = S + D\, q_g$$

$$S_a = 1.151\left[\frac{m(P_i) - m(P_{1hr})}{m} - \log\left(\frac{k}{\phi\mu_p(P_i)c_g(P_i){r_w}^2}\right) + 3.23\right] \quad (8)$$

7. Radius of investigation (r_i):

$$r_i = \left(\frac{kt}{948\phi\mu_i c_{ti}}\right)^{0.5} \quad (10)$$

Ramey - Fligelman method

Ramey comments that above conventional method of analyzing drawdown test gives an approximated values of permeability and skin not the exact values and modifies the conventional method as follows..

8. Using slope, $m(P_{1hr})$ and $m(Pi)$ from same semi-log graph calculate Bq_D and b_D with following equations:

$$Bq_D = 2.715x10^{-15}\frac{\beta k}{r_w}\frac{MP_{SC}}{2\mu_{pi}T_{SC}}\frac{q_{SC}}{h} \quad (11)$$

and

$$b_D = \frac{m(P_i) - m\log\left[\frac{k}{\phi\mu_p(P_i)c_g(P_i){r_w}^2}\right] - m(P_{1hr})}{q_D m(P_i)} \quad (12)$$

Where M is the molecular wt. of gas (lb_m/mol) and m is from step 2 and:

$$q_D = 50{,}330\frac{q_{SC}P_{SC}T}{khT_{SC}m(P_i)} \quad (13)$$

9. Read S from fig.2 (Bq_D *Vs* b_D) for the values calculated

10. Read $m[P_D(1, t_D)]_{turb}$ from fig.3 for S and Bq_D. Interpolate if necessary

11. Calculate m_D:

$$m_D = \frac{m\left[P_D(1, t_D)\right]_{turb} - b_D + S + 0.4045}{\log t_D} + 1.151 \quad (14)$$

OR calculate the slope (m_D) from the semi-log graph of $m[P_D(1, t_D)]$ vs t_D.

$$t_D = \frac{kt}{\phi \mu_p(P_i) c_g(P_i) r_w^2} \tag{15}$$

and

$$m[P_D(1, t_D)] = \frac{m(P_i) - m(P_{wf})}{q_D m(P_i)} \tag{16}$$

12. Calculate k using following equation:

$$k = 5.033x10^4 \frac{T}{mh} \frac{q_{SC} P_{SC}}{T_{SC}} m_D \tag{17}$$

13. To get true value of k iterate from step 8 using k from step 11. It converges after two or three iterations.

EXAMPLE

1. From semi-log graph (fig.1)
2. $m = 50 \times 10^6$ $psia^2/cp$

   $m(P_{1hr}) = 736 \times 10^6$ $psia^2/cp$ and $m(P_i) = 1364 \times 10^6$ $psia^2/cp$
3. Permeability, k

$$k = 50{,}330 \frac{P_{SC}}{T_{SC}} \frac{q_g T}{mh} = 50{,}330 \frac{14.7}{520} \frac{(5{,}000)(715)}{(50x10^6)(12.4)} = 9.4 \ md$$

5. Turbulent coefficient, β:

$$\ln(\beta) = -1.201 \ln(k) + 23.83 = -1.201 \ln(9.4) + 23.83$$

$$\beta = 1.5 \times 10^9 \ ft^{-1}$$

6. Apparent skin factor (S_a)

$$S_a = 1.151\left[\frac{m(P_i) - m(P_{1hr})}{m} - \log\left(\frac{k}{\phi\mu_p(P_i)c_g(P_i)r_w{}^2}\right) + 3.23\right]$$

$$= 1.151\left[\frac{1364 - 736}{50} - \log\left(\frac{9.4}{(0.15)(3.307x10^{-6})(1/3)^2}\right) + 3.23\right] = +8..7$$

7. Radius of investigation (r_i) can be calculated at any time. At $t = 10\ hr$:

$$r_i = \left(\frac{kt}{948\phi\mu_i c_{ti}}\right)^{0.5} = \left\{\frac{(9.4)(10)}{948(0.15)(0.0242)(3.6x10^{-6})}\right\}^{0.5} = 2754.57\,ft$$

Ramey-Fligelman method

8. Using slope, $m(P_{1hr})$ and $m(Pi)$ from same semi-log graph calculate Bq_D and b_D:

$$Bq_D = 2.715x10^{-15}\frac{\beta k}{r_w}\frac{MP_{sc}}{\mu_{pi}T_{sc}}\frac{q_{sc}}{h} =$$

$$= 2.715x10^{-15}\frac{(1.513x10^9)(9.4)}{(1/3)}\frac{(28.96x0.7)(14.7)}{(0.0242)(520)}\frac{(5{,}000)}{12.43} = 1.104$$

and

$$b_D = \frac{m(P_i) - m\log\left[\frac{k}{\phi\mu_p(P_i)c_g(P_i)r_w{}^2}\right] - m(P_{1hr})}{q_D m(P_i)} =$$

$$= \frac{(2.715x10^6) - (50x10^6)\log\left[\frac{9.4}{(0.15)(3.307x10^{-6})(1/3)^2}\right] - 736x10^6}{(0.032)(1364x10^6)} = 9.06$$

Where

$$q_D = 50{,}330\frac{q_{SC}P_{SC}T}{khT_{SC}m(P_i)} = 50{,}330\frac{(5{,}000)(14.7)(715)}{(9.4)(12.43)(520)(1364x10^6)} = 0.032$$

9. Reading S from fig.2 (Bq_D *Vs* b_D) for the values calculated in step 8, $S = +5$

10. Read $m[P_D(1, t_D)]_{turb}$ from fig.3. For $Bq_D = 1.104$, and $S = +5$ curve, $m[P_D(1, t_D)]_{turb} = 4$

11. Calculate m_D:

$$m_D = \frac{m[P_D(1,t_D)]_{turb} - b_D + S + 0.4045}{\log t_D} + 1.151$$

and

$$t_D{}^* = t_D\phi = \frac{0.0002637k}{\mu c_t r_w{}^2} = \log(t_D{}^*) = \log\left(\frac{0.0002637(9.4)}{(0.0242)(3.307x10^{-6})(1/3)^2}\right) = 5.44$$

$$m_D = \frac{4 - 9.06 + 5 + 0.4045}{5.44} + 1.151 = 1.214$$

12. Calculate k using following equation:

$$k = 5.033x10^4 \frac{T}{mh}\frac{q_{SC}P_{SC}}{T_{SC}}m_D = 5.033x10^4 \frac{715}{(50x10^6)(12.43)}\frac{(5{,}000)(14.7)}{520}1.214 = 9.9md$$

13. Non-Darcy Flow Factor, D:

$$D = \frac{2.715x10^{-15}\beta kMP_{SC}}{h\mu_{p_{wf}} r_w T_{SC}} = \frac{2.715x10^{-15}(1.513x10^9)(9.9)(28.96x0.7)(14.7)}{(12.43)(0.019)(1/3)(520)}$$

$$= 28.12x10^{-5}(Mscf/D)^{-1}$$

and

$$Dq_{SC} = (28.12x10^{-5})(5{,}000) = 1.41$$

and

$$S = S_a - Dq_{SC} = 8.7 - 1.41 = 7.29$$

The above value of S is almost twice the Value obtained by Ramey-Fligeman method. D calculated from field data is twice the value calculated from cores. Following may be the reasons:

1. Effect of damaged zones on high velocity flow
2. Stress sensitive permeability
3. Reduced permeability from condensation near wellbore.

3. PRESSURE BUILDUP TESTING

Introduction

Introduced by hydrologists, most widely used pressure transient test in oil and gas industry is the pressure buildup test. Basically test is conducted by producing the well at constant rate followed by shutting the well and recording the pressure response at the well bore with pressure recording equipment. Most widely equation used to calculate reservoir properties is Horner equation. Although this equation assumes an infinite acting reservoir but works equally for finite reservoirs.

Purpose

To determine:

Permeability, K

Skin factor, S

Initial Reservoir Pressure, P_i

Non-Darcy turbulence factor, D

Flow efficiency of the well, FE

Damage ratio, R_d

Governing Equation

Although flow of gas is modeled most rigorously in terms of adjusted pressure and adjusted time or equally rigorous but less user friendly pseudofunctions, following equations can be used for test design and are sufficiently accurate when gas properties are estimated at average pressure.

$$P_{wf} = P_i - 70.6\frac{B_g q_g \mu}{k_g h}\left[\ln\left(\frac{k_g t}{1{,}688\phi\mu c_t {r_w}^2}\right) + 2S_a\right] \tag{1}$$

where,

$$S_a = S + Dq_g \tag{2}$$

Assumptions

- Infinite acting reservoir
- D is constant
- Gas properties are estimated at P_{av} $\left(P_{av} = \frac{P_i + P_{wf}}{2}\right)$

Test Procedure:

- Determine the packer locations, tubing, casing size and T_D.
- Stabilize the pressure at constant rate, q_g
- Lower the pressure recording equipment
- Shut the well and read the pressure(P_{ws}) just before the shut in ($\Delta t=0$)
- Read shut in pressure P_{ws} at interval of time as short as possible, 10-15 seconds for first few minutes(15-60 min), 15-30 sec for the next 2-5 hours and then every hour for remaining

Note:

- Recording interval may vary in tight gas formations because of slow response of the reservoir.Generally time interval depends upon the purpose of the test.

Analysis Procedure

1. Plot P_{ws} Vs Δt on a semilog paper
2. Calculate slope, m
3. Read P_i (Y-intercept) by extrapolating the straight line portion
4. Calculate K_g

$$K_g = 162.6\frac{B_g q_g \mu_g}{mh} \qquad (3)$$

5. Calculate apparent skin, S_a

$$S_a = 1.153\left[\frac{[P_i - P_{wf}(\Delta t = 0)}{m} - \log(\frac{k_g}{\phi\mu_g c_t r_w^{\ 2}}) + 3.23\right] \quad (4)$$

6. Calculate non-Darcy turbulence factor, D

$$D = \frac{9.106x10^{-9}\gamma_g}{K_g^{\frac{1}{3}}\mu_{g,w}r_w} \quad (5)$$

7. Calculate skin,S

$$S=S_a\text{-}Dq_g \quad (6)$$

8. Investigation radius, r_i

$$r_i = \left(\frac{K_g t}{377\phi\mu_g c_t}\right)^{\frac{1}{2}} \quad (7)$$

9. Time to end wellbore storage effects, t_{ws}

$$t_{wbs} = \frac{(200{,}000 + 12{,}000S_a)C}{(k_g h/\mu_g)} \quad (8)$$

$$C = c_{wb}.V_{wb} \quad (9)$$

where,

V_{wb} = wellbore volume

c_{wb} = gas comp: in wellbore

$c_{wb} = c_g$ at P_{av}

10. Calculate pressure drop due to skin, ΔP_s

$$\Delta P_S = \frac{141.2q_g\mu_g B_g S}{K_g h} \quad (10)$$

11. Flow efficiency of the well, FE

$$FE = 1 - \left(\frac{\Delta P_S}{\Delta P}\right) \quad (11)$$

12. Damage Factor, DF

$$DF=1-FE \tag{12}$$

13. Damage ratio, R_d

$$R_d=1/FE \tag{13}$$

14. Time to end the transient state, t_{end}:

$$t_{end} = \frac{273\phi\mu c_t r_e^{\,2}}{K_g} \tag{14}$$

EXAMPLE

Well, rock, and fluid properties :

P_i = 6500 psia $\quad$ h = 25 ft

P_{wf} = 707 psia $\quad$ T = 202 °F

q_g = 190 Mcf/D $\quad$ t_p = 1200

c_{wb} = $2.2556x10^{-4}$ $psia^{-1}$ $\quad$ γ_g = 0.65

c_{ti} = 8.28×10^{-5} $psia^{-1}$ $\quad$ μ_g = 0.0241 cp

r_w = 0.25 ft $\quad$ ϕ = 0.075

V_{wb} = 131 bbl $\quad$ B_g = 0.447 RB/Mscf

r_e = 3115 ft

Solution

1. Fig.1 shows semilog graph

2. Slope, m = 140 psia/cycle

3. Reading P_i (Y-intercept) by extrapolating the straight line portion ,P_i= 6500 psia

4. Permeability, $K_g = 162.6\frac{B_g q_g \mu_g}{mh} = 162.6\frac{(0.447)(190)(0.0241)}{(140)(25)} = 0.095md$

5. Apparent skin,S_a

$$S_a = 1.1513\left[\frac{P_i - P_{wf}(\Delta t = 0)}{m} - \log(\frac{k_g}{\phi\mu_g c_t {r_w}^2}) + 3.23\right]$$

$$S_a = 1.1513\left[\frac{6140 - 707}{140} - \log[\frac{(0.095)}{(0.75)(0.0241)(8.28x10^{-5})(0.25)^2}) + 3.23\right] = 35$$

6. Non-Darcy turbulence factor, D

$$D = \frac{9.106x10^{-9}\gamma_g}{K_g^{\frac{1}{3}}\mu_{g,w}r_w} = \frac{9.106x10^{-9}(0.65)}{(0.095)^{\frac{1}{3}}(0.0241)(0.25)} = 0.00000021$$

7. Skin,$S = S_a - Dq_g = 35 - (0.00000021)(190) = 34.8$

8. Radius of investigation, r_i, after 100 hours

$$r_i = \left(\frac{k_g t}{948\phi\mu_g c_t}\right)^{\frac{1}{2}} = \left(\frac{(0.095)(100)}{948(0.075)(0.0241)(8.28x10^{-5})}\right)^{\frac{1}{2}} = 259ft$$

t (hr)	r_i(ft)
10	81
50	182
100	259

9. Time to end wellbore storage effects, t_{wbs}

$$t_{wbs} = \frac{(200{,}000 + 12{,}000S_a)C}{(k_g h / \mu_g)}$$

where

$$C = c_{wb} \cdot V_{wb} = 2.2556x10^{-4})(131) = 0.0295$$

$$t_{wbs} = \frac{(200{,}000 + 12{,}000x39.7)0.0295}{(0.095x25 / 0.0241)} = 203 hours$$

10. Calculate pressure drop due to skin, ΔP_s

$$\Delta P_S = \frac{141.2 q_g \mu_g B_g S}{K_g h} = \frac{141.2(190)(0.0241)(0.447)(34.8)}{(0.095)(25)} = 4234 psia$$

11. Flow efficiency, *FE*

$$FE = 1 - \left(\frac{\Delta P_S}{\Delta P}\right) = 1 - \left(\frac{4234}{5793}\right) = 0.4417 = 44.17\%$$

12. Damage Factor, *DF*

$$DF = 1 - FE = 1 - 0.4417 = 0.558$$

13. Damage ratio, R_d

$$R_d = 1/FE = 1/0.4417 = 2.26$$

14. Time to end the transient state, t_{end}:

$$r_e = 3{,}115 ft$$

$$t_{end} = \frac{237 \phi \mu c_t r_e^2}{K_g} = \frac{237(0.075)(0.0241)(8.28x10^{-5})(3{,}115)^2}{0.095} = 3623 hours$$

4. PRESSURE AND PRESSURE DERIVATIVE (DIRECT SYNTHESIS TECHNIQUE)

Procedure:

1. Calculate $t*\Delta P'$ using Bourdet algorithm.
2. Plot ΔP and $t*\Delta P'$ Vs t on log-log graph.
3. Draw the unit slope, radial, and infinite acting lines (fig.2)
4. Read the following points.

   t_x, $(t*\Delta P')_x$, t_i, $(t*\Delta P')_i$, $(t*\Delta P')_r$, *and* $(\Delta P)_r$

   $(t*\Delta P')_x = 2700\ psi$ $(t*\Delta P')_i = 58\ psi$ $(\Delta P)_r = 5800\ psi$

   $t_x = 29\ hr$ $t_i = 0.22\ hr$ $t_r = 500\ hr$ $(t*\Delta P')_r = 58\ psi$

5. Calculate permeability, k

$$k = \frac{70.6q\mu B}{(t\cdot\Delta P')_i h} = \frac{70.6(190)(0.0241)(0.447)}{(58)(25)} = 0.099 \tag{15}$$

or

$$k = 9416.2\left(\frac{\mu C}{ht_x}\right)\left[0.5\frac{(t\cdot\Delta P')_x}{(t\cdot\Delta P')_r} + 0.42\right] = 9416.2\left(\frac{0.0241x0.0133}{25x29}\right)\left[0.5\frac{2700}{58} + 0.42\right] = 0.098$$

6. Calculate wellbore storage coefficient, C

$$C = \frac{t_{ii}kh}{1695\mu} = \frac{(0.22)(0.099)(25)}{1695(0.0241)} = 0.013 \tag{17}$$

or

$$C = \frac{0.015qBt_x}{(t*\Delta P')_x + 0.84(t*\Delta P')_r} = \frac{0.015(190)(0.447)(29)}{2700 + 0.84(58)} = 0.0134 \tag{18}$$

6. Calculate skin, S

$$S = 0.171\left(\frac{t_x}{t_i}\right)^{1.24} - 0.5\ln\left[\frac{0.8935C}{\phi hc_t r_w{}^2}\right]$$
$$= 0.171(29/0.22)^{1.24} - 0.5\ln\left[\frac{0.8935x0.0133}{0.075x25x8.28x10^{-5}x0.25^2}\right] = 69 \tag{19}$$

or

$$S = \left\{ \frac{\Delta P_x}{(t * \Delta P')_r} - \ln\left(\frac{kt_r}{\phi \mu c_t {r_w}^2} \right) + 7.43 \right\} \tag{20}$$

$$S = 0.5\left\{ \frac{5800}{58} - \ln\left(\frac{0.099(500)}{(0.075)(0.0241)(8.28x10^{-5}(0.25)^2} \right) + 7.43 \right\} = 40.7$$

II. PRESSURE TRANSIENT ANALYSIS (CO_2 RESERVOIRS)

1. INTRODUCTION

CO_2 reservoirs in New Mexico, Colorado, Utah, Wyoming, and Texas are the main natural source of CO_2 for EOR Projects and other industrial applications. Unlike HC gases, CO_2 affects the skin zone both physically and chemically, in most cases favorably. CO_2 reacts with fresh water from mud filtrate and forms weak carbonic acid.

$$H_2O + CO_2 = H_2CO_3$$

Carbonic acid reacts with limestone and dolomites and increases permeability, provides rapid cleanup, which helps remove muds and silts from the well bottom. Chances of perforation plugging are greatly reduced due to presence of CO_2.

Pressure data, when analyzed by conventional diffusivity equation, gives under estimated values of reservoir transmissivity and excessive values of skin. CO_2 behaves differently with changing pressure and temperature. It is necessary to evaluate pseudopressure functions for the CO_2 properties to estimate true flow potential of the reservoir.

Purpose

Purpose of pressure transient analysis in CO_2 containing reservoirs is the same as for natural gas reservoirs i-e to determine reservoir rock properties:

- Permeability, k
- Reservoir transmissivity, kh
- Skin factor, S
- Drainage radius, r_e
- Economic loss due to skin, etc.

2. PRESSURE DRAWDOWN TEST

- **Governing equation** in terms of pseudopreuure function, *m(p)*

$$m(P_{wf}) = m(Pi) - \frac{1637}{kh}\frac{qT}{}\left[\log\left(\frac{kt}{\phi_i \mu c_{ti} r^2{}_w}\right) - 3.23 + 0.87S_t\right]$$

(A)

$$m(P) = \left(\frac{2M_t}{\mu_a}\right)P^2 \tag{1}$$

where

$$M_t = (M_c + M_r)T_{pr} \tag{2}$$

$$M_r = 0.5\left(\frac{C_{pr}}{P_{pr}} - 1\right) \tag{3}$$

$$M_c = \Sigma_{j=1}^{6} C_j (C_o + 1)^{j-1} \tag{4}$$

- C_{pr} is Reduced Press: Correlation factor fig. 1-5
- C_j is the reduced pressure correlation factor (Table 1).
- C_o is the mole fraction of CO_2 and H_2S.
- μ_a is the corrected viscosity of gas at 1 atmosphere.
- P_{pr} and T_{pr} are Pseudoreduced pressure and Temperature respectively.
- *m(P)* is the pseudopressure function for CO_2 containing (Sour gas) natural.

Assumptions:

- Homogeneous and isotropic reservoir
- Infinite acting reservoir
- Well fully penetrates the producing formation
- Turbulent factor, *D*, is constant.

How To Calculate *M(P)*

1. Calculate the corrected viscosity(μ_a) of gas at 1 atm (fig. 6)
2. Determine the T_{pc} and P_{pc} at average reservoir conditions using gas composition.
3. Find reduced pressure correlation factors (C_j) from Table 1.
4. Calculate M_c from equation 4.
5. Read C_{pr} from figures 1-10
6. Calculate M_r from eq: 3.
7. Calculate M_t from eq: 2.
8. Calculate *m(P)* from eq: 1.

Analysis Procedure

1. Plot $m(P_{wf})$ vs t on a semi-log graph.
2. Calculate the slope (m)
3. Read $m(P_{1hr})$
4. Read $m(P_i)$, y-intercept by extrapolating it
5. Calculate k:

$$kh = \frac{1637Tq}{m} \tag{5}$$

7. Apparent skin factor (S_a)

$$S_a = S + Dq_g \tag{6}$$

$$S_a = 1.1513\left[\frac{m(P_i) - m(P_{1hr})}{m} - \log\left(\frac{k}{\phi\mu\ c_t {r_w}^2}\right) + 3.23\right] \tag{7}$$

8. Flow Efficiency, E_f

$$E_f = 1 - \frac{0.87mS_t}{m(P_i) - m(P_{wf})} \tag{8}$$

9. Radius of investigation *(r_i)*:

$$r_i = \left(\frac{kt}{948\phi\mu_i c_{ti}}\right)^{0.5} \tag{9}$$

3.BUILDUP TEST ANALYSIS

Governing Equation

$$m(P_{ws}) = m(Pi) - \frac{1637}{kh}\frac{qT}{}\left[\log\left(\frac{t+\Delta t}{\Delta t}\right)\right] \tag{10}$$

Analysis Procedure

1. Plot $m(P_{ws})$ vs. $\left(\frac{t+\Delta t}{\Delta t}\right)$ on semi-log graph

2. Read $m(P_{ws})_1$ and $m(P_{ws})_0$ at $\Delta t=1$ and $\Delta t=0$ respectively

3. Calculate *kh:*

$$kh = \frac{1637T}{m}q \tag{11}$$

4. Apparent skin factor S_a,

$$S_a = 1.1513\left[\frac{m(P_{ws})_1 - m(P_{ws})_0}{m} - \log\left(\frac{k}{\phi\mu\ c_t r_w{}^2}\right) + \frac{3.23}{}\right] \tag{12}$$

Actual skin (s) is the calculated as:

$$S = S_a - Dq_g \tag{13}$$

EXAMPLE

A pressure buildup test was conducted in the Moqui No.1, located in the McElmo Dome field, Montenzuma county, Colorado, after it's acidization. The well produced for 96 hours at an average rate of 8,400 *Mscf/D.* BHP recorded prior shut in, was 2490 *psig.* Test was run to determine effetiveness of the acid job and permeability of the formation. Other pertinent data are:

$T = 168\ ^\circ F$ $SG = 1.518$ $S_g = 0.84$

$P_{av} = 2533$ psig $h = 86$ ft $\phi = 013$

The gas composition is:

$CO_2 = 98.25\ \%$

$CH_4 = 0.138\ \%$

$N_2 = 1.606\ \%$

Solution

Corrected viscosity(μ_a) of gas at 1 atm.

$\mu_a = 0.041744$ cp (fig.6)

1. T_{pc} and P_{pc} *at* average reservoir conditions using gas composition

   $T_{pc} = 542.14\ ^\circ R$ $P_{pc} = 1.158$

2. Reduced pressure correlation factors (C_j) from Table 1

   $C_1 = 0.6918$ $C_2 = -0.41645$ $C_3 = 0.24265$

   $C_4 = 0.04922$ $C_5 = -0.085213$ $C_6 = 0.019954$

3. M_c from equation 4.

   $M_c = 0.4981$

4. Calculate C_{pr} from fig. 1-5 for range of P_{pr}

5. Calculate M_r from eq: 3 for the range of C_{pr} and P_{pr}

6. Calculate M_t from eq: 2.
7. Calculate $m(P)$ from eq: 1.

Analysis

1. From fig. 7
2. $m(P)_{1hr} = 342.2\ MM\ psi^2/cp$ and $m(P)_0 = 337\ MM\ psi^2/cp$
3. $kh = 1637\ T\ q/m = 1637\ (628)(8400)/2.1 \times 10^6 = 4128\ \ md\text{-}ft$

   $k = 48\ \ md\ \ [h=86\ ft]$
4. Apparent Skin(S_a)

$$S_a = 1.1513\left[\frac{m(P_{ws})_1 - m(P_{ws})_0}{m} - \log\left(\frac{k}{\phi\mu\ c_t r_w^{\ 2}}\right) + 3.23\right]$$

$$S_a = 1.1513\left[\frac{342.2x10^6 - 337x10^6}{2.1x10^6} - \log\left(\frac{48}{(0.13)(0.044)(2.8x10^{-4})(0.33)^2}\right) + 3.23\right] = -3$$

Nomenclature

A = Drainage area, ft

C = wellbore Storage Coefficient, Mscf/psi

C_o = Mole fraction CO_2, N_2, H_2S

C_j = Correlation coefficients, table 1

C_{pr} = Reduced correlation factor

c_t = Total system compressibility, psi^{-1}

D = Non- Darcy flow factor, $(Mscf/D)^{-1}$

h = Pay zone thickness, ft

k_g = Gas permeability, md

M = Molecular Weight

M_c = Concentration correlation factor

M_r = Reduced properties correlation factor

M_t = $(M_c+M_r)T_{pr}$

m = Slope, psia/cycle

P_{pc} = Pseudocritical pressure, psi

P_{pr} = Pseudoreduced pressure, dimentionless

P_i = Initial reservoir pressure, psia

P_{wf} = Wellbore flowing pressure, psia

P_{ws} = Shut-in wellbore pressure, psia

P_{av} = Average Reservoir pressure, psia

q_g = Gas flow rate, Mscf/D

r_w = Wellbore radius, ft

r_e = Drainage radius, ft

r_i = Radius of investigation, ft

S_a = Apparent skin

S = Skin

T = Reservoir temperature, °R

T_{pc} = Pseudocritical temperature, °R

Δt = Shut-in time, hr

t_{wbs} = Time to end wellbore storage effects, hr

t_{end} = Time to end transient state, hr

V_{wb} = Wellbore volume, bbl

z = Gas deviation factor

ϕ = Porosity

μ_a = Gas viscosity at 1 atmosphere, cp

γ_g = Gas gravity

Table 3

Δt	P_{ws}	ΔP	$t*\Delta P'$
hr	**psi**	**psi**	**psi**
0	707	5793	
0.072	720	5780	
0.288	759	5741	344.0043
0.936	872	5628	184.3851
2.23	1088	5412	379.5795
3.58	1304	5196	550.5099
4.97	1521	4979	717.518
6.41	1739	4761	889.9476
7.92	1957	4543	1078.038
9.46	2176	4324	1282.45
11	2395	4105	1393.643
12.7	2615	3885	1618.278
14.4	2834	3666	1765.772
16.1	3054	3446	1990.523
17.8	3272	3228	2108.508
19.6	3491	3009	2255.624
21.5	3707	2793	2393.831
23.4	3922	2578	2449.282
25.4	4136	2364	2527.585
27.6	4346	2154	2554.53
29.9	4556	1944	2567.087
32.3	4760	1740	2501.333
35	4961	1539	2461.469

38	5158	1342	2294.235
41.4	5348	1152	2066.535
45.6	5530	970	1854.81
50.6	5702	798	1498.779
57.2	5861	639	1219.87
66.6	6001	499	882.5742
81.6	6118	382	591.9357
110	6210	290	351.3768
181	6283	217	175.0975
301	6334	166	76.83577
421	6363	137	56.2185
541	6383	117	56.66542
661	6397	103	54.69873
781	6408	92	51.44546
901	6417	83	45.97031
1021	6424	76	36.61029
1141	6429	71	
1200	6432	68	

APPENDIX D

FUNDAMENTALS OF DIRECT SYNTHESIS FOR COMPRESSIBLE FLUIDS

FUNDAMENTALS OF DIRECT SYNTHESIS FOR COMPRESSIBLE FLUIDS

1. INTRODUCTION AND BASIC EQUATIONS

In terms of **pseudo-pressure**, the dimensionless wellbore pressure for a well with storage and skin, $m(p_{wD})$, and its derivative, $dm(p_{wD})/dt$, are obtained from

$$m(p_D) = \frac{4}{\pi^2}\int_0^\infty \left(\frac{1-e^{-u2t_D}}{u^3 U_J}\right) du \tag{1.1}$$

and

$$\frac{dm(p_D)}{dt_D} = \frac{4}{\pi^2}\int_0^\infty \left(\frac{e^{-u2t_D}}{uU_J}\right) du \tag{1.2}$$

where

$$U_J = \left[uC_D J_0(u) - (1 - C_D s u^2) J_1(u)\right]^2 + \left[uC_D Y_0(u) - \left(1 - C_D s u^2\right) Y_1(u)\right]^2 \tag{1.3}$$

the dimensionless pressure, $m(p_{wD})$, dimensionless time, t_D and dimensionless wellbore storage coefficient are expressed as follows:

$$m(P_D) = \left(\frac{kh}{141.2quB}\right)\Delta m(p) \tag{1.4}$$

$$t_D = \left(\frac{0.0002637k}{\phi\mu c_t r_W^2}\right) t \tag{1.5}$$

$$C_D = \left(\frac{0.8935}{\phi c_t h r_W^2}\right) C \tag{1.6}$$

The factors C and S are respectively the wellbore storage coefficient and skin.

2. CHARACTERISTIC POINTS AND STRAIGHT LINES

The log-log plot of dimensionless pressure and pressure derivatives versus time, Fig. B1, has several unique features:

(1) The pressure curve has a unit slope line during early time. This line corresponds to pure wellbore storage flow. The equation of this straight line is

$$m(p_D)=\frac{t_D}{C_D} \tag{2.1}$$

Combining Eqs. 1.5 and 1.6 gives

$$\frac{t_D}{C_D}=\left(2.95\times10^{-4}\frac{h}{\mu}\right)\frac{t}{C} \tag{2.2}$$

Substituting Eqs. 1.4 and 2.2 into Eq. 2.1 and solving for the wellbore storage coefficient C we obtain:

$$C=\left(0.483\frac{qT}{\mu}\right)\frac{t}{\Delta m(p)} \tag{2.3}$$

2) The pressure derivative curve also has an early time straight line of unit slope. The equation of this line is obtained by taking the derivative of Eq. 2.1 with respect to the natural log of t_D/C_D Thus:

$$\left(\frac{t_D}{C_D}\right)\Delta m(p'_D)=\frac{t_D}{C_D} \tag{2.4}$$

where the dimensionless pressure derivative is

$$m(p'_D)=\left(2.32\frac{\phi(\mu c_t)_i hr_w^2}{qT}\right)\Delta m(p') \tag{2.5}$$

The left-hand side of Eq. 2.4 can be expressed in real units by combining Eqs. 2.2 and 2.5

$$\left(\frac{t_D}{C_D}\right)m(p'_D)=\left(6.106x10^{-4}\frac{kh}{qT}\right)[t\cdot\Delta m(p')] \tag{2.6}$$

It is obvious from Fig. B.1 that the early-time unit slope line is the same for both pressure and pressure derivative curves. Combining Eqs. 2.4, 2.5 and 2.6 and solving for C we obtain an equation similar to Eq. 2.3 where $\Delta m(p)$ is replaced with $t\cdot\Delta m(p')$.

3) The infinite acting radial flow portion of the pressure derivative is a horizontal straight line. For a homogeneous reservoir, the equation of this line is:

$$\left[\left(\frac{t_D}{C_D}\right)m(p'_D)\right]_r=0.5 \tag{2.7}$$

Combining Eqs. 2.6 and 2.7 and solving for the permeability yields:

$$k=818.866\frac{qT}{h(t\cdot\Delta m(p'))_r} \tag{2.8}$$

where the subscript r stands for radial flow line. In terms of pressure, the equation of this line is:

$$m(p_{Dr})=0.5\left[\ln\left(\frac{t_D}{C_D}\right)_r+0.80907+\ln\left(C_De^{2s}\right)\right] \tag{2.9}$$

4) The starting time of the infinite acting line of the pressure derivative curve is approximately given by:

$$\left(\frac{t_D}{C_D}\right)_{SR}=10\log\left(C_De^{2s}\right)^{10} \tag{2.10}$$

This equation is obtained by plotting the values of t_D/C_D corresponding to the first point where Eq. 2.9 is valid, i.e. at the start of the horizontal line for different values of $C_De^{2s} > 10^2$. Values of t_D/C_{SR} were obtained from the second derivative of Eq. 1.1. Substituting for C_D and t_D and solving for t_{SR} gives:

$$t_{SR} = \frac{\mu C}{6.9\times10^{-5}kh}\left[\ln\left(\frac{0.8935C}{\phi c_t h r_w^2}\right)+2s\right] \tag{2.11}$$

where t_{SR} is the starting time of the infinite acting radial flow line.

Vongvuthipornchai and Raghavan (1988) showed that the starting time of the semilog straight line is best determined from

$$\left(\frac{t_D}{C_D}\right)_{SR} = \frac{1}{\alpha}\left[\ln\left(C_D e^{2s}\right)+\ln\left(\frac{t_D}{C_D}\right)_{SR}\right] \tag{2.12}$$

where α is the tolerance (fraction) used to determine the value of t_{DSR} at which Eq. 2.7 is valid. For α=0.05 they found that Eq. 2.12 (approximate solution) can predict the value of t_{DSR} within 8 percent of the value predicted by Eq. 1.2 (exact solution).

The semilog straight line will always appear to start earlier than the horizontal portion of the pressure derivative curve. The difference can be as much as fifty percent.

The wellbore storage coefficient may be estimated from Eq. 2.12 by letting α=0.05 and solving for C:

$$C = 0.056\phi c_t h r_w^2\left(\frac{t_{DSR}}{2s+\ln t_{DSR}}\right) \tag{2.13}$$

where t_{DSR} is calculated from Eq. 1.5 at $t=t_{SR}$.

5) The early-time unit slope line and the late-time infinite acting line of the pressure derivative, i.e. the horizontal line, intersect at:

$$\left(\frac{t_D}{C_D}m(p'_D)\right)_i = 0.5 \tag{2.14}$$

$$\left(\frac{t_D}{C_D}\right)_i = 0.5 \tag{2.15}$$

where the subscript *i* stands for "intersection". In real units the coordinates of this

intersection point are obtained from

and

$$\left(t \cdot \Delta m(p')\right)_i = 0.41\frac{qT}{kh} \tag{2.16}$$

and

$$t_i = \frac{1695\mu C}{kh} \tag{2.17}$$

These equations can be derived, respectively, from Eqs. 2.8, 2.2 and 2.15. Thus, the intersection point can be used to determine k from Eq. 2.16 and C from Eq. 2.17. Since the unit slope line is the same for pressure and pressure derivative curves, at the intersection point we have:

$$\Delta m(p)_i = t \cdot \Delta m(p')_i = t \cdot \Delta m(p')_r \tag{2.18}$$

6) Between the early-time and late-time straight lines, the derivative curves have specific shapes for different values of C_De^{2s}. In this study, the coordinates of the "peaks" for $C_de^{2s} > 10^2$ were obtained from the second derivative and plotted on a cartesian graph. The equation of this line is

$$\left(\frac{t_D}{C_D} m(p'_D)\right)_x = 0.36\left(\frac{t_D}{C_D}\right)_x - 0.42 \tag{2.19}$$

Combining Eqs. 2.2, 2.6 and 2.19 yields:

$$\left(t \cdot \Delta m(p')\right)_x = \left(0.174\frac{t_x}{C}\right) - 687.85\frac{qT}{kh} \tag{2.20}$$

and $(t \cdot \Delta m(p'))_x$ and t_x are the coordinates of the maximum point (peak) of the pressure derivative curve. It is obvious from Eq. 2.20 that we can calculate the wellbore storage coefficient or the permeability from the coordinates of the peak.

Solving Eq. 2.20 for k yields:

$$k = \left(\frac{687.85qT}{h}\right)\frac{1}{(0.174qT/\mu)\frac{t_x}{C} - (t\cdot\Delta m(p'))_x} \tag{2.22}$$

This equation should be used to calculate k only if the late-time infinite acting radial flow line is not observed, such as in a short test, or there is too much noise in the late-time derivative values.

Solving Eq. 2.20 for C yields:

$$C = \frac{0.174qT}{(t\cdot\Delta m(p'))_x + 687.85qT/(kh)}\frac{t_x}{\mu} \tag{2.23}$$

This equation should be used in cases where k is known from other sources and the early time unit slope line is not observed.

7) A log-log plot of log (C_De^{2s}) versus the coordinates of the peaks yielded the following equations:

$$\log\left(C_De^{2s}\right) = 0.35\left(\frac{t_D}{C_D}\right)_x^{1.24} \tag{2.23}$$

and

$$\log\left(C_De^{2s}\right) = 1.71\left(\frac{t_D}{C_D}m(p'_D)\right)_x^{1.10} \tag{2.24}$$

Substituting Eqs. 2.2 and 2.6 into Eqs. 2.23 and 2.24 yields two new expressions. Combining these new expressions with Eqs. 2.16 and 2.17 gives:

$$\log C_De^{2s} = 0.1485\left(\frac{t_x}{t_i}\right)^{1.24} \tag{2.25}$$

and

$$\log C_D e^{2s} = 0.80\left[\frac{(t\cdot\Delta m(p'))_x}{(t\cdot\Delta m(p'))_i}\right]^{1.10} \tag{2.26}$$

Thus the coordinates of the maximum point (peak) of the pressure derivative can be used also to calculate skin. Solving for skin Eqs. 2.25 and 2.26 give respectively:

$$s = 0.171\left(\frac{t_x}{t_i}\right)^{1.24} - 0.5\ln\left(\frac{0.8935C}{\phi hc_t r_w^2}\right) \tag{2.27}$$

and

$$s = 0.921\left[\frac{(t\cdot\Delta m(p))_x}{(t\cdot\Delta m(p))_i}\right]^{1.1} - 0.5\ln\left(\frac{0.8935C}{\phi hc_t r_w^2}\right) \tag{2.28}$$

Because in some pressure tests the wellbore storage hump may appear to be flat at the "peak", it is possible to read the right value of $(t\cdot\Delta m(p'))_x$ but the wrong value of t_x. In this case, it is a good practice to calculate s from both equations. If they give different values then obtain a new value of t_x and repeat the calculations until the two equations give the same value of skin.

8) An expression relating the infinite-acting radial flow line portion of the pressure derivative curve and the peaks for different values of C_De^{2S} can be derived by dividing Eq. 2.19 with Eq. 2.7:

$$\frac{\left(\frac{t_D}{C_D}m(p'_D)\right)_x}{\left(\frac{t_D}{C_D}m(p'_D)\right)_r} = 2\left[0.36\left(\frac{t_D}{C_D}\right)_x - 0.42\right] \tag{2.29}$$

Using Eqs. 2.2 and 2.6 with Eq. 2.29 we have:

$$\frac{(t\cdot\Delta m(p'))_x}{(t\cdot\Delta m(p'))_r}=2\left[1.062\times10^{-4}\left(\frac{kh}{\mu}\right)\frac{t_x}{C}-0.42\right] \tag{2.30}$$

Eq. 2.30 can be used to calculate C or k. Substituting for kh/μ from Eq. 2.8 and solving for C gives:

$$C=\frac{0.174qT}{(t\cdot\Delta m(p'))_x+0.84(t\cdot\Delta m(p'))_r}\frac{t_x}{\mu} \tag{2.31}$$

Thus, the wellbore storage coefficient can be determined even if the unit slope line is not observed for mechanical reasons or due to lack of early time pressure data. Solving for k Eq. 2.30 yields:

$$k=9416.2\frac{\mu C}{ht_x}\left[0.5\frac{(t\cdot\Delta m(p'))_x}{(t\cdot\Delta m(p'))_r}+0.42\right] \tag{2.32}$$

9) An expression relating the infinite-acting radial flow line portions of the pressure and pressure derivative curves can be derived by dividing Eq. 2.9 with Eq. 2.7:

$$\frac{m(p_{Dr})}{(t_D/C_D)m(p'_D))_r}=\ln t_{Dr}+2s+0.80907 \tag{2.33}$$

Using Eqs. 1.4, 2.2 and 2.6 with Eq. 2.33 and solving for skin we have:

$$s=0.5\left[\frac{\Delta m(p_r)}{(t\cdot\Delta m(p'))_r}-\ln\left(\frac{kt_r}{\phi\mu c_t r_w^2}\right)+7.43\right] \tag{2.34}$$

where t_r is any convenient time during the infinite acting radial flow line and Δp_r is the value of Δp corresponding to t_r.

3. PROCEDURE

The following step-by-step procedure is for the ideal case where both the early time unit-slope line and the late time infinite acting radial flow line have **definitely** been observed, and are **well defined**.

Step 1 - Plot $\Delta m(p)$ and $t \cdot \Delta m(p')$ versus time on a log-log graph.

Step 2 - Draw the unit-slope line corresponding to the wellbore storage flow regime using early-time pressure and pressure derivative points. If there is too much noise in the derivative values, it is recommended to draw the unit-slope line using only pressure points.

Step 3 - Draw the infinite acting radial flow line using late-time pressure derivative points. This line is, of course, horizontal.

Step 4 - Read the coordinates of the point where the unit-slope line and the infinite-acting horizontal line intersect: t_i and $\Delta m(p_i)$. Note that $\Delta m(p_i) = (t \cdot \Delta m(p'))_i = (t \cdot \Delta m(p'))_r$ in all steps.

Step 5 - Read the coordinates of the maximum point (peak) on the pressure derivative curve: t_x and $(t \cdot \Delta m(p'))_x$

Step 6 - Select any convenient time t_r during infinite acting radial flow and read $\Delta m(p_r)$ from the pressure curve.

Step 7 - Calculate the permeability from Eq. 2.8.

Step 8 -Calculate the wellbore storage coefficient from Eq. 2.3 using t_i and $\Delta m(p_i)$, or any convenient t and $\Delta m(p)$ values on the unit slope line.

Step 9 - Calculate the skin factor from Eq. 2.34.

Step 10 - This step is used to verify the correctness and accuracy of the permeability, skin and wellbore storage. This step is necessary only if there is considerable noise in the pressure derivative value. Recalculate permeability using Eq. 2.32. If the values of k obtained from Eqs. 2.8 and 2.32 are approximately equal, this means the peak, the unit-slope and horizontal lines are in their correct "location", and therefore, the values of k, s and C are correct. However, if the two values of k are significantly different, obtain a

new peak and/or shift one or both straight lines and repeat Steps 4 through 9 until the values of t_i and $\Delta m(p_i)$ give similar values of k. The decision of which straight lines should be shifted or whether a new peak should be obtained is really a function of the quality of data. For instance, if the infinite-acting line (horizontal line) portion of the derivative curve is well defined, the value of k and s obtained in Steps 7 and 9 are correct. In this case the unit slope line should be shifted and/or a new peak selected and a new value of C calculated such that the value of k obtained from Eq. 2.32 is similar to the one obtained in Step 7.

5. NOMENCLATURE

b_x See Eq. 2.21

c_t Total system compressibility, psi^{-1}

C Wellbore storage coefficient, RB/psi

C_D Dimensionless storage constant

h Formation thickness, feet

$J_0(u)$ Bessel function of the first kind, order zero

$J_1(u)$ Bessel function of the first kind, order one

k Formation permeability

$m(P_D)$ Dimensionless wellbore pseudo-pressure drop

$m(P_D')$ Dimensionless wellbore pseudo-pressure derivative

$m(P_i)$ Initial pseudo-pressure, psi

$m(P_{wf})$ Wellbore flowing pseudo-pressure, psi

q Surface rate, STB/day

r_w Wellbore radius, ft

s skin factor

t Test time, h

t_D Dimensionless time

t_{DSR} Dimensionless time reflecting time at which storage effects can be assumed to be negligible or start of infinite acting line

$Y_0(u)$ Bessel function of second kind, order zero

$Y_1(u)$ Bessel function of second kind, order one

α Tolerance, fraction

m Viscosity, cp

f Porosity, fraction of bulk volume

Subscripts

D	Dimensionless quantity
i	Initial conditions or intersection
w	Well
wf	Flowing conditions
ws	Shut-in condition
x	Maximum point or peak
r	radial flow
SR	Start of radial flow line

Determining Pressure Derivatives

The derivative at a point is determined by finding a weighted mean of the slopes to a preceding point and a following point (**Fig. F-1**). The parameter L defines the minimum abscissa distance to these points, smoothing out "noise" in the neighborhood of the central point. Thus, L can be defined as $\Delta(\ln t)$ for a flow test or as $\Delta(\ln \Delta t_e)$ for a buildup test. Experience indicates that $0.1 \le L \le 0.3$ often is a satisfactory compromise between being too far from the central point so that detail is lost and being too near the central point so that a great amount of noise is introduced. However, trial and error may indicate that other values of L are more appropriate in a given situation.

The pressure derivative calculation procedure is best illustrated with an example taken from field data. Suppose that we want to determine the derivative $-dp_{wf}/d\ \ln t = d(\Delta p)/d\ \ln(\Delta t)$ at $\Delta t = 23.96$ hours from the drawdown data in **Table F-1** and that we choose $L = \Delta(\ln t) = 0.3$. We first calculate $\ln(\Delta t)$ for all test times, obtaining $\ln(23.96) = 3.1764$ at $\Delta t = 23.96$ hours. Then $3.1764 - L = 3.1764 - 0.3 = 2.8764$, and $3.1764 + L = 3.1764 + 0.3 = 3.4764$, as shown in the last column of Table F-1, creating a "window" around the central point. We use the data points just beyond this window to calculate the pressure derivative, m_P:

$$\Delta t_L = 3.1764 - 2.7713 = 0.4051.$$

$$\frac{\Delta p_L}{\Delta t_L} = \frac{(850-839)}{0.4051} = 27.1538 = m_L.$$

$$\Delta t_R = 3.6859 - 3.1764 = 0.5095.$$

$$\frac{\Delta p_R}{\Delta t_R} = \frac{(864-850)}{0.5095} = 27.4779 = m_R.$$

$$m_P = \frac{m_L \Delta t_R + m_R \Delta t_L}{\Delta t_L + \Delta t_R}$$

$$= \frac{(27.1538)(0.5095) + (27.4779)(0.4051)}{(0.4051 + 0.5095)} = 27.30.$$

SI Metric Conversion Factor

psi × 6.894 767 E+00 = kPa

TABLE F-1—DATA FOR DERIVATIVE CALCULATION

Δt (hours)	Δp (psi)	ln(Δt)	Derivative Window
11.99	830	2.4841	
15.98	839	2.7713	
			2.8764
19.97	845	2.9942	
23.96	850	3.1764	3.1764
29.93	859	3.3989	
			3.4764
39.88	864	3.6859	
49.32	869	3.8983	

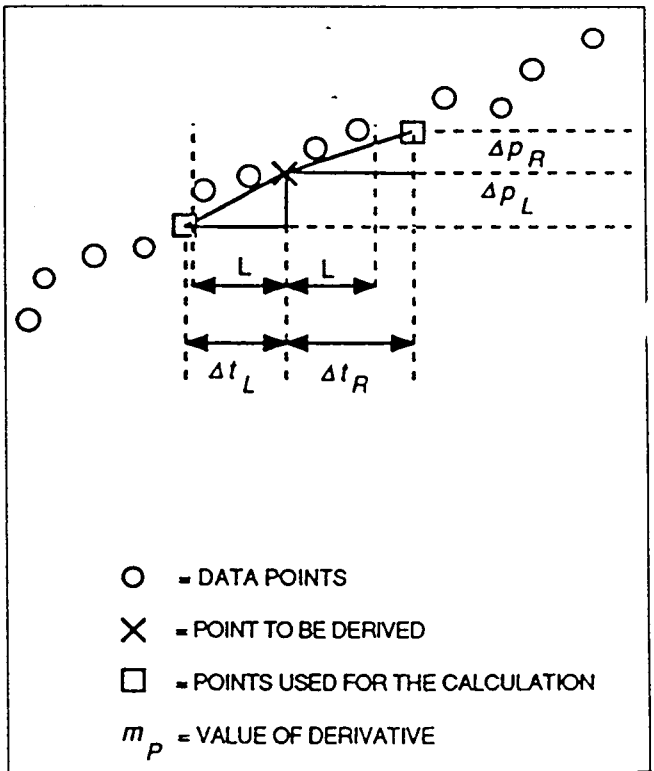

Fig. F-1—Calculation of pressure derivative.

EXAMPLE

A build-up test was run in a gas well located in the center of a large circular reservoir with low-permeability.

Given well and reservoir data:

$T = 673^{o}R$

$h = 20$ ft

$\phi = 0.10$

$r_e = 2640$

$r_w = 0.29$

$p_i = 3732$ psia

$m(p_i) = 872.7 \times 10^6$ psi^2/cp

$q = 5650$ Mscf/D

$\mu_i = 0.0208$ cp

$c_i = 22 \times 10^{-5}$ psi^{-1}

$SG = 0.68$

$p_{ws}(dt = 0) = 3295$ psia

$m(p_{ws})_0 = 709.77 \times 10^6$ psia^2/cp

$t_p = 120.53$ hrs

$c_{ws} = 45 \times 10^{-5}$ psi^{-1} (wellbore fluid comp)

$D = 12{,}000$ ft

Table D1 includes the pressure and pseudo-pressure data.

Find

1. Wellbore storage coefficient, C
2. Reservoir permeability, k
3. Skin factor, s

Solution

A. Using the Pressure Approach

Procedure:

1. Calculate t*ΔP' using Bourdet algorithm (Table of data).
2. Plot ΔP and t*ΔP' vs. t on log-log graph as in Fig.1.
3. Draw the unit slope, and infinite acting lines
4. Read the following points.

t_x , $(t^*\Delta P')_x$, t_i , $(t^*\Delta P')_i$, $(t^*\Delta P')_r$, and $(\Delta P)_r$

$(t^*\Delta P')_x$ = 280 psi, t_x = 2.6 hr

a) $(t^*\Delta P')_r$= 58 psi $(\Delta P)_r$ = 335 psia t_r = 9.07 hr

b) $(t^*\Delta P')_r$= 30 psi $(\Delta P)_r$ = 381 psia t_r =29.33 hr

B_g = 0.6744, calculated as a function of T, SG, T_{pc}, P_{pc},, z.

5. Calculate permeability, k

a) $$k = \frac{70.6q\mu B_g}{(t\cdot\Delta P')_r h} = \frac{70.6(5650)(0.0208)(0.6744)}{(58)(20)} = 4.83 \text{ md}$$

b) $$k = \frac{70.6q\mu B_g}{(t\cdot\Delta P')_r h} = \frac{70.6(5650)(0.0208)(0.6744)}{(30)(20)} = 9.32 \text{ md}$$

6. Calculate wellbore storage coefficient, C

$$C = \frac{0.015qBt_x}{(t*\Delta P')_x + 0.84(t*\Delta P')_r} = \frac{0.015(5650)(0.6744)(2.6)}{280+0.84(58)} = 0.452$$

7. Calculate skin, S

a)

$$S = \left\{\frac{\Delta P_r}{(t*\Delta P')_r} - \ln\left(\frac{kt_r}{\phi\mu c_t r_w{}^2}\right) + 7.43\right\} =$$

$$0.5\left\{\frac{335}{58} - \ln\left(\frac{4.83(9.07)}{(0.1)(0.0208)(22x10^{-5}(0.29)^2}\right) + 7.43\right\} = -4.33$$

b)

$$S = \left\{\frac{\Delta P_r}{(t*\Delta P')_r} - \ln\left(\frac{kt_r}{\phi\mu c_t r_w{}^2}\right) + 7.43\right\}$$

$$= 0.5\left\{\frac{381}{30} - \ln\left(\frac{9.32(29.33)}{(0.1)(0.0208)(22x10^{-5}(0.29)^2}\right) + 7.43\right\} = -2.55$$

B. Using the Pseudo-Pressure Approach

Procedure:

1. Calculate t*Δm(P)' using Bourdet algorithm (Table of data).
2. Plot Δm(P) and t*Δm(P)' Vs t on log-log graph as in Fig. 2.
3. Draw the unit slope, and infinite acting lines
4. Read the following points

t_x , $(t^*\Delta m(P)')_x$, t_i , $(t^*\Delta m(P)')_i$, $(t^*\Delta m(P)')_r$, and $(\Delta m)P))_r$

$(t^*\Delta m(P)')_x$ = 280 psiam, t_x = 2.6 hr

a) $(t^*\Delta m(P)')_r$= 21.8 x10^6 psia $(\Delta m(P))_r$ =125 psia, t_r = 9.07 hr

b) $(t^*\Delta m(P)')_r$=11.23x10^6 psia $(\Delta m(P))_r$ =142 psia, t_r = 29.33 hr

5. Calculate permeability, k

a) $$k = 818.866\frac{qT}{(t\cdot\Delta m(P)')_r h} = \frac{818.866(5650)(673)}{(21.8)(20)} = 7.13 \text{ md}$$

b) $$k = 818.866\frac{qT}{(t\cdot\Delta m(P)')_r h} = \frac{818.866(5650)(673)}{(11.23)(20)} = 13.86 \text{ md}$$

6. Calculate wellbore storage coefficient, C

$$C = \frac{0.174qTt_x/\mu}{(t\cdot\Delta m(p'))_x + 687.85qT/(kh)} =$$

$$= \frac{0.174(5650)(673)}{(100x10^6) + (687.85)(5650)(673)/[(7.13)(20)]}\frac{2.6}{0.0208} = 0.698$$

7. Calculate skin, S

a)

$$s = 0.5\left[\frac{\Delta m(p_r)}{(t\cdot\Delta m(p'))_r} - \ln\left(\frac{kt_r}{\phi\mu c_t r_w^2}\right) + 7.43\right] =$$

$$0.5\left\{\frac{125}{21.8} - \ln\left(\frac{7.13(9.07)}{(0.1)(0.0208)(22x10^{-5}(0.29)^2}\right) + 7.43\right\} = -4.039$$

b)

$$s = 0.5\left[\frac{\Delta m(p_r)}{(t\cdot\Delta m(p'))_r} - \ln\left(\frac{kt_r}{\phi\mu c_t r_w^2}\right) + 7.43\right] =$$

$$0.5\left\{\frac{142}{11.23} - \ln\left(\frac{13.86(29.33)}{(0.1)(0.0208)(22x10^{-5}(0.29)^2}\right) + 7.43\right\} = -1.503$$

TABLE OF DATA

dt	(tp+dt)/dt	P_{ws}	Dp_{ws}	dt*Dp'	$m(p_{ws})$,	$Dm(p_{ws})$,	$t*Dm'(p_{ws})$
hrs		psia	psia	psia	$psia^2/cpx10^{-6}$	$psia^2/cpx10^{-6}$	$psia^2/cpx10^{-6}$
1.6	76.33	3385	90	181.2318	742.69	32.92	689.5374827
2.67	46.14	3547	252	265.6492	802.81	93.04	802.81
4.27	29.23	3582	287	76.55714	815.94	106.17	815.94
6.4	19.83	3609	314	67.46384	826.1	116.33	826.1
9.07	14.29	3630	335	57.98746	834.01	124.24	834.01
12	11.04	3644	349	50.85313	839.3	129.53	839.3
14.67	9.22	3654	359	50.45183	843.08	133.31	843.08
16.53	8.29	3660	365	42.89478	845.35	135.58	845.35
18.67	7.46	3664	369	31.85572	846.87	137.1	846.87
21.33	6.65	3668	373	29.61823	848.38	138.61	848.38
24.53	5.91	3672	377	26.57417	849.9	140.13	849.9
29.33	5.11	3676	381	29.67917	851.41	141.64	851.41
35.73	4.37	3684	389	32.83456	854.45	144.68	854.45
45.87	3.63	3688	393	29.78925	855.97	146.2	855.97
49.87	3.42	3691	396		857.1	147.33	

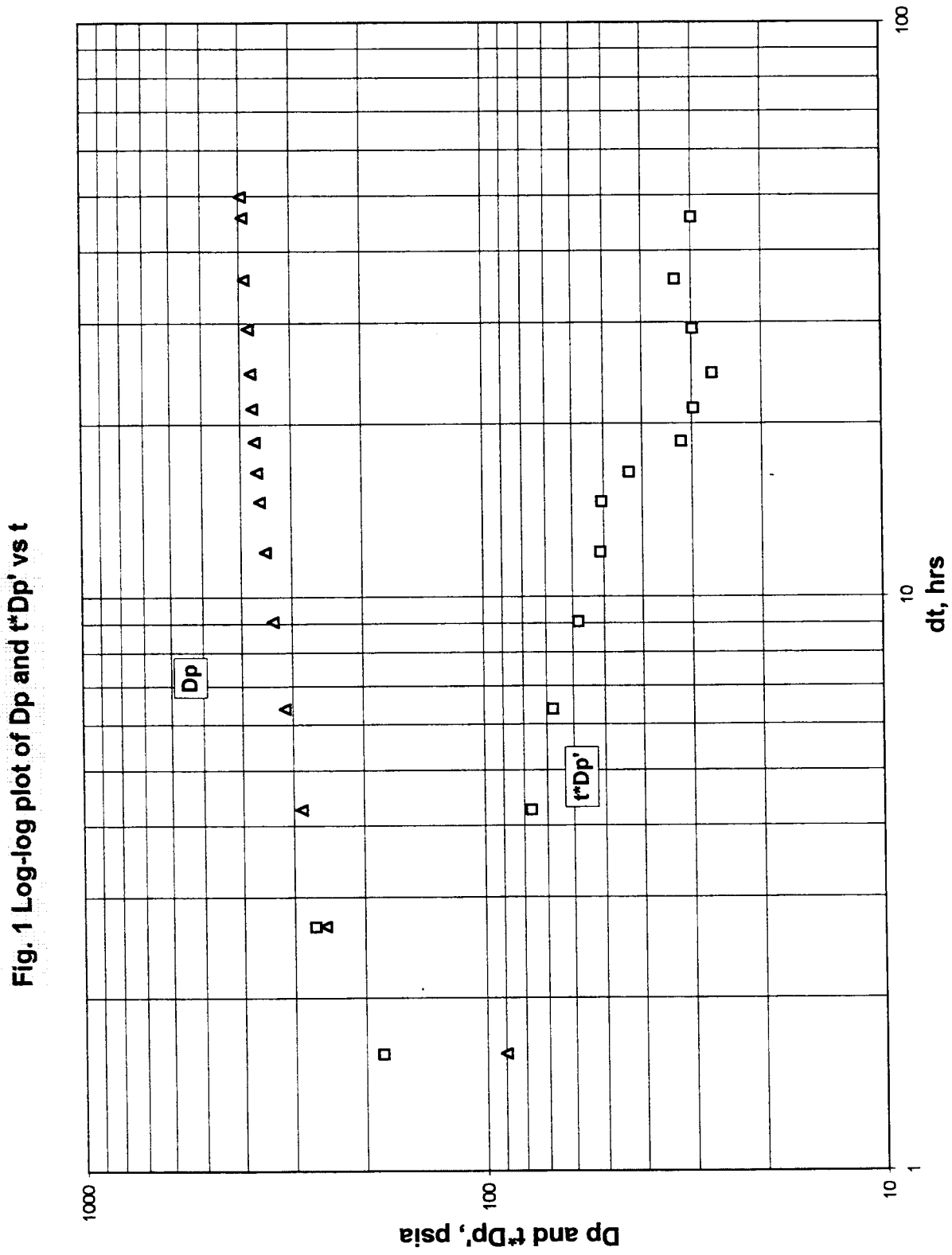

Fig. 1 Log-log plot of Dp and t*Dp' vs t

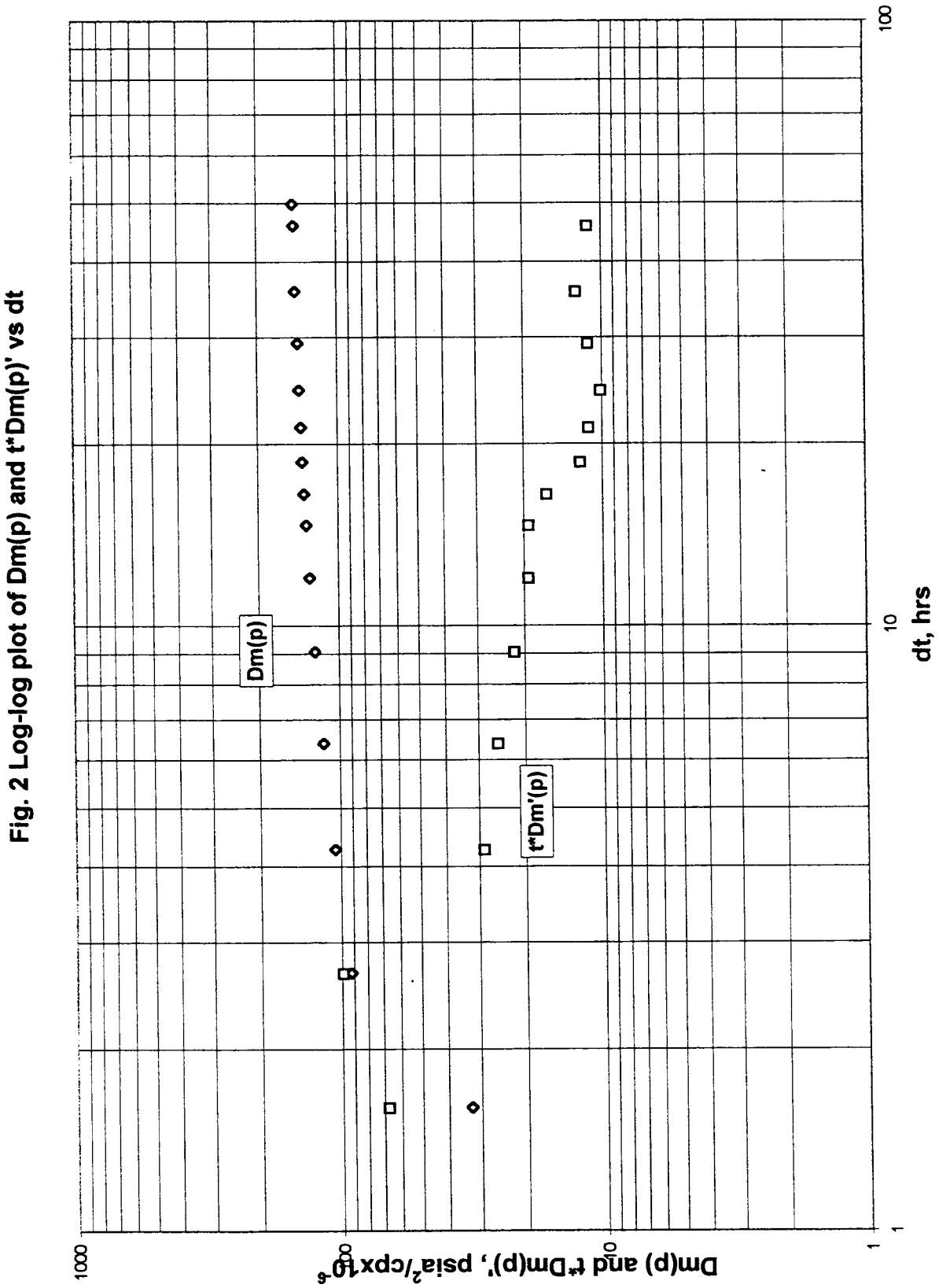

Fig. 2 Log-log plot of Dm(p) and t*Dm(p)' vs dt

Fig. 3a. Semilog plot of Pws vs (tp+dt)/dt

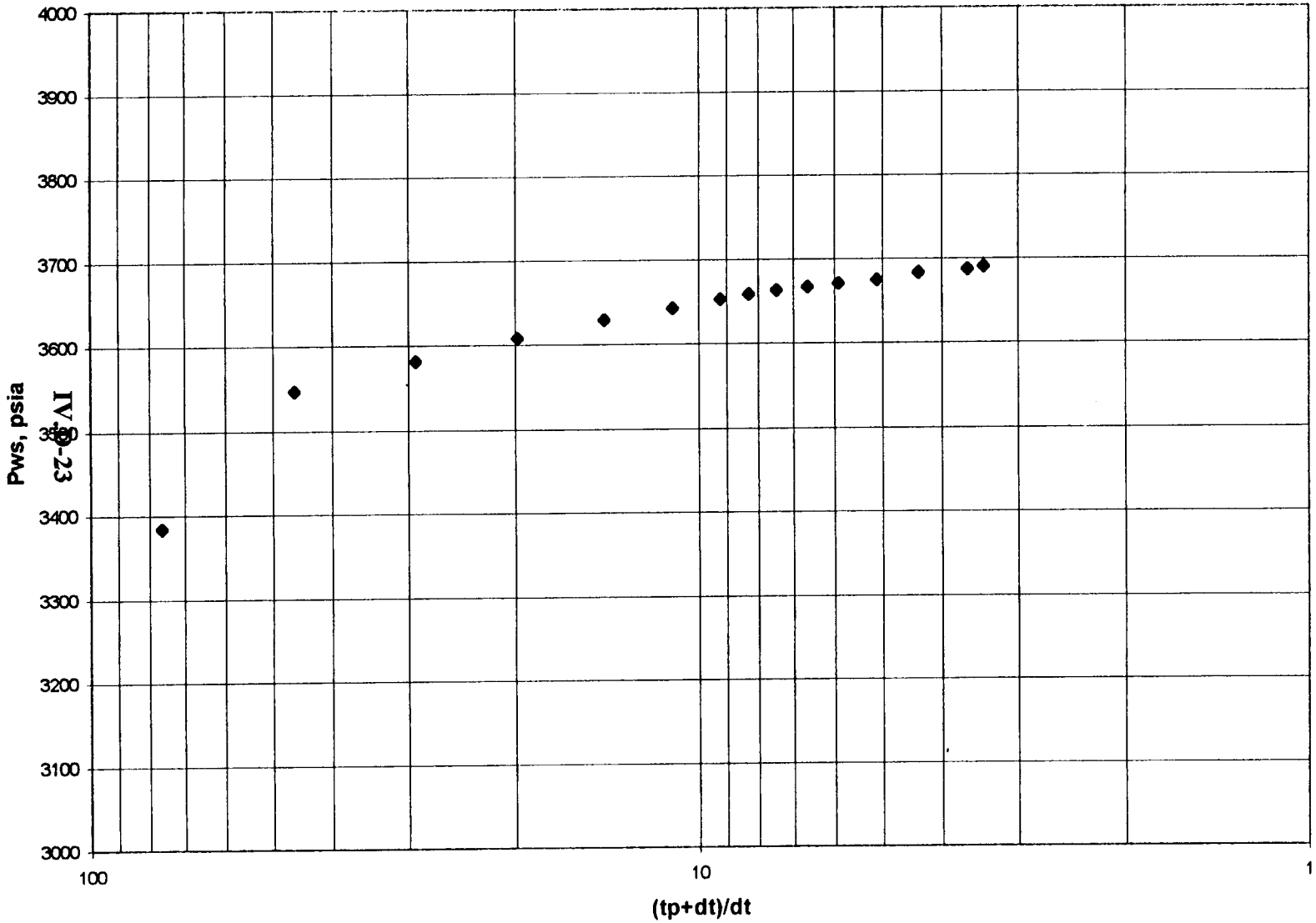

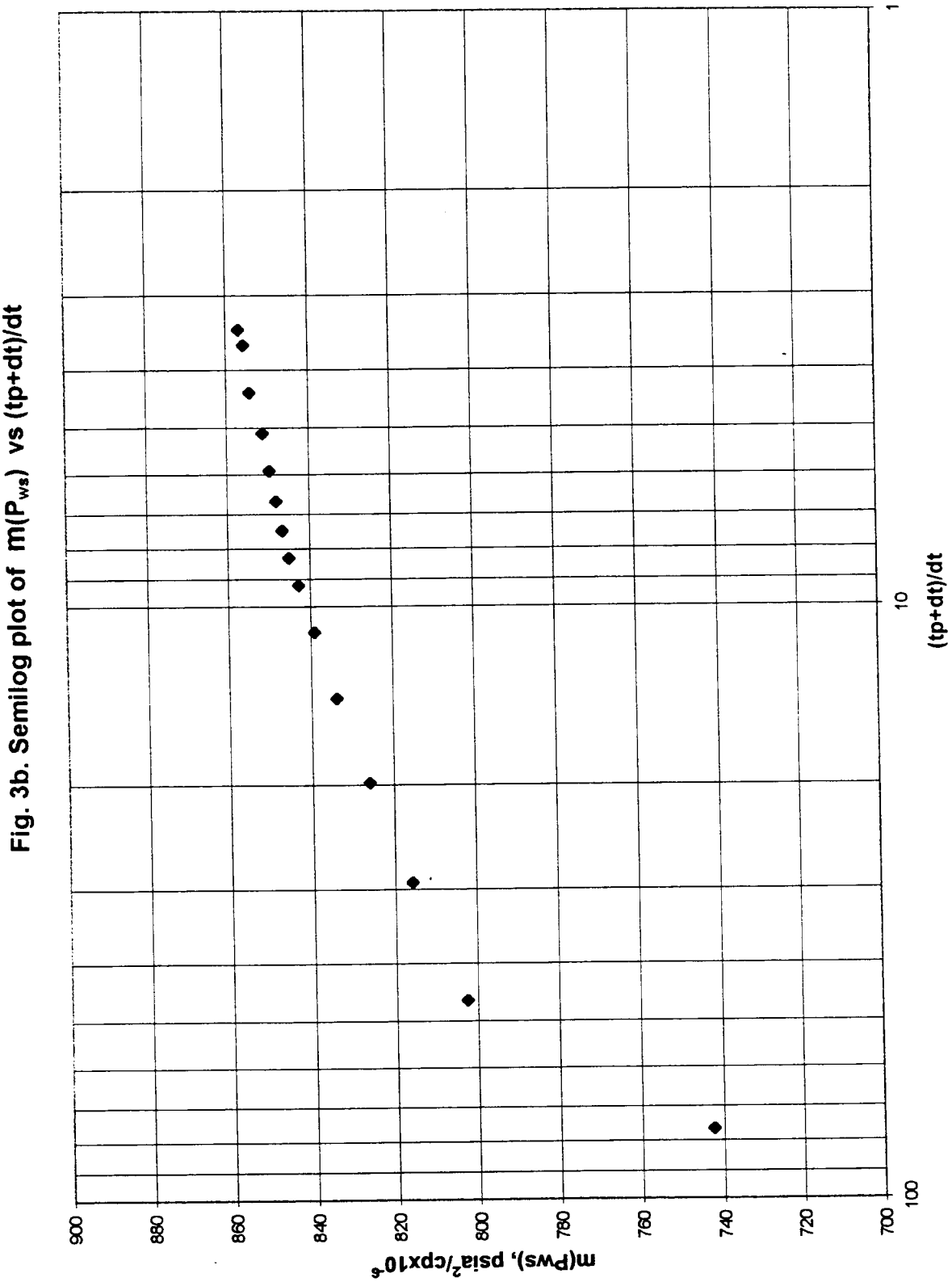

Fig. 3b. Semilog plot of $m(P_{ws})$ vs (tp+dt)/dt

PART 5

DELIVERABILITY TESTING

OF GAS WELLS

DELIVERABILITY TESTING OF GAS WELLS

5.1 TYPES AND PURPOSES OF DELIVERABILITY TESTS

Deliverability testing refers to the testing of a gas well to measure its production capabilities under specific conditions of reservoir and bottomhole flowing pressures (BHFP's). A common productivity indicator obtained from these tests is the absolute open-flow (AOF) potential. The AOF is the maximum rate at which a well could flow against a theoretical atmospheric backpressure at the sandface. Although in practice the well cannot produce at this rate, regulatory agencies often use the AOF to establish field proration schedules or to set maximum allowable production rates for individual wells.

Another, and possibly more important, application of deliverability testing is to generate a reservoir inflow performance relationship (IPR) or gas backpressure curve. The IPR curve describes the relationship between surface production rate and BHFP for a specific value of reservoir pressure (i.e., either the original pressure or the current average value). The IPR curve can be used to evaluate gas-well current deliverability potential under a variety of surface conditions, such as production against a fixed backpressure. In addition, the IPR can be used to forecast future production at any stage in the reservoir's life.

Several deliverability testing methods have been developed for gas wells. Flow-after-flow tests are conducted by producing the well at a series of different stabilized flow rates and measuring the stabilized bottomhole pressure (BHP). Each flow rate is established in succession without an intermediate shut-in period. A single-point test is conducted by flowing the well at a single rate until the BHFP is stabilized. This type of test was developed to overcome the limitation of long testing times required to reach stabilization in the flow-after-flow test.

The isochronal and modified isochronal tests also were developed to shorten test times for wells that need long periods to stabilize.

An isochronal test consists of a series of single-point tests usually conducted by alternately producing at a stabilized (or slowly declining) sandface rate and then shutting in and allowing the well to build to the average reservoir pressure before the next flow period. The modified isochronal test is conducted similarly, except the flow periods are of equal duration and the shut-in periods are of equal duration (but not necessarily the same as the flow periods).

5.2 THEORY OF DELIVERABILITY TEST ANALYSIS

This section summarizes the theoretical and empirical gas-flow equations used to analyze deliverability tests. The theoretical equations, developed by Houpeurt,[1] are exact solutions to the generalized radial-flow diffusivity equation, while the Rawlins and Schellhardt[2] equation is derived empirically. All basic equations presented here were developed with radial flow in a homogeneous, isotropic reservoir assumed and therefore are not applicable to the analysis of deliverability tests from reservoirs with heterogeneities, such as natural fractures or layered pay zones. These equations also cannot be used to analyze tests from hydraulically fractured wells, especially during the initial, fracture-dominated, linear flow period. Finally, these equations assume that wellbore-storage effects have ceased. Unfortunately, wellbore-storage distortion may affect the entire test period in short tests, especially those conducted in low-permeability reservoirs.

5.2.1 **Theoretical Deliverability Equations.** The generalized diffusivity equation for radial flow of a real gas through a homogeneous, isotropic porous medium is

$$\frac{1}{r}\frac{\partial}{\partial r}\left(r\frac{p}{\mu_g z}\frac{\partial p}{\partial r}\right)\frac{1}{0.0002637}=\frac{\phi c_t p}{k_g z}\frac{\partial p}{\partial t}, \tag{5.1}$$

Because of the pressure dependence of the gas properties, Eq. 5.1 is a nonlinear partial-differential equation; however, Eq. 5.1 can be linearized partially with several limiting assumptions. If we assume that the quantity $p/\mu_g z$ is constant with respect to pressure and that $\mu_g c_t$, can be evaluated at $\bar{p}$ and treated as constant, Eq. 5.1 can be solved in terms of pressure. With these assumptions, Eq. 5.1 becomes

$$\frac{1}{r}\frac{\partial}{\partial r}\left(r\frac{\partial p}{\partial r}\right)=\frac{\phi\mu_g c_t}{0.0002637k_g}\frac{\partial p}{\partial t}, \tag{5.2}$$

which is the same linear differential equation that we solve for slightly compressible liquid flow. The solution is the familiar exponential integral (E_i) solution.

The assumptions made to obtain Eq. 5.2 generally are valid only for very high pressures and temperatures. Figs. 5.1 through 5.3, which show the relationship between pressure and $p/\mu_g z$ at different temperatures for various gas gravities, illustrate that $p/\mu_g z$ is essentially constant with pressure at pressures exceeding 3,000 psia for 100°F, 5,000 psia for 200°F, and 6,500 psia for 300°F.

Note that $p/\mu_g z$ varies with pressure more at high gas gravity. Figs. 5.1 through 5.3 imply that the solutions to the real-gas diffusivity equation in terms of pressure should be used only for gases at very high pressures.

As an alternative solution, we can rewrite Eq. 5.1 in terms of pressure-squared variables using the following relationships:

$$p\frac{\partial p}{\partial r}=\frac{1}{2}\frac{\partial p^2}{\partial r}, \tag{5.3}$$

$$p\frac{\partial p}{\partial t} = \frac{1}{2}\frac{\partial p^2}{\partial t}, \tag{5.4}$$

Substituting Eqs. 5.3 and 5.4 into Eq. 5. I yields the resulting equation:

$$\frac{1}{r}\frac{\partial}{\partial r}\left(\frac{r}{\mu_g z}\frac{\partial p^2}{\partial r}\right) = \frac{\phi c_t}{0.0002637 k_g z}\frac{\partial p^2}{\partial t}, \tag{5.5}$$

If we assume that , $\mu_g z$ is constant with pressure and that $\mu_g c_g$ can be evaluated at $\bar{p}$ and treated as constant, Eq. 5.5 becomes

$$\frac{1}{r}\frac{\partial}{\partial r}\left(r\frac{\partial p^2}{\partial r}\right) = \frac{\phi \mu_g c_t}{0.0002637 k_g}\frac{\partial p^2}{\partial t}, \tag{5.6}$$

which is a linear differential equation in the variable p2 and thus has the familiar Ei-function solution. The assumption of constant $\mu_g z$ is valid only for very low pressures and gas gravities at high temperatures. Figs. 5.4 through 5.6 illustrate the variation of the product $\mu_g z$ with pressure for different gas gravities at 100, 20O, and 300°F, respectively. Note that $\mu_g z$ is essentially constant with pressure at pressures < 1,200 psia for 100°F, < 1,750 psia for 200°F, and <2,200 psia for 300°F. The ~gz product varies with pressure more at higher gas gravities. Therefore, solutions to the real-gas diffusivity equation should be used in terms of pressure squared only at very low pressures and gas gravities at high temperatures.

A more rigorous method of linearizing Eq. 5.1 is with the real gas pseudopressure transformation introduced by Al-Hussainy et al.,[3]

$$p = 2\int_{p_o}^{p} \frac{p}{\mu_g z} dp, \tag{5.7}$$

With the pseudopressure transformation, Eq. 5.1 can be solved without the limiting assumptions that certain gas properties are constant with pressure. Eq. 5.1 can be written in terms of the pseudopressure function as

$$\frac{1}{r}\frac{\partial}{\partial r}\left(r\frac{\partial p_p}{\partial r}\right) = \frac{\phi\mu_g(p)c_t(p)}{k_g}\frac{\partial p_p}{\partial t}, \tag{5.8}$$

Eq. 5.8 is not completely linear because $\mu_g(p)c_t(p)$ depends on pressure and pseudopressure. An acceptable approximation is the assumption that $\mu_g c_t$ is constant and can be evaluated at some p. We denote this product $\mu_g z$. Thus, familiar solutions, such as the Ei-function solution, are reasonably accurate for gas wells when we use the pseudopressure transformation.

The early-time or transient solution to Eq. 5.8 for constant-rate production from a well in a reservoir with closed outer boundaries is

$$p_p(p_s) - p_p(p_{wf}) = \frac{1.422x10^6 qT}{k_g h} x\left[1.151\cdot\log\left(\frac{k_g t}{1{,}688\phi\bar{\mu}_g\bar{c}_t r_w^2}\right) + s + Dq\right] \tag{5.9}$$

where p_S=the stabilized shut-in BHP measured before the deliverability test. In new reservoirs with little or no pressure depletion, this shut-in pressure equals the initial reservoir pressure (ps =P~), while in developed reservoirs, Ps <Pi

The late-time or pseudo steady-state solution to Eq. 5.8 is

$$p_p(\bar{p}) - p_p(p_{wf}) = \frac{1.422x10^6 qT}{k_g h} x\left[1.151 \cdot \log\left(\frac{10.06A}{C_A r_w^2}\right) - \frac{3}{4} + s + Dq\right] \quad (5.10)$$

where p_s = current drainage area pressure. Gas wells cannot reach true pseudosteady state because $\mu_g(p)c_t(p)$ changes asp decreases. Note that, unlike $\bar{p}$(which decreases during a pseudosteady-state flow test), p_s remains constant.

Eqs. 5.9 and 5.10 are quadratic in terms of the gas flow rate, q. For convenience, Houpeurt[1] wrote the transient flow equation as

$$\Delta p_p = p_p(p_s) - p_p(p_{wf}) = a_t q + bq^2 \quad (5.11)$$

and the pseudosteady state flow equation as

$$\Delta p_p = p_p(\bar{p}) - p_p(p_{wf}) = aq + bq^2 \quad (5.12)$$

where

$$a_t = \frac{1.422x10^6 T}{k_g h} x\left[1.151 \cdot \log\left(\frac{k_g t}{1{,}688\phi\bar{\mu}_g \bar{c}_t r_w^2}\right) + s\right] \quad (5.13)$$

$$a = \frac{1.422x10^6 T}{k_g h} x\left[1.151 \cdot \log\left(\frac{10.06A}{C_A r_w^2}\right) - \frac{3}{4} + s\right] \quad (5.14)$$

and

$$b = \frac{1.422x10^6 TD}{k_g h} \quad (5.15)$$

The coefficients of q(at for transient flow and a for pseudosteady state flow) include the Darcy flow and skin effects and are measured in (psia2-cp)/(MMscf-D) when q is in MMscf/D. The coefficient of the q2 term represents the inertial and turbulent flow effects and is measured in (psia2-cp)/(MMscf-D)2 when q is in MMscf/D. Commonly called non-Darcy effects, the inertial and turbulent flow effects result from high gas velocities near the wellbore and consequently cannot be modeled with Darcy's law. The non-Darcy flow coefficient, D, is defined in terms of a turbulence factor, β, which has been correlated with rock properties, permeability, and porosity,[4]

$$D = \frac{2.715 \times 10^{-12} \beta k_g M p_{sc}}{h \mu_g (p_{wf}) r_w T_{sc}} \tag{5.16}$$

$$\beta = 1.88 \times 10^{10} k^{-1.47} \phi^{-0.53} \tag{5.17}$$

where μ_g is evaluated at P_{wf}. Note that, because ,μ_g is not constant with respect to pressure, D and the coefficient b are not strictly constant at different BHFP's; however, the assumption of a constant D is adequate for most practical applications.

The Houpeurt equations also can be written in terms of pressure squared and are derived directly from the solutions to the gas diffusivity equation, assuming that $\mu_g z$ is constant over the pressure range considered. For transient flow,

$$\Delta p^2 = p_s^2 - p_{wf}^2 = a_t q + D q^2, \tag{5.18}$$

and for pseudosteady-state flow,

$$\Delta p^2 = \bar{p}^2 - p_{wf}^2 = aq + bq^2, \tag{5.19}$$

Then flow coefficients are

$$a_t = \frac{1.422x10^6 \bar{\mu}_g \bar{z}\bar{T}}{k_g h} x\left[1.151 \cdot \log\left(\frac{k_g t}{1{,}688\bar{\phi}\bar{\mu}_g \bar{c}_t r_w^2}\right) + s\right] \tag{5.20}$$

$$a = \frac{1.422x10^6 \bar{\mu}_g \bar{z}\bar{T}}{k_g h} x\left[1.151 \cdot \log\left(\frac{10.06A}{C_A r_w^2}\right) - \frac{3}{4} + s\right] \tag{5.21}$$

and

$$b = \frac{1.422x10^6 \bar{\mu}_g \bar{z}\bar{T}D}{k_g h} \tag{5.22}$$

When the Houpeurt equation is presented in terms of pressures squared, the coefficients of q are measured in psia^2/(MMscf-D) when q is in MMscf/D, while the coefficient of q^2 is measured in units of psia^2/(MMscf-D)^2 when q is in MMscf/D. The units of the flow coefficients given by Eqs. 5.11 through 5.13 and 5.18 through 5.20 vary depending on the units of flow rate and whether the pseudopressure or pressure-squared formulation is used. For consistency, all equations and example problems in this chapter are presented with q measured in MMscf/D.

Recall from previous discussions that, because of the nonlinear behavior of the gas properties at high pressures, the pressure-squared form of the equation should be used only for gas reservoirs at low pressures and high temperatures. To eliminate doubt about which equations to choose, we recommend using the pseudopressure equations, which are applicable at all pressures and temperatures. Consequently, all the analysis procedures in

this chapter are presented in terms of pseudopressure. The same procedures and example problems, however, are presented in terms of pressure squared (Examples 5.5-5.9).

An advantage of the pseudopressure form of the theoretical deliverability equation is that the flow coefficients are independent of the average reservoir pressure and therefore do not change as p- decreases during a flow test conducted under pseudosteady-state flow unless s, k, or A changes. Because of the dependency of the non-Darcy flow coefficient on $\mu_g(P_{wf})$, only the coefficient b will change slightly if the BHFP is changed. Conversely, because of the pressure dependency of the gas properties on average reservoir pressure, the flow coefficients for the pressure-squared form of the deliverability equation must be recalculated for every new $\bar{p}$ value. When s, k, or A changes with time, the only way to update the deliverability curve is to retest the well.

5.2.2 Empirical Deliverability Equations.

In 1935, Rawlins and Schellhardt[2] presented an empirical relationship that is used frequently in deliverability test analysis. The original form of their relation given by Eq. 5.23 in terms of pressure squared, is applicable only at low pressures:

$$q = C\left(\bar{p}^2 - p_{wf}^2\right)^n \tag{5.23}$$

In terms of pseudopressure, Eq. 5.23 becomes

$$q = C\left[p_p(\bar{p}) - p_p(p_{wf})\right]^n \tag{5.24}$$

which is applicable over all pressure ranges. In Eqs. 5.23 and 5.24, C = stabilized performance coefficient and n = inverse slope of the line on a log-log plot of the change

in pressure squared or pseudopressure vs. gas flow rate. Depending on the flowing conditions, the theoretical value of n ranges from 0.5, indicating turbulent or non-Darcy flow, to 1.0, indicating flow behavior described by Darcy's equation. Note that the value of C changes depending on the units of flow rate and whether Eq. 5.23 or 5.24 is used. Again, all equations and example problems in this chapter are presented with q measured in MMscf/D.

Houpeurt proved that neither Eq. 5.23 nor Eq. 5.24 can be derived from the generalized diffusivity equation for radial flow of real gas through porous media. Although the Rawlins and Schellhardt equation is not theoretically rigorous, it is still used widely in deliverability analysis and has worked well over the years, especially when the test rates approach the AOF potential of the well and the extrapolation is minimal.

5.3 STABILIZATION TIME

Unlike pressure-transient tests, the analysis techniques for conventional flow-after-flow and single-point tests require data obtained under stabilized flowing conditions. Although isochronal and modified isochronal tests were developed to circumvent the requirement of stabilized flow, they still may require a single, stabilized flow period at the end of the test. Consequently, we must understand the meaning of stabilization time and have a method to estimate its value.

Stabilization time is defined as the time when the flowing pressure is no longer changing or is no longer changing significantly. Physically, stabilized flow can be interpreted as the time when the pressure transient is affected by a no-flow boundary, either a natural reservoir boundary or an artificial boundary created by active wells surrounding the tested well. Consider a graph of pressure as a function of radius for constant-rate flow at various times since the beginning of flow. As Fig. 5.7 shows, the pressure in the wellbore continues to decrease as flow time increases. Simultaneously, the area from which fluid is drained increases, and the pressure transient moves further out into the reservoir.

The radius of investigation, the point in the formation beyond which the pressure drawdown is negligible, is a measure of how far a transient has moved into a formation following any rate change in a well. The approximate position of the radius of investigation at any time is estimated by[5]

$$r_i = \sqrt{\frac{k_g t_s}{948\phi\bar{\mu}_g\bar{c}_t}} \tag{5.25}$$

Stabilized flowing conditions occur when the radius of investigation equals or exceeds the distance to the no-flow boundary of the well, i.e., $r_i \geq r_e$ Substituting r_e and rearranging Eq. 5.25, we can develop an equation for estimating the stabilization time, t_s, for a well centered in a circular drainage area:

$$t_s = \frac{948\phi\bar{\mu}_g\bar{c}_t r_e^2}{k_g} \tag{5.25}$$

As long as the radius of investigation is less than the distance to the no-flow boundary, stabilization has not been attained and the pressure behavior is transient. To illustrate the importance of stabilization times in deliverability testing, we calculated stabilization times as a function of permeability and drainage area for a well producing a gas with a specific gravity of 0.6 from a formation at 210°F and an average pressure of 3,500 psia (μ_g = 0.02 cp and $\bar{c}_g = 2.468\text{x}10^{-4}$ psia^{-1}), with a porosity of 10%. Table 5.1 shows that, for wells completed in low-permeability reservoirs, several days, if not years, are required to reach stabilized flow, while wells completed in high-permeability reservoirs stabilize in a short time.

A more general equation for calculating stabilization time is

$$t_s = \frac{\phi \bar{\mu}_g \bar{c}_t A t_{DA}}{0.0002637 k_g} \tag{5.25}$$

where t_{DA} = dimensionless time for the beginning of pseudosteadystate flow. Values for t_{DA} are given in Appendix for various reservoir shapes and well locations. [5,6] The time required for the pseudosteady-state equation to be exact is found from the entry in the column "Exact for t_{DA} > "

We should emphasize that the Rawlins-Schellhardt and Houpeurt deliverability equations assume radial flow. If pseudoradial flow has been achieved, however, these analysis techniques can be used for hydraulically fractured wells. The time to reach the pseudoradial flow regime, t_{prf}, occurs [7,8] at $t_{LfD} = 3$ and is estimated with

$$t_{prf} = \frac{11{,}400 \phi \bar{\mu}_g \bar{c}_t L_f^2}{k_g} \tag{5.25}$$

To illustrate the importance of achieving pseudoradial flow during a deliverability test, we calculated values of t_{prf} for a hydraulically fractured well completed in a reservoir with $\phi = 0.15$, $\bar{\mu}_g = 0.03 cp$, and $\bar{c}_t = 1 x 10^{-4}\ psia^{-1}$ and with the range of permeabilities and hydraulic fracture half-lengths in Table 5.2. The results illustrate that a well with a long fracture in a low-permeability formation will take far too long to stabilize for conventional deliverability testing.

5.4 ANALYSIS OF DELIVERABILITY TESTS

This section discusses the implementation and analysis of the flowafter-flow, single-point, isochronal, and modified isochronal tests. We present both the Rawlins and

Schellhardt and Houpeurt analysis techniques in terms of pseudopressures. The same analysis techniques are presented in terms of pressure squared.

5.5.1 Flow-After-Flow Tests

Flow-after-flow tests, sometimes called gas backpressure or four-point tests, are conducted by producing the well at a series of different stabilized flow rates and measuring the stabilized BHFP at the sandface. Each different flow rate is established in succession either with or without a very short intermediate shut-in period. Conventional flow-after-flow tests oflen are conducted with a sequence of increasing flow rates; however, if stabilized flow rates are attained, the rate sequence does not affect the test. 9 The requirement that the shut-in and flowing periods be continued until stabilization is a major limitation of the flow-afler-flow test, especially in low-permeability formations that take long times to reach stabilized flowing conditions. Fig. 5.8 illustrates a flow-after-flow test.

a) Rawlins-Schellhardt Analysis Technique. Recall the empirical equation introduced by Rawlins and Schellhardt:

$$q = C\left[p_p(\bar{p}) - p_p(p_{wf})\right]^n \tag{5.24}$$

Taking the logarithm of both sides of Eq. 5.24, we obtain the equation that forms the basis for the Rawlins-Schellhardt analysis technique:

$$\log(q) = \log(C) + n\left\{\log\left[p_p(\bar{p}) - p_p(p_{wf})\right]\right\} \tag{5.29}$$

The form of Eq. 5.29 suggests that, if we plot log (q) vs. log(Δp_p), we will obtain a straight line with a slope n and an intercept of log(C). The conventional graphical method for analyzing flow-after-flow test data, however, is to plot log(Δp_p), vs. log (q), giving a straight line of slope 1/n and an intercept of {-1/n [log(C)] }. The AOF potential is estimated from the extrapolation of the straight line to (Δp_p), evaluated at a P_{wf} equal to atmospheric pressure (sometimes called base pressure), P_b. This analysis technique is described in the next section and is illustrated with Example 5.1. In addition, we present the same example in Example 5.5) in terms of pressure squared.

Analysis Procedure.

1. Plot $\Delta p_p = p_p(\bar{p}) - p_p(p_{wf})$ vs. q on log-log graph paper. Construct the best-fit line through the data points. Some of the data points at the lower rates may not fit on the same straight lini the later points. In this case, the points at the lower rates sho be ignored for all subsequent calculations.

2. Determine the deliverability exponent, n, by simply calcu ing the slope of the best-fit straight line through the data points with least-squares regression analysis. For a regression analysis,

$$n = \frac{N\sum_{j=1}^{N}\left(\log(q)\cdot\log(\Delta p_p)\right)_j - \sum_{j=1}^{N}\log(q_j)\sum_{j=1}^{N}\log(\Delta p_p)_j}{N\sum_{j=1}^{N}\left(\log(\Delta p_p)\right)_j^2 - \left[\sum_{j=1}^{N}\log(\Delta p_p)_j\right]^2} \qquad (5.30)$$

Alternatively, l/n is the slope of the graph of log(Δp_p) vs. log(q). If (q_1, Δp_{p1}) and (q_2, Δp_{p1}) are two points on the perceived "best" straight line fitting the test data, then

$$\frac{1}{n} = \frac{\log(\Delta p_{p2}) - \log(\Delta p_{p1})}{\log(q_2) - \log(q_1)}$$

or the reciprocal of the slope

$$n = \frac{\log(q_2) - \log(q_1)}{\log(\Delta p_{p2}) - \log(\Delta p_{p1})} = \frac{\log(q_2 / q_1)}{\log(\Delta p_{p1} / \Delta p_{p1})} \tag{5.31}$$

The value of n should be between 0.5 and 1.0. A value of 0.5 indicates turbulent flow throughout the entire drainage area (improbable), while a value of 1.0 indicates completely laminar flow.

If n does not lie in this range, we recommend conducting the test again at flow rates higher than the highest rate achieved in the first test. If absolutely necessary, the original test can be analyzed with approximate techniques outlined in Step 4.

3. If $0.5 \le n \le 1$, calculate the AOF using either Step 3A or 3B.

A. Estimate the stabilized AOF potential of the well from the extrapolated straight line on the deliverability plot to the flow rate that corresponds to $\Delta p_p = p_p(\bar{p}) - p_p(p_b)$, where $p_p(p_b)$ is the pseudopressure evaluated at Pb

B. Alternatively, determine the stabilized performance coefficient, C:

$$C = 10^{\alpha}, \tag{5.32}$$

where α is determined from least-squares regression analysis of the points on the best-fit straight line,

$$\alpha = \frac{\sum_{j=1}^{N} \log(q_j) \sum_{j=1}^{N} \left(\log(\Delta p_p)\right)_j^2 - \sum_{j=1}^{N} \log(\Delta p_p)_j \sum_{j=1}^{N} \left[\log(q_j)\log(\Delta p_p)_j\right]}{N \sum_{j=1}^{N} \left(\log(\Delta p_p)\right)_j^2 - \left[\sum_{j=1}^{N} \log(\Delta p_p)_j\right]^2} \tag{5.33}$$

Alternatively (and less accurately), we can determine C from a perceived "best" straight line using the value of n determined in Step 2, one point $\left(q_1, \Delta p_{pl}\right)$ on the straight line, and

$$C = q_1 / \left(\Delta p_{pl}\right)^n \tag{5.34}$$

We can then calculate the AOF potential with

$$q_{AOF} = C\left[p_p(\bar{p}) - p_p(p_b)\right]^n \tag{5.35}$$

where $p_p(p_b)$ = pseudopressure evaluated at P_b.

4. If $n < 0.5$, set $n = 0$. S and construct a line with a slope of 2.0 through the data point corresponding to the highest flow rate. Similarly, if $n > 1.0$, set $n = 1.0$ and construct a line with slope of 1.0 through the data point corresponding to the highest flow rate. Determine the stabilized AOF potential of the well from the extrapolated straight line on the deliverability plot to the flow rate corresponding to $\Delta p_p = p_p(\bar{p}) - p_p(p_b)$ Alternatively, calculate C with $n = 0.5$ or 1.0:

$$C = \frac{q}{\left[p_p(\bar{p}) - p_p(p_{wf})\right]^n} \tag{5.36}$$

where $p_p(p_{wf})$ is the point through which the line was constructed. Calculate the AOF potential with Eq. 5.35 using C from Eq. 5.36 and n = 0.5 or 1.0.

b) Houpeurt Analysis Technique.

Flow-afler-flow tests require stabilized data or data measured during pseudosteady-state flow. Recall that Houpeurt gives the theoretical equation for pseudosteadystate flow, which was derived directly from the gas diffusivity equation, as

$$\Delta p_p = p_p(\bar{p}) - p_p(p_{wf}) = aq + bq^2 \tag{5.12}$$

In addition, recall that coefficients a and b have theoretical bases and can be estimated if reservoir properties are known. We can also determine these stabilized flow coefficients from flow-aflerflow test data. Dividing both sides of Eq. 5.12 by the flow rate, q, and rearranging, we obtain the equation that is the basis for the Houpeurt analysis technique:

$$\frac{\Delta p_p}{q} = \frac{p_p(\bar{p}) - p_p(p_{wf})}{q} = a + bq \tag{5.37}$$

The form of Eq. 5.37 suggests that, if we plot $\frac{\Delta p_p}{q}$ vs. q, we will obtain a straight line with a slope b and an intercept a. The AOF is estimated in the Houpeurt deliverability analysis by solving Eq. 5.12 for $q = q_{AOF}$ at $P_{wf} = P_b$

Analysis Procedure.

1 Plot $\Delta p_p / q = \left[p_p(\bar{p}) - p_p(p_{wf}) \right] / q$ vs. q on Cartesian graph paper. Construct the best-fit line through the data points. Some of the data points at the lower rates may not fit on the same straight line as the points corresponding to the higher rates.

In this case, ignore the points at the lower rates and use only the points at the higher rates for all subsequent calculations.

2. Calculate a and b by least-squares regression analysis (Eqs. 5.38 and 5.39, respectively) of the points on the best-fit line.

$$a = \frac{\sum_{j=1}^{N} \left(\frac{\Delta p_p}{q} \right)_j \sum_{j=1}^{N} (q_j)^2 - \sum_{j=1}^{N} (q_j) \sum_{j=1}^{N} \left[(\Delta p_p)_j \right]}{N \sum_{j=1}^{N} (q_j)^2 - \left[\sum_{j=1}^{N} q_j \right]^2} \tag{5.38}$$

$$\text{and } b = \frac{N \sum_{j=1}^{N} (\Delta p_p)_j - \sum_{j=1}^{N} q_j \sum_{j=1}^{N} \left(\frac{\Delta p_p}{q} \right)_j}{N \sum_{j=1}^{N} (q_j)^2 - \left[\sum_{j=1}^{N} q_j \right]^2} \tag{5.39}$$

An alternative but less accurate method is to use two points, $\left[q_1, (\Delta p_p / q)_1 \right]$ and $\left[q_2, (\Delta p_p / q)_2 \right]$, on the perceived "best" line through the test data and the following equations:

$$b = \frac{\left(\frac{\Delta p_p}{q}\right)_2 - \left(\frac{\Delta p_p}{q}\right)_1}{q_2 - q_1} \tag{5.40}$$

$$\text{and } a = \left(\frac{\Delta p_p}{q}\right)_1 - bq_1 \tag{5.41}$$

3. Calculate the AOF with Eq. 5 42, where $p_p(p_b)$ is the pseudopressure evaluated at P_b and a and b are from Step 2:

$$q_{AOF} = \frac{-a + \sqrt{a^2 + 4b\left[p_p(\bar{p}) - p_p(p_b)\right]}}{2b} \tag{5.42}$$

(See Example 5.1)

5.4.2 Single-Point Tests.

A single-point test is an attempt to overcome the limitation of long test times. A single-point test is conducted by flowing the well at a single rate until the sandface pressure is stabilized. One limitation of this test is that it requires prior knowledge of the well's deliverability behavior, either from previous well producing in the same field under similar conditions. We also must ensure that the well has flowed long enough to be out of wellbore storage and in the pseudosteady-state flow regime. Similarly, for hydraulically fractured wells, we must ensure that the well has flowed long enough be in the pseudoradial flow regime.

To analyze a single-point test with the Rawlins-Schellhardt method, n must be known or estimated. An estimate of n can be obtained either from a previous deliverability test on the well or from correlations with similar wells producing from the same formation under similar conditions. The calculation procedure is similar to that presented for

flow-after-flow tests. The AOF can be estimated graphically by drawing a stMight line through the single flow point with a slope of l/n and extrapolating it to the flow rate at $\Delta p_p / q = \left[p_p(\bar{p}) - p_p(p_b) \right] / q$ .Or the AOF can be calculated with Eq. 5.35, where C is estimated with Eq. 5.36. To use the Houpeurt analysis technique, the slope, b, of the line on a plot of $\Delta p_p / q = \left[p_p(\bar{p}) - p_p(p_{wf}) \right] / q$ vs. q must be known. We have only one point from a single-point test, so we must estimate b using Eq. 5.15. Note that we must have estimates of the formation properties to use Eq. 5.15. The remaining analysis procedure is similar to that for flow-afler-flow tests. The AOF can be calculated with Eq. 5.42 where the intercept, a, is estimated with Eq. 5.41.

5.4.3 **Isochronal Tests**

The isochronal test is a series of single point tests developed to estimate stabilized deliverability characteristics without actually flowing the well for the time required to achieve stabilized conditions. The isochronal test is conducted by alternately producing the well, then shutting in the well and allowing it to build to the average reservoir pressure before the beginning of the next production period. Pressures are measured at several time increments during each flow period. The times at which the pressures are measured should be the same relative to the beginning of each flow period. Because less time is required to build to essentially initial pressure afler short flow periods than to reach stabilized flow in a flow-after-flow test, the isochronal test is more practical for low-permeability formations. Although not required for analyzing the test, a final stabilized flow point often is obtained at the end of the test. Fig. 5.12 illustrates an isochronal test.

The isochronal test is based on the principle that the radius of investigation established during each flow period is not a function of the flow rate but depends only on the length of time for which the well is flowed. Consequently, the pressures measured at the same

time periods during each different rate correspond to the same drainage radius. Under these conditions, isochronal test data can be analyzed using the same theory as a flow-after-flow test, even though stabilized flow is not attained. In theory, we should obtain a stabilized deliverability curve from transient data if a single stabilized rate and the corresponding BHP have been measured and are available.

Recall that the transient solution to the real-gas diffusivity equation in terms of pseudopressures is

$$p_p(p_s) - p_p(p_{wf}) = \frac{1.422 \times 10^6 qT}{k_g h} x \left[1.151 \cdot \log\left(\frac{k_g t}{1{,}688 \phi \bar{\mu}_g \bar{c}_t r_w^2} \right) + s + Dq \right] \tag{5.9}$$

where p_S = stabilized BHP measured before the test. We can rewrite the transient equation in a form similar to the late-time solution (Eq. 5.10):

$$p_p(p_s) - p_p(p_{wf}) = \frac{1.422 \times 10^6 qT}{k_g h} x \left[1.151 \cdot \log\left(\frac{k_g t}{1{,}688 \phi \bar{\mu}_g \bar{c}_t r_w^2} \right) - \frac{3}{4} + s + Dq \right] \tag{5.10}$$

Further, we define an effective drainage radius as

$$r_d = \sqrt{\frac{k_g t}{377 \phi \bar{\mu}_g \bar{c}_t}} \tag{5.44}$$

If we substitute Eq. 5.44 into Eq. 5.43 and rearrange, the transient solution becomes

$$p_p(p_s) - p_p(p_{wf}) = \frac{1.422 \times 10^6 qT}{k_g h} x \left[\ln\left(\frac{r_d}{r_w} \right) - \frac{3}{4} + s + Dq \right] \tag{5.45}$$

only, not flow rate. Note that rd has no physical significance but is simply the radius that forces the pseudosteady-state equation to resemble the transient equation. io In addition, do not confuse rd with r,, which is the transient radius of investigation given by Eq. Similar to Houpeurt's equations, we can rewrite Eq. 5.45 as

$$p_p(p_s) - p_p(p_{wf}) = aq + bq^2 \tag{5.46}$$

where

$$a_t = \frac{1.422x10^6 T}{k_g h} x\left[\ln\left(\frac{r_d}{r_w}\right) - \frac{3}{4} + s\right] \tag{5.47}$$

and $$b = \frac{1.422x10^6 TD}{k_g h} \tag{5.15}$$

Note that b is not a function of time and will remain constant. Similarly, the intercept a, is constant for each fixed time line or isochron.

The theory of isochronal test analysis implies that the transient pressures corresponding to the same elapsed time during each different flow period will plot as a straight line with a slope b. In addition, the slopes of each line or isochron representing a fixed flow time will have the same value. The intercept a' will increase with increasing time. Therefore, we can draw a line with the same slope, b, through the final, stabilized data point, and use the coordinates of the stabilized point and the slope to calculate a stabilized intercept, a, independent of time, where the stabilized flow coefficient is defined by

$$a = \frac{1.422x10^6 T}{k_g h} x\left[\ln\left(\frac{r_d}{r_w}\right) - \frac{3}{4} + s\right] \tag{5.48}$$

a) Rawlins-Schellhardt Analysis.

Recall the empirical equation introduced by Rawlins and Schellhardt for analysis of flow-after-flow test data:

$$\log(q) = \log(C) + n\left\{\log\left[p_p(\bar{p}) - p_p(p_{wf})\right]\right\} \tag{5.29}$$

For isochronal tests, we plot transient data measured at different flow rates but taken at the same time increments relative to the beginning of each flow period. Therefore, the lines drawn through data points corresponding to the same f~xed flow time are parallel, so the value of n remains constant and is independent of time. However, the intercept, log (C), is a function of time, so we must calculate a different intercept for each isochronal line. We call this the "transient" intercept, log (C_t). In terms of this transient intercept, Eq. 5.29 becomes

$$\log(q) = \log(C_t) + n\left\{\log\left[p_p(p_s) - p_p(p_{wf})\right]\right\} \tag{5.49}$$

The conventional Rawlins-Schellhardt method of isochronal test analysis is to plot $\log\left[\Delta p_p = p_p(\bar{p}) - p_p(p_{wf})\right]$ vs. log (q) for each time, giving a straight line of slope l/n and an intercept of { - 1/n[log(C_t)] }.

Analysis Procedure.

1. Plot $\Delta p_p = p_p(p_s) - p_p(p_{wf})$ vs. q on log-log graph paper. Also plot $\Delta p_{ps} = p_p(p_s) - p_p(p_{wf,s})$ vs. q_s, which corresponds to the stabilized, extended flow

point ($p_{wf,S}$, q_S). Construct the bestfit line through the data points for the same flow times, i.e., draw the best-fit line through the isochrons. Ignore the data points at the lower flow rates if they do not follow the same trend as the higher flow rates.

2. Determine the deliverability exponent, n, for each line or isochron either by drawing the perceived best-fit line through the data and calculating the slope (Eq. 5.31) or by least-squares regression analysis (Eq. 5.30).

The theoretical value of n should be between 0.5 and 1.0. If n is not in this range for any of the times chosen, we recommend conducting the test again at flow rates higher than the highest rates achieved in the first test. If absolutely necessary, this test can be analyzed using approximate techniques outlined in Step 4.

3. Calculate an arithmetic average of the n values, $\bar{n}$, from Step 2.

4. If $0.5 \le \bar{n} \le 1.0$, estimate the AOF using either Step 4A or 4B.

A. Calculate the pseudopressure at P_b. Draw a line of slope I /nthrough the stabilized, extended flow point, extrapolate the line to the flow rate at $\Delta p_p = p_p(p_s) - p_p(p_b)$, and read the AOF directly from the graph.

B. Alternatively, determine C using the coordinates of the stabilized, extended flow point and $n = \bar{n}$.

$$C = \frac{q_s}{\left[p_p(p_s) - p_p(p_{wf})\right]^n} \tag{5.36}$$

Calculate the AOF potential using calculated values of $n = \bar{n}$ from Step 3 and C from Eq. 5.36.

$$q_{AOF} = C\left[p_p(p_s) - p_p(p_b)\right]^n \tag{5.35}$$

5. If $\bar{n} < 0.5$, set n = 0.5 and construct a line with a slope of 2.0 through the extended flow data point. Similarly, if $\bar{n} > 1.0$, set n = 1.0 and construct a line with slope of 1.0 through the extended flow data point. Extrapolate this line to the flow rate at $\Delta p_p = \left|p_p(p_s) - p_p(p_b)\right|$ and read the AOF directly from the graph. Alternatively, calculate C using Eq. 5.36 with either n =0.5 or 1.0 where $\Delta p_p = p_p(p_{wf,s}) - p_p(p_b)$ is the pseudopressure evaluated at the extended flow point. The AOF potential of the well is computed with Eq. 5.35.

b) Houpeurt Analysis.

Recall that the Houpeurt equation for analyzing flow-after-flow tests is

$$\frac{\Delta p_p}{q} = \frac{p_p(\bar{p}) - p_p(p_{wf})}{q} = a + bq \tag{5.37}$$

Remember that Eq. 5.37 assumes stabilized flow conditions; however, in isochronal testing, we are measuring transient data. Consequently, for each isochronal (or fixed time) line, the equation for transient flow conditions is

$$\frac{\Delta p_p}{q} = \frac{p_p(p_s) - p_p(p_{wf})}{q} = a_t + bq \tag{5.50}$$

where

$$a_t = \frac{1.422x10^6 T}{k_g h} x\left[\ln\left(\frac{r_d}{r_w}\right) - \frac{3}{4} + s\right] \tag{5.47}$$

and $$b = \frac{1.422x10^6 TD}{k_g h} \tag{5.15}$$

The form of Eq. 5.50 suggests that a plot of $\Delta p_p = \left[p_p(p_s) - p_p(p_{wf})\right]/q$ vs. q will yield a straight line with slope b and intercept a,. We can then extend this theory to the stabilized point and calculate a stabilized intercept, a, using the coordinates of the stabilized point. The slope b remains the same.

Analysis Procedure.

1. Plot $\Delta p_p = \left[p_p(p_s) - p_p(p_{wf})\right]/q$ vs. q on log-log graph paper. Also plot $\Delta p_{ps}/q = \left[p_p(p_s) - p_p(p_{wf,s})\right]/q_s$ vs. q_s, which corresponds to the stabilized, extended flow point ($p_{wf,S}$, q_S). Construct best-fit lines through the data points for the same flow times, ignoring the lower flow rates that do not follow the same trend as the higher flow rates.

2. Calculate the slopes b for each time line by least-squares regression analysis (Eq. 5.39), or use two points use two points, $\left[q_1, (\Delta p_p/q)_1\right]$ and $\left[q_2, (\Delta p_p/q)_2\right]$, on the perceived "best" line through the test data and Eq. 5.40. Calculate the arithmetic average value of the slopes.

3. Calculate the stabilized isochronal deliverability line intercept using the average b from Step 2.

$$a = \left[p_p(p_s) - p_p(p_{wf,s})\right]/q_s - bq_s \tag{5.51}$$

The AOF is calculated by Eq. 5.42

$$q_{AOF} = \frac{-a + \sqrt{a^2 + 4b\left[p_p(p_s) - p_p(p_b)\right]}}{2b}$$

(See Example 5.2)

5.4.4 Modified Isochronal Tests

The time to build up to the average reservoir pressure before flowing for a certain period of time still may be impractical, even after short flow periods. Consequently, a modification[12] of the isochronal test was developed to shorten test times further. The objective of the modified isochronal test is to obtain the same data as in an isochronal test without using the sometimes lengthy shut-in periods required to reach the average reservoir pressure in the drainage area of the well.

The modified isochronal test (Fig. 5.17) is conducted like an isochronal test, except the shut-in periods are of equal duration and the flow periods are of equal duration. The shut-in periods, however, should equal or exceed the length of the flow periods. Because the well does not build up to average reservoir pressure after each flow period, the shut-in sandface pressures recorded immediately before each flow period rather than the average reservoir pressure are used in the test analysis. As a result, the modified isochronal test is

less accurate than the isochronal test. Note that, as the duration of the shut-in periods increases, the accuracy of the modified isochronal test also increases. Again, a final stabilized flow point usually is obtained at the end of the test but is not required for analyzing the test data.

The well does not build up to the average reservoir pressure during shut-in; the analysis techniques for the modified isochronal tests are derived empirically. Recall the transient flow equation, expressed in terms of the reservoir pressure at the start of flow, on which isochronal testing is based:

$$p_p(p_s) - p_p(p_{wf}) = \frac{1.422 \times 10^6 qT}{k_g h} x \left[\ln\left(\frac{r_d}{r_w}\right) - \frac{3}{4} + s + Dq \right] \qquad (5.45)$$

In new reservoirs with little or no pressure depletion, Ps equals the initial reservoir pressure ($p_S = p_i$) in developed reservoirs, ($p_S < p_i$) In addition, the transient drainage radius, r_d, in Eq. 5.45 is defined as

$$r_d = \sqrt{\frac{k_g t}{377 \phi \bar{\mu}_g \bar{c}_t}} \qquad (5.44)$$

Because rd is a function only of time and not flow rate, Eq. 5.45 is valid at any fixed time. F modified isochronal tests, Eq. 5.45 is approximated by Eq. 5.52 where the stabilized shut-in BH p_s, is replaced with the shut-in BHP, p_{ws}, measured before each flow period, where $p_{ws} \leq p_s$,

$$p_p(p_{ws}) - p_p(p_{wf}) = \frac{1.422 \times 10^6 qT}{k_g h} x \left[\ln\left(\frac{r_d}{r_w}\right) - \frac{3}{4} + s + Dq \right] \qquad (5.52)$$

We can rewrite Eq. 5.52 as

$$p_p(p_s) - p_p(p_{wf}) = a_t q + bq^2 \tag{5.53}$$

where

$$a_t = \frac{1.422x10^6 T}{k_g h} x\left[\ln\left(\frac{r_d}{r_w}\right) - \frac{3}{4} + s\right] \tag{5.47}$$

$$\text{and } b = \frac{1.422x10^6 TD}{k_g h} \tag{5.15}$$

Eq. 5.15 indicates that b is independent of time and will remain which gives constant during the test. Similarly, Eq. 5.47 illustrates that a_t is constant for a fixed time. The similarity of Eqs. 5.46 and 5.53 for the isochronal and modified isochronal tests, respectively, suggests that the modified isochronal test data can be analyzed like those from an isochronal test.

The theory developed for the modified isochronal test implies that, if the empirical approximation of using p_{ws} instead of p_s is valid, the transient data will plot as straight line for each time having the same slope, b.

The intercept, a_t, will increase with increasing time. Therefore, we can draw a line with slope b through the stabilized data point and use the coordinates of the stabilized point and the slope to calculate a stabilized intercept, a, that is independent of time, where

$$a = \frac{1.422x10^6 T}{k_g h}\left[\ln\left(\frac{r_d}{r_w}\right) - \frac{3}{4} + s\right] \tag{5.48}$$

To calculate the AOF of the well, we use the average reservo pressure, Ps, measured before the test instead of the p_{ws} value, or

$$q_{AOF} = \frac{-a + \sqrt{a^2 + 4b\left[p_p(p_s) - p_p(p_b)\right]}}{2b} \qquad (5.42)$$

We now consider two variations of the modified isochronal tesl tests with a stabilized flow point obtained at the end of the test an' tests run without that final point.

a) Modified Isochronal Tests With a Stabdized Flow Point.

a1) Rawlins Schellhardt Analysis.

Recall the empirical Rawlins and Schellhard equation in terms of transient isochronal test data:

$$\log(q) = \log(C) + n\left\{\log\left[p_p(\bar{p}) - p_p(p_{wf})\right]\right\} \qquad (5.49)$$

As in the graphical analysis techniques for isochronal tests, we plot several trends of data taken at different times during a modi fied isochronal test. The slope n of each line through points at equa] time values will be constant. However, the intercept, log (C_t), is a function of time but not flow rate. Therefore, we must calculate a different intercept for each isochronal line. In addition, for modified isochronal tests, we use $P_P(P_{ws})$ instead of $P_P(P_S)$ in Eq 5 49,which gives

$$\log(q) = \log(C_t) + n\left\{\log\left[p_p(p_s) - p_p(p_{wf})\right]\right\} \qquad (5.49)$$

The conventional analysis technique for modified isochronal test data is to plot $p_p(p_s) - p_p(p_b)$ vs. log (q) for each time, giving a straight line of slope 1/n and an intercept of $\{-1/n[\log(C_t)]\}$.

The Rawlins-Schellhardt analysis procedure for modified isochronal tests with a stabilized flow point is similar to that presented for isochronal tests, except the plotting functions are developed in terms of the shut-in pressure measured immediately before the next flow period. Only the stabilized, extended flow point is plotted in terms of the average reservoir pressure measured before the test. Example 5.3 illustrates the procedure.

a2) Houpeurt Analysis.

As shown previously, the Houpeurt deliverability equation in terms of transient isochronal test data is

$$\frac{\Delta p_p}{q} = \frac{p_p(p_s) - p_p(p_{wf})}{q} = a_t + bq \tag{5.50}$$

For modified isochronal test data, we must modify Eq. 5.50 with the assumption that we can use $p_p(p_{ws})$ instead of $p_p(p_s)$. With this assumption, Eq. 5.50 becomes

$$\frac{\Delta p_p}{q} = \frac{p_p(p_{ws}) - p_p(p_{wf})}{q} = a_t + bq \tag{5.55}$$

where

$$a_t = \frac{1.422x10^6 T}{k_g h}\left[\ln\left(\frac{r_d}{r_w}\right) - \frac{3}{4} + s\right] \tag{5.47}$$

and $$b = \frac{1.422x10^6 TD}{k_g h} \tag{5.15}$$

The form of Eq. 5.55 suggests that, if we plot $\Delta p_p / q = p_p(p_s) - p_p(p_{wf}) / q$ vs. q, we will obtain a straight line with a slope b and intercept a_t. We also can extend this theory to the stabilized point and calculate a stabilized intercept, a_t using the coordinates of the stabilized point, or

$$a = \frac{p_p(p_{ws}) - p_p(p_{wf})}{q} - bq = \frac{\Delta p_p}{q} - bq$$

The slope b of the line through the stabilized point should remain the same. In addition, we must use the average reservoir pressure, which is measured before the test, to evaluate the pseudopressure, $p_p(p_s)$, in Eq. 5.51. Example 5.3 illustrates the Houpeurt analysis procedure for modified isochronal tests with a stabilized flow point, which is similar to that presented for isochronal tests. (See Example 5.3)

b) Modified Isochronal Tests Without a Stabilized Flow Point.

Because the well is not required to build up to the average reservoir pressure between the flow periods, the modified isochronal approximation shortens test times considerably. However, the test analysis relies on obtaining one stabilized flow point. Under some conditions, environmental or economic concerns prohibit flaring produced gas to the atmosphere during a long production period, thus preventing measurement of a stabilized flow point. These conditions often occur when new wells are tested before being connected to a pipeline.

Two methods have been developed to analyze modified isochronal tests without a stabilized flow point. The Brar and Aziz[13] method was developed for the Houpeurt analysis, while the stabilized C method[4] was developed for the Rawlins and Schellhardt analysis. The stabilized C method requires that we have prior knowledge of permeability and skin factor or that we determine these properties using the methods Brar and Aziz proposed for analyzing modified isochronal tests. Both methods require knowledge of the drainage area shape and size.

b1) Brar and Aziz Method - Houpeurt Analysis.

The Brar and Aziz method is based on the transient Houpeurt deliverability equation,

$$\Delta p_p = p_p(p_s) - p_p(p_{wf}) = a_t q + bq^2 \tag{5.11}$$

where

$$a_t = \frac{1.422x10^6 T}{k_g h} x\left[1.151 \cdot \log\left(\frac{k_g t}{1{,}688\phi\bar{\mu}_g \bar{c}_t r_w^2}\right) + s\right] \tag{5.13}$$

and

$$b = \frac{1.422x10^6 TD}{k_g h} \tag{5.15}$$

and Ps = stabilized BHP measured before the deliverability test.

The transient-gas-flow equation derived from the diffusivity equation for a homogeneous-acting, isotropic reservoir producing at a constant sandface rate is

$$p_p(p_s) - p_p(p_{wf}) = \frac{1.422x10^6 qT}{k_g h} x\left[1.151 \cdot \log\left(\frac{k_g t}{1{,}688\phi\bar{\mu}_g \bar{c}_t r_w^2}\right) + s + Dq\right] \tag{5.9}$$

The form of Eq. 5.9 suggests that, for a single and constant flow rate, a plot of $\Delta p_p = p_p(p_s) - p_p(p_{wf})$ vs. log t will be a straight line with slope m, where

$$m = \frac{1.422x10^6(1.151)T}{k_g h} = \frac{1.632x10^6 T}{k_g h} \tag{5.56}$$

Equating Eqs. 5.9 and 5.11 yields

$$a_t + bq^2 = \frac{1.422x10^6 qT}{k_g h} x\left[1.151 \cdot \log\left(\frac{k_g t}{1{,}688\phi\bar{\mu}_g\bar{c}_t r_w^2}\right) + s + Dq\right] \tag{5.57}$$

Dividing Eq. 5.57 by rate, q gives

$$a_t = m'\log(t) + c' \tag{5.58}$$

where

$$m' = \frac{1.632x10^6 T}{k_g h} \tag{5.59}$$

$$\text{and } c' = \frac{1.422x10^6 T}{k_g h}\left[1.151 \cdot \log\left(\frac{k_g t}{1{,}688\phi\bar{\mu}_g\bar{c}_t r_w^2}\right) + s + Dq\right] - bq \tag{5.60}$$

Substituting the definition of b (Eq. 5.15) into Eq. 5.60 gives an equation for the intercept, c':

$$c' = \frac{1.422x10^6 T}{k_g h}\left[1.151 \cdot \log\left(\frac{k_g t}{1{,}688\phi\bar{\mu}_g\bar{c}_t r_w^2}\right) + s\right] - bq \tag{5.61}$$

m' and c' can be calculated using regression analysis of Eq. 5.58. Alternatively, these variables can be computed from a plot of a, vs. log t. We then can calculate the permeability from the slope,

$$k_g = \frac{1.632x10^6 T}{m'h} \quad .. \tag{5.62}$$

Combining Eqs. 5.59 and 5.61 yields an equation for the skin factor,

$$s = 1.151\left[\left(\frac{c'}{m'}\right) - \log\left(\frac{k_g}{\phi\bar{\mu}_g\bar{c}_t r_w^2}\right) + 3.23\right] \tag{5.63}$$

Estimating the AOF potential of the well requires that we have a stabilized value of a. If we know the drainage area shape, we can use the gas permeability calculated from Eq. 5.62 and the skin factor from Eq. 5.63 to calculate

$$a = \frac{1.422x10^6 T}{k_g h}\left[1.151 \cdot \log\left(\frac{10.06A}{C_A r_w^2}\right) - \frac{3}{4} + s\right] \tag{5.14}$$

Appendix gives shape factors, CA, for various reservoir shapes and well locations. This stabilized value of a then is used in Eq. 5.42 to calculate the AOF of the well:

$$q_{AOF} = \frac{-a + \sqrt{a^2 + 4b\left[p_p(p_s) - p_p(p_b)\right]}}{2b} \tag{5.42}$$

Analysis Procedure

1 Plot $\Delta p_p / q = \left[p_p(p_s) - p_p(p_b) \right] / q$ vs. q on Cartesian graph paper. Construct best-fit lines through the modified isochronal data points for each time, ignoring the data at the lower rates that do not follow the trend of the data at higher rates.

2. Determine the slopes, b of the lines for each time by least squares regression analysis (Eq. 5.39) or simply by drawing the best-fit line through the data. Calculate the arithmetic average of the slopes, $\bar{b}$.

.3. Calculate the transient deliverability line intercepts, a,, for each isochronal line either directly from the graph or with Eq. 5.64.

$$a_t = \frac{\sum_{j=1}^{N} \left(\frac{\Delta p_p}{q} \right)_j \sum_{j=1}^{N} (q_j)^2 - \sum_{j=1}^{N} (q_j) \sum_{j=1}^{N} \left[(\Delta p_p)_j \right]}{N \sum_{j=1}^{N} (q_j)^2 - \left[\sum_{j=1}^{N} q_j \right]^2} \qquad (5.64)$$

4. Plot a, vs. Iog t and draw the best-fit line through the data. If the earliest-time data do not lie on the straight line, these data should be omitted from subsequent calculations. Calculate the slope m' and intercept, c', of the line either directly from the graph or using Eqs. 5.65 and 5.66, respectively.

$$m' = \frac{\sum_{j=1}^{N} (a_t \log t)_j - \sum_{j=1}^{N} (a_t)_j \sum_{j=1}^{N} (\log t)_j}{N \sum_{j=1}^{N} (\log t_j)^2 - \left[\sum_{j=1}^{N} \log t_j\right]^2} \qquad (5.65)$$

and

$$c' = \frac{\sum_{j=1}^{N} (a_t)_j \sum_{j=1}^{N} (\log t)_j - \sum_{j=1}^{N} (a_t \log t)_j \sum_{j=1}^{N} (\log t)_j}{N \sum_{j=1}^{N} (\log t_j)^2 - \left[\sum_{j=1}^{N} \log t_j\right]^2} \qquad (5.66)$$

5. Calculate the formation permeability to gas using the slope of the semilog straight line, m from the plot of a, vs. log t.

$$k_g = \frac{1.632 \times 10^6 T}{m' h} \qquad (5.62)$$

6. Calculate the skin factor using c'.

$$s = 1.151\left[\left(\frac{c'}{m'}\right) - \log\left(\frac{k_g}{\phi \bar{\mu}_g \bar{c}_t r_w^2}\right) + 3.23\right] \qquad (5.63)$$

7. Calculate the stabilized line intercept, a

$$a = \frac{1.422 \times 10^6 T}{k_g h} x \left[1.151 \cdot \log\left(\frac{10.06A}{C_A r_w^2} \right) - \frac{3}{4} + s \right] \tag{5.14}$$

8. Calculate the AOF potential using b from Step 2 and the stabilized a value from Step 7.

$$q_{AOF} = \frac{-a + \sqrt{a^2 + 4b\left[p_p(p_s) - p_p(p_b) \right]}}{2b} \tag{5.42}$$

where $p_p(p_b)$ = pseudopressure evaluated at p_p.

b2) Stabilized C Method - Rawlins-Schellhardt Analysis.

Although the Houpeurt equation has a theoretical basis and is rigorously correct, the more familiar but empirically based Rawlins and Schellhardt equation continues to be used and is indeed favored by the natural gas industry. Consequently, in this section we combine the Houpeurt and Rawlins-Schellhardt analysis techniques and develop a more accurate version of the Rawlins-Schellhardt method for analyzing modified isochronal tests. This analysis technique, called the stabilized C method, t4 is derived by equating the stabilized Rawlins and Schellhardt empirical backpressure equation with the stabilized theoretical Houpeurt equation to obtain equations for the deliverability exponent, n, and the stabilized flow coefficient, C, in terms of the Houpeurt flow coefficients, a and b.

To obtain an equation for the exponent n, we begin by taking the logarithm of both sides of the stabilized Rawlins and Schellhardt empirical backpressure equation (Eq. 5.24),

$$\log(q) = \log(C) + n\left\{ \log\left[p_p(\bar{p}) - p_p(p_{wf}) \right] \right\} \tag{5.67}$$

Rearranging Eq. 5.67 and solving for n, we see that n is the slope of a log-log plot of q vs. Δp_p Alternatively, n can be expressed as the derivative of log q with respect to $\log\left(\Delta p_p\right)$.

$$n = \frac{d\log(q)}{d\log\left[p_p(\bar{p}) - p_p(p_{wf})\right]} = \frac{1}{q}\frac{dq}{d\log\left[p_p(\bar{p}) - p_p(p_{wf})\right]} \tag{5.68}$$

Similarly, if we take logarithms of both sides of the stabilized Houpeurt equation given by Eq. 5.12, we obtain

$$\log\left[p_p(\bar{p}) - p_p(p_{wf})\right] = \log\left[aq + bq^2\right] \tag{5.69}$$

Differentiating $\log \Delta p_p$ with respect to q gives

$$\frac{d\log\left[p_p(\bar{p}) - p_p(p_{wf})\right]}{dq} = \frac{1}{aq + bq^2}\frac{d\left(aq + bq^2\right)}{dq} = \frac{a + 2bq}{aq + bq^2} \tag{5.70}$$

Equating Eqs. 5.68 and 5.70 shows that n can be expressed terms of the gas flow rate and the Houpeurt flow coefficients,

$$n = \frac{1}{q}\left(\frac{aq + bq^2}{a + 2bq}\right) = \frac{a + bq}{a + 2bq^2} \tag{5.71}$$

Note that n is different for different rates, but we will clear up this difficulty shortly. To develop an expression for the performance coefficient, C, we first take the logarithm of the original Rawlins and Schellhardt equation in terms of pseudopressures, or

$$\log\left(\frac{q}{C}\right) = n\left\{\log\left[p_p(\bar{p}) - p_p(p_{wf})\right]\right\} \tag{5.72}$$

Similarly, taking the logarithm of the Houpeurt equation in terms of pseudopressures gives

$$\log\left[p_p(\bar{p}) - p_p(p_{wf})\right] = \log\left[aq + bq^2\right] \tag{5.73}$$

Equating Eqs. 5.72 and 5.73 and solving for C yields

$$C = \frac{q_e}{\left(aq_e + bq_e^2\right)^n} \tag{5.74}$$

where q_e = the unique rate at which the pseudopressure drops from Eqs. 5.72 and 5.73 are equal. In terms of the Houpeurt coefficients and the deliverability exponent, from Eq. 5.71,

$$q_e = \frac{a(1-n)}{b(2n-1)} \tag{5.75}$$

To apply the stabilized C method, we must assume that the slope, n, of the empirical deliverability plot remains constant with time. This assumption implies that, if we can

calculate values of a and b for given reservoir properties, we can calculate a flow rate from Eq. 5.75 where the change in pseudopressure calculated by the Rawlins-Schellhardt equation is equal to the change in pseudopressure calculated by the theoretical Houpeurt equation. We then substitute this flow rate into Eq. 5.74 and calculate a stabilized C value. We use the constant n and calculated stabilized C to calculate a value of AOF:

$$q_{AOF} = C\left[p_p(\bar{p}) - p_p(p_b)\right]^n \tag{5.35}$$

The stabilized C method is limited by the need for values of reservoir properties determined before the deliverability test. However, these properties can be estimated either from drawdown or buildup test analysis or from the Brar and Aziz method.

Analysis Procedure

1. Plot $\Delta p_p = \left[p_p(p_s) - p_p(p_b)\right]$ vs. q on log-log graph paper. Construct the best-fit line through the data points for each isochron. Some of the data points at lower rates may not agree with the general trend of the data at higher rates, so the data points at the lower rates should be ignored in all subsequent calculations.

2. Determine the deliverability exponent, n, with least-squares regression analysis (Eq. 5. 30) or simply by taking the slope of the perceived "best-fit" line through the test data. In addition, calculate the arithmetic average of the exponents, $\bar{n}$.

3. Determine the theoretical values of the Houpeurt coefficients, a and b, using permeability, skin, and non-Darcy flow coefficient values obtained from drawdown and buildup tests on the well, or alternatively from the modified isochronal test data using the Brar and Aziz method.

$$a = \frac{1.422x10^6 T}{k_g h}\left[1.151 \cdot \log\left(\frac{10.06A}{C_A r_w^2}\right) - \frac{3}{4} + s\right] \tag{5.14}$$

and

$$b = \frac{1.422x10^6 TD}{k_g h} \tag{5.15}$$

4. Calculate the rate at which the change in pseudopressure, Δp_p, determined with the Rawlins-Schellhardt equation is equal to the change in pseudopressure determined using the Houpeurt equation. Use the average slope, $\bar{n}$, of the deliverability plot and theoretical stabilized a and b values from Eqs. 5.14 and 5.15, respectively.

$$q_e = \frac{a(1-n)}{b(2n-1)} \tag{5.75}$$

5. Calculate the stabilized C value using $\bar{n}$ from Step 2.

$$C = \frac{q_e}{\left(aq_e + bq_e^2\right)^n} \tag{5.74}$$

6. Substitute the stabilized C value from Step 5 into Eq. 5.35 to calculate the AOF potential of the well. Use $\bar{n}$ from Step 2.

$$q_{AOF} = C\left[p_p(\bar{p}) - p_p(p_b)\right]^n \tag{5.35}$$

5.5 NUMERICAL - APPLICATIONS

A. PSEUDOPRESSURE TECHNIQUES

EXAMPLE 1.

ANALYSIS OF A FLOW-AFTER-FLOW TEST.

Estimate the initial stabilized AOF potential of a well having the well and reservoir properties listed below. Use both the Rawlins-Schellhardt and the Houpeurt analysis techniques. In addition, estimate the AOF potential 10 years later when the static drainage area pressure has decreased to 350 psia. Evaluate the AOF potential at P_b = 14.65 psia. Table 5.3 summarizes the flow-after-flow test data.

$\gamma_g = 0.715$

$L = 3{,}050$ ft

$r_w = 0.5$ ft

$M_a = 20.71$ lbm / lbm − mol

$A = 640$ Ac.

$\phi = 0.25$

$T_{f,wf} = 90°F.$

$C_A = 30.8828$

$h = 200$ ft

Current $\bar{p} = 407.6$ psia, $p_p(\bar{p} = 407.6) = 1.6173 \times 10^7$ psia^2 / cp.

$\bar{p}$ after 10 years = 350 psia, $p_p(\bar{p} = 350) = 1.2239 \times 10^7$ psia^2 / cp.

$p_b = 14.65$ psia, $p_p(p_b) = 2{,}674.8$ psia^2 / cp.

Solution.

1. Rawlins-Schellhardt Analysis.

Plot Δp_p vs. q on log-log graph paper (Fig. 5.9). Table 5.4 gives the plotting functions. Construct the best-fit line through the data points. Note that all data points lie on the best-fit line and will be used for all subsequent calculations.

2. Determine the deliverability exponent using least-squares regression analysis (Eq. 5.30). Table 5.5 summarizes the calculations.

$$n = \frac{N\sum_{j=1}^{N}\left(\log(q)\cdot\log(\Delta p_p)\right)_j - \sum_{j=1}^{N}\log(q_j)\sum_{j=1}^{N}\log(\Delta p_p)_j}{N\sum_{j=1}^{N}\left(\log(\Delta p_p)\right)_j^2 - \left[\sum_{j=1}^{N}\log(\Delta p_p)_j\right]^2} = \frac{4(25.5319)-(4.0958)(24.5507)}{4(151.2710)-(24.5507)^2} = 0.67$$

Alternatively, because Points I and 4 both lie on the perceived "best" straight line through the test data, the reciprocal slope is estimated to be

$$n = \frac{\log(q_2/q_1)}{\log(\Delta p_{pl}/\Delta p_{pl})} = \frac{\log(20.177/4.288)}{\log(3.582\text{x}10^6/3.560\text{x}10^5)} = 0.671$$

3. Now, calculate the AOF of the well. Because $0.5 \le n \le 1$, we can calculate C using either regression analysis or a point from the best-fit straight line through the test data.

A. We can estimate C with regression analysis using Eq. 5.33 where the exponent α is

$$\alpha = \frac{\sum_{j=1}^{N} \log(q_j) \sum_{j=1}^{N} \left(\log(\Delta p_p)\right)_j^2 - \sum_{j=1}^{N} \log(\Delta p_p)_j \sum_{j=1}^{N} \left[\log(q_j)\log(\Delta p_p)_j\right]}{N \sum_{j=1}^{N} \left(\log(\Delta p_p)\right)_j^2 - \left[\sum_{j=1}^{N} \log(\Delta p_p)_j\right]^2} =$$

$$= \frac{(4.0958)(25.5319) - (24.5507)(25.5319)}{4(151.2710) - (24.5507)^2} = -3.09$$

The stabilized performance coefficient is

$$C = 10^{\alpha} = 10^{(-3.09)} = 8.13 \times 10^{-4}$$

B. We also can estimate C using Point 4 from the best-fit line and Eq. 5.34.

$$C = \frac{q_4}{\left(\Delta p_{p4}\right)^n} = \frac{20.177}{\left(3.582 \times 10^6\right)^{0.671}} = 8.07 \times 10^{-4}$$

4. To update the AOF to a new average reservoir pressure, recall that, for pseudopressure analysis, both C and n do not change as drainage area pressure decreases. Therefore, recalculate AOF for the new drainage area pressure using Eq. 5.35.

$$q_{AOF} = \left[p_p(\bar{p}) - p_p(14.65)\right]^n = 8.13 \times 10^{-4}\left(1.673 \times 10^7 - 2.6748 \times 10^3\right)^{0.67} = 45.6 \text{ MMscf / D}$$

at $\bar{p} = 350$ psia

2. Houpeurt Analysis.

1. Plot $\Delta p / q$ vs. q on Cartesian graph paper (Fig. 5.10). Ta ble 5.6 gives the plotting functions. Construct the best-fit line through the last three data points. The first point, corresponding to the lowest flow rate, does not follow the trend and will be ignored in subsequent analyses.

2. Determine the deliverability coefficients, a and b, from a least squares regression analysis (Eqs. 5.38 and 5.39, respectively) ol the points used to develop the best-fit straight line. Table 5.7 summarizes the calculations. Note that Point I is not included in the calculations.

$$a = \frac{\sum_{j=1}^{N}\left(\frac{\Delta p_p}{q}\right)_j \sum_{j=1}^{N}(q_j)^2 - \sum_{j=1}^{N}(q_j)\sum_{j=1}^{N}\left[(\Delta p_p)_j\right]}{N\sum_{j=1}^{N}(q_j)^2 - \left[\sum_{j=1}^{N} q_j\right]^2} = \frac{(4.574x10^5)(734.82) - (44.994)(7.160x10^6)}{3(734.82) - (44.994)^2} =$$

$$= 7.75x10^4 \text{ psia}^2 / \text{cp(MMscf} - \text{D)}$$

$$b = \frac{N\sum_{j=1}^{N}(\Delta p_p)_j - \sum_{j=1}^{N} q_j \sum_{j=1}^{N}\left(\frac{\Delta p_p}{q}\right)_j}{N\sum_{j=1}^{N}(q_j)^2 - \left[\sum_{j=1}^{N} q_j\right]^2} = \frac{3(7.160x10^6) - (4.574x10^5)(44.994)}{3(734.82) - (44.994)^2} =$$

$$= 5.00x10^3 \text{ psia}^2 / \text{cp(MMscf} - \text{D)}$$

Alternatively, we can use Points 2 and 4 from the line drawn through the test data to calculate a and b using Eqs. 5.40 and 5.41, respectively.

$$b = \frac{\left(\frac{\Delta p_p}{q}\right)_2 - \left(\frac{\Delta p_p}{q}\right)_1}{q_2 - q_1} = \frac{1.775x10^5 - 1.232x10^5}{20.177 - 9.265} = 4.976x10^3 \text{ psia}^2 / \text{cp} / (\text{MMscf} - \text{D})^2$$

$$a = \left(\frac{\Delta p_p}{q}\right)_1 - bq_1 = 1.775x10^5 - (4{,}976)(20.177) = 7.71x10^4 = psia^2 / cp / (MMscf - D)^2$$

3. From Eq. 5.42,

$$q_{AOF} = \frac{-a + \sqrt{a^2 + 4b\left[p_b(\bar{p}) - p_b(p_b)\right]}}{2b} =$$

$$= \frac{-\left(7.75x10^4\right) + \sqrt{\left(7.75x10^4\right)^2 + 4\left(5.00x10^4\right)\left[1.62x10^7 - 2{,}674.8\right]}}{2\left(5.00x10^3\right)} =$$

$$= 49.7 \text{ MMscf / Day at } \bar{p} = 407.6 \text{psia.}$$

4. To update the AOF, recall for pseudopressure analysis that both a and b do not change as drainage area pressure changes. Therefore, the AOF for the new drainage area pressure is

$$q_{AOF} = \frac{-a + \sqrt{a^2 + 4b\left[p_b(\bar{p}) - p_b(p_b)\right]}}{2b} =$$

$$= \frac{-\left(7.75x10^4\right) + \sqrt{\left(7.75x10^4\right)^2 + 4\left(5.00x10^4\right)\left[1.2239x10^7 - 2{,}674.8\right]}}{2\left(5.00x10^3\right)} =$$

$$= 42.2 \text{ MMscf / Day at } \bar{p} = 350 \text{psia.}$$

A comparison (Fig. 5.11) of the results from example 1shows that the Rawlins-Schellhardt equation appears to be valid for this range of test data; however, the line representing the Houpeurt equation deviates from the Rawlins-Schellhardt equation as BHFP decreases. Although the Rawlins-Schellhardt method is valid under many testing conditions, this deviation suggests that, when we extrapolate the empirical equation over large variations in pressure, we may not predict well behavior correctly.

EXAMPLE 2

ANALYSIS OF ISOCHRONAL TESTS.

Estimate the AOF of this well[11] using both the Rawlins-Schellhardt and the Houpeurt analyses. Table 5.8 summarizes the isochronal test data. Assume P_b=14.65 psia.

$$\bar{p} = 352.4 \text{ psia}, \; p_p(\bar{p}) \approx p_p(p_s) = 9.975 \text{x} 10^6 \text{ psia}^2 / \text{cp}.$$

$$p_b = 14.65 \text{ psia}, \; p_p(p_b) = 2{,}674.8 \text{ psia}^2 / \text{cp}.$$

Solution.

1. Rawlins-Schellhardt Analysis Technique.

1. First, plot $\Delta p_p = \left[p_p(p_s) - p_p(p_{wf}) \right]$ vs. q on log-log graph paper (Fig. 5.13) and include the single stabilized, extended flow point. Table 5.9 gives the plotting functions.

2. Calculate the deliverability exponent, n, for each line or isochron using least-squares regression analysis (Eq. 5.30). Note that, because the first data point for each isochron does not align with the data points at the last three flow rates (Fig. 5.13), the first data point is ignored in all subsequent calculations.

For example, at t=0.5 hours, the deliverability exponent is calculated as follows (see Table 5.10):

$$n = \frac{N\sum_{j=1}^{N}\left(\log(q)\cdot\log(\Delta p_p)\right)_j - \sum_{j=1}^{N}\log(q_j)\sum_{j=1}^{N}\log(\Delta p_p)_j}{N\sum_{j=1}^{N}\left(\log(\Delta p_p)\right)_j^2 - \left[\sum_{j=1}^{N}\log(\Delta p_p)_j\right]^2} =$$

$$= \frac{3(10.2445)-(1.6625)(18.4165)}{3(113.0999)-(18.4165)^2} = 0.88$$

Table 5.11 summarizes the deliverability exponents determined with a least-squares regression analysis for each isochron.

3. The arithmetic average of the n values in Table 5.11 is

$$\bar{n} = \frac{n_1 + n_2 + n_3 + n_4}{4} = \frac{0.88 + 0.91 + 0.89 + 0.88}{4} = 0.89$$

4. Because $0.5 \le \bar{n} \le 1.0$, estimate the AOF either using Eq. 5.35 or graphically using Fig. 5.14. For this example, we use Eq. 5.35. First, determine the stabilized performance coefficient using the coordinates of the stabilized, extended flow point and $n = \bar{n}$

$$C = \frac{q_s}{\left[p_p(p_s) - p_p\left(p_{wf,s}\right)\right]^n} = \frac{1.156}{\left(2.443x10^6\right)^{0.89}} = 2.39x10^{-6}$$

Calculate the AOF potential using Eq. 5.35.

$$q_{AOF} = C\left[p_p\left(p_s\right) - p_p\left(p_b\right)\right]^n = 2.39x10^{-6}\left(9.9715x10^6 - 2{,}098.7\right)^{0.89} = 4.04 \text{MMscf / D.}$$

To determine the AOF graphically, first calculate the pseudopressure at P_b and compute

$$\Delta p_p = \left[p_p(p_s) - p_p(p_b) \right] = 9.9715 \text{x} 10^6 - 2{,}098.7 = 9.969 \text{x} 10^6$$

Then, draw a line of slope $1/\bar{n}$ through the stabilized flow point, extrapolate the line to the flow rate at $\Delta p_p = \left[p_p(p_s) - p_p(p_b) \right]$, and read the AOF directly from the graph.

2. Houpeurt Analysis Technique.

1 Plot $\Delta p_p / q = \left[p_p(p_s) - p_p(p_b) \right] / q$ vs. q on Cartesian graph paper (Fig. 5.15). Table 5.12 gives the plotting functions. Construct best-fit lines through the isochronal data points for each time. Note that, for each flow time, the point corresponding to the lowest rate does fit on the same straight line, so all four data points will be used for the analysis of each isochron.

2. Determine the slope b of each line or isochron. For this example, use least-squares regression analysis (Eq. 5.39). For example, at t=0.5 hour (see Table 5.13):

$$b = \frac{N \sum_{j=1}^{N} \left(\Delta p_p \right)_j - \sum_{j=1}^{N} q_j \sum_{j=1}^{N} \left(\frac{\Delta p_p}{q} \right)_j}{N \sum_{j=1}^{N} \left(q_j \right)^2 - \left[\sum_{j=1}^{N} q_j \right]^2} = \frac{4\left(4.6239 \text{x} 10^6\right) - (12.050)\left(14.293 \text{x} 10^5\right)}{4(44.108) - (12.050)^2} =$$

$$= 1.644 \text{x} 10^4 \text{ psia}^2 / \text{cp} / (\text{MMscf} - \text{D})^2.$$

Other values of b are summarized in Table 5.14.

3. The arithmetic average value of the slopes in table 5.14 is

$$\bar{b} = \frac{b_1 + b_2 + b_3 + b_4}{4} = \frac{(1.644 + 1.904 + 2.255 + 2.492)x10^4}{4} = 2.074x10^4 \text{ psia}^2 / \text{cp} / (\text{MMscf} -$$

4. Calculate the stabilized isochronal deliverability line intercept using

$\Delta p_p / q = 2.113x10^6$ psia^2 / cp / (MMscf – D)^2 at the extended, stabilized point.

$$a = \Delta p_p / q - bq = 2.113x10^6 - \left(2.074x10^4\right)(1.156) = 2.109x10^6 \text{ psia} / \text{cp} / (\text{MMscf} - \text{D})$$

5. Calculate the AOF potential using the average value of b from Step 3 and the stabilized value of a calculated from Step 4.

$$q_{AOF} = \frac{-a + \sqrt{a^2 + 4b\left[p_p(p_s) - p_p(p_b)\right]}}{2b} =$$

$$= \frac{-\left(2.109x10^6\right) + \sqrt{\left(2.109x10^6\right)^2 + 4\left(2.074x10^4\right)\left(9.97x10^6\right)}}{2\left(2.074x10^4\right)} = 4.53 \text{ MMscf / D.}$$

Fig. 5.16 illustrates the results.

EXAMPLE 3

ANALYSIS OF A MODIFIED ISOCHRONAL TEST WITH A STABILIZED FLOW POINT.

Using the following data taken from Well 4 of Ref. 13, calculate the AOF using both Rawlins and Schellhardt and Houpeurt analysis techniques. Assume P_b = 14.65 psia, where $p_p(p_b)$=5.093 x 10^7 psia2/cp. Table 5.15 gives the test data.

$h = 6$ ft

$r_w = 0.1875$ ft

$\phi = 0.2714$

$T_{f,wf} = 540°\,R(80°\,F)$.

$\bar{p} \approx p_s = 706.6$ psia.

$\bar{\mu}_g = 0.015$ cp

$\bar{z} = 0.97$

$\bar{c}_g = 1.5 \times 10^{-3}$ psia^{-1}

$\gamma_g = 0.75$

$S_w = 0.3$

$c_f = 3 \times 10^{-6}$ psia^{-1}

$A = 640$ acres

Assume that the well is centered in a square drainage area.

Solution.

1. Rawlins-Schellhardt Analysis.

1 Plot $\Delta p_p = p_p(p_s) - p_p(p_{wf})$ vs. q on log-log graph paper (Fig. 5.18). Table 5.16 gives the plotting functions. In addition, plot on the same graph the value of Δp_p that corresponds to the stabilized, extended flow point evaluated at P_S.

$$\Delta p_p = p_p(p_s) - p_p(p_{wf}) = 5.093 \times 10^7 - 3.276 \times 10^7 = 1.817 \times 10^7 \text{ psia}^2/\text{cp}.$$

For each time, construct the best-fit line through the data points. Because the first data point for each isochron does not follow the trend of the higher rate points, it will be ignored for all subsequent calculations.

2. Calculate the deliverability exponent, n, for each line or isochron. For this example, we use least-squares regression analysis (Eq. 5.30). For example, at t=O.5 hour (see Table 5.17)

$$n = \frac{N\sum_{j=1}^{N}\left(\log(q)\cdot\log(\Delta p_p)\right)_j - \sum_{j=1}^{N}\log(q_j)\sum_{j=1}^{N}\log(\Delta p_p)_j}{N\sum_{j=1}^{N}\left(\log(\Delta p_p)\right)_j^2 - \left[\sum_{j=1}^{N}\log(\Delta p_p)_j\right]^2} =$$

$$= \frac{(3)(8.8963) - (1.2336)(21.5753)}{(3)(155.1988) - (21.5753)^2} = 0.72$$

Table 5.18 summarizes deliverability exponents.

3. The arithmetic average $\bar{n}$ of the n values in Table 5.18 is

$$\bar{n} = \frac{n_1 + n_2 + n_3 + n_4}{4} = \frac{0.72 + 0.74 + 0.74 + 0.78}{4} = 0.74$$

4. Because $0.5 \le \bar{n} \le 1.0$, determine the stabilized performance coefficient, C, using the coordinates of the stabilized, extended flow point and $n = \bar{n}$. Note that the pseudopressure used to calculate the stabilized C value is evaluated at P_S measured at the beginning oi the test, rather than P_{ws} From Eq. 5.36,

$$C = \frac{q}{\left[p_p(p_s) - p_p(p_{wf})\right]^n} = \frac{2.665}{\left(5.093x10^7 - 3.276x10^7\right)^{0.74}} = 1.132x10^{-5}$$

From Eq. 5.35.

$$q_{AOF} = C\left[p_p(p_s) - p_p(p_b)\right]^n = 1.132x10^{-5}\left(5.0935x10^7 - 2{,}766.6\right)^{0.74} = 5.7\,\text{MMscf / D}$$

We can also determine the AOF graphically by drawing a line of slope $1/\bar{n}$ through the extended flow point, extrapolating the line to the flow rate at $\Delta p_p = p_p(p_s) - p_p(p_b)$, and reading the AOF directly from the graph (Fig. 5.19).

2. Houpeurt Analysis.

1 Plot $\Delta p_p / q = \left[p_p(p_s) - p_p(p_b)\right] / q$ vs. q on Cartesian graph paper (Fig. 5.20). In addition, plot the $\Delta p_p / q$ value that corresponds to the stabilized, extended flow point. Table 5.19 gives the plotting functions. Construct best-fit lines through the modified isochronal data points for each time. The first data point at the

lowest rate for each isochron does not fit on the same straight line as the last three rate points and is ignored in subsequent calculations.

2. Determine the slopes of the lines, b, for each isochron by leastsquares regression analysis of the best-fit lines through the data points. For example, at t=0.5 hour (see Table 5.20),

$$b = \frac{N\sum_{j=1}^{N}\left(\Delta p_p\right)_j - \sum_{j=1}^{N} q_j \sum_{j=1}^{N}\left(\frac{\Delta p_p}{q}\right)_j}{N\sum_{j=1}^{N}\left(q_j\right)^2 - \left[\sum_{j=1}^{N} q_j\right]^2} = \frac{3\left(4.807x10^7\right) - (7.8751)\left(1.851x10^7\right)}{3(21.138) - (7.581)^2} =$$

$$= 9.654x10^5 \text{ psia}^2 / \text{cp} / (\text{MMscf} - \text{D})^2.$$

Table 5.21 summarizes the slopes of the isochrons.

The arithmetic average value of the slopes in Table 5.21 is

$$\bar{b} = \frac{b_1 + b_2 + b_3}{3} = \frac{(8.678 + 8.711 + 8.78)x10^5}{3} = 8.723x10^5 \text{ psia}^2 / \text{cp} / (\text{MMscf} - \text{D})^2$$

3. Calculate the stabilized isochronal deliverability line intercept,

$$a = \frac{p_p(p_s) - p_p(p_{wf})}{q} - bq = \frac{1.817x10^7}{2.665} - \left(8.723x10^5\right)(2.665) =$$

$$= 4.493x10^6 \text{ psia}^2 / \text{cp} / (\text{MMscf} - \text{D}).$$

Calculate the AOF potential using b from Step 2 and the stabilized a value:

$$q_{AOF} = \frac{-a + \sqrt{a^2 + 4b\left[p_p(\bar{p}) - p_p(14.65)\right]}}{2b} =$$

$$= \frac{-\left(4.493x10^6\right) + \sqrt{\left(4.493x10^6\right)^2 + 4\left(8.723x10^5\right)\left[\left(5.093x10^7\right) - 2{,}766.6\right]}}{2\left(8.723x10^5\right)} = 5.5 \text{ MMscf / D.}$$

Fig. 5.21 shows the data for this example.

EXAMPLE 4.

ANALYSIS OF A MODIFIED ISOCHRONAL TEST WITHOUT A STABILIZED DATA POINT.

The purpose of this example is to compare results obtained from the analysis of a modified isochronal test (see Table 5.22) with and without an extended, stabilized data point. Calculate the AOF for the following modif~ed isochronal test data without the extended flow point. Use both the Brar and Aziz and the stabilized C methods. Compare these results with the results obtained by using the extended flow point. This example is Well 8 taken from Ref. 13. Only the last four flow points from the test are used in the analysis. Reservoir data are summarized below. In addition, the results from a drawdown test in this well indicate kg=4.23 md and s= - 5.2.

$h = 454$ ft

$r_w = 0.2615\,\text{ft}$

$\phi = 0.0675$

$T_{f,wf} = 718°\,\text{R}\left(258°\,\text{F}\right).$

$\bar{p} = 4{,}372.6$ psia.

$\bar{\mu}_g = 0.023$ cp

$\bar{z} = 0.87$

$\bar{c}_g = 1.69\text{x}10^{-4}$ cp

$\gamma_g = 0.65$

$S_w = 0.3$

$A = 640$ acres.

$C_A = 30.8828$. (assume that the well is centered in a square drainage area).

The Rawlins and Schellhardt analysis with extended flow point gave $C=2.426x10^{-3}$, n=0.54, and q_{AOF} = 180.1 MMscf/D.

The Houpeurt analysis with extended flow point gave a= $1.455x10^{6}$ $psia^2/cp/MMscf-D$, b=$1.774x10^{4}$ $psia^2/cp/(MMscf-D)^2$, and q_{AOF}=205.6 MMscf/D.

Solution.

1. Brar and Aziz Method.

1 Plot $\Delta p_p / q = \left[p_p(p_s) - p_p(p_b)\right]/q$ vs. q on Cartesian graph paper (Fig. 5.22). Table 5.23 gives the plotting functions. Construct best-fit lines through the modified isochronal data points for each time. Although the data are scattered, we used all flow rates for each isochron.

2. Determine the slopes of the lines, b, for each time by leastsquares regression analysis. For example, at t=3.0 hours (see Table 5.24),

$$b = \frac{N\sum_{j=1}^{N}\left(\Delta p_p\right)_j - \sum_{j=1}^{N} q_j \sum_{j=1}^{N}\left(\frac{\Delta p_p}{q}\right)_j}{N\sum_{j=1}^{N}\left(q_j\right)^2 - \left[\sum_{j=1}^{N} q_j\right]^2} = \frac{4\left(3.167x10^{8}\right) - (202.477)\left(5.961x10^{6}\right)}{4\left(1.107x10^{4}\right) - (202.477)^2} =$$

$$= 1.823x10^{4}\ psia^2/cp/(MMscf-D)^2.$$

Table 5.25 summarizes the slopes for all isochrons. The arithmetic average value of the b values in Table 5.25 is

$$\bar{b} = \frac{b_1 + b_2 + b_3 + b_4}{4} = \frac{(1.823 + 1.870 + 1.881 + 1.939)x10^4}{4} =$$

$$= 1.878x10^4 \text{ psia}^2 / \text{cp} / (\text{MMscf} - \text{D})^2$$

3. Using Eq. 5.64, calculate the transient deliverability line intercepts for each isochronal line. For example, at t=3.0 hours (see Table 5.26),

$$a_t = \frac{\sum_{j=1}^{N}\left(\frac{\Delta p_p}{q}\right)_j \sum_{j=1}^{N}(q_j)^2 - \sum_{j=1}^{N}(q_j)\sum_{j=1}^{N}\left[(\Delta p_p)_j\right]}{N\sum_{j=1}^{N}(q_j)^2 - \left[\sum_{j=1}^{N} q_j\right]^2} =$$

$$= \frac{(5.961x10^6)(1.107x10^4) - (202.477)(3.167x10^6)}{(4)(1.107x10^4) - (202.477)^2} =$$

$$= 5.677x10^5 \text{ psia}^2 / \text{cp} / (\text{MMscf} - \text{D}).$$

Table 5.27 gives the intercepts for each isochron.

4. Prepare a graph of a, vs. log t (Fig. 5.23) and draw the bestfit line through the data. Using all four data points, calculate m' and c' of the best-fit line of the plot of a, vs. log t using leastsquares regression analysis (Eqs. 5.65 and 5.66, respectively) (see Table 5.28).

$$m' = \frac{\sum_{j=1}^{N}\left(a_t \log t\right)_j - \sum_{j=1}^{N}\left(a_t\right)_j \sum_{j=1}^{N}(\log t)_j}{N\sum_{j=1}^{N}\left(\log t_j\right)^2 - \left[\sum_{j=1}^{N}\log t_j\right]^2} = \frac{(4)\left(1.651\text{x}10^6\right) - \left(2.533\text{x}10^6\right)(2.556)}{(4)(1.684) - (2.556)^2} =$$

$$= 3.871\text{x}10^5 \text{ psia}^2/(\text{cp} - \text{MMscf}/\text{D})/\text{cycle}$$

$$c' = \frac{\sum_{j=1}^{N}(a_t)_j \sum_{j=1}^{N}(\log t)_j - \sum_{j=1}^{N}\left(a_t \log t\right)_j \sum_{j=1}^{N}(\log t)_j}{N\sum_{j=1}^{N}\left(\log t_j\right)^2 - \left[\sum_{j=1}^{N}\log t_j\right]^2} = \frac{\left(2.553\text{x}10^6\right)(1.684) - \left(1.651\text{x}10^6\right)(2.556)}{(4)(1.684) - (2.556)^2} =$$

$$= 3.909\text{x}10^5 \text{ psia}^2/(\text{cp} - \text{MMscf}/\text{D})$$

5. Calculate the formation permeability to gas using the slope of the semilog straight line.

$$k_g = \frac{1.632\text{x}10^6 T}{m'h} = \frac{\left(1.632\text{x}10^6\right)(718)}{\left(3.871\text{x}10^5\right)(454)} = 6.6 \text{ md},$$

which compares with kg=4.23 md estimated from the drawdown test analysis.

6. Calculate the skin factor with Eq. 5.63.

$$s = 1.151\left[\left(\frac{c'}{m'}\right) - \log\left(\frac{k_g}{\phi\bar{\mu}_g\bar{c}_t r_w^2}\right) + 3.23\right] =$$

$$= 1.151\left[\left(\frac{3.909\text{x}10^5}{3.871\text{x}10^5}\right) - \log\left(\frac{6.6}{(0.0675)(0.023)(0.000169)(0.2615)^2}\right) - 3.23\right] = -5.0$$

This value agrees with s= -5.2 estimated from the drawdown test analysis.

7. Calculate the stabilized flow coefficient, a. Assume that the well is centered in a square drainage area with CA =30.8828.

$$a = \frac{1.422x10^6 T}{k_g h} x\left[1.151 \cdot \log\left(\frac{10.06A}{C_A r_w^2}\right) - \frac{3}{4} + s\right] =$$

$$= \frac{(1.422x10^6)(718)}{(6.6)(454)}\left\{1.151 \cdot \log\frac{(10.06)(640)(43,560)}{(30.8828)(0.2615)^2} - \frac{3}{4} - 5.0\right\}$$

$$= 1.227x10^6 \text{ psia}^2 / \text{cp} / (\text{MMscf} - \text{D}).$$

8. Now, calculate the AOF potential using $\bar{b}$ from Step 2 and the stabilized a value calculated in Step 7.

$$q_{AOF} = \frac{-a + \sqrt{a^2 + 4b\left[p_p(p_s) - p_p(p_b)\right]}}{2b} =$$

$$= \frac{-(1.277x10^6) + \sqrt{(1.277x10^6)^2 + 4(1.878x10^4)[1.049x10^9 - 2,003.81]}}{2(1.878x10^4)} =$$

$$= 205.9 \text{ MMscf / D.}$$

2. Stabilized C Method.

1. Plot $\Delta p_p = \left[p_p(p_s) - p_p(p_b)\right]$ vs. q on log-log graph paper (Fig. 5.24). Table 5.29 gives the plotting functions. Construct best fit lines through the data.

2. Calculate the deliverability exponent, n, for each line. For this example, use least-squares regression analysis of all points for each isochron. For example, for t=3.0 hours (see Table 5.30),

$$n = \frac{N\sum_{j=1}^{N}\left(\log(q)\cdot\log(\Delta p_p)\right)_j - \sum_{j=1}^{N}\log(q_j)\sum_{j=1}^{N}\log(\Delta p_p)_j}{N\sum_{j=1}^{N}\left(\log(\Delta p_p)\right)_j^2 - \left[\sum_{j=1}^{N}\log(\Delta p_p)_j\right]^2} =$$

$$= \frac{(4)(53.0561)-(6.7435)(31.4091)}{(4)(246.7983)-(31.4091)^2} = 0.63$$

Table 5.31 summarizes values of the deliverability exponent for each isochron. The arithmetic average slope of the values in Table 5.31 is

$$\bar{n} = \frac{n_1+n_2+n_3+n_4}{4} = \frac{0.63+0.64+0.65+0.65}{4} = 0.64$$

3. Calculate the theoretical value of the Houpeurt coefficient, a using permeability and skin factor values calculated previously with the Brar and Aziz analysis (i.e., k_g=6.6 md, s=-5.0).

$$a = \frac{1.422x10^6 T}{k_g h} x\left[1.151\cdot\log\left(\frac{10.06A}{C_A r_w^2}\right) - \frac{3}{4} + s\right] =$$

$$= \frac{\left(1.422x10^6\right)(718)}{(6.6)(454)}\left\{1.151\cdot\log\frac{(10.06)(640)(43,560)}{(30.8828)(0.2615)^2} - \frac{3}{4} - 5.0\right\}$$

$$= 1.227x10^6 \text{ psia}^2/\text{cp}/(\text{MMscf}-\text{D}).$$

Use the average value for the coefficient, $b=1.873x10^4$ $psia^2/(cp\text{-}MMscf/D^2)$, obtained from the Brar and Aziz analysis.

4. Calculate the rate at which the change in pseudopressure determined with the Rawlins-Schellhardt equation equals the change in pseudopressure determined with the Houpeurt equation. Use the average value for the coefficient $b=1.873x10^4$ $psia^2/(cp\text{-}MMscf/D^2)$, obtained from the Brar and Aziz analysis and the a coefficient from Step 3.

$$q_e = \frac{a(1-n)}{b(2n-1)} = \frac{1.227x10^6(1-0.64)}{1.873x10^4[2(0.64)-1]} = 84.2 \text{ MMscf / D.}$$

5. Calculate the stabilized C value.

$$C = \frac{q_e}{\left(aq_e + bq_e{}^2\right)^n} = \frac{84.2}{\left[\left(1.227x10^6\right)(84.2)+\left(1.873x10^4\right)(81.2)\right]^{0.64}} = 3.69x10^{-4}$$

6. Calculate the AOF potential of the well using $\bar{n}$ from Step 2.

$$q_{AOF} = C\left[p_p(\bar{p}) - p_p(p_b)\right]^n = \left(3.69x10^{-4}\right)\left[1.049x10^9 - 2{,}003.8\right]^{0.64} = 218.7 \text{ MMscf / D.}$$

Table 5.32 compares the results of the analyses with and without the extend, stabilized flow point. In general, the results are comparable and illustrate the validity of the Brar and Aziz and the stabilized C methods for modified isochronal tests with no extended, stabilized flow point.

B. PRESSURE-SQUARED TECHNIQUES

EXAMPLE 5.5

ANALYSIS OF A FLOW-AFTER-FLOW TEST.

Estimate the initial stabilized AOF potential of a well having the well and reservoir properties listed below. Use both the Rawlins-Schellhardt and the Houpeurt analysis techniques. Evaluate the AOF potential at P_b = 14.65 psia. Table 5.37 summarizes the flow-after-flow test data.

$\gamma_g = 0.715$

$L = 3{,}050$ ft

$r_w = 0.5$ ft

$M_a = 20.71$ lbm / lbm – mol

$A = 640$ Ac.

$\phi = 0.25$

$T_{f,wf} = 90°$F.

$C_A = 30.8828$

$h = 200$ ft

Solution

a) Rawlins-Schellhardt Analysis.

1. First, plot $\Delta p^2 = \bar{p}^2 - p_{wf}^2$ vs. q on log-log graph paper (Fig. 5.25). Table 5.38 gives the plotting functions. Construct the best-fit line through the data points. Note that all data points lie on the best-fit line and will be used for all subsequent calculations.

2. Using least-squares regression analysis, determine the deliverability exponent (Eq. 5.30). Table 5.39 summarizes the calculations.

3. Because $0.5 \le n \le 1.0$, we can calculate the stabilized performance coefficient, C, where the exponent α is

$$\alpha = \frac{\sum_{j=1}^{N} \log(q_j) \sum_{j=1}^{N} \left(\log(\Delta p^2)\right)_j^2 - \sum_{j=1}^{N} \log(\Delta p^2)_j \sum_{j=1}^{N} \left[\log(q_j)\log(\Delta p^2)_j\right]}{N \sum_{j=1}^{N} \left(\log(\Delta p^2)\right)_j^2 - \left[\sum_{j=1}^{N} \log(\Delta p2)_j\right]^2} =$$

$$= \frac{(4.096)(69.307) - (16.579)(17.372)}{4(69.307) - (16.579)^2} = -1.746$$

The stabilized performance coefficient is

$$C = 10^{\alpha} = 10^{(-1.746)} = 1.795 \text{x} 10^{-2}$$

4. The stabilized AOF potential is

$$AOF = \left[\bar{p}^2 - (14.65)^2\right]^n = 1.795 \text{x} 10^{-2} \left(1.659 \text{x} 10^5\right)^{0.668} = 55.1 \text{ MMscf / D}$$

b) Houpeurt Analysis.

1. Plot $\Delta p^2 / q = \left[\bar{p}^2 - p_{wf}^2\right] / q$ vs. q on Cartesian graph paper (Fig. 5.26).

Table 5.40 summarizes the plotting functions. Construct the best-fit line through the last three data points. The first point, corresponding to the lowest flow rate, does not follow the trend and will be ignored in subsequent analyses.

2. Determine the deliverability coefficients, a and b, by leastsquares regression analysis of the last three points. The calculations are summarized in Table 5.41.

3. The AOF Dotential is

$$q_{AOF} = \frac{-a + \sqrt{a^2 + 4b\left[\bar{p}^2 - (14.65)^2\right]}}{2b} =$$

$$= \frac{-(7.797x10^2) + \sqrt{(7.797x10^2)^2 + 4(51.739)\left[1.661x10^5 - 214.6223\right]}}{2(51.739)} =$$

$$= 49.6 \text{ MMscf / Day}$$

SINGLE POINT TESTS

To analyze a single-point test with the Rawlins-Schellhardt method, the stabilized deliverability exponent, n, must be known or estimated. We can estimate n from either a previous deliverability test on the well or correlations with similar wells producing from the same formation under similar conditions. The calculation procedure is similar to that presented for flow-after-flow tests. The AOF can be estimated graphically by drawing a straight line through the single flow point with a slope of l/n and extrapolating it $\Delta p^2 = \left[\bar{p}^2 - p_b^2\right]$, or the AOF can be calculated with

$$q_{AOF} = C\left[\bar{p}^2 - p_b^2\right]^n$$

$$C = \frac{q}{\left[\bar{p}^2 - p_b^2\right]^n}$$

To use Houpert analysis technique, the slope of the line, b, on a plot of $\Delta p^2 / q = \left[\bar{p}^2 - p_{wf}^2\right] / q$ vs q must be known. We have only one point from a

single-point test, so we must estimate b using Eq. 5.22, which requires estimates of the formation properties. The remaining analysis procedure is similar to that for flow-after-flow tests. The AOF can be calculated with

$$q_{AOF} = \frac{-a + \sqrt{a^2 + 4b\left[\bar{p}^2 - p_b^2\right]}}{2b}$$

where the intercept, a, is estimated with Eq. 5.21.

EXAMPLE 5.6

ANALYSIS OF ISOCHRONAL TESTS

Using the isochronal data in Table 5.42, estimate the AOF of this well with both the Rawlins-Schellhardt and the Houpeurt analyses. Assume P_b=14.65 psia.

$\bar{p} \approx p_s = 532.4$ psia.

Solution.

a) Rawlins-Schellhardt Analysis Technique.

1. Plot $\Delta p^2 = \left[\bar{p}^2 - p_b^2\right]$ vs. q on log-log graph paper. (Fig. 5.27) shows the test data, and Table 5.43 gives the plotting functions. Note that all data point for each flow time can be fit with straight lines. Therefore, we will use all data points for subsequent calculations.

2. Calculate the deliverability exponent, n, for each isochron using least-squares regression analysis (Eq. 5.30). For example, Table 5.44 gives the calculations for t=0.5 hours. Deliverability exponents for all flow tiomes are given in Table 5.45.

3. The arithmetic average of the n values summarized in Table 5.45 is

$$\bar{n} = \frac{n_1 + n_2 + n_3 + n_4}{4} = \frac{0.88 + 0.91 + 0.89 + 0.88}{4.} = 0.89$$

4. Because $0.5 \le \bar{n} \le 1.0$, estimate the AOF with the following procedure. First, determine C:

$$C = \frac{q}{\left[p_s^2 - p_{wf}^2\right]^n} = \frac{1.156}{\left[3.933 \times 10^4\right]^{0.93}} = 6.164 \times 10^{-5}$$

Calculate the AOF potential using Eq. 5.35.

$$q_{AOF} = C\left[p_s^2 - (14.65)^2\right]^n = 6.164x10^{-5}\left[1.24x10^5\right]^{0.93} = 3.36 \text{ MMscf / D}$$

Alternatively, we can determine the AOF graphically. Draw a line of slope $1/\bar{n} = 1.08$ through the stabilized, extended flow point and extrapolate this line to the flow rate at $\Delta p^2 = p_s^2 - p_b^2 = (352.4)^2 - (14.65)_b^2 = 1.24x10^5$. From Fig. 5.28, qAOF=3.4 MMscf/D.

b) Houpeurt Analysis Technique.

1 Plot $\Delta p^2 / q = \left[p_s^2 - p_{wf}^2\right] / q$ vs. q on Cartesian graph paper (Fig. 5.29), including the stabilized, extended flow point (Table 5.46).

2. Compute the slopes of the lines, b, of each time by least squares regression analysis of the points on the best fit-line. For example, Table 5.47 gives the calculations for t=0.5 hours. Table 5.48 gives the slopes of all isochrons.

3. The arithmetic average value of the slopes in Table 5.48 is

$$\bar{b} = \frac{b_1 + b_2 + b_3 + b_4}{4} = \frac{(2.625 + 3.022 + 3.435 + 3.755)x10^2}{4} = 3.209x10^2 \text{ psia}^2 / \text{cp} / (\text{MMscf} -$$

4. Calculate the stabilized isochronal deliverability line intercept

$$a = \Delta p^2 / q - bq = 3.402x10^4 - (3.209x10^2)(1.156) = 3.365x10^4 \text{ psia / cp / (MMscf - D)}$$

5. Calculate the AOF potential.

$$q_{AOF} = \frac{-a + \sqrt{a^2 + 4b\left[p_s{}^2 - p_b{}^2\right]}}{2b} =$$

$$= \frac{-\left(3.365x10^4\right) + \sqrt{\left(3.365x10^4\right)^2 + 4\left(3.209x10^2\right)\left(1.240x10^5 - 214.623\right)}}{2\left(3.209x10^2\right)} = 3.56 \text{ MMscf / D.}$$

EXAMPLE 5.7

MODIFIED ISOCHRONAL TEST WITH A STABILIZED FLOW POINT

Calculate the AOF of well 4 using both Rawlins and Schellhardt and Houpeurt analysis techniques (Table 5.49). Assume $P_b = 14.65$ psia.

$h = 6$ ft

$r_w = 0.1875$ ft

$\phi = 0.2714$

$T_{f,wf} = 540°R\left(80°F\right).$

$\bar{p} \approx p_s = 706.6$ psia.

$\bar{\mu}_g = 0.015$ cp

$\bar{z} = 0.97$

$\bar{c}_g = 1.5x10^{-3}$ psia^{-1}

$\gamma_g = 0.75$

$S_w = 0.3$

$c_f = 3x10^{-6}$ psia^{-1}

$A = 640$ acres

Assume that the well is centered in a square drainage area.

Solution.

a). Rawlins-Schellhardt Analysis.

1 Plot $\Delta p^2 = \left[p_{ws}^2 - p_{wf}^2\right]$ vs. q on log-log graph paper (Fig. 5.30).

In addition, plot the value of Δp^2 that corresponds to the stabilized, extended flow

point, $\Delta p^2 = \left[p_{ws}^2 - p_{wf}^2\right] = 1.770 \text{x} 10^5 \text{e}$, q=2.665 MMscf/D. Table 5.51 summarizes the plotting functions. The first data points do not follow the trend of points taken at the higher rates and will be ignored for all subsequent calculations.

2. Determine the deliverability exponent, n, for each line by least-squares regression analysis of the last three points. For example see Table 5.51 for calculations at t=O.5 hours. Slopes of all isochrones are given in Table 5.52.

3. Calculate an arithmetic average, $\bar{n}$ of the n values.

$$\bar{n} = \frac{n_1 + n_2 + n_3 + n_4}{4} = \frac{0.837 + 0.698 + 0.694 + 0.758}{4} = 0.746$$

4. Because $0.5 \le \bar{n} \le 1.0$, we estimate the AOF as follows. First, determine C using the coordinates of the stabilized extended flow point and $n = \bar{n}$. Note that we are using P_S, not P_{ws}.

$$C = \frac{q}{\left[p_s^2 - p_{wf}^2\right]^n} = \frac{2.665}{\left[1.770 \text{x} 10^5\right]^{0.746}} = 3.241 \text{x} 10^{-4}$$

The AOF is

$$q_{AOF} = C\left[p_s^2 - (14.65)^2\right]^n = 3.241 \text{x} 10^{-4}\left(4.993 \text{x} 10^5 - 214.623\right)^{0.746} = 5.8 \text{ MMscf / D.}$$

Alternatively, we can also draw a line of slope $1/\bar{n} = 1.34$ through the stabilized, extended flow point and extrapolate this line to the flow rate at $\Delta p^2 = p_s^2 - p_b^2 = (352.4)^2 - (14.65)_b^2 = 1.24 \times 10^5$. or AOF=5.8 MMscf/D (Fig. 5.30)

b) Houpeurt Analysis Technique.

1 Plot $\Delta p^2 / q = \left[p_{ws}^2 - p_{wf}^2 \right] / q$ vs. q on Cartesian graph paper (Fig. 5.31), In addition, plot the stabilized, extended flow point. Table 5.53 summarizes the plotting function. Construct best-fit lines through the modified isochronal data points for each time. Note that the early data points at the lowest rate do not fit on the same straight line as the last three rate points. Consequently, these points are ignored in subsequent.

2. Determine the slopes of the lines for each time by leastsquares regression analysis of the last three data points. For example, Table 5.54 gives values for t=0.5 hour.

The arithmetic average value of the slopes in Table 5.55 is

$$\bar{b} = \frac{b_1 + b_2 + b_3 + b_4}{4} = \frac{(8.817 + 8.313 + 8.488 + 8.538) \times 10^3}{4} = 8.539 \times 10^3 \text{ psia}^2 / \text{cp} / (\text{MMscf} -$$

3. Calculate the stabilized isochronal deliverability line intercept

$$a = \left(p_s^2 - p_{wf}^2 \right) / q - bq = \frac{1.770 \times 10^5}{2.665} - (8.539 \times 10^3)(2.665) = 4.366 \times 10^4 \text{ psia / cp / (MMscf - D)}$$

5. Calculate the AOF potential using the average b value from Step 2 and the stabilized a value.

$$q_{AOF} = \frac{-a + \sqrt{a^2 + 4b\left[p_s{}^2 - (14.65)^2\right]}}{2b} =$$

$$= \frac{-\left(4.366x10^4\right) + \sqrt{\left(4.366x10^4\right)^2 + 4\left(8.539x10^3\right)\left(4.993x10^5 - 214.623\right)}}{2\left(8.539x10^3\right)} = 5.5 \text{ MMscf / D.}$$

EXAMPLE 5.8
MODIFIED ISOCHRONAL TEST WITH NO STABILIZED DATA POINT

The purpose of this example is to compare results obtained from the analysis of a modified isochronal test with and without an extended, stabilized data point. Calculate the AOF for the following modified isochronal test data without the extended flow point. Use both the Brar and Aziz and the stabilized C methods. Compare these results with the results obtained by with the extended flow point (Table 5.56). This example is Well 8 in the Brar and Aziz paper. Only the last four flow points from the test are used in the analysis. Reservoir data are summarized below. In addition, the results from a drawdown test in this well indicate k_g=4.23 md and s = - 5.2.

$h = 454$ ft

$r_w = 0.2615$ ft

$\phi = 0.0675$

$T_{f,wf} = 718°R\left(258°F\right)$.

$\bar{p} = 4{,}372.6$ psia.

$\bar{\mu}_g = 0.023$ cp

$\bar{z} = 0.87$

$\bar{c}_g = 1.69 \times 10^{-4}$ cp

$\gamma_g = 0.65$

$S_w = 0.3$

$A = 640$ acres.

$C_A = 30.8828$. (assume that the well is centered in a square drainage area).

The Rawlins and Schellhardt analysis with extended flow point gave $C=2.426x10^{-3}$, n=0.54, and q_{AOF} = 180.1 MMscf/D. The Houpeurt analysis with extended flow point gave a= $1.455x10^{6}$ $psia^2/cp/MMscf-D$, b=$1.774x10^{4}$ $psia^2/cp/(MMscf-D)^2$, and q_{AOF}=205.6 MMscf/D.

Solution

a) Brar and Aziz Method

1 Plot $\Delta p_p / q = \left[p_p(p_s) - p_p(p_b)\right]/q$ vs. q on Cartesian graph paper (Fig. 5.32). The plotting functions are summarized in Table 5.57. Construct best-fit lines through the modified isochronal data points for each time. The data points at the first rate (31.612 MMscf/D) do not fit on the same straight line as the other three points. Consequently, the first flow rates at each isochron have been ignored, we used all flow rates for each isochron in the subsequent calculations.

2. Determine the slopes of the lines for each time by least-squares regression analysis of the points on the best fit line (the last three data points). See Table 5.58 for values at t=3.0 hours. Table 5.59 gives the slopes of all isochrons. Determine the arithmetic average value of the slopes from Table 5.59.

$$\bar{b} = \frac{b_1 + b_2 + b_3 + b_4}{4} = \frac{(4.803 + 5.238 + 5.302 + 5.535)x10^2}{4} =$$

$$= 5.220x10^2 \text{ psia}^2 / \text{cp} / (\text{MMscf} - \text{D})^2$$

3. Calculate the transient deliverability line intercepts, a_t, for each isochronal line. For example, see Table 5.60 for values at t=3 hours. Table 5.61 gives the values of a_t.

4. Plot a_t vs. log t (Fig. 5.33) and draw the bestfit line through the data. Because of the scatered data, we use the last three data points in our regression analysis to determine the slope, m', and intercept c'. The calculations are summarized in Table 5.62.

5. Calculate the formation permeability to gas using the slope of the semilog straight line.

$$k_g = \frac{1.632x10^6 \bar{\mu}_g \bar{z}T}{m'h} = \frac{(1.632x10^6)(0.023)(0.87)(718)}{(1.193x10^3)(454)} = 43.29 \text{ md},$$

which compares with k_g=4.23 md estimated from the drawdown test analysis.

6. Calculate the skin factor with Eq. 5.63.

$$s = 1.151\left[\left(\frac{c'}{m'}\right) - \log\left(\frac{k_g}{\phi\bar{\mu}_g \bar{c}_t r_w^2}\right) + 3.23\right] =$$

$$= 1.151\left[\left(\frac{6.449x10^3}{1.193x10^3}\right) - \log\left(\frac{43.29}{(0.0675)(0.023)(0.000169)(0.2615)^2}\right) + 3.23\right] = -0.19$$

This value agrees with s= -5.2 estimated from the drawdown test analysis.

7. Calculate the stabilized flow coefficient, a. Assume that the well is centered in a square drainage area with CA =30.8828

$$a = \frac{1.422x10^6 \bar{\mu}_g \bar{z}\bar{T}}{k_g h} x\left[1.151 \cdot \log\left(\frac{10.06A}{C_A r_w^2}\right) - \frac{3}{4} + s\right] = \frac{\left(1.422x10^6\right)(0.023)(0.87)(718)}{(43.29)(454)}$$

$$\left\{1.151 \cdot \log\frac{(10.06)(640)(43{,}560)}{(30.8828)(0.2615)^2} - \frac{3}{4} - 0.19\right\} = 8.742x10^3 \text{ psia}^2 / \text{cp} / (\text{MMscf} - \text{D}).$$

8. Now, calculate the AOF potential using $\bar{b}$ from Step 2 and the stabilized a value calculated in Step 7.

$$q_{AOF} = \frac{-a + \sqrt{a^2 + 4b\left[\bar{p}^2 - (14.65)^2\right]}}{2b} =$$

$$\frac{-\left(8.742x10^3\right) + \sqrt{\left(8.742x10^3\right)^2 + 4(522)\left[1.912x10^9 - 214.623\right]}}{2\left(522x10^4\right)} = 83.23 \text{ MMscf / D.}$$

b) Stabilized C Method

1. Plot $\Delta p^2 = \left[p_{ws}^2 - p_{wf}^2\right]$ vs. q on log-log graph paper (Fig. E.5.34). Use values of p_{ws} for each flow period as the shut-in bottom-hole pressures measured immediately before that flow period. Table 5.63 summarizes the plotting functions. Note that the first data point for each isochron does not follow the trend of the higher-rate points and is ignored in all subsequent calculations.

2. Calculate the deliverability exponent, n, for each line using least-squares regression analysis of the last three points. For example, Table E.5.28 gives values for t=3 hours. Table 5.65 summarizes the deliverability exponents for each isochron.

The arithmetic average slope, $\bar{n}$, of the values in Table 5.65 is

$$\bar{n} = \frac{n_1 + n_2 + n_3 + n_4}{4} = \frac{0.544 + 0.554 + 0.536 + 0.502}{4} = 0.534$$

3. Use the value for the stabilized flow coefficienta, a and b, obtained from the Brar-Aziz analysis: a= 8.742x103 psia2/(MMscf/D) and b=1.873x10^4 psia^2/(cp-MMscf/D)^2, obtained from the Brar and Aziz analysis.

4. Calculate the rate at which the change in pressure squared determined with the Rawlins-Schellhardt equation equals the change in pressure squared determined with the Houpeurt equation.

$$q_e = \frac{a(1-n)}{b(2n-1)} = \frac{8.742x10^3(1-0.534)}{5.220x10^4[2(0.534)-1]} = 114.77 \text{ MMscf / D.}$$

5. Calculate the stabilized C value.

$$C = \frac{q_e}{\left(aq_e + bq_e^{\,2}\right)^n} = \frac{84.2}{\left[\left(8.742x10^3\right)(114.77) + \left(5.220x10^2\right)(114.77)^2\right]^{0.534}} = 2.383x10^{-2}$$

6. Calculate the AOF potential of the well using $\bar{n}$ from Step 2.

$$q_{AOF} = C\left[\bar{p}^2 - p_b^2\right]^n = \left(2.383x10^{-2}\right)\left[1.912x10^7 - 214.623\right]^{0.534} = 184.3 \text{ MMscf / D.}$$

Table 5.66 compares the results of the analysis with and without the extended stabilized flow point. In general, the results are comparable and illustrate the validity of the Brar-Aziz and stabilized C methods in terms of pressure squared. Note, however, that the permeability and skin factor estimated from the Brar-Aziz method using pressure squared did not agree with the drawdown analysis or the Brar-Aziz analysis.

Nomenclature

a = stabilized deliverability coefficient, (psia2cp)/(MMscf-D) for calculations in terms of pseudopressure or psia2/(MMscf-D) for calculations in terms of pressure squared

a_t = transient deliverability coefficient, (psia2cp)/(MMscf-D) for calculations in terms of pseudopressure or psia2/(MMscf-D) for calculations in terms of pressure squared

A = drainage area of well, ft^2

b = deliverability equation coefficient, (psia2cp)/(MMscf-D)2 for calculations in terms of pseudopressure or psia2/(MMscf-D)2 for calculations in terms of pressure squared

c' = constant in Eq. 5.58

C_f = formation compressibility, psia

c_g = gas compressibility, $psia^{-1}$

c-g = gas compressibility at average reservoir pressure, psia

c' = total system compressibility, $psia^{-1}$

C_W = water compressibility, $psia^{-1}$

C = stabilized performance coefficient, (MMscfD)/(psia2-cp)n for calculations in terms of pseudopressure or (MMscf-D)/psia2n for calculations in terms of pressure squared

CA = shape constant or factor for well drainage area

C_t = transient performance coefficient, (Mmscf D)/(psia2-cp)n for calculations in terms of pseudopressure or (MMscf-D)/psia2n for calculations in terms of pressured squared

D = non-Darcy flow constant, D/MMscf h = net formation thickness, ft j = summation parameter

k_g = reservoir effective permeability to gas, md

L = flow-string length from surface to middle of perforations, ft

m = slope of at or (at+by) vs. log (t) plot, $(psia^2cp)/(MMscf\text{-}D)$ per cycle for calculations in terms of pseudopressure or $psia^2/(MMscf\text{-}D)$ per cycle for calculations in terms of pressure squared

m' = constant in Eq. 5.58

n = inverse slope (exponent) of deliverability curve

N = number of data points used in regression analysis

p = pressure, psia

Pa = atmospheric pressure, psia

P_b = base pressure, psia

P_i = initial reservoir pressure, psia

p_p = gas pseudopressure, $psia^2/cp$

$p_p(\bar{p})$ = average reservoir pseudopressure, $psia^2/cp$

$P_p(P_{wf})$ = flowing sandface pseudopressure, $psia^2/cp$

$P_p(P_{wS})$ = static sandface pseudopressure, $psia^2/cp$

$\bar{p}$ = average reservoir pressure, psia

P_S = stabilized shut-in BHP measured before the deliverability test, psia

Δp^2 = difference of squared static and flowing pressures, $psia^2$

Δp_p = difference of static and flowing sandface pseudopressures, $psia^2/cp$

P_{tf} = flowing wellhead pressure, psia

P_{wf} = BHFP, psia

P_{ws} = shut-in BHP, psia

q = total wellstream gas flow rate, MMscf/D

q_{AOF} = AOF potential, MMscf/D

q_e = rate at which pressure drops from Houpeurt and Rawlins-Schellhardt equations are equal, MMscf/D

r = radial distance from center of wellbore, ft

r_d = effective (transient) radius of drainage, ft

r_e = external radius of drainage, ft

r_i = radius of investigation, ft

r_w = wellbore radius, ft

s = skin factor, dimensionless

S_g = gas saturation, fraction of PV

S_O = oil saturation, fraction of PV

S_w = water saturation, fraction of PV t = elapsed time, hours

t_D = dimensionless time

t_{LfD} = dimensionless time calculated with fracture half length

t_S = well stabilization time, hours

T= temperature, °R

T_f = temperature, °F

z = gas-law deviation factor, dimensionless

$\bar{z}$ = gas-law deviation factor at average reservoir pressure and temperature, dimensionless

α = exponent in Eq. 5.32

β = turbulence factor

γ_g = gas specific gravity (air= 1.0)

μ_g = gas viscosity, cp

$\bar{\mu}_g$ = gas viscosity at average reservoir pressure and temperature, cp

ϕ = porosity of reservoir rock, fraction

References

1. Houpeurt, A.: "On the Flow of Gases in Porous Media," Revue de L'Institut Francais du Petrole (1959) XIV (11), 1468-1684.
2. Rawlins, E.L. and Schellhardt, M.A.: Backpressure Data on Natural Gas Wells and TheirApplicatuan to Production Practices, Monograph Series, USBM (1935)
3. Al-Hussainy, R., Ramey, H.J. Jr., and Crawford, P.B.: "The Flow of Real Gases Through Porous Media," JPT (May 1966) 624-36 Trans., AIME, 237.
4. Jones, S.C.: "Using the Inertial Coefficient, §, To Characterize Heterogeneity in Reservoir Rock," paper SPE 16949 presented at the 1987 SPE Annual Technical Conference and Exhibition, Dallas, Sept. 27-30.
5. Lee, W.J.: Well Testing, Textbook Series, SPE, Richardson, TX (1977) 1.
6. Earlougher, R.C. Jr.: Advances in Well TestAnalysis, Monograph Series, SPE, Richardson, TX (1977) 5.
7. Gringarten, A.C., Ramey, H.J. Jr., and Raghavan, R.: "UnsteadyState Pressure Distributions Created by a Well With a Single InfiniteConductivity Vertical Fracture," SPEJ (Aug. 1974) 347-60; Trans., AIME, 257.
8. Gringarten, A.C., Ramey, H.J. Jr., and Raghavan, R.: "Applied Pressure Analysis for Fractured Wells," JPT(July 1975) 887-92; Trans., AIME, 259.
9. Theory and Proaice of the Testing of Gas Wells, third edition, Energy Resources and Conservation Board, Calgary (1978).
10. Jennings, J.W. et al.: "Deliverability Testing of Natural Gas Wells, " prepared for the Texas Railroad Commission, Petroleum Engineering Dept., Texas A&M U., College Station, TX (Aug. 1989).
I I. Cullender, M.H.: "The Isochronal Performance Method of Determining the Flow Characteristics of Wells, " Trans., AIME (1955) 204, 137-42.
12. Katz, D.L. et al.: Handbook of Natural Gas Engineering, McGrawHill Publishing Co., New York City (1959).

13. Brar, G.S. and Aziz, K.: "Analysis of Modified Isochronal Tests To Predict the Stabilized Deliverability Potential of Gas Wells Without Using StabilizedFlowData,"JPT(Feb. 1978)297-304; Trans.,AIME 265.

14. Johnston, J.L., Lee, W.J., and Blasingame, T.A.: "Estimating the Stabilized Deliverability of a Gas Well Using the Rawlins and Schellhardt Method: An Analytical Approach," paper SPE 23440 presented at the 1991 SPE Eastern Regional Meeting, Lexington, Oct. 22-25.

15. Donohue, D.A.T. and Ertekin, T.: Gaswell Testing, Intl. Human Resources Development Corp., Boston, MA (1982).

APPENDIX A

FIGURES AND TABLES

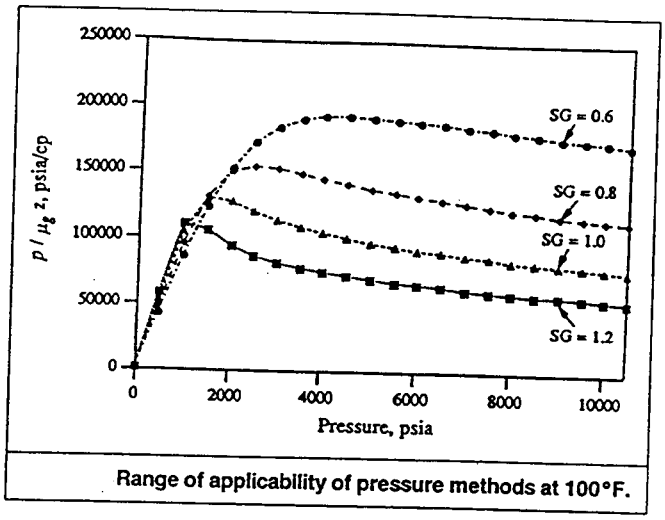
250000
200000
150000
100000
50000
0
$p / \mu_g z$, psia/cp
SG = 0.6
SG = 0.8
SG = 1.0
SG = 1.2
0
2000
4000
6000
8000
10000
Pressure, psia
Range of applicability of pressure methods at 100°F.

FIG. 5.1

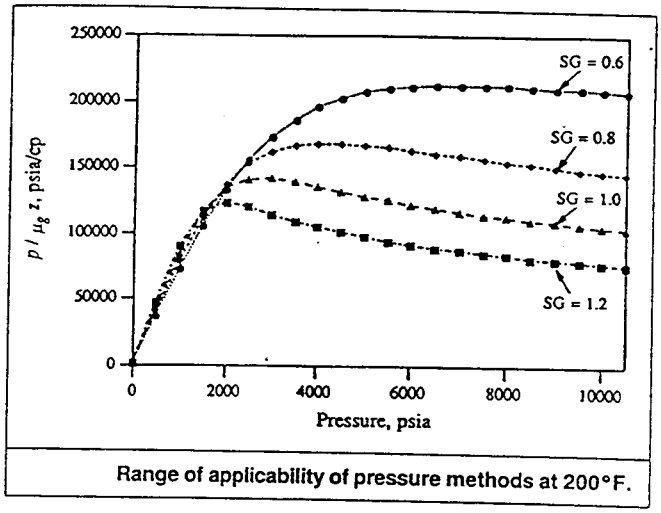
250000
200000
150000
100000
50000
0
$p / \mu_g z$, psia/cp
SG = 0.6
SG = 0.8
SG = 1.0
SG = 1.2
0
2000
4000
6000
8000
10000
Pressure, psia
Range of applicability of pressure methods at 200°F.

FIG. 5.2

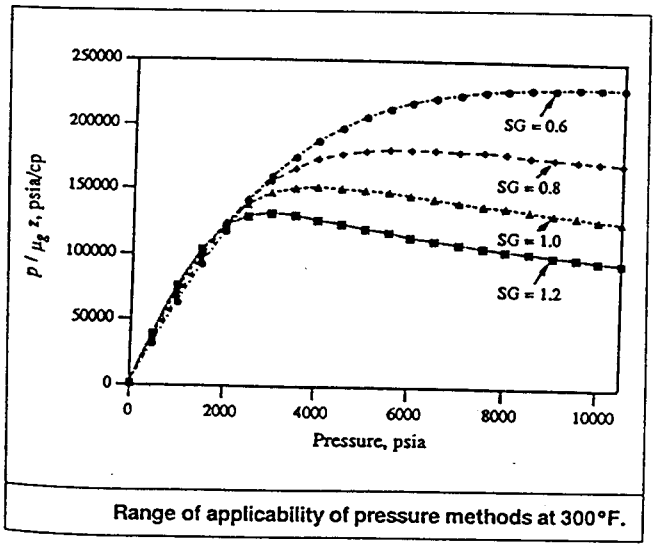

Range of applicability of pressure methods at 300°F.

FIG. 5.3

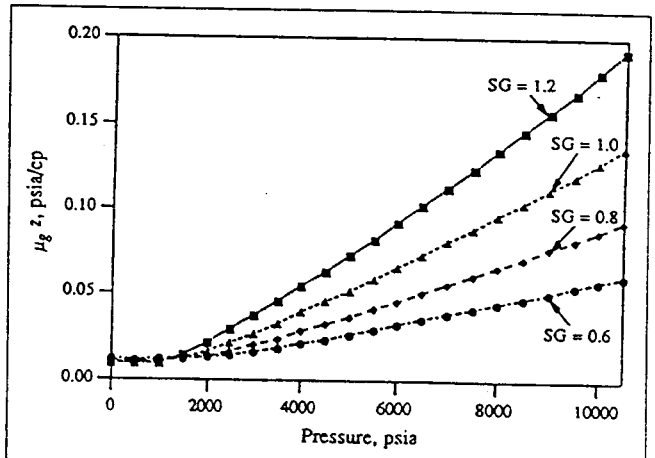

Range of applicability of pressure-squared methods at 100°F.

FIG. 5.4

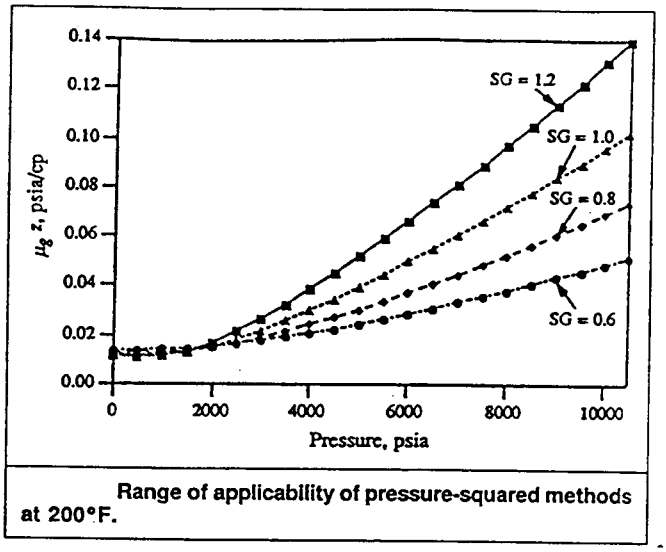

Range of applicability of pressure-squared methods at 200°F.

FIG. 5.5

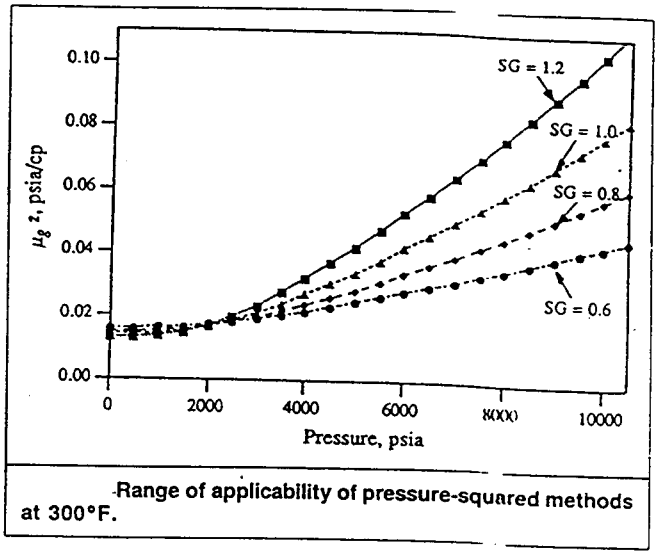

Range of applicability of pressure-squared methods at 300°F.

FIG. 5.6

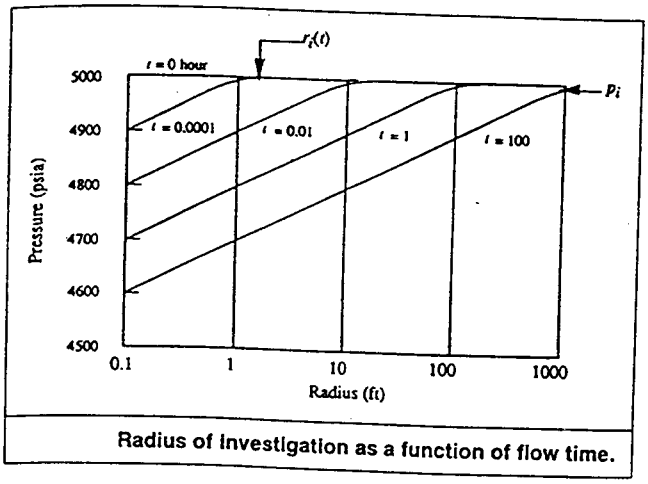

Radius of investigation as a function of flow time.

FIG. 5.7

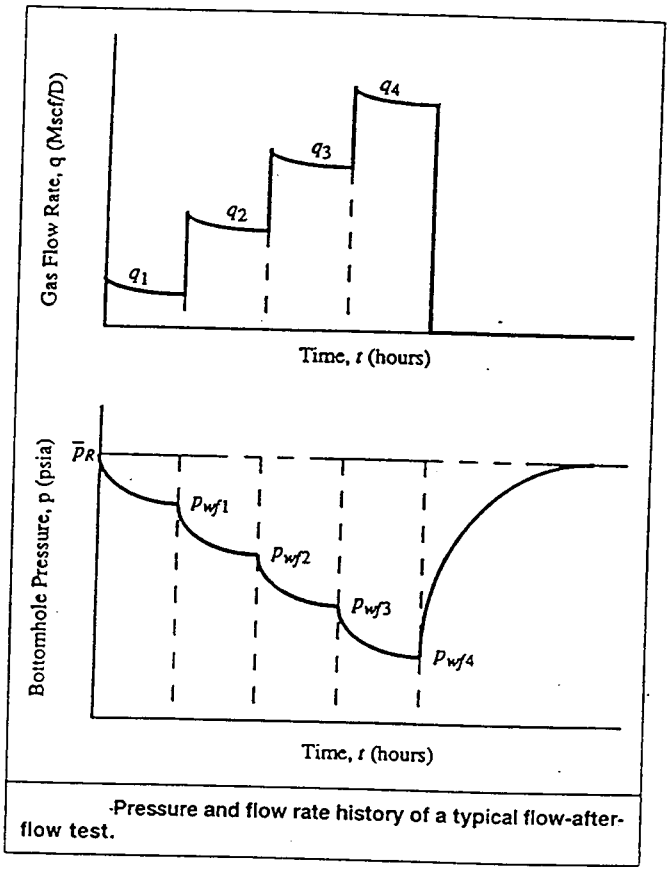

Pressure and flow rate history of a typical flow-after-flow test.

FIG. 5.8

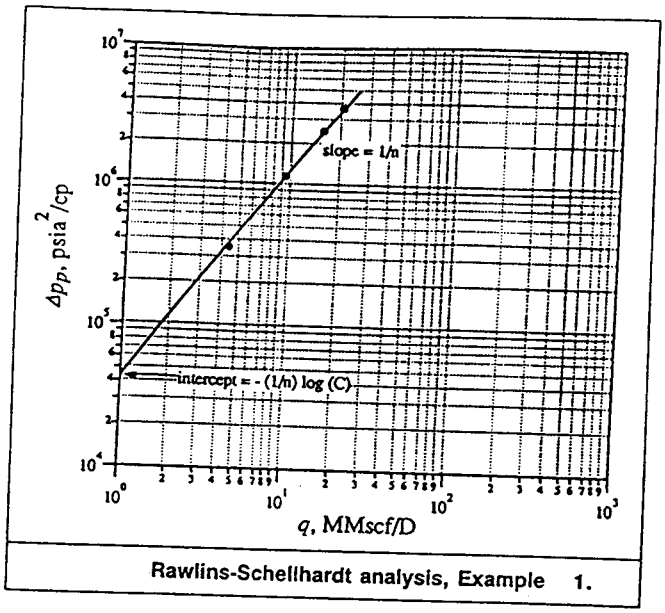

Rawlins-Schellhardt analysis, Example 1.

FIG. 5.9

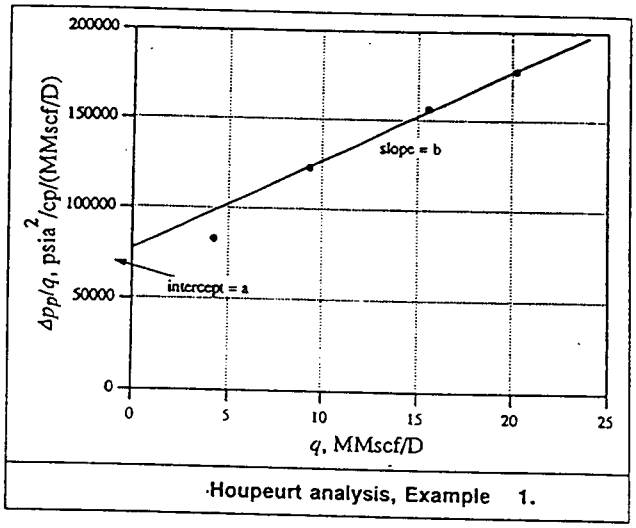

Houpeurt analysis, Example 1.

FIG. 5.10

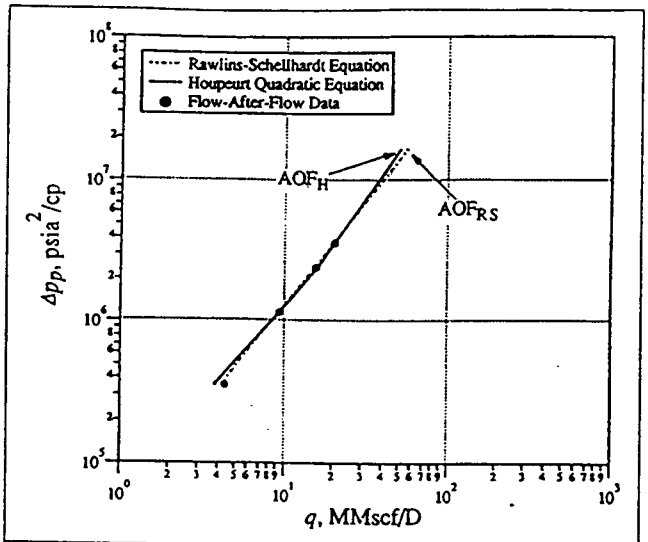

Comparison of results from the Rawlins-Schellhardt and Houpeurt methods, Example 7.1.

FIG. 5.11

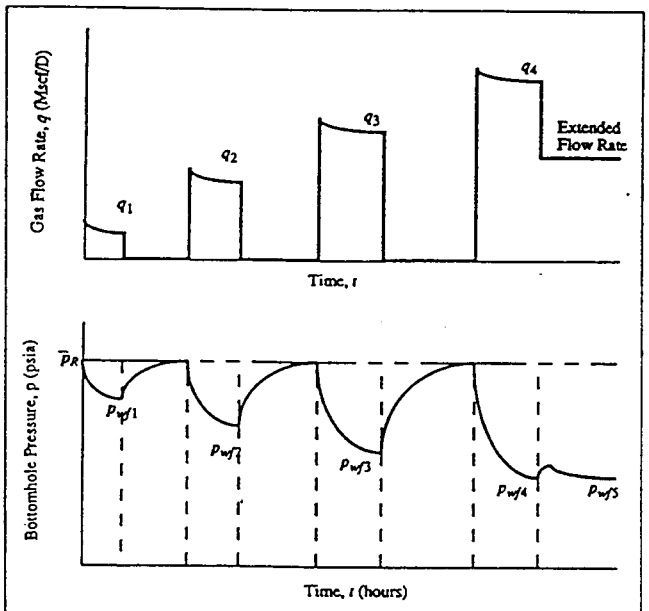

Pressure and flow rate history of a typical isochronal test.

FIG. 5.12

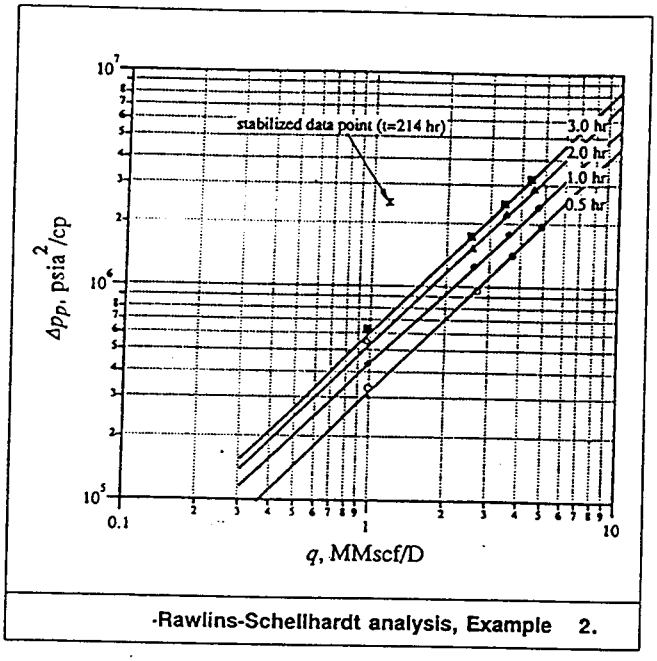

FIG. 5.13

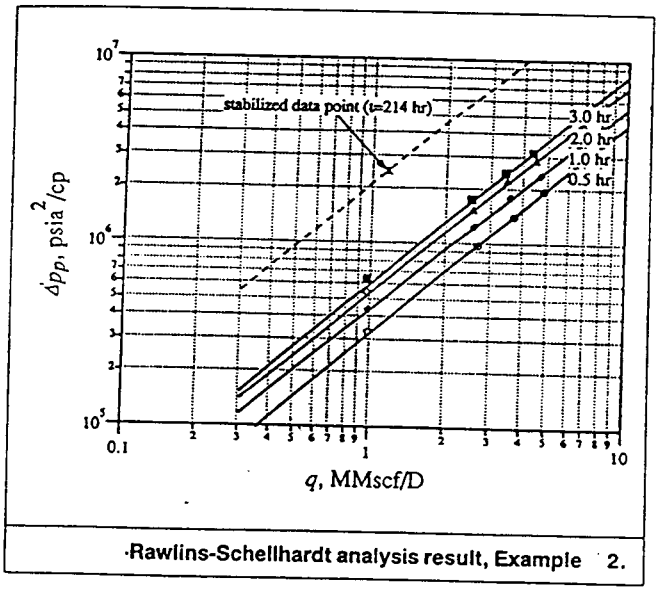

FIG. 5.14

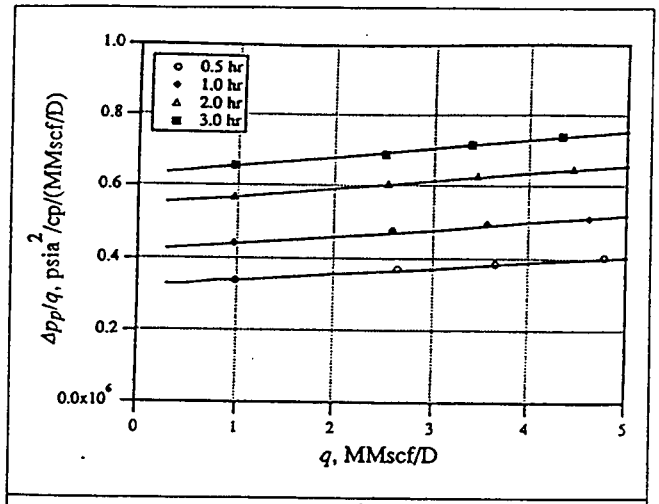

Houpeurt analysis of isochronal test data, Example 2.

FIG. 5.15

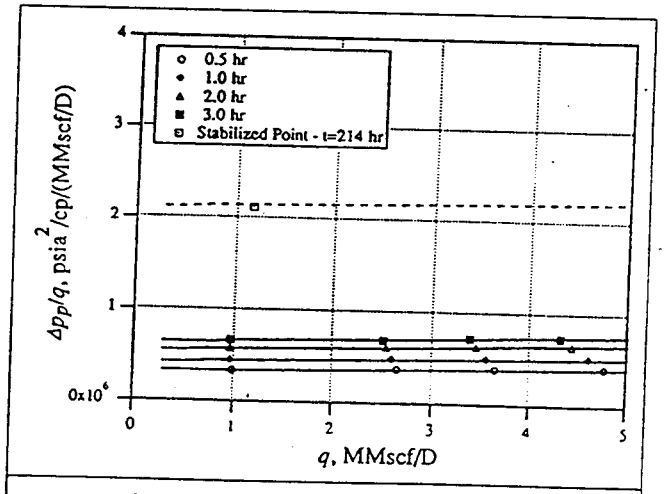

Example 2. Houpeurt analysis of isochronal test data result,

FIG. 5.16

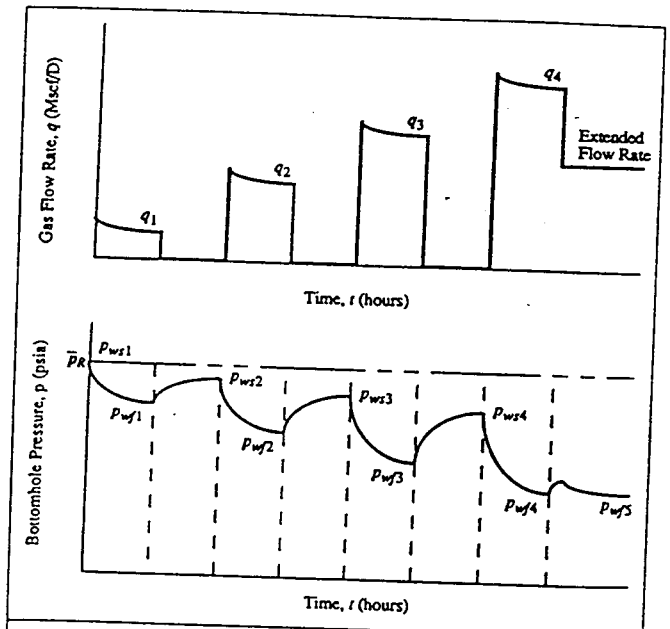

Pressure and flow rate history of a typical modified isochronal test.

FIG. 5.17

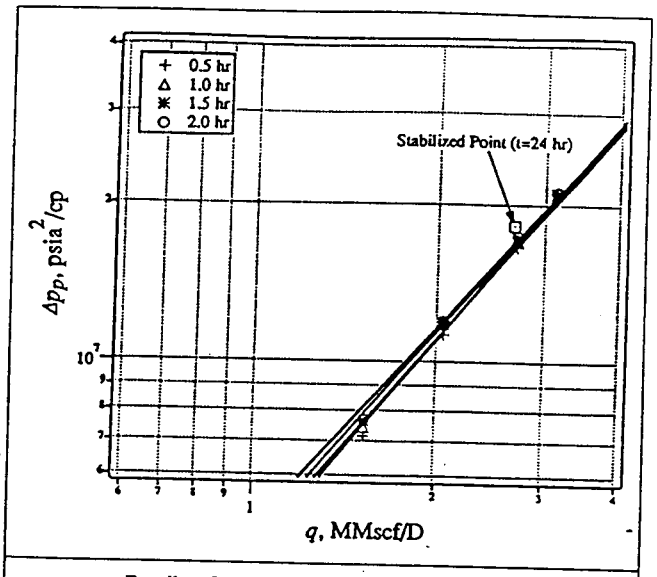

Rawlins-Schellhardt plot of the modified isochronal test data, Example 3.

FIG. 5.18

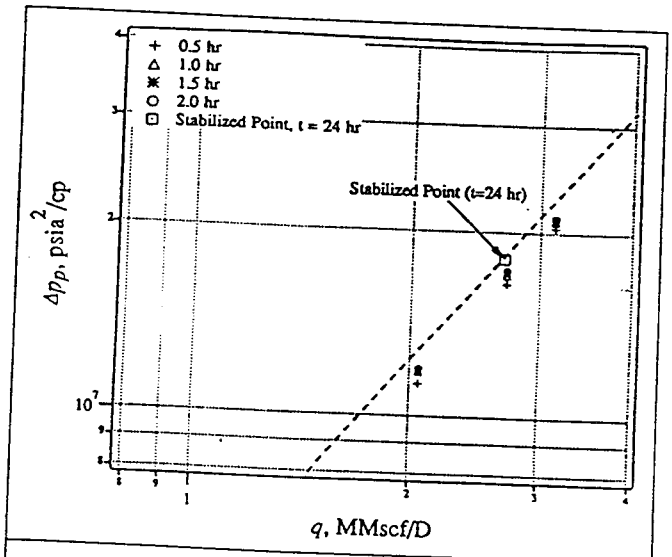

Rawlins-Schellhardt analysis of a modified isochronal test, Example 3.

FIG. 5.19

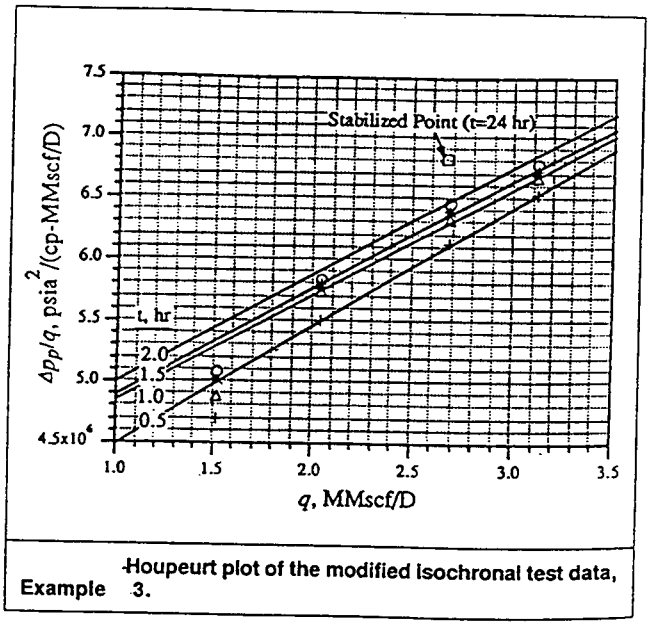

Example 3. Houpeurt plot of the modified isochronal test data,

FIG. 5.20

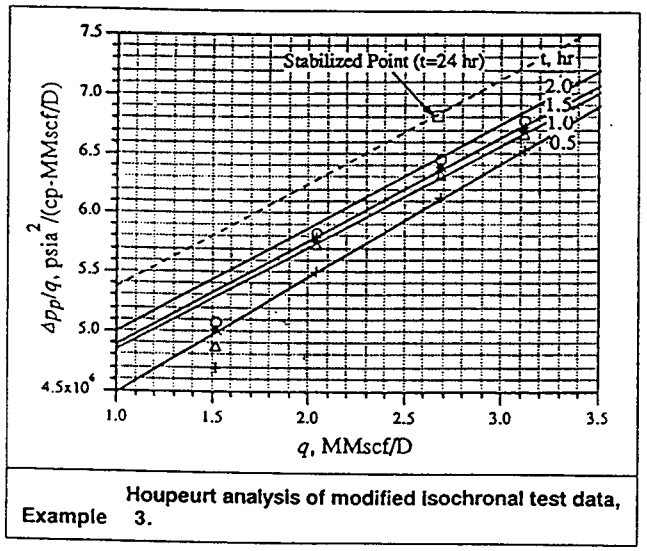

Example 3. Houpeurt analysis of modified isochronal test data,

FIG. 5.21

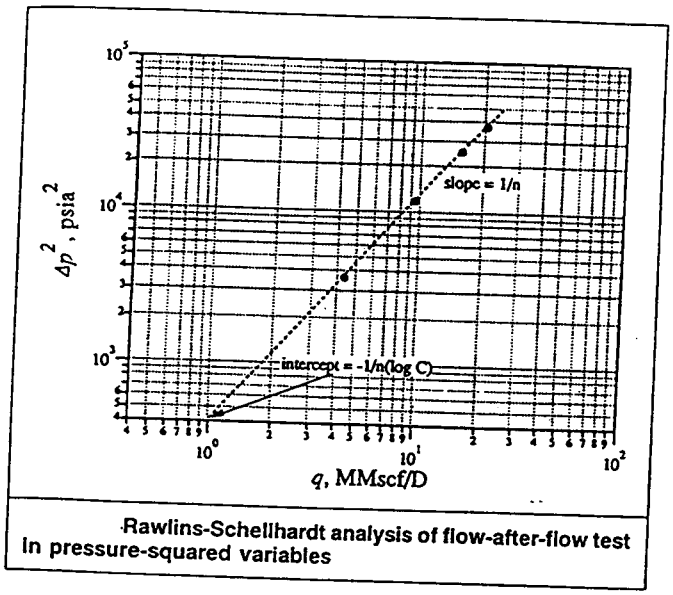

Rawlins-Schellhardt analysis of flow-after-flow test in pressure-squared variables

FIG. 5.25

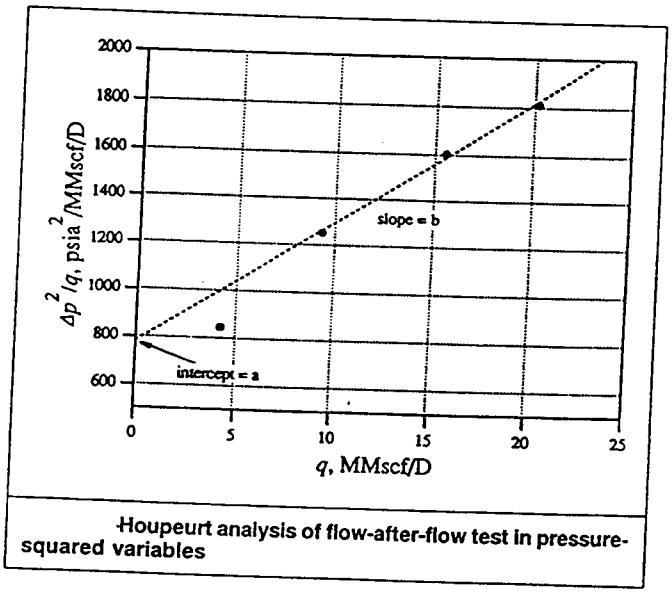

Houpeurt analysis of flow-after-flow test in pressure-squared variables

FIG. 5.26

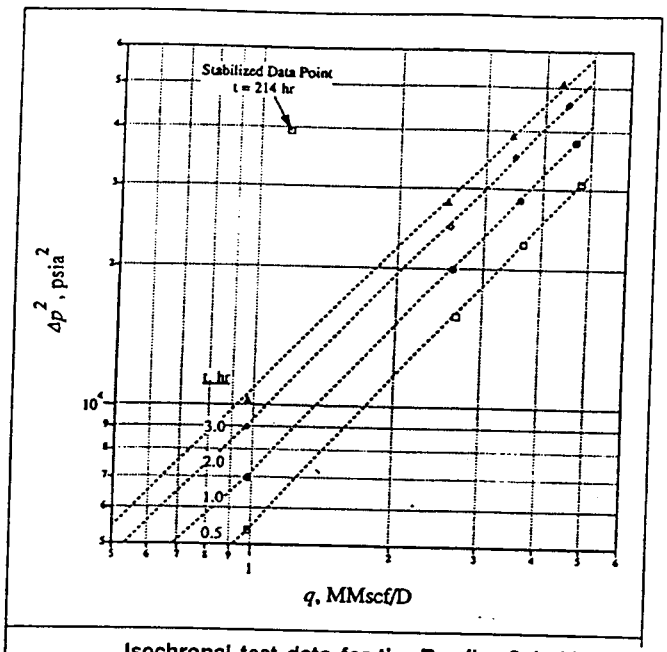

Isochronal test data for the Rawlins-Schellhardt analysis

FIG. 5.27

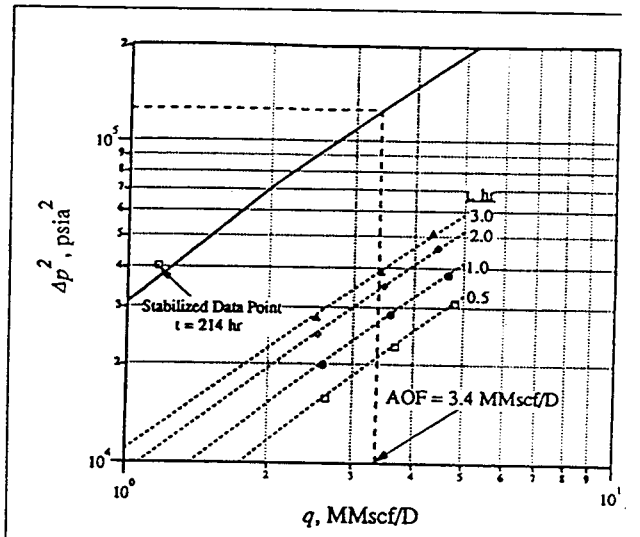

-Rawlins-Schellhardt analysis of isochronal test.

FIG. 5.28

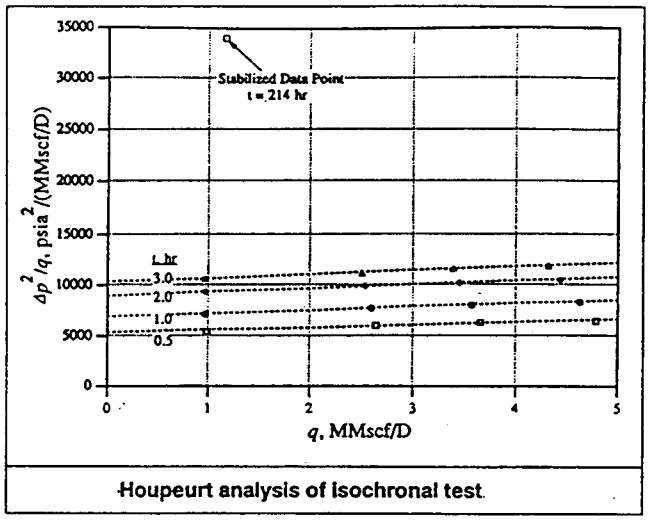
35000
30000
25000
20000
15000
10000
5000
0
Stabilized Data Point
t = 214 hr
t, hr
3.0
2.0
1.0
0.5
$\Delta p^2/q$, psia^2/(MMscf/D)
0
1
2
3
4
5
q, MMscf/D
Houpeurt analysis of isochronal test

FIG. 5.29

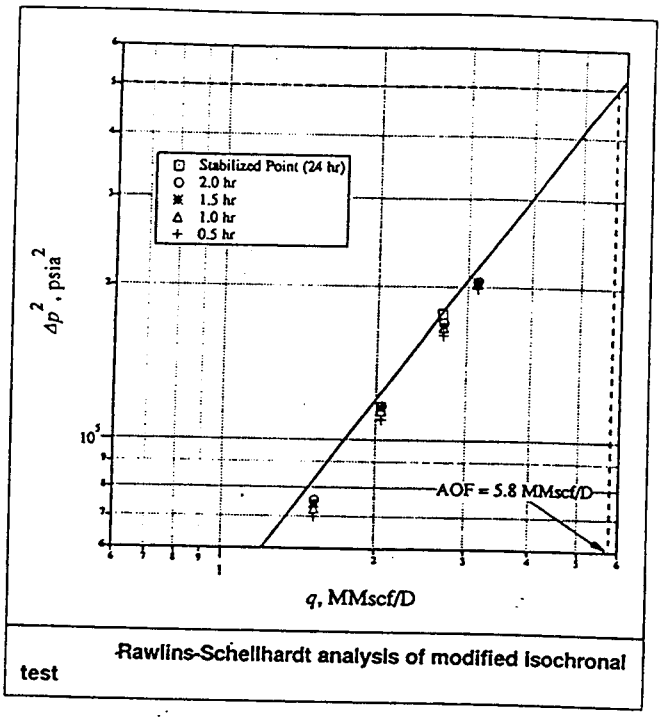

Rawlins-Schellhardt analysis of modified isochronal test

FIG. 5.30

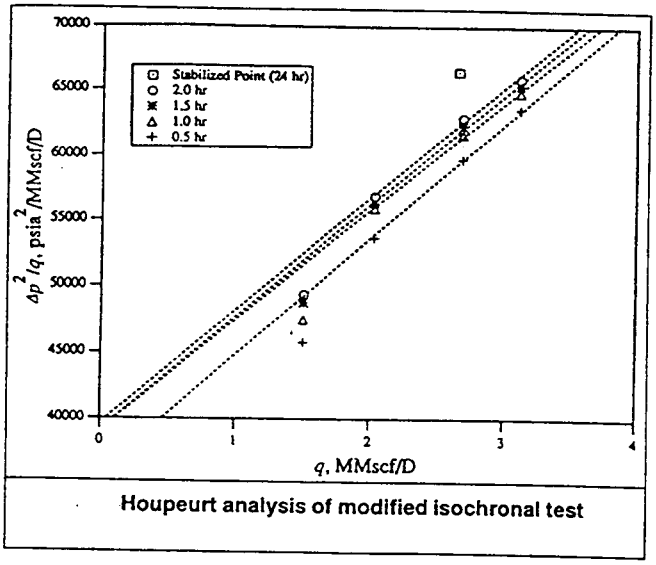

Houpeurt analysis of modified isochronal test

FIG. 5.31

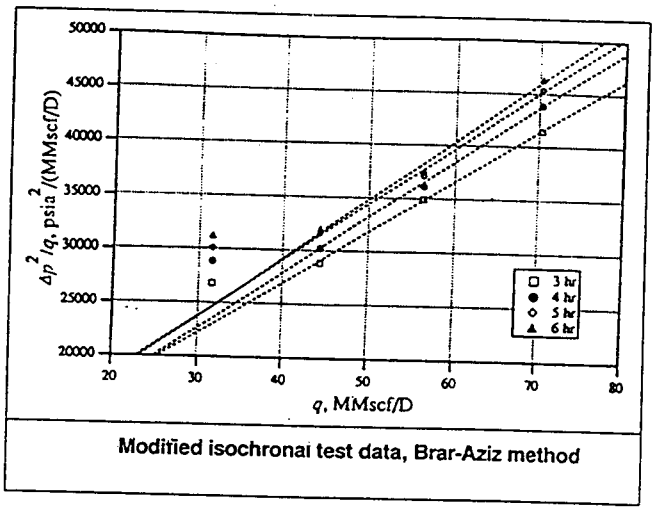
50000
45000
40000
35000
30000
25000
20000
20
30
40
50
60
70
80
$\Delta p^2/q$, psia^2/(MMscf/D)
q, MMscf/D
3 hr
4 hr
5 hr
6 hr
Modified isochronal test data, Brar-Aziz method

FIG. 5.32

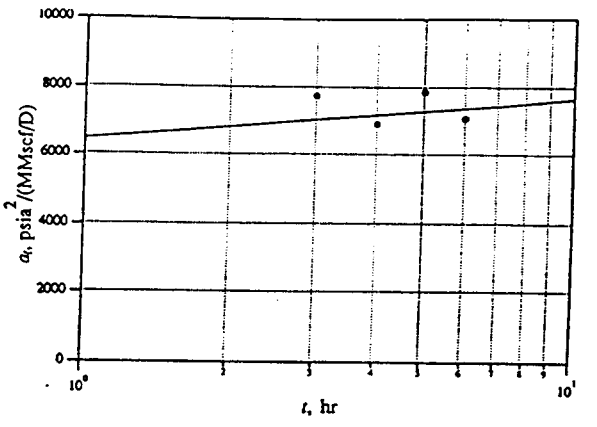

Fig. H-9—Brar-Aziz plot of a_t vs. t, Example H-4.

FIG. 5.33

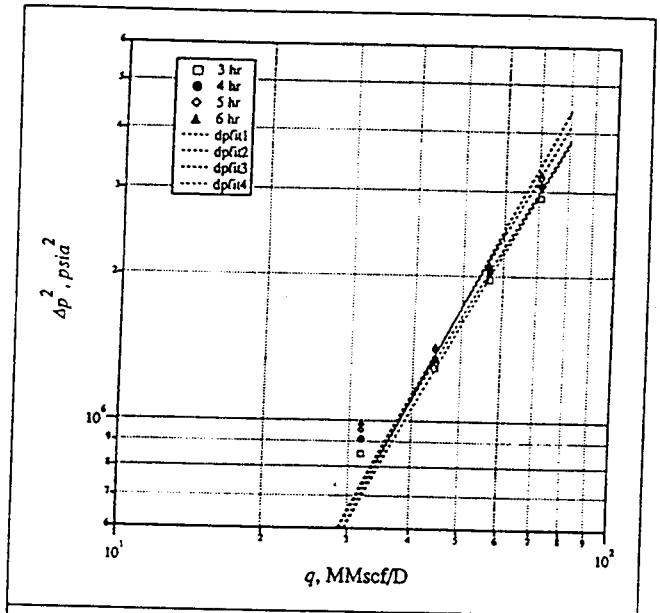

Fig. H-10—Stabilized C analysis of modified Isochronal test, Example H-4.

FIG. 5.34

TABLE 5.1

EFFECTS OF PERMEABILITY AND DRAINAGE AREA ON STABILIZATION TIME

k (md)	A (acres)	t_s (hours)
0.01	40	25,953 (3 years)
0.01	640	415,242 (47 years)
0.1	40	2,595 (108 years)
0.1	640	41,524 (4.7 years)
1.0	40	259.5 (10.8 years)
1.0	640	4,152.4 (173 days)
10.0	40	25.95 (1.1 days)
10.0	640	415.2 (17.3 days)
100.0	40	2.59 (0.11 days)
100.0	640	41.52 (1.73 days)
1,000.0	40	0.259 (0.011 days)
1,000.0	640	4.15 (0.173 days)

TABLE 5.2

EFFECTS OF PERMEABILITY AND HYDRAULIC FRACTURE HALF-LENGTH ON TIME TO REACH PSEUDORADIAL FLOW

Case	k (md)	L_f (ft)	t_{prf} (hours)
1	1	100	51.2
2	0.01	100	5,120 (213 days)
3	0.01	1,000	512,000 (58 years)

TABLE 5.3

FLOW-AFTER-FLOW TEST DATA, EXAMPLE 1

q (MMscf/D)	$T_{f,ff}$ (°F)	p_{ff} (psia)	p_{wf} (psia)	$p_p(p_{wf})$ (psia²/cp)
0	75	375.2	$p = 407.60$	1.6173×10^7
4.288	70	371.2	403.13	1.5817×10^7
9.265	73	361.3	393.03	1.5032×10^7
15.552	77	343.8	375.79	1.3736×10^7
20.177	77	327.1	359.87	1.2591×10^7

TABLE 5.4

PLOTTING FUNCTIONS FOR RAWLINS-SCHELLHARDT ANALYSIS, EXAMPLE 1

q (MMscf/D)	$\Delta p_p = p_p(\bar{p}) - p_p(p_{wf})$ (psia²/cp)
4.288	3.560×10^5
9.265	1.141×10^6
15.552	2.437×10^6
20.177	3.582×10^6

TABLE 5.5

LEAST-SQUARES REGRESSION, RAWLINS-SCHELLHARDT ANALYSIS, EXAMPLE 1

Point	log q	log Δp_p	(log Δp_p)²	log q log Δp_p
1	0.6323	5.5514	30.8186	3.5102
2	0.9668	6.0573	36.6909	5.8562
3	1.1918	6.3879	40.8053	7.6131
4	1.3049	6.5541	42.9562	8.5524
$\Sigma =$	4.0958	24.5507	151.2710	25.5319

TABLE 5.6

TABLE 7.6—PLOTTING FUNCTIONS FOR THE HOUPEURT ANALYSIS, EXAMPLE 7.1	
q (MMscf/D)	$\frac{\Delta p_p}{q} = \frac{p_p(\bar{p}) - p_p(p_{wf})}{q}$ (psia²/cp)/(MMscf/D)
4.288	0.8302×10^5
9.265	1.232×10^5
15.552	1.567×10^5
20.177	1.775×10^5

TABLE 5.7

TABLE 7.7—LEAST-SQUARES REGRESSION, HOUPEURT ANALYSIS, EXAMPLE 7.1				
Point	q	q^2	Δp_p	$\Delta p_p/q$
2	9.265	85.84	1.141×10^6	1.232×10^5
3	15.552	241.87	2.437×10^6	1.567×10^5
4	20.177	407.11	3.582×10^6	1.775×10^5
$\Sigma =$	44.994	734.82	7.160×10^6	4.574×10^5

TABLE 5.8

TABLE 7.8—ISOCHRONAL TEST DATA, EXAMPLE 7.2			
Time (hours)	q (MMscf/D)	p_{wf} (psia)	$p_p(p_{wf})$ (psia²/cp)
0.5	0.983	344.7	9.6386×10^6
1.0	0.977	342.4	9.5406×10^6
2.0	0.970	339.5	9.4179×10^6
3.0	0.965	337.6	9.3381×10^6
0.5	2.631	329.5	9.0027×10^6
1.0	2.588	322.9	8.7351×10^6
2.0	2.533	315.4	8.4371×10^6
3.0	2.500	310.5	8.2458×10^6
0.5	3.654	318.7	8.5674×10^6
1.0	3.565	309.5	8.2071×10^6
2.0	3.453	298.6	7.7922×10^6
3.0	3.390	291.9	7.5435×10^6
0.5	4.782	305.5	8.0534×10^6
1.0	4.625	293.6	7.6136×10^6
2.0	4.438	279.6	7.0990×10^6
3.0	4.318	270.5	6.7797×10^6
214 (Extended flow point)	1.156	291.6	7.5285×10^6

TABLE 5.9

PLOTTING FUNCTIONS FOR THE RAWLINS-SCHELLHARDT ANALYSIS, EXAMPLE 2

t (hours)	q (MMscf/D)	Δp_p (psia^2/cp)	t (hours)	q (MMscf/D)	Δp_p (psia^2/cp)
0.5	0.983	0.3329×10^6	2.0	3.654	1.4041×10^6
	0.977	0.4309×10^6		3.565	1.7644×10^6
	0.970	0.5536×10^6		3.453	2.1793×10^6
	0.965	0.6334×10^6		3.390	2.4280×10^6
1.0	2.631	0.9688×10^6	3.0	4.782	1.9181×10^6
	2.588	1.2364×10^6		4.625	2.3579×10^6
	2.533	1.5344×10^6		4.438	2.8725×10^6
	2.500	1.7257×10^6		4.318	3.1918×10^6
			214	1.156	2.443×10^6

TABLE 5.10

LEAST-SQUARES REGRESSION, RAWLINS-SCHELLHARDT ANALYSIS, EXAMPLE 2

Point	log q	log Δp_p	(log Δp_p)^2	log q log Δp_p
2	0.4201	5.9862	35.8346	2.5148
3	0.5628	6.1474	37.7905	3.4598
4	0.6796	6.2829	39.4748	4.2699
Σ =	1.6625	18.4165	113.0999	10.2445

TABLE 5.11

DELIVERABILITY EXPONENTS FOR VARIOUS FLOWING TIMES, EXAMPLE 2

t (hours)	n
0.5	0.88
1.0	0.91
2.0	0.89
3.0	0.88

TABLE 5.12

PLOTTING FUNCTIONS FOR HOUPEURT ANALYSIS, EXAMPLE 2

t (hours)	q (MMscf/D)	$\Delta p_p/q$ (psia^2/cp/MMscf-D)	t (hours)	q (MMscf/D)	$\Delta p_p/q$ (psia^2/cp/MMscf-D)
0.5	0.983	3.387×10^5	2.0	0.970	5.707×10^5
	2.631	3.682×10^5		2.533	6.058×10^5
	3.654	3.843×10^5		3.453	6.311×10^5
	4.782	4.011×10^5		4.438	6.473×10^5
1.0	0.977	4.410×10^5	3.0	0.965	6.564×10^5
	2.588	4.777×10^5		2.500	6.903×10^5
	3.565	4.949×10^5		3.390	7.162×10^5
	4.625	5.098×10^5		4.318	7.392×10^5
			214	1.156	2.113×10^6

TABLE 5.13

LEAST-SQUARES REGRESSION, HOUPEURT ANALYSIS, EXAMPLE 2

Point	q	q^2	Δp_p	$\Delta p_p/q$
1	0.983	0.966	0.3320×10^6	3.387×10^5
2	2.631	6.922	0.9688×10^6	3.682×10^5
3	3.654	13.352	1.4041×10^6	3.843×10^5
4	4.782	22.868	1.9181×10^6	4.011×10^5
$\Sigma=$	12.050	44.108	4.6239×10^6	14.923×10^5

TABLE 5.14

SLOPES, b, OF ISOCHRONS, EXAMPLE 2	
t (hours)	b [psia^2/(MMscf-D)^2]
0.5	1.644×10^4
1.0	1.904×10^4
2.0	2.255×10^4
3.0	2.492×10^4

TABLE 5.15

MODIFIED ISOCHRONAL TEST DATA, EXAMPLE 3

Time (hours)	p_{wf} (psia)			
	$q = 1.520$ MMscf/D	$q = 2.041$ MMscf/D	$q = 2.688$ MMscf/D	$q = 3.122$ MMscf/D
0 (p_{ws})	706.6	706.6	703.5	701.2
0.5	655.6	624.5	578.5	541.7
1.0	653.6	620.7	573.9	537.8
1.5	652.1	619.9	572.3	536.3
2.0	651.3	619.1	570.8	534.7
	$p_p(p_{wf})$ (psia)			
0[$p_p(p_{ws})$]	5.093×10^7	5.093×10^7	5.093×10^7	5.015×10^7
0.5	4.379×10^7	3.970×10^7	3.403×10^7	2.979×10^7
1.0	4.352×10^7	3.922×10^7	3.348×10^7	2.936×10^7
1.5	4.332×10^7	3.911×10^7	3.330×10^7	2.919×10^7
2.0	4.321×10^7	3.901×10^7	3.312×10^7	2.902×10^7

Extended Flow Point

$p_{wf} = 567.7$ psia	$t = 24$ hours
$\bar{p} = 706.6$ psia	$q = 2.665$ MMscf/D
$p_p(p_{wf}) = 3.276 \times 10^7$ psia^2/cp	$p_p(14.65) = 2{,}766.6$ psia^2/cp

TABLE 5.16

PLOTTING FUNCTIONS FOR RAWLINS-SCHELLHARDT ANALYSIS, EXAMPLE 3

Time (hours)	Δp_p (psia^2/cp)			
	$q = 1.520$ MMscf/D	$q = 2.041$ MMscf/D	$q = 2.688$ MMscf/D	$q = 3.122$ MMscf/D
0.5	0.714×10^7	1.123×10^7	1.645×10^7	2.039×10^7
1.0	0.741×10^7	1.171×10^7	1.700×10^7	2.082×10^7
1.5	0.761×10^7	1.182×10^7	1.718×10^7	2.099×10^7
2.0	0.772×10^7	1.192×10^7	1.736×10^7	2.113×10^7

TABLE 5.17

LEAST-SQUARES REGRESSION, RAWLINS-SCHELLHARDT ANALYSIS, EXAMPLE 3

Point	log q	log Δp_p	(log Δp_p)^2	log q log Δp_p
2	0.3098	7.0503	49.7067	2.1842
3	0.4294	7.2162	52.0735	3.0986
4	0.4944	7.3088	53.4186	3.6135
$\Sigma =$	1.2336	21.5753	155.1988	8.8963

TABLE 5.18

SLOPES, n, OF ISOCHRONS, EXAMPLE 3

t (hours)	n
0.5	0.72
1.0	0.74
1.5	0.74
2.0	0.78

TABLE 5.19

PLOTTING FUNCTIONS FOR HOUPEURT ANALYSIS, EXAMPLE 3

Time (hours)	$\Delta p_p/q$ [psia^2/(cp1MMscf/D)]			
	$q = 1.520$ MMscf/D	$q = 2.041$ MMscf/D	$q = 2.688$ MMscf/D	$q = 3.122$ MMscf/D
0.5	0.470×10^7	0.550×10^7	0.612×10^7	0.653×10^7
1.0	0.488×10^7	0.574×10^7	0.632×10^7	0.667×10^7
1.5	0.501×10^7	0.579×10^7	0.639×10^7	0.672×10^7
2.0	0.508×10^7	0.584×10^7	0.646×10^7	0.678×10^7

TABLE 5.20

LEAST-SQUARES REGRESSION, HOUPEURT ANALYSIS, EXAMPLE 3

Point	q	q^2	Δp_p	$\Delta p_p/q$
2	2.041	4.166	1.123×10^7	0.550×10^7
3	2.688	7.225	1.645×10^7	0.612×10^7
4	3.122	9.747	2.039×10^7	0.653×10^7
$\Sigma =$	7.851	21.138	4.807×10^7	1.815×10^7

SLOPES, b, OF THE ISOCHRONS, EXAMPLE 3

t (hours)	b [psia^2/cp/(MMscf-D)^2]
0.5	9.654×10^5
1.0	8.678×10^5
1.5	8.711×10^5
2.0	8.780×10^5

TABLE 5.21

TABLE 5.22

MODIFIED ISOCHRONAL TEST DATA, EXAMPLE 4

Time (hours)	p_{wf} (psia) $q=31.612$ MMscf/D	$q=44.313$ MMscf/D	$q=56.287$ MMscf/D	$q=70.265$ MMscf/D
0 (p_{ws})	4,372.6	4,356.0	4,344.3	4,343.6
3.0	4,274.1	4,206.5	4,111.8	3,994.6
4.0	4,266.8	4,199.3	4,103.3	3,973.3
5.0	4,262.5	4,192.0	4,097.0	3,959.6
6.0	4,258.3	4,190.4	4,093.5	3,951.9
	$p_p(p_{wf})$ (psia^2/cp)			
0[$p_p(p_{ws})$]	1.049×10^9	1.042×10^9	1.038×10^9	1.037×10^9
3.0	1.011×10^9	9.848×10^8	9.488×10^8	9.047×10^8
4.0	1.008×10^9	9.821×10^8	9.456×10^8	8.968×10^8
5.0	1.006×10^9	9.793×10^8	9.433×10^8	8.916×10^8
6.0	1.005×10^9	9.787×10^8	9.419×10^8	8.888×10^8

Extended Flow Point

$p_{wf}=3{,}794.0$ psia
$p=4{,}372.6$ psia
$p_p(p_{wf})=8.303\times10^8$ psia^2/cp
$t=72$ hours
$q=77.346$ MMscf/D
$p_p(14.65)=2{,}003.8$ psia^2/cp

TABLE 5.23

PLOTTING FUNCTIONS FOR BRAR AND AZIZ ANALYSIS, EXAMPLE 4

Time (hours)	$\Delta p_p/q$ [psia^2/(cp-MMscf/D)] $q=31.612$ MMscf/D	$q=44.313$ MMscf/D	$q=56.287$ MMscf/D	$q=70.265$ MMscf/D
3.0	1.202×10^6	1.291×10^6	1.585×10^6	1.883×10^6
4.0	1.297×10^6	1.352×10^6	1.642×10^6	1.995×10^6
5.0	1.360×10^6	1.415×10^6	1.682×10^6	2.069×10^6
6.0	1.392×10^6	1.428×10^6	1.707×10^6	2.121×10^6

TABLE 5.24

LEAST-SQUARES REGRESSION FOR SLOPES, EXAMPLE 4

Point	q	q^2	Δp_p	$\Delta p_p/q$
1	31.612	0.999×10^3	3.800×10^7	1.202×10^6
2	44.313	1.965×10^3	5.724×10^7	1.291×10^6
3	56.287	3.168×10^3	8.920×10^7	1.585×10^6
4	70.265	4.937×10^3	1.323×10^7	1.883×10^6
$\Sigma =$	202.477	1.107×10^4	3.167×10^8	5.961×10^6

TABLE 5.25

SLOPES, b, OF THE ISOCHRONS, EXAMPLE 4

t (hours)	b [psia^2/(cp-MMscf/D)]
3.0	1.823×10^4
4.0	1.870×10^4
5.0	1.881×10^4
6.0	1.939×10^4

TABLE 5.26

LEAST-SQUARES REGRESSION FOR INTERCEPTS, EXAMPLE 4

Point	q	q^2	Δp_p	$\Delta p_p/q$
1	31.612	0.999×10^3	3.800×10^7	1.202×10^6
2	44.313	1.965×10^3	5.724×10^7	1.291×10^6
3	56.287	3.168×10^3	8.920×10^7	1.585×10^6
4	70.265	4.937×10^3	1.323×10^7	1.883×10^6
$\Sigma =$	202.477	1.107×10^4	3.167×10^8	5.961×10^6

TABLE 5.27

TRANSIENT DELIVERABILITY LINE INTERCEPTS, a_t, OF THE ISOCHRONS, EXAMPLE 4

t (hours)	b (psia^2/cp/MMscf-D)
3.0	5.677×10^5
4.0	6.247×10^5
5.0	6.794×10^5
6.0	6.807×10^5

TABLE 5.28

LEAST-SQUARES REGRESSION ON TRANSIENT INTERCEPTS, a_t, EXAMPLE .4

Point	log(t)	[log(t)]^2	a_t	a_t log(t)
1	0.477	0.228	5.677×10^5	2.708×10^5
2	0.602	0.362	6.247×10^5	3.761×10^5
3	0.699	0.489	6.794×10^5	4.749×10^5
4	0.778	0.605	6.807×10^5	5.296×10^5
$\Sigma =$	2.556	1.684	2.553×10^6	1.651×10^6

TABLE 5.29

PLOTTING FUNCTIONS FOR STABILIZED C METHOD, EXAMPLE .4

	Δp_p (psia^2/cp)			
Time (hours)	$q = 31.612$ MMscf/D	$q = 44.313$ MMscf/D	$q = 56.287$ MMscf/D	$q = 70.265$ MMscf/D
3.0	3.800×10^7	5.720×10^7	8.920×10^7	1.323×10^8
4.0	4.100×10^7	5.990×10^7	9.240×10^7	1.402×10^8
5.0	4.300×10^7	6.270×10^7	9.470×10^7	1.454×10^8
6.0	4.400×10^7	6.330×10^7	9.610×10^7	1.490×10^8

TABLE 5.30

LEAST-SQUARES REGRESSION, STABILIZED C METHOD, EXAMPLE .4

Point	log q	log Δp_p	(log Δp_p)^2	log q log Δp_p
1	1.4999	7.5789	57.4531	11.3686
2	1.6465	7.7574	60.1773	12.7726
3	1.7504	7.9504	63.2089	13.9164
4	1.8467	8.1216	65.9604	14.9982
$\Sigma =$	6.7435	31.4091	246.7983	53.0561

TABLE 5.31

DELIVERABILITY EXPONENTS, n, OF THE ISOCHRONS, EXAMPLE 4

t (hours)	n
3.0	0.63
4.0	0.64
5.0	0.65
6.0	0.65

TABLE 5.32

COMPARISON OF RESULTS FROM EXAMPLE 4

Parameter	Without Stabilized Data		With Stabilized Data	
	Stabilized C Method	Brar and Aziz Method	Rawlins-Schellhardt	Houpeurt
n	0.64	—	0.54	—
C, (MMscf/D)/(psia^2/cp)^n	3.60×10^{-4}	—	2.426×10^{-3}	—
a, psia^2/(cp-MMscf/D)	1.227×10^6	1.227×10^6	—	1.455×10^6
b, psia^2/(cp-MMscf/D^2)	1.873×10^4	1.873×10^4	—	1.774×10^4
AOF, MMscf/D	218.7	205.9	180.1	205.6

TABLE 5.33

ISOCHRONAL TEST DATA, PROBLEM .2

t (hours)	q (MMscf/D)	p_{wf} (psia)	$p_p(p_{wf})$ (psia^2/cp)	Δp_p (psia^2/cp)	$\Delta p_p/q$ (psia^2/cp-MMscf/D)
1	1.224	425.75	1.4692×10^7	0.538×10^6	4.395×10^5
2	1.215	422.37	1.4483×10^7	0.747×10^6	6.148×10^5
3	1.200	416.32	1.4116×10^7	1.114×10^6	9.283×10^5
1	4.262	371.08	1.1577×10^7	3.653×10^6	8.571×10^5
2	4.114	355.77	1.0797×10^7	4.433×10^6	1.078×10^6
3	4.022	345.89	1.0313×10^7	4.917×10^6	1.223×10^6
1	1.710	414.47	1.4004×10^7	1.226×10^6	7.170×10^5
2	1.691	409.59	1.3715×10^7	1.515×10^6	8.959×10^5
3	1.680	406.33	1.3523×10^7	1.707×10^6	1.016×10^6
1	2.107	407.35	1.3583×10^7	1.647×10^6	7.817×10^5
2	2.073	400.45	1.3183×10^7	2.047×10^6	9.875×10^5
3	2.054	396.01	1.2931×10^7	2.299×10^6	1.119×10^6
1	3.057	389.91	1.2590×10^7	2.640×10^6	8.636×10^5
2	2.986	379.66	1.2031×10^7	3.199×10^6	1.071×10^6
3	2.942	373.04	1.1679×10^7	3.551×10^6	1.207×10^6
72 (Extended flow point)	3.238	259.79	0.6883×10^7	8.347×10^6	2.579×10^6

TABLE 5.34

MODIFIED ISOCHRONAL TEST DATA, PROBLEM .4

t (hours)	q (MMscf/D)	p_{wf} (psia)	$p_p(p_{wf})$ (psia^2/cp)
2	1.9	2,910	5.7135×10^8
2	2.7	2,860	5.5415×10^8
2	3.6	2,804	5.3509×10^8
2	4.5	2,750	5.1690×10^8
16	4.5	2,630	4.7720×10^8
(Extended flow point)			

TABLE 5.35

MODIFIED ISOCHRONAL TEST DATA, PROBLEM .5

Reservoir Data

$h = 4$ ft	$p = 1{,}188.5$ psia	$A = 640$ acres (assume well is centered in a square drainage area)
$r_w = 0.12$ ft	$\bar{\mu} = 0.015$ cp	
$\phi = 0.19$	$z = 0.902$	
$T = 602°R$ (142°F)	$c_g = 8.8 \times 10^{-4}$ psia^{-1}	

Modified Isochronal Test Data

Time (hours)	p_{wf} (psia)			
	$q = 2.104$ MMscf/D	$q = 3.653$ MMscf/D	$q = 4.026$ MMscf/D	$q = 5.079$ MMscf/D
0 (p_{ws})	1,188.5	1,187.1	1,186.4	1,186.0
0.5	1,072.9	954.0	887.2	721.1
1.0	1,072.6	946.9	883.5	715.5
1.5	1,071.4	944.4	882.5	713.5
2.0	1,070.6	944.2	882.3	713.2
	$p_p(p_{wf})$ psia^2/cp			
0[$\Delta p_p(p_{ws})$]	11.230×10^7	11.204×10^7	11.191×10^7	11.184×10^7
0.5	9.1846×10^7	7.2776×10^7	6.2940×10^7	4.1355×10^7
1.0	9.1795×10^7	7.1700×10^7	6.2414×10^7	4.0704×10^7
1.5	9.1593×10^7	7.1323×10^7	6.2272×10^7	4.0473×10^7
2.0	9.1458×10^7	7.1293×10^7	6.2243×10^7	4.0438×10^7

Extended Flow Point

$p_{wf} = 738.0$ psia	$t = 7$ hours
$p = 1{,}188.5$ psia	$q = 4.964$ MMscf/D
$p_p(p_{wf}) = 4.3353 \times 10^7$ psia^2/cp	$\Delta p_p/q = 1.3889 \times 10^7$ psia^2/cp/MMscf-D
$\Delta p_p(p) = 6.8947 \times 10^7$ psia^2/cp	$p_p(14.65) = 2{,}326.6$ psia^2/cp

TABLE 5.36

MODIFIED ISOCHRONAL TEST DATA, PROBLEM 7

Reservoir Data

$h = 35$ ft	$p = 7{,}121$ psia	$A = 160$ acres
$r_w = 0.1875$ ft	$\bar{\mu} = 0.0286$ cp	(assume well is
$\phi = 0.08$	$\bar{z} = 1.145$	centered in a square
$T = 715°R$	$\bar{c}_g = 7.4 \times 10^{-5}$ psia^{-1}	drainage area)

Modified Isochronal Test Data

Time (hours)	p_{wf} (psia) $q = 8.584$ MMscf/D	$q = 9.879$ MMscf/D	$q = 12.867$ MMscf/D
0 (p_{ws})	7,121	7,101	7,085
6.0	6,250	6,006	5,388
7.0	6,238	5,989	5,360
8.0	6,226	5,975	5,338
9.0	6,216	5,965	5,319
	$p_p(p_{wf})$ psia^2/cp		
0[$\Delta p_p(p_{ws})$]	2.1545×10^9	2.1470×10^9	2.1411×10^9
6.0	1.8297×10^9	1.7358×10^9	1.5018×10^9
7.0	1.8233×10^9	1.7293×10^9	1.4912×10^9
8.0	1.8188×10^9	1.7240×10^9	1.4828×10^9
9.0	1.8150×10^9	1.7203×10^9	1.4756×10^9

Extended Flow Point

$p_{wf} = 5845$ psia	$t = 120$ hours
$\bar{p} = 7121$ psia	$q = 9.225$ MMscf/D
$p_p(p_{wf}) = 1.5054 \times 10^9$ psia^2/cp	$p_p(14.65) = 13{,}788$ psia^2/cp

TABLE 5.37

FLOW-AFTER-FLOW DATA			
q (MMscf/D)	$T_{f,tf}$ (°F)	p_{tf} (psia)	p_{wf} (psia)
0	75	375.2	407.60
4.288	70	371.2	403.13
9.265	73	361.3	393.03
15.552	77	343.8	375.79
20.177	77	327.1	359.87

TABLE 5.38

PLOTTING FUNCTIONS FOR RAWLINS-SCHELLHARDT ANALYSIS.		
q (MMscf/D)	p_{wf}^2 (psia^2)	$\Delta p^2 = \bar{p}^2 - p_{wf}^2$ (psia^2)
0	1.661×10^5	0
4.288	1.625×10^5	0.360×10^4
9.265	1.545×10^5	1.160×10^4
15.552	1.412×10^5	2.490×10^4
20.177	1.295×10^5	3.660×10^4

TABLE 5.39

CALCULATION OF n				
Point	$\log q$	$\log \Delta p^2$	$(\log \Delta p^2)^2$	$\log q \log \Delta p^2$
1	0.632	3.556	12.645	2.247
2	0.967	4.064	16.516	3.930
3	1.192	4.396	19.325	5.240
4	1.305	4.563	20.821	5.955
$\Sigma =$	4.096	16.579	69.307	17.372

$$n = \frac{N \sum_{j=1}^{N} (\log q \log \Delta p^2)_j - \sum_{j=1}^{N} \log q_j \sum_{j=1}^{N} (\log \Delta p^2)_j}{N \sum_{j=1}^{N} (\log \Delta p^2)_j^2 - \left[\sum_{j=1}^{N} (\log \Delta p^2)_j \right]^2}$$

$$= \frac{4(17.372) - (4.096)(16.579)}{4(69.307) - (16.579)^2}$$

$$= 0.668.$$

TABLE 5.40

PLOTTING FUNCTIONS FOR HOUPEURT ANALYSIS	
q (MMscf/D)	$\Delta p^2/q=(\bar{p}^2-p_{wf}^2)/q$ (psia^2)/(MMscf/D)
4.288	0.8302×10^5
9.265	1.232×10^5
15.552	1.567×10^5
20.177	1.775×10^5

TABLE 5.41

CALCULATIONS FOR a AND b				
Point	q	q^2	Δp^2	$\Delta p^2/q$
2	9.265	85.84	1.160×10^4	1.252×10^3
3	15.552	241.87	2.490×10^4	1.601×10^3
4	20.177	407.11	3.660×10^4	1.814×10^3
$\Sigma=$	44.994	734.82	7.310×10^4	4.667×10^3

TABLE 5.42

ISOCHRONAL TEST DATA			
Time (hours)	Rate (MMscf/D)	p_{wf} (psia)	p_{wf}^2 (psia^2/cp)
0.5	0.983	344.7	1.188×10^5
1.0	0.977	342.4	1.172×10^5
2.0	0.970	339.5	1.153×10^5
3.0	0.965	337.6	1.140×10^5
0.5	2.631	329.5	1.086×10^5
1.0	2.588	322.9	1.043×10^5
2.0	2.533	315.4	9.948×10^4
3.0	2.500	310.5	9.641×10^4
0.5	3.654	318.7	1.016×10^5
1.0	3.565	309.5	9.579×10^4
2.0	3.453	298.6	8.916×10^4
3.0	3.390	291.9	8.521×10^4
0.5	4.782	305.5	9.333×10^4
1.0	4.625	293.6	8.620×10^4
2.0	4.438	279.6	7.818×10^4
3.0	4.318	270.5	7.317×10^4
214	1.156	291.3	8.486×10^4

TABLE 5.43

PLOTTING FUNCTIONS FOR THE RAWLINS-SCHELLHARDT ANALYSIS			
Rate (MMscf/D)	Δp^2 (psia^2/cp)	Rate (MMscf/D)	Δp^2 (psia^2/cp)
0.983	5.368×10^3	3.654	2.262×10^4
0.977	6.948×10^3	3.565	2.840×10^4
0.970	8.926×10^3	3.453	3.502×10^4
0.965	1.021×10^4	3.390	3.898×10^4
2.631	1.562×10^4	4.782	3.086×10^4
2.588	1.992×10^4	4.625	3.798×10^4
2.533	2.471×10^4	4.438	4.601×10^4
2.500	2.778×10^4	4.318	5.102×10^4
		1.156	3.933×10^4

TABLE 5.44

CALCULATION OF n

Point	$\log q$	$\log \Delta p^2$	$(\log \Delta p^2)^2$	$\log q \log \Delta p^2$
1	−0.007	3.730	13.911	−0.026
2	0.420	4.194	17.586	1.762
3	0.563	4.354	18.961	2.451
4	0.680	4.489	20.154	3.051
$\Sigma =$	1.656	16.767	70.612	7.238

$$n_1 = \frac{N \sum_{j=1}^{N} (\log q \log \Delta p^2)_j - \sum_{j=1}^{N} \log q_j \sum_{j=1}^{N} (\log \Delta p^2)_j}{N \sum_{j=1}^{N} (\log \Delta p^2)_j^2 - \left[\sum_{j=1}^{N} (\log \Delta p^2)_j \right]^2}$$

$$= \frac{4(7.238) - (1.656)(16.767)}{4(70.612) - (16.767)^2}$$

$$= 0.901.$$

DELIVERABILITY EXPONENTS FOR VARIOUS FLOWING TIMES

t (hours)	n
0.5	0.901
1.0	0.917
2.0	0.939
3.0	0.961

TABLE 5.45

TABLE 5.46

HOUPEURT PLOTTING FUNCTIONS					
t (hours)	q (MMscf/D)	$\Delta p^2/q$ (psia^2/MMscf/D)	t (hours)	q (MMscf/D)	$\Delta p^2/q$ (psia^2/MMscf/D)
0.5	0.983	0.546×10^4	2.0	0.970	0.920×10^4
	2.631	0.594×10^4		2.533	0.976×10^4
	3.654	0.619×10^4		3.453	1.014×10^4
	4.782	0.645×10^4		4.438	1.037×10^4
1.0	0.977	0.711×10^4	3.0	0.965	1.058×10^4
	2.588	0.770×10^4		2.500	1.111×10^4
	3.565	0.797×10^4		3.390	1.150×10^4
	4.625	0.821×10^4		4.318	1.181×10^4
			214	1.156	3.402×10^4

TABLE 5.47

LEAST-SQUARES REGRESSION ANALYSIS FOR COMPUTING b				
Point	q	q^2	Δp^2	$\Delta p^2/q$
1	0.983	0.966	0.537×10^4	0.546×10^3
2	2.631	6.922	1.562×10^4	0.594×10^3
3	3.654	13.352	2.262×10^4	0.619×10^3
4	4.782	22.868	3.086×10^4	0.645×10^4
$\Sigma =$	12.050	44.108	7.447×10^4	2.404×10^4

TABLE 5.48

SLOPES OF ISOCHRONS	
t (hours)	b (psia^2/(MMscf/D)^2)
0.5	2.625×10^2
1.0	3.022×10^2
2.0	3.435×10^2
3.0	3.755×10^2

TABLE 5.49

MODIFIED ISOCHRONAL TEST DATA,

Time (hours)	p_{wf} (psia) $q = 1.520$ MMscf/D	$q = 2.041$ MMscf/D	$q = 2.688$ MMscf/D	$q = 3.122$ MMscf/D
0(p_{ws})	706.6	706.6	703.5	701.2
0.5	655.6	624.5	578.5	541.7
1.0	653.6	620.7	573.9	537.8
1.5	652.1	619.9	572.3	536.3
2.0	651.3	619.1	570.8	534.7

Extended Flow Point
$p_{wf} = 567.7$ psia
$\bar{p} = 706.6$ psia
$p_{wf}^2 = 3.223 \times 10^5$ psia^2
$t = 24$ hr
$q = 2.665$ MMscf/D

TABLE 5.50

PLOTTING FUNCTIONS FOR RAWLINS-SCHELLHARDT ANALYSIS

Time (hours)	Δp^2 (psia^2) $q = 1.520$ MMscf/D	$q = 2.041$ MMscf/D	$q = 2.688$ MMscf/D	$q = 3.122$ MMscf/D
0.5	0.695×10^5	1.093×10^5	1.603×10^5	1.982×10^5
1.0	0.721×10^5	1.140×10^5	1.656×10^5	2.025×10^5
1.5	0.741×10^5	1.150×10^5	1.674×10^5	2.041×10^5
2.0	0.751×10^5	1.160×10^5	1.691×10^5	2.058×10^5

TABLE 5.51

CALCULATION OF n

Point	$\log q$	$\log \Delta p^2$	$(\log \Delta p^2)^2$	$\log q \log \Delta p^2$
2	0.310	5.039	25.387	1.562
3	0.429	5.205	27.090	2.233
4	0.494	5.297	28.060	2.617
$\Sigma =$	1.233	15.541	80.537	6.412

$$n_t = \frac{N \sum_{j=1}^{N} (\log q \log \Delta p^2)_j - \sum_{j=1}^{N} \log q_j \sum_{j=1}^{N} (\log \Delta p^2)_j}{N \sum_{j=1}^{N} (\log \Delta p^2)_j^2 - \left[\sum_{j=1}^{N} (\log \Delta p^2)_j \right]^2}$$

$$= \frac{3(6.412) - (1.233)(15.541)}{3(80.537) - (15.541)^2}$$

$$= 0.837.$$

TABLE 5.52

SLOPES OF ISOCHRONS

t (hours)	n
0.5	0.837
1.0	0.698
2.0	0.694
3.0	0.758

TABLE 5.53

PLOTTING FUNCTIONS FOR HOUPEURT ANALYSIS

Time (hours)	$\Delta p^2/q$ [psia^2/(MMscf/D)] $q = 1.520$ MMscf/D	$q = 2.041$ MMscf/D	$q = 2.688$ MMscf/D	$q = 3.122$ MMscf/D
0.5	4.571×10^4	5.354×10^4	5.962×10^4	6.350×10^4
1.0	4.743×10^4	5.586×10^4	6.159×10^4	6.485×10^4
1.5	4.872×10^4	5.635×10^4	6.227×10^4	6.536×10^4
2.0	4.940×10^4	5.683×10^4	6.291×10^4	6.591×10^4

TABLE 5.54

CALCULATION OF b

Point	q	q^2	Δp^2	$\Delta p^2/q$
2	2.041	4.166	1.093×10^5	5.354×10^4
3	2.688	7.225	1.603×10^5	5.962×10^4
4	3.122	9.747	1.982×10^5	6.350×10^4
$\Sigma =$	7.851	21.138	4.678×10^5	17.676×10^4

$$b_1 = \frac{N \sum_{j=1}^{N} (\Delta p^2)_j - \sum_{j=1}^{N} q_j \sum_{j=1}^{N} \left(\frac{\Delta p^2}{q}\right)_j}{N \sum_{j=1}^{N} (q_j)^2 - \left(\sum_{j=1}^{N} q_j\right)^2}$$

$$= \frac{3(4.678 \times 10^5) - (7.851)(17.676 \times 10^4)}{3(21.138) - (7.851)^2}$$

$= 8.817 \times 10^3$ psia^2/(MMscf/D).

TABLE 5.55

SLOPES OF THE ISOCHRONS

t (hours)	b [psia^2/(MMscf/D)]
0.5	8.817×10^3
1.0	8.313×10^3
2.0	8.488×10^3
3.0	8.538×10^3

TABLE 5.56

MODIFIED ISOCHRONAL TEST DATA,

Time (hours)	p_{wf} (psia) $q=31.612$ MMscf/D	$q=44.313$ MMscf/D	$q=56.287$ MMscf/D	$q=70.265$ MMscf/D
0(p_{ws})	4,372.6	4,356.0	4,344.3	4,343.6
0.5	4,274.1	4,206.5	4,111.8	3,994.6
1.0	4,266.8	4,199.3	4,103.3	3,973.3
1.5	4,262.5	4,192.0	4,097.0	3,959.6
2.0	4,258.3	4,190.4	4,093.5	3,951.9
	p_{wf}^2 (psia)^2			
0(p_{ws}^2)	1.912×10^7	1.897×10^7	1.887×10^7	1.887×10^7
3.0	1.827×10^7	1.769×10^7	1.691×10^7	1.596×10^7
4.0	1.821×10^7	1.763×10^7	1.684×10^7	1.579×10^7
5.0	1.817×10^7	1.757×10^7	1.679×10^7	1.568×10^7
6.0	1.813×10^7	1.756×10^7	1.676×10^7	1.562×10^7

Extended Flow Point
$p_{wf}=3,794.0$ psia
$\bar{p}=4,372.6$ psia
$p_{wf}^2=1.439\times10^7$ psia^2
$t=72$ hours
$q=77.346$ MMscf/D

TABLE 5.57

PLOTTING FUNCTIONS FOR THE BRAR-AZIZ ANALYSIS

Time (hours)	$\Delta p^2/q$, psia^2/(MMscf/D) $q=31.612$ MMscf/D	$q=44.313$ Mscf/D	$q=56.287$ MMscf/D	$q=70.265$ MMscf/D
3.0	2.694×10^4	2.889×10^4	3.493×10^4	4.142×10^4
4.0	2.891×10^4	3.025×10^4	3.617×10^4	4.383×10^4
5.0	3.007×10^4	3.164×10^4	3.709×10^4	4.538×10^4
6.0	3.121×10^4	3.194×10^4	3.760×10^4	4.624×10^4

TABLE 5.58

VALUES FOR $t = 3$ hours

Point	q	q^2	Δp^2	$\Delta p^2/q$
2	44.313	1.964×10^3	1.280×10^6	2.889×10^4
3	56.287	3.168×10^3	1.966×10^6	3.493×10^4
4	70.265	4.937×10^3	2.910×10^6	4.142×10^4
$\Sigma =$	170.865	10.069×10^3	6.156×10^6	10.524×10^4

$$b_1 = \frac{N \sum_{j=1}^{N} (\Delta p^2)_j - \sum_{j=1}^{N} q_j \sum_{j=1}^{N} \left(\frac{\Delta p^2}{q} \right)_j}{N \sum_{j=1}^{N} (q_j)^2 - \left(\sum_{j=1}^{N} q_j \right)^2}$$

$$= \frac{3(6.156 \times 10^6) - (170.865)(10.524 \times 10^4)}{3(10.069 \times 10^3) - (170.865)^2}$$

$$= 4.803 \times 10^2 \text{ psia}^2/(\text{MMscf/D})^2.$$

TABLE 5.59

SLOPES OF THE ISOCHRONS

t (hours)	b [psia^2/(MMscf/D)^2]
3.0	4.803×10^2
4.0	5.238×10^2
5.0	5.302×10^2
6.0	5.535×10^2

TABLE 5.60

VALUES FOR $t = 3.0$

Point	q	q^2	Δp^2	$\Delta p^2/q$
2	44.313	1.964×10^3	1.280×10^6	2.889×10^4
3	56.287	3.168×10^3	1.966×10^6	3.493×10^4
4	70.265	4.937×10^3	2.910×10^6	4.142×10^4
$\Sigma =$	170.865	10.069×10^3	6.156×10^6	10.524×10^4

$$a_{t1} = \frac{\sum_{j=1}^{N} \left(\frac{\Delta p^2}{q}\right)_j \sum_{j=1}^{N} (q_j)^2 - \sum_{j=1}^{N} q_j \sum_{j=1}^{N} (\Delta p_2)_j}{N \sum_{j=1}^{N} (q_j)^2 - \left(\sum_{j=1}^{N} q_j\right)^2}$$

$$= \frac{(10.524 \times 10^4)(10.069 \times 10^3) - (170.865)(6.156 \times 10^6)}{3(10.069 \times 10^3) - (170.865)^2}$$

$$= 7.723 \times 10^3 \text{ psia}^2/(\text{MMscf/D}).$$

TABLE 5.61

VALUES OF a_t

t (hours)	a_t [psia^2/(MMscf/D)]
3.0	7.723×10^3
4.0	6.919×10^3
5.0	7.842×10^3
6.0	7.067×10^3

TABLE 5.62

CALCULATION OF m' AND c'

Point	log(t)	[log(t)]^2	a_t	a_t log(t)
2	0.602	0.362	6.919×10^3	4.165×10^3
3	0.699	0.489	7.842×10^3	5.482×10^3
4	0.778	0.605	7.067×10^3	5.498×10^3
$\Sigma =$	2.079	1.456	21.828×10^3	15.145×10^3

$$m' = \frac{N \sum_{j=1}^{N} (a_t \log t)_j - \sum_{j=1}^{N} (a_t)_j \sum_{j=1}^{N} (\log t)_j}{N \sum_{j=1}^{N} (\log t_j)^2 - \left(\sum_{j=1}^{N} \log t_j \right)^2}$$

$$= \frac{3(15.145 \times 10^3) - (21.828 \times 10^3)(2.079)}{3(1.456) - (2.079)^2}$$

$$= 1.193 \times 10^3 \text{ psia}^2/(\text{MMscf/D})/\text{cycle}$$

$$c' = \frac{N \sum_{j=1}^{N} (a_t)_j \sum_{j=1}^{N} (\log t_j) - \sum_{j=1}^{N} (a_t \log t)_j \sum_{j=1}^{N} (\log t)_j}{N \sum_{j=1}^{N} (\log t_j)^2 - \left(\sum_{j=1}^{N} \log t_j \right)^2}$$

$$= \frac{(21.828 \times 10^3)(1.456) - (15.145 \times 10^3)(2.079)}{3(1.456) - (2.079)^2}$$

$$= 6.449 \times 10^3 \text{ psia}^2/(\text{MMscf/D})$$

TABLE 5.63

PLOTTING FUNCTIONS FOR STABILIZED C METHOD

Time (hours)	Δp^2 (psia^2) $q=31.612$ MMscf/D	$q=44.313$ MMscf/D	$q=56.287$ MMscf/D	$q=70.265$ MMscf/D
3.0	0.852×10^6	1.280×10^6	1.966×10^6	2.910×10^6
4.0	0.914×10^6	1.341×10^6	2.036×10^6	3.080×10^6
5.0	0.951×10^6	1.402×10^6	2.088×10^6	3.188×10^6
6.0	0.987×10^6	1.415×10^6	2.116×10^6	3.249×10^6

TABLE 5.64

VALUES FOR $t=3$ hours

Point	$\log q$	$\log \Delta p^2$	$(\log \Delta p^2)^2$	$\log q \log \Delta p^2$
2	1.647	6.107	37.298	10.056
3	1.750	6.294	39.609	11.016
4	1.847	6.464	41.782	11.937
$\Sigma=$	5.244	18.865	118.690	33.009

$$n_1 = \frac{N\sum_{j=1}^{N}(\log q \log \Delta p^2)_j - \sum_{j=1}^{N}\log q_j \sum_{j=1}^{N}(\log \Delta p^2)_j}{N\sum_{j=1}^{N}(\log \Delta p^2)_j^2 - \left[\sum_{j=1}^{N}(\log \Delta p^2)_j\right]^2}$$

$$= \frac{3(33.009) - (5.244)(18.865)}{3(118.690) - (18.865)^2}$$

$$= 0.544.$$

TABLE 5.65

DELIVERABILITY EXPONENTS, *n*	
t (hours)	*n*
3.0	0.544
4.0	0.554
5.0	0.536
6.0	0.502

TABLE 5.66

COMPARISON OF RESULTS				
	Without Stabilized Data		With Stabilized Data	
Parameter	Stabilized C Method	Brar-Aziz Method	Rawlins-Schellhardt	Houpeurt
n	0.534	—	0.534	—
C	2.397×10^{-2}	—	2.109×10^{-2}	—
a, psia^2/(cp-MMscf/D)	8.019×10^3	8.019×10^3	—	2.078×10^4
b, psia^2/(cp-MMscf/D)^2	5.220×10^2	5.220×10^2	—	5.220×10^2
q_{AOF}, MMscf/D	184.3	183.9	163.1	172.5